UC Santa Barbara

UC Santa Barbara Electronic Theses and Dissertations

Title

Total Syntheses of N-Desmethyl Thalassospiramide C, Isotopically Labeled (+)-Anatoxin-a, and Xestospongin-type Natural Products

Permalink

https://escholarship.org/uc/item/79c7x38r

Author

Chen, Karen Yir Jing

Publication Date

2022

Peer reviewed|Thesis/dissertation

eScholarship.org Powered by the California Digital Library
University of California

UNIVERSITY OF CALIFORNIA

Santa Barbara

Total Syntheses of *N*-Desmethyl Thalassospiramide C, Isotopically Labeled (+)-Anatoxin-a, and Xestospongin-type Natural Products

A dissertation submitted in partial satisfaction of the
requirements for the degree Doctor of Philosophy
in Chemistry

by

Karen Yir Jing Chen

Committee in charge:
Professor Armen Zakarian, Chair
Professor Liming Zhang
Professor Thomas R. R. Pettus
Professor Gabriel Ménard

June 2022

The dissertation of Karen Yir Jing Chen is approved.

Liming Zhang

Thomas R. R. Pettus

Gabriel Ménard

Armen Zakarian, Committee Chair

May 2022

Total Syntheses of *N*-Desmethyl Thalassospiramide C, Isotopically Labeled (+)-Anatoxin-a,
and Xestospongin-type Natural Products

Copyright © 2022

by

Karen Yir Jing Chen

ACKNOWLEDGEMENTS

My research presented in this dissertation would not have been possible without the assistance of many individuals that I interacted with during the course of my graduate career at UC Santa Barbara. First and foremost, I would like to thank my research advisor, Professor Armen Zakarian, for whom there are no words to convey my gratitude and respect. His support and insight guided my journey of becoming an independent researcher, and the wealth of knowledge that he imparted to me will continue to be invaluable in my future career pursuits.

I would like to thank my thesis committee, Professors Liming Zhang, Thomas R. R. Pettus, and Gabriel Ménard, for the direction and constructive criticism throughout my time at UCSB. Their feedback helped me develop a broader perspective on my research than what was possible within the lab. I am also grateful to those whose past advice and mentorship continue to shape and motivate me: Professors David Lombard, Jye-Shane Yang, and Chi-Huey Wong, and Drs. Jeongsoon Park and Hui-Min Yu.

While it is impossible to list all of those who have had an impact on my career thus far, I would like to extend my sincere thanks to colleagues in the Zakarian group, past and present, for constant encouragement, friendship, and stimulating chemistry discussions. In particular, I would like to thank Dr. Jeremy Fournier for guidance even exceeding my first project on thalassospiramides, and Dr. Artur Mailyan for his tutelage far beyond our work on the (+)-[$^{13}C_4$]-anatoxin-a project. It was also a great pleasure working with Drs. Jacob Lacharity and Maša Podunavac, and Alana Borum.

To my family, I cannot begin to express my thanks; each and every one of them have always stood by me with endless love, support, and faith. I am extremely grateful for my mom, Hsiou-Ann Hu, who with her unconditional love and confidence would do anything and has never failed to lift my spirits up, for my dad, Dr. Chin-Wen Chen, who is the constant inspiration and role model I look up to even in aspects greater than life, and for my brother, William Chen, who with his admirable character motivates me to do better every day. I would not have been able to make it this far without their unwavering nurture. Finally, Dr. Sean Jason Weinberg [Chen], my husband, was instrumental in helping me stride through this journey with kindness, love, and tears of joy, and has repeatedly and faithfully provided words of encouragements and wisdom. Thank you for being such a great cheerleader and life coach.

Curriculum Vitae

Karen Yir Jing Chen

Department of Chemistry and Biochemistry, University of California, Santa Barbara, CA 93106
karenychen@ucsb.edu · +1 (917) 699-1393

EDUCATION

University of California, Santa Barbara **Sept. 2016 – June 2022**
Doctor of Philosophy in Chemistry

University of Michigan – Ann Arbor **Aug. 2013 – Apr. 2016**
Bachelor of Science in Biochemistry

PUBLICATIONS

1. Lacharity, J. J.; Mailyan, A. K.; **Chen, K. Y.**; Zakarian, A. Concise Synthesis of (+)-[$^{13}C_4$]-Anatoxin-a by Dynamic Kinetic Resolution of a Cyclic Iminium Ion. *Angew. Chem. Int. Ed.* **2020**, *59*, 11364–11368.
2. Fournier, J.; **Chen, K.**; Mailyan, A. K.; Jackson, J. J.; Buckman, B. O.; Emayan, K.; Yuan, S.; Rajagopalan, R.; Misialek, S.; Adler, M.; Blaesse, M.; Griessner, A.; Zakarian, A. Total Synthesis of Covalent Cysteine Protease Inhibitor *N*-Desmethyl Thalassospiramide C and Crystallographic Evidence for Its Mode of Action. *Org. Lett.* **2019**, *21*, 508–512.
3. Tsai, T.-I.; Li, S.-T.; Liu, C.-P.; **Chen, K. Y.**; Shivatare, S. S.; Lin, C.-W.; Liao, S.-F.; Lin, C.-W.; Hsu, T.-L.; Wu, Y.-T.; Tsai, M.-H.; Lai, M.-Y.; Lin, N.-H.; Wu, C.-Y.; Wong, C.-H. An Effective Bacterial Fucosidase for Glycoprotein Remodeling. *ACS Chem. Biol.* **2017**, *12* (1), 63–72.

RESEARCH EXPERIENCE

Prof. Armen Zakarian **Sept. 2016 – June 2022**
University of California, Santa Barbara, Department of Chemistry and Biochemistry | PhD Candidate

1. Total Synthesis of *N*-Desmethyl Thalassospiramide C

   Established the synthesis of *N*-desmethyl thalassospiramide C; its X-ray crystal structure led to the elucidation of the mode of action of these thalassospiramide natural products. This work was published in *Org. Lett.* in 2019.

2. Total Synthesis of (+)-[$^{13}C_4$]-Anatoxin-a

   Established the synthesis of (+)-[$^{13}C_4$]-anatoxin-a for a more precise cyanotoxin determination method to be established. Developed a dynamic kinetic resolution type enantioselective cyclization of a cyclic iminium, a late-stage key intermediate, to furnish the bicyclic structure of (+)-anatoxin-a. Various chiral sulfides were designed and synthesized for the optimization of the enantioselective cyclization. This work was published in *Angew. Chem. Int. Ed.* in 2020.

3. Synthesis of Xestospongin-type Natural Products and Derivatives

   Implemented an established modular synthetic approach for the large-scale synthesis of xestospongin-type natural products. Optimized for more efficient access of key early phase intermediates in shorter steps, higher yields, and high diastereoseletivity for the large-scale synthesis.

Prof. David Lombard **Sept. 2013 – May 2016**
University of Michigan – Ann Arbor, Department of Pathology | Undergraduate Researcher

1. Sirtuin Longevity Proteins in Modulation of Responses to Diet
2. The Sirtuin Sirt5 Plays an Essential Role in Melanoma Cell Proliferation

Prof. Jye-Shane Yang **May 2016 – August 2016**
National Taiwan University, Department of Chemistry | Summer Research Intern

1. Photochemical Analysis and Synthesis of Green Fluorescent Protein-like Chromophore Derivatives

Prof. Chi-Huey Wong **Summer of 2012, 2013, 2015**
Academia Sinica, Genomics Research Center | Summer Research Assistant

1. Breast Cancer Drug Development Targeting Thrombin-PAR-1 Pathway
2. A Versatile Fucosidase for Glycoprotein Remodeling and Glycan Sequencing

---

LEADERSHIP AND INSTRUCTIONAL EXPERIENCE

Teaching Assistant **Sept. 2016 – Dec. 2020**
University of California, Santa Barbara, Department of Chemistry and Biochemistry
General Chemistry Laboratory (1AL, 1BL, 1CL) | Instructor: Dr. Petra Van Koppen
Organic Chemistry Laboratory (6AL, 6BL, 6CL) | Instructor: Dr. Morgan Gainer

Head Teaching Assistant **Sept. 2021 – June 2022**
University of California, Santa Barbara, Department of Chemistry and Biochemistry
Organic Chemistry Laboratory (6AL, 6BL, 6CL) | Instructor: Dr. Morgan Gainer

ABSTRACT

Total Syntheses of *N*-Desmethyl Thalassospiramide C, Isotopically Labeled (+)-Anatoxin-a, and Xestospongin-type Natural Products

By

Karen Yir Jing Chen

Chemical synthesis of structurally complex and biologically active natural products plays a critical role in bridging innovative synthetic methodologies with real-world applications, particularly in medicinal fields. However, limited availability of many natural products impedes further studies of their biological activities and possible therapeutic utilization. Synthetic strategies for natural products have the potential to mitigate their scarcity and, at the same time, provide new insights into complex molecules and their practical uses. This dissertation features the synthetic developments of three natural products: thalassospiramide C, anatoxin-a, and xestospongins. The syntheses of these natural products are widely impactful: while thalassospiramide C and xestospongins are marine natural products with promising clinical significance for drug developments, isotopically labeled anatoxin-a is a key to developing a precise quantification analysis for toxins in fresh water.

The first chapter of this dissertation focuses on the total synthesis of the *N*-desmethyl thalassospiramide C, a first in the family of thalassospiramides natural products. Moreover, its mode of binding was elucidated by the crystallography adduct of *N*-desmethyl thalassospiramide C with cathepsin K. The great inhibitory activity of thalassospiramides against

cysteine proteases was clearly depicted through a covalent addition of cysteine residue to the α,β-unsaturated amide of the macrocycle. Our successful chemical synthesis allowed further evaluation of the bioactivities of this macrocyclic cysteine protease inhibitor and addressed the unique 12-membered depsipeptide macrocyclic core as a pharmacophore unit.

The second chapter highlights the asymmetric total synthesis of (+)-[$^{13}C_4$]-anatoxin-a, the first isotopically labeled synthesis for this commonly found freshwater cyanotoxin. Two enantioselective synthetic approaches were introduced: a route centered around retaining the enantiopurity of materials established through a Sharpless asymmetric epoxidation of an early-stage allylic alcohol, and an approach employing a penultimate enantioselective intramolecular cyclization enabled late-stage stereocontrol. The paramount aza-Morita–Baylis–Hillman cyclization strategically maneuvered a dynamic kinetic resolution of cyclic iminiums to construct the bicyclic core of anatoxin-a. Our novel and robust synthesis demonstrated high scalability, and the successful isotopically labeled synthesis allows for a more precise anatoxin-a quantification method to be established.

The last chapter of this dissertation describes an ongoing study towards a 2nd generation large-scale synthesis of xestospongin-type natural products, a family of marine alkaloid with promising cancer therapeutics. Two key early-stage intermediates were identified as targets for synthesis optimizations—the α-alkoxy acid intermediate and the common azidoalcohol intermediate responsible for a non-symmetrical synthetic design. Optimized routes for both intermediates showcased synthetic efficiencies, with the synthesis of the azidoalcohol featuring a titanium–salalen catalyzed asymmetric epoxidation with hydrogen peroxide of a typically challenging terminal and non-conjugated olefin intermediate. The accomplished shortened and greater yielding synthetic routes for the two intermediates ensures the overall scalability and synthetic ease for the ultimate synthetic access of various xestospongins.

TABLE OF CONTENTS

ACKNOWLEDGEMENTS iv

Curriculum Vitae vi

ABSTRACT viii

TABLE OF CONTENTS x

List of Abbreviations xiii

List of Figures xix

List of Schemes xx

List of Tables xxiii

Chapter 1. Total Synthesis of *N*-Desmethyl Thalassospiramide C 1

- 1.1. Introduction 2
  - 1.1.1. Background 2
  - 1.1.2. Biological Studies and Synthesis Motivation 3
- 1.2. Total Synthesis Approach 5
  - 1.2.1. Synthetic Considerations 5
  - 1.2.2. Synthesis of Lipopeptide Side Chain **4** 8
  - 1.2.3. Preparation of the Precursors **15a** and **15b** Containing **3** 8
  - 1.2.4. Construction of the Macrocycle **9** 9
  - 1.2.5. Completion of the Total Synthesis 13
- 1.3. Analyses of the Bioactivity and Mode of Binding of **8** 14
- 1.4. Conclusion 18
- References 19

Chapter 2. Total Synthesis of (+)-[$^{13}C_4$]-Anatoxin-a via a Dynamic Kinetic Resolution of a Cyclic Iminium Ion 22

2.1. Introduction 23

2.1.1. Background 23

2.1.2. Previous Syntheses 25

2.1.3. Motivation for an Isotopically Labeled (+)-Anatoxin-a Synthesis 28

2.2. Total Synthesis of (+)-[$^{13}C_4$]-Anatoxin-a 30

2.2.1. Synthesis Plan 30

2.2.2. Synthesis of Allylic Alcohol [$^{13}C_4$]-**44** 31

2.2.3. Completion of the Asymmetric Total Synthesis of [$^{13}C_4$]-**23** 34

2.3. A Dynamic Kinetic Resolution Enantioselective aza-Morita–Baylis–Hillman (aza-MBH) Cyclization 36

2.3.1. Initial Studies of Cyclic Iminium Ion Racemization 36

2.3.2. Proposed Dynamic Kinetic Resolution Design 41

2.3.3. Optimization of the Enantioselective aza-MBH Cyclization 44

2.4. Conclusion 49

References 50

Chapter 3. Large Scale Synthesis Efforts Towards Xestospongin-type Marine Natural Products 54

3.1. Introduction 55

3.1.1. Isolation and Biological Activity 55

3.1.2. Biological Studies and Background 57

3.1.3. Motivation for a Large-Scale Chemical Synthesis 59

3.2. Previous Syntheses 60

3.2.1. Hoye's C_2-Symmetric Synthesis of (−)-Xestospongin A 61

3.2.2. Baldwin's C_2-Symmetric Synthesis of (−)-Xestospongin A 63

3.2.3. Zakarian's C_2-Asymmetric Synthesis of (+)-Desmethylxestospongin B 66

3.3. A 2nd Generation Total Synthesis Approach 70

3.3.1. Merits of a 2nd Generation Synthesis 70

3.3.2. Shortened Synthesis of the α-Alkoxy Valeric Acid Intermediate.......................... 73

3.3.3. An Improved Synthesis Design for the Azidoalcohol **95** 75

3.3.4. Future Optimization Studies 82

3.4. Conclusion 85

References 86

Experimental Procedures 91

References 212

^{1}H NMR and ^{13}C NMR Spectra 214

List of Abbreviations

[α]	specific rotation
Å	angstrom
Ac	acetyl
acac	acetylacetone (ligand)
Alloc	allyloxy carbonyl
AMP	adenosine 5'-monophosphate
AMPK	5' adenosine monophosphate-activated protein kinase
Arg	arginine
Asn	asparagine
ATP	adenosine 5'-triphosphate
BINAP	2,2'-bis(diphenylphosphino)-1,1'-binaphthyl (ligand)
Bn	benzyl
Boc	*tert*-butyl carbonate
br	broad (spectra)
Bu	butyl
Bz	benzoyl
c	concentration
calcd	calculated
COMU	1-[(1-(cyano-2-ethoxy-2-oxoethylideneaminooxy)-dimethylamino-morpholinomethylene)]methanaminium hexafluorophosphate
CSA	10-camphorsulfonic acid
Cys	cysteine
δ	chemical shift(s) in parts per million

°	degrees
°C	degrees Celsius
d	doublet (spectra)
D	dexter (configuration)
dba	dibenzylideneacetone (ligand)
DBU	2,3,4,6,7,8,9,10-octahydropyrimido[1,2-*a*]azepine
DCC	*N*,*N*'-dicyclohexylmethanediimine
DDQ	4,5-dichloro-3,6-dioxocyclohexa-1,4-diene-1,2-dicarbonitrile
DEAD	diethyl azodicarboxylate
(−)-DIPT	(−)-diisopropyl D-tartrate
DMAP	*N*,*N*-4-dimethylaminopyridine
DMF	dimethylformamide
DMPU	*N*,*N*'-dimethylpropyleneurea
DMSO	dimethyl sulfoxide
dr	diastereomeric ratio
DTE	dithioerythritol
E	entgegen (configuration)
EDCI·HCl	3-{[(ethylimino)methylidene]amino}-*N*,*N*-dimethylpropan-1-amine hydrochloride
ee	enantiomeric excess
EPA	Environmental Protection Agency
ER	endoplasmic reticulum
ESI	electrospray ionization
Et	ethyl

g	gram(s)
Gln	glutamine
Gly	glycine
h	hour(s); heptet (spectra)
HATU	(1-[bis(dimethylamino)methylene]-1*H*-1,2,3-triazolo[4,5-*b*]pyridinium 3-oxide hexafluorophosphate
HBTU	3-[bis(dimethylamino)methyliumyl]-3*H*-benzotriazol-1-oxide hexafluorophosphate
HMPA	hexamethylphosphoramide
HOAt	3*H*-[1,2,3]-triazolo[4,5-*b*]pyridin-3-ol
HOBt	1*H*-1,2,3-benzotriazol-1-ol
HPLC	high-performance liquid chromatography
HRMS	high-resolution mass spectrometry
Hz	hertz
i	iso
i.p.	intraperitoneally
IC_{50}	half maximal inhibitory concentration
IP_3	inositol-1,4,5-triphosphate
IP_3R	inositol-1,4,5-triphosphate receptor
J	coupling constant (spectra)
L	laevus (configuration)
LD_{50}	dose that is lethal to 50% of test subjects
LDA	lithium diisopropylamide

LRMS	low-resolution mass spectrometry
μL	microliter(s)
m	multiplet (spectra)
M	molar
[M + H]	molecular mass + hydrogen
m/*z*	mass/charge
Me	methyl
MES	2-morpholinoethanesulfonic acid
mg	milligram(s)
MHz	megahertz
min	minute(s)
mL	milliliter(s)
mmHg	millimeters of mercury (measure of pressure)
mmol	millimole(s)
mol	mole(s)
Ms	methylsulfonyl
MS	molecular sieves
n	normal
NBS	*N*-bromosuccinimide
nM	nanomolar
NMR	nuclear magnetic resonance
PDB	Protein Data Bank
PMB	*para*-methoxybenzyl
Ph	phenyl

PPTS	pyridinium *para*-toluenesulfonate
Pr	propyl
PyBOP	(benzotriazol-1-yloxy)tripyrrolidinophosphonium hexafluorophosphate
q	quartet (spectra)
quant	quantitative
R	generic functional group
R	rectus (configurational)
RCM	ring-closing metathesis
s	singlet (spectra)
S	sinister (configurational)
salen	*N*,*N*'-bis(salicylidene)ethylenediaminato (ligand)
sat. FA	saturated fatty acid at the *N*-terminus
Ser	serine
sp.	species (singular)
t	triplet (spectra)
TBS	*tert*-butyldimethylsilyl
TCA	tricarboxylic acid cycle
TEMPO	(2,2,6,6-tetramethylpiperidin-1-yl)oxyl
Tf	trifluoromethanesulfonyl
Th	thienyl (ligand)
THF	tetrahydrofuran
TLC	thin-layer chromatography
Ts	4-toluenesulfonyl
Tyr	tyrosine

Val	valine
wt	weight
Z	zusammen (configuration)

List of Figures

Figure 1. Structures of Thalassospiramides A–F with reported IC_{50} values. 2

Figure 2. Protease inhibitors with Michael acceptors targeting cysteine residues for covalent C–S binding: the electrophilic warheads (α,β-unsaturated carbonyls) are highlighted in blue. 4

Figure 3. a) Ring conformation of macrocycle **5** showing large ring strain and b) the inward orienting N–Me of **5**. 6

Figure 4. Focused view of the crystal structure of **8** bound to cathepsin K (PDB entry 6hgy). 15

Figure 5. a) Enlarged view of crystal structure of cathepsin K and **8**; b–e) superpositions of other homologous cysteine proteases on the crystal structure of the adduct between **8** and cathepsin K. 17

Figure 6. Four most commonly found cyanotoxins in the U.S. identified by the EPA. 24

Figure 7. Xestospongin-type marine natural products. 55

Figure 8. The step counts and yields from the reported synthesis of dmXe B (**69b**) for the three critical intermediates identified in Zakarian's synthesis design: **102**, **103**, and **95**. 70

Figure 9. Comparison of the step counts and yields of the two routes for accessing key synthetic intermediates. 83

Figure 10. Crystal electron density map for the covalent complex of **8** with cathepsin K. 118

Figure 11. Specific rotations of 2,5-disubstituted thiolanes. 159

List of Schemes

Scheme 1. Evaluation of Activity by Chemical Modifications of Active Sites. 3

Scheme 2. a) Two Key Synthetic Targets and b) Construction of the Lipopeptide Side Chain **3**. 5

Scheme 3. Synthesis Plan for the Cyclization of Macrocycles **9a** and **9b**. 7

Scheme 4. Synthesis of the Lipopeptide Side Chain **4**. 8

Scheme 5. Preparation of Precursors Incorporating **3**. 9

Scheme 6. Incorporation of L-Serine and L-Valine Residues. 9

Scheme 7. Preparation of the Linear Depsipeptides **12a** and **12b**. 10

Scheme 8. Synthesis of Macrocycle **9a** via Path A and Path B. 11

Scheme 9. Completion of the Total Synthesis of **8**. 13

Scheme 10. Previous Synthetic Approaches to Construct the Bicyclic System of **23**, and Potential Incorporation of Isotopes for a Synthesis of an Isotopically Labeled **23**. 28

Scheme 11. Synthesis Plan for [$^{13}C_4$]-**23**. 31

Scheme 12. Precursors Synthesis for the Development of the Chiral Alcohol [$^{13}C_4$]-**44**. 32

Scheme 13. Three Enantioselective Approaches for the Preparation of Chiral Alcohol [$^{13}C_4$]-**44**. 32

Scheme 14. Completion of the Total Synthesis of [$^{13}C_4$]-**23**. 35

Scheme 15. a) Observed Racemization During aza-MBH Cyclization, b) Tanner's Observed Racemization, and c) Tanner's Proposed Iminium Racemization Mechanism 37

Scheme 16. Proposed Acid-Catalyzed Isomerization of Iminiums at Temperatures at or Above −30 °C. 40

Scheme 17. a) Proposed Enantioselective aza-MBH Cyclization through a Dynamic Kinetic Resolution; b) Synthesis of (±)-[$^{13}C_4$]-**39** from Direct Access of (±)-[$^{13}C_4$]-**44**. 42

Scheme 18. The Relative Energy Profiles for Our Proposed Dynamic Kinetic Resolution aza-MBH Explained by the Curtin–Hammett Principle. 43

Scheme 19. a) Hoye's Dimerization Approach and b) the Key Condensation Reaction for Constructing the 1-Oxaquinolizidine Rings in Hoye's Synthesis. 61

Scheme 20. Hoye's Macrocyclic Dimerization: a) With and b) without Rigid Modifiers. 62

Scheme 21. a) Baldwin's Biomimetic Synthesis Plan and b) Baldwin's Dimeric Synthesis of Dehydroxestospongin **90** from 3-Alkylpyridine Monomers. 64

Scheme 22. Baldwin's Synthesis: Access to the C_2-Symmetric *ent*-**68a** and *ent*-**70a**, and Their C9/C9' Epimer, *ent*-**71a**. 65

Scheme 23. Zakarian's Synthesis Design for Xestospongin-type Natural Products with Varying Substitution and Stereochemistry at the C9/C9' Positions. 67

Scheme 24. Zakarian's Synthesis of the Hydroxylated and C_2-Asymmetrical **69b**. 69

Scheme 25. Reported Synthesis of Acyl Chloride **102**, the α-Alkoxy Valeric Acid Intermediate. 71

Scheme 26. Reported Synthesis of the Common Intermediate Azidoalcohol **95**. 73

Scheme 27. Synthesis of the α-Alkoxy Valeric Acid Intermediate **117** in the 2nd Generation Synthesis. 74

Scheme 28. The 2nd Generation Synthesis of Azidoalcohol **95**: a) Synthesis Plan and b) Synthetic Access to the Terminal Alkene Precursor **121**. 76

Scheme 29. Asymmetric Epoxidation Methods Attempted on the Terminal Alkene **121**. 77

Scheme 30. Optimized Synthesis Route for the Azidoalcohol **95** in the 2nd Generation Synthesis. 80

Scheme 31. Superior Synthetic Access of Our New and Improved 2nd Generation Synthesis for Azidoalcohol **95**, Compared to That of the Previously Reported Synthesis. 81

Scheme 32. Possible Epimerization Mechanism of Thiolane **62.** 197

List of Tables

Table 1. Macrocyclization Reagents Tested with **12b**. 12

Table 2. Biochemical Potencies of **8** Against Calpain and Cathepsin Proteases (IC_{50}, nM). 14

Table 3. Parameter Optimization for the aza-MBH Cyclization of **39**..39

Table 4. Optimization of the Chiral Sulfides Used for the Enantioselective aza-MBH Cyclization. 45

Table 5. Reaction Condition Optimizations of the Asymmetric Epoxidation of Olefin **121** for the Large-Scale Preparation of Azidoalcohol **95**. 79

Table 6. Enzyme and Reagents with Assay Conditions..115

Table 7. Crystallographic Data Collection and Refinement Statistics. (PDB code 6HGY) 117

Table 8. Enantioselective aza-MBH Cyclization Conditions with Various Chiral Sulfides. 192

Chapter 1.

Total Synthesis of *N*-Desmethyl Thalassospiramide C

1.1. Introduction

1.1.1. Background

In 2007, the Fenical group isolated and characterized thalassospiramides A (**1**) and B from the marine bacteria *Thalassospira* sp. CNJ-328.[1] The works of Qian and Moore in 2013 revealed the biosynthesis of thalassospiramides, along with the identification of additional 14 members of this family of marine natural products isolated from marine α-proteobacteria *Thalassospira* and *Tristella*.[2,3] Thalassospiramides were shown to have great inhibitory activity against human calpain 1 proteases with IC$_{50}$ values as low as 3.4 nM for thalassospiramide C (**2**, Figure 1). Thalassospiramides are characterized by a shared 12-membered depsipeptide macrocyclic core (highlighted in blue) containing a unique (4*R*)-4-amino-5-hydroxy-2-pentenoic acid **3**, and a (3*Z*)-decenyl lipid residue (highlighted in red).

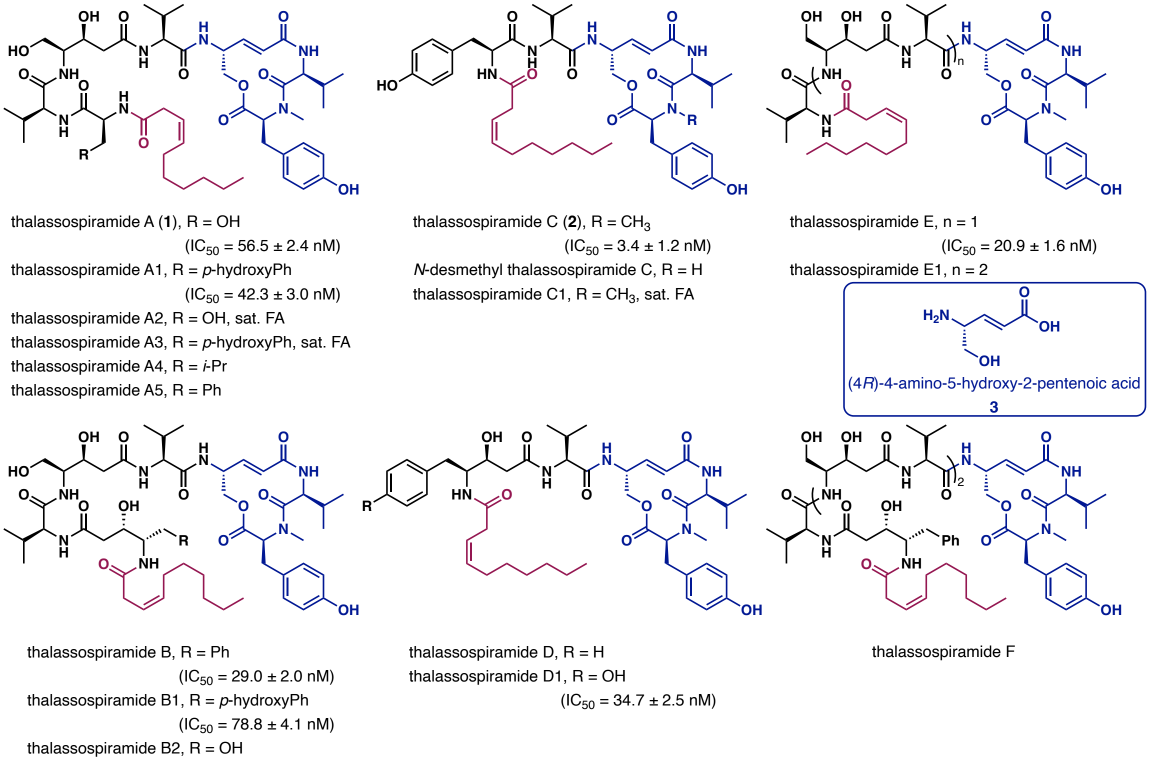
thalassospiramide A (1), R = OH
(IC$_{50}$ = 56.5 ± 2.4 nM)
thalassospiramide A1, R = *p*-hydroxyPh
(IC$_{50}$ = 42.3 ± 3.0 nM)
thalassospiramide A2, R = OH, sat. FA
thalassospiramide A3, R = *p*-hydroxyPh, sat. FA
thalassospiramide A4, R = *i*-Pr
thalassospiramide A5, R = Ph

thalassospiramide C (2), R = CH$_3$
(IC$_{50}$ = 3.4 ± 1.2 nM)
N-desmethyl thalassospiramide C, R = H
thalassospiramide C1, R = CH$_3$, sat. FA

thalassospiramide E, n = 1
(IC$_{50}$ = 20.9 ± 1.6 nM)
thalassospiramide E1, n = 2

(4*R*)-4-amino-5-hydroxy-2-pentenoic acid
3

thalassospiramide B, R = Ph
(IC$_{50}$ = 29.0 ± 2.0 nM)
thalassospiramide B1, R = *p*-hydroxyPh
(IC$_{50}$ = 78.8 ± 4.1 nM)
thalassospiramide B2, R = OH

thalassospiramide D, R = H
thalassospiramide D1, R = OH
(IC$_{50}$ = 34.7 ± 2.5 nM)

thalassospiramide F

Figure 1. Structures of Thalassospiramides A–F with reported IC$_{50}$ values.

1.1.2. Biological Studies and Synthesis Motivation

Calpains are a family of calcium-dependent cysteine proteases catalyzing the proteolysis processes, and are vital in the calcium-mediated signal transductions pathways.[3,4] Unlike other cysteine proteases, such as cathepsins,[5] much of calpains' precise physiological roles in cell regulation and their therapeutic potentials remain unclear.[4] Nevertheless, both calpains and cathepsins are therapeutic targets for numerous conditions including neurodegenerative diseases, fibrosis, cancer, osteoporosis, cardiovascular diseases, muscular dystrophies, and more.[4–6]

In evaluating thalassospiramides' inhibitory activities as calpain inhibitors, Qian and Moore identified the α,β-unsaturated carbonyl moiety present in **3** within the macrocyclic unit, as the pharmacological active site responsible for the nanomolar concentration inhibition.[3,7] This was supported by a 100-fold decrease in inhibitory activity upon hydrogenation of the C17 double bond (Scheme 1).[3] Additionally, the congested cyclic system was revealed to be critical for the observed bioactivity; hydrolysis of the C1 macrocyclic ester resulted in loss of bioactivity.[3]

Scheme 1. Evaluation of Activity by Chemical Modifications of Active Sites.

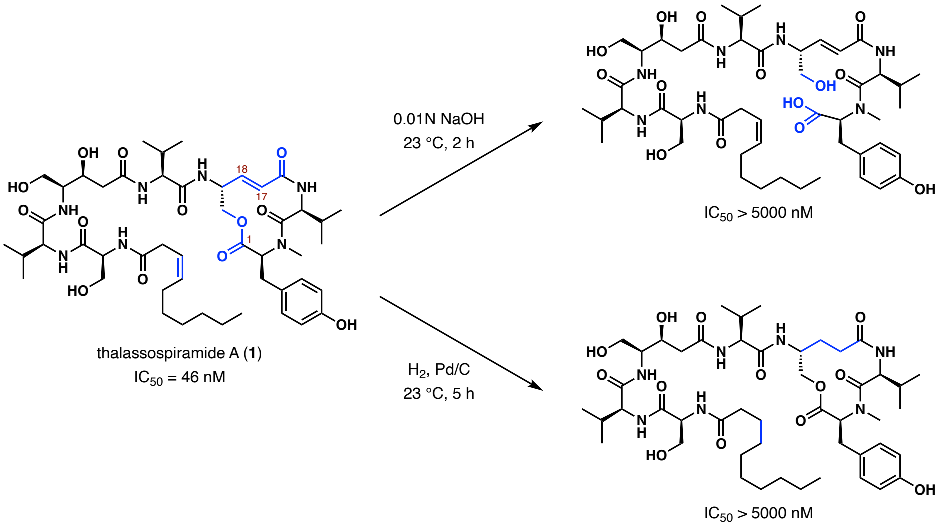

Thus, Qian and Moore proposed that the inhibitory activity of thalassospiramides stems from a covalent bonding between the Cys115 of calpain and the α,β-unsaturated amide of the macrocyclic unit via a Michael-type 1,4-addition.[3,7] Cysteine protease inhibitors commonly feature electrophilic moieties for covalent binding with the catalytic cysteine residues.[6–8] These functional groups that account for the reactivity of these bioactive molecules are typically termed "warheads," where they become targets in drug designs.[8] Michael acceptors (particularly for hetero-Michael addition reactions) are gaining increasing interest as candidates for targeted covalent inhibitors.[7] While there are many reported protease inhibitors with α,β-unsaturated carbonyls as electrophilic warheads targeting cysteine residues (representative compounds in Figure 2: the anti-tumor natural product hypothemycin contains a macrocyclic enone, and the synthetic drug afatinib used to treat non-small-cell lung cancer features a dimethylacrylamide), bioactive molecules with cyclic α,β-unsaturated amide moieties are rather unusual in both nature and synthesis.[3,6–8] This makes thalassospiramides distinctively unique targets, from both therapeutic and synthesis perspectives.

We believe a synthesis of the 12-membered macrocyclic system of thalassospiramides bearing the α,β-unsaturation of **3** would not only promote investigations of the activities of calpains and cathepsins cysteine proteases but would also offer further insights into these cyclic Michael acceptors as electrophilic warheads in related drug designs.

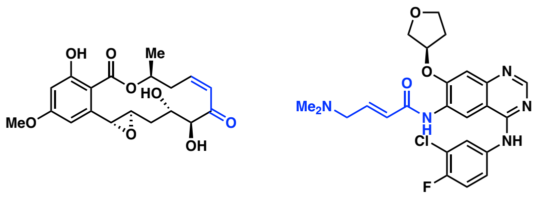

hypothemycin

afatinib

Figure 2. Protease inhibitors with Michael acceptors targeting cysteine residues for covalent C–S binding: the electrophilic warheads (α,β-unsaturated carbonyls) are highlighted in blue.

1.2. Total Synthesis Approach

1.2.1. Synthetic Considerations

Scheme 2. a) Two Key Synthetic Targets and b) Construction of the Lipopeptide Side Chain **3**.

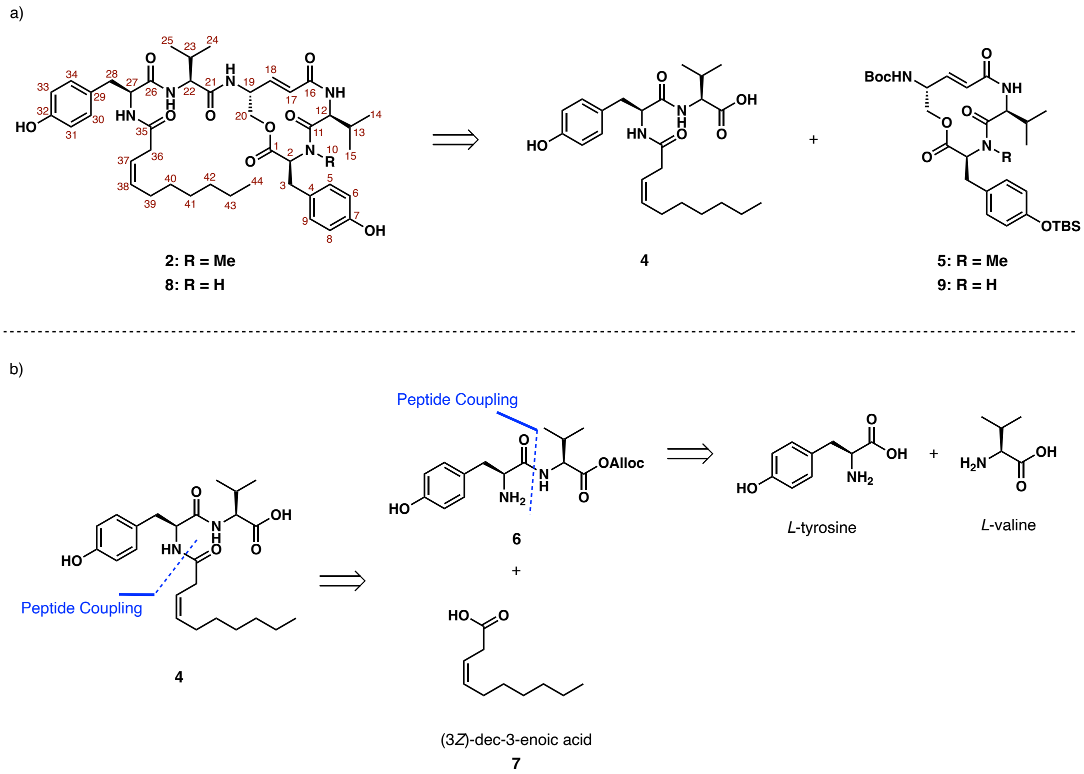
a)
2: R = Me
8: R = H
4
BocHN
OTBS
5: R = Me
9: R = H
b)
Peptide Coupling
Peptide Coupling
4
OAlloc
6
L-tyrosine
L-valine
(3Z)-dec-3-enoic acid
7

We envisioned a relatively straightforward synthetic approach through an amide coupling between lipopeptide side chain **4** and the 12-membered macrocyclic unit **5**, where **4** would come from the coupling between the amino acid L-tyrosine-L-valine **6** and (3*Z*)-dec-3-enoic acid **7** (Scheme 2). The construction of the cyclic depsipeptide core **5** is rather strategically remarkable. Conformational studies have indicated that this macrocycle would be synthetically challenging. Work done by Fenical revealed that this 12-membered cycle exhibits substantial ring strain, where the rigid C17–18 double bond allowed a strained ring conformation with a *s*-cis C16 N–H amide and a *s*-trans C11 N–Me amide.[2] In addition, these 2D NMR studies identified that the C10 methyl group of the C11 N–Me amide is oriented into the ring (Figure 3).[2] Thus, our focus was directed to the synthesis of the *N*-desmethyl congener of **2** (the most potent inhibitor of the thalassospiramide family), the *N*-desmethyl thalassospiramide C **8**, with **9** being the targeted intermediate for the synthesis of the macrocyclic unit.

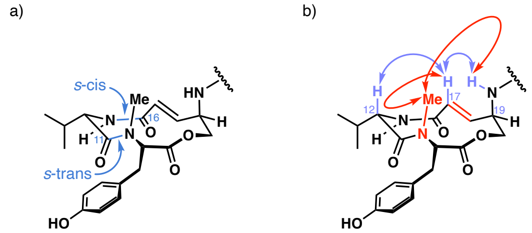

Figure 3. a) Ring conformation of macrocycle **5** showing large ring strain and b) the inward orienting N–Me of **5**.

Bearing the structural features of **9** in mind, macrolactonization forming the C1 ester was deemed highly impractical; the acyclic *seco*-acid precursor would be highly rigid with the highly strained conformation of the two amides, making cyclization extremely difficult.[9] Macrolactamization at the C16 amide would also be impractical; preliminary results showed a rapid fragmentation of the amino acid precursor **10** forming a diketopiperazine **11** and a derivative of **3** (red in Scheme 3). This leaves the disconnection at the C11 amide to be the most promising approach to construct this macrocycle **9**. Additionally, to further evaluate the conformational ring strain brought on by the C17–18 unsaturation, we envisaged an exploration of two macrolactamization pathways: path A (blue in Scheme 3) would involve the cyclization of the α,β-unsaturated amide **9a** from the α,β-unsaturated amino acid precursor **12a**, and path B (green in Scheme 3) would involve the cyclization of the β-phenylthio amide **9b** from the β-phenylthio amino acid precursor **12b**. We expected to experience difficulties with the macrocyclization via path A due to the high rigidity of **12a**, which would lead to an unfavorable macrocyclization process. We believed the introduction of the phenylthiol group would alleviate the strain of the unsaturation of the acyclic **12b**, therefore, increasing the success of macrocyclization via path B. This was encouraged by the structure of **9b** closely resembling that of a strain-relieving conjugated addition to the macrocycle by a cysteine residue—a proposed mode of action for thalassospiramides.

Scheme 3. Synthesis Plan for the Cyclization of Macrocycles **9a** and **9b**.

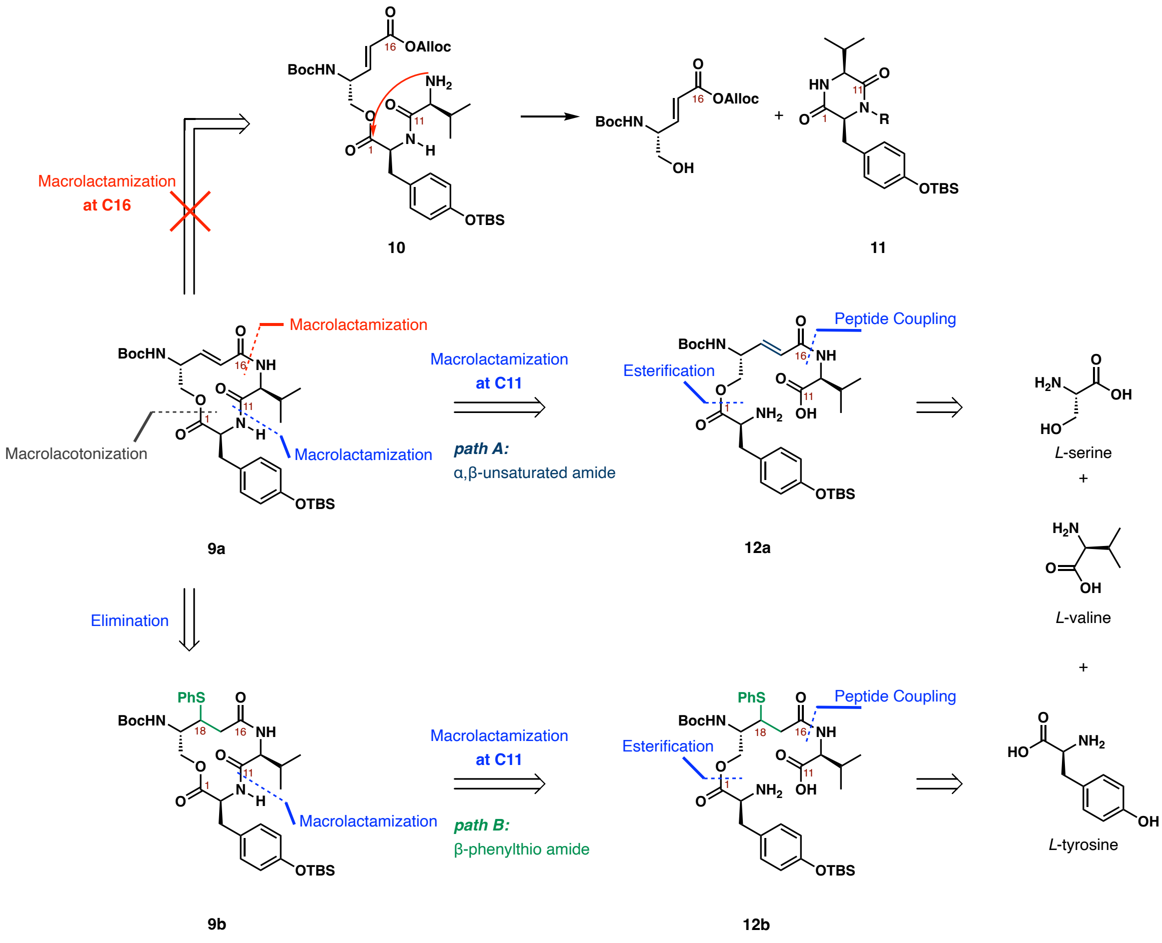

BocHN
OAlloc
NH₂
16
11
1
N
H
OTBS
10
OH
HN
N
R
11
Macrolactamization
at C16
Macrolactamization
NH
Macrolacotonization
Macrolactamization
9a
Macrolactamization
at C11
path A:
α,β-unsaturated amide
Peptide Coupling
Esterification
NH₂
OH
12a
H₂N
OH
HO
L-serine
+
L-valine
+
NH₂
L-tyrosine
Elimination
PhS
18
9b
path B:
β-phenylthio amide
12b

Both the acyclic **12a** and **12b** consist of L-serine, L-valine, and L-tyrosine. The dipeptide resulted from the peptide coupling of L-serine and L-valine residue would embody the α,β-unsaturation of **3**, and esterification with the L-tyrosine residue would deliver the amino acid precursors.

1.2.2. Synthesis of Lipopeptide Side Chain 4

The lipopeptide side chain **4** was achieved as outlined above in Scheme 2b. The amino acid L-tyrosine-L-valine **6** was established through a peptide coupling between *N*-Boc-L-tyrosine **13** and allyl L-valinate **14** followed by the removal of the Boc group. Appendage of **7** was accomplished using HATU as the coupling reagent, and ester hydrolysis afforded the side chain **4** (Scheme 4).

Scheme 4. Synthesis of the Lipopeptide Side Chain **4**.

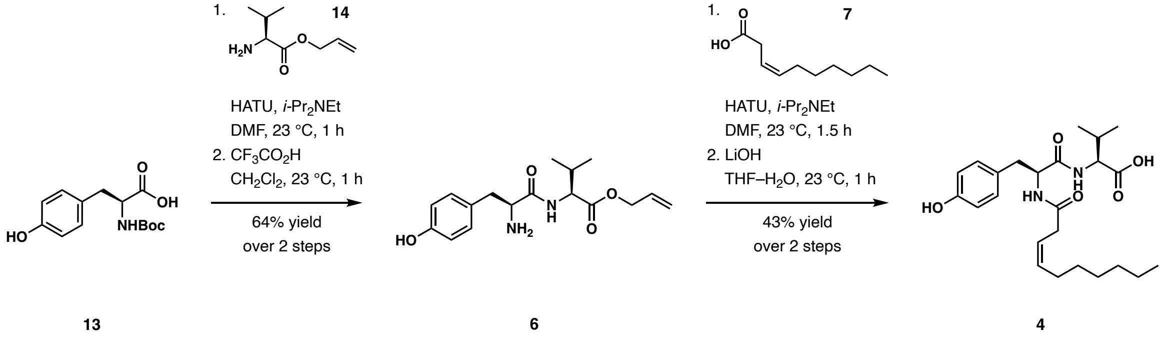
1.
14
H2N
O
HATU, i-Pr2NEt
DMF, 23 °C, 1 h
2. CF3CO2H
CH2Cl2, 23 °C, 1 h
64% yield
over 2 steps
1.
O
7
HO
HATU, i-Pr2NEt
DMF, 23 °C, 1.5 h
2. LiOH
THF–H2O, 23 °C, 1 h
43% yield
over 2 steps
HO
O
OH
NHBoc
13
HO
NH2
N
H
O
6
HO
HN
N
H
OH
O
4

1.2.3. Preparation of the Precursors 15a and 15b Containing 3

Following our synthesis plan to explore the conformational ring strain effect on macrocycle **9**, two precursors comprising **3** were first prepared for the two macrocyclization pathways (see Scheme 3). Starting with the L-serine derived Garner's aldehyde, olefination with methyl (triphenylphosphoranylidene)acetate followed by ester hydrolysis established carboxylic acid **15a** as a single *E* isomer in 97% yield. This α,β-unsaturated acid **15a** would later be derived to partake in the macrocyclization via path A. The phenylthio group was introduced to **15a** via a conjugate addition reaction, yielding a mixture of diastereomers (dr 4:1) in 91% yield with **15b** as the major product.[i]

Scheme 5. Preparation of Precursors Incorporating **3**.

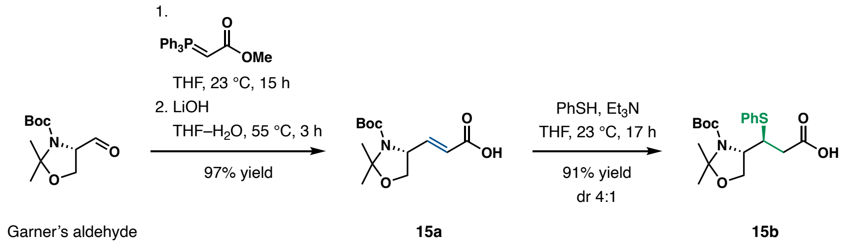

1.
Ph3P
O
OMe
THF, 23 °C, 15 h
2. LiOH
THF–H2O, 55 °C, 3 h
97% yield
PhSH, Et3N
THF, 23 °C, 17 h
91% yield
dr 4:1
Boc
N
O
PhS
OH
Garner's aldehyde
15a
15b

1.2.4. Construction of the Macrocycle 9

Scheme 6. Incorporation of L-Serine and L-Valine Residues.

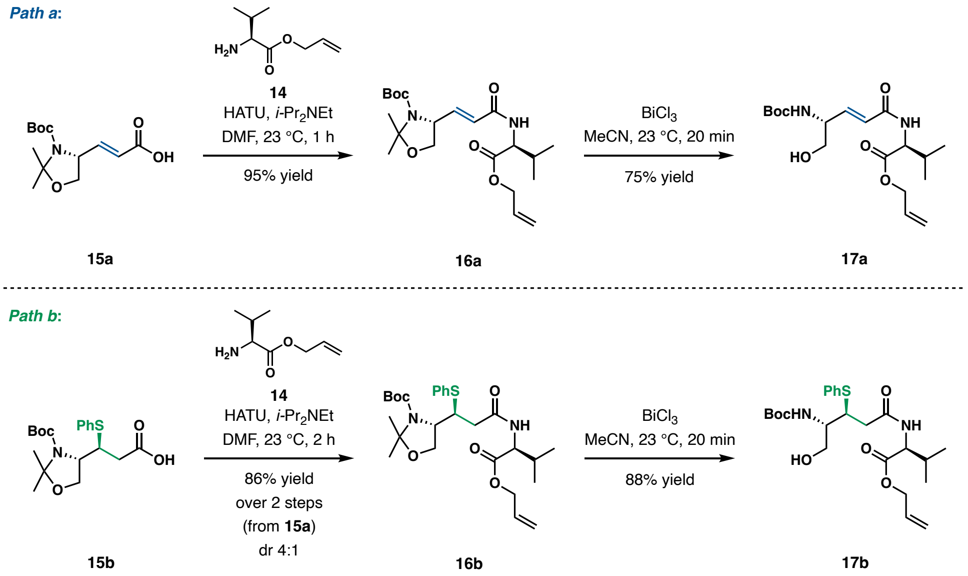

Path a:
H2N
O
14
HATU, i-Pr2NEt
DMF, 23 °C, 1 h
95% yield
BiCl3
MeCN, 23 °C, 20 min
75% yield
Boc
N
OH
NH
BocHN
HO
15a
16a
17a
Path b:
14
HATU, i-Pr2NEt
DMF, 23 °C, 2 h
86% yield
over 2 steps
(from 15a)
dr 4:1
BiCl3
MeCN, 23 °C, 20 min
88% yield
PhS
15b
16b
17b

Intermediates **15a** and **15b** were advanced towards the amino acid precursors **12a** and **12b** concurrently for the investigation of the two macrocyclization pathways, which is depicted in

---

[i] Attempted hydrolysis of the β-(phenylthio) ester resulted in the recovery of **15a**.

Schemes 6 and 7. Peptide coupling of **15a** and **15b** with **14** afforded acetonides **16a** and **16b**[ii] in great yields. Selective cleavage of the acetonides was successfully achieved using bismuth trichloride, affording **17a** and **17b** while leaving other acid sensitive groups intact. Other acid hydrolysis conditions led to a mixture of products with partial cleavages of the acetonide, the *N*-Boc and the *O*-Alloc groups (Scheme 6).

Scheme 7. Preparation of the Linear Depsipeptides **12a** and **12b**.

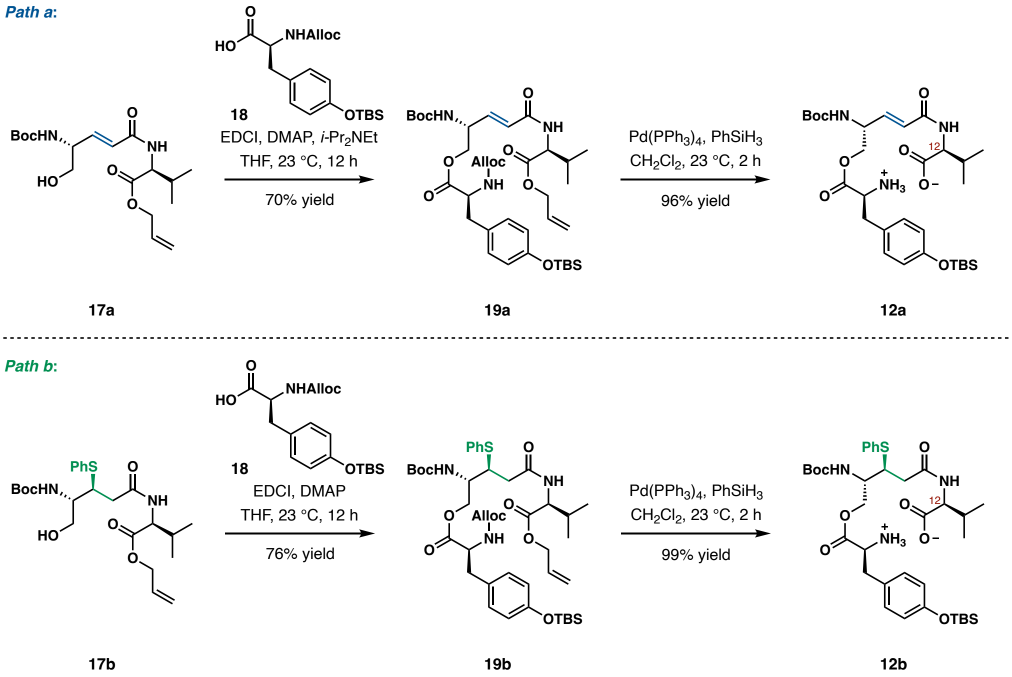
Path a:
18
EDCI, DMAP, i-Pr2NEt
THF, 23 °C, 12 h
70% yield
Pd(PPh3)4, PhSiH3
CH2Cl2, 23 °C, 2 h
96% yield
17a
19a
12a
Path b:
18
EDCI, DMAP
THF, 23 °C, 12 h
76% yield
Pd(PPh3)4, PhSiH3
CH2Cl2, 23 °C, 2 h
99% yield
17b
19b
12b

The primary alcohols **17a** and **17b** readily underwent esterification with the *N*-Alloc derivative of L-tyrosine **18**, forming the linear depsipeptides **19a** and **19b**. Reductive cleavage with 5 mol % of Pd(PPh$_3$)$_4$ simultaneously established de-esterification of the *O*-Alloc group and decarboxylation of the *N*-Alloc group, affording the desired amino acid precursors **12a** and **12b** (Scheme 7).

[ii] The two diastereomers resulted from the addition of thiophenol were separated in this step to give acetonide **16b** as the major diastereomer.

We began our investigation into the two macrolactamization pathways by submitting the zwitterionic precursors **12a** and **12b** for macrolactamization for various ring closure strategies and employing innumerable coupling reagents.[10] Unfortunately, as we had expected, macrocyclization via path A proved to be exceedingly difficult; no traces of **9a** was ever observed, and multiple coupling conditions led to the decomposition of **12a**. To our relief, macrocyclization via path B afforded product **9b**, though the reaction progression was extremely slow (Scheme 8).

Scheme 8. Synthesis of Macrocycle **9a** via Path A and Path B.

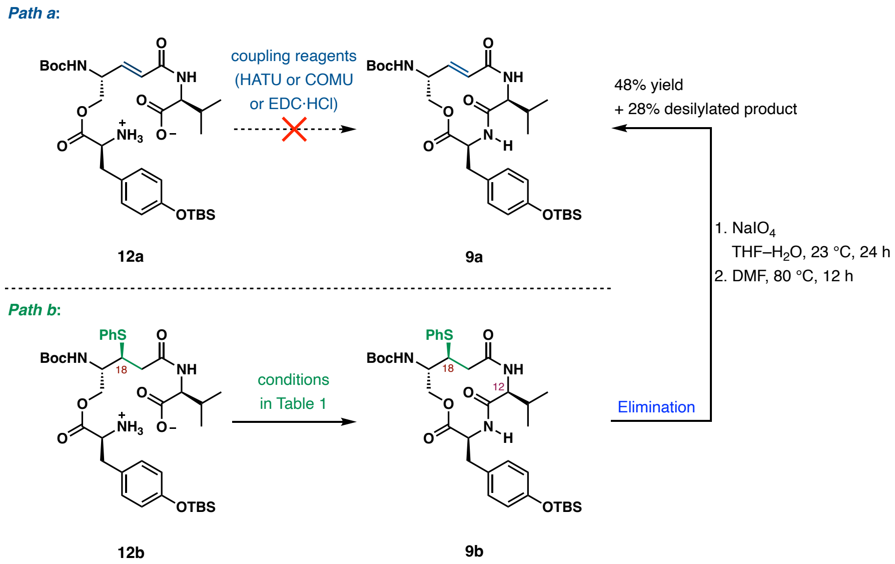
Path a:
BocHN
O
NH
O
O
$\overset{+}{N}H_3$
O−
OTBS
12a
coupling reagents
(HATU or COMU
or EDC·HCl)
BocHN
NH
N
H
OTBS
9a
48% yield
+ 28% desilylated product
1. $NaIO_4$
THF–H_2O, 23 °C, 24 h
2. DMF, 80 °C, 12 h
Elimination
Path b:
PhS
18
BocHN
NH
$\overset{+}{N}H_3$
O−
OTBS
12b
conditions
in Table 1
PhS
18
12
BocHN
NH
N
H
OTBS
9b

Our endeavors to selecting the most suitable macrocyclization condition for path B are detailed in Table 1.[10] The use of peptide coupling reagents HATU, HBTU and PyBOP (entries 1–3) delivered the cyclized product of **12b** in approximately 50% yields. However, a closer inspection of the product indicated an inseparable mixture of diastereomers: macrocycle **9b** and the C12 epimer **9c**. While the reaction was less yielding when COMU and EDCI·HCl–HOAt were used (entries 4 and 5), significantly less amount of **9c** was produced.

The β-phenylthio macrocycle **9b** was then submitted for elimination to synthesize **9a** with the α,β-unsaturated amide (see Schemes 8 and 9). The epimerization observed at the C12 valine unit also revealed to have complicated this elimination step: difficult purification and lower yields were observed when the mixture of diastereomers **9b** and **9c** were submitted to the reaction. This established COMU to be the optimal macrocyclization reagent for the synthesis of our macrocycle **9b**. Oxidation of the pure sulfide **9b** afforded the sulfoxide, which then undergoes thermolysis in DMF to restore the C17–18 unsaturation in **9a**.

Table 1. Macrocyclization Reagents Tested with **12b**.

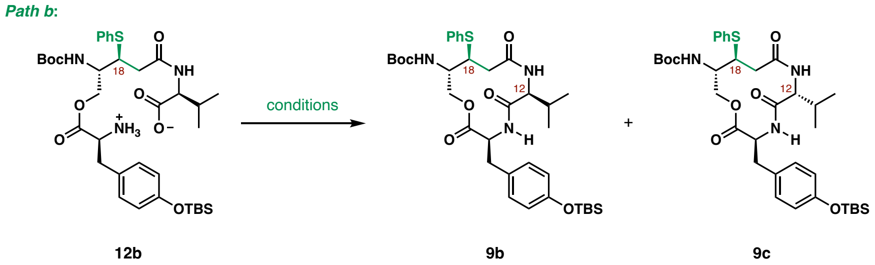
Path b:
PhS
O
BocHN
18
NH
O
O
O
$\overset{+}{N}H_3$
O–
OTBS
12b
conditions
PhS
O
BocHN
18
NH
12
O
O
N
H
O
OTBS
9b
+
PhS
O
BocHN
18
NH
12
O
O
N
H
O
OTBS
9c

entry[a]	reagents	solvent[b]	yield	dr (**9b**:**9c**)
1	HATU, *i*-Pr_2NEt	DMF	50%	2:1
2	HBTU, *i*-Pr_2NEt	DMF	52%	1:1
3	PyBOP, *i*-Pr_2NEt	DMF	41%	1:1
4	COMU, *i*-Pr_2NEt	DMF	26%	> 30:1
5	EDCI·HCl, HOAt	CH_2Cl_2	23%	> 30:1
6[c]	C_6F_5OH, EDCI·HCl	PhMe	no reaction	—

[a]All reactions were performed at 23 °C for 4 days, unless otherwise noted. [b]All reactions were carried out in diluted concentrations (0.005 M), unless otherwise noted. [c]Reaction was performed 23 °C for 10 h, followed by heating at 110 °C overnight.

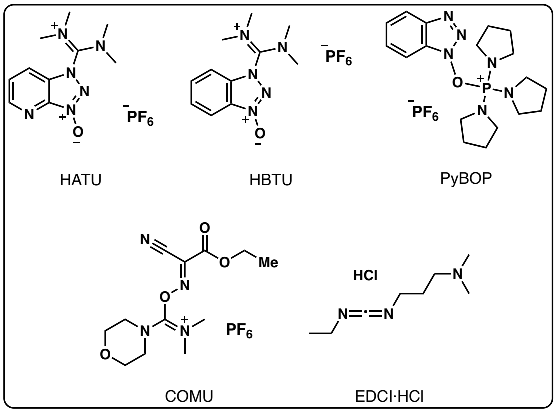
$\overset{-}{P}F_6$
HATU
$\overset{-}{P}F_6$
HBTU
$\overset{-}{P}F_6$
PyBOP
Me
PF_6
COMU
HCl
EDCI·HCl

Our ability to cyclize **9b** from **12b**, but not **9a** from the C17–18 unsaturated amide **12a**, indicates the β-phenylthio group was critical in the notably lessened macrocyclic ring strain, making the path B macrolactamization feasible. Our macrocyclization efforts discussed here solidified our plan to synthesize a less strained macrocyclic target that emulated the reduced ring strain seen in the proposed cysteine adduct to the C17–18 unsaturation of the 12-membered macrocycle of thalassospiramides.

Scheme 9. Completion of the Total Synthesis of **8**.

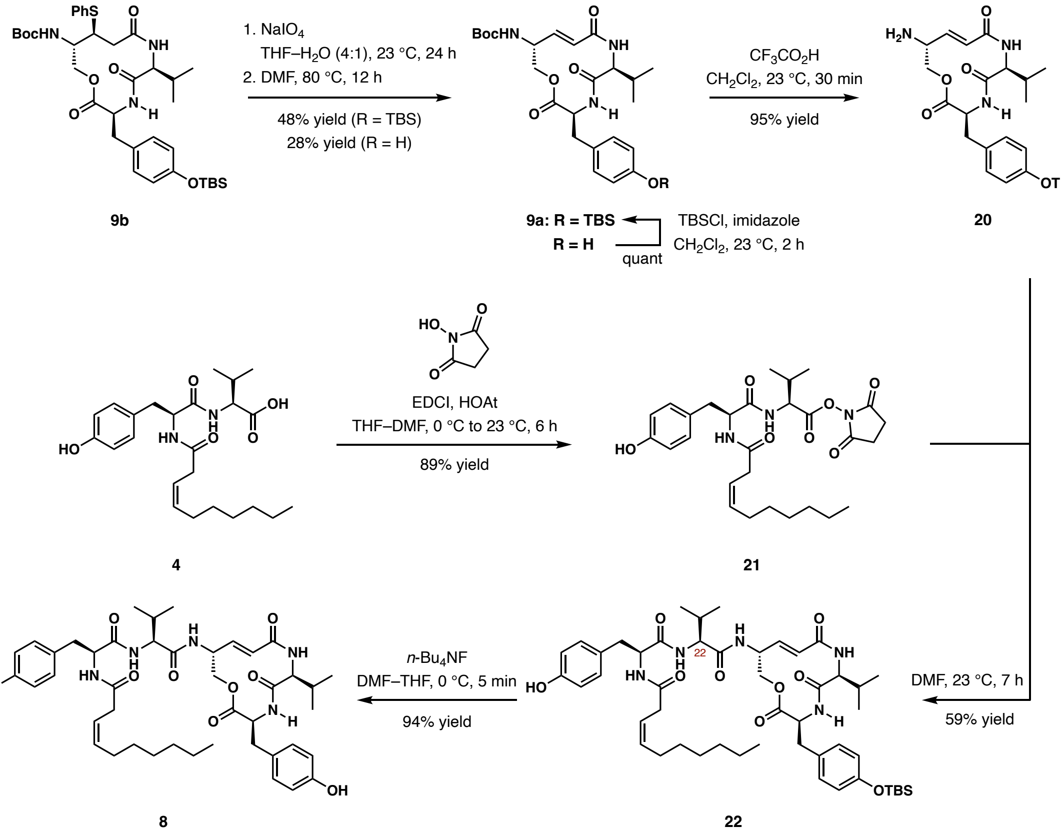
PhS
BocHN
OTBS
9b
1. NaIO4
THF–H2O (4:1), 23 °C, 24 h
2. DMF, 80 °C, 12 h
48% yield (R = TBS)
28% yield (R = H)
BocHN
OR
9a: R = TBS
R = H
quant
TBSCl, imidazole
CH2Cl2, 23 °C, 2 h
CF3CO2H
CH2Cl2, 23 °C, 30 min
95% yield
H2N
OTBS
20
HO
OH
4
EDCI, HOAt
THF–DMF, 0 °C to 23 °C, 6 h
89% yield
21
DMF, 23 °C, 7 h
59% yield
22
OTBS
22
n-Bu4NF
DMF–THF, 0 °C, 5 min
94% yield
8
OH

1.2.5. Completion of the Total Synthesis

To complete the synthesis of **8**, a final peptide coupling between the lipopeptide side chain **4** and the primary amine of the macrocyclic unit **9a** was performed (Scheme 9). The macrocycle though strained, was stable under acidic conditions evident by the removal of the Boc group with trifluoroacetic acid achieving the amine **20**. Incorporation of the side chain was accomplished through coupling of **20** with the activated hydroxy-succinate ester **21**. Other coupling methods had resulted in epimerization at C22. Finally, desilylation of the resulting depsipeptide **22**[iii] concluded the synthesis of **8**, providing us with 20 mg of *N*-desmethyl thalassospiramide C (**8**).

1.3. Analyses of the Bioactivity and Mode of Binding of 8

With sufficient synthetic quantities of **8**, a detailed crystallography study of **8** with cysteine proteases was followed, providing the molecular underpinnings of the bioactivity of **8** as a cysteine protease inhibitor. Successful X-ray crystal structure with cathepsin K further substantiates the previously proposed mode of action: the strained macrocycle of thalassospiramides acts as covalent Michael acceptor for binding.

The bioactivity of **8** as a cysteine protease inhibitor was evaluated, and the results are summarized in Table 2. The synthesized **8** showed potent inhibition towards calpains and cathepsins in nanomolar concentrations. Though the potencies against calpains 1 and 2 were approximately 60-fold less than the reported 3.4 nM for thalassospiramide C (**2**), which is likely due to the substitution of the C11 N–Me amide with an N–H amide, the *N*-desmethyl congener **8** showed significant selectivity for cathepsins K and L.[1–3]

Table 2. Biochemical Potencies of **8** Against Calpain and Cathepsin Proteases (IC_{50}, nM).

Protease Inhibitor	Calpain 1	Calpain 2	Cathepsin K	Cathepsin B	Cathepsin S	Cathepsin L
IC_{50}, nM	175	210	3	65	46	1

We were able to successfully obtain the X-ray crystallography analysis of the adduct between **8** and cathepsin K, and this high-resolution structural detail reveals the mode of action. Two different orientations of this adduct highlighting the underlying interactions are depicted in Figure 4: cathepsin K is shown as green cartoon representation, and **8** is shown in ball and stick figures; the dotted lines represent intermolecular H–bonds. In Figure 4a, cathepsin K is shown in bright green, and the tyrosine of the macrocycle of **8** (carbon backbone in orange) is oriented upwards in this view with the fatty acid of the lipopeptide side chain (cropped out of this view) extending towards the viewer. In Figure 4b, cathepsin K is shown in dark green, and the tyrosine of the macrocycle of **8** (carbon backbone in grey) is oriented leftwards in this view with the tyrosine of the lipopeptide side chain extending towards the viewer. The Schechter and Berger nomenclature[11] is used in Figure 4a to identify the cleavage sites by the cysteine proteases.

[iii] The byproduct with free phenolic OH can be silylated in > 95% yield and used productively in the next step of the synthesis (see Scheme 9).

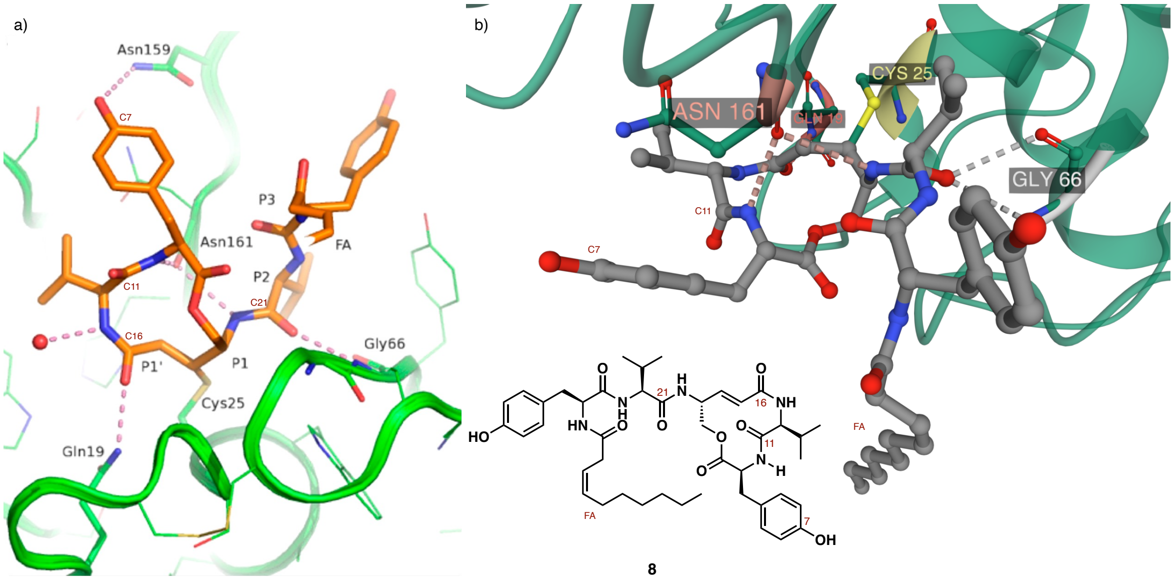

Figure 4. Focused view of the crystal structure of **8** bound to cathepsin K (PDB entry 6hgy). Color code: C (cathepsin K): green; C (**8**): orange in a), gray in b); O: red; N: blue; S: yellow.

As shown in Figure 4, the macrocyclic core of **8** sits right in the P1' substrate binding site[iv] of cathepsin K, allowing the active site Cys25 to covalently bind to C18. The torsional angle at the C17–18 double bond was measured at 105°, reaffirming our conjecture that the large macrocyclic strain arose from this unsaturation would be liberated with the addition of a cysteine residue. The C7 tyrosine phenolic OH of the macrocycle forms a weak H–bond with Asn159 (3.4 Å). Additionally, with **8** being the *N*-desmethyl congener, the C11 N–H amide forms a hydrogen bond to the backbone Asn161 (2.7 Å) that would differ from the binding with the *N*-methylated thalassospiramide C (**2**). While models indicate local shifts of ~1 Å or more with the methyl group at the C11 N–Me amide, the overall macrocyclic conformation of **8** bound to cathepsin K highly resembles the 2D NMR analysis of the solution structure of thalassospiramide A (**1**).[1]

The S1–S3 subsites of cathepsin K can be seen in Figure 4a binding to the lipopeptide side chain of **8**. The interactions at P1–P2 depict a conserved motif for this family of proteases and coincide with many other crystallographic structures reported.[12,13] The C21 N–H amide hydrogen bonds with the backbone carbonyl group of Asn161, and the C21 carbonyl forms a H–bond with the amide group of Gly66. The C22 valine isopropyl group sits deep in the P2 site, which is in accordance with the generally characterized hydrophobic S2 pocket of these papain-like proteases.[5a,12–14] The P3 site shows much less H–bonding interactions, as explained by the weak electron density at the side chain tyrosine and lipid residues of **8** (see Figure 10 in the Experimental Procedures section). Overall, these observed binding interactions between cathepsin K and **8** correspond to those of papain-like cysteine proteases and typical peptidomimetics.[5a,12–15]

[iv] P1', P1, P2, and P3 refer to the amino acids of the substrate that are interacting with the binding sites of the protease, which are referred to as S1', S1, S2, and S3, respectively. The residues at the *C*-terminal are primed (denoted by '). The P1–P1' peptide bond is cleaved via hydrolysis.

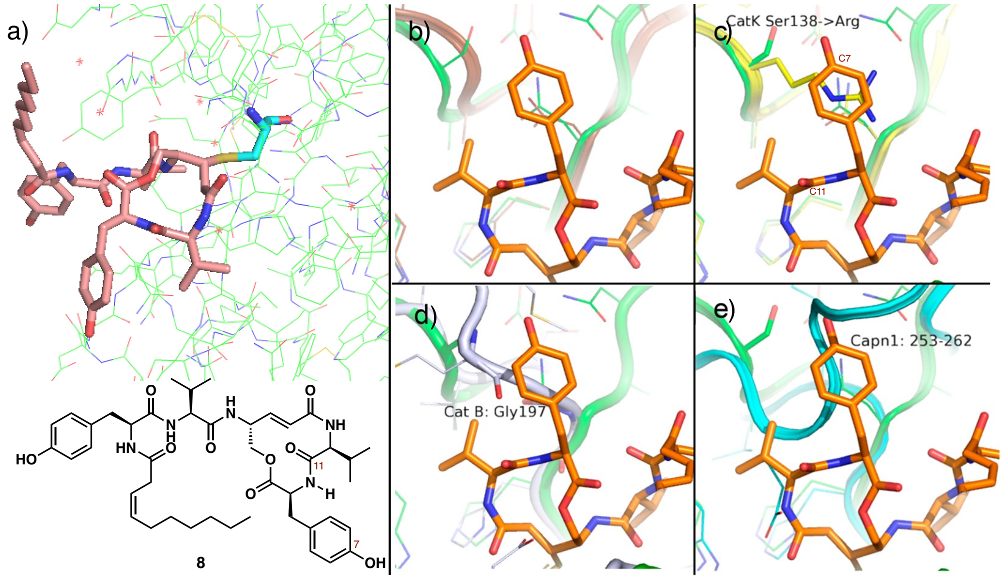

Figure 5. a) Enlarged view of crystal structure of cathepsin K and **8**; b–e) superpositions of other homologous cysteine proteases on the crystal structure of the adduct between **8** and cathepsin K.

b) Cathepsin L (brown, PDB entry 2xu3); c) cathepsin S (yellow, PDB entry 4p6g); d) cathepsin B (gray, PDB entry 1gmy); e) calpain 1 (cyan, PDB entry 1zcm). Cathepsin K is shown as green cartoon representation, and **8** is shown in ball and stick figures.

To further understand the inhibition potencies of **8** and its selectivity for cysteine proteases, the crystal structure of cathepsin K and **8** was superimposed on published structures of other homologous cysteine proteases (Figure 5). Cathepsin L is closely related to cathepsin K in both their 3D structures and their catalytic domains.[5a,16,17] As shown in Figure 5b, the crystal structure of cathepsin L poses a very similar S1' site to that of cathepsin K.[18] In particularly, the lack of backbone steric interference with the macrocycle of **8** indicates an even stronger P1'–S1' binding affinity, which explains the high potency against cathepsin L. Whereas in the case with cathepsin S, which is also structurally similar to cathepsin K,[16] the Ser138 → Arg substitution results in an intruding backbone as seen in Figure 5c.[19] This would impede the binding at the C11 amide and

C7 tyrosine phenol region, explaining the more than 10-fold loss of inhibitory activity. Figure 5d depicts the binding with cathepsin B with its a distinctive occluding loop.[20] This led to a different structural fold at the S1' site preventing strong interactions with the macrocyclic core (P1'), thus explaining the much lowered potency we observed.

The differences between conventional calpains (calpains 1 and 2) and cathepsins in the chemical reactivity of the active site cysteine residues and the structural differences at their S1' regions can explain the lowered potency of **8** for calpains.[13,21] Though the catalytic domains of conventional calpains are reported to be quite similar to that of cathepsins in their structural homology, as shown in Figure 5e, the P1' binding site is partially obstructed by the characteristic gating loop[v] at residues 253–262 in human calpain 1.[13,22,23]

1.4. Conclusion

We reported the chemical synthesis of *N*-desmethyl thalassospiramide C (**8**), the first in this family of marine natural products characterizing a 12-membered cyclic depsipeptide.[24] The successful macrocyclization validated our mode of action inspired approach: targeting a less strained macrocycle **9b**. We were able to achieve the key α,β-unsaturated macrocycle **9a**, first by constructing the β-phenylthio congener (**9b**) from the amino acid precursor **12b**, followed by an effective elimination of the β-phenylthio group to restore the unsaturation. The completion of the synthesis of **8** enabled a detailed analysis of the biochemical potencies of **8**, which was further illuminated by structural analyses of the crystallography structure of the adduct of **8** and cathepsin K. Calpains and cathepsins are of considerable interest as therapeutic targets, as numerous cysteine proteases are correlated with many conditions including neurodegenerative disorders, fibrosis and cancer.[4,5a] Evaluation of the X-ray crystal structure allowed the structural features necessary for strong covalent interactions with cysteine proteases to be determined. In addition, it elucidated the mode of binding: inhibition of cysteine proteases via a covalent addition of an active site cysteine residue to the electrophilic α,β-unsaturated amide of the macrocycle. Ultimately, our resolve accomplished the goal to further evaluate the bioactivity of this 12-membered cyclic Michael acceptor. Our work stipulates meaningful insights for drug design specifically targeting these cysteine proteases.

---

[v] This characteristic loop for calpains has also exhibit conformational heterogeneity in different crystal forms of the rodent calpains.[22,23]

References

[1] Oh, D.-C.; Strangman, W. K.; Kauffman, C. A.; Jensen, P. R.; Fenical, W. *Org. Lett.* **2007**, *9*, 1525–1528.

[2] Ross, A. C.; Xu, Y.; Lu, L.; Kersten, R. D.; Shao, Z.; Al-Suwailem, A. M.; Dorrestein, P. C.; Qian, P.-Y.; Moore, B. S. *J. Am. Chem. Soc.* **2013**, *135*, 1155–1162.

[3] Lu, L.; Meehan, M. J.; Gu, S.; Chen, Z.; Zhang, W.; Liu, L.; Huang, X.; Dorrestein, P. C.; Xu, Y.; Moore, B. S.; Qian, P.-Y. *Sci. Rep.* **2015**, *5*, 8783.

[4] Ono, Y.; Saido, T. C.; Sorimachi, H. *Nat. Rev. Drug Discovery* **2016**, *15*, 854–876.

[5] (a) Turk, V.; Stoka, V.; Vasiljeva, O.; Renko, M.; Sun, T.; Turk, B.; Turk, D. *Biochim. Biophys. Acta, Proteins Proteomics* **2012**, *1824*, 68–88. (b) Vidak, E.; Javoršek, U.; Vizovišek, M.; Turk, B. *Cells* **2019**, *8*, 264.

[6] (a) Siklos, M.; BenAissa, M.; Thatcher, G. R. J. *Acta Pharm. Sin. B* **2015**, *5*, 506–519.

[7] Jackson, P. A.; Widen, J. C.; Harki, D. A.; Brummond, K. M. *J. Med. Chem.* **2017**, *60*, 839–885.

[8] Drug designs of cysteine protease inhibitors: (a) Silva, D. G.; Ribeiro, J. F. R.; De Vita, D.; Cianni, L.; Franco, C. H.; Freitas-Junior, L. H.; Moraes, C. B.; Rocha, J. R.; Burtoloso, A. C. B.; Kenny, P. W.; Leitão, A.; Montanari, C. A. *Bioorg. Med. Chem. Lett.* **2017**, *27*, 5031–5035. (b) Ábrányi-Balogh, P.; Petri, L.; Imre, T.; Szijj, P.; Scarpino, A.; Hrast, M.; Mitrović, A.; Fonovič, U. P.; Németh, K.; Barreteau, H.; Roper, D. I.; Horváti, K.; Ferenczy, G. G.; Kos, J.; Ilaš, J.; Gobec, S.; Keserű, G. M. *Eur. J. Med. Chem.* **2018**, *160*, 94–107. (c) Chaikuad, A.; Koch, P.; Laufer, S. A.; Knapp, S. *Angew. Chem. Int. Ed.* **2018**, *57*, 4372–4385.

[9] This hypothesis was also borne out by preliminary studies. Examples of macrolactonization in cyclic depsipeptide synthesis are rare: (a) Hamada, Y.; Shioiri, T. *Chem. Rev.* **2005**, *105*, 4441–4442. (b) Li, W.; Schlecker, A.; Ma, D. *Chem. Commun.* **2010**, *46*, 5403. (c) Davies, J. S. *J. Pept. Sci.* **2003**, *9*, 471–501. (d) Batiste, S. M.; Johnston, J. *N. Proc. Natl. Acad. Sci. U. S. A.* **2016**, *113*, 14893−14897. Yakovleva, M. P.; Denisova, D. S.; Vydrina, V. A.; Tolstikov, A. G.; Ishmuratov, G. Y. *Russ. J. Org. Chem.* **2021**, *57*, 679–729.

[10] El-Faham, A.; Albericio, F. *Chem. Rev.* **2011**, *111*, 6557–6602.

[11] The Schechter and Berger nomenclature: (a) Scheter, I.; Berger, A. *Biochem. Biophys. Res. Commun.* **1967**, *27*, 157–162. (b) Scheter, I.; Berger, A. *Biochem. Biophys. Res. Commun.* **1968**, *32*, 898–902.

[12] Boros, E. E.; Deaton, D. N.; Hassell, A. M.; McFauyden, R. B.; Miller, A. B.; Miller, L. R.; Paulick, M. G.; Shewchuk, L. M.; Thompson, J. B.; Willard, D. H., Jr.; Wright, L. L. *Bioorg. Med. Chem. Lett.* **2004**, *14*, 3425−3429.

[13] Li, Q.; Hanzlik, R. P.; Weaver, R. F.; Schönbrunn, E. *Biochemistry* **2006**, *45*, 701−708.

[14] Turk, D.; Gunčar, G.; Podobnik, M.; Turk, B. *Biol. Chem.* **1998**, *379*, 137–147.

[15] (a) Yamashita, D. S.; Smith, W. W.; Zhao, B.; Janson, C. A.; Tomaszek, T. A.; Bossard, M. J.; Levy, M. A.; Oh, H.-J.; Carr, T. J.; Thompson, S. K.; Ijames, C. F.; Carr, S. A.; McQueney, M.; D'Alessio, K. J.; Amegadzie, B. Y.; Hanning, C. R.; Abdel-Meguid, S.; DesJarlais, R. L.; Gleason, J. G.; Veber, D. F. *J. Am. Chem. Soc.* **1997**, *119*, 11351–11352. (b) Thompson, S. K.; Halbert, S. M.; Bossard, M. J.; Tomaszek, T. A.; Levy, M. A.; Zhao, B.; Smith, W. W.; Abdel-Meguid, S. S.; Janson, C. A.; D'Alessio, K. J.; McQueney, M. S.; Amegadzie, B. Y.; Hanning, C. R.; DesJarlais, R. L.; Briand, J.; Sarkar, S. K.; Huddleston, M. J.; Ijames, C. F.; Carr, S. A.; Garnes, K. T.; Shu, A.; Heys, J. R.; Bradbeer, J.; Zembryki, D.; Lee-Rykaczewski, L.; James, I. E.; Lark, M. W.; Drake, F. H.; Gowen, M.; Gleason, J. G.; Veber, D. F. *Proc. Natl. Acad. Sci. U. S. A.* **1997**, *94*, 14249–14254. (c) Novinec, M.; Korenč, M.; Caflisch, A.; Ranganathan, R.; Lenarčič, B.; Baici, A. *Nat. Commun.* **2014**, *5*, 3287.

[16] Guay, J.; Falgueyret, J.-P.; Ducret, A.; Percival, M. D.; Mancini, J. A. *Eur. J. Biochem.* **2000**, *267*, 6311–6318.

[17] Lecaille, F.; Chowdhury, S.; Purisima, E.; Brömme, D.; Lalmanach, G. *Protein Sci.* **2007**, *16*, 662–670.

[18] Hardegger, L. A.; Kuhn, B.; Spinnler, B.; Anselm, L.; Ecabert, R.; Stihle, M.; Gsell, B.; Thoma, R.; Diez, J.; Benz, J.; Plancher, J.-M.; Hartmann, G.; Banner, D. W.; Haap, W.; Diederich, F. *Angew. Chem. Int. Ed.* **2011**, *50*, 314–318.

[19] Jadhav, P. K.; Schiffler, M. A.; Gavardinas, K.; Kim, E. J.; Matthews, D. P.; Staszak, M. A.; Coffey, D. S.; Shaw, B. W.; Cassidy, K. C.; Brier, R. A.; Zhang, Y.; Christie, R. M.; Matter, W. F.; Qing, K.; Durbin, J. D.; Wang, Y.; Deng, G. G. *ACS Med. Chem. Lett.* **2014**, *5*, 1138–1142.

[20] (a) Greenspan, P. D.; Clark, K. L.; Tommasi, R. A.; Cowen, S. D.; McQuire, L. W.; Farley, D. L.; van Duzer, J. H.; Goldberg, R. L.; Zhou, H.; Du, Z.; Fitt, J. J.; Coppa, D. E.; Fang, Z.; Macchia, W.; Zhu, L.; Capparelli, M. P.; Goldstein, R.; Wigg, A. M.; Doughty, J. R.; Bohacek, R. S.; Knap, A. K. *J. Med. Chem.* **2001**, *44*, 4524–4534. (b) Schmitz, J.; Gilberg, E.; Löser, R.; Bajorath, J.; Bartz, U.; Gütschow, M. *Bioorg. Med. Chem.* **2019**, *27*, 1–15.

[21] Sorimachi, H.; Mamitsuka, H.; Ono, Y. *Biol. Chem.* **2012**, *393*, 853–871.

[22] Cuerrier, D.; Moldoveanu, T.; Inoue, J.; Davies, P. L.; Campbell, R. L. *Biochemistry* **2006**, *45*, 7446–7452.

[23] (a) Moldoveanu, T.; Gehring, K.; Green, D. R. *Nature* **2008**, *456*, 409-412. (b) Hanna, R. A.; Campbell, R. L.; Davies, P. L. *Nature* **2008**, *456*, 409–412.

[24] Fournier, J.; Chen, K.; Mailyan, A. K.; Jackson, J. J.; Buckman, B. O.; Emayan, K.; Yuan, S.; Rajagopalan, R.; Misialek, S.; Adler, M.; Blaesse, M.; Griessner, A.; Zakarian, A. *Org. Lett.* **2019**, *21*, 508–512.

Chapter 2.

Total Synthesis of (+)-[$^{13}C_4$]-Anatoxin-a via a Dynamic Kinetic Resolution of a Cyclic Iminium Ion

2.1. Introduction

2.1.1. Background

Anatoxin-a (**23**) is a cyanobacterial toxin (cyanotoxin) produced by several genera of cyanobacteria such as *Chrysosporum (Aphanizomenon) ovalisporum*, *Raphidiopsis*, *Cylindrospermum*, and *Dolichospermum (previously Anabaena) flos-aquae*.[25,26] It is one of the four most commonly found cyanotoxins in the United States according to the Environment Protection Agency (EPA), along with microcystin-L, cylindrospermopsin, and saxitoxin, shown in Figure 6.[26,27] Anatoxin-a (**23**) is a potent agonist to nicotinic acetylcholine receptors with widely distributed effects. Exposure to **23** results in overstimulation of these receptors, causing continuous excitation at neuromuscular junctions and blockage of further electrical transmissions.[28,29] Acute exposure can lead to muscle paralysis and death by asphyxiation within minutes.[27–29] Anatoxin-a and other cyanotoxin poisonings through accidental ingestion while recreating in cyanobacteria-contaminated water have been widely documented to have broad health effects on humans, livestock, and domestic animals.[26,27]

In recent years, there have been increasing occurrences of cyanobacterial algal blooms threatening freshwater systems, causing widespread health, social and economic impacts.[26,27,30] While algal blooms are naturally occurring events, these algal blooms become harmful when the survival of other organisms are threatened by the toxins these algae produce.[30] Increasing nutrient loading from fertilizer runoff as well as various other human activities have all been reported to be major factors for harmful algal blooms, and these factors are further exacerbated by the rapid growth of global population.[30] The resulting escalation of cyanotoxin threat to our drinking and recreational freshwater has led to changes in agency policies and response plans, including efforts in building monitor programs tracking these harmful algal blooms and raising awareness with publicly issued health advisories.[26,27,30] More importantly, having highly accurate and accessible methods for detecting and quantifying cyanotoxins with immense precision is critical in establishing safer public health guidelines.[27,29]

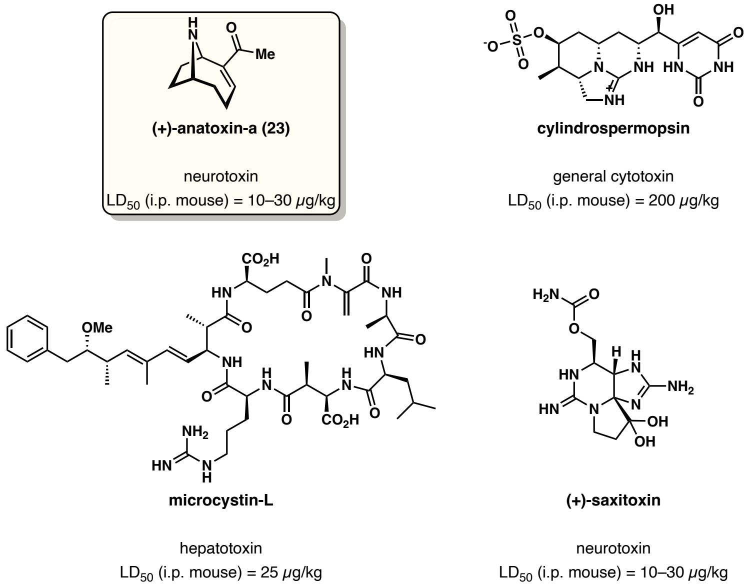
(+)-anatoxin-a (23)
neurotoxin
LD_{50} (i.p. mouse) = 10–30 μg/kg
cylindrospermopsin
general cytotoxin
LD_{50} (i.p. mouse) = 200 μg/kg
microcystin-L
hepatotoxin
LD_{50} (i.p. mouse) = 25 μg/kg
(+)-saxitoxin
neurotoxin
LD_{50} (i.p. mouse) = 10–30 μg/kg

Figure 6. Four most commonly found cyanotoxins in the U.S. identified by the EPA.

While a range of analytical methods have been approved by the EPA to detect and identify cyanotoxins in drinking and ambient freshwater, methods employing liquid chromatography combined with mass spectrometry (LC/MS) with a deuterated internal standard as reference remain the most accurate.[31] Unfortunately, the accuracy and reproducibility of this method is hampered by sample matrix interference[vi], and more importantly, the varying sensitivity and susceptibility between the analyte and the internal standard.[32,33] Due to the internal standard (L-phenylalanine-d_5, in the case with anatoxin-a) having drastically different structures from the analyte (anatoxin-a), matrix effect[vii] results in disproportional loss of cyanotoxin analyte and internal standard, leading to incorrect interpretations of cyanotoxins levels.[31] These issues can be addressed by using an isotope-dilution method, where an isotopic form of the analyte is used as the referencing internal standard.[34] An isotopically labeled cyanotoxin would, in principle, behave identically to the cyanotoxins collected from water samples throughout the detection and quantification process.[35] The development of isotope-dilution methods for cyanotoxins determination and the use of such methods hinge upon the availability of isotopically labeled forms of these cyanotoxin analytes.[36] Our group has reported the total synthesis of [$^{15}N_5$]-cylindrospermopsin and demonstrated superior detection limits using this labeled form of cylindrospermopsin compared to that of the currently approved and available methods.[37]

[vi] Another factor that can contribute to an inaccurate determination of the amount of cyanotoxins is deuterium–hydrogen exchange. While this factor does not directly affect the determination of anatoxin-a (L-phenylalanine-d_5 does not have exchangeable deuterium), certain internal standards used for other cyanotoxins, such as uracil-d_5 for cylindrospermopsin determination, can easily be subjected to deuterium–hydrogen exchanges leading to false measurements of the internal standards.

However, prior to our work detailed in this chapter, no such labeled form of anatoxin-a (**23**) was easily available. Additionally, no synthetic approach for a labeled anatoxin-a (**23**) had ever been derived.

2.1.2. Previous Syntheses

Since the first synthesis of anatoxin-a (**23**) was reported by the Edwards group in 1977 (this group is also credited for the first isolation and characterization efforts for anatoxin-a),[38] a myriad of synthetic methods have been developed.[39] As shown in Scheme 10, the construction of the iconic bridged, bicyclic system of **23** can broadly be classified in three approaches: ring expansion of tropanes (shaded in gray, Scheme 10a), cyclization of cyclooctanes (shaded in blue, Scheme 10b), and cyclization of 2,5-disubsitituted pyrrolidines (shaded in green, Scheme 10c).[39] Selected syntheses featuring novel strategies are also depicted in Scheme 10.

[vii] Matrix effect describes the typically negative impact of non-sample components on the effectiveness and the reliability of the analysis of the sample. These effects are interferences that could apply at various stages of the analysis, such as sample preparation, sample inlet, and/or ion suppression.[32,33]

One of the shortest syntheses of anatoxin-a to date was developed by Seitz (Scheme 10a).[40] This 8-step synthesis was based on the tropane ring expansion approach starting with the chiral tropane (−)-cocaine (**24**) hydrochloride.[40] A successful ring expansion of tropanone **25** followed by hydrolysis furnished the azabicyclo[4.2.1]nonan-2-one **26**, and further transformations afforded **23** in a 26% overall yield.[40] Extensive efforts have contributed towards utilizing cyclooctane intermediates for the formation of the azabicyclic system in anatoxin-a (**23**). The syntheses developed by Trost[41] and Aggarwal[42] are representatives of such efforts (Scheme 10b). In Trost's approach, an intramolecular asymmetric allylic alkylation was accomplished to form this bicyclic system, allowing their total synthesis of *ent*-**23** to be achieved from 4-bromo-1-butene (**27**) in 16 steps with an overall yield of 13%.[41] The key enantioselective Pd-catalyzed amination of the racemic allylic cyclooctane (±)-**28** gave bicyclic scaffold (−)-**29** in 88% ee.[41] Aggarwal et al. reported an 8-step formal synthesis of **23**, beginning with *cis*-1,5-cycloocatanediol (**30**).[42] Eventually, this synthesis would afford **23** in 11 steps and 39% yield after adopting a literature procedure from Rapoport.[43] The critical step in Aggarwal's synthesis was the asymmetric induction of the aminocyclooctanone **31** via an enantioselective deprotonation with the chiral lithium amide of (*R*,*R*)-**32**.[42] The resulting enolate was quenched with diphenyl chlorophosphite to form the corresponding enol phosphate, which was then transformed into an enol ether through a Stille coupling reaction.[42] A hydrolysis of the enol ether revealed the enone and simultaneously removed the amine protecting group; finally, an intramolecular conjugate addition provided Rapoport's known bicyclic ketone **33** in 89% ee.[42,43]

Another attractive approach to establish the azabicyclic skeleton of anatoxin-a (**23**) is through the cyclization of a 2,5-disubstituted pyrrolidine (**34**), shown in Scheme 10c. Using intermediate **34**, an iminium ion cyclization is one method that forges the connection at the bridge head of **23** to accomplish the bicyclic system.[39] Works done by Rapoport,[43,44] Somfai,[45] Skrinjar,[46] Stockman,[47] and others[39,48,49] are examples of such cyclization method. An iminium generated from the pyrrolidine precursor **35** under acidic conditions would undergo a Mannich-type cyclization to establish the bicyclic structure **36**.[50] Many have also demonstrated productive asymmetric syntheses of **23** through the cyclization of chiral pyrrolidiniums, where the enantioselectivity stems from the chiral amino acid starting material used, eventually achieving **23** in 8–15 steps.[43–49] Other methods of this cyclization approach focused on directly cyclizing the second ring on the side chains of intermediate **34**, thereby forging the critical bicyclic system.[39,51,52] Martin and co-workers utilized a ring-closing enyne metathesis of the pyrrolidine intermediate **37** to construct the bicyclic skeleton in **38**.[52] Subsequent dihydroxylation of the terminal alkene, followed by oxidative cleavage of the resulting diol and removal of the *N*-carbamoyl group afforded **23**.[52] This approach achieved enantiopure **23** in 9 steps and a 27% overall yield from D-methyl pyroglutamate, and is arguably one of the most efficient synthesis till now.[52]

Many of these effective and elegant synthetic efforts were exemplary of revolutions in chemistry at the time, and some continue to be inspiring even in the contemporary context. The rich history associated with the syntheses of anatoxin-a serves as motivations for novel strategies to be developed.

Scheme 10. Previous Synthetic Approaches to Construct the Bicyclic System of **23**, and Potential Incorporation of Isotopes for a Synthesis of an Isotopically Labeled **23**.

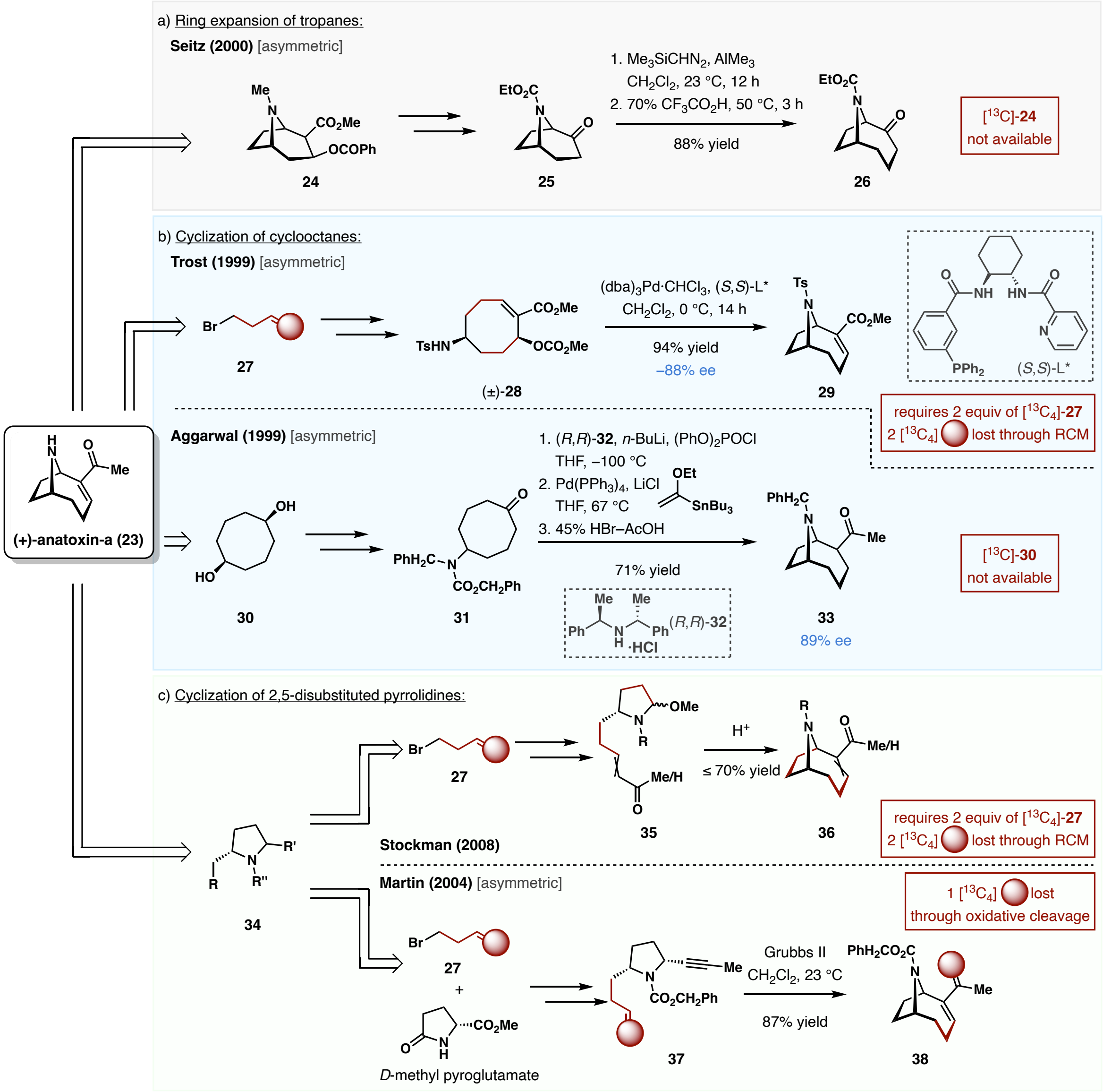
a) Ring expansion of tropanes:
Seitz (2000) [asymmetric]
Me
N
CO2Me
OCOPh
24
EtO2C
N
O
25
1. Me3SiCHN2, AlMe3
CH2Cl2, 23 °C, 12 h
2. 70% CF3CO2H, 50 °C, 3 h
88% yield
EtO2C
N
O
26
[13C]-24
not available
b) Cyclization of cyclooctanes:
Trost (1999) [asymmetric]
Br
27
TsHN
CO2Me
OCO2Me
(±)-28
(dba)3Pd·CHCl3, (S,S)-L*
CH2Cl2, 0 °C, 14 h
94% yield
–88% ee
Ts
N
CO2Me
29
O
NH
HN
O
N
PPh2
(S,S)-L*
requires 2 equiv of [13C4]-27
2 [13C4] lost through RCM
Aggarwal (1999) [asymmetric]
H
N
O
Me
(+)-anatoxin-a (23)
OH
HO
30
1. (R,R)-32, n-BuLi, (PhO)2POCl
THF, –100 °C
2. Pd(PPh3)4, LiCl
OEt
SnBu3
THF, 67 °C
3. 45% HBr–AcOH
71% yield
O
PhH2C
N
CO2CH2Ph
31
Me
Me
Ph
N
H
Ph
·HCl
(R,R)-32
PhH2C
N
O
Me
33
89% ee
[13C]-30
not available
c) Cyclization of 2,5-disubstituted pyrrolidines:
R'
N
R
R''
34
Br
27
OMe
N
R
Me/H
O
35
H+
≤ 70% yield
R
N
O
Me/H
36
Stockman (2008)
requires 2 equiv of [13C4]-27
2 [13C4] lost through RCM
Martin (2004) [asymmetric]
1 [13C4] lost
through oxidative cleavage
Br
27
+
CO2Me
O
N
H
D-methyl pyroglutamate
Me
N
CO2CH2Ph
37
Grubbs II
CH2Cl2, 23 °C
87% yield
PhH2CO2C
N
Me
38

2.1.3. Motivation for an Isotopically Labeled (+)-Anatoxin-a Synthesis

Our objective was to develop a chemical synthesis to easily access an isotopically labeled form of **23**, which would be used as the internal standard of a more precise anatoxin-a quantification method. Biosynthetic methods to procure labeled forms of cyanotoxins have shown to be slow and ineffective.[53,54] Thus, at this point, a chemical synthesis of an isotopically labeled **23** is the logical approach for an effective and scalable method to consistently access isotopically enriched **23**. To synthetically achieve such a labeled form of **23** efficiently, the incorporation of isotopes must be carefully strategized.[37] The isotopically labeled **23** would require a mass difference of at least 4 atomic units relative to the natural **23** collected from water supplies. This is to ensure that when using the labeled **23** as the internal standard in determining the cyanotoxin levels, the signal generated in mass spectrometry would be distinguishable from the signal generated from the unlabeled analyte. The incorporation of these labeled atoms would also need to be at non-exchangeable positions throughout the entire synthesis.[viii] This is to warrant a uniform molecular mass of the final labeled **23**.

Considering these two isotope incorporation requirements to ensure analytical success and structural integrity of the isotopically labeled **23**, as well as the availability of stable isotope starting materials, we re-evaluated the numerous existing syntheses discussed in Chapter 2.1.2 (see Scheme 10). While many past synthetic approaches elegantly and efficiently afforded **23**, none would allow a synthesis of the labeled **23** without isotope loss. As identified in Scheme 10, many established syntheses employed starting materials that are not commercially available in their isotopically labeled forms, such as (−)-cocaine (**24**) and *cis*-1,5-cyclooctanediol (**30**). One exception is the case of the starting material 4-bromo-1-butene (**27**) that was utilized by Trost,[41] Speckamp,[48] Martin,[52] and Stockman[47] where the [$^{13}C_4$]-**27** is commercially available. However, if applied to the synthesis of [$^{13}C_4$]-**23**, one or more of the labeled ^{13}C would have been lost during their syntheses. Evidently, there was no effective method to introduce stable isotopes and to reliably transform isotopically enriched materials to a labeled form of **23**.

[viii] This excludes deuterium as our stable isotope choice. Of the 15 hydrogens, 10 carbons, 1 oxygen and 1 nitrogen that formulate **23**, labeling the carbons with ^{13}C was deemed the most reasonable.

We thus were prompted to develop a de novo chemical synthesis of [$^{13}C_4$]-anatoxin-a ([$^{13}C_4$]-**23**) that would supply ample quantities of this labeled cyanotoxin, facilitating the development of a new analytical method.

2.2. Total Synthesis of (+)-[$^{13}C_4$]-Anatoxin-a

2.2.1. Synthesis Plan

Our synthetic approach depicted in Scheme 11 was motivated by many previous successful syntheses.[39–52] In particular, the bicyclic structure of [$^{13}C_4$]-**23** would be established through a Mannich-type iminium cyclization of a 2,5-disubstituted pyrrolidine precursor [$^{13}C_4$]-**39**.[39,43–50] After thoughtful assessment of commercial stable isotope sources and factoring in considerations discussed in Chapter 2.1.3, we envisioned that the four carbons (highlighted in red in Scheme 11) located on the side chain portion of vinyl ketone [$^{13}C_4$]-**39** would be relatively safe positions to incorporate isotopes. The pyrrolidine [$^{13}C_4$]-**39** would be established through a cyclic hemiaminal formation of the amine [$^{13}C_4$]-**40**, which would be derived from a Curtius rearrangement of the carboxylic acid [$^{13}C_4$]-**41**. The acid [$^{13}C_4$]-**41** would be the result of an Ireland–Claisen rearrangement of the allylic ester [$^{13}C_4$]-**42**, of which the ester C–O bond would arise from the coupling between the carboxylic acid **43** and the chiral alcohol [$^{13}C_4$]-**44**. We identified that [$^{13}C_4$]-**44** would originate from the commercially available ethyl [$^{13}C_4$]-acetoacetate ([$^{13}C_4$]-**45**), and the four labeled carbons (in red) would be transformed without complications to the enone positions of the final [$^{13}C_2$, $^{13}C_3$, $^{13}C_{10}$, $^{13}C_{11}$]-**23**. These four isotopes were chosen as they are placed at non-exchangeable positions throughout the full synthesis plan, ensuring full retention of the isotopic labels.

Scheme 11. Synthesis Plan for [^{13}C$_4$]-**23**.

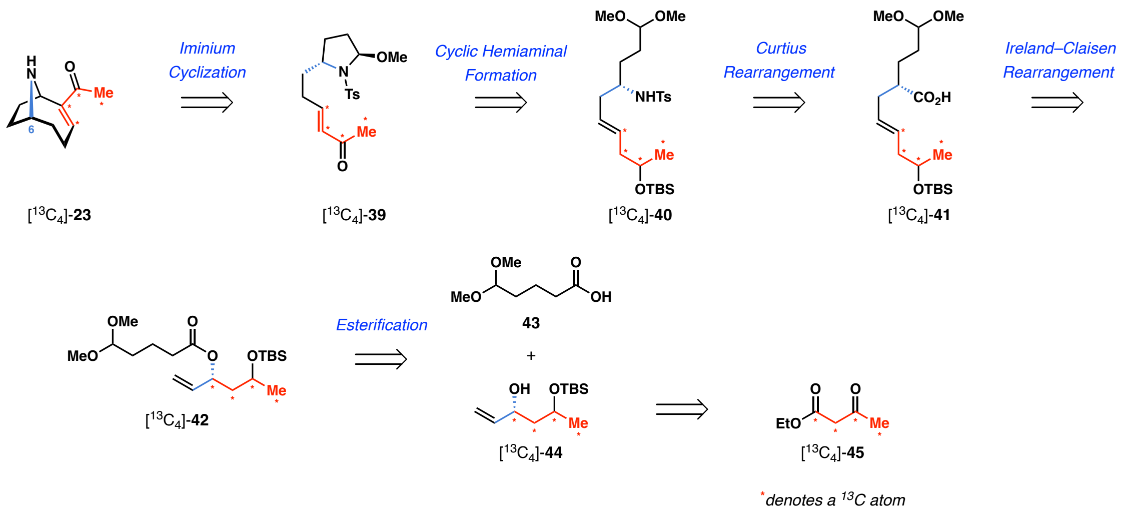

[^{13}C$_4$]-23
Iminium Cyclization
[^{13}C$_4$]-39
Cyclic Hemiaminal Formation
[^{13}C$_4$]-40
Curtius Rearrangement
[^{13}C$_4$]-41
Ireland–Claisen Rearrangement
[^{13}C$_4$]-42
Esterification
43
+
[^{13}C$_4$]-44
[^{13}C$_4$]-45
*denotes a ^{13}C atom

The chirality of **23** is also notable in this synthetic plan: the chiral [^{13}C$_4$]-**44** is pivotal to the success of this asymmetric synthesis in establishing the C6 stereocenter of [^{13}C$_4$]-**23** (highlighted in blue in Scheme 11).

2.2.2. Synthesis of Allylic Alcohol [^{13}C$_4$]-44

The synthesis of the chiral allylic alcohol [^{13}C$_4$]-**44** is of particular importance. Our synthesis began with the sodium borohydride reduction of [^{13}C$_4$]-**45** followed by TBS silylation of the resulting alcohol, affording [^{13}C$_4$]-**46** in 97% yield over 2 steps (Scheme 12). With this ester [^{13}C$_4$]-**46** in hand, we commenced three enantioselective approaches for the chiral development of [^{13}C$_4$]-**44**: an asymmetric reduction of ketone [^{13}C$_4$]-**47**, an enantioselective vinyl addition of aldehyde [^{13}C$_4$]-**48**, and a Sharpless asymmetric epoxidation of allylic alcohol [^{13}C$_4$]-**49**. A Kulinkovich cyclopropanation of [^{13}C$_4$]-**46** followed by electrophilic ring-opening achieved ketone [^{13}C$_4$]-**47**. A partial reduction of [^{13}C$_4$]-**46** gave aldehyde [^{13}C$_4$]-**48**, of which homologation followed by reduction of the resulting α,β-unsaturated ester accomplished the allylic alcohol [^{13}C$_4$]-**49**.

Scheme 12. Precursors Synthesis for the Development of the Chiral Alcohol [^{13}C$_4$]-**44**.

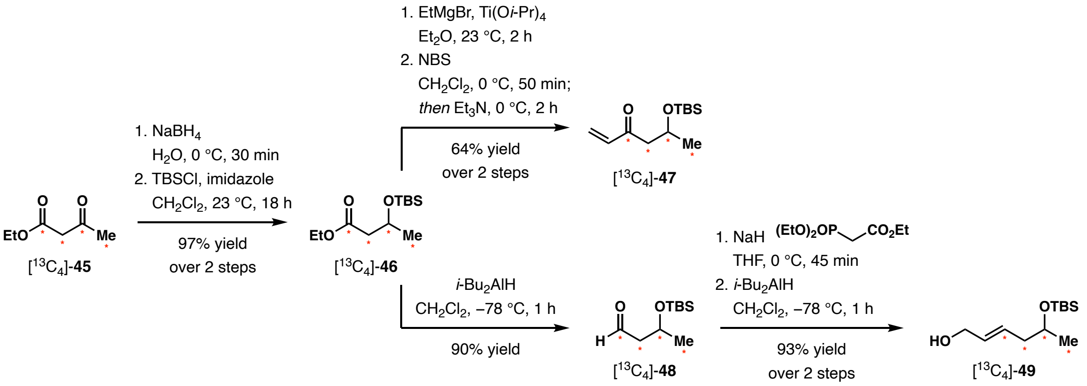

EtO
O
O
Me
[^{13}C$_4$]-**45**
1. NaBH$_4$
H$_2$O, 0 °C, 30 min
2. TBSCl, imidazole
CH$_2$Cl$_2$, 23 °C, 18 h
97% yield
over 2 steps
OTBS
[^{13}C$_4$]-**46**
1. EtMgBr, Ti(O*i*-Pr)$_4$
Et$_2$O, 23 °C, 2 h
2. NBS
CH$_2$Cl$_2$, 0 °C, 50 min;
then Et$_3$N, 0 °C, 2 h
64% yield
over 2 steps
[^{13}C$_4$]-**47**
i-Bu$_2$AlH
CH$_2$Cl$_2$, –78 °C, 1 h
90% yield
H
[^{13}C$_4$]-**48**
1. NaH (EtO)$_2$OP CO$_2$Et
THF, 0 °C, 45 min
2. *i*-Bu$_2$AlH
CH$_2$Cl$_2$, –78 °C, 1 h
93% yield
over 2 steps
HO
[^{13}C$_4$]-**49**

We initially pictured a rather straightforward one-step transformation of either the ketone [^{13}C$_4$]-**47** or the aldehyde [^{13}C$_4$]-**48**. However, this simple, rosy outlook was quickly met with unforeseen challenges. Our attempts to quickly derivatize to the chiral alcohol material [^{13}C$_4$]-**44** is summarized in Scheme 13.

Scheme 13. Three Enantioselective Approaches for the Preparation of Chiral Alcohol [^{13}C$_4$]-**44**.

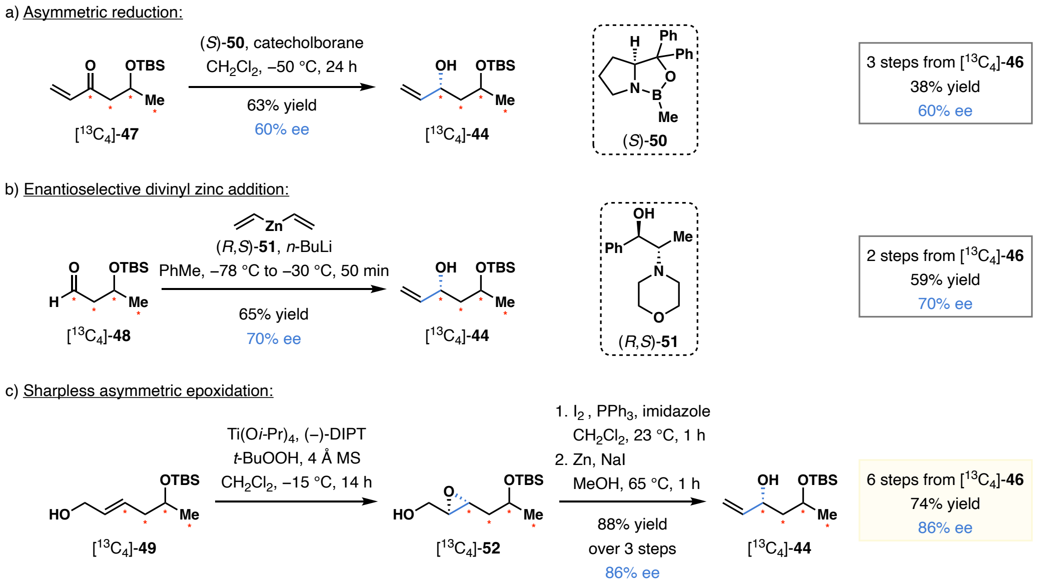

a) Asymmetric reduction:
O
OTBS
Me
[^{13}C$_4$]-**47**
(*S*)-**50**, catecholborane
CH$_2$Cl$_2$, –50 °C, 24 h
63% yield
60% ee
OH
[^{13}C$_4$]-**44**
H
Ph
Ph
O
N
B
Me
(*S*)-**50**
3 steps from [^{13}C$_4$]-**46**
38% yield
60% ee
b) Enantioselective divinyl zinc addition:
Zn
(*R*,*S*)-**51**, *n*-BuLi
PhMe, –78 °C to –30 °C, 50 min
65% yield
70% ee
H
[^{13}C$_4$]-**48**
[^{13}C$_4$]-**44**
OH
Ph
Me
N
O
(*R*,*S*)-**51**
2 steps from [^{13}C$_4$]-**46**
59% yield
70% ee
c) Sharpless asymmetric epoxidation:
HO
[^{13}C$_4$]-**49**
Ti(O*i*-Pr)$_4$, (–)-DIPT
t-BuOOH, 4 Å MS
CH$_2$Cl$_2$, –15 °C, 14 h
O
[^{13}C$_4$]-**52**
1. I$_2$, PPh$_3$, imidazole
CH$_2$Cl$_2$, 23 °C, 1 h
2. Zn, NaI
MeOH, 65 °C, 1 h
88% yield
over 3 steps
86% ee
[^{13}C$_4$]-**44**
6 steps from [^{13}C$_4$]-**46**
74% yield
86% ee

Our initial strategy was to utilize an enantioselective reductive method of ketone [$^{13}C_4$]-**47** (Scheme 13a).[55] A Corey–Bakshi–Shibata asymmetric reduction of [$^{13}C_4$]-**47** using the methyl oxazaborolidine catalyst (*S*)-**50** with borane dimethylsulfide showed significant oligomerization, likely due to competing hydroboration reactions. The terminally positioned α,β-unsaturation of **47** conceivably made this asymmetric reduction even more difficult. Using a milder reducing agent catecholborane, the reaction was performed at −50 °C to give the chiral allylic alcohol [$^{13}C_4$]-**44** in 63% yield and a displeasing 60% ee.[ix] Another seemingly promising one-step approach we imagined was an enantioselective addition of divinyl zinc to the aldehyde [$^{13}C_4$]-**48** (Scheme 13b). To our surprise, a literature survey revealed limited chiral ligands that are compatible with vinyl zinc reagents.[56,57] Use of lithium alkoxide of the norephedrine-derived ligand (*R*,*S*)-**51** reported by Myers,[57] afforded the chiral [$^{13}C_4$]-**44** in 65% yield but a hardly adequate 70% ee.[x]

Dissatisfied by these direct transformations, we turned our efforts to a Sharpless asymmetric epoxidation of the allylic alcohol [$^{13}C_4$]-**44** (Scheme 13c), which established the chirality in epoxide [$^{13}C_4$]-**52.**[58] Subsequent subjection to iodination followed by reduction with zinc resulted in epoxide-opening, accomplishing the chiral [$^{13}C_4$]-**44** in 88% yield over 3 steps and a gratifying 86% ee.

Though longer steps are required to achieve chiral alcohol [$^{13}C_4$]-**44** from the ethyl ester [$^{13}C_4$]-**46**, the Sharpless asymmetric epoxidation approach gave superior results overall. The enantiopurity of alcohol [$^{13}C_4$]-**44** obtained from the 6 steps involving a Sharpless asymmetric epoxidation step was 86% with an overall yield of 74% (Scheme 13c), which is greater than that obtained from the two-step transformation with an enantioselective divinyl zinc addition reaction

---

[ix] Noyori's hydrogen transfer was also attempted to asymmetrically reduce this ketone **47**. However, only the reduced alkene and none of the alcohol **44** was detected by ^1H NMR.

[x] Oppolzer's (+)-camphor derived chiral diaminoalcohol ligand, which has shown to be compatible with divinyl zinc additions to benzaldehyde, was unable to give any selectivity in our allylic alcohol **44.**[56a,c]

(70% enantiopurity with an overall yield of 59%, Scheme 13b). With these isotopically labeled materials being more costly and precious, it was especially critical for us to identify the most practical and reliable synthesis route. To that end, we believe the implementation of Sharpless asymmetric epoxidation step is the most efficient method to obtain chiral alcohol [$^{13}C_4$]-**44**.

2.2.3. Completion of the Asymmetric Total Synthesis of [$^{13}C_4$]-23

In accordance with our synthesis plan, after successfully procuring the chiral allylic alcohol intermediate [$^{13}C_4$]-**44**, it was advanced to afford the ester [$^{13}C_4$]-**42** in 97% yield via a DCC coupling with acid **43** (Scheme 14). The allylic ester [$^{13}C_4$]-**42** was subjected to an Ireland–Claisen rearrangement first by the formation of the silyl ketene acetal intermediate via deprotonation by LDA and silylation with TBSCl; the silyl ketene acetal was subsequently rearranged to give the carboxylic acid [$^{13}C_4$]-**41** in 95% yield. Repeated experimentation found it crucial to ensure the rearrangement step took place without excess base to prevent racemization, which would arise from deprotonation of the rearranged silyl ester intermediate. Thus, methanol was introduced to quench any excess LDA to retain the enantiopurity of the carboxylic acid [$^{13}C_4$]-**41** (81% ee).[xi] Treatment of diphenylphosphoryl azide formed the corresponding acyl azide, and a Curtius rearrangement was performed at elevated temperatures. Effective hydrolysis of the resulting isocyanate intermediate was achieved with $NaOSiMe_3$ forming the primary amine, which was quickly tosylated to afford amine [$^{13}C_4$]-**40** in 83% yield over two steps.[59] Acid catalyzed cyclization of the tosyl amine [$^{13}C_4$]-**40** constructed the pyrrolidine structure with concurrent desilylation, and the following TEMPO oxidation furnished ketone [$^{13}C_4$]-**53**. Exposure to DBU promoted a double bond migration yielding the α,β-unsaturated ketone [$^{13}C_4$]-**39**.

[xi] We believe the minor erosion of enantiopurity was likely the result of a competitive boat-like transition state during the rearrangement process of the *E*-silyl ketene acetal intermediate.

Scheme 14. Completion of the Total Synthesis of [$^{13}C_4$]-**23**.

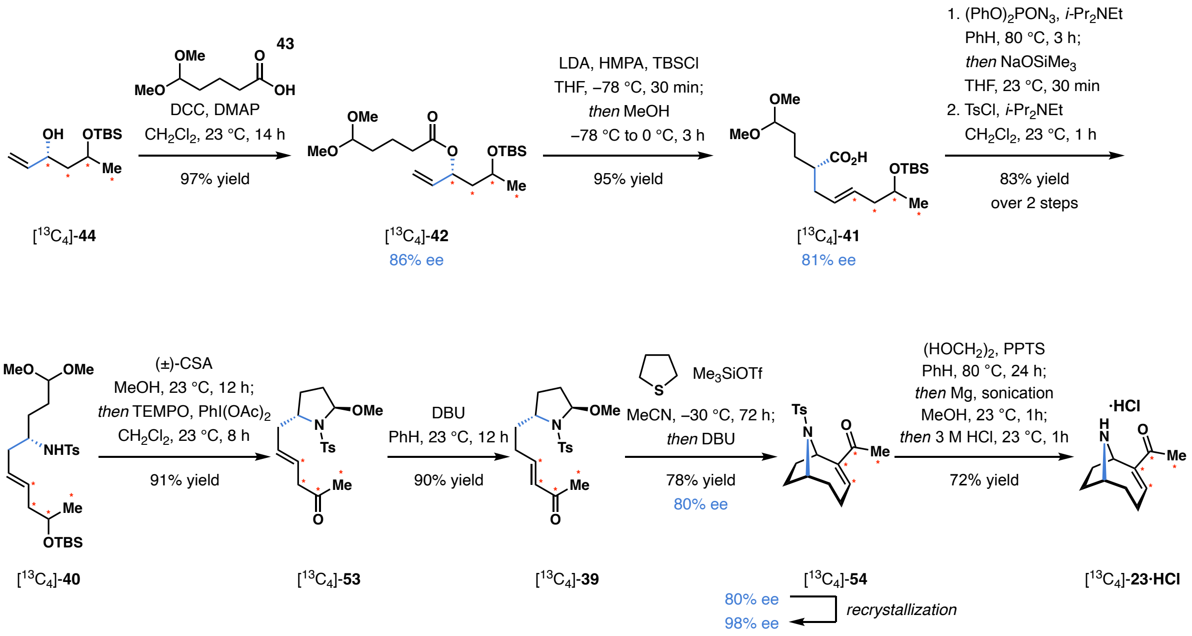

[13C4]-44
43
DCC, DMAP
CH2Cl2, 23 °C, 14 h
97% yield
[13C4]-42
86% ee
LDA, HMPA, TBSCl
THF, –78 °C, 30 min;
then MeOH
–78 °C to 0 °C, 3 h
95% yield
[13C4]-41
81% ee
1. (PhO)2PON3, i-Pr2NEt
PhH, 80 °C, 3 h;
then NaOSiMe3
THF, 23 °C, 30 min
2. TsCl, i-Pr2NEt
CH2Cl2, 23 °C, 1 h
83% yield
over 2 steps
[13C4]-40
(±)-CSA
MeOH, 23 °C, 12 h;
then TEMPO, PhI(OAc)2
CH2Cl2, 23 °C, 8 h
91% yield
[13C4]-53
DBU
PhH, 23 °C, 12 h
90% yield
[13C4]-39
Me3SiOTf
MeCN, –30 °C, 72 h;
then DBU
78% yield
80% ee
[13C4]-54
80% ee
98% ee
recrystallization
(HOCH2)2, PPTS
PhH, 80 °C, 24 h;
then Mg, sonication
MeOH, 23 °C, 1h;
then 3 M HCl, 23 °C, 1h
72% yield
[13C4]-23·HCl

At this point, we have reached the key synthetic intermediate [$^{13}C_4$]-**39** in our synthesis plan. As mentioned in previous sections (Chapters 2.1.3 and 2.2.1), many have successfully formed the azabicyclic structure from cyclization of iminiums generated from 2,5-disubstituted pyrrolidines.[43–49] Most notably, Somfai reported a successful tandem iminium cyclization performed in methanol saturated with hydrochloric acid.[45] This strongly acidic condition, however, appeared to be unreliable to consistently provide the cyclized product in high yields, and more importantly maintaining high enantiopurity of the product.[47,49] Stockman and Tanner reported the yields of the cyclization step to be less than ideal (a mere 51% yield).[47,49] More significantly, Tanner reported a complete loss of enantiopurity after cyclization under this HCl–MeOH condition (see Scheme 15b).[49] Explorations for a suitable Michael-type nucleophile for an aza-Morita–Baylis–Hillman (aza-MBH) cyclization step revealed tetrahydrothiophene to be compatible with our enone **39**.[60] In the presence of a Lewis acid Me_3SiOTf at −30 °C, the tosyl iminium was generated in situ, to which an addition of the enolate activated by tetrahydrothiophene accomplished the cyclized [$^{13}C_4$]-**54** in 78% yield while preserving the enantiopurity (80% ee). Recrystallization of [$^{13}C_4$]-**54** enriched the enantiopurity to give a 98% enantiopure *N*-tosylanatoxin-a. Treatment of the enone [$^{13}C_4$]-**54** with ethylene diol and pyridinium *p*-toluenesulfonate at 80 °C formed the acetal, which was critical in preventing decomposition. In the same pot, reduction with magnesium removed the *N*-tosyl moiety, and hydrolysis of the acetal afforded the [$^{13}C_4$]-anatoxin-a hydrochloric salt ([$^{13}C_4$]-**23**·HCl) in 72% yield.

A high-resolution mass spectral analysis presented a 99.1% carbon-13 incorporation at all four positions, validating our synthetic strategy (see page 157 in the Experimental Procedures section for HRMS results). We were able to prepare 0.110 grams of [$^{13}C_4$]-**23** using this approach, demonstrating the scalability of this labeled synthesis. This approach represents the first synthesis of [$^{13}C_4$]-**23**: a 16-step synthesis with an overall yield of 25%. The successful synthesis of [$^{13}C_4$]-**23** attained our initial intention to facilitate the development of a more precise anatoxin-a quantification method, while ensuring the ease and accessibility when employing said method.

2.3. A Dynamic Kinetic Resolution Enantioselective aza-Morita–Baylis–Hillman (aza-MBH) Cyclization

2.3.1. Initial Studies of Cyclic Iminium Ion Racemization

In our acid-catalyzed aza-MBH cyclization of the enantiopure pyrrolidinyl enone **39** for the formation of the bicyclic *N*-tosylanatoxin-a **54**, the conservation of enantiopurity proved to be somewhat problematic: we were astonished to observe a significant 41% decrease in the enantiopurity of product **54** from an 81% enantiopure precursor **39** (Scheme 15a). Our experience was consistent with that reported by Tanner in their synthesis of anatoxin-a, during which their enantiopure *N*-methoxycarbonyl pyrrolidine (**55**) cyclized to form the *N*-methoxycarbonyl anatoxin-a (**56**) after treatment of DBU (Scheme 15b); other acidic conditions Tanner explored failed to prevent racemization of their product **56**.[49] This observed racemization of the cyclized product was a result of cyclization of the two enantiomeric iminiums in equilibrium: iminiums **i** and **ii**. Tanner proposed that iminium **ii** would arise from [1,3]-hydride shifts between carbocations **iii**, **iv**, and **v** (Scheme 15c).[49] This is not apparent to us as very few [1,3]-hydride shifts have been reported; a suprafacial [1,3]-hydride shift is symmetry forbidden, and an antrafacial [1,3]-hydride shift would involve a highly strained transition state of a cyclic system, making it also extremely unlikely.[61]

Scheme 15. a) Observed Racemization During aza-MBH Cyclization, b) Tanner's Observed Racemization, and c) Tanner's Proposed Iminium Racemization Mechanism.

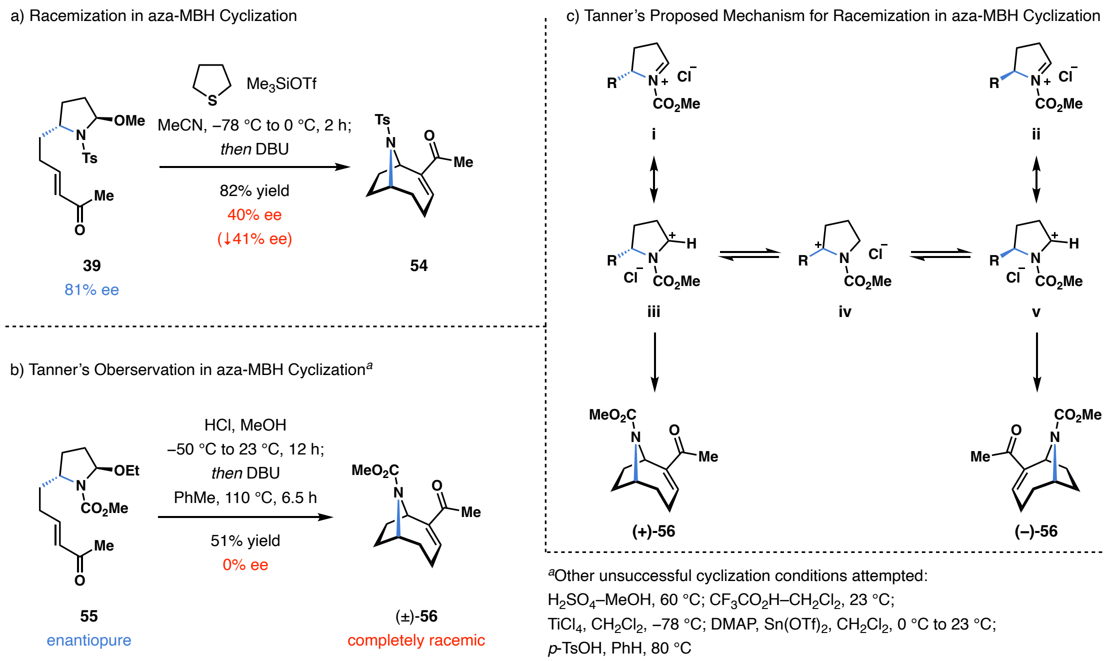
a) Racemization in aza-MBH Cyclization
OMe
N
Ts
Me
O
39
81% ee
S
Me3SiOTf
MeCN, –78 °C to 0 °C, 2 h;
then DBU
82% yield
40% ee
(↓41% ee)
Ts
N
O
Me
54
b) Tanner's Oberservation in aza-MBH Cyclization^a
OEt
N
CO2Me
Me
O
55
enantiopure
HCl, MeOH
–50 °C to 23 °C, 12 h;
then DBU
PhMe, 110 °C, 6.5 h
51% yield
0% ee
MeO2C
N
O
Me
(±)-56
completely racemic
c) Tanner's Proposed Mechanism for Racemization in aza-MBH Cyclization
R
N+
Cl–
CO2Me
i
ii
+
H
Cl–
iii
iv
v
MeO2C
CO2Me
(+)-56
(–)-56

^{a}Other unsuccessful cyclization conditions attempted:
H_2SO_4–MeOH, 60 °C; CF_3CO_2H–CH_2Cl_2, 23 °C;
$TiCl_4$, CH_2Cl_2, –78 °C; DMAP, $Sn(OTf)_2$, CH_2Cl_2, 0 °C to 23 °C;
p-TsOH, PhH, 80 °C

We were curious to identify factors that could account for this puzzling racemization phenomenon as there are no discernible epimerizable carbon centers in either Tanner or our pyrrolidine precursors. We began to investigate this discrepancy in the enantiopurity, proceeding with Me_3SiOTf as the Lewis acid and tetrahydrothiophene as the nucleophile (Table 3). While changes in solvents had little effect on the racemization of the iminiums, the isolated yields were superior with less byproduct formation when the reactions were performed in the more polar acetonitrile. After extensive experimentation in parameter adjustments, we found that the reaction temperature is critical in determining the enantiopurity of the cyclized **54**. When the reaction temperature was maintained at −20 °C for the entire 2-hour duration, we observed a 29% drop in the enantiopurity of the cyclized **54** compared to that of the enone **39** before subjecting to the reaction (entries 1 and 2). However, when the reaction was performed at −40 °C, there appeared to be no change of the enantiopurity of the product **54** with respect to that of the starting material **39**, though the yields suffered from slow reaction progression with a bare 50% conversion (entries 3 and 4). These results signify that racemization took place at temperatures at or above −20 °C but suppressed at temperatures at or below −40 °C, though at which point the reaction progress, too, was inhibited. We were delighted to find that when the reaction was performed at −30 °C, full conversion of **39** was achieved after 72 hours while the enantiopurity of **54** was preserved (entry 5). Also to note, in the two racemized reactions shown in Scheme 15a,b, both reactions were initially performed at low temperatures (−78 °C in our initial case, and −50 °C in Tanner's reaction) and were gradually warmed to higher temperatures to ensure full conversion of the precursors (0 °C for us, and 23 °C for Tanner).[49]

Table 3. Parameter Optimization for the aza-MBH Cyclization of **39**.

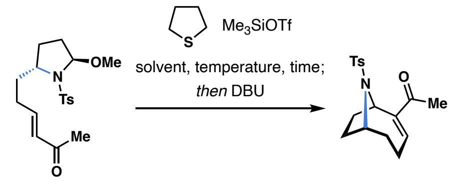

39
56% ee

54

entry^a	solvent	temperature (time)	yield	ee (change in ee)
1	MeCN	−20 °C (2 h)	83%	27% **(↓29%)**
2	CH_2Cl_2	−20 °C (1 h)	70%	31% **(↓25%)**
3	MeCN	−40 °C (44 h)	27%	55% **(no change)**
4	CH_2Cl_2	−40 °C (7 h)	69%	51% **(↓5%)**
5	MeCN	−30 °C (72 h)	78%	56% **(no change)**

^{a}Reactions were performed by treating a solution of **39** and 1.5 equiv of tetrahydrothiophene in solvent (0.1 M) with 2.5 equiv of Me$_3$SiOTf at the indicated temperature.

We theorized that an isomerization pathway facilitated by the presence of Lewis acids could help explain this racemization process (Scheme 16). The chiral pyrrolidinyl enone **39** first forms the cyclic iminium **vi** (analog of Tanner's iminium **i**) upon exposure to Me$_3$SiOTf. At temperatures above −30 °C, an acid-catalyzed isomerization could take place through the formation of the more stable *C*-disubstituted iminium **vii**, which would then re-form iminium **vi** while forming the enantiomeric iminium **viii** (analog of Tanner's iminium **ii**). A considerably elevated reaction temperature would thus allow both iminiums **vi** and **viii** to cyclize equally (through the transition states **TS1** and **TS2**, respectively), and a completely racemic **54** would form. Our findings in Table 3 are consistent with this proposed racemization construct: when the reaction temperature was raised above −30 °C, cyclic iminiums **vi** and **viii** were in rapid equilibrium, leading to the formation of both enantiomers of the azabicycle **54**, decreasing its enantiopurity; when the reaction temperature was cooled to −30 °C or below, isomerization of the cyclic iminium **vi** was impeded, forming the enantiopure azabicycle **54** with no erosion of enantiopurity. For these to be true, the rate of racemization between iminiums **vi**, **vii**, and **viii** must be greater than that of the irreversible cyclization step (**TS1** to (+)-**54** and **TS2** to (−)-**54**) at temperatures above −30 °C. Unsurprisingly, we never observed the azaspirocycle **57** that would form via the supposedly less reactive iminium **vii**,[62] and neither did Tanner with their *N*-methoxycarbonyl substrate **55**.[49]

Scheme 16. Proposed Acid-Catalyzed Isomerization of Iminiums at Temperatures at or Above −30 °C.

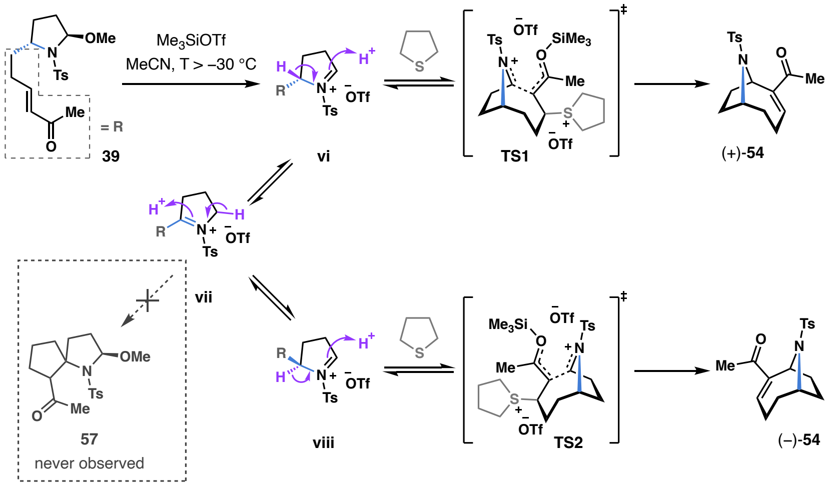
OMe
N
Ts
Me
O
= R
39
Me_3SiOTf
MeCN, T > –30 °C
H
R
N+
Ts
OTf
H+
vi
S
Ts
OTf
$SiMe_3$
O
N+
Me
S
+
OTf
TS1
‡
Ts
N
O
Me
(+)-54
H+
H
R
N+
OTf
Ts
vii
OMe
N
Ts
Me
O
57
never observed
R
H
N+
Ts
OTf
H+
viii
Me_3Si
OTf
Ts
O
+N
Me
S
+
OTf
TS2
‡
Me
O
Ts
N
(–)-54

Our synthesis for $[^{13}C_4]$-**23** was therefore accomplished by performing this aza-MBH cyclization on enone $[^{13}C_4]$-**39** at −30 °C to deliver the *N*-tosylanatoxin-a $[^{13}C_4]$-**54** with no loss in enantiopurity (see Scheme 14). While the exact origin of the epimerization is not yet accounted for, we are also not completely convinced that this racemization of iminiums occurred through [1,3]-hydride shifts suggested by Tanner.[49] We believe our proposed isomerization process presents a highly plausible explanation for the racemization observed in the aza-MBH cyclization of these pyrrolidines.

2.3.2. Proposed Dynamic Kinetic Resolution Design

Our asymmetric total synthesis plan for **23** relied on preserving the chirality of the C6 stereocenter originating from chiral allylic alcohol **44**, which was installed through a Sharpless asymmetric epoxidation (see Scheme 13c). Furthermore, to retain the enantiopurity of the cyclized **54**, the reaction was performed at −30 °C; this slowed the process of the unexpected iminium racemization to a rate that was negligible to that of the cyclization step. Even though this racemization of cyclic iminiums was initially presented to us as somewhat of a challenge in ensuring the enantiopurity of materials (through the last 8 steps of the entire synthesis from the chiral allylic alcohol **44** shown in Scheme 14), it occurred to us that this might be an opportunity in disguise. We were inspired to capitalize on this apparent predicament by applying this supposed inconvenience as the premise for realizing a dynamic kinetic resolution. We postulated that an enantioselective aza-MBH cyclization could be achieved by controlling the rates of cyclization of the two enantiomeric iminiums (iminiums **vi** and **viii**).

The two enantiomeric transition states **TS1** and **TS2** in Scheme 16 have identical energy levels and cyclize to product **54** at identical rates. However, with the introduction of a chiral nucleophile (chiral sulfide SR_2* labeled orange in Scheme 17a), transition states **TS3** and **TS4** (arising from iminiums **vi** and **viii**, respectively) are now diastereomeric and have different energy levels. These two transition states would cyclize to form product **54** at different rates, hence allowing us to modulate the rates of product formation to favor the cyclization for one enantiomer of *N*-tosylanatoxin-a **54** over the other (Scheme 17a). The chirality of the cyclized product (**54**) would be induced by the chiral nucleophile, thus circumventing the use of chiral materials up to this point. This is synthetically advantageous as it allows for a late-stage stereocontrol synthesis. Therefore, the racemic pyrrolidine (±)-[$^{13}C_4$]-**39** was prepared instead from the racemic form of the allylic alcohol (±)-[$^{13}C_4$]-**44**, which was obtained via a one-step Grignard addition of vinylmagnesium bromide to our aldehyde [$^{13}C_4$]-**48** (Scheme 17b). This shortens the total synthesis steps by 4 steps.

Scheme 17. a) Proposed Enantioselective aza-MBH Cyclization through a Dynamic Kinetic Resolution; b) Synthesis of (±)-[$^{13}C_4$]-**39** from Direct Access of (±)-[$^{13}C_4$]-**44**.

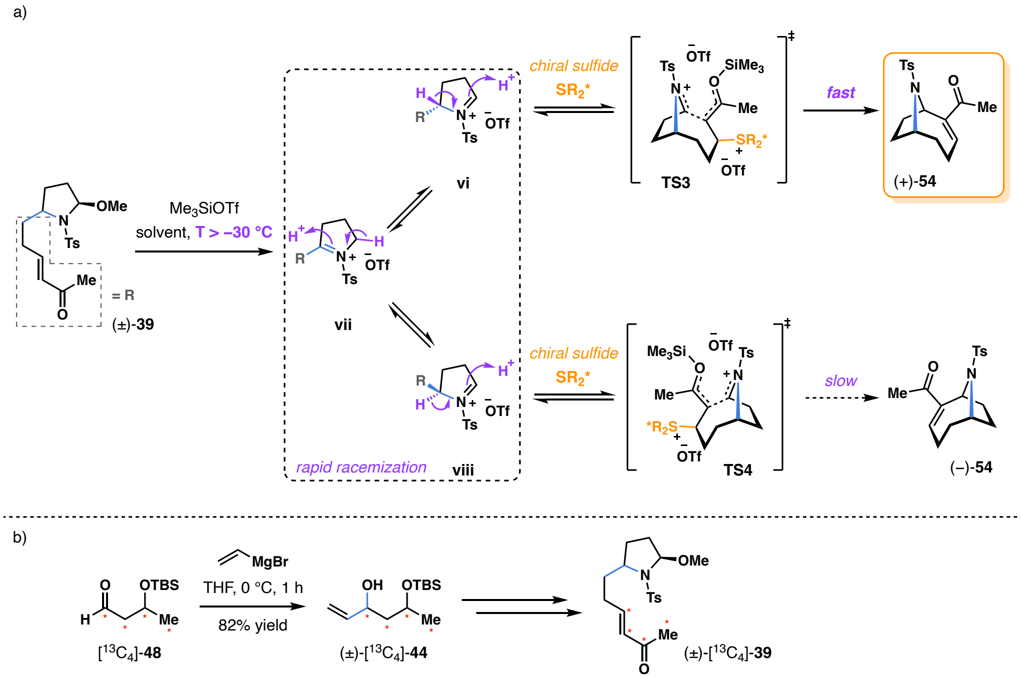
a)
OMe
N
Ts
Me
O
= R
(±)-39
Me3SiOTf
solvent, T > −30 °C
H+
R
N+
OTf
Ts
H
vii
vi
viii
rapid racemization
chiral sulfide
SR2*
TS3
TS4
SiMe3
Me
fast
slow
(+)-54
(−)-54
b)
H
OTBS
[13C4]-48
MgBr
THF, 0 °C, 1 h
82% yield
OH
(±)-[13C4]-44
(±)-[13C4]-39

To further establish the basis of our idea, we extended the Curtin–Hammett principle to our dynamic kinetic resolution design, as depicted in Scheme 18.[63] Since the key to accomplish our proposed enantioselective aza-MBH cyclization via a dynamic kinetic resolution is to take advantage of the rapid racemization process between cyclic iminiums **vi**, **vii**, and **viii**, the reactions would need to take place at temperatures above −30 °C. As we have established, at temperatures above −30 °C, the rate of these iminiums equilibrating is significantly faster than that of the cyclization to the β-sulfonium intermediates (+)-**58** and (−)-**58**, which eventually eliminate to afford azabicyclic enones (+)-**54** and (−)-**54**, respectively. According to the Curtin–

Hammett principle, the distribution of our cyclized (+)-**54** and (−)-**54** relies solely on the energy differences of the two diastereomeric transition states **TS3** and **TS4** of the irreversible cyclization step.[63] This energy difference between **TS3** and **TS4** is attributed to the chiral nucleophile used.

Scheme 18. The Relative Energy Profiles for Our Proposed Dynamic Kinetic Resolution aza-MBH Explained by the Curtin–Hammett Principle.

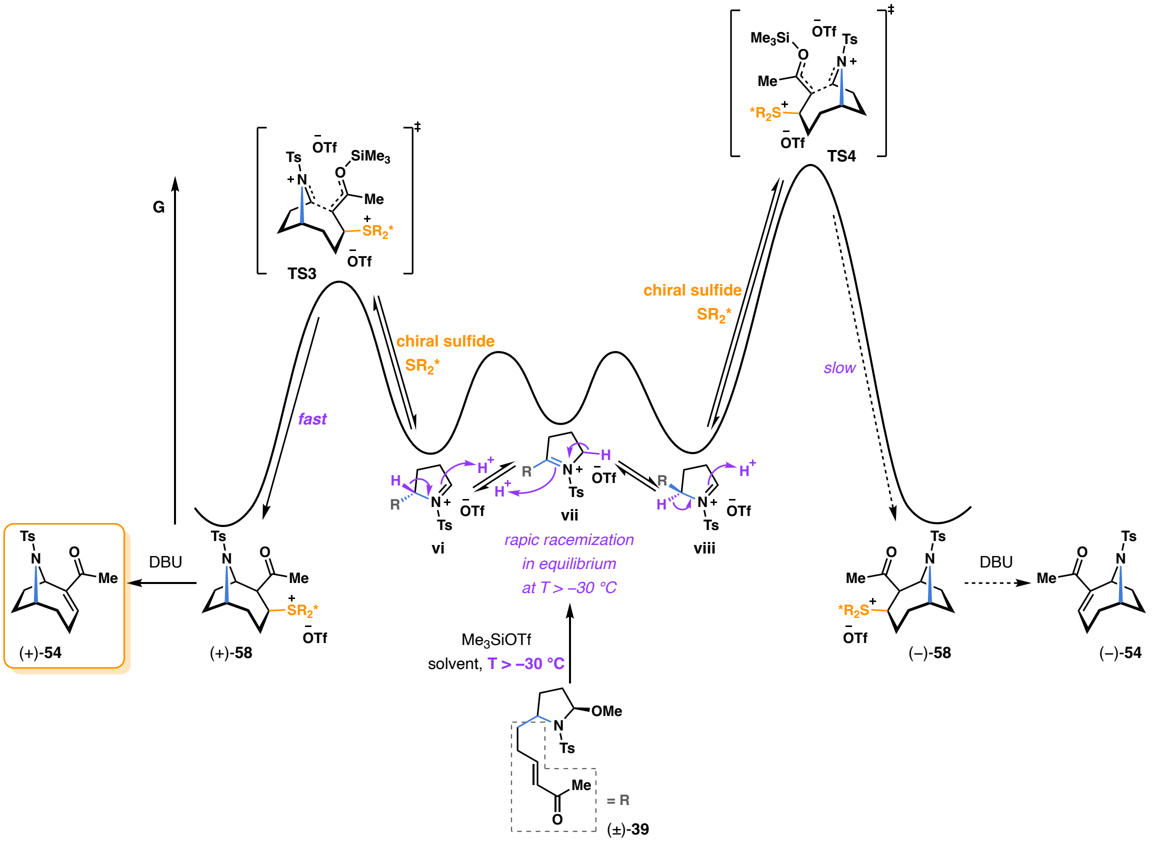
G
TS3
Ts
OTf
SiMe3
Me
SR2*
OTf
TS4
Me3Si
OTf
Ts
Me
*R2S
OTf
fast
chiral sulfide
SR2*
chiral sulfide
SR2*
slow
H
R
N+
Ts
OTf
H+
H+
vi
R
N+
H
Ts
OTf
vii
R
H
N+
Ts
OTf
H+
viii
rapic racemization
in equilibrium
at T > –30 °C
Ts
N
O
Me
(+)-54
DBU
Ts
N
O
Me
SR2*
OTf
(+)-58
O
Ts
Me
N
*R2S
OTf
(–)-58
DBU
Ts
O
Me
N
(–)-54
Me3SiOTf
solvent, T > –30 °C
OMe
N
Ts
Me
O
= R
(±)-39

Building on this intriguing phenomenon of rapidly racemizing cyclic iminiums in equilibrium, we began to investigate an enantioselective aza-MBH cyclization for (+)-**54** through a dynamic kinetic resolution of the cyclic iminiums generated from racemic (±)-**39**, where the chiral nucleophile used plays a critical role.

2.3.3. Optimization of the Enantioselective aza-MBH Cyclization

The energy difference between transition states **TS3** and **TS4** reflects the composition of the cyclized products (+)-**54** and (−)-**54**, as predicted by the Curtin–Hammett principle.[63] In our case, the goal is for the enantiomer (+)-**54** to prevail as the major product formed from the cyclization of the racemic pyrrolidinyl enone (±)-**39**: to achieve a greater energy barrier to **TS4** from iminium **viii** and a smaller energy barrier to **TS3** from iminium **vi**, thereby favoring the cyclized product of (+)-**54**. The extent to which we succeed is based on the energy profiles of the transition states, which is contingent on the chiral nucleophile implemented. Our optimization objective was to assess an array of chiral nucleophiles, where the ultimate chiral nucleophile is one that would allow significant preferences for the lower energy process of iminium **vi** cyclizing via **TS3** to form β-sulfonium (+)-**58**, and eventually our intended cyclized product (+)-**54** (see Scheme 18).

Given our success in using tetrahydrothiophene as the nucleophile for the aza-MBH cyclization of the chiral enone (+)-**39** to (+)-**54**, we directed our focus to sulfur-containing chiral nucleophiles for the development of the enantioselective variant of this transformation. We began a systematic search for the ideal chiral sulfide by first assessing the optimal geometry of the chiral sulfide nucleophile used, and in turn, the ideal geometries for the two transition states **TS3** and **TS4** to have distinct energy levels. The chiral sulfide isothiocine **59** is commercially available, and its ability to induce superior selectivity in asymmetric epoxidation reactions is well documented.[64,65] When the chiral sulfide **59** was implemented in our aza-MBH cyclization condition, we saw the reaction efficiently go to completion within 2 hours at 0 °C in acetonitrile (Table 4, entry 1). The cyclized **54** was isolated in 85% yield, but little to no selectivity was observed. Chiral oxathiane **60** possessing a different general steric feature, was revealed to be incompatible with our acidic reaction conditions.[64,66] We were unable to recover this chiral sulfide following work up, likely due to an acid-catalyzed hydrolysis of the thioacetal.[66] The chiral sulfide

60 gave azabicycle **54** in only 24% yield and a low −14% enantioselectivity (entry 2). The bulky camphor-derived sulfide **61** developed by Aggarwal and colleagues is another widely used chiral sulfide for sulfur ylide-mediated asymmetric carbon–carbon bond formation reactions.[64,67] We were further encouraged by Aggarwal's successful implementation of chiral sulfide **61** in an intermolecular aza-MBH reaction between iminiums and various α,β-unsaturated ketones.[68] When chiral sulfide **61** was used with our pyrrolidinyl enone (±)-**39**, the cyclized product **54** was isolated with good yield, but woefully presented no enantioselectivity (entry 3).

Table 4. Optimization of the Chiral Sulfides Used for the Enantioselective aza-MBH Cyclization.

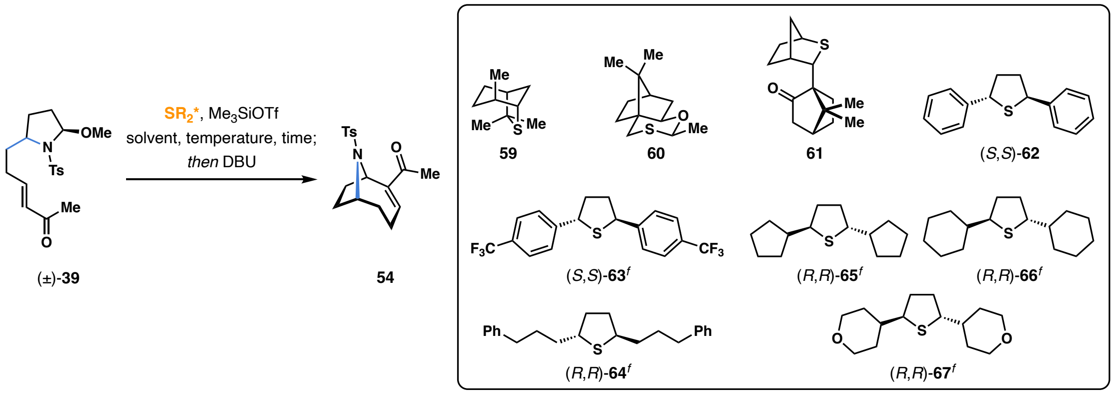

entry[a]	solvent	SR_2*	temperature	(time)	yield	ee
1	MeCN	**59**	0 °C	(2 h)	85%	–4%
2[b]	MeCN	**60**	0 °C	(3 h)	24%	–14%
3[c]	MeCN	**61**	0 °C	(4 h)	85%	0%
4[d]	MeCN	**62**	–20 °C	(22 h)	53%	–21%
5	MeCN–CH_2Cl_2 (1:1)	**63**	–15 °C	(24 h)	19%	0%
6	MeCN	**64**	0 °C	(2 h)	68%	–9%
7	MeCN–CH_2Cl_2 (1:1)	**65**	0 °C	(3 h)	59%	44%
8	MeCN–CH_2Cl_2 (1:1)	**65**	–10 °C	(6 h)	42%	26%
9	MeCN–CH_2Cl_2 (1:1)	**65**	–20 °C	(6 h)	68%	9%
10	MeCN–PhMe (1:1)	**66**	0 °C	(3 h)	40%	62%
11	MeCN–CH_2Cl_2 (1:1)	**67**	0 °C	(3 h)	29%	82%
12	MeCN–PhMe (1:1)	**66**	–48 °C	(24 h)	42%	70%
13	MeCN–CH_2Cl_2 (1:1)	**67**	–78 °C	(4 h)	28%	93%
14[e]	MeCN–CH_2Cl_2 (1:1)	**67**	0 °C	(2.5 h)	50%	78%

[a] Reactions were performed by treating a solution of (±)-**39** and 1.5 equiv of chiral sulfide (SR_2*) in solvent (0.1 M) with 2.5 equiv of Me_3SiOTf at the indicated temperature. [b] Chiral sulfide **59** was destroyed under the acidic reaction condition. [c] Epimerization of chiral sulfide **60** was observed. [d] TBSOTf was used instead of Me_3SiOTf. [e] Me_3SiOTf was added at –78 °C, and the reaction was performed at –78 °C for 1 h, then warmed to 0 °C to stir at 0 °C for another 75 min. [f] Thiolane configurations are proposed based on their optical rotations.

The C_2-asymmetric *trans*-2,5-disubstituted thiolanes represent another group of chiral sulfides with distinct geometric properties.[64] Chiral diphenyl thiolane (*S*,*S*)-**62** gave the cyclized product **54** in a moderate 53% yield with −21% ee (entry 4).[69] Yet, upon detailed examination, we noticed the recovered sulfide **62** had epimerized: the recovered sulfide **62** was a mixture of the *cis*- and *trans*-2,5-diphenylthiolane (**62**) (dr 14:86), with the *trans*-**62** losing 10% enantiopurity (from a 99% ee prior to the reaction to an 89% ee when recovered after the reaction). We believe that when the diphenyl thiolane **62** acted as a nucleophile to form the intermediate adduct, a ring-opening mechanism resulted in a benzylic carbocation formation (see page 197 in the Experimental Procedures section for full detail of epimerization of thiolane **62**). Thus, we synthesized the chiral sulfide (*S*,*S*)-**63**, a similar sulfide to **62** but with *para*-CF_3 electron-withdrawing groups that would discourage the carbocation formation, thereby preventing the loss of enantiopurity of the chiral sulfide, whose enantiopurity critically determines that of the cyclized product. Though, we were indeed able to inhibit epimerization of the sulfide, chiral sulfide **63** gave a measly 19% yield and no enantioselectivity (entry 5). The comparatively less bulky primary alkyl disubstituted thiolane (*S*,*S*)-**64** gave the cyclized **54** in 68% yield and a −6% ee (entry 6). Nonetheless, at this point, these C_2-asymmetric chiral sulfides (sulfides **62**–**64**, entries 4–6) appeared more compatible with our pyrrolidinyl enone **39**. Therefore, we sought to explore additional C_2-asymmetric thiolanes.

The results from implementing sulfides **62**–**64** directed our designs for the next set of C_2-asymmetric *trans*-2,5-disubstituted thiolanes. Hoping to improve the selectivity, we focused on incorporating congested substitutions at the C2 and C5 positions, hence targeting thiolanes with cyclic substituents. Employing the dicyclopentyl thiolane **65** at 0 °C yielded azabicycle product **54** with a promising 44% enantiopurity (entry 7), the highest induced enantioselectivity that we had seen thus far. As expected, this enantioselectivity is highly correlated with reaction temperature: the induced enantioselectivity decreases as temperature decreases. When the reaction temperature was lowered to −10 °C (entry 8) from 0 °C (entry 7), enantioselectivity was reduced by 18% (from 44% ee to 26% ee). When the reaction temperature was lowered even further to −20 °C (entry 9), there was essentially no enantioselectivity (9% ee). These observations substantiate the principles of our design for a dynamic kinetic resolution process. The racemization rate between the enantiomeric iminiums **vi** and **viii** in equilibrium slows as reaction temperature lowers, and when the reaction was performed at −20 °C, the rate of racemization slowed to no longer supersede the rates of cyclization. In other words, at −20 °C, the iminium **viii** generated in situ begins cyclizing to form the (−)-**54** quicker than it is isomerizing to the enantiomeric iminium **vi**, thus corroding the enantioselectivity. The dicyclohexyl thiolane **66** was presented with increased steric bulk which we aspired would further widen the energy differences between the two transition states **TS3** and **TS4**. The use of chiral sulfide **66** at 0 °C gave the cyclized **54** in 40% yield with a 62% ee (entry 10). We then varied the 6-membered cyclic system of the thiolane substituents and synthesized the bis(4-tetrahydropyranyl) thiolane **67**. The reaction using chiral sulfide **67** at 0 C successfully achieved azabicycle **54** with a remarkable 82% ee, however, at the expense of a low 29% yield (entry 11).

We also explored conditions for a simple kinetic resolution, a process where racemization between the two enantiomeric iminiums (iminiums **vi** and **viii**) was completely inhibited. This was accomplished by simply lowering the reaction temperature to below −30 °C. When the racemic precursor (±)-**39** was cyclized at −48 °C using dicyclohexyl thiolane **66**, product **54** was isolated in 42% yield with a modest increased in selectivity of 70% ee (entry 12) compared to the 62% ee attained when the reaction was performed at 0 °C (entry 10). In the case with the bis(4-tetrahydropyranyl) thiolane **67**, the reaction performed at −78 °C accomplished azabicycle **54** with an excellent 93% ee and a 28% yield (entry 13), a similar isolated yield (29%) to that obtained when the reaction was performed at 0 °C (entry 11).[xii] This led to a curious attempt where we first opted for a simple kinetic resolution-type cyclization by performing the reaction with chiral sulfide **67** at −78 °C for 1 hour,[xiii] during which the racemization between the iminiums **vi** and **viii** was completely suppressed. The reaction was subsequently warmed to 0 °C and stirred for an additional 75 minutes. At this temperature, the process of rapid racemization of iminiums was restored, allowing for a dynamic kinetic resolution to take place. Using this hybrid strategy, we were able to isolate product **54** with a 50% yield, a non-trivial improvement from the 29% yield accomplished with dynamic kinetic resolution at 0 °C for 3 hours (entry 10), while maintaining a good enantioselectivity of 78% (entry 14).[xiv]

[xii] Full conversion of the reaction was achieved when performed at 0 °C with thiolane **67** (Table 4, entry 11), but not when the reactions were performed at −40 °C with thiolane **66** (entry 12) or at −78 °C with thiolane **67** (entry 13). In these two cases, the recovered starting material **59** were also enantioenriched.

The cyclization findings with our C_2-asymmetric *trans*-2,5-disubstituded thiolanes occupying bulky substituents at the C2 and C5 positions concur with the assumptions we established in our chiral sulfide designs (Table 4, entries 7–14): increased bulkiness of the chiral sulfide nucleophile would result in greater enantioselectivity but in diminishing yields. Steric hindrance obstructed the approach of the bulkier sulfur-containing nucleophiles, impeding the rate of conjugate addition to vinyl ketone **39**. While we were never able to isolate any other side products (none of the azaspirocycle **57** in Scheme 16), in accounting for the remaining mass balance for some of the lower yielding reactions, we believe decomposition and oligomerization took place as a result of the encumbered nucleophilic activation of the enone of **39**, which likely participated in unstable side reactions.

Our optimization was expansive in applying a diverse range of chiral sulfides that exhibit varying geometries, and our results exemplify a complementary method for asymmetric induction in *N*-heterocycle formations, which stereoselective intramolecular aza-MBH reactions have limited literature presence.[70] We demonstrated a successful dynamic kinetic resolution approach for an enantioselective aza-MBH cyclization of the racemic pyrrolidinyl enone (±)-**39**. This unique strategy not only sets our total synthesis of (+)-**23** apart from the profusion of previous synthetic efforts, but also completes our asymmetric total synthesis of [$^{13}C_4$]-**23** in just 12 steps from the commercially available [$^{13}C_4$]-**45**, with a 16% overall yield.

[xiii] Performing the reaction at −78 °C for 1 hour afforded enantioenriched product in 14% yield. Compared to the 28% isolated yield when reacting for 4 hours at −78 °C (Table 4, entry 13), this result pointed to the scenario where greater reaction progression took place within the first hour.

[xiv] When the reaction was performed at −78 °C for 1 hour followed by an additional 30 minutes at 0 °C, product **54** was isolated in 36% yield with 83% ee.

2.4. Conclusion

We developed a scalable and robust synthesis of (+)-[$^{13}C_4$]-anatoxin-a ([$^{13}C_4$]-**23**), the first chemical synthesis of an isotopically labeled anatoxin-a.[71] Moreover, a paramount enantioselective aza-MBH cyclization method was established for the construction of the distinctive bicyclic structure of [$^{13}C_4$]-**23**.[71] The scalability of our synthesis was demonstrated by the 0.110 grams of [$^{13}C_4$]-**23** prepared from the commercially available [$^{13}C_4$]-**45**. The current EPA-adopted analytical method for cyanotoxin determination is limited by the lack of widely available high-performance internal standards that operate identical to the cyanotoxins in fresh water sources. With our synthesis providing a direct route to efficiently access high quality [$^{13}C_4$]-**23**, a more reliable method to more accurately detect and quantify freshwater anatoxin-a can be developed using our isotopically labeled probe. We accomplished our goal of bridging the gaps presented in the current method while acknowledging that this isotope-dilution method, once developed, will only be practically viable when such an isotopic form of anatoxin-a becomes prevalent. The peculiar constraints set forth by isotope incorporation instigated our novel and practical synthesis design—an approach embarked upon easily and commercially accessible starting material with at least four atoms isotopically labeled, as well as relying on effective transformations for conservation of all stable isotopes. A 16-step synthesis with an overall yield of 25% from [$^{13}C_4$]-**45** was established, where the enantioselectivity was accomplished by a Sharpless asymmetric epoxidation. Additionally, we devised a unique late-stage enantioselective

C–C bond formation method by exploiting the rapidly racemizing cyclic iminiums that was initially an impediment to the synthesis. The characteristic azabicycle of **23** was assembled through a penultimate intramolecular aza-MBH cyclization maneuvering a dynamic kinetic resolution of the cyclic iminiums generated from (±)-**39**, where the high enantioselectivity of this approach was brought about by the chiral sulfide used, in particular thiolanes **66** and **67**. This novel design unveils unique asymmetric applications for the syntheses of *N*-heterocyclic frameworks. Ultimately, our unusual discovery of the isomerization of cyclic iminiums empowered an improved and fascinating synthesis of [$^{13}C_4$]-**23** in 12 steps and a 16% overall yield.

References

[25] (a) Carmichael, W. W.; Biggs, D. F. *Science* **1975**, *187*, 542–544. (b) Devlin, J. P.; Edwards, O. E.; Gorham, P. R.; Hunter, N. R.; Pike, R. K.; Starvric, B. *Can. J. Chem.* **1977**, *55*, 1367–1371.

[26] (a) U.S. Environmental Protection Agency. http://www.epa.gov (accessed Dec 8, 2021). (b) U.S. EPA Cyanobacterial Harmful Algal Blooms (CyanoHABs) in Water Bodies https://www.epa.gov/cyanohabs (accessed Dec 8, 2021). (c) U.S. EPA Office of Water. https://arcg.is/0TPW0u0 (accessed Dec 8, 2021). (d) Cyanobacteria and Cyanotoxins: Information for Drinking Water Systems. EPA-810F11001. https://www.epa.gov/sites/default/files/2019-07/documents/cyanobacteria_and_cyanotoxins_fact_sheet_for_pws_final_06282019.pdf.pdf

[27] *Health Effects Support Document for the Cyanobacterial Toxin Anatoxin-A*; EPA 820R15104; U.S. Environmental Protection Agency, Office of Water: Washington, DC, June 2015. https://www.epa.gov/sites/production/files/2017-06/documents/anatoxin-a-report-2015.pdf

[28] (a) Albuquerque, E. X.; Pereira, E. F. R.; Alkondon, M.; Rogers, S. W. *Physiol. Rev.* **2009**, *89*, 73–120. (b) Harris, J. Neuromuscular Junctions (NMJ): A Target for Natural and Environmental Toxins in Humans. In *Encyclopedia of Neuroscience*; Squire, L. R., Ed.; Elsevier: Amsterdam, 2009; pp 539–549.

[29] Osswald, J.; Rellán, S.; Cago, A.; Vasconcelos, V. *Environ. Int.* **2007**, *33*, 1070–1089.

[30] (a) Cheung, M. Y.; Liang, S.; Lee, J. *J. Microbiol.* **2013**, *51*, 1–10. (b) Grahan, J. L.; Dubrovsky, N. M.; Eberts, S. M. *Cyanobacterial harmful algal blooms and U.S. Geological Survey Science Capabilities*; US Geological Survey: Reston, VA, 2016.

[31] Method 545: Determination of Cylindrospermopsin and Anatoxin-a in Drinking Water by Liquid Chromatography Electrospray Ionization Tandem Mass Spectrometry (LC/ESI–MS/MS); EPA 815-R-15-009; U.S. Environmental Protection Agency, Office of Water: Washington, DC, April 2015.

[32] (a) Smeraglia, J.; Baldrey, S. F.; Watson, D. *Chromatographia* **2002**, *55*, S95–S99. (b) Matuszewski, B. K.; Constanzer, M. L.; Chavez-Eng, C. M. *Anal. Chem.* **2003**, *75*, 3019–3030. (c) Bienvenu, J.-F.; Provencher, G.; Bélanger, P.; Bérubé, R.; Dumas, P.; Gagné, S.; Gaudreau, É.; Fleury, N. *Anal. Chem.* **2017**, *89*, 7560–7568.

[33] Annesley, T. M. *Clin. Chem.* **2003**, *49*, 1041–1044.

[34] (a) De Bièvre, P. Chapter 8 Isotope Dilution Mass Spectrometry (IDMS). In *Trace Element Analysis in Biological Specimens*; Herber, R. F. M.; Stoeppler, M., Eds.; Elsevier: Amsterdam, 1994; pp 169–183. (b) Vogl, J.; Rosner, M.; Pritzkow, W. *Anal. Bioanal. Chem.* **2013**, *405*, 2763–2770. (c) Panda, D.; Dash, B. P.; Manickam, S.; Boczkaj, G. *Mass Spectrom. Rev.* **2021**, 1–38.

[35] Stevens, D. K.; Krieger, R. I. *Toxicon* **1991**, *29*, 167–179.

[36] Haddad, S. P.; Bobbitt, J. M.; Taylor, R. B.; Lovin, L. M.; Conkle, J. L.; Chambliss, C. K.; Brooks, B. W. *J. Chromatogr. A* **2019**, *1599*, 66–74.

[37] Mailyan, A. K.; Chen, J. L.; Li, W.; Keller, A. A.; Sternisha, S. M.; Miller, B. G.; Zakarian, A. *J. Am. Chem. Soc.* **2018**, *140*, 6027–6032.

[38] Campbell, H. F.; Edwards, O. E.; Kolt, R. *Can. J. Chem.* **1977**, *55*, 1372–1379.

[39] (a) Mansell, H. L. *Tetrahedron* **1996**, *52*, 6025–6061. (b) Fonseca, C.; Aureliano, M.; Abbas, F.; Furey, A. Recent Insights into Anatoxin-a Chemical Synthesis, Biomolecular Targets, Mechanisms of Action and LC-MS Detection. In *Phycotoxins: Chemistry and Biochemistry*, 2nd ed.; Botana, L. M.; Alfonso, A., Eds.; John Wiley & Sons: New York, 1994; 137–180.

[40] Wegge, T.; Schwarz, S.; Seitz, G. *Tetrahedron: Asymmetry* **2000**, *11*, 1405–1410.

[41] Trost, B. M.; Oslob, J. D. *J. Am. Chem. Soc.* **1999**, *122*, 3057–3064.

[42] Aggarwal, V. K.; Humphries, P. S.; Fenwick, A. *Angew. Chem. Int. Ed.* **1999**, *38*, 1985–1986.

[43] Sardina, F. J.; Howard, M. H.; Koskinen, A. M. P.; Rapoport, H. *J. Org. Chem.* **1989**, *54*, 4654–4660.

[44] (a) Bates, H. A.; Rapoport, H. *J. Am. Chem. Soc.* **1979**, *101*, 1259–1265. (b) Petersen, J. S.; Fels, G.; Rapoport, H. *J. Am. Chem. Soc.* **1984**, *106*, 4539–4547.

[45] Somfai, P.; Åhman, J. *Tetrahedron Lett.* **1992**, *33*, 3791–3794.

[46] Skrinjar, M.; Nilsson, C.; Wistrand, L.-G. *Tetrahedron: Asymmetry* **1992**, *3*, 1263–1270.

[47] Roe, S. J.; Stockman, R. A. *Chem. Commun.* **2008**, 3432–3434.

[48] Melching, K. H.; Hiemstra, H.; Klaver, W. J.; Speckamp, W. N. *Tetrahedron Lett.* **1986**, *27*, 4799–4802.

[49] Hjelmgaard, T.; Søtofte, I.; Tanner, D. *J. Org. Chem.* **2005**, *70*, 5688–5697.

[50] Speckamp, W. N.; Hiemstra, H. *Tetrahedron* **1985**, *41*, 4367–4416.

[51] (a) Vernon, P.; Gallagher, T. *J. Chem. Soc., Chem. Commun.* **1987**, 245–246. (b) Huby, N. J. S.; Kinsman, R. G.; Lathbury, D.; Vernon, P. G.; Gallagher, T. *J. Chem. Soc., Perkin Trans. 1* **1991**, 145–155.

[52] (a) Brenneman, J. B.; Martin, S. F. *Org. Lett.* **2004**, *6*, 1329–1331. (b) Brenneman, J. B.; Machauer, R.; Martin, S. F. *Tetrahedron* **2004**, *60*, 7301–7314.

[53] Kittler, K.; Hoffmann, H.; Lindemann, F.; Koch, M.; Rohn, S.; Maul, R. *Anal. Bioanal. Chem.* **2014**, *406*, 5765–5774.

[54] Incorporation experiments of [U-^{13}C, ^{15}N]-L-proline into anatoxin-a (**23**) present a mixture of labeled and unlabeled forms of anatoxin-a: (a) Méjean, A.; Dalle, K.; Paci, G.; Bouchonnet, S.; Mann, S.; Pichon, V.; Ploux, O. *J. Nat. Prod.* **2016**, *79*, 1775–1782. (b) Kust, A.; Méjean, A.; Ploux, O. *J. Nat. Prod.* **2020**, *83*, 142–151.

[55] Corey, E. J.; Helal, C. J. *Angew. Chem. Int. Ed.* **1998**, *37*, 1986–2012.

[56] (a) Oppolzer, W.; Radinov, R. N. *Tetrahedron Lett.* **1988**, *29*, 5645–5648. (b) Layton, M. E.; Morales, C. A.; Shair, M. D. *J. Am. Chem. Soc.* **2002**, *124*, 773–775. For a review of enantioselective organozinc reagents addition to aldehydes, see: (c) Soai, K.; Niwa, S. *Chem. Rev.* **1992**, *92*, 833–856.

[57] Brubaker, J. D.; Myers, A. G. *Org. Lett.* **2007**, *9*, 3523–3525.

[58] (a) Katsuki, T.; Sharpless, K. B. *J. Am. Chem. Soc.* **1980**, *102*, 5974–5976. (b) Hanson, R. M.; Sharpless, K. B. *J. Org. Chem.* **1986**, *51*, 1922–1925.

[59] (a) Ma, B.; Lee, W.-C. *Tetrahedron Lett.* **2010**, *51*, 385–386. (b) Gluyas, J. B. G.; Burschka, C.; Dörrich, S.; Vallet, J.; Gronemeyer, H.; Tacke, R. *Org. Biomol. Chem.* **2012**, *10*, 6914–6929.

[60] (a) Myers, E. L.; Butts, C. P.; Aggarwal, V. K. *Chem. Commun.* **2006**, 4434–4436. (b) Myers, E. L.; de Vries, J. G.; Aggarwal, V. K. *Angew. Chem. Int. Ed.* **2007**, *46*, 1893–1896. (c) Kitulagoda, J. E.; Palmelund, A.; Aggarwal, V. K. *Tetrahedron* **2010**, *66*, 6293–6299.

[61] Woodward, R. B.; Hoffmann, R. *Angew. Chem. Int. Ed.* **1969**, *8*, 781–932.

[62] Kværnø, L.; Norrby, P.-O.; Tanner, D. *Org. Biomol. Chem.* **2003**, *1*, 1041–1048.

[63] (a) Seeman, J. I. *Chem. Rev.* **1983**, *83*, 83–134. (b) Caddick, S.; Jenkins, K. *Chem. Soc. Rev.* **1996**, *25*, 447–456.

[64] Illa, O.; Namutebi, M.; Saha, C.; Ostovar, M.; Chen, C. C.; Haddow, M. F.; Nocquet-Thibault, S.; Lusi, M.; McGarrigle, E. M.; Aggarwal, V. K. *J. Am. Chem. Soc.* **2013**, *135*, 11951–11966.

[65] Illa, O.; Arshad, M.; Ros, A.; McGarrigle, E. M.; Aggarwal, V. K. *J. Am. Chem. Soc.* **2010**, *132*, 1828–1830.

[66] (a) Aggarwal, V. K.; Ford, J. G.; Thompson, A.; Jones, R. V. H.; Standen, M. C. H. *J. Am. Chem. Soc.* **1996**, *118*, 7004–7005. (b) Aggarwal, V. K.; Ford, J. G.; Fonquerna, S.; Adams, H.; Jones, R. V. H.; Fieldhouse, R. *J. Am. Chem. Soc.* **1998**, *120*, 8328–8339.

[67] (a) Aggarwal, V. K.; Alonso, E. Hynd, G.; Lydon, K. M.; Palmer, M. J.; Porcelloni, M.; Studley, J. R. *Angew. Chem. Int. Ed.* **2001**, *40*, 1430–1433. (b) Aggarwal, V. K.; Fang, G.; Kokotos, C. G.; Richardson, J.; Unthank, M. U. *Tetrahedron* **2006**, *62*, 11297–11303.

[68] Myers, E. L.; de Vries, J. G.; Aggarwal, V. K. *Angew. Chem. Int. Ed.* **2007**, *46*, 1893–1896.

[69] Periasamy, M.; Ramani, G.; Muthukumaragopal, G. P. *Synthesis* **2009**, 1739–1743.

[70] For a review of aza-MBH reactions, see: (a) Declerck, V.; Martinez, J.; Lamaty, F. *Chem. Rev.* **2009**, *109*, 1–48. For reviews on the applications of MBH reactions in cyclization reactions and syntheses of natural products, see: (b) Wang, F.-J.; Wei, Y.; Shi, M. In *The Chemistry of the Morita–Baylis–Hillman Reaction*; Spivey, J. J. Ed.; RSC Catalysis Series No. 8; Royal Society of Chemistry: Cambridge, U.K., 2011; 325–551.

[71] Lacharity, J. J.; Mailyan, A. K.; Chen, K. Y.; Zakarian, A. *Angew. Chem. Int. Ed.* **2020**, *59*, 11364–11368.

Chapter 3.

Large Scale Synthesis Efforts Towards Xestospongin-type Marine Natural Products

3.1. Introduction

3.1.1. Isolation and Biological Activity

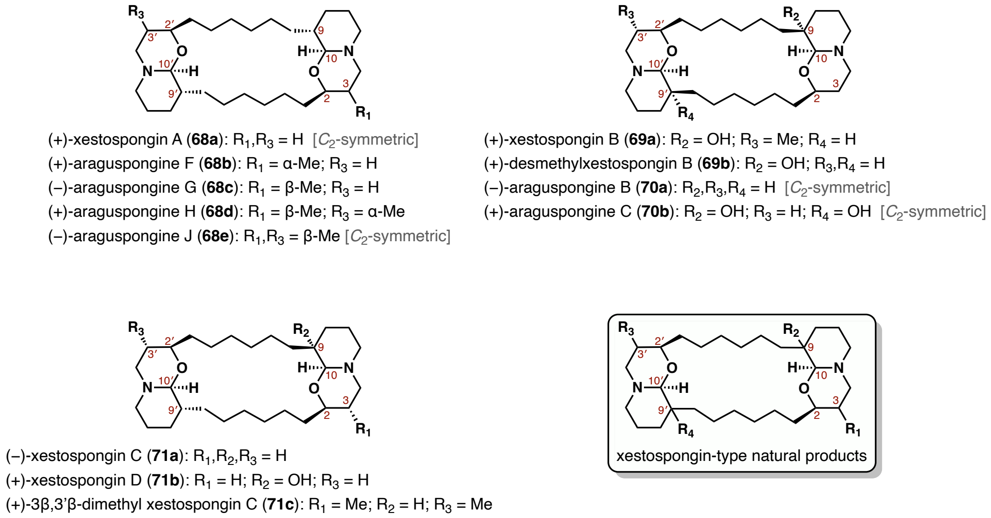

(+)-xestospongin A (**68a**): $R_1,R_3 = H$ [C_2-symmetric]
(+)-araguspongine F (**68b**): R_1 = α-Me; R_3 = H
(−)-araguspongine G (**68c**): R_1 = β-Me; R_3 = H
(+)-araguspongine H (**68d**): R_1 = β-Me; R_3 = α-Me
(−)-araguspongine J (**68e**): R_1,R_3 = β-Me [C_2-symmetric]

(+)-xestospongin B (**69a**): R_2 = OH; R_3 = Me; R_4 = H
(+)-desmethylxestospongin B (**69b**): R_2 = OH; R_3,R_4 = H
(−)-araguspongine B (**70a**): R_2,R_3,R_4 = H [C_2-symmetric]
(+)-araguspongine C (**70b**): R_2 = OH; R_3 = H; R_4 = OH [C_2-symmetric]

(−)-xestospongin C (**71a**): R_1,R_2,R_3 = H
(+)-xestospongin D (**71b**): R_1 = H; R_2 = OH; R_3 = H
(+)-3β,3′β-dimethyl xestospongin C (**71c**): R_1 = Me; R_2 = H; R_3 = Me

Figure 7. Xestospongin-type marine natural products.

Xestospongin-type natural products are a group of marine alkaloids isolated from the sponges *Xestospongia* sp.[72] These alkaloids, which include xestospongins and araguspongins, feature a characteristic macrocyclic core of two 1-oxaquinolizidine units joined together with saturated alkylidene chains (Figure 7 inset).[72] All isolated xestospongin-type natural products display (*R*)-configurations at the C2/C2' positions and (*S*)-configurations at the C10/C10' positions, but each differs in oxidation and stereochemistry at the C3, C9, C3', and C9' positions.[72d] By categorizing the substitution and ring junction patterns at the C2/C2' and C9/C9' positions of the 1-oxaquinolizidine units, a general structural division can be made to identify these alkaloids (Figure 7): the bis-*trans*-fused system represented in (+)-xestospongin A (Xe A, **68a**), the bis-*cis*-fused system shown in (+)-xestospongin B (Xe B, **69a**) and (−)-araguspongine B (Ar B, **70a**), and lastly, the *cis*–*trans*-fused system presented in (−)-xestospongin C (Xe C, **71a**).[72d,73] More notably, Xe A (**68a**), (−)-araguspongine J (Ar J, **68e**), Ar B (**70a**), and (+)-araguspongine C (Ar C, **70b**) are C_2-symmetric, while the remaining alkaloids of this family lacks this symmetry.[72d]

The family of xestospongin-type natural products has been associated with a wide spectrum of biological activities.[73] Initially uncovered as vasodilators by Nakagawa and co-workers in 1984 when xestospongins A–D were first isolated,[72a,72e,74] these marine alkaloids featuring macrocyclic bis-1-oxaquinolizidines have since been reported to express additional biological properties, including growth inhibition.[72b,75] Interest grew with findings identifying these marine alkaloids as a distinct class of potent modulators of inositol-1,4,5-triphosphate receptors (IP_3Rs) in calcium signaling.[73,76,77] Gafni et al. also suggested that the bis-1-oxaquinolizidine structure of these marine alkaloids were responsible for the effective inhibition of IP_3R-mediated calcium ion (Ca^{2+}) release from the endoplasmic reticulum (ER) while not interacting with the binding sites of IP_3Rs.[73] IP_3 receptors have been extensively studied for their role as Ca^{2+} release channels: the intricate intracellular Ca^{2+} signaling begins with the release of Ca^{2+} from the ER via IP_3Rs to the cytosol and other organelles, triggering a series of Ca^{2+}-regulated signaling cascades.[78] Recent discoveries have unfolded the role of IP_3Rs in autophagy, a major cellular process that regulates homeostasis.[79,80] Autophagy as a result of inhibition of Ca^{2+} release mediated by IP_3Rs implicates an attractive target in cancer therapy.[80,81] As inhibitors of IP_3R-mediated calcium signaling, xestospongin-type marine alkaloids are thus presented as potential therapeutics, and also as compelling modulators in assisting research advances in cancer cell biology.[79–81] Most intriguingly, the specific IP_3R inhibitor xestospongin B (Xe B, **69a**) demonstrated unparalleled ability to induce autophagy; perhaps more pertinently, Xe B-induced autophagy selectively led to cancer cell death while normal cells appeared to be unaffected by treatment of **69a**.[77,81–82]

3.1.2. Biological Studies and Background

Calcium ions command many cellular functions by initiating cascade events, and the intracellular flow of calcium is directed by IP_3Rs.[78,79] The peculiar ability of xestospongin-type natural products to modulate calcium signaling as inhibitors of IP_3Rs enables the regulation of autophagy in cancer cells, thereby positioning them as prominent therapeutic targets.[78–82] This prospect of promoting cancer cell death is apropos to the Ca^{2+} transfer from the ER to the mitochondria through IP_3Rs.[79]

Research in cancer therapy targets the hallmark features of cancer, and one of these characteristics of cancer cells is their uncontrolled metabolic rates to meet the high growth demands.[83] The Warburg effect describes the increased occurrence of anaerobic glycolysis in cancer cells as a means to sustain their proliferation.[84] Initially believed to have originated from defected mitochondrial functions, studies presently show that the mitochondria's role in oxidative phosphorylation for adenosine triphosphate (ATP) production is critical in cancer cells' ability to prosper with elevated rates.[84] Despite inefficiently producing ATP, this re-programmed metabolism promotes the biosynthesis of metabolic macromolecules for the rapid growth of cancer cells.[84] Many research directions have thus focused on targeting oxidative phosphorylation and ATP production in cancer metabolism.[79–83,85]

Since the major finding of the constitutive Ca^{2+} transfer between the ER and the mitochondria by the Cardenas group,[79a] there is considerable propensity for regulating mitochondrial metabolism, one of the hallmark features of cancer, by modulating the Ca^{2+} flux mediated by IP_3Rs.[81,83] An influx of Ca^{2+} to the mitochondria is necessary to bioenergetically regulate the mitochondrial respirations, where the Ca^{2+}-dependent tricarboxylic acid cycle (TCA) can be activated for the production of ATP by oxidative phosphorylation.[78] This constitutive IP_3R-mediated Ca^{2+} transfer between the ER and the mitochondria is essential for the survival of the cell and a disruption to this continuous mitochondrial uptake of Ca^{2+} results in the activation of a degradation pathway, and autophagy is induced upon the cell.[79] This autophagic process is indicated by the expression of the adenosine monophosphate (AMP)-activated protein kinase (AMPK), an enzyme that is pivotal in cellular homeostasis by sensing the intracellular AMP:ATP ratio.[79] The inhibition of IP_3Rs interferes with the constitutive Ca^{2+} transfer to the mitochondria, lowering ATP production and activating AMPK.[79] Metabolic stress resulting from a lack of Ca^{2+} flow to the mitochondria has different cellular responses in normal and cancer cells.[79–81] Normal cells enter the pro-survival autophagy to recycle metabolites for maintaining ATP levels and necessary synthesis for metabolic intermediates; apoptosis is avoided as the cell cycle is arrested.[79–81] Instead, cancer cells demonstrate uninhibited progression to the cell cycle; the lack of sufficient metabolic building blocks, nucleotides in particular, leads to mitotic cell death in cancer cells.[79–82]

Increased expression of IP_3Rs has been associated with tumorigenesis, and its inhibition slowed the progression of cancer.[86] The Cardenas group examined the metabolic response of IP_3R inhibition both in vitro and in vivo.[81a] Bioenergetic stress was introduced to non-tumorigenic and tumorigenic cells by treatment with the IP_3R-specific inhibitor, Xe B (**69a**).[77,81,82] As expected, induced autophagy was observed across a wide range of cell lines[xv] as demonstrated by increased AMPK activation (phosphorylation of AMPK).[81a] Shrinkages and diminished formation of cancer cell colonies, as well as the eventual cancer cell-specific killing resulted from necrosis during mitosis of cell cycles, were observed upon Xe B (**69a**) inhibition of IP_3Rs; in contrast, the absence of morphological changes to normal cells allowed them to survive after exposure of Xe B (**69a**).[81a] In vivo studies of Xe B (**69a**)-treated mice tumors also presented bioenergetic distress and activation of autophagy; moreover, the tumors injected with Xe B (**69a**) were significantly reduced in size compared to the untreated, control tumors.[81a] IP_3R-mediated Ca^{2+} intracellular signaling is vital not only to supporting the metabolic bioenergetics, but also to regulating cell cycle progression.[72–81,87] This key difference in the cellular fates of normal and cancer cells under cellular distress lies in cancer cells' ability to bypass Ca^{2+}-regulated cell cycle checkpoints.[81,87]

[xv] This investigation included various cell lines: human breast- (nontumorigenic MCF10A; tumorigenic MCF7, T46D, and HS578T), human prostate- (nontumorigenic PNT2, tumorigenic PC3 and DU145), mouse skin (melanoma B16F10), human cervical- (tumorigenic HeLa) cancer cells and more.[81a]

Therefore, xestospongin-type marine alkaloids are distinctly valuable in further elucidating the therapeutic significance of IP_3R-regulated cancer cell metabolism.

3.1.3. Motivation for a Large-Scale Chemical Synthesis

Secondary metabolites produced from marine natural sources showcase expansive biological activities; however, the therapeutic aptitude of these natural products are often thwarted by limited isolated quantities.[88] The vast marine environment is credited for the diversity of these bioactive molecules, and this same reason also complicates their sustained supply.[88] Re-isolation of these molecules is thus not guaranteed. As a result, novel chemical synthetic strategies prevail as the most practical approach to provide ample amounts of such bioactive molecules.

Xestospongin-type alkaloids isolated from marine sponges suffer a similar fate of scarcity. Owing to the pharmaceutical potentials of these macrocyclic bis-1-oxaquinolizidines, chemical syntheses to access these structurally complex alkaloids are in great demand to further advance progress of their medicinal applications. Captivated particularly by the remarkable remedies shown by the C_2-asymmetric Xe B (**69a**), we undertook a synthetic strategy focusing on scalability and divergence, that would enable sizable procurement of the various alkaloids within the xestospongin family. We envision that such a versatile chemical synthesis will not only illuminate the clinical roles of these marine alkaloids but also further progress in cancer research.

3.2. Previous Syntheses

Several synthetic efforts studying the unique 1-oxaquinolizidine ring system of xestospongin-type natural products have been published.[89,90] However, to date, there are only three successful chemical synthesis documentations of xestospongin-type natural products: two of which are C_2-symmetrical syntheses (Hoye in 1994[91] and 1996[92], and Baldwin in 1998[93]), and the third being a C_2-non-symmetrical synthesis (Zakarian in 2020).[94]

The first ever chemical synthesis reported for this family of xestospongins was by Hoye for Xe A (**68a**).[91] Their method was later expanded for the synthesis of the epimer Xe C (**71a**).[92] Baldwin reported a biomimetic synthesis approach for Xe A (**68a**), Xe C (**71a**), and Ar B (**70a**).[93] After extensive structural characterizations done by Baldwin, they determined that their three synthetic compounds, as well as Hoye's products, were actually the enantiomeric forms of the natural isomers (*ent*-**68a**, *ent*-**71a**, and *ent*-**70a** by Baldwin; *ent*-**68a** and *ent*-**71a** by Hoye).[93]

The two previous syntheses of Hoye and Baldwin elucidated the absolute configurations of these structurally intriguing marine alkaloids.[91–93] Nonetheless, synthetic access to other members of this family of marine alkaloids beyond the three synthesized by Hoye and Baldwin (Xe A, Xe C, and Ar B) remained largely unexplored.[91–93] It was only until the recent work published by the Zakarian Group that it became possible to access a diverse range of natural and non-natural derivatives of xestospongins.[94] Zakarian's synthesis design features scalability and flexibility in substitution control, where an approach that accesses xestospongins of varying stereochemical and oxidation patterns at the C9/C9' positions was reported.[94] This was demonstrated by the synthesis of two members of xestospongins—the (+)-Ar C (**70b**) and the (+)-desmethylxestospongin B (dmXe B, **69b**)—both have not been previously chemically synthesized.[94]

3.2.1. Hoye's C_2-Symmetric Synthesis of (−)-Xestospongin A

Scheme 19. a) Hoye's Dimerization Approach and b) the Key Condensation Reaction for Constructing the 1-Oxaquinolizidine Rings in Hoye's Synthesis.

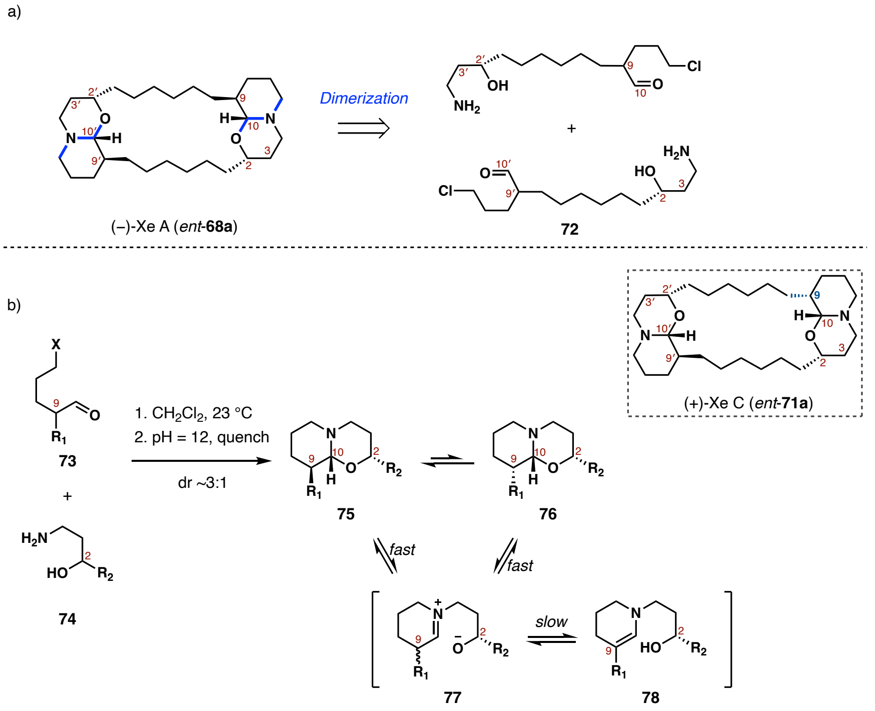

Hoye adopted a dimerization strategy to construct the macrocycle of **68a** by taking advantage of its C_2-symmetric nature.[91,92] In both accounts of Hoye's xestospongin total synthesis, including the initial step-wise approach and the subsequent direct approach, the bifunctional monomer **72** was identified as the key intermediate for the macrocyclization of *ent*-**68a** (Scheme 19a, bonds highlighted in blue represent the dimerization disconnections).[91,92] The key bis-*trans*-fused 1-oxaquinolizidines were cyclized via a condensation reaction between a 5-halovaleraldehyde **73** and a 1,3-aminoalcohol **74**, which monomer **72** carries both the aldehyde and the aminoalcohol moieties (Scheme 19b).[90–92] Conformational studies of the stereochemical patterns of the

2,9-disubstituted 1-oxaquinolizidine ring system revealed a strong thermal preference (dr 3:1) for a 2,9-*trans* disubstituted system (**75**), and the relative stereochemistries at C2, C9, and C10 were established by the configuration of C2.[90–92] The C9 epimer (**76**) was the result of a rapid and reversible ring-opening at the aminal carbon forming iminium **77**, followed by a slower reversible proton transfer step forming enamine **78**.[90–92] The C9 epimer of *ent*-**68a**, *ent*-**71a** (Scheme 19 inset, C9 highlighted in blue), was obtained through this equilibrating process when forging the macrocyclic bis-1-oxaquinolizidines.[92]

Scheme 20. Hoye's Macrocyclic Dimerization: a) With and b) without Rigid Modifiers.

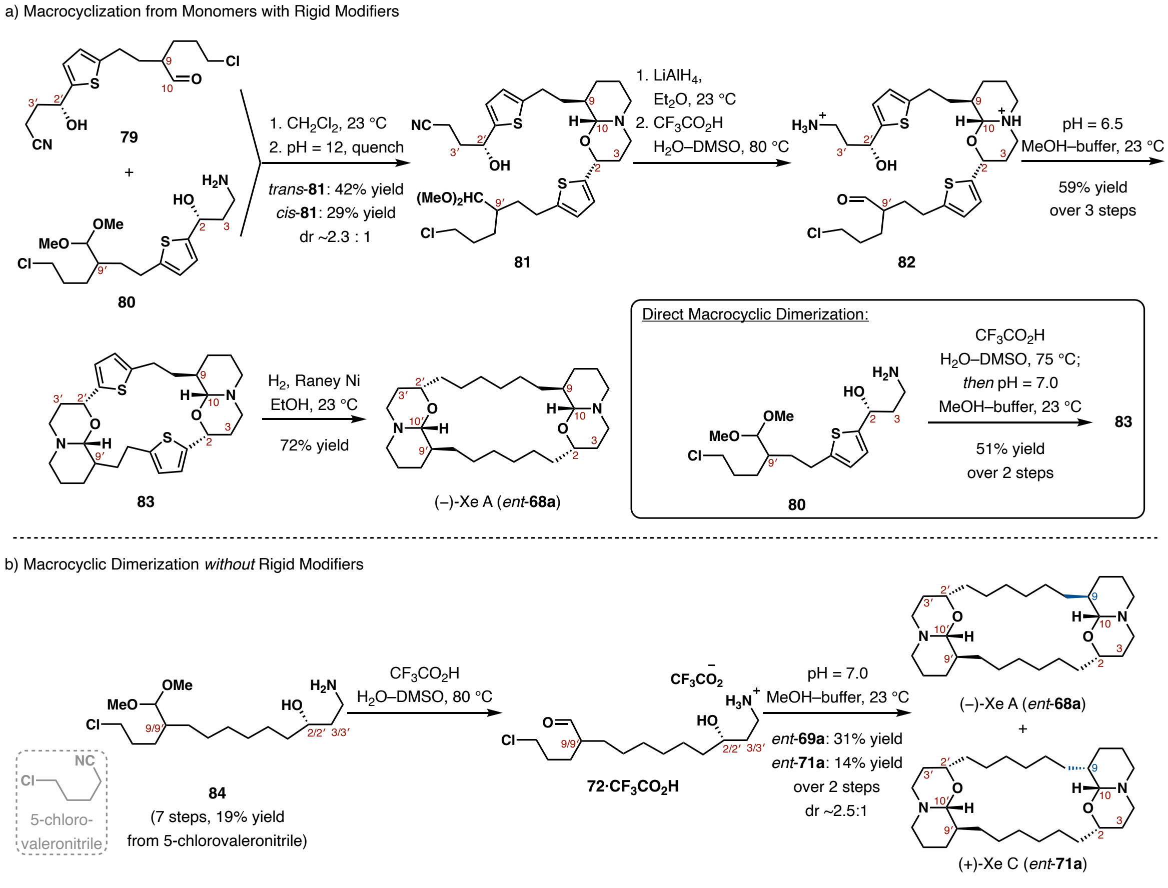
a) Macrocyclization from Monomers with Rigid Modifiers
79
80
1. CH_2Cl_2, 23 °C
2. pH = 12, quench
trans-81: 42% yield
cis-81: 29% yield
dr ~2.3 : 1
81
1. $LiAlH_4$, Et_2O, 23 °C
2. CF_3CO_2H H_2O–DMSO, 80 °C
82
pH = 6.5
MeOH–buffer, 23 °C
59% yield over 3 steps
83
H_2, Raney Ni
EtOH, 23 °C
72% yield
(−)-Xe A (*ent*-68a)
Direct Macrocyclic Dimerization:
CF_3CO_2H
H_2O–DMSO, 75 °C;
then pH = 7.0
MeOH–buffer, 23 °C
51% yield over 2 steps
80
83
b) Macrocyclic Dimerization *without* Rigid Modifiers
84
(7 steps, 19% yield from 5-chlorovaleronitrile)
5-chloro-valeronitrile
CF_3CO_2H
H_2O–DMSO, 80 °C
72·CF_3CO_2H
pH = 7.0
MeOH–buffer, 23 °C
ent-69a: 31% yield
ent-71a: 14% yield
over 2 steps
dr ~2.5:1
(−)-Xe A (*ent*-68a)
+
(+)-Xe C (*ent*-71a)

Hoye's initial approach involved a more conservative, step-wise macrocyclization, where thiophene was introduced as a rigid modifier to hinder intramolecular monocyclization of the monomers and to encourage the macrocyclization of dimers.[91,92] The thiophene-containing monomers **79** and **80** condensed to forge the first 1-oxaquinolizidine ring, affording the *trans*-**81** in 42% yield and its *cis*-diastereomer in 29% yield.[91,92] The bis-ammonium ion **82** was submitted to another condensation reaction for the second 1-oxaquinolizidine formation after removal of the acetal and nitrile protecting groups (Scheme 20a).[91,92] The C_2-symmetric macrocyclic bis-thiophene **83** was then reduced to give *ent*-**68a**.[91,92] A more direct macrocyclization of dimers was also achieved using the thiophene-containing monomer **80** to first generate an ammonium ion intermediate, where the protonated amine served as a protecting group allowing for a pH-mediated macrocyclization for the bis-thiophene **83** (Scheme 20a inset).[92]

Hoye and co-workers later explored the dimeric macrocyclization without the rigidifying thiophenes (Scheme 20b).[92] The less rigid acetal monomer **84** was synthesized from 5-chlorovaleronitrile in 7 steps and in 19% yield (compared to the monomers **79** and **80**, each synthesized in 5% yields over 9 steps from the same 5-chlorovaleronitrile starting material)[xvi].[91,92] Subsequent acid-catalyzed hydrolysis achieved the trifluoroacetate ammonium salt of monomer **72** (**72**·CF_3CO_2H), which was successfully dimerized and cyclized in one-pot to give the *ent*-**68a** and its C9 epimer, *ent*-**71a**, in 31% and 14% yields, respectively (dr 2.3:1).[92] This demonstrates that rigidifiers had little impact on the effectiveness of macrocyclization under this diluted, pH-regulated condition, and this report completed the synthesis in 9 steps with an overall yield of 9%.[92]

3.2.2. Baldwin's C_2-Symmetric Synthesis of (−)-Xestospongin A

The dimeric total synthesis reported by Baldwin is a biosynthetically inspired strategy.[93] Highly acclaimed for his works on biomimetic synthesis, Baldwin put forth numerous syntheses of bioactive natural products isolated from marine sponges. Baldwin and co-workers, too, exploited the C_2 symmetry presented in Xe A (**68a**) and Ar B (**70a**), and proposed the bis-hydroxypyridinium dimer **85** as a biosynthetic intermediate constructed from monomer **86** (Scheme 21a).[93] Consisting of 3-alkylpyridines, the dimer **85** shares these units with many other macrocyclic and polymeric natural products isolated from marine sponges,[xvii] substantiating it as a probable biosynthesis precursor to members of the xestospongin family.[93,95]

[xvi] Monomers **79**, **80**, and **84** were all measured to be ≥ 95% enantiopure.[91,92]

Scheme 21. a) Baldwin's Biomimetic Synthesis Plan and b) Baldwin's Dimeric Synthesis of Dehydroxestospongin **90** from 3-Alkylpyridine Monomers.

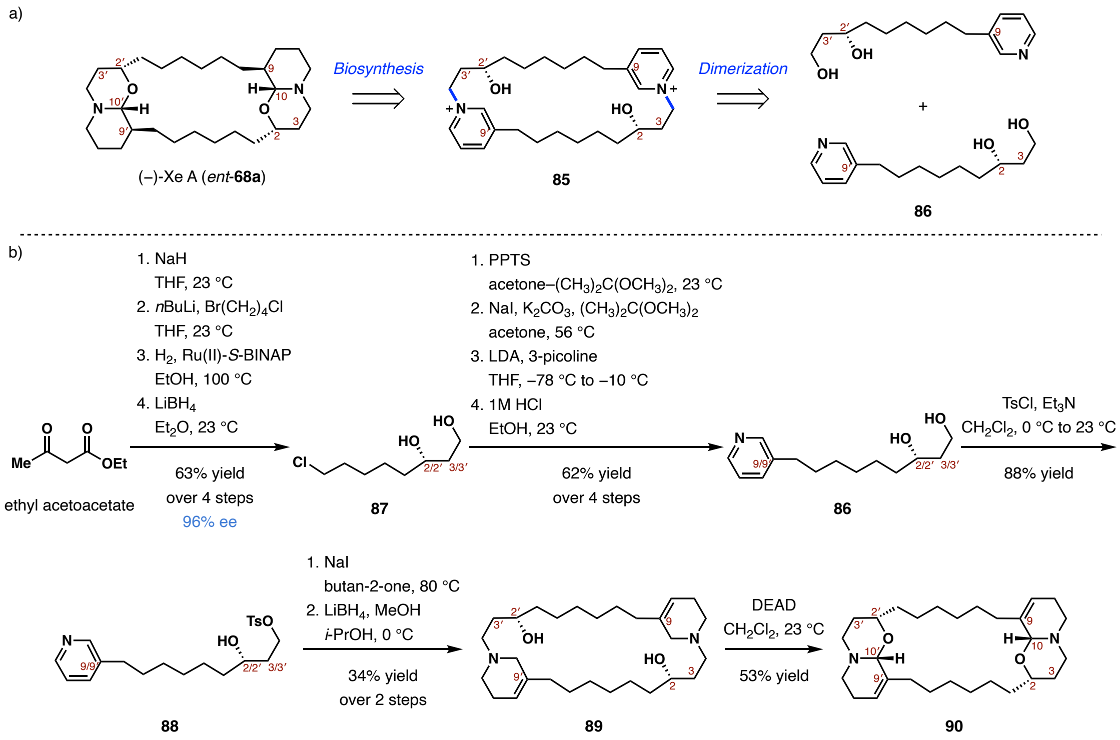
a)
(−)-Xe A (*ent*-**68a**)
Biosynthesis
85
Dimerization
86
b)
1. NaH
THF, 23 °C
2. *n*BuLi, Br(CH$_2$)$_4$Cl
THF, 23 °C
3. H$_2$, Ru(II)-*S*-BINAP
EtOH, 100 °C
4. LiBH$_4$
Et$_2$O, 23 °C
63% yield
over 4 steps
96% ee
ethyl acetoacetate
87
1. PPTS
acetone–(CH$_3$)$_2$C(OCH$_3$)$_2$, 23 °C
2. NaI, K$_2$CO$_3$, (CH$_3$)$_2$C(OCH$_3$)$_2$
acetone, 56 °C
3. LDA, 3-picoline
THF, −78 °C to −10 °C
4. 1M HCl
EtOH, 23 °C
62% yield
over 4 steps
86
TsCl, Et$_3$N
CH$_2$Cl$_2$, 0 °C to 23 °C
88% yield
88
1. NaI
butan-2-one, 80 °C
2. LiBH$_4$, MeOH
i-PrOH, 0 °C
34% yield
over 2 steps
89
DEAD
CH$_2$Cl$_2$, 23 °C
53% yield
90

[xvii] The interesting stereochemistry and substitution patterns of xestspongins could possibly be explained by using this bis-hydroxypyridinium **85** as the biodivergent precursor, where the (*R*)-configured C2/C2' were set by enzymic hydroxylation.[72d,95]

The synthesis of the monomeric diol **86** identified in the biomimetic synthesis plan was prepared from ethyl acetoacetate in 39% yield over 8 steps, where the C2/C2' hydroxy stereocenter was established in diol **87** using Noyori's asymmetric hydrogenation (Scheme 21b).[93] Diol **86** was selectively tosylated and submitted to the critical dimerization step, which was achieved through slow addition of a solution of monotosylate **88** in butan-2-one to a highly diluted, refluxing sodium iodide solution in butan-2-one.[93] A mixture of dimers containing the bis-hydroxypyridinium **85**, the proposed biosynthetic precursor, was obtained and reduced to produce the bis-tetrahydropyridine **89**.[93] The *N*-alkyltetrahydropyridine **89** was subjected to diethyl azocarboxylate (DEAD) to form an iminium, and cyclization of the iminium afforded the dehydro-bis-oxquinolizidine **90**.[93,96]

Scheme 22. Baldwin's Synthesis: Access to the C_2-Symmetric *ent*-**68a** and *ent*-**70a**, and Their C9/C9' Epimer, *ent*-**71a**.

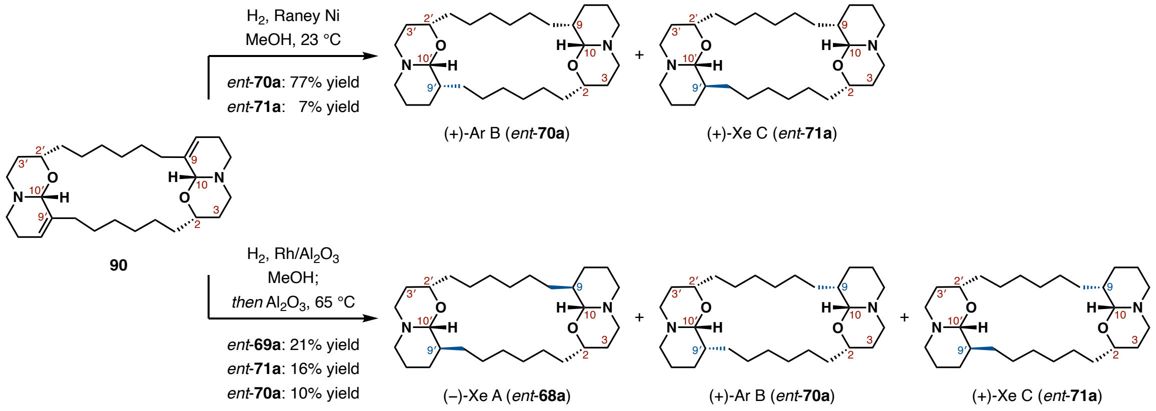

H_2, Raney Ni
MeOH, 23 °C
ent-**70a**: 77% yield
ent-**71a**: 7% yield
(+)-Ar B (*ent*-**70a**)
(+)-Xe C (*ent*-**71a**)
90
H_2, Rh/Al_2O_3
MeOH;
then Al_2O_3, 65 °C
ent-**69a**: 21% yield
ent-**71a**: 16% yield
ent-**70a**: 10% yield
(−)-Xe A (*ent*-**68a**)
(+)-Ar B (*ent*-**70a**)
(+)-Xe C (*ent*-**71a**)

The dehydro-bis-oxaquinolizidine **90** with established stereochemistries at C2 and C2' positions and the *trans*-fused ring junctions (at C10 and C10') served as the platform to access xestospongins, which would arise from the reduction of the tetrahydropyridine (Scheme 22).[93] Hydrogenation of the unsaturation at C9 and C9' of the dehydroxestospongin **90** afforded mixtures of diastereomeric xestospongins separated by preparative HPLC: hydrogenation with Raney nickel gave the C9' epimers (+)-Ar B (*ent*-**70a**) and (+)-Xe C (*ent*-**71a**); hydrogenation with rhodium on alumina produced the C9' epimeric pairs (*ent*-**70a** and *ent*-**71a**), and the (−)-Xe A (*ent*-**68a**), which is also the C9 epimer of *ent*-**71a.**[93] This synthesis described a biomimetic approach that yielded xestospongins in 13 steps with a 2% overall yield for *ent*-**70a** and *ent*-**71a**, and was concluded with the reassignment of the absolute configurations of the naturally occurring counterparts of their synthesized compounds.[93]

3.2.3. Zakarian's C_2-Asymmetric Synthesis of (+)-Desmethylxestospongin B

The two dimerization syntheses described previously (Chapters 3.2.1 and 3.2.2) are marked by synthetic finesse. However, both Hoye and Baldwin prepared xestospongins in only small quantities, no more than 15 milligrams each[xviii].[91–93] Furthermore, neither synthetic routes were able to obtain the C_2-non-symmetrical congeners, nor the hydroxylated xestospongins (see Figure 7).[91–93] These relatively more synthetically challenging xestospongins include the (+)-Ar C (**70b**), on which limited biological studies have been conducted, and also the (+)-Xe B (**69a**), whose anticancer properties piqued our interest.[82,97] Aiming to gain access to those previously synthetically unattainable xestospongins, the Zakarian Group utilized a modular design and reported a scalable synthesis strategy to derive several members of the xestospongin family: (+)-Ar C (**70b**), the C9 and C9' bis-hydroxylated congener of (−)-Ar B (**70a**), and perhaps more notably, the C9 hydroxylated C_2-asymmetric (+)-dmXe B (**69b**).[94]

With the goal of developing a more general strategy to access both the C_2-symmetrical and C_2-non-symmetrical xestospongins, as well as the hydroxylated and nonhydroxylated congeners,

---

[xviii] Roughly 10 mg or less were synthesized for each of these xestospongins, with the exception of *ent*-**70a**, where 50 mg was prepared with Baldwin's synthesis.[91–93]

Zakarian's synthesis focused on incorporating different substitutions at the C9/C9' positions.[94] It was also posited that the C3/C3' methyl groups have little effects on the bioactivity of these bis-1-oxaquinolizidines.[94] This design entailed a late-stage 1-oxaquinolizidine cyclization of the macrocyclic bis-lactam **91**, which was accomplished from the macrolactamization of **92** (Scheme 23).[94] The key to this synthesis plan relied on a convergent strategy coupling the two ω-amino acids **93** and **94**, each with independently functionalized C9 and C9' stereogenic centers, but derived from a common azidoalcohol **95**.[94] The stereochemistries of C9 in **93** and C9' in **94** were established through Ireland–Claisen rearrangements of the esters **96** and **97**, respectively.[94] Esterification between the azidoalcohol **95** with carboxylic acids **98** and **99** afforded the esters with differing substituents.[94]

Scheme 23. Zakarian's Synthesis Design for Xestospongin-type Natural Products with Varying Substitution and Stereochemistry at the C9/C9' Positions.

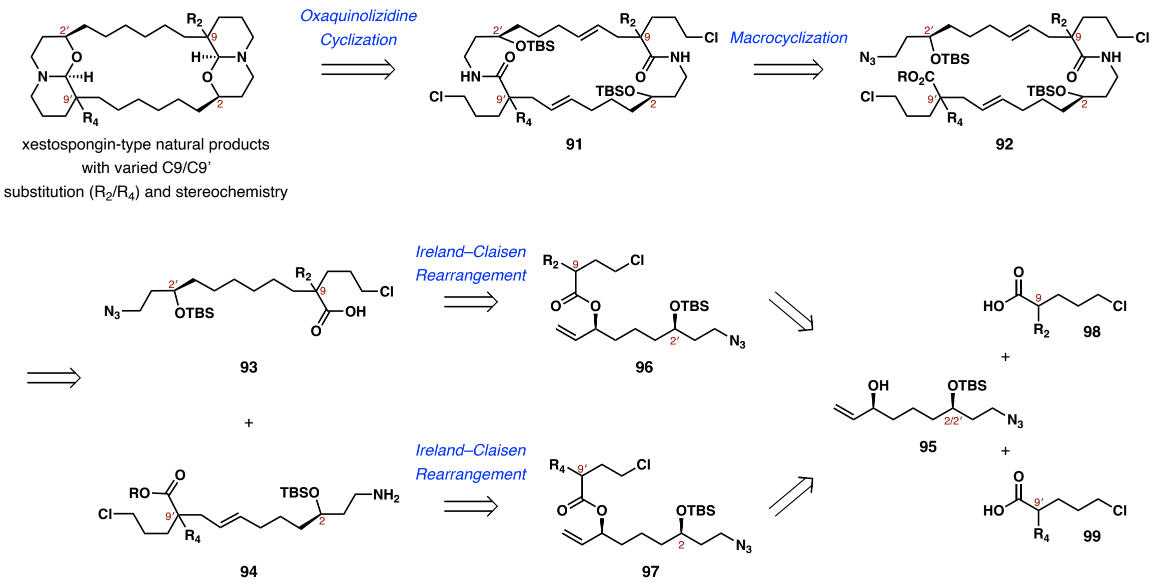
xestospongin-type natural products with varied C9/C9' substitution (R_2/R_4) and stereochemistry
Oxaquinolizidine Cyclization
Macrocyclization
91
92
93
94
Ireland–Claisen Rearrangement
Ireland–Claisen Rearrangement
96
97
95
98
99
OTBS
TBSO
R_2
R_4
Cl
N_3
NH_2
HN
NH
RO_2C
RO
OH
HO
2
2'
9
9'
2/2'
+

The most distinguishable feature of this modular approach is the ability to access hydroxylated and C_2-asymmetric xestospongins, as demonstrated by the synthesis of the non-symmetrical dmXe B (**69b**, R_2 = OH, R_4 = H) with a C9 hydroxy group depicted in Scheme 24.[94] The two ω-amino acids **100** and **101** were derived from the common azidoalcohol **95**, which esterification with valeric acids **102** (R_2 = OBn) and **103** (R_4 = H) delivered esters **104** and **105**, respectively.[94] The stereochemistries of the amino acids at C9 and C9' positions were established during the Ireland–Claisen rearrangements of the corresponding esters, where diastereoselectivity was achieved through the stereochemical control of the enolates formed.[98] In the well-established Ireland–Claisen rearrangement of esters, the chirality of the α-carbon of the carboxylic acid product (C9 and C9' in this case) is transferred from that of the carbinol center of the ester precursor.[98] Treatment of the allylic ester **105** with LDA in THF yielded the corresponding carboxylic acid (87% yield, dr 6:1); derivatization to the methyl ester followed by azide reduction gave the amino acid **101**.[94] The amino acid **100** (the α-benzyloxy counterpart) was prepared in a similar fashion, while noting the selective enolizations of α-alkoxy esters that was previously observed (also by the Zakarian Group).[94,99] The use of $KN(SiMe_3)_2$ base in toluene provided the rearranged products of α-alkoxy esters formed from *Z*-enolates, a result of the metal cation chelating with the alkoxy and the carbonyl oxygen atoms.[99] Application of this chelation-controlled enolization method to the α-alkoxy ester **104** gave the amino acid **100** in 82% yield and with great diastereoselectivity (dr 10:1).[94,99]

The formation of the macrocycle was accomplished through sequential amide formations, first through the coupling of the two amino acid fragments **100** and **101** giving amide **106** in 81% yield.[94] Azide reduction followed by hydrolysis of the methyl ester allowed the resulting amino acid to undergo macrolactamization, forging the macrocyclic bis-lactam **107** which was isolated as a single diastereomer.[94] *N*-Alkylation of the macrocyclic amides of **107** and subsequent desilylation produced the macrocyclic diol **108**.[94] The 1-oxaquinolizidine ring system was constructed via cyclization of the hemiaminal ensued from reductive conditions.[94] Birch reduction with lithium and ammonia successfully performed the semireduction of lactams while achieving *O*-debenzylation in the same pot.[94] A final hydrogenation with rhodium on alumina in ethyl acetate achieved the natural product (+)-dmXe B (**69b**) in 60% yield over 2 steps.[94] During the semireduction of **108**, the α-dehydroxylated product was also isolated (12% yield), which afforded (−)-Ar B (**70a**) upon subjecting to hydrogenation.[94]

Scheme 24. Zakarian's Synthesis of the Hydroxylated and *C*2-Asymmetrical **69b**.

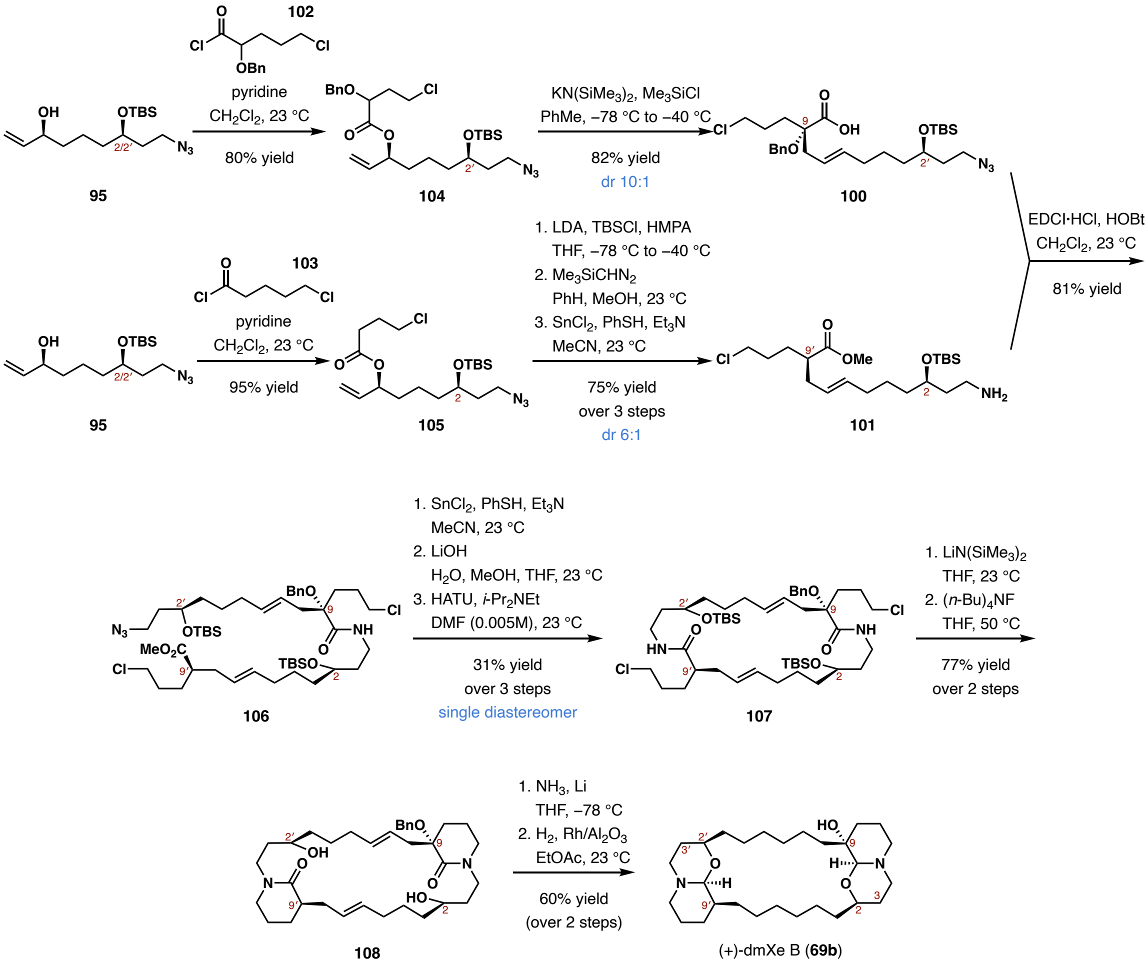
102
pyridine
CH_2Cl_2, 23 °C
80% yield
95
104
$KN(SiMe_3)_2$, Me_3SiCl
PhMe, −78 °C to −40 °C
82% yield
dr 10:1
100
EDCI·HCl, HOBt
CH_2Cl_2, 23 °C
81% yield
103
pyridine
CH_2Cl_2, 23 °C
95% yield
95
105
1. LDA, TBSCl, HMPA
THF, −78 °C to −40 °C
2. Me_3SiCHN_2
PhH, MeOH, 23 °C
3. $SnCl_2$, PhSH, Et_3N
MeCN, 23 °C
75% yield
over 3 steps
dr 6:1
101
106
1. $SnCl_2$, PhSH, Et_3N
MeCN, 23 °C
2. LiOH
H_2O, MeOH, THF, 23 °C
3. HATU, *i*-Pr_2NEt
DMF (0.005M), 23 °C
31% yield
over 3 steps
single diastereomer
107
1. $LiN(SiMe_3)_2$
THF, 23 °C
2. $(n\text{-}Bu)_4NF$
THF, 50 °C
77% yield
over 2 steps
108
1. NH_3, Li
THF, −78 °C
2. H_2, Rh/Al_2O_3
EtOAc, 23 °C
60% yield
(over 2 steps)
(+)-dmXe B (**69b**)

Zakarian's modular approach allowed for the first total synthesis of the *C*2-asymmetric, C9 hydroxylated (+)-dmXe B (**69b**) in 22 steps (longest linear sequence) and a 1.2% overall yield.[94]

Attesting to the versatility of this approach, the *C*$_2$-symmetric, C9 and C9' bis-hydroxylated (+)-Ar C (**70b**, R$_2$ and R$_4$ = OH) was also successfully synthesized for the first time.[94]

3.3.A 2nd Generation Total Synthesis Approach

3.3.1. Merits of a 2nd Generation Synthesis

The key to the synthesis design of Zakarian's *C*$_2$-asymmetric access of hydroxylated xestospongins (see Schemes 23 and 24) was the independently derivatized ω-amino acids **93** and **94** from one common azidoalcohol **95**.[94] Three imperative synthetic intermediates can be identified in this design: azidoalcohol **95**, and 5-chlorovaleric acids with and without α-alkoxy moieties.[94] The scalability of this synthetic strategy for xestospongin-type natural products is thus highly dependent on easy and robust access to these early-stage intermediates.

The synthetic steps and yields of these three pivotal intermediates are summarized in Figure 8. While acyl chloride **103** can easily be achieved in a one-step transformation from 5-chlorovaleric acid, accessing chloride **102** and azidoalcohol **95** requires a lengthier synthesis (8 and 10 steps, respectively), which is not ideal for the purpose of having these synthetically attained natural products supplying the investigations of bioactivities.[94]

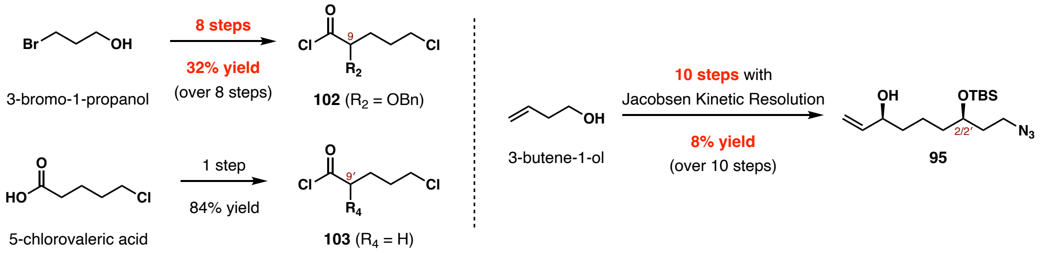
Br
OH
3-bromo-1-propanol
8 steps
32% yield
(over 8 steps)
O
Cl
9
Cl
R2
102 (R2 = OBn)
O
HO
Cl
5-chlorovaleric acid
1 step
84% yield
O
Cl
9'
Cl
R4
103 (R4 = H)
OH
3-butene-1-ol
10 steps with
Jacobsen Kinetic Resolution
8% yield
(over 10 steps)
OH
OTBS
2/2'
N3
95

Figure 8. The step counts and yields from the reported synthesis of dmXe B (**69b**) for the three critical intermediates identified in Zakarian's synthesis design: **102**, **103**, and **95**.

While access to valeric chloride **103** is straightforward, the synthesis of chloride **102**, the α-alkoxy counterpart, is much more challenging. An 8-step synthesis was reported to accomplish this α-benzyloxy valeric chloride **102** in 32% yield from commercially available 3-bromo-1-propanol and 2-(benzyloxy)acetic acid (Figure 8 and Scheme 25).[94] Iodide **109** was accomplished in 2 steps in 90% yield.[94] Alkylation of the *tert*-butyl ester **110**, which was derived from 2-(benzyloxy)-acetic acid in one step, with iodide **109** at −95 °C afforded ester **111** in 45% yield under optimized conditions.[94] Due to the thermal instability of the α-alkoxy ester enolates formed, this alkylation reaction is low yielding even when performed at low temperatures.[94] Desilylation and mesylation followed by chloride substitution yielded ester **112** in 3 steps and 84% yield.[94] Hydrolysis and the final chlorodehydroxylation gave acyl chloride **102**.[94]

In addition to this α-benzyloxy valeric acid being synthetically demanding, the selective and effective *O*-debenzylation at a later stage of the synthesis also proved difficult.[94] In the reported synthesis, debenzylation was only achieved under harsh reductive conditions and α-dehydroxylation was also observed.[94] While a 32% yield over 8 steps is acceptable, it is undesirable for an early-stage intermediate. Further examination of a more suitable synthesis approach for more robust transformations and for possible yield improvements is thus warranted.

Scheme 25. Reported Synthesis of Acyl Chloride **102**, the α-Alkoxy Valeric Acid Intermediate.

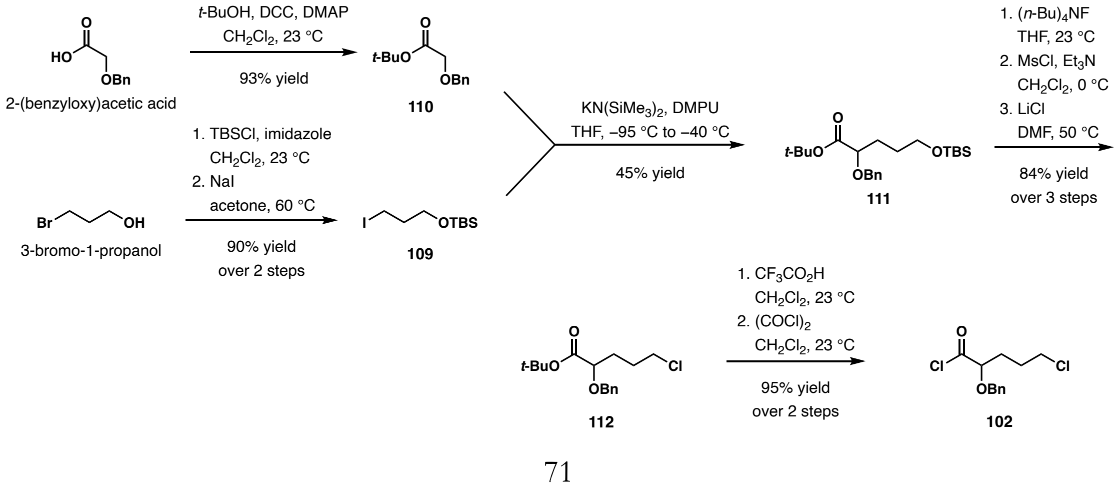

HO
OBn
2-(benzyloxy)acetic acid
t-BuOH, DCC, DMAP
CH2Cl2, 23 °C
93% yield
t-BuO
OBn
110
Br
OH
3-bromo-1-propanol
1. TBSCl, imidazole
CH2Cl2, 23 °C
2. NaI
acetone, 60 °C
90% yield
over 2 steps
I
OTBS
109
KN(SiMe3)2, DMPU
THF, −95 °C to −40 °C
45% yield
t-BuO
OBn
OTBS
111
1. (n-Bu)4NF
THF, 23 °C
2. MsCl, Et3N
CH2Cl2, 0 °C
3. LiCl
DMF, 50 °C
84% yield
over 3 steps
t-BuO
OBn
Cl
112
1. CF3CO2H
CH2Cl2, 23 °C
2. (COCl)2
CH2Cl2, 23 °C
95% yield
over 2 steps
Cl
OBn
Cl
102

Since the azidoalcohol **95** diverges to non-symmetrically form the ω-amino acids necessary for this asymmetric design (see Schemes 23 and 24), a concise and highly yielding synthesis of **95** is important. The reported stereoselective synthesis of azidoalcohol **95** from 3-butene-1-ol was achieved in 10 steps and a mere 8% yield (see Figure 8 and Scheme 26), not what one would consider an efficient route for accessing a highly critical, early-stage intermediate.[94] In this synthesis, chloride **113** was easily obtained from 3-butene-1-ol and epoxidized to the racemic epoxide **114**.[94] The C2/C2' stereochemistry was established through a Jacobsen hydrolytic kinetic resolution of the racemic epoxide **114**, achieving the (*S*)-**114** in 30% yield and 92% ee over 3 steps from commercially available 3-butene-1-ol.[94] This chiral epoxide (*S*)-**114** served as a point of divergence in the synthesis of azidoalcohol **95**, where a portion of it was transformed into iodide **115** before coupling with the remainder of the epoxide **114**.[94] Part of (*S*)-**114** was subjected to ring-opening conditions to form the corresponding allylic alcohol, and subsequent electrophilic benzylation and iodination gave the chiral iodide **115** in 3 steps and 71% yield.[94] Coupling of epoxide **114** with iodide **115** via a higher order cuprate addition opened up the epoxide and formed the chloroalcohol **116**.[94] Substitution with sodium azide was followed by silylation of the alcohol, and lastly, the oxidative removal of the *para*-methoxybenzyl (PMB) group accomplished the azidoalcohol **95**.[94]

The azidoalcohol **95** was synthesized in 10 steps with an overall yield of 8%.[94] This was primarily limited by the use of Jacobsen kinetic resolution, which halves the yield each time performed.[94] Furthermore, this synthesis design fundamentally calls for the low yielding Jacobsen hydrolytic kinetic resolution twice, considering that the carbon skeleton of azidoalcohol **95** was constructed through the cuprate coupling of the enantiopure materials epoxide **114** and iodide

115, both of which established their chiralities from (*S*)-**114**.[94] Evidently, further explorations and optimizations of this synthetic route for azidoalcohol **95** is warranted.

Scheme 26. Reported Synthesis of the Common Intermediate Azidoalcohol **95**.

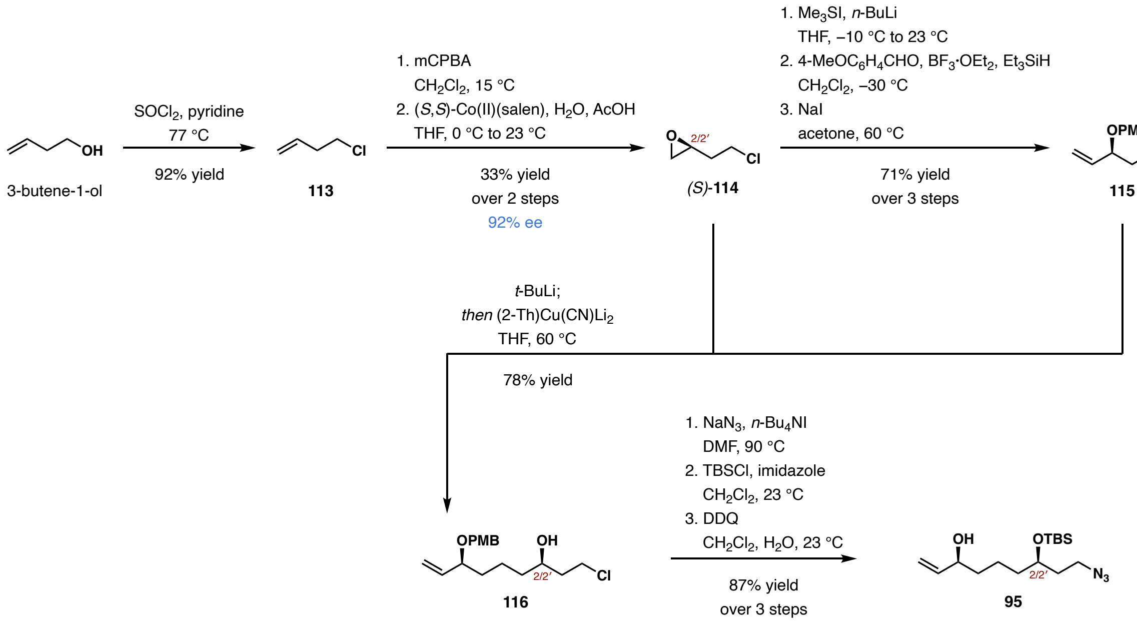

SOCl2, pyridine
77 °C
92% yield
3-butene-1-ol
113
1. mCPBA
CH2Cl2, 15 °C
2. (S,S)-Co(II)(salen), H2O, AcOH
THF, 0 °C to 23 °C
33% yield
over 2 steps
92% ee
(S)-114
1. Me3SI, n-BuLi
THF, −10 °C to 23 °C
2. 4-MeOC6H4CHO, BF3·OEt2, Et3SiH
CH2Cl2, −30 °C
3. NaI
acetone, 60 °C
71% yield
over 3 steps
115
t-BuLi;
then (2-Th)Cu(CN)Li2
THF, 60 °C
78% yield
116
1. NaN3, n-Bu4NI
DMF, 90 °C
2. TBSCl, imidazole
CH2Cl2, 23 °C
3. DDQ
CH2Cl2, H2O, 23 °C
87% yield
over 3 steps
95
OH
Cl
OPMB
I
OTBS
N3
2/2′

Therefore, we devised an optimized route for the 2nd generation synthesis of xestospongins, focusing on the inefficiencies of the developed synthesis highlighted in this section. We envisioned a more concise, higher yielding synthesis by allowing easier access to key early-stage intermediates—the α-alkoxy valeric acid and the azidoalcohol **95**.

3.3.2. Shortened Synthesis of the α-Alkoxy Valeric Acid Intermediate

The α-alkoxy valeric acid intermediate in the established synthesis is the α-benzyloxy valeric chloride **102**, which requires 8 steps from commercially available starting materials with an overall yield of 32% (see Figure 8 and Scheme 25).[94] In addition to the suboptimal yield after a lengthy synthesis sequence, this particular alkoxy group appeared to complicate the total synthesis during debenzylation.[94] The lower yield was primarily due to the instability of the enolate formed during the alkylation step, where the enolate intermediate was observed to decompose even at low temperatures. This hindered the ability to effectively perform the synthesis on larger scales. We thus anticipated that a different α-alkoxy moiety, such as a *para*-methoxybenzyl (PMB) ether, could allow for more selective removal in revealing the free hydroxy group. Moreover, it could offer modest improvements to the stability of the enolate formed during alkylation, thereby decreasing the number of steps and increasing the overall yield to the α-alkoxy valeric acid intermediate. To that end, we aimed to synthesize the α-*p*-methoxybenzyloxy valeric chloride **117**.

As shown in Scheme 27, the α-alkoxy valeric acid intermediate **117** was obtained through an alkylation of the α-*p*-methoxybenzyloxy acetic acid **118** with commercially available 1-chloro-3-iodopropane (**119**). The thermal instability of enolates formed from α-benzyloxy esters observed previously was indeed lessened with the use of *p*-methoxybenzyloxy ether. Additionally, due to the increased stability observed for the α-*p*-methoxybenzyloxy enolate, the extensive steps concerning protecting groups was omitted. Acid **118** was smoothly derived from 2-bromoacetic acid in 92% yield in one step.[100] The enolate derived from **118** was able to form at −78 °C, as opposed to the −90 °C required in the reported synthesis.[94] Facile alkylation with iodide **119** achieved the valeric acid **117** at −40 °C in 4 hours with an isolated yield of 45%, even on large scales (10 grams).

Scheme 27. Synthesis of the α-Alkoxy Valeric Acid Intermediate **117** in the 2nd Generation Synthesis.

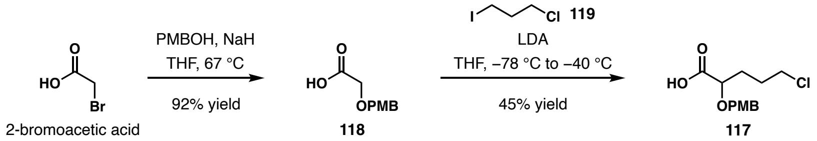

Overall, employing the *p*-methoxybenzyloxy ether in **117** (R_2 = OPMB) shortened the synthetic access to the α-alkoxy valeric acid intermediate to just 2 steps, from the previously reported 8 steps (for acyl chloride **102**, R_2 = OBn). This new approach is more concise by excluding unnecessary functional group manipulations.[101] With this simplified synthetic route, our goal to obtain the α-alkoxy valeric acid intermediate **117** was achieved through a more direct path in 42% yield.

3.3.3. An Improved Synthesis Design for the Azidoalcohol 95

The azidoalcohol **95** serves a pivotal role in divergently providing non-symmetrical ω-amino acids for assembling the carbon skeleton of xestospongins (see Schemes 23 and 24).[94] The established synthesis of this linchpin azidoalcohol **95** relied on the cuprate coupling of the (*S*)-epoxide **114** and the (*S*)-iodide **115** (see Scheme 26).[94] The two stereocenters arose from the Jacobsen kinetic resolution reaction, which reliably afforded the chiral epoxide in great enantiopurity (92% ee), albeit limiting in yield.[94] With azidoalcohol **95** being the critical precursor for establishing both amino acids, the difficulty in easily obtaining this important synthon **95** in large quantities greatly impedes the scalability of the synthesis for xestospongin-type natural products. We therefore pursued a novel, alternate pathway with the goal of making the synthesis more efficient in both synthetic sequence and overall yield.

In the established synthesis, the (*S*)-iodide **115** functions to provide one of two stereocenters as well as the carbons necessary for the framework of azidoalcohol **95**.[94] On the other hand, in the new 2nd generation synthesis plan for azidoalcohol **95**, we envisaged that the second stereocenter would be established in chiral epoxide **120** from a diastereoselective epoxidation of alkene **121** (Scheme 28a). The carbons previously installed by the (*S*)-iodide **115** during the cuprate coupling step with (*S*)-epoxide **114** (see Scheme 26) would instead be introduced by a Grignard reagent derived from 3-butene-1-ol, the same starting material used to derive the (*S*)-epoxide **114**. Analogous to the formation of the precursor chloride **113**, an alcohol substitution reaction gave bromide **122**, which was quickly transformed into the butenyl Grignard **123** (Scheme 28b). A copper-catalyzed coupling reaction with the (*S*)-**114** regioselectively opened the epoxide, and subsequent silylation of the resulting alcohol yielded the terminal alkene **121** in 87% yield over 2 steps.[102] With the olefin precursor **121** in hand, we sought to explore asymmetric epoxidation conditions.

Scheme 28. The 2nd Generation Synthesis of Azidoalcohol **95**: a) Synthesis Plan and b) Synthetic Access to the Terminal Alkene Precursor **121**.

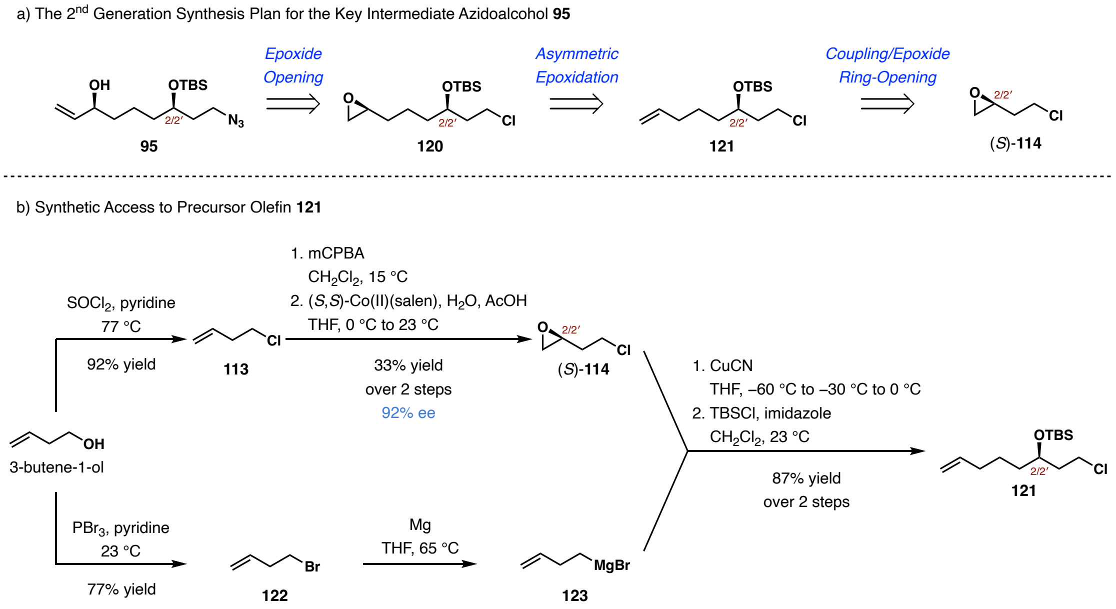
a) The 2nd Generation Synthesis Plan for the Key Intermediate Azidoalcohol 95
OH
OTBS
2/2′
N3
95
Epoxide Opening
O
OTBS
2/2′
Cl
120
Asymmetric Epoxidation
OTBS
2/2′
Cl
121
Coupling/Epoxide Ring-Opening
O
2/2′
Cl
(S)-114
b) Synthetic Access to Precursor Olefin 121
SOCl2, pyridine
77 °C
92% yield
Cl
113
1. mCPBA
CH2Cl2, 15 °C
2. (S,S)-Co(II)(salen), H2O, AcOH
THF, 0 °C to 23 °C
33% yield
over 2 steps
92% ee
O
2/2′
Cl
(S)-114
OH
3-butene-1-ol
PBr3, pyridine
23 °C
77% yield
Br
122
Mg
THF, 65 °C
MgBr
123
1. CuCN
THF, –60 °C to –30 °C to 0 °C
2. TBSCl, imidazole
CH2Cl2, 23 °C
87% yield
over 2 steps
OTBS
2/2′
Cl
121

To truly achieve the goal of enhancing the efficiency of the synthesis of azidoalcohol **95**, the asymmetric epoxidation of **121** needs to be both highly yielding and highly stereoselective. More importantly, it must be easily scalable. Our asymmetric epoxidation design is also presented with additional challenges: olefin **121** is not only non-conjugated but also terminally positioned. The

Sharpless asymmetric epoxidation is an effective method for allylic alcohols, but little success and progress has been documented for aliphatic olefins with longer carbon chains.[103] Literature precedents utilizing transition-metal catalysts have reported productive epoxidations of allylic and homoallylic alcohols,[104] and even bishomoallylic alcohols with olefins three carbons away from the hydroxy group.[105] Initially, we intended to achieve an induced diastereoselective epoxidation that would take advantage of the already established chirality of the alcohol in olefin **124** with its free alcohol moiety at the C2/C2' position. However, epoxidation to the epoxide **125** proved to be more difficult than we imagined, even with an increased loading of catalyst and oxidant, likely due to the chiral alcohol being four carbons apart from the hydroxy group (Scheme 29a).

Scheme 29. Asymmetric Epoxidation Methods Attempted on the Terminal Alkene **121**.

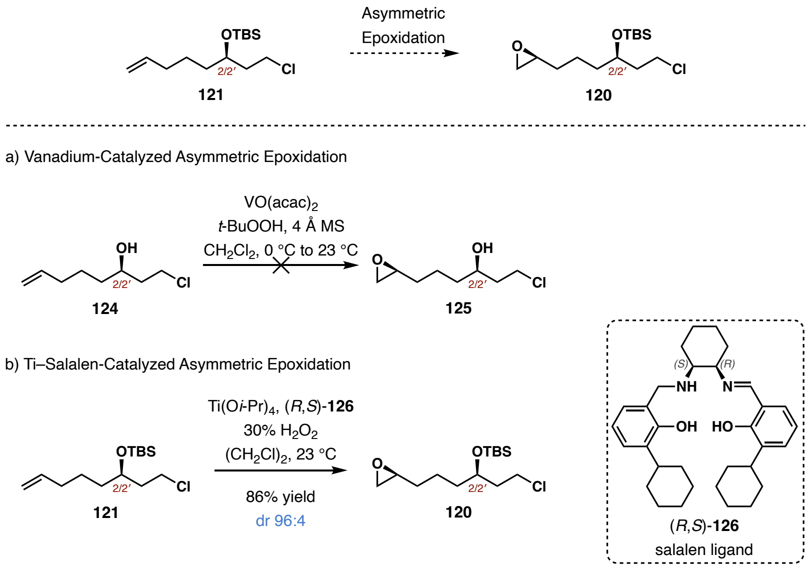
OTBS
2/2'
Cl
121
Asymmetric
Epoxidation
O
OTBS
2/2'
Cl
120
a) Vanadium-Catalyzed Asymmetric Epoxidation
VO(acac)₂
t-BuOOH, 4 Å MS
CH₂Cl₂, 0 °C to 23 °C
OH
2/2'
Cl
124
O
OH
2/2'
Cl
125
b) Ti–Salalen-Catalyzed Asymmetric Epoxidation
Ti(Oi-Pr)₄, (R,S)-126
30% H₂O₂
(CH₂Cl)₂, 23 °C
86% yield
dr 96:4
OTBS
2/2'
Cl
121
O
OTBS
2/2'
Cl
120
(S)
(R)
NH
N
OH
HO
(R,S)-126
salalen ligand

Due to the electron-deficient nature of terminal and non-conjugated olefins, very few asymmetric epoxidation methods are suitable for epoxidizing these more challenging olefins.[106,107] The titanium(salalen)-catalyzed epoxidation method using aqueous hydrogen peroxide that was first developed by Katsuki showed promising results with non-activated, aliphatic olefins.[107]

Berkessel and co-workers built on Katsuki's success and reported an improved method utilizing salalen ligands derived from *cis*-1,2-diaminocyclohexane.[108] Inspired by the Ti–salalen catalysis approach, we attempted this asymmetric epoxidation method on our olefin **121**.[xix] The titanium complex was generated in situ using 10 mol % of Ti(O*i*-Pr)$_4$ and (*R*,*S*)-**126**, the salalen ligand derived from *cis*-1,2-diaminocyclohexane with 3-cyclohexylsalicylic aldehyde substituents.[108] Subjecting olefin **121** to catalytic amount of this titanium–salalen in dichloroethane with aqueous hydrogen peroxide as oxidant gave epoxide **120** in 86% yield with a diastereomeric ratio of 96 to 4 (Scheme 29b).

The good yield and high selectivity of this asymmetric epoxidation method substantiate our 2nd generation synthesis plan. In particular, the use of the easy-to-handle and environmentally friendly aqueous hydrogen peroxide (readily available as 30% aqueous solution) is attractive for our ultimate goal of performing large scale-up synthesis of the azidoalcohol **95**. This successful asymmetric epoxidation of **121** was only performed on a 27 mg (0.1 mmol) scale and the reaction time was 100 hours. The scalability of this asymmetric epoxidation was faced with undue challenges: when performed on a 1-gram scale (3.6 mmol), epoxide **120** was obtained only in 67% yield with 33% of the olefin precursor **121** being recovered (Table 5, entry 1). This incomplete conversion of **121** was not resolved by extending the reaction time (up to 120 hours).

We believe that the biphasic nature of this reaction likely hindered the progression of the epoxidation reaction when scaled up. The addition of a more polar co-solvent, acetonitrile, was presumed to be able to help homogenize the reaction mixture. However, the improvement was minimal (73% yield, entry 2). When the reaction was performed at an elevated temperature of

---

[xix] When this epoxidation method was attempted on olefin **124** with the alcohol unsilylated, the formation of the epoxide product was observed by TLC and crude NMR. However, the major product isolated appeared to contain a tetrahydropyran, which would result from an epoxidation–cyclization sequence where the unprotected alcohol cyclized to form the 6-membered ring through an epoxide-opening reaction.

65 °C, an improved 80% isolated yield was observed while the amount of Ti–salalen catalyst needed was reduced to 5 mol % (entry 3). We next explored the effects of additives on the efficiency and scalability of this asymmetric epoxidation reaction on our olefin **121**.[108b,109] The presence of additive tetrabutyl ammonium hydrogen sulfide shortened the reaction time to 80 hours, although the isolated yield remained unaffected (77% yield, entry 4). Additive pentafluorobenzoic acid satisfyingly gave epoxide **120** in 87% yield while simultaneously accelerating the reaction to complete in just 48 hours (entry 5). More importantly, this optimized epoxidation condition giving highly diastereoselective epoxide **120** in high yields and in reduced reaction time was reproducible on a 1-gram scale (3.6 mmol), and even on a 10-gram scale (36 mmol) (entries 6 and 7, respectively).

Table 5. Reaction Condition Optimizations of the Asymmetric Epoxidation of Olefin **121** for the Large-Scale Preparation of Azidoalcohol **95**.

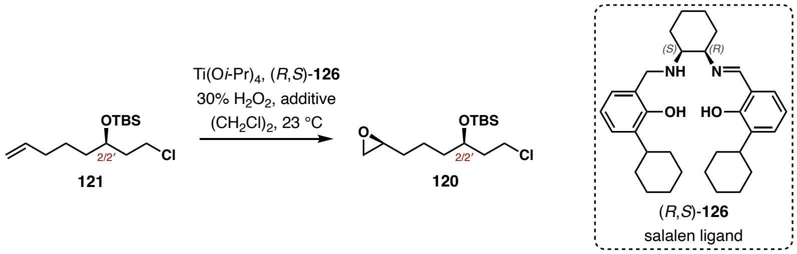

entry[a]	Ti–salalen (mol %)[b]	solvent	additive[c]	time	yield	dr[d]
1[e]	10	$(CH_2Cl)_2$	–	100 h	67%	96:4
2	10	MeCN–$(CH_2Cl)_2$ (1:3)	–	100 h	73%	96:4
3[f]	5	$(CH_2Cl)_2$	–	100 h	80%	96:4
4	5	$(CH_2Cl)_2$	$(n\text{-Bu})_4NHSO_4$	80 h	77%	96:4
5	5	$(CH_2Cl)_2$	$C_6F_5CO_2H$	48 h	87%	96:4
6[e,g]	5	$(CH_2Cl)_2$	$C_6F_5CO_2H$	40 h	87%	96:4
7[g,h]	5	$(CH_2Cl)_2$	$C_6F_5CO_2H$	50 h	85%	96:4

[a] All reactions were performed by treating a solution of **121** and Ti–salalen catalyst in solvent (2 M) with additives and 4.5 equiv of 30% H_2O_2 at 23 °C in 8 mL vials and on 0.9 mmol scales, 0.25 g of **121**, unless otherwise noted. [b] Catalysts were prepared using the in situ/vac procedure described by Berkessel.[108] [c] Additives were added equimolar to the Ti–salalen catalyst. [d] The dr values were measured using chiral HPLC analysis of the allylic alcohol after a two-step derivatization. [e] Reactions were performed on 3.6 mmol scales, 1 g of **121**. [f] Reaction was carried out at 65 °C. [g] Reactions were performed in 6 M $(CH_2Cl)_2$. [h] Reaction was performed on a 36 mmol scale, 10 g of **121**.

The successful asymmetric epoxidation of 10 grams of olefin **121** yielded 9.3 grams (85% yield) of epoxide **120** (Table 5, entry 7 and Scheme 30). Olefination with trimethylsulfonium iodide opened the epoxide to afford allylic alcohol **127** in good yields, and the eventual azide substitution concluded this new synthesis approach for azidoalcohol **95**.

Scheme 30. Optimized Synthesis Route for the Azidoalcohol **95** in the 2nd Generation Synthesis.

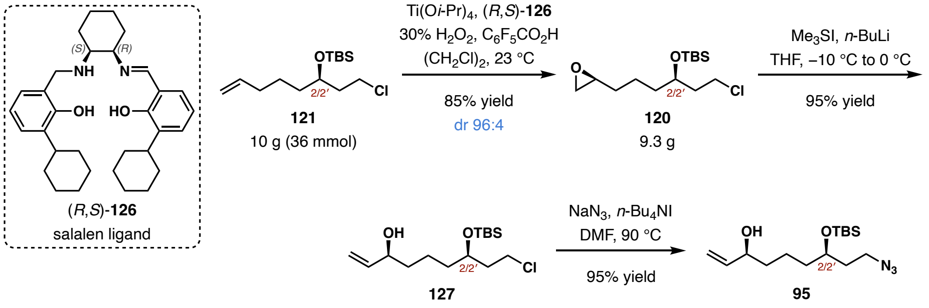

(S)
(R)
NH
N
OH
HO
(R,S)-126
salalen ligand
OTBS
2/2'
Cl
121
10 g (36 mmol)
Ti(Oi-Pr)4, (R,S)-126
30% H2O2, C6F5CO2H
(CH2Cl)2, 23 °C
85% yield
dr 96:4
O
OTBS
2/2'
Cl
120
9.3 g
Me3SI, n-BuLi
THF, −10 °C to 0 °C
95% yield
OH
OTBS
2/2'
Cl
127
NaN3, n-Bu4NI
DMF, 90 °C
95% yield
OH
OTBS
2/2'
N3
95

Overall, the ability to scale up this asymmetric epoxidation reaction, which is essential to the 2nd generation synthesis plan, allowed quicker and more atom-efficient access to azidoalcohol **95**. This new and improved synthesis route was able to achieve azidoalcohol **95** in 8 steps while involving only 1 Jacobsen kinetic resolution step, as opposed to the 10 steps and 2 Jacobsen reactions of the established synthesis.[94] More remarkable is the synthetic efficiency in the overall obtained yields of azidoalcohol **95**: 5 grams (16 mmol) of azidoalcohol **95** would have required 14.3 grams (197 mmol) of 3-butene-1-ol, but would now only require 8.5 grams (117 mmol) of this same starting material. The 3-butene-1-ol starting material required to access large quantities of azidoalcohol **95** is 40% less than the previously reported method. Alternatively, from the perspective of product quantities, 10 grams (139 mmol) of starting material 3-butene-1-ol would previously only be able to synthesize 3.5 grams (11 mmol) of azidoalcohol **95**. The same amount of 3-butene-1-ol can provide 5.9 grams (19 mmol) of azidoalcohol **95**, which is a 68% increase in the amount of this critical intermediate obtained. This difference in yield (40% less of the 3-butene-1-ol needed, or almost 70% more azidoalcohol **95** synthesized) becomes substantially more significant for larger scale synthesis, our primary goal for optimizations.

Scheme 31. Superior Synthetic Access of Our New and Improved 2nd Generation Synthesis for Azidoalcohol **95**, Compared to That of the Previously Reported Synthesis.

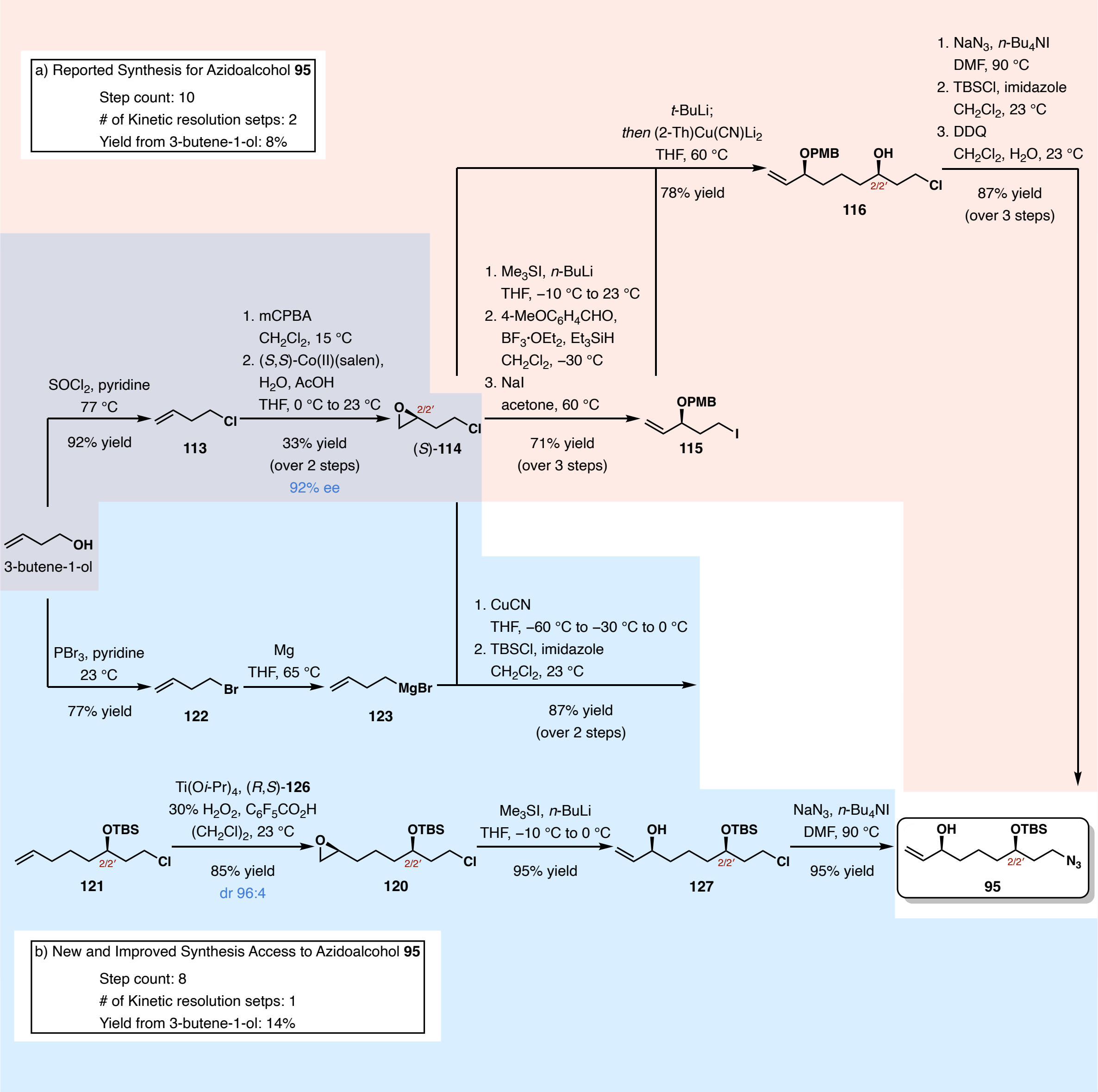
a) Reported Synthesis for Azidoalcohol 95
Step count: 10
# of Kinetic resolution setps: 2
Yield from 3-butene-1-ol: 8%
3-butene-1-ol
OH
SOCl$_2$, pyridine
77 °C
92% yield
113
Cl
1. mCPBA
CH$_2$Cl$_2$, 15 °C
2. (S,S)-Co(II)(salen),
H$_2$O, AcOH
THF, 0 °C to 23 °C
33% yield
(over 2 steps)
92% ee
(S)-114
O
2/2′
1. Me$_3$SI, n-BuLi
THF, −10 °C to 23 °C
2. 4-MeOC$_6$H$_4$CHO,
BF$_3$·OEt$_2$, Et$_3$SiH
CH$_2$Cl$_2$, −30 °C
3. NaI
acetone, 60 °C
71% yield
(over 3 steps)
OPMB
I
115
t-BuLi;
then (2-Th)Cu(CN)Li$_2$
THF, 60 °C
78% yield
OPMB
OH
116
1. NaN$_3$, n-Bu$_4$NI
DMF, 90 °C
2. TBSCl, imidazole
CH$_2$Cl$_2$, 23 °C
3. DDQ
CH$_2$Cl$_2$, H$_2$O, 23 °C
87% yield
(over 3 steps)
PBr$_3$, pyridine
23 °C
77% yield
Br
122
Mg
THF, 65 °C
MgBr
123
1. CuCN
THF, −60 °C to −30 °C to 0 °C
2. TBSCl, imidazole
CH$_2$Cl$_2$, 23 °C
87% yield
(over 2 steps)
OTBS
121
Ti(Oi-Pr)$_4$, (R,S)-126
30% H$_2$O$_2$, C$_6$F$_5$CO$_2$H
(CH$_2$Cl)$_2$, 23 °C
85% yield
dr 96:4
120
Me$_3$SI, n-BuLi
THF, −10 °C to 0 °C
95% yield
127
NaN$_3$, n-Bu$_4$NI
DMF, 90 °C
95% yield
N$_3$
95
b) New and Improved Synthesis Access to Azidoalcohol 95
Step count: 8
# of Kinetic resolution setps: 1
Yield from 3-butene-1-ol: 14%

Depicted in Scheme 30 is a side-by-side comparison of the synthesis design between the first generation approach (the reported synthesis), and the 2nd generation approach for the azidoalcohol **95** developed in this work. Beyond the ability to access larger quantities of this linchpin azidoalcohol **95** more promptly and in fewer steps, this new approach conforms to many of the modern measures of a practical and efficient synthetic design.[101] The primary design change was in devising a new coupling partner for the (*S*)-epoxide **114**. The cuprate addition used in the previous synthesis where 2.2 equivalents of *t*-BuLi was required is bypassed. Instead, the Grignard reagent **123** was employed in place of the coupling with the (*S*)-**114** through a more direct and less complex chemical transformation. The second stereocenter was installed following the coupling and was achieved with the Ti–salalen catalyzed asymmetric epoxidation with hydrogen peroxide, an accessible and feasible maneuver with the perk of being environmentally benign.[101] The use of this epoxidation reaction also avoided protecting group manipulations, making this pathway far more economical in the synthetic efficiency sense.[101]

3.3.4. Future Optimization Studies

We have thus far accomplished the optimizations for accessing the two synthons—the α-alkoxy acid **98** and the azidoalcohol **95** (Figure 9, boxed). These two intermediates were identified in Chapter 3.2.3 as two of the three critical synthetic intermediates for Zakarian's synthesis of xestospongins (see Scheme 23) and in Chapter 3.3.1 as the two foremost areas for a more concise synthesis to access various members of the xestospongin-type marine natural products. Future developments of synthetic access to other xestospongins, both natural and non-natural congeners, will benefit from the improvements outlined in this 2nd generation synthesis plan.

The α-alkoxy acid intermediate bearing a C9 hydroxy group was previously established as the α-benzyloxy valeric chloride **102** (R_2 = OBn).[94] The α-benzyloxy ether moiety was identified as contributing to selectivity issues during the reductive oxaquinolizidine formation at a later stage of the synthesis; this is on top of the already difficult synthesis of this α-alkoxy acid synthon **102**. A new α-alkoxy acid intermediate **117** (R_2 = OPMB) bearing an α-methoxybenzyloxy ether at the C9 position, was chosen as the α-alkoxy acid intermediate for the 2nd generation synthesis. The most critical intermediate of the synthesis, the azidoalcohol **95** is now accessed in substantial synthetic efficiency (yielding 68% more of **95** in 2 fewer steps than previously, see Scheme 31), with greater capacity for synthesis on larger scales.

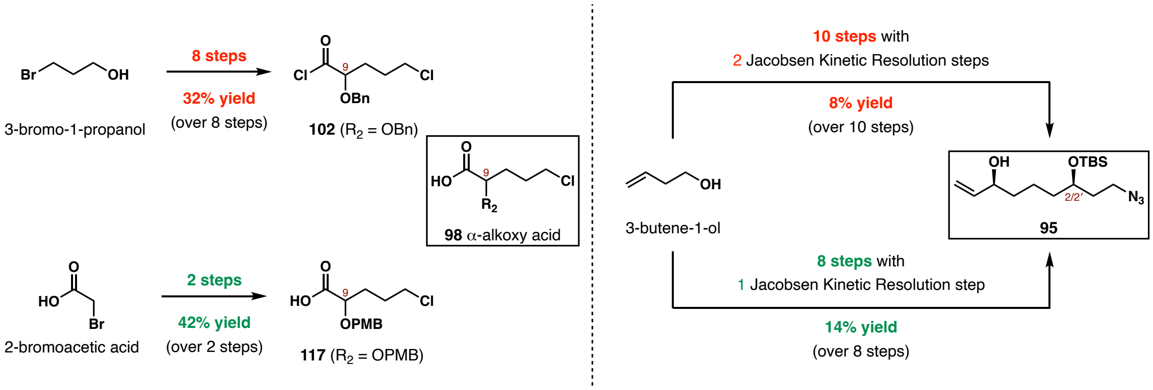

3-bromo-1-propanol
8 steps
32% yield
(over 8 steps)
102 (R2 = OBn)
98 α-alkoxy acid
2-bromoacetic acid
2 steps
42% yield
(over 2 steps)
117 (R2 = OPMB)
10 steps with
2 Jacobsen Kinetic Resolution steps
8% yield
(over 10 steps)
3-butene-1-ol
95
8 steps with
1 Jacobsen Kinetic Resolution step
14% yield
(over 8 steps)
Br
OH
Cl
O
OBn
HO
R2
Br
OPMB
OTBS
N3
9
2/2'

Figure 9. Comparison of the step counts and yields of the two routes for accessing key synthetic intermediates. The previously reported route in red, and the 2nd generation route in green.

We have shown the improved efficiency employing this new α-*p*-methoxybenzyloxy ether moiety in the 2nd generation synthesis up to the point of accessing synthon **117**. While the direct comparison of the synthesis of the α-alkoxy acid synthon is significantly shorter (8 steps versus 2 steps) with incremental yields (42% yield versus 38% yield), the comprehensive effects of having this α-*p*-methoxybenzyloxy ether group on later parts of the synthesis remains to be examined.

In particular, during the oxaquinolizidine formation step, the α-dehydroxylated byproduct would no longer be observed under reductive conditions. With the precursor for the oxaquinolizidine formation step now being a free alcohol or an α-*p*-methoxybenzyloxy ether at the C9 position, as opposed to the α-benzyloxy ether in the previous generation synthesis, the ring formation step would most likely behave differently. This could lead to a widened search for other suitable methods to be utilized for this oxaquinolizidine formation step.

In considering optimizing the overall yield of the synthesis, an investigation of different carboxylic acid protecting group would be beneficial (see Scheme 23, the R group of amino acid **94**). The coupling between the two ω-amino acids **100** and **101** utilized a methyl ester to facilitate the desired sequential coupling design (see Scheme 24); hydrolysis of the methyl ester revealed the carboxylic acid for the 2nd coupling to form the macrocycle. This basic hydrolysis was found to form undesirable products,[xx] lowering the yield. Hence, implementation of a different protecting group could more effectively provide the macrocycle intermediate.

Eventually, future studies will entail the completion of the 2nd generation total synthesis of the desmethylxestospongin B (dmXe B, **69b**), as well as other hydroxylated congeners of xestospongins found in nature. The non-natural bis-fluoroxestospongin with fluoro groups at the C9 and C9' positions is also an intriguing target, due to the known pharmacological impacts of fluorine substituents.[110] Application of our 2nd generation total synthesis basing on the improvements framed in Chapter 3.3 allows for easier access to many synthetic derivatives of xestospongin-type natural products. This will aid the structure–activity relationship studies and help further elucidate the clinical roles of these alkaloids featuring bis-1-oxaquinolizidine units.

[xx] Side products observed include the diol resulted from desilylation of the alcohols at C2 and C2' positions, as well as the terminal alcohol resulted from a hydroxy substation of the chloride.

3.4. Conclusion

We have completed the key optimization goals for Zakarian's 2nd generation synthesis of xestospongin-type natural products, a family of marine alkaloids with distinct bis-1-oxaquinolizidine skeletons. The versatility of the synthetic design is vital in accessing various congeners for structure–activity relationship studies, and the scalability of the synthesis is critical in providing ample amounts of natural products for biological studies, which is an increasingly pressing matter due to the scarce quantities of existing xestospongins isolated naturally from marine sponges. A 2nd generation synthesis aiming for large-scale adaptations while preserving flexibility in design was therefore developed. This new synthesis improved the synthetic access to critical early-stage intermediates while satisfying modern principles of synthetic efficiencies—a simpler synthesis for the α-alkoxy valeric acid intermediate and an enhanced design to better yield the azidoalcohol **95**. A modification to the synthetic target of the α-alkoxy valeric acid led to a more direct 2-step synthesis void of any functional group manipulations. This allowed a 10-gram synthesis of α-*p*-methoxybenzyloxy valeric acid **117** to be performed with ease. As the common intermediate to divergently install the non-symmetrical nature of the two ω-amino acid coupling partners, the azidoalcohol **95** plays a vital role in the overall success of this synthesis, with the scalability of the entire synthesis hinging on the successful synthesis of **95**. We were able to establish a contemporary synthesis route refined to improve synthetic efficiencies. The optimized large-scale synthesis design is characterized by easily maneuvered chemistry and atom efficiency, while ensuring high stereoselectivity: chiral resolution reactions were reduced to being utilized once, and the second stereocenter was introduced through a titanium–salalen catalyzed asymmetric epoxidation with aqueous hydrogen peroxide, which is a considerably more sustainable method. This novel and progressive synthesis approach provided the critical azidoalcohol intermediate **95** with a 1.7-fold enhancement in yield. The overall improvement of this 2nd generation synthesis will rely on the completion of the total synthesis. Nevertheless, the optimizations made thus far have shown to significantly improve the synthesis, with the core foundation of this new generation synthesis now established. The numerous analogs of xestospongins synthetically accessed with our 2nd generation synthesis will ultimately better our knowledge of xestospongins and their role in cancer biology.

References

[72] Isolations and characterizations of new xestospongins: (a) Nakagawa, M.; Endo, M. Tanaka, N.; Gen-Pei, L. *Tetrahedron Lett.* **1984**, *25*, 3227–3230. (b) Quirion, J.-C.; Sevenet, T.; Husson, H.-P.; Weniger, B.; Debitus, C. *J. Nat. Prod.* **1992**, *55*, 1505–1508. (c) Reddy, M. V. R.; Faulkner, D. J. *Nat. Prod. Lett.* **1997**, *11*, 53–59. (d) Moon, S.-S.; MacMillan, J. B.; Olmstead, M. M.; Ta, T. A.; Pessah, I. N.; Molinski, T. F. *J. Nat. Prod.* **2002**, *65*, 249–254. Isolations and characterizations of new araguspongins: (e) Kobayashi, M.; Kawazoe, K.; Kitagawa, I. *Chem. Pharm. Bull.* **1989**, *37*, 1676–1678. (f) Venkateswarlu, Y.; Reddy, M. V. R.; Rao, J. V. *J. Nat. Prod.* **1994**, *57*, 1283–1285. (g) Kobayashi, M.; Miyamoto, Y.; Aoki, S.; Murakami, N.; Kitagawa, I.; In, Y.; Ishida, T. *Heterocycles* **1998**, *47*, 195–203.

[73] Gafni, J.; Munsch, J. A.; Lam, T. H.; Catlin, M. C.; Costa, L. G.; Molinski, T. F.; Pessah, I. N. *Neuron* **1997**, *19*, 723–733.

[74] Endo, M.; Nakagawa, M.; Hamamoto, Y.; Ishihama, M. *Pure Appl. Chem.* **1986**, *58*, 387–394.

[75] (a) Petit, G. R.; Orr, B.; Herald, D. L.; Doubek, D. L.; Tackett, L.; Schmidt, J. M.; Boyd, M. R.; Pettit, R. K.; Hooper, J. N. A. *Bioorg. Med. Chem. Lett.* **1996**, *6*, 1313–1318. (b) Orabi, K. Y.; El Sayed, K. A.; Hamann, M. T.; Dunbar, D. C.; Al-Said, M. S.; Higa, T.; Kelly, M. *J. Nat. Prod.* **2002**, *65*, 1782–1785.

[76] For selected examples of IP_3R inhibition by xestospongin C (Xe C, **71a**) in a wide-range of cell types, see: (a) De Smet, P.; Parys, J. B.; Callewaert, G.; Weidema, A. F.; Hill, E.; De Smedt, H.; Erneux, C.; Sorrentino, V.; Missiaen, L. *Cell Calcium* **1999**, *26*, 9–13. (b) Miyamoto, S.; Izumi, M.; Hori, M.; Kobayashi, M.; Ozaki, H.; Karaki, H. *Br. J. Pharmacol.* **2000**, *130*, 650–654. (c) Rosado, J. A.; Sage, S. O. *Biochem. J.* **2000**, *350*, 631–635. (d) Schäfer, M.; Bahde, D.; Bosche, B.; Ladilov, Y.; Schäfer, C.; Piper, H. M.; Noll, T. *Am. J. Physiol.: Heart Circ. Physiol.* **2001**,

280, H1002–H1010. (e) Oka, T.; Sato, K.; Hori, M.; Ozaki, H.; Karaki, H. *Br. J. Pharmacol.* **2002**, *135*, 1959–1966. (f) Ozaki, H.; Masatoshi, H.; Kim, Y.-S.; Kwon, S.-C.; Ahn, D.-S.; Nakazawa, H.; Kobayashi, M.; Karaki, H. *Br. J. Pharmacol.* **2002**, *137*, 1207–1212.

[77] Jaimovich, E.; Mattei, C.; Liberona, J. L.; Cardenas, C.; Estrada, M.; Barbier, J.; Debitus, C.; Laurent, D.; Molgó, J. *FEBS Lett.* **2005**, *579*, 2051–2057.

[78] For reviews on the role calcium signaling in cancer, see: (a) Monteith, G. R.; Prevarskaya, N.; Roberts-Thomson, S. J. *Nat. Rev. Cancer* **2017**, *17*, 367–380. (b) Kania, E.; Roest, G.; Vervliet, T.; Parys, J. B.; Bultynck, G. *Front. Oncol.* **2017**, *7*, 140.

[79] (a) Cárdenas, C.; Miller, R. A.; Smith, I.; Bui, T.; Molgó, J.; Müller, M.; Vais, H.; Cheung, K.-H.; Yang, J.; Parker, I.; Thompson, C. B.; Birnbaum, M. J.; Hallows, K. R.; Foskett, J. K. *Cell* **2010**, *142*, 270–283. (b) Parys, J. B. Decuypere, J.-P.; Bultynck, G. *Cell Commun. Signaling* **2012**, *10*, 17. (c) Lovy, A.; Foskett, J. K.; Cárdenas, C. *Mol. Cell. Oncol.* **2016**, *3*, e1185563.

[80] For an overall review of the role of autophagy in cancer, see: (a) Matthew, R.; Karantza-Wadsworth, V.; White, E. *Nat. Rev. Cancer* **2007**, *7*, 961–967. (b) White, E. *J. Clin. Invest.* **2015**, *125*, 42–46. For reviews on targeting autophagy in cancer therapy, see: (c) Amaravadi, R. K.; Kimmelman, A. C.; Debnath, J. *Cancer Discovery* **2019**, *9*, 1167–1181. (d) Mulcahy Levy, J. M.; Thorburn, A. *Cell Death Differ.* **2020**, *27*, 843–857. (e) Lim, S. M.; Mohamad Hanif, E. A.; Chin, S.-F. *Cell Biosci.* **2021**, *11*, 56.

[81] (a) Cárdenas, C.; Müller, M.; McNeal, A.; Lovy, A.; Jaňa, F.; Bustos, G.; Urra, F.; Smith, N.; Molgó, J.; Diehl, J. A.; Ridky, T. W.; Foskett, J. K. *Cell Rep.* **2016**, *14*, 2313–2324. (b) Bustos, G.; Cruz, P.; Lovy, A.; Cárdenas, C. *Front. Oncol.* **2017**, *7*, 199.

[82] (a) Criollo, A.; Maiuri, M. C.; Tasdemir, E.; Vitale, I. Fiebig, A. A.; Andrews, D. Molgó, J.; Díaz, J.; Lavandero, S.; Harper, F.; Pierron, G.; di Stefano, D.; Rizzuto, R.; Szabadkai, G.; Kroemer, G. *Cell Death Differ.* **2007**, *14*, 1029–1039. (b) Vicencio, J. M.; Ortiz, C.; Criollo, A.; Jones, A. W. E.; Kepp, O.; Galluzzi, L.; Joza, N.; Vitale, I.; Morselli, E.; Tailler, M.; Castedo, M.; Maiuri, M. C.; Molgó, J.; Szabadkai, G.; Lavandero, S.; Kroemer, G. *Cell Death Differ.* **2009**, *16*, 1006–1017. (c) Cardenas, C.; Lovy, A.; Silva-Pavez, E.; Urra, F.; Mizzoni, C.; Ahumada-Caster, U.; Bustos, G.; Jaňa, F.; Cruz, P.; Farias, P.; Mendoza, E.; Huerta, H.; Murgas, P.; Hunter, M.; Rios, M.; Cerda, O.; Georgakoudi, I.; Zakarian, A.; Molgó, J.; Foskett, J. K. *Sci. Signaling* **2020**, *13*, eaay1212.

[83] (a) Jones, R. G.; Thompson, C. B. *Genes Dev.* **2009**, *23*, 537–548. (b) Boroughs, L. K.; DeBerardinis, R. J. *Nat. Cell. Biol.* **2015**, *17*, 351–359. (c) Pavlova, N. N.; Thompson, C. B. *Cell Metab.* **2016**, *23*, 27–47.

[84] (a) Vander Heiden, M. G.; Cantley, L. C.; Thompson, C. B. *Science* **2009**, *324*, 1029–1033. (b) Koppenol, W. H.; Bounds, P. L.; Dang, C. V. *Nat. Rev. Cancer* **2011**, *11*, 325–337.

[85] For selective works of cancer therapeutics targeting mitochondrial functions, see: (a) Naguib, A.; Mathew, G.; Reczek, C. R.; Watrud, K.; Ambrico, A.; Herzka, T.; Salas, I. C.; Lee, M. F.; El-Amine, N.; Zheng, W.; Di Francesco, M. E.; Marszalek, J. R.; Pappin, D. J.; Chandel, N. S.; Trotman, L. C. *Cell Rep.* **2018**, *23*, 58–67. (b) Ippolito, L.; Morandi, A.; Taddei, M. L.; Parri, M.; Comito, G.; Iscaro, A.; Raspollini, M. R.; Magherini, F.; Rapizzi, E.; Masquelier, J.; Muccioli, G. G.; Sonveaux, P.; Chiarugi, P.; Giannoni, E. *Oncogene* **2019**, *38*, 5339–5355. (c) Ref 81.

[86] Various cancers have identified the upregulation of IP$_3$R: for glioblastoma see: (a) Kang, S. S.; Han, K.-S.; Ku, B. M.; Lee, Y. K.; Hong, J.; Shin, H. Y.; Almonte, A. G.; Woo, D. H.; Brat, D. J.; Hwang, E. M.; Yoo, S. H.; Chung, C. K.; Park, S.-H.; Paek, S. H.; Roh, E. J.; Lee, S. J.; Park, J.-Y.; Traynelis, S. F.; Lee, C. J. *Cancer Res.* **2010**, *70*, 1173–1183. For gastric cancer, see: (b) Sakakura, C.; Hagiwara, A.; Fukuda, K.; Shimomura, K.; Takagi, T.; Kin, S.; Nakase, Y.; Fujiyama, J.; Mikoshiba, K.; Okazaki, Y.; Yamagishi, H. *Anticancer Res.* **2003**, *23*, 3691–3697. For small and non-small cell lung cancer, see: (c) Bergner, A.; Kellner, J.; Tufman, A. Huber, R. M. *J. Exp. Clin. Cancer Res.* **2009**, *28*, 25. For colorectal cancer, see: (d) Shibao, K.; Fiedler, M. J.; Nagata, J.; Minagawa, N.; Hirata, K.; Nakayama, Y.; Iwakiri, Y.; Nathanson, M. H.; Yamaguchi, K. *Cell Calcium* **2010**, *48*, 315–323. For breast cancer, see: (e) DeWald, D. B.; Torabinejad, J.; Samant, R. S.; Johnston, D.; Erin, N.; Shope, J. C.; Xie, Y.; Welch, D. R. *Cancer Res.* **2005**, *65*, 713–717. (f) Szatkowski, C.; Parys, J. B.; Ouadid-Ahidouch, H.; Matifat, F. *Mol. Cancer* **2010**, *9*, 156. (g) Mound, A; Rodat-Despoix, L.; Bougarn, S.; Ouadid-Ahidouch, H.; Matifat, F. *Eur. J. Cancer* **2013**, *49*, 3738–3751. For breast and prostate cancer, see: (h) ref 81a.

[87] (a) Resende, R. R.; Adhikari, A.; da Costa, J. L.; Lorençon, E.; Ladeira, M. S.; Guatimosim, S.; Kihara, A. H.; Ladeira, L. O. *Biochim. Biophys. Acta, Mol. Cell Res.* **2010**, *1803*, 246–260. (b) Lagos-Cabré, R.; Ivanova, A.; Taylor, C. W. *Cell Rep.* **2020**, *33*, 108483.

[88] Molinski, T. F.; Dalisay, D. S.; Lievens, S. L.; Saludes, J. P. *Nat. Rev. Drug Discovery* **2009**, *8*, 69–85.

[89] For related studies on the construction of the oxaquinolizidine ring of xestospongins, see (a) Ahn, K. H.; Lee, S. J. *Tetrahedron Lett.* **1992**, *33*, 507–510. (b) Börjesson, L.; Welch, C. J. *Tetrahedron* **1992**, *48*, 6325–6334. (c) Bentley,

N.; Singh, G.; Howarth, O. W. *Tetrahedron* **1993**, *49*, 4315–4320. (d) Börjesson, L.; Csöregh, I. Welch, C. J. *J. Org. Chem.* **1995**, *60*, 2989–2999.

[90] (a) Hoye, T. R.; North, J. T. *Tetrahedron Lett.* **1990**, *31*, 4281–4284. (b) Hoye, T. R.; North, J. T.; Yao, L. J. *J. Org. Chem.* **1994**, *59*, 6904–6910.

[91] Hoye, T. R.; North, J. T.; Yao, L. J. *J. Am. Chem. Soc.* **1994**, *116*, 2617–2618.

[92] Hoye, T. R.; Ye, Z.; Yao, L. J.; North, J. T. *J. Am. Chem. Soc.* **1996**, *118*, 12074–12081.

[93] Baldwin, J. E.; Melman, A.; Lee, V.; Firkin, C. R.; Whitehead, R. C. *J. Am. Chem. Soc.* **1998**, *120*, 8559–8560.

[94] Podunavac, M.; Mailyan, A. K.; Jackson, J. J.; Lovy, A.; Farias, P.; Huerta, H.; Molgó, J.; Cardenas, C.; Zakarian, A. *Angew. Chem. Int. Ed.* **2021**, *60*, 11278–11282.

[95] (a) Baldwin, J. E.; Whitehead, R. C. *Tetrahedron Lett.* **1992**, *33*, 2059–2062. (b) Sepčić, K. Guella, G.; Mancini, I.; Pietra, F.; Serra, M. D.; Menestrina, G.; Tubbs, K.; Maček, P.; Turk, T. *J. Nat. Prod.* **1997**, *60*, 991–996. (c) Baldwin, J. E.; Claridge, T. D. W.; Culshaw, A. J.; Heupel, F. A.; Lee, V.; Spring, D. R.; Whitehead, R. C.; Boughtflower, R. J.; Mutton, I. M.; Upton, R. J. *Angew. Chem. Int. Ed.* **1998**, *37*, 2661–2663.

[96] For examples of DEAD-promoted dehydrogenation of tertiary amines, see (a) Smissman, E. E.; Makriyannis, A. *J. Org. Chem.* **1973**, *38*, 1652–1657. (b) Xu, X.; Li, X.; Ma, L.; Ye, N.; Weng, B. *J. Am. Chem. Soc.* **2008**, *130*, 14048–14049.

[97] For related work done to access the effects of hydroxy substituents in IP$_3$R inhibition, see: Ta, T. A.; Feng, W.; Molinski, T. F.; Pessah, I. N. *Mol. Pharmacol.* **2006**, *69*, 532–538.

[98] (a) Ireland, R. E.; Mueller, R. H.; Willard, A. K. *J. Am. Chem. Soc.* **1976**, *98*, 2868–2877. (b) Ilardi, E. A.; Stivala, C. E.; Zakarian A. *Chem. Soc. Rev.* **2009**, *38*, 3133–3148.

[99] Podunavac, M.; Lacharity, J. J.; Jones, K. E.; Zakarian, A. *Org. Lett.* **2018**, *20*, 4867–4870.

[100] Stockley, M.; Clegg, W.; Fontana, G.; Golding, B. T.; Martin, N.; Rigoreau, L. J. M.; Smith, G. C. M.; Griffin, R. J. *Bioorg. Med. Chem. Lett.* **2001**, *11*, 2837–2841.

[101] Kuttruff, C. A.; Eastgate, M. D.; Baran, P. S. *Nat. Prod. Prep.* **2014**, *31*, 419.

[102] Kobayashi, Y.; Nakano, M.; Kumar, G. B.; Kishihara, K. *J. Org. Chem.* **1998**, *63*, 7505–7515.

[103] (a) Katsuki, T.; Sharpless, K. B. *J. Am. Chem. Soc.* **1980**, *102*, 5974–5976. (b) Hanson, R. M.; Sharpless, K. B. *J. Org. Chem.* **1986**, *51*, 1922–1925.

[104] For selective examples of asymmetric epoxidations of homoallylic alcohols, see (a) Zhang, W.; Yamamoto, H. *J. Am. Chem. Soc.* **2007**, *129*, 286–287. (b) Chen, X.; Xiong, F.; Zheng, C.; Li, J.; Chen, F. *Tetrahedron* **2014**, *70*, 5794–5799. (c) Wang, C.; Yamamoto, H. *J. Am. Chem. Soc.* **2014**, *136*, 1222–1225.

[105] For selective examples of asymmetric epoxidations of bishomoallylic alcohols, see (a) Hanessian, S.; Cooke, N. G. DeHoff, B.; Sakito, Y. *J. Am. Chem. Soc.* **1990**, *112*, 5276–5290. (b) Li, Z; Yamamoto, H. *J. Am. Chem. Soc.* **2010**, *132*, 7878–7880.

[106] (a) Tian, H.; She, X.; Yu, H.; Shu, L.; Shi, Y. *J. Org. Chem.* **2002**, *67*, 2435–2446. (b) Barlan, A. U.; Basak, A.; Yamamoto, H. *Angew. Chem. Int. Ed.* **2006**, *45*, 5849–5852. (c) Colladon, M.; Scarso, A.; Sgarbossa, P.; Michelin, R. A.; Strukul, G. *J. Am. Chem. Soc.* **2006**, *128*, 14006–14007.

[107] (a) Matsumoto, K.; Sawada, Y.; Saito, B.; Sakai, K.; Katsuki, T. *Angew. Chem. Int. Ed.* **2005**, *44*, 4935–4939. (b) Sawada, Y.; Matsumoto, K.; Katsuki, T. *Angew. Chem. Int. Ed.* **2007**, *46*, 4559–4561.

[108] (a) Berkessel, A.; Günther, T.; Wang, Q.; Neudörfl, J.-M. *Angew. Chem. Int. Ed.* **2013**, *52*, 8467–8471. For a review of catalytic asymmetric epoxidation of olefins using Ti–salalen and hydrogen peroxide, see (b) Berkessel, A. *Aldrichimica Acta* **2019**, *52*, 23–31.

[109] Lansing, M.; Engler, H.; Leuther, T. M.; Neudörfl, J.-M.; Berkessel, A. *ChemCatChem* **2016**, *8*, 3706–3709.

[110] (a) Shah, P.; Westwell, A. D. *J. Enzyme Inhib. Med. Chem.* **2007**, *22*, 527–520. (b) Inoue, M.; Sumii, Y.; Shibata, N. *ACS Omega* **2020**, *5*, 10633–10640.

Experimental Procedures

General Information: All reactions were carried out under an inert atmosphere of dry argon in oven or flame-dried glassware, unless the reaction procedure states otherwise. Tetrahydrofuran (THF) and diethyl ether (Et_2O) were distilled from sodium–benzophenone in a continuous still under an atmosphere of argon. Dichloromethane (CH_2Cl_2), diisopropylamine (*i*-Pr_2NH), *N*,*N*-diisopropylethylamine (*i*-Pr_2NEt), triethylamine (Et_3N), and acetonitrile (MeCN) were distilled from calcium hydride in a continuous still under an atmosphere of argon. Reaction temperatures were controlled by IKA ETS-D4 fuzzy thermo couples. Analytical thin-layer chromatography (TLC) was performed using pre-coated TLC plates with Silica Gel 60 F_{254} (EMD no. 5715-7) and visualized using combinations of UV, anisaldehyde, ceric ammonium molybdate (CAM), potassium permanganate and iodine staining. Flash column chromatography was preformed using 40–63 μm silica gel (Merck, Geduran, no. 11567-1) as the stationary phase. Reversed-phase chromatography was performed using SiliCycle SiliaSphere PC, C18 monomeric, 25 μm 90 Å functionalized spherical silica gel. Proton nuclear magnetic resonance spectra were recorded at 400, 500, and 600 MHz on Varian Unity Inova spectrometers. Carbon nuclear magnetic resonance spectra were recorded at 100 MHz, 125 MHz, and 150 MHz on Varian Unity Inova spectrometers. All Chemical shifts were reported in δ units relative to tetramethylsilane. Optical rotations were measured on a Rudolph Autopol III polarimeter. High-resolution mass spectral data were obtained using Waters Xevo G2-XS Tof mass spectrometer at the University of California, Santa Barbara. Ethyl-[$^{13}C_4$]-acetoacetate ([$^{13}C_4$]-**45**, $^{13}C_4$, 99.1% isotope purity) was purchased from Cambridge Isotope Laboratories. Sulfide **59** was purchased from TCI America. * denotes the ^{13}C isotope.

CHAPTER 1 EXPERIMENTAL PROCEDURES

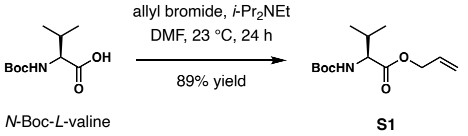

Allyl (*tert*-butoxycarbonyl)-L-valinate (S1): *i*-Pr$_2$NEt (2.4 mL, 13.8 mmol, 2.0 equiv) was added to a solution of *N*-Boc-L-valine (1.5 g, 6.9 mmol) in DMF (34 mL) at 23 °C, followed by the addition of allyl bromide (1.2 mL, 13.8 mmol, 2.0 equiv). The reaction mixture was stirred at 23 °C for 24 h, then diluted with EtOAc (100 mL) and water (150 mL). The product was extracted with EtOAc (3 × 50 mL), and the combined organic layers were washed with water (4 × 150 mL) and brine (100 mL), dried over Na$_2$SO$_4$, and concentrated to dryness under reduced pressure. The crude product was purified by column chromatography on silica gel (10% EtOAc in hexanes) to afford **S1** (1.57 g, 6.1 mmol, 89% yield).

$[\alpha]^{23}_{D}$ −2.3 (*c* 1.0, CH$_2$Cl$_2$). ^{1}H NMR (500 MHz, CDCl$_3$): δ 5.98–5.83 (m, 1H), 5.33 (dd, *J* = 17.2, 1.4 Hz, 1H), 5.25 (d, *J* = 10.4 Hz, 1H), 5.01 (d, *J* = 8.3 Hz, 1H), 4.70–4.55 (m, 2H), 4.24 (dd, *J* = 9.1, 4.6 Hz, 1H), 2.21–2.08 (m, 1H), 1.44 (s, 9H), 0.96 (d, *J* = 6.9 Hz, 3H), 0.89 (d, *J* = 6.9 Hz, 3H). ^{13}C NMR (125 MHz, CDCl$_3$): δ 172.2, 155.8, 131.9, 118.9, 79.9, 65.8, 58.7, 31.5, 28.5, 19.2, 17.7. HRMS–ESI (*m/z*): [M + Na]$^+$ calcd for C$_{13}$H$_{23}$NO$_4$Na, 280.1525; found, 280.1520.

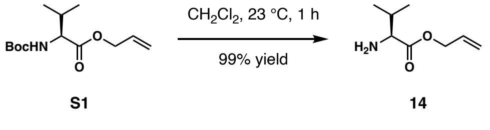

Allyl L-valinate (14): Trifluoroacetic acid (4 mL) was added to a solution of allyl (*tert*-butoxycarbonyl)-L-valinate **S1** (1.5 g, 5.8 mmol) in CH$_2$Cl$_2$ (16 mL) at 23 °C. The reaction mixture was stirred at 23 °C for 1 h. A saturated aqueous solution of NaHCO$_3$ (150 mL) was then poured into the reaction mixture and vigorously stirred for 10 min. The product was extracted with CH_2Cl_2 (4 × 50 mL). The combined organic layers were dried over Na_2SO_4 and concentrated to dryness under reduced pressure (10 mmHg). The residue was dried under vacuum (1 mmHg) for 20 min to remove residual solvent to give allyl L-valinate **14** (0.91 g, 0.58 mmol, 99% yield) as a yellowish liquid.

$[\alpha]_D^{23}$ +23.4 (*c* 1.0, $CHCl_3$). ^{1}H NMR (500 MHz, $CDCl_3$): δ 6.02–5.82 (m, 1H), 5.32 (d, *J* = 17.2 Hz, 1H), 5.23 (d, *J* = 10.4 Hz, 1H), 4.66–4.52 (m, 2H), 3.30 (d, *J* = 5.0 Hz, 1H), 2.13–1.94 (m, 1H), 1.41 (s, 2H), 0.97 (d, *J* = 6.9 Hz, 3H), 0.90 (d, *J* = 6.9 Hz, 3H). ^{13}C NMR: (125 MHz, $CDCl_3$) δ 175.4, 132.2, 118.7, 65.4, 60.1, 32.3, 19.4, 17.3. HRMS–ESI (*m/z*): [M + Na]$^+$ calcd for $C_8H_{16}NO_2Na$, 158.1181; found, 158.1181.

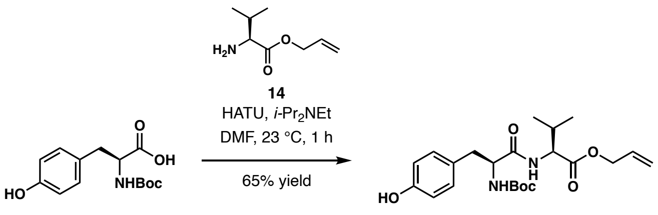

13

S2

***N*-Boc-L-Tyr-L-Val-*O*-Alloc (S2):** Ally L-valinate **14** (0.300 g, 1.90 mmol, 1.05 equiv) was added to a solution of *N*-Boc-L-tyrosine **13**[111] (0.511 g, 1.81 mmol) in DMF (9 mL) at 23 °C, followed by the addition of *i*-Pr_2NEt (0.95 mL, 5.45 mmol, 3.0 equiv) and HATU (0.760 g, 2.00 mmol, 1.1 equiv). The reaction mixture was stirred at 23 °C for 1 h, then diluted with water (100 mL), and extracted with EtOAc (3 × 70 mL). The combined organic layers were washed with brine (100 mL), dried over Na_2SO_4, and concentrated to dryness under reduced pressure. The crude product was purified by column chromatography on silica gel (40% EtOAc in hexanes) to give **S2** (0.503 g, 1.19 mmol, 65% yield).

$[\alpha]^{23}_{\mathrm{D}}$ −1.4 (*c* 1.0, $CHCl_3$). ^1H NMR (600 MHz, $CDCl_3$): δ 7.02 (d, *J* = 8.3 Hz, 2H), 6.72 (d, *J* = 8.3 Hz, 2H), 6.45 (m, 1H), 6.33 (m, 1H), 5.88 (ddt, *J* = 16.5, 10.6, 5.9 Hz, 1H), 5.32 (d, *J* = 16.5, 1H), 5.25 (d, *J* = 10.6 Hz, 1H), 5.11 (s, 1H), 4.59 (d, *J* = 5.9 Hz, 2H), 4.47 (m, 1H), 4.31 (m, 1H), 2.97 (m, 2H), 2.12 (m, 1H), 1.42 (s, 9H), 0.89 (dd, *J* = 7.2 Hz, 3H), 0.85 (dd, *J* = 7.2 Hz, 3H). ^{13}C NMR (125 MHz, $CDCl_3$): δ 171.8, 171.2, 155.8, 155.4, 131.7, 130.5 (2C), 128.1, 119.2, 115.8 (2C), 80.6, 66.06, 57.5, 56.2, 37.5, 31.5, 28.4 (3C), 19.0, 17.9. LRMS–ESI (*m*/*z*): $[M + Na]^+$ calcd for $C_{22}H_{32}N_2O_6Na$, 443.2158; found, 443.30.

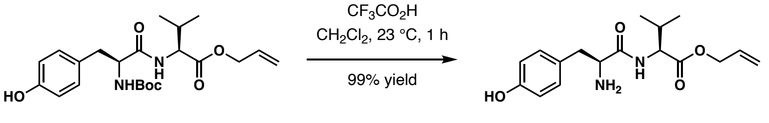

S2

6

L-Tyr-L-Val-*O*-Alloc (6): Trifluoroacetic acid (3 mL) was added to a solution of dipeptide **S2** (0.502 g, 1.19 mmol) in CH_2Cl_2 (9 mL) at 23 °C and the reaction mixture was stirred at 23 °C for 1 h. The resulting solution was then quenched with a solution of saturated aqueous $NaHCO_3$ (20 mL) and extracted with CH_2Cl_2 (3 × 30 mL). The combined organic layers were dried over Na_2SO_4 and concentrated to dryness under reduced pressure, affording **6** (0.378 g, 1.18 mmol, 99% yield).

$[\alpha]^{23}_{\mathrm{D}}$ −32.3 (*c* 1.0, $CHCl_3$). ^1H NMR (400 MHz, $CDCl_3$): δ 7.87 (d, *J* = 9.0 Hz, 1H), 7.03 (d, *J* = 8.3 Hz, 2H), 6.79 (d, *J* = 8.3 Hz, 2H), 5.90 (ddt, *J* = 16.4, 10.4, 5.8 Hz, 1H), 5.34 (d, *J* = 16.4 Hz, 1H), 5.25 (d, *J* = 10.4 Hz, 1H), 4.70–4.57 (m, 2H), 4.54 (dd, *J* = 9.0, 4.8 Hz, 1H), 3.59 (dd, *J* = 9.3, 3.9 Hz, 1H), 3.15 (dd, *J* = 13.8, 3.9 Hz, 1H), 2.61 (dd, *J* = 13.8, 9.3 Hz, 1H), 2.20 (m, 1H), 0.93 (d, *J* = 10.2 Hz, 3H), 0.90 (d, *J* = 10.2 Hz, 3H). ^{13}C NMR (100 MHz, $CDCl_3$): δ 175.1, 171.9, 155.4, 131.7, 130.5 (2C), 129.05, 119.2, 115.9 (2C), 66.1, 57.1, 56.8, 40.3, 31.3, 19.3, 17.9. HRMS–ESI (*m*/*z*): $[M + H]^+$ calcd for $C_{17}H_{25}N_2O_4$, 321.1814; found, 321.1804.

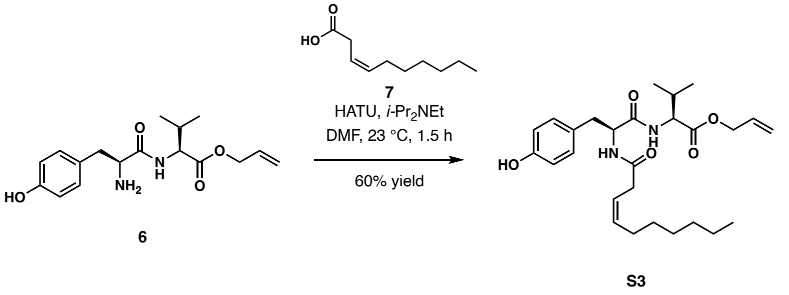

Lipopeptide allyl ester S3. (3*Z*)-3-Decenoic acid **7** (0.072 g, 0.42 mmol, 1.14 equiv) was added to a solution of L-Tyr-L-Val-*O*-Alloc **6** (0.120 g, 0.37 mmol, 1.0 equiv) in DMF (4.4 mL) at 23 °C, followed by the addition of *i*-Pr_2NEt (1.0 mL, 1.10 mmol, 2.5 equiv) and HATU (0.184 g, 0.49 mmol, 1.1 equiv). The reaction mixture was stirred at 23 °C for 1.5 h, then diluted with water (50 mL), and extracted with EtOAc (3 × 50 mL). The combined organic layers were washed with brine (70 mL), dried over Na_2SO_4, and concentrated to dryness under reduced pressure. The crude product was purified by column chromatography on silica gel (40% ethyl acetate in hexanes) to afford **S3** (0.106 g, 0.22 mmol, 60% yield).

$[\alpha]_D^{23}$ −6.5 (*c* 1.0, $CHCl_3$). ^1H NMR (600 MHz, $CDCl_3$): δ 7.03 (d, *J* = 8.0 Hz, 2H), 6.79 (s, 1H), 6.72 (d, *J* = 8.0 Hz, 2H), 6.41 (m, 2H), 5.89 (ddt, *J* = 17.2, 10.4, 5.9 Hz, 1H), 5.65 (m, 1H), 5.44 (m, 1H), 5.34 (d, *J* = 17.2 Hz, 1H), 5.26 (d, *J* = 10.4 Hz, 1H), 4.65 (q, *J* = 7.2 Hz, 1H), 4.61 (d, *J* = 6.0 Hz, 2H), 4.44 (dd, *J* = 8.5, 5.0 Hz, 1H), 2.98 (dd, *J* = 21.1, 7.3 Hz, 4H), 2.12 (m, 1H), 1.95 (m, 2H), 1.36– 1.18 (m, 8H), 0.94–0.78 (m, 9H). ^{13}C NMR (125 MHz, $CDCl_3$): δ 171.6, 171.2, 171.1, 155.6, 136.2, 131.7, 130.5 (2C), 127.8, 120.8, 119.3, 115.8 (2C), 66.1, 57.7, 54.8, 37.6, 35.2, 31.9, 31.3, 29.4, 29.1, 27.5, 22.8, 19.1, 17.9, 14.3. LRMS–ESI (*m/z*): $[M + Na]^+$ calcd for $C_{27}H_{40}N_2O_5Na$, 495.2835; found, 495.40.

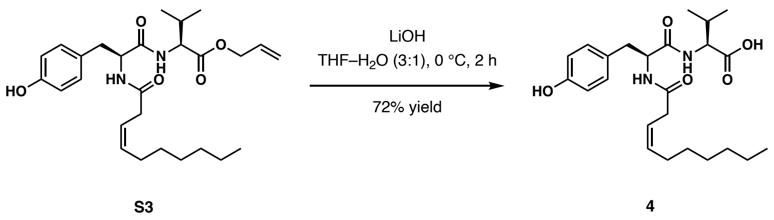

Lipopeptide 4. Lithium hydroxide monohydrate (0.020 g, 0.48 mmol, 3.0 equiv) was added to a solution of ester **S3** (0.076 g, 0.16 mmol, 1.0 equiv) in THF–H_2O (3:1, 1.6 mL) at 0 °C, and the reaction mixture was stirred at 0 °C for 2 h. The resulting solution was quenched with a solution of aqueous 3 M NaOH and washed with EtOAc. The aqueous layer was then acidified to pH = 1 with 1 M aqueous hydrochloric acid solution and re-extracted with EtOAc (3 × 5 mL) and brine. The combined organic layers were washed with brine, dried over Na_2SO_4, and concentrated to dryness under reduced pressure. The crude product **4** (0.050 mg, 0.12 mmol, 72% yield) was used without further purification.

$[\alpha]_D^{23}$ −13.5 (*c* 1.0, $CHCl_3$). ^{1}H NMR (600 MHz, CD_3OD): δ 8.07 (d, *J* = 8.6 Hz, 1H), 7.78 (d, *J* = 7.9 Hz, 1H), 7.05 (d, *J* = 8.1 Hz, 2H), 6.69 (d, *J* = 8.1 Hz, 2H), 5.54 (m, 1H), 5.41 (m, 1H), 4.65 (m, 1H), 4.33 (m, 1H), 3.35 (s, 1H), 3.06 (dd, *J* = 14.1, 5.3 Hz, 1H), 2.95 (d, *J* = 7.3 Hz, 2H), 2.80 (dd, *J* = 14.1, 9.0 Hz, 1H), 2.17 (m, 1H), 1.99 (q, *J* = 7.2 Hz, 2H), 1.38–1.23 (m, 8H), 1.02–0.92 (m, 6H), 0.86 (t, *J* = 6.9 Hz, 3H). ^{13}C NMR (150 MHz, CD_3OD): δ 174.6, 174.0, 173.8, 157.2, 134.9, 131.3 (2C), 128.9, 122.7, 116.1 (2C), 55.9, 55.9, 37.9, 35.3, 32.9, 31.9, 30.4, 30.0, 28.3, 23.7, 19.6, 18.3, 14.4. LRMS–ESI (*m/z*): $[M + Na]^+$ calcd for $C_{24}H_{36}N_2O_5Na$, 455.2522; found, 455.20.

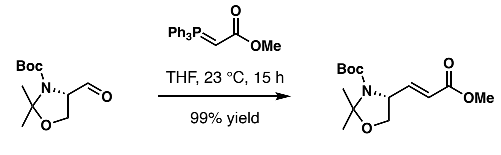

***tert*-Butyl (4*R*)-4-[(1*E*)-3-methoxy-3-oxoprop-1-en-1-yl]-2,2-dimethyl-1,3-oxazolidine-3-carboxylate (S4):** Methyl (triphenylphosphoranylidene)acetate (3.00 g, 8.9 mmol, 1.2 equiv) was added to a solution of Garner's aldehyde[112] (1.70 g, 7.4 mmol, 1.0 equiv) in THF (24 mL) at 23 °C, and the reaction mixture was stirred at 23 °C for 15 h. The reaction mixture was concentrated under reduced pressure, and the residue was directly subjected to column chromatography on silica gel (15% EtOAc in hexanes) to afford **S4** (2.1 g, 7.4 mmol, 99% yield).

$[\alpha]_D^{23}$ −69.2 (*c* 1.0, CHCl$_3$). ^{1}H NMR (500 MHz, C$_6$D$_6$, 60 °C): δ 6.94 (dd, *J* = 15.2, 6.2 Hz, 1H), 6.02 (br. s, 1H), 4.28–3.93 (m, 4H), 3.58 (dd, *J* = 8.9, 6.5 Hz, 1H), 3.36 (dd, *J* = 8.9, 2.4 Hz, 1H), 1.62 (s, 3H), 1.49 (s, 3H), 1.37 (s, *J* = 15.2 Hz, 9H). ^{13}C NMR (125 MHz, C$_6$D$_6$, 60 °C): δ 165.8, 151.9, 146.3, 122.9, 79.9, 67.5, 60.3, 58.4, 28.4, 26.9, 24.2, 14.3. HRMS–ESI (*m*/*z*): [M + Na]$^+$ calcd for C$_{14}$H$_{23}$O$_5$Na, 308.1474; found, 308.1469.

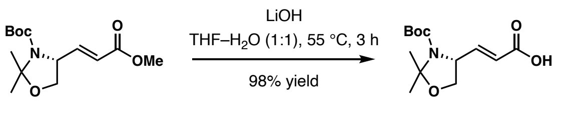

S4 **15a**

(*R*,*E*)-3-(3-(*tert*-Butoxycarbonyl)-2,2-dimethyloxazolidin-4-yl)acrylic acid (15a): Lithium hydroxide monohydrate (0.74 g, 17.5 mmol, 5.0 equiv) was added to a solution of **S4** (1.0 g, 3.5 mmol) in a mixture of THF (17.5 mL) and water (17.5 mL) at 23 °C, and the reaction mixture was stirred vigorously at 55 °C until complete hydrolysis was observed by TLC analysis (approximately 3 h). The reaction mixture was then cooled to room temperature, diluted with water (50 mL), and extracted with EtOAc (50 mL). The aqueous layer was acidified to pH = 1 with 1 M aqueous hydrochloric acid solution and re-extracted with EtOAc (3 × 20 mL). The combined organic layers were washed with brine (100 mL), dried over Na$_2$SO$_4$, and concentrated to dryness under reduced pressure to afford carboxylic acid **15a** (2.1 g, 7.4 mmol, 98% yield).

$[\alpha]_D^{23}$ −66.7 (*c* 1.0, CHCl$_3$). ^{1}H NMR (500 MHz, C$_6$D$_6$, 60 °C): δ 6.96 (dd, *J* = 15.4, 6.9 Hz, 1H), 5.95 (br. s, 1H), 4.01 (br. s, 1H), 3.56 (dd, *J* = 9.0, 6.6 Hz, 1H), 3.32 (dd, *J* = 9.1, 2.6 Hz, 1H), 1.61 (s, 3H), 1.49 (s, 3H), 1.36 (s, 9H). ^{13}C NMR (125 MHz, C$_6$D$_6$, 60 °C): δ 171.0, 151.9, 149.0, 122.0, 80.2, 67.3, 58.33, 58.31, 28.4, 26.7, 24.4. HRMS–ESI (*m/z*): [M + Na]$^+$ calcd for C$_{13}$H$_{21}$NO$_5$Na, 294.1317; found, 294.1317.

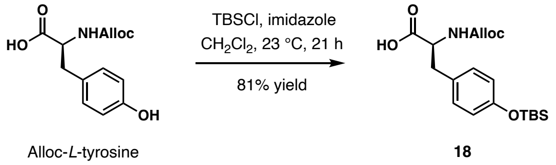

(*S*)-2-(((allyloxy)carbonyl)amino)-3-(4-((*tert*-butyldimethylsilyl)oxy)phenyl)propanoic acid (18): Alloc-L-tyrosine[113] (1.5 g, 5.65 mmol) was dissolved in CH$_2$Cl$_2$ (60 mL) and the solution was cooled to 0 °C. Imidazole (1.16 g, 16.96 mmol, 3.0 equiv) and TBSCl (1.87 g, 12.44 mmol, 2.2 equiv) were added sequentially at 0 °C. The reaction mixture was then stirred at 23 °C until full consumption of starting material was observed by TLC (approximately 21 h). The solvent was evaporated under reduced pressure, and the dry residue was dissolved in a mixture of THF (20 mL) and water (40 mL) at 23 °C. The solution was then treated with K$_2$CO$_3$ (390 mg, 2.83 mmol, 0.5 equiv) and stirred at 23 °C for 90 min. The resulting mixture was then acidified to pH = 2 with 1 M aqueous hydrochloric acid solution, and the aqueous layer was extracted with EtOAc (3 × 50 mL). The combined organic layers were washed with brine, dried over Na$_2$SO$_4$, and concentrated to dryness under reduced pressure. The crude product was purified by column chromatography on silica gel (30% EtOAc in hexanes with 5% formic acid) to afford **18** (1.72 g, 4.58 mmol, 81% yield).

$[\alpha]_D^{23}$ +22.7 (*c* 1.0, CHCl$_3$). ^{1}H NMR (500 MHz, C$_6$D$_6$, 60 °C): δ 9.31 (br. s, 1H), 6.99 (d, *J* = 7.3 Hz, 2H), 6.76 (d, *J* = 7.3 Hz, 2H), 5.70 (br. s, 1H), 5.27 (br. s, 1H), 5.09 (d, *J* = 17.1 Hz, 1H), 4.96 (d, *J* = 10.4 Hz, 1H), 4.70 (br. s, 1H), 4.43 (br. s, 2H), 3.08 (dd, *J* = 14.0, 5.0 Hz, 1H), 2.87 (dd, *J* = 13.1, 7.0 Hz, 1H), 0.96 (s, 9H), 0.10 (s, 6H). ^{13}C NMR (125 MHz, C_6D_6, 60 °C): δ 176.0, 156.5, 155.3, 133.1, 130.8, 129.4, 120.5, 117.6, 66.2, 55.6, 37.5, 25.9, 18.4, −4.3. HRMS–ESI (*m*/*z*): $[M + Na]^+$ calcd for $C_{19}H_{29}NO_5SiNa$, 402.1713; found, 402.1728.

Procedures for the Synthesis of Intermediates (16a–12a) for Macrocyclization Path A:

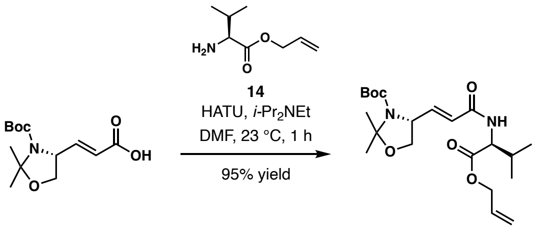

15a 16a

Acetonide 16a. Ally L-valinate **14** (0.43 g, 2.74 mmol, 1.05 equiv) was added to a solution of **15a** (0.70 g, 2.58 mmol) in DMF (12 mL) at 23 °C, followed by the addition of i-Pr$_2$NEt (1.35 mL, 7.75 mmol, 3.0 equiv) and HATU (1.08 g, 2.84 mmol, 1.1 equiv). The reaction mixture was stirred at 23 °C for 1 h, then diluted with water (130 mL), and extracted with EtOAc (3 × 30 mL). The combined organic layers were washed with water (3 × 50 mL) and brine (50 mL), dried over Na$_2$SO$_4$, and concentrated to dryness under reduced pressure. The crude product was purified by column chromatography on silica gel (30% EtOAc in hexanes) to give **16a** (1.01 g, 2.46 mmol, 95% yield).

$[\alpha]^{23}_{D}$ −21.9 (*c* 1.0, CHCl$_3$). ^{1}H NMR (500 MHz, C$_6$D$_6$, 60 °C): δ 6.95 (dd, *J* = 14.5, 7.0 Hz, 1H), 6.08 (s, 1H), 5.83 (br. s, 1H), 5.73–5.58 (m, 1H), 5.09 (d, *J* = 17.2 Hz, 1H), 4.95 (d, *J* = 10.4 Hz, 1H), 4.88 (s, 1H), 4.44 (dd, *J* = 12.5, 5.2 Hz, 1H), 4.36 (dd, *J* = 13.0, 5.3 Hz, 1H), 4.19 (br. s, 1H), 3.70 (dd, *J* = 8.1, 7.1 Hz, 1H), 3.47 (d, *J* = 8.0 Hz, 1H), 2.18–2.03 (m, 1H), 1.62 (s, 3H), 1.52 (s, 3H), 1.39 (s, 9H), 0.89 (d, *J* = 6.2 Hz, 3H), 0.83 (d, *J* = 6.8 Hz, 3H). ^{13}C NMR (125 MHz, C$_6$D$_6$, 60 °C): δ 172.0, 164.9, 152.0, 143.0, 132.3, 125.1, 118.4, 94.5, 79.8, 67.7, 65.6, 58.6, 57.7, 31.8, 28.5, 26.9, 24.6, 19.1, 18.1. HRMS–ESI (*m*/*z*): [M + Na]$^+$ calcd for C$_{21}$H$_{34}$N$_2$O$_6$Na, 433.2315; found, 433.2303.

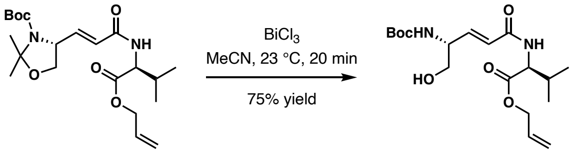

16a 17a

Alcohol 17a. Bismuth (III) chloride (0.99 g, 3.14 mmol, 1.0 equiv) was added to a solution of acetonide **16a** (1.29 g, 3.14 mmol) in MeCN (10 mL) at 23 °C, and the reaction mixture was stirred at 23 °C for 20 min. The resulting mixture was quenched with a saturated aqueous solution of $NaHCO_3$ (20 mL), diluted with EtOAc (50 mL), and filtered through Celite to remove the inorganic precipitate. The layers were separated, and the aqueous layer was extracted with EtOAc (4 × 50 mL). The combined organic layers were washed with brine, dried over Na_2SO_4, and concentrated to dryness under reduced pressure. The crude product was purified by column chromatography on silica gel (70% EtOAc in hexanes) to afford **17a** (0.87 g, 2.35 mmol, 75% yield).

$[\alpha]^{23}_{D}$ −0.4 (*c* 1.0, $CHCl_3$). ^1H NMR (500 MHz, C_6D_6, 60 °C): δ 6.95 (dd, *J* = 15.4, 6.0 Hz, 1H), 6.68 (br. s, 1H), 6.04 (d, *J* = 15.4 Hz, 1H), 5.80–5.63 (m, 1H), 5.40 (br. s, 1H), 5.14 (dd, *J* = 17.2, 1.5 Hz, 1H), 5.00 (dd, *J* = 10.4, 1.2 Hz, 1H), 4.82 (dd, *J* = 8.5, 5.3 Hz, 1H), 4.62–4.32 (m, 3H), 3.56 (br. s, 2H), 3.22 (br. s, 1H), 2.26–2.07 (m, 1H), 1.44 (s, 9H), 0.93 (d, *J* = 6.8 Hz, 3H), 0.90 (d, *J* = 6.9 Hz, 3H). ^{13}C NMR (125 MHz, C_6D_6, 60 °C): δ 172.3, 165.9, 156.0, 142.9, 132.3, 125.1, 118.5, 79.5, 65.8, 64.8, 58.0, 54.4, 31.6, 28.6, 19.2, 18.2. HRMS–ESI (*m/z*): $[M + Na]^+$ calcd for $C_{18}H_{30}N_2O_6Na$, 393.2002; found, 393.2010.

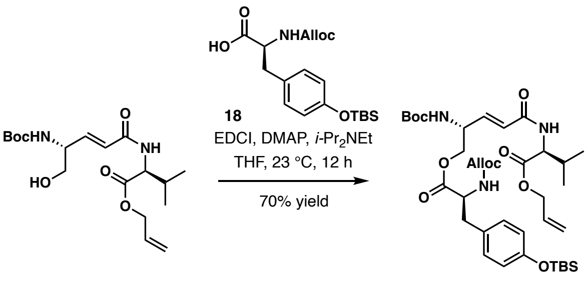

17a 19a

Depsipeptide 19a. *i*-Pr$_2$NEt (0.141 mL, 0.82 mmol, 3.0 equiv), DMAP (50 mg, 0.41 mmol, 1.5 equiv), and EDCI hydrochloride (78 mg, 0.41 mmol, 1.5 equiv) were added to a solution of acid **18** (0.154 g, 0.41 mmol, 1.5 equiv) in THF (2 mL) at 23 °C. The mixture was stirred at 23 °C for 30 min before a solution of **17a** (0.100 g, 0.27 mmol) in THF (0.9 mL) was added. The reaction mixture was stirred 23 °C for 12 h. The resulting solution was quenched with 1 M aqueous hydrochloric acid solution (10 mL) and diluted with EtOAc (15 mL). The layers were separated, and the aqueous layer was extracted by EtOAc (3 × 10 mL). The combined organic layers were washed with a saturated aqueous solution of NaHCO$_3$ (20 mL), dried over Na$_2$SO$_4$, and concentrated to dryness under reduced pressure. The crude product was purified by column chromatography on silica gel (30% EtOAc in hexanes) to afford **19a** (0.131 g, 0.19 mmol, 70% yield).

$[\alpha]_D^{23}$ +2.7 (*c* 1.0, CHCl$_3$). ^{1}H NMR (500 MHz, CDCl$_3$): δ 6.99 (d, *J* = 8.4 Hz, 2H), 6.75 (d, *J* = 8.4 Hz, 2H), 6.69 (dd, *J* = 15.4, 5.4 Hz, 1H), 6.46 (d, *J* = 8.6 Hz, 1H), 6.03 (dd, *J* = 15.4, 1.1 Hz, 1H), 5.97–5.79 (m, 2H), 5.37–5.11 (m, 4H), 5.03 (dd, *J* = 7.7 Hz, 1H), 4.73–4.56 (m, 4H), 4.58–4.43 (m, 3H), 4.34–4.09 (m, 2H), 3.05 (dd, *J* = 14.1, 5.6 Hz, 1H), 2.95 (dd, *J* = 14.1, 7.1 Hz, 1H), 2.28–2.13 (m, 1H), 1.44 (s, 9H), 0.95 (s, 9H), 0.94 (d, *J* = 6.9 Hz, 3H), 0.91 (d, *J* = 6.9 Hz, 3H), 0.16 (s, 6H). ^{13}C NMR (125 MHz, CDCl$_3$): δ 171.8, 171.7, 165.0, 155.9, 155.2, 154.9, 140.0, 132.6, 131.7, 130.3, 128.3, 125.3, 120.4, 119.1, 118.0, 80.3, 66.0, 66.0, 57.3, 55.1, 50.5, 37.2, 31.5, 29.8, 28.5, 25.8, 19.1, 18.3, 18.0, −4.3. HRMS–ESI (*m*/*z*): $[M + Na]^+$ calcd for $C_{37}H_{57}N_3O_{10}SiNa$, 754.3711; found, 754.3690.

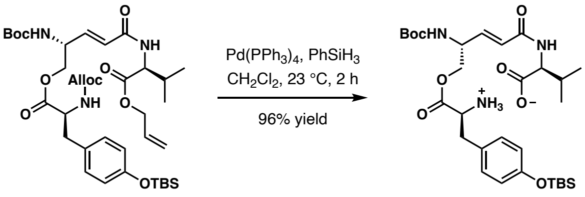

19a **12a**

Amino acid 12a. Phenylsilane (0.126 mL, 1.16 mmol, 4.0 equiv) and $Pd(PPh_3)_4$ (17 mg, 0.015 mmol, 0.05 equiv) were added to a solution of **19a** (0.20 g, 0.29 mmol) in CH_2Cl_2 (3 mL) at 23 °C. The reaction mixture was stirred at 23 °C for 2 h, and the mixture was concentrated under reduced pressure. The residue was directly subjected to column chromatography on silica gel (100% EtOAc to 15% MeOH in CH_2Cl_2) to afford **12a** (0.170 g, 0.28 mmol, 96% yield).

$[\alpha]_D^{23}$ −10.6 (*c* 1.0, MeOH). ^{1}H NMR (500 MHz, CD_3OD): δ 7.09 (d, *J* = 8.4 Hz, 2H), 6.80 (d, *J* = 8.5 Hz, 2H), 6.70 (dd, *J* = 15.5, 5.5 Hz, 1H), 6.30 (dd, *J* = 15.5, 1.4 Hz, 1H), 4.58 (br. s, 1H), 4.33–4.19 (m, 2H), 4.21–4.09 (m, 1H), 3.88–3.78 (m, 1H), 3.05 (dd, *J* = 13.9, 5.5 Hz, 1H), 2.89 (dd, *J* = 13.9, 7.4 Hz, 1H), 2.27–2.10 (m, 1H), 1.45 (s, 9H), 0.98 (s, 9H), 0.95 (d, *J* = 6.8 Hz, 3H), 0.93 (d, *J* = 6.8 Hz, 3H), 0.19 (s, 6H). ^{13}C NMR (125 MHz, CD_3OD): δ 174.2, 167.3, 157.6, 156.1, 140.9, 131.5, 131.4, 130.4, 126.5, 121.3, 80.6, 67.1, 61.8, 56.5, 52.0, 39.8, 32.2, 28.8, 26.2, 20.3, 19.0, 18.6, −4.3. HRMS–ESI (*m*/*z*): $[M + Na]^+$ calcd for $C_{30}H_{49}N_3O_8SiNa$, 630.3187; found, 630.3189.

Procedures for the Synthesis of Intermediates (15b–12b) for Macrocyclization Path B:

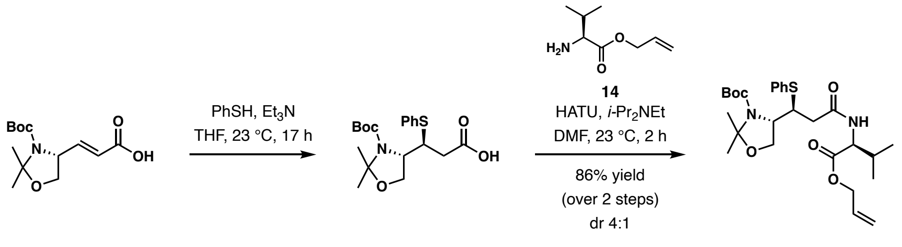

15a **15b** **16b**

Acetonide 16b. Triethylamine (4.4 mL, 32.4 mmol, 3.05 equiv) and thiophenol (1.6 mL, 16.2 mmol, 1.5 equiv) were added to a solution of the crude acid **15a** (2.87 g, 10.6 mmol) in THF (21 mL) at 23 °C, and the reaction mixture was stirred 23 °C for 17 h. 1 M aqueous NaOH solution (20 mL) was then added to the reaction mixture, and the aqueous layer was extracted with EtOAc (2 × 30 mL). The aqueous layer was acidified to pH = 1 with a 1 M aqueous hydrochloric acid solution and re-extracted with EtOAc (3 × 50 mL). The combined organic layers were washed with brine, dried over Na_2SO_4, concentrated to dryness under reduced pressure to afford a mixture of diastereomers **15b** without further purification.

15b: ^{1}H NMR (500 MHz, $CDCl_3$): δ 7.49 (d, *J* = 7.35 Hz, 2H), 7.29 (m, 3H), 4.15 (m, 4H), 2.91 (dd, *J* = 16.5, 3.9 Hz, 1H), 2.46 (m, 1H), 1.43 (m, 15H). ^{13}C NMR (125 MHz, $CDCl_3$): δ 177.4, 152.3, 133.2, 130.7, 129.2, 128.0, 95.5, 80.2, 64.4, 59.0, 46.6, 34.2, 28.4, 26.2, 22.5.

Ally L-valinate **14** (1.80 g, 11.5 mmol, 1.07 equiv) was added to a solution of crude **15b** in DMF (30 mL) at 23 °C, followed by the addition of *i*-Pr$_2$NEt (7.5 mL, 42.9 mmol, 4.0 equiv) and HATU (4.89 g, 12.9 mmol, 1.2 equiv). The reaction mixture was stirred at 23 °C for 2 h, then diluted with water (300 mL), and extracted with EtOAc (3 × 40 mL). The combined organic layers were washed with brine, dried over Na_2SO_4, and concentrated to dryness under reduced pressure. The crude product was purified by column chromatography on silica gel (15% EtOAc in hexanes to 30% EtOAc in hexanes) to afford **16b** (3.76 g, 7.22 mmol, 67% yield, major diastereomer) and its diastereomer (0.93 g, 1.79, 17% yield, minor diastereomer).

16b: $[\alpha]^{23}_{\mathrm{D}}$ +15.9 (*c* 0.57, $CHCl_3$). ^{1}H NMR (600 MHz, CD_3CN): δ 7.52 (d, *J* = 7.5 Hz, 2H), 7.32 (dd, *J* = 7.5, 7.5 Hz, 2H), 7.27 (t, *J* = 7.5 Hz, 1H), 6.70 (d, *J* = 8.6 Hz, 1H), 5.96 (ddt, *J* = 16.4, 10.8, 5.6 Hz, 1H), 5.36 (d, *J* = 16.4, 1H), 5.25 (d, *J* = 10.8 Hz, 1H), 4.68–4.59 (m, 2H), 4.45 (dd, *J* = 8.5, 5.7 Hz, 1H), 4.24–4.13 (m, 2H), 4.12–4.03 (m, 2H), 2.71 (d, *J* = 15.6 Hz, 1H), 2.41 (dd, *J* = 15.6, 11.4 Hz, 1H), 2.16 (m, 1H), 1.59 (s, 3H), 1.42 (s, 3H), 1.41 (s, 9H), 0.99 (d, *J* = 7.0 Hz, 3H), 0.98 (d, *J* = 7.0 Hz, 3H). ^{13}C NMR (150 MHz, CD_3CN): δ 172.4, 171.6, 133.6, 130.2 (4C), 128.3, 118.8, 118.0 (2C), 96.0, 81.3, 66.3 (2C), 65.5, 60.6, 59.1, 36.5, 31.9, 28.9 (5C), 19.7, 18.7. LRMS–ESI (*m/z*): [M + Na]$^+$ calcd for $C_{27}H_{40}N_2O_5SNa$, 520.2607; found, 520.26.

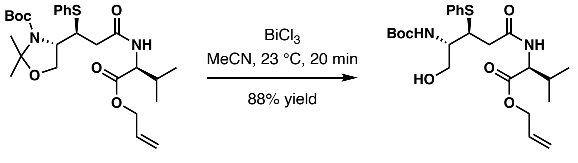

16b **17b**

Alcohol 17b. Bismuth (III) chloride (1.66 g, 5.28 mmol, 1.0 equiv) was added to a solution of acetonide **16b** (2.75 g, 5.28 mmol) in MeCN (18 mL) at 23 °C, and the reaction mixture was stirred at 23 °C for 20 min. The resulting mixture was quenched with a saturated aqueous solution of $NaHCO_3$ (40 mL), diluted with EtOAc (80 mL), and filtered through Celite to remove the inorganic precipitate. The layers were separated, and the aqueous layer was extracted with EtOAc (3 × 70 mL). The combined organic layers were washed with brine, dried over Na_2SO_4, and concentrated to dryness under reduced pressure. The crude product was purified by column chromatography on silica gel (40% EtOAc in hexanes) to afford **17b** (2.24 g, 4.66 mmol, 88% yield).

$[\alpha]_D^{23}$ −22.4 (*c* 1.0, $CHCl_3$). ^1H NMR (600 MHz, $CDCl_3$): δ 7.57 (d, *J* = 8.5 Hz, 1H), 7.49–7.44 (m, 2H), 7.33–7.28 (m, 2H), 7.23 (m, 1H), 5.91 (ddt, *J* = 17.2, 10.3, 5.8 Hz, 1H), 5.34 (d, *J* = 17.2 Hz, 1H), 5.25 (d, *J* = 10.3 Hz, 1H), 5.09 (d, *J* = 9.4 Hz, 1H), 4.63 (qd, *J* = 13.1, 5.7 Hz, 2H), 4.48 (m, 1H), 4.35 (m, 1H), 3.82 (m, 1H), 3.76 (m, 1H), 3.68 (m, 1H), 2.68 (dd, *J* = 13.7, 9.8 Hz, 1H), 2.57 (dd, *J* = 13.7, 4.7 Hz, 1H), 2.36 (m, 1H), 2.26 (m, 1H), 1.46 (s, 9H), 0.98 (d, *J* = 7.2 Hz, 3H), 0.96 (d, *J* = 7.2 Hz, 3H). ^{13}C NMR (125 MHz, $CDCl_3$, 60 °C): δ 172.2, 171.3, 157.0, 134.3, 131.94, 131.3, 129.4 (4C), 127.4, 119.0, 80.5, 66.0, 64.0, 58.1, 54.5, 49.4, 41.3, 30.5, 29.9, 28.5 (3C), 19.4, 17.8. HRMS–ESI (*m*/*z*): $[M + Na]^+$ calcd for $C_{24}H_{36}N_2O_6SNa$, 503.2192; found, 503.2177.

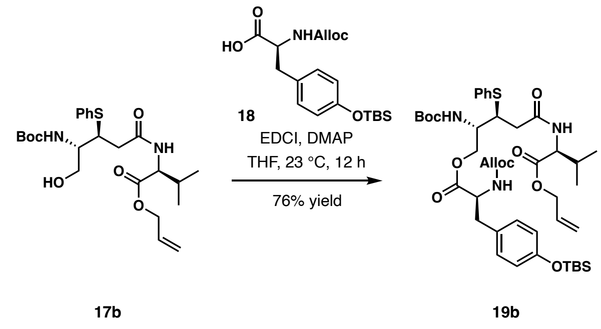

Depsipeptide 19b. EDCI hydrochloride (1.31 g, 0.41 mmol, 1.5 equiv), DMAP (56 mg, 0.46 mmol, 0.1 equiv), and acid **18** (2.60 g, 6.86 mmol, 1.5 equiv) in THF (23 mL) were added to a solution of **17b** at 23 °C. The reaction mixture was stirred 23 °C for 12 h. The resulting solution was quenched with 1 M aqueous hydrochloric acid solution (20 mL) and diluted with EtOAc. The layers were separated, and the aqueous layer was extracted by EtOAc (3 × 40 mL). The combined organic layers were washed with a saturated aqueous solution of $NaHCO_3$, dried over Na_2SO_4, and concentrated to dryness under reduced pressure. The crude product was purified by column chromatography on silica gel (25% EtOAc in hexanes) to afford **19b** (2.92 g, 3.47 mmol, 76% yield).

$[\alpha]_D^{23}$ −12.9 (*c* 1.0, $CHCl_3$). ^{1}H NMR (600 MHz, CD_3CN): δ 7.55–7.47 (m, 2H), 7.36–7.30 (m, 2H), 7.27 (m, 1H), 7.11 (m, 1H), 7.06 (d, *J* = 8.1 Hz, 2H), 6.77 (d, *J* = 8.1 Hz, 2H), 6.00–5.78 (m, 3H), 5.58 (m, 1H), 5.34 (d, *J* = 17.2 Hz, 1H), 5.26–5.19 (m, 2H), 5.15 (d, *J* = 10.2 Hz, 1H), 4.67–4.54 (m, 2H), 4.51–4.41 (m, 2H), 4.41–4.32 (m, 2H), 4.28 (s, 1H), 4.21–4.12 (m, 2H), 3.81 (m, 1H), 2.99 (dd, *J* = 14.2, 5.0 Hz, 1H), 2.77 (dd, *J* = 14.2, 9.3 Hz, 1H), 2.61 (dd, *J* = 15.0, 6.1 Hz, 1H), 2.48 (dd, *J* = 15.0, 8.4 Hz, 1H), 2.13 (m, 1H), 1.42 (s, 9H), 0.94 (s, 9H), 0.95–0.90 (m, 6H), 0.18 (s, 6H). ^{13}C NMR (125 MHz, CD_3CN): δ 172.4, 172.3, 171.2, 156.8, 156.7, 155.5, 135.7, 134.2, 133.35, 132.3 (2C), 131.3 (2C), 130.6, 130.2 (2C), 128.2, 120.9 (2C), 118.2 (2C) 80.2, 66.2, 66.1, 65.0, 58.7, 56.5, 53.4, 49.1, 39.28, 37.2, 31.4, 28.6 (3C), 26.0 (3C), 19.4, 18.8, 18.3, −4.2, −4.2. HRMS–ESI (*m*/*z*): $[M + Na]^+$ calcd for $C_{43}H_{63}N_3O_{10}SSiNa$, 864.3901; found, 865.3877.

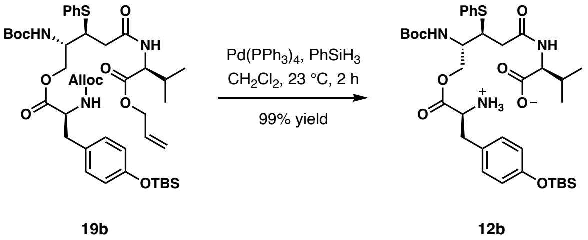

Amino acid 12b. Phenylsilane (0.530 mL, 4.28 mmol, 4.0 equiv) and $Pd(PPh_3)_4$ (62 mg, 0.054 mmol, 0.05 equiv) were added to a solution of **19b** (0.901 g, 1.07 mmol) in CH_2Cl_2 (11 mL) at 23 °C. The reaction mixture was stirred at 23 °C for 2 h, and the mixture was concentrated under reduced pressure. The residue was directly subjected to column chromatography on silica gel (100% EtOAc to 15% MeOH in CH_2Cl_2) to afford **12b** (0.770 g, 1.06 mmol, 99% yield).

$[\alpha]_D^{23}$ −10.9 (*c* 1.0, MeOH). ^{1}H NMR (600 MHz, CD_3OD): δ 7.56–7.49 (m, 2H), 7.34–7.27 (m, 2H), 7.24 (m, 1H), 7.06 (d, *J* = 8.1 Hz, 2H), 6.80 (d, *J* = 8.1, 2H), 4.37–4.13 (m, 4H), 3.87 (m, 1H), 3.78 (m, 1H), 2.97 (dd, *J* = 13.8 6.2 Hz, 1H), 2.84 (dd, *J* = 13.8, 6.2 Hz, 1H), 2.68 (dd, *J* = 14.5, 7.0 Hz, 1H), 2.54 (dd, *J* = 14.5, 8.1 Hz, 1H), 2.21 (m, 1H), 1.46 (s, 9H), 1.14–0.78 (m, 15H), 0.19 (s, 6H). ^{13}C NMR (125 MHz, CD_3OD): δ 178.1, 172.9, 172.7, 158.2, 156.4, 136.6, 132.9, 132.3, 131.5 (2C), 130.2, 130.0, 129.2, 127.8, 121.5 (2C), 80.3, 65.8, 62.8, 61.1, 57.1, 55.8, 40.4, 38.3, 32.0, 28.8 (3C), 26.1 (3C), 20.2, 19.0, 18.3, −4.3 (2C). HRMS–ESI (*m*/*z*): $[M + H]^+$ calcd for $C_{36}H_{56}N_3O_8SSi$, 718.3557; found, 718.3553.

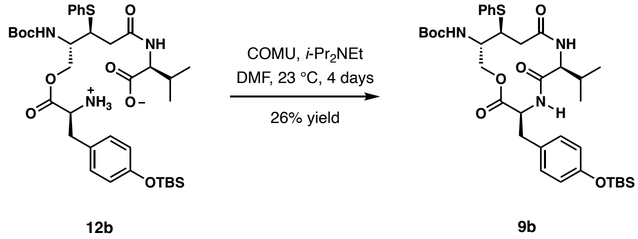

Macrocyclic depsipeptide 9b. *i*-Pr_2NEt (0.636 mL, 3.62 mmol, 4.0 equiv) was added to a solution of acid **12b** (0.650 g, 0.90 mmol) in DMF (220 mL) at 23 °C, followed by the addition of COMU (0.775 g, 1.81 mmol, 2.0 equiv). The reaction mixture was stirred 23 °C for 4 days, then diluted with water (80 mL) and concentrated under reduced pressure. The resulting aqueous layer was then extracted with EtOAc. The combined organic layers were washed with water, brine, dried over Na_2SO_4, and concentrated to dryness under reduced pressure. The crude product was purified by column chromatography on silica gel (10% EtOAc in CH_2Cl_2) to afford **9b** (0.16 g, 0.23 mmol, 26% yield).

^{1}H NMR (600 MHz, $CDCl_3$): δ 7.47–7.39 (m, 2H), 7.36–7.29 (m, 2H), 7.27 (m, 1H), 6.98 (d, *J* = 8.0 Hz, 2H), 6.78 (m, 1H), 6.73 (d, *J* = 8.0 Hz, 2H), 6.58 (m, 1H), 5.35 (m, 1H), 4.38 (d, *J* = 10.2 Hz, 1H), 4.12 (m, 1H), 4.00 (m, 2H), 3.84 (m, 1H), 3.74 (m, 1H), 3.29–3.15 (m, 2H), 2.69–2.56 (m, 2H), 2.14 (m, 1H), 1.45 (s, 9H), 0.97 (m, 15H), 0.17 (s, 6H). ^{13}C NMR (125 MHz, $CDCl_3$): δ 172.8, 171.7, 170.0, 155.8, 154.5, 133.9, 131.4 (2C), 130.5, 130.4 (2C), 129.6 (2C), 127.7, 120.1 (2C), 80.5, 64.6, 61.0, 56.0, 52.1, 49.6, 41.2, 35.3, 28.5 (3C), 27.8, 25.8 (3C), 19.5, 19.1, 18.3, −4.3 (2C). HRMS–ESI (*m*/*z*): $[M + Na]^+$ calcd for $C_{36}H_{53}N_3O_7SSiNa$, 722.3271; found, 722.3292.

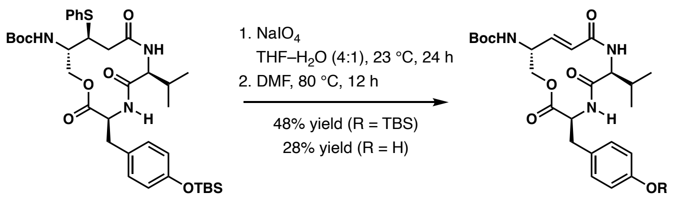

9b

9a: R = TBS

Unsaturated macrocyclic depsipeptide 9a. Sodium periodate (134 mg, 0.63 mmol, 10 equiv) was added to a solution of **9b** (44 mg, 0.063 mmol) in THF (4 mL) and water (1 mL) at 23 °C, and the reaction mixture was stirred at 23 °C for 24 h. The resulting solution was then quenched with a saturated aqueous solution of NaHCO$_3$ (5 mL) and extracted with EtOAc (3 × 5 mL). The combined organic layers were washed with water, dried over Na$_2$SO$_4$, and concentrated to dryness under reduced pressure. The residue was quickly filtered through a pad a silica gel with EtOAc and concentrated.

The crude residue was redissolved in DMF (2 mL), and the solution was heated at 80 °C for 12 h. The reaction mixture was cooled to room temperature, and a solution of a saturated aqueous NaHCO$_3$ (5 mL). The aqueous layer was then extracted with EtOAc (3 × 5 mL). The combined layers were washed with water, brine, dried over Na$_2$SO$_4$, and concentrated to dryness under reduced pressure. The crude product was purified by column chromatography on silica gel (50% EtOAc in CH$_2$Cl$_2$) to afford **9a** (17.8 mg, 0.030 mmol, 48% yield) and the desilylated product (R = H) (8.3 mg, 0.018 mmol, 28% yield).

9a (R = TBS): $[\alpha]_D^{23}$ −37.0 (*c* 1.0, MeOH). ^{1}H NMR (600 MHz, CD$_3$OD): δ 7.08 (d, *J* = 8.4 Hz, 2H), 6.95 (m, 1H), 6.74 (d, *J* = 8.4 Hz, 2H), 6.47 (dd, *J* = 15.6, 4.2 Hz, 1H), 6.28 (d, *J* = 15.6 Hz, 1H), 4.70 (m, 1H), 4.64–4.44 (m, 2H), 3.87–3.76 (m, 2H), 3.21–3.03 (m, 2H), 1.82 (m, 1H), 1.45 (s, 9H), 0.98 (s, 9H), 0.88 (d, *J* = 6.9 Hz, 3H), 0.77 (d, *J* = 6.9 Hz, 3H), 0.17 (s, 6H). ^{13}C NMR (100 MHz, CD$_3$OD): δ 174.1, 171.5, 157.1, 155.6 (2C), 142.0, 131.8, 131.3 (2C), 125.3, 121.0 (2C), 80.8, 78.1, 64.7, 56.2, 52.3, 34.9, 31.6, 30.8, 28.7 (3C), 26.2 (3C), 19.3, 19.1, −4.3 (2C). HRMS–ESI (*m*/*z*): $[M + Na]^+$ calcd for $C_{30}H_{47}N_3O_7SiNa$, 612.3081; found, 612.3084.

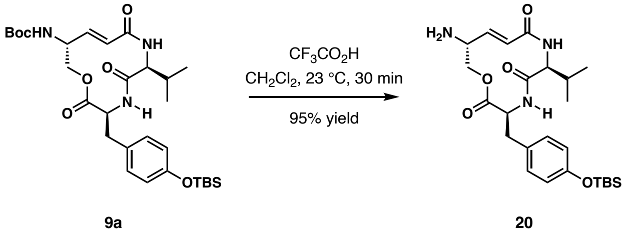

Amino macrocyclic depsipeptide 20: Trifluoroacetic acid (0.1 mL) was added to a solution of **9a** (16.5 mg, 0.028 mmol) in CH_2Cl_2 (0.40 mL) at 23 °C and the reaction mixture was stirred at 23 °C for 30 min. The resulting solution was then quenched with a solution of saturated aqueous $NaHCO_3$ (2 mL) and extracted with CH_2Cl_2 (3 × 5 mL). The combined organic layers were dried over Na_2SO_4 and concentrated to dryness under reduced pressure, affording **20** (13 mg, 0.027 mmol, 95% yield).

$[\alpha]_D^{23}$ −26.2 (*c* 1.0, MeOH). ^{1}H NMR (600 MHz, CD_3OD): δ 7.06 (d, *J* = 8.4 Hz, 2H), 6.72 (d, *J* = 8.4 Hz, 2H), 6.51 (dd, *J* = 15.6, 4.0 Hz, 1H), 6.32 (d, *J* = 15.6 Hz, 1H), 4.64 (d, *J* = 11.0 Hz, 1H), 4.43 (m, 1H), 3.86–3.71 (m, 3H), 3.12 (m, 2H), 1.78 (m, 1H), 0.96 (s, 9H), 0.88 (d, *J* = 6.8 Hz, 3H), 0.75 (d, *J* = 6.8 Hz, 3H), 0.15 (s, 6H). ^{13}C NMR (125 MHz, CD_3OD): δ 173.9, 172.9, 171.7, 155.6, 144.7, 131.90, 131.2 (2C), 124.8, 121.0 (2C), 66.1, 64.6, 55.7, 52.5, 34.9, 31.6, 30.7, 26.2 (3C), 19.3, 19.1, −4.3 (2C). LRMS–ESI (*m*/*z*): $[M + H]^+$ calcd for $C_{25}H_{40}N_3O_5Si$, 490.2737; found, 490.20.

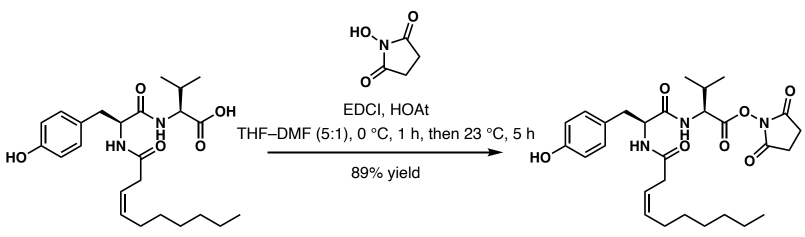

4

21

N-Hydroxysuccinimide ester 21. *N*-Hydroxysuccinimide (12 mg, 0.106 mmol, 2.0 equiv), HOAt (11 mg, 0.0795 mmol, 1.5 equiv), and EDCI hydrochloride (15 mg, 0.0795 mmol, 1.5 equiv) were added to a solution of acid **4** (23 mg, 0.0532 mmol) in THF (1 mL) and DMF (0.2 mL) at 0 °C. The reaction mixture was stirred at 0 °C for 1 h and then at 23 °C for 5 h. The resulting mixture was quenched with a saturated aqueous solution of NH_4Cl (5 mL), and the aqueous layer was extracted with CH_2Cl_2 (3 × 10 mL). The combined organic layers were washed with brine, dried over Na_2SO_4, and concentrated to dryness under reduced pressure. The crude product was purified by column chromatography on silica gel (60% EtOAc in hexanes) to give **21** (25 mg, 0.0473 mmol, 89% yield).

$[\alpha]_D^{23}$ −6.7 (*c* 1.0, $CHCl_3$). ^1H NMR (600 MHz, $CDCl_3$): δ 7.03 (d, *J* = 8.2 Hz, 2H), 6.73 (d, *J* = 8.2 Hz, 2H), 6.42 (d, *J* = 13.4, 8.1 Hz, 2H), 6.05 (s, 1H), 5.67 (m, 1H), 5.46 (m, 1H), 4.77 (dd, *J* = 8.5, 4.7 Hz, 1H), 4.62 (q, *J* = 7.5 Hz, 1H), 3.07–2.89 (m, 4H), 2.84 (s, 4H), 2.27 (m, 1H), 1.98 (m, 2H), 1.36–1.23 (m, 8H), 0.97 (d, *J* = 7.2 Hz, 3H), 0.95 (d, *J* = 7.2 Hz, 3H), 0.88 (t, *J* = 6.9 Hz, 3H). ^{13}C NMR (125 MHz, $CDCl_3$): δ 171.63, 171.27, 168.96, 167.04, 155.38, 136.05, 130.49, 127.77, 120.79, 115.90, 55.75, 54.91, 37.62, 35.08, 31.83, 31.51, 29.37, 29.09, 27.46, 25.75, 22.74, 18.74, 17.51, 14.22.

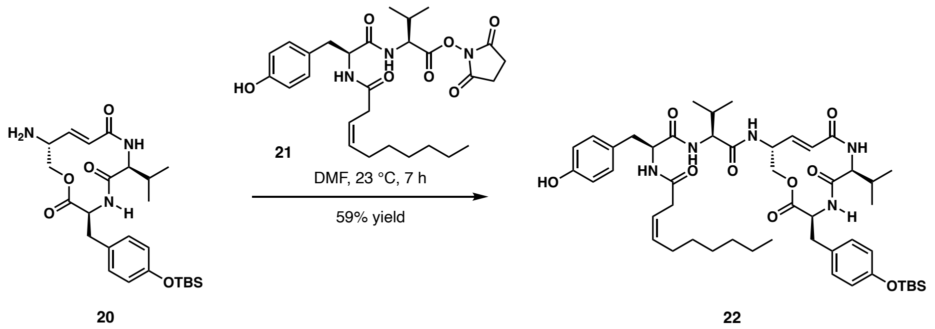

***O*-TBS-*N*-desmethyl thalassospiramide 22.** *N*-Hydroxysuccinimide ester **21** (12 mg, 0.0226 mmol, 1.7 equiv) was added to a solution of macrocyclic amine **20** (6.5 mg, 0.0133 mmol) in DMF (0.5 mL) at 23 °C. The reaction mixture was stirred at 23 °C for 7 h concentrated to dryness under reduced pressure. The crude residue was purified by column chromatography on silica gel (60% EtOAc in hexanes to 100% EtOAc) to afford **22** (7.1 mg, 0.00785 mmol, 59% yield).

$[\alpha]_D^{23}$ −23.3 (*c* 1.0, MeOH). ^{1}H NMR (600 MHz, CD_3OD): δ 7.09 (d, *J* = 8.2 Hz, 2H), 7.04 (d, *J* = 8.2 Hz, 2H), 6.74 (d, *J* = 8.2 Hz, 2H), 6.68 (d, *J* = 8.2 Hz, 2H), 6.49 (dd, *J* = 15.7, 4.3 Hz, 1H), 6.22 (d, *J* = 15.6 Hz, 1H), 5.52 (m, 1H), 5.41 (m, 1H), 4.84 (m, 1H), 4.78 (m, 1H), 4.60 (dd, *J* = 9.0, 5.5 Hz, 2H), 4.20 (m, 1H), 3.84 (dd, *J* = 11.7, 2.1 Hz, 1H), 3.78 (d, *J* = 5.8 Hz, 1H), 3.16 (dd, *J* = 14.5, 5.2 Hz, 1H), 3.08 (dd, *J* = 14.0, 5.7 Hz, 2H), 2.99–2.96 (m, 2H), 2.86–2.81 (m, 1H), 2.11 (h, *J* = 6.8 Hz, 1H), 1.99 (q, *J* = 7.0 Hz, 2H), 1.83 (h, *J* = 6.7 Hz, 1H), 1.38–1.22 (m, 8H), 1.04–0.80 (m, 21H), 0.75 (d, *J* = 6.9 Hz, 3H), 0.17 (s, 6H). ^{13}C NMR (125 MHz, CD_3OD): δ 174.3, 174.0, 173.9, 172.8, 171.5, 157.3, 155.7, 141.1, 135.0, 131.7, 131.3 (2C), 131.3 (2C), 128.8, 125.5, 122.7 (2C), 121.1 (2C), 116.2 (2C), 64.8, 64.0, 60.2, 56.4, 55.3, 51.2, 37.6, 35.3, 35.1, 32.9, 32.0, 31.6, 30.5, 30.1, 28.3, 26.2 (3C), 23.7, 19.9, 19.3, 19.2, 19.1, 18.6, 14.4, −4.3 (2C). HRMS–ESI (*m*/*z*): $[M + Na]^+$ calcd for $C_{49}H_{73}N_5O_9SiNa$, 926.5075; found, 926.5063.

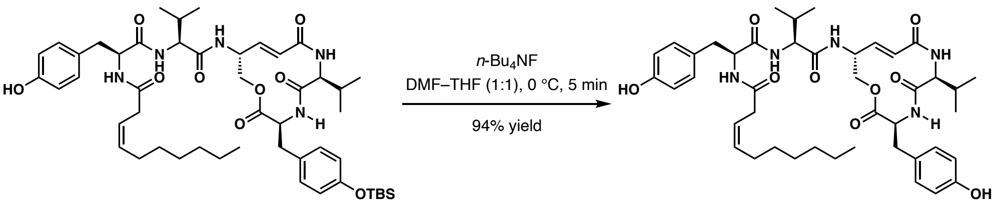

22 → 8

N-Desmethyl thalassospiramide C 8. Tetra-*n*-butylammonium fluoride (1.0 M in THF, 0.041 mL, 0.041 mmol, 1.5 equiv) was added to a solution of silyl ether **22** (24.8 mg, 0.027 mmol) in DMF (1.4 mL) and THF (1.4 mL) at 0 °C. The resulting mixture was stirred at 0 °C for 5 min, then quenched with a solution of saturated aqueous NH_4Cl and diluted with EtOAc. The aqueous layer was extracted with EtOAc. The combined organic layers were washed with brine, dried over Na_2SO_4, and concentrated to dryness under reduced pressure. The crude product was purified by column chromatography on silica gel (2% MeOH in EtOAc) to give **8** (0.020 g, 0.025 mmol, 94% yield).

$[\alpha]^{23}_{D}$ −25.6 (*c* 1.0, $CHCl_3$). ^{1}H NMR (600 MHz, $(CD_3)_2SO$): δ 9.15 (br, 2H), 8.42 (br, 1H), 7.98–7.92 (m, 3H) 7.06 (br, 1H), 6.99 (d, *J* = 12 Hz, 2H), 6. 96 (d, *J* = 12 Hz, 2H), 6.62 (d, *J* = 12 Hz, 2H), 6.59 (d, *J* = 12 Hz, 2H), 6.32 (dd, 1H), 6.27 (d, 1H), 5.43–5.32 (m, 2H), 4.78 (br, 1H), 4.45 (m, 2H), 4.22–4.15 (m, 2H), 3.69–3.68 (m, 2H), 3.05–3.02 (m, 2H), 2.91 (d, 1H), 2.85 (d, 1H), 2.65 (m, 1H), 2.00 (m, 1H), 1.94 (m, 2H), 1.77 (m, 1H), 1.30–1.20 (m, 8H), 0.88–0.78 (m, 12H), 0.7 (d, 3H). ^{13}C NMR (125 MHz, $(CD_3)_2SO$): δ 171.7, 171.28, 170.42, 170.33, 170.13, 162.31, 155.71, 155.66, 138.16, 131.79, 130.07 (2C), 129.91 (2C), 128.36, 127.83, 125.44, 123.05, 114.85 (2C), 114.73, 63.07, 62.16, 57.79, 54.21, 53.17, 48.34, 36.43, 34.11, 33.27, 31.15, 30.82, 28.84, 28.33, 26.82, 25.59, 22.08, 20.05, 19.23, 18.86, 18.37, 18.14, 13.96. HRMS–ESI (*m*/*z*): $[M + Na]^+$ calcd for $C_{43}H_{59}N_5O_9Na$, 812.4210; found, 812.4191.

Biochemical Potencies of *N*-Desmethyl Thalassospiramide C (8):

Materials and Methods:

All assays were performed in 384 well format and utilized peptide substrates that liberate fluorescence upon protease catalyzed cleavage. FLIPR plate readers (Molecular Devices Inc.) were used to monitor reactions and extract initial rates, which were then fit (four parameter logistic function) to obtain IC_{50} values. IC_{50} values are the average of 2 or more determinations. All enzymes are human. Calpain 2 was cloned, expressed, and purified at Blade Therapeutics. Biochemical potencies against calpain and cathepsin proteases are summarized in Table 2 (see page 14). All other enzymes and reagents were obtained commercially and are summarized with assay conditions in Table 6.

Table 6. Enzyme and Reagents with Assay Conditions.

Enzyme	Enzyme Conc (nM)	Substrate (conc 1 μM)	Assay Buffer
Calpain 1	10	5-FAM/QXL520 Calpain	Tris–HCl 50 mM, NaCl 100 mM, 2mM $CaCl_2$ DTT 1 mM, Brij-35 0.02%, pH 7.4
Calpain 2	30	5-FAM/QXL520 Calpain	Tris–HCl 50 mM, NaCl 100 mM, 2mM $CaCl_2$ DTT 1 mM, Brij-35 0.02%, pH 7.4
Cathepsin B	25	QXL520/HiLyteFluor488 CatB	25 mM MES, 5 mM DTT, pH 5.0
Cathepsin K	10	QXL520/HiLyte Fluor 488 CatK	50 mM NaOAc, pH 5.5, 2.5 mM EDTA, 1 mM DTT, 0.01% TritonX-100
Cathepsin L	0.025	QXL™ 520/HiLyte Fluor™ 488 CatL	50 mM MES, 5 mM DTT, 1 mM EDTA, 0.005% (w/v) Brij-35, pH 6.0
Catehpsin S	6	5-Fam/QXL520 CatS	50 mM NaOAc, 5 mM DTT, 250 mM NaCl, pH 4.5
All enzymes were pre-incubated with inhibitor for 30 minutes prior to substrate addition.			

Protein Production, Crystallization and Structure Determination:

Human Cathepsin K (16-329) was produced by refolding from inclusion bodies as described in literature.[114] In short, refolded protein was auto activated at pH = 4.0 to Cathepsin K (115-329) followed by a two-step purification including ion exchange chromatography and size exclusion chromatography. Purified protein was concentrated to 8 mg/mL in 50 mM sodium acetate pH 5.5 and flash frozen in liquid nitrogen for storage at –80 °C. For crystallization experiments Cathepsin K (115-329) (8 mg/mL) was incubated with 0.5 mM compound **8** (2753) and 2 mM DTE on ice for 1 h, followed by mixing of 0.1 µL protein solution (8.0 mg/mL CatK; 50 mM NaOAc pH 5.5, 0.5 mM ligand) with 0.1 µL precipitant solution (0.05 M MES pH 6.0, 0.1 M Na–Oxalate, 0.1 M $CaCl_2$). Crystallization drops were equilibrated against 50 µl precipitant solution and incubated at 4 °C. Plate shaped crystals appeared within 4 days and grew to full size within 7 days. Crystals were cryo-protected by precipitant solution supplemented with 25% (v/v) glycerol and flash frozen in liquid nitrogen. A complete dataset was collected at the Swiss Light Source under cryogenic conditions. The crystals belong to space group P 2_1 and the data were processed using the programs XDS and XSCALE.[115] The phase information necessary to determine and analyze the structure was obtained by molecular replacement and subsequent model building and refinement was performed with the software packages CCP4[116] and COOT[117].

Table 7. Crystallographic Data Collection and Refinement Statistics. (PDB code 6HGY)

	6HGY
Data Collection	
X-ray source	PXII/X10SA (SLS[1])
Wavelength [Å]	0.9999
Detector	PILATUS 6M
Temperature [K]	100
Space group	$P\ 2_1$
Unit cell parameters	
a; b; c; [Å]	45.55; 44.94; 49.97
A, β, γ [°]	90.0; 115.9; 90.0
Resolution range [Å]	2.17 (2.42–2.17)
Unique reflections	8527 (2101)
Multiplicity	3.8 (3.9)
Completeness [%]	86.9 (77.8)
R_{sym} [%]	11.4 (42.5)
R_{meas} [%]	13.4 (49.3)
$CC_{1/2}$	98.8 (87.4)
<1/σ(l)>	7.69 (3.15)
Refinement	
Resolution [Å]	44.97–2.17
Number of reflections (working/test)	6790/782
R_{work} [%]	25.0
R_{free} [%]	31.0
Total number of atoms:	
Protein	1657
Water	19
Ligand	57
Deviation from ideal geometry:	
Bond lengths [Å]	0.011
Bond angles [°]	1.61
Bonded B's [Å^2]	1.2
Ramachandran plot:	
Most favored regions [%]	84.0
Additional allowed regions [%]	16.0
Generously allowed regions [%]	0.0
Disallowed regions [%]	0.0

The crystal electron density map of **8** with cathepsin K is depicted in Figure 10. Wherein the ligand molecule is shown superimposed with the refined 2Fo-Fc electron density map contoured at 1.0 s.

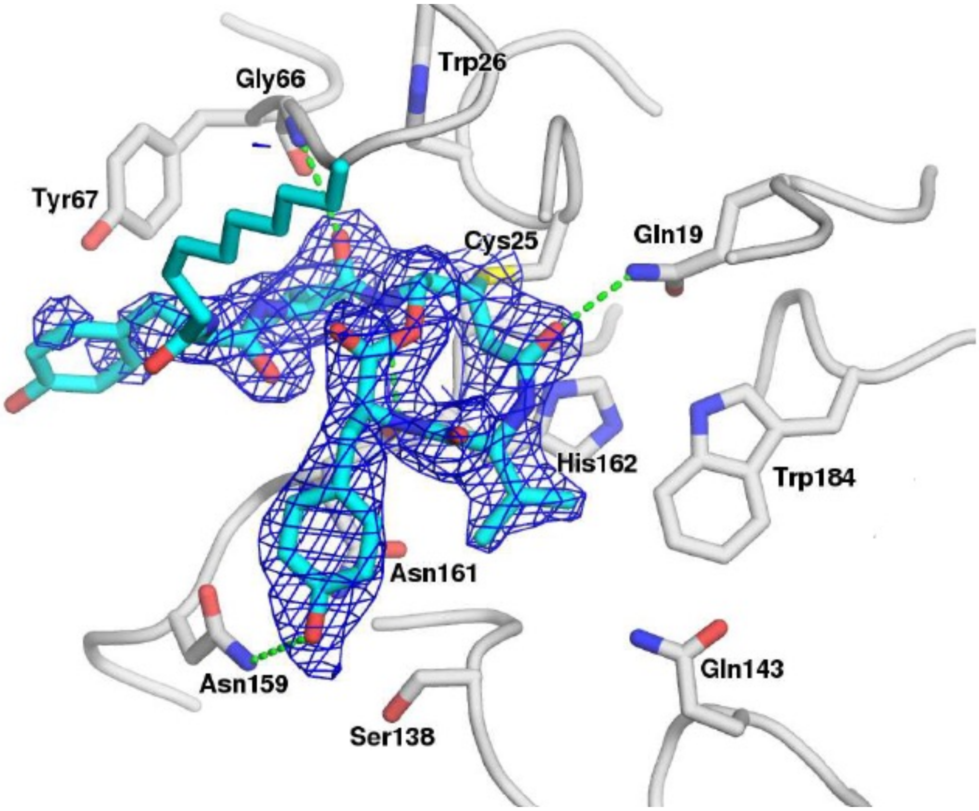
Gly66
Trp26
Tyr67
Cys25
Gln19
His162
Trp184
Asn161
Asn159
Gln143
Ser138

Figure 10. Crystal electron density map for the covalent complex of **8** with cathepsin K.

CHAPTER 2 EXPERIMENTAL PROCEDURES

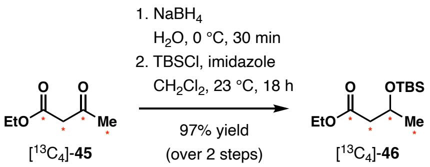

[$^{13}C_4$]-**45** [$^{13}C_4$]-**46**

Ethyl ester [$^{13}C_4$]-46. A solution of sodium borohydride (93 mg, 2.50 mmol, 0.33 equiv) in water (1.0 mL) was added in three portions over 5 min to a heterogeneous mixture of commercially available ethyl [$^{13}C_4$]-acetoacetate ([$^{13}C_4$]-**45**, 1.00 g, 7.5 mmol) and water (2.0 mL) at 0 °C. The reaction mixture was stirred at 0 °C for 30 min, and then carefully quenched by slow addition of 1 M aqueous hydrochloric acid solution (2 mL), followed by the addition of solid NaCl (1.35 g). The product was extracted with CH_2Cl_2 (6 × 15 mL), and the combined organic layers were dried over Na_2SO_4 and concentrated under reduced pressure at 0 °C. The crude product was submitted to the next step without further purification.

The crude β-hydroxyester was dissolved in CH_2Cl_2 (15 mL) and the solution was cooled to 0 °C. Imidazole (1.23 g, 17.6 mmol, 2.4 equiv) and TBSCl (1.36 g, 9.02 mmol, 1.2 equiv) were added sequentially at 0 °C. The reaction mixture was stirred at 0 °C for 30 min, then warmed to 23 °C and left to stir for another 12 h. The resulting solution was quenched with water (50 mL), and the product was extracted with CH_2Cl_2 (3 × 50 mL). The combined organic layers were dried over Na_2SO_4 and concentrated to dryness under reduced pressure. The crude product was purified by column chromatography on silica gel (5% EtOAc in hexanes) to give ethyl ester [$^{13}C_4$]-**46** (1.80 g, 7.2 mmol, 97% yield over 2 steps) as a colorless liquid.

^{1}H NMR (500 MHz, $CDCl_3$) δ 4.25 (dm, *J* = 151.7 Hz, 1H), 4.16–4.04 (m, 2H), 2.44 (dm, *J* = 134.0 Hz, 1H), 2.34 (dm, *J* = 126.4 Hz, 1H), 1.24 (t, *J* = 10 Hz, 6H), 1.17 (ddd, *J* = 125.9, 10.5, 4.6 Hz, 1H), 0.85 (s, 9H), 0.05 (s, 3H), 0.03 (s, 3H). ^{13}C NMR (125 MHz, $CDCl_3$): δ 171.8 (dd, *J*

= 57.6, 3.5 Hz), 66.0 (td, *J* = 39.2, 1.3 Hz), 60.4 (d, *J* = 2.4 Hz), 45.1 (ddd, *J* = 57.7, 38.9, 1.8 Hz), 25.9, 24.1 (ddd, *J* = 39.4, 3.5, 1.7 Hz), 18.1, 14.3, −4.4, −4.9. HRMS–ESI (*m/z*): $[M + H]^+$ calcd for $^{13}C_4C_8H_{26}O_3SiNa$, 273.1683; found, 273.1683.

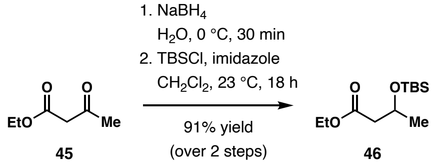

Ethyl ester 46. The title compound was obtained using the procedure described above for its $^{13}C_4$ analog starting from 9.05 g (69.6 mmol) of ethyl acetoacetate **45** (natural isotope), 0.87 g (23.0 mmol, 0.33 equiv) of sodium borohydride, and 27.0 mL of water for the first step. The second step was performed using 12.6 g (83.5 mmol, 1.2 equiv) of TBSCl, and 11.4 g (167.0 mmol, 2.4 equiv) of imidazole in 135 mL of CH_2Cl_2. Ethyl ester **46** was obtained in 91% yield (15.6 g, 63.3 mmol) over 2 steps.

^1H NMR (500 MHz, $CDCl_3$): δ 4.30–4.24 (m, 1H), 4.16–4.07 (m, 2H), 2.45 (dd, *J* = 14.5, 7.6 Hz, 1H), 2.35 (dd, *J* = 14.5, 5.3 Hz, 1H), 1.26 (t, *J* = 7.15 Hz, 3H), 1.19 (d, *J* = 6.15 Hz, 3H), 0.86 (s, 9H), 0.06 (s, 3H), 0.04 (s, 3H). ^{13}C NMR (125 MHz, $CDCl_3$): δ 171.8, 66.0, 60.4, 45.1, 25.8, 24.1, 18.1, 14.3, −3.4, −4.9. HRMS–ESI (*m/z*): $[M + Na]^+$ calcd for $C_{12}H_{26}O_3SiNa$, 269.1549; found, 269.1553.

Allylic Alcohol 44:

Chiral Allylic Alcohol [$^{13}C_4$]-**44**:

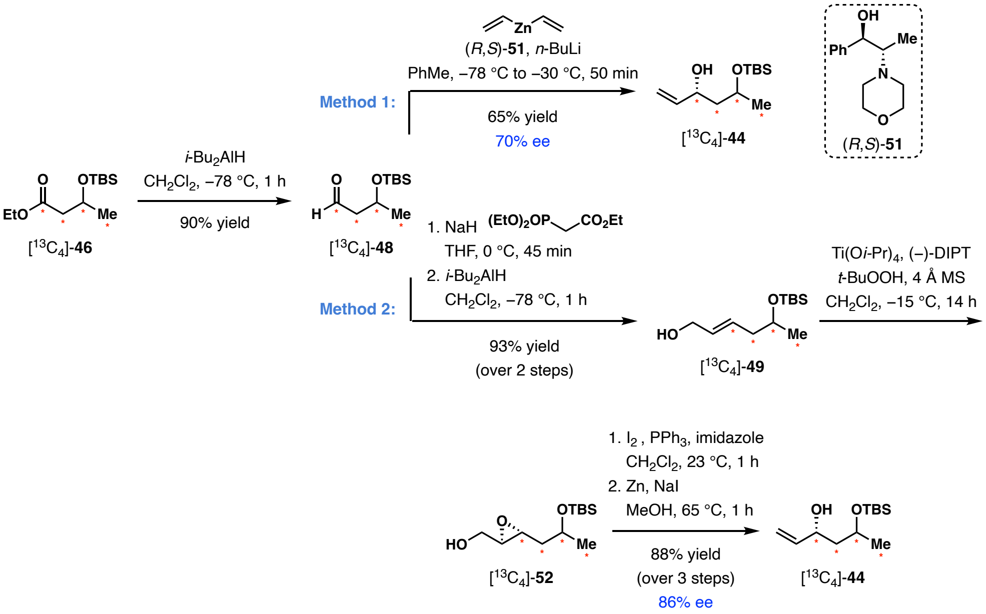
(R,S)-51, n-BuLi
PhMe, –78 °C to –30 °C, 50 min
Method 1:
65% yield
70% ee
[13C4]-44
(R,S)-51
i-Bu2AlH
CH2Cl2, –78 °C, 1 h
90% yield
[13C4]-46
[13C4]-48
1. NaH (EtO)2OP CO2Et
THF, 0 °C, 45 min
2. i-Bu2AlH
CH2Cl2, –78 °C, 1 h
Method 2:
93% yield
(over 2 steps)
[13C4]-49
Ti(Oi-Pr)4, (–)-DIPT
t-BuOOH, 4 Å MS
CH2Cl2, –15 °C, 14 h
1. I2, PPh3, imidazole
CH2Cl2, 23 °C, 1 h
2. Zn, NaI
MeOH, 65 °C, 1 h
88% yield
(over 3 steps)
86% ee
[13C4]-52
[13C4]-44

Racemic Allylic Alcohol (±)-[$^{13}C_4$]-**44**:

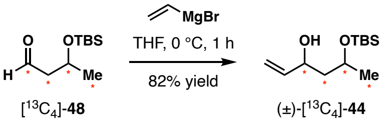
MgBr
THF, 0 °C, 1 h
82% yield
[13C4]-48
(±)-[13C4]-44

Chiral Allylic Alcohol 44 – Method 1 (via Enantioselective Divinyl Zinc Addition):

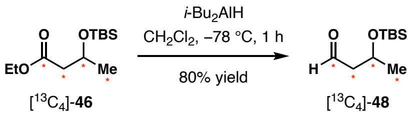
i-Bu2AlH
CH2Cl2, –78 °C, 1 h
80% yield
[13C4]-46
[13C4]-48

Aldehyde [$^{13}C_4$]-48. *i*-Bu$_2$AlH (1.27 mL, 7.10 mmol, 1.05 equiv) was added dropwise over 30 min to a solution of ethyl ester [$^{13}C_4$]-**46** (1.68 g, 6.80 mmol) in CH$_2$Cl$_2$ (40 mL) at −78 °C. The resulting solution was stirred at −78 °C for 1 h before 2 mL of MeOH was added dropwise over 2 min. After 5 min, the reaction mixture was warmed to 23 °C, and a saturated solution of potassium sodium tartrate (20 mL) was added. The resulting heterogeneous mixture was stirred vigorously at 23 °C for 1 h. The layers were separated, and the aqueous layer was extracted with CH_2Cl_2 (4 × 30 mL). The combined organic layers were dried over Na_2SO_4, and the solvent was removed under reduced pressure on a rotary evaporator (bath temperature 7 °C). The crude product was purified by column chromatography on silica gel (5% EtOAc in hexanes) to give [$^{13}C_4$]-**48** (1.05 g, 5.19 mmol, 80% yield).

^{1}H NMR (400 MHz, $CDCl_3$): δ 9.80 (s, 1H), 4.45–4.30 (m, 1H), 2.63–2.38 (m, 2H), 1.24 (d, *J* = 6.12 Hz, 3H), 0.98 (s, 9H), 0.08 (s, 3H), 0.06 (s, 3H). ^{13}C NMR (125 MHz, $CDCl_3$): δ 202.3, 64.7, 53.1, 25.9, 24.3, 18.1, −4.2, −4.8. HRMS–ESI (*m/z*): [M + Na + CH_3OH]$^+$ calcd for $^{13}C_4C_7H_{26}O_3SiNa$, 261.1683; found, 261.1675.

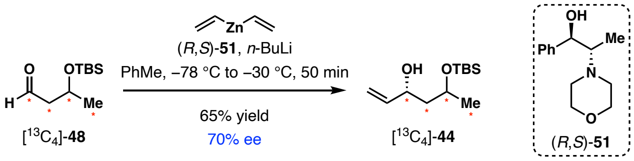

Chiral allylic alcohol [$^{13}C_4$]-44. A solution of *n*-butyllithium in hexanes (2.50 M, 0.350 mL, 0.872 mmol, 2.0 equiv) was added dropwise over 3 min to a solution of (1*R*,2*S*)-2-morpholin-4-yl-1-phenylpropanol **51** (0.193 g, 0.872 mmol, 2.0 equiv) in toluene (1 mL) at 0 °C. The resulting solution was stirred for 30 min at 0 °C before a divinyl zinc solution[118] (0.289 M, 3.02 mL, 0.872 mmol, 2.0 equiv) was added dropwise over 5 min at 0 °C. The resulting solution was then stirred at 0 °C for an additional 1 h before it was cooled to −78 °C. A solution of aldehyde [$^{13}C_4$]-**48** (88 mg, 0.436 mmol) in toluene (0.55 mL) was added to the reaction mixture. The reaction mixture was stirred at −78 °C for 40 min, and then raised to −30 °C to stir for another 10 min. An aqueous citric acid solution (30% by weight, 5 mL) was then added slowly to the reaction solution, and the solution was diluted with EtOAc (5 mL). The aqueous layer was extracted with EtOAc (3 × 5 mL). The combined organic layers were washed with 1 M aqueous NaOH solution (4 × 5 mL), brine (5 mL), dried over Na_2SO_4, and concentrated to dryness under reduced pressure. The crude product was purified by column chromatography on silica gel (1% EtOAc in hexanes to 5% EtOAc in hexanes) to give $[^{13}C_4]$-**44** (65 mg, 0.282 mmol, 65% yield). The enantiopurity of the material (70% ee) was measured by HPLC trace analysis after derivatization to compound $[^{13}C_4]$-**S7** (see page 132).

^1H NMR (600 MHz, $CDCl_3$, a mixture of diastereomers): δ 5.90–5.80 (m, 2H), 5.29–5.22 (m, 2H), 5.10–5.03 (m, 2H), 4.58–3.9 (m, 4H), 3.31 (br. s, 2H), 1.81–1.65 (m, 2H), 1.58–1.46 (m, 2H), 1.22 (ddd, *J* = 125.6, 6.2, 4.3 Hz, 3H), 1.18 (ddd, *J* = 125.7, 6.9, 4.5 Hz), 0.89 (s, 9H), 0.89 (s, 9H), 0.11 (s, 3H), 0.10 (s, 3H), 0.08 (s, 3H), 0.08 (s, 3H). ^{13}C NMR (150 MHz, $CDCl_3$, mixture of diastereomers): δ 141.3 (dd, *J* = 47.0, 3.7 Hz), 140.86 (dd, *J* = 47.6, 4.1 Hz), 114.0 (dd, *J* = 31.5, 2.9 Hz), 72.3 (ddd, *J* = 37.0, 3.7, 1.2 Hz), 69.7 (ddd, *J* = 37.2, 2.7, 2.0 Hz), 69.6 (td, *J* = 39.3, 1.1 Hz), 67.2 (td, *J* = 39.1, 1.9 Hz), 46.1 (dd, *J* = 38.9, 37.4 Hz), 44.6 (dd, *J* = 38.4, 37.3 Hz), 25.95, 25.94, 24.6 (ddd, *J* = 38.8, 3.7, 0.9 Hz), 23.21 (ddd, *J* = 39.0, 2.7, 0.8 Hz), 18.06 (d, *J* = 0.8 Hz), 18.03 (d, *J* = 0.9 Hz), −3.7, −4.3, −4.7, −4.8. HRMS–ESI (*m/z*): $[M + Na]^+$ calcd for $^{13}C_4C_8H_{26}O_2SiNa$, 257.1734; found, 257.1727.

Chiral Allylic Alcohol 44 – Method 2 (via Sharpless Asymmetric Epoxidation):

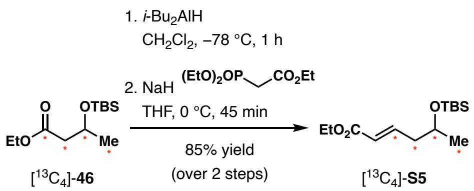

Ethyl ester $[^{13}C_4]$-S5. *i*-Bu_2AlH (1.27 mL, 7.10 mmol, 1.05 equiv) was added dropwise over 30 min to a solution of ethyl ester $[^{13}C_4]$-**46** (1.68 g, 6.80 mmol) in CH_2Cl_2 (40 mL) at −78 °C.

The resulting solution was stirred at −78 °C for 1 h before 2 mL of MeOH was added dropwise over 2 min. After 5 min, the reaction mixture was warmed to 23 °C, and a saturated solution of potassium sodium tartrate (20 mL) was added. The resulting heterogeneous mixture was stirred vigorously at 23 °C for 1 h. The layers were separated, and the aqueous layer was extracted with CH_2Cl_2 (4 × 30 mL). The combined organic layers were dried over Na_2SO_4, and the solvent was removed under reduced pressure on a rotary evaporator (bath temperature 7 °C). The crude aldehyde was submitted to the next step without further purification.

Triethyl phosphonoacetate (1.98 g, 8.83 mmol, 1.3 equiv) was added dropwise over 10 min to a suspension of sodium hydride (0.33 g, 8.15 mmol, 1.2 equiv; 60% sodium hydride suspension in mineral oil was used) in THF (20 mL) at 0 °C. The mixture was stirred until homogeneity was observed (approximately 30 min). A solution of the crude aldehyde from the previous step in THF (3 mL) was then added, and the reaction mixture was stirred at 0 °C for 30 min. A saturated aqueous solution of NH_4Cl (20 mL) was added to the reaction mixture, and the aqueous layer was extracted with EtOAc (4 × 30 mL). The combined organic layers were dried over Na_2SO_4 and concentrated to dryness under reduced pressure. The crude product was purified by column chromatography on silica gel (1% EtOAc in hexanes to 5% EtOAc in hexanes) to give [$^{13}C_4$]-**S5** (1.60 g, 5.77 mmol, 85% yield over 2 steps) as a colorless liquid.

^{1}H NMR (500 MHz, $CDCl_3$): δ 6.90 (dddd, *J* = 155.6, 15.3, 7.5, 2.7 Hz, 1H), 5.78 (dd, *J* = 15.6, 5.5 Hz, 1H), 4.14 (q, *J* = 7.2 Hz, 2H), 3.87 (dm, *J* = 140.5 Hz, 1H), 2.27 (d, *J* = 127.7, 2H), 1.24 (t, *J* = 7.1 Hz, 3H), 1.11 (ddd, *J* = 125.3, 5.9, 4.5 Hz, 3H), 0.84 (s, 9H), 0.01 (s, 3H), 0.00 (s, 3H). ^{13}C NMR (125 MHz, $CDCl_3$): 166.5 (d, *J* = 6.4 Hz), 146.13 (d, J = 42.3 Hz), 123.3 (dd, *J* = 70.4, 2.2 Hz), 67.8 (d, *J* = 39.9, 38.1, 2.0 Hz), 60.2, 42.55 (ddd, *J* = 42.3, 38.1, 1.3 Hz), 25.9, 23.9 (ddd, *J* = 39.7, 2.6, 1.2 Hz), 18.2, 14.4, −4.4, −4.7. HRMS–ESI (*m/z*): [M + Na]$^+$ calcd for $^{13}C_4C_{10}H_{28}O_3SiNa$, 299.1840; found, 299.1843.

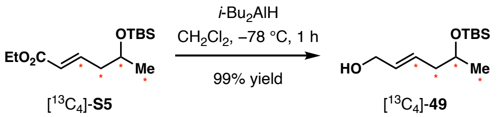

OTBS
EtO2C
Me
[13C4]-S5
i-Bu2AlH
CH2Cl2, −78 °C, 1 h
99% yield
OTBS
HO
Me
[13C4]-49

Allylic alcohol [$^{13}C_4$]-49. *i*-Bu$_2$AlH (2.40 mL, 13.3 mmol, 2.3 equiv) was added dropwise over 5 min to a solution of ethyl ester [$^{13}C_4$]-**S5** (1.60 g, 5.80 mmol) in CH_2Cl_2 (115 mL) at −78 °C. The resulting solution was stirred at −78 °C for 1 h, and a saturated solution of potassium sodium tartrate (60 mL) was added. The resulting heterogeneous mixture was stirred vigorously at 23 °C for 3 h. The layers were separated, and the aqueous layer was extracted with CH_2Cl_2 (3 × 70 mL). The combined organic layers were dried over Na_2SO_4 and concentrated to dryness under reduced pressure. The crude product was purified by column chromatography on silica gel (30% EtOAc in hexanes) to afford product [$^{13}C_4$]-**49** (1.35 g, 5.76 mmol, 99% yield) as a pale yellow oil.

^{1}H NMR (500 MHz, $CDCl_3$): δ 5.71–5.61 (m, 1H), 5.68 (dm, *J* = 153.4, 1H), 4.12–4.07 (m, 2H), 3.84 (dm, *J* = 139.9, 1H), 2.17 (dm, *J* = 125.9 Hz, 2H), 1.43 (br. s, 1H), 1.12 (ddd, *J* = 125.5, 6.0, 4.4 Hz, 3H), 0.88 (s, 9H), 0.04 (s, 3H), 0.03 (s, 3H). ^{13}C NMR (125 MHz, $CDCl_3$): δ 131.3 (dt, *J* = 71.6, 2.5 Hz), 129.9 (dt, *J* = 43.5, 2.2 Hz), 68.5 (ddd, *J* = 40.1, 38.5, 2.0 Hz), 63.9 (dd, *J* = 5.7, 1.5 Hz), 42.7 (ddd, *J* = 43.4, 38.5, 1.1 Hz), 37.7 (ddd, *J* = 42.7, 39.0, 1.3 Hz), 26.0, 23.6 (ddd, *J* = 39.8, 2.4, 1.2 Hz), −4.4, −4.6. HRMS–ESI (*m*/*z*): $[M + Na]^+$ calcd for $^{13}C_4C_8H_{26}O_2SiNa$, 257.1734; found, 257.1739

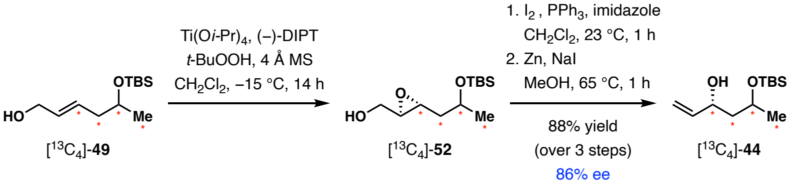

OTBS
HO
Me
[13C4]-49
Ti(Oi-Pr)4, (−)-DIPT
t-BuOOH, 4 Å MS
CH2Cl2, −15 °C, 14 h
O
OTBS
HO
Me
[13C4]-52
1. I2 , PPh3, imidazole
CH2Cl2, 23 °C, 1 h
2. Zn, NaI
MeOH, 65 °C, 1 h
88% yield
(over 3 steps)
86% ee
OH
OTBS
Me
[13C4]-44

Chiral allylic alcohol [$^{13}C_4$]-44. Crushed 4 Å molecular sieves (0.27 g) and Ti(O*i*-Pr)$_4$ (0.24 mL, 0.81 mmol, 0.14 equiv) were added sequentially to a solution of (−)-diisopropyl D-tartrate

(0.24 g, 1.03 mmol, 0.18 equiv) in CH_2Cl_2 (9 mL) at −5 °C, and the mixture was stirred at −5 °C for 15 min. The mixture was then cooled to −20 °C and *t*-BuOOH[119] (2.1 mL of 5.5 M solution, 11.4 mmol, 2.0 equiv) was added to stir at −20 °C for 15 min. A solution of alcohol [$^{13}C_4$]-**49** (1.34 g, 5.72 mmol) in CH_2Cl_2 (2.5 mL) was added, and the reaction mixture was stirred at −15 °C for 24 h. The reaction mixture was then diluted with Et_2O (25 mL) and quenched by the addition of a saturated solution of Na_2SO_4 (15 mL). After stirring at 23 °C for 1 h, the aqueous layer was extracted with EtOAc (4 × 30 mL). The combined organic layers were dried over Na_2SO_4 and concentrated to dryness under reduced pressure. The crude product [$^{13}C_4$]-**52** was submitted to the next step without further purification.

Triphenylphosphine (4.50 g, 17.16 mmol, 3.0 equiv) and imidazole (2.92 g, 42.9 mmol, 7.5 equiv) were added sequentially to a solution of the crude epoxide [$^{13}C_4$]-**52** in CH_2Cl_2 (57 mL) at 23 °C. The mixture was then cooled to 0 °C and crushed iodine (4.36 g, 17.16 mmol, 3.0 equiv) was added. The reaction mixture was stirred at 0 °C for 10 min before warming to 23 °C to let stir for another 1 h. The reaction mixture was then diluted with CH_2Cl_2 (80 mL) and washed with a 1:1 mixture of saturated aqueous solutions of $NaHCO_3$ and $Na_2S_2O_3$ (100 mL). The layers were separated, and the aqueous layer was extracted with CH_2Cl_2 (3 × 30 mL). The combined organic layers were dried over Na_2SO_4 and concentrated to dryness under reduced pressure. Et_2O (30 mL) was added to the dry solid residue and crushed with a spatula. The precipitate was filtered and washed with an additional portion of Et_2O (20 mL). The filtrate was concentrated under reduced pressure, and the crude product was purified by column chromatography on silica gel (3% EtOAc in hexanes to 8% EtOAc in hexanes) to produce the unstable iodide that was immediately submitted to the next step.

Zinc (1.86 g, 28.6 mmol, 5.0 equiv) and sodium iodide (2.15 g, 14.3 mmol, 2.5 equiv) were added sequentially to a solution of the iodide from the previous step in MeOH (29 mL) at 23 °C.

The reaction mixture was heated to reflux and vigorously stirred for 1 h. The mixture was then cooled to 23 °C, and the solvent was evaporated under reduced pressure. Water (20 mL) and CH_2Cl_2 were added to dry residue, and the white precipitate formed was then filtered and washed with CH_2Cl_2 (2 × 20 mL). The layers of the filtrate were then separated, and the aqueous layer was extracted with CH_2Cl_2 (2 × 15 mL). The combined organic layers were dried over Na_2SO_4 and concentrated to dryness under reduced pressure. The crude product was purified by column chromatography on silica gel (5% EtOAc in hexanes to 15% EtOAc in hexanes) to give [$^{13}C_4$]-**44** (1.18 g, 5.03 mmol, 88% yield over 3 steps) as a pale yellow oil. The enantiopurity of the material (86% ee) was measured by HPLC trace analysis after derivatization to compound [$^{13}C_4$]-**S7** (see page 132). The ^{1}H NMR, ^{13}C NMR, and mass spectral data are in full agreement with those for the compound obtained by method 1 (see page 123).

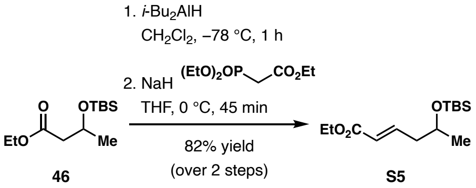

Ethyl ester S5. The title compound was obtained using the procedure described above for its $^{13}C_4$ analog starting from 4.88 g (19.8 mmol) of ethyl ester **46** and 3.71 mL (20.8 mmol, 1.05 equiv) of *i*-Bu_2AlH in 115 mL of CH_2Cl_2 for the first step. The second step was performed using 0.95 g (23.8 mmol, 1.2 equiv) of 60% sodium hydride suspension in mineral oil, and 5.8 g (25.7 mmol, 1.3 equiv) of triethyl phosphonoacetate in 66 mL of THF. Ethyl ester **S5** was obtained in 82% yield (4.42 g, 16.2 mmol) over 2 steps.

^{1}H NMR (500 MHz, $CDCl_3$): δ 6.99–6.87 (m, 1H), 5.84 (d, *J* = 15.65 Hz, 1H), 4.17 (q, *J* = 7.15 Hz, 2H), 3.96–3.89 (m, 1H), 2.38–2.24 (m, 2H), 1.28 (t, *J* = 16.1 Hz, 3H), 1.15 (d, *J* = 6.1 Hz, 3H), 0.88 (s, 9H), 0.04 (s, 3H), 0.04 (s, 3H). ^{13}C NMR (125 MHz, $CDCl_3$): δ 166.6, 146.2, 123.4, 67.8, 60.3, 42.6, 26.0, 23.9, 18.2, 14.4, −4.4, −4.7. HRMS–ESI (*m/z*): $[M + Na]^+$ calcd for $C_{14}H_{28}O_3SiNa$, 295.1705; found, 295.1711.

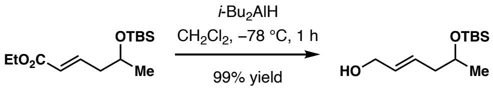
OTBS
EtO2C
Me
i-Bu2AlH
CH2Cl2, −78 °C, 1 h
99% yield
HO
OTBS
Me

S5 **49**

Allylic alcohol 49. The title compound was obtained using the procedure described above for its $^{13}C_4$ analog using 5.7 g (20.9 mmol) of ethyl ester **S5** and 8.6 mL (48.1 mmol, 2.3 equiv) of *i*-Bu_2AlH in 420 mL of CH_2Cl_2. Allylic alcohol **49** was obtained in 99% yield (4.8 g, 20.83 mmol).

^1H NMR (500 MHz, $CDCl_3$): δ 5.75–5.60 (m, 2H), 4.11–4.08 (m, 2H), 3.86–3.80 (m, 1H), 2.25–2.09 (m, 2H), 1.13 (d, *J* = 6.1 Hz, 3H), 0.88 (s, 9H), 0.04 (s, 3H), 0.04 (s, 3H). ^{13}C NMR (125 MHz, $CDCl_3$): δ 131.3, 130.0, 68.6, 64.0, 42.7, 26.0, 23.6, 18.3, −4.4, −4.6. HRMS–ESI (*m/z*): $[M + Na]^+$ calcd for $C_{12}H_{26}O_2SiNa$, 253.1600; found, 253.1605.

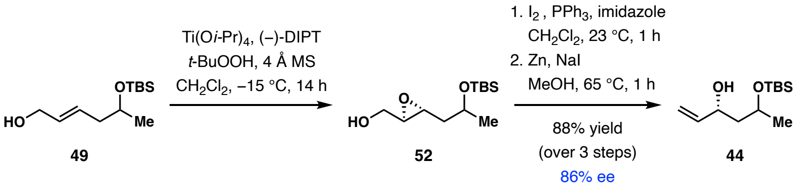
OTBS
HO
Me
Ti(Oi-Pr)4, (–)-DIPT
t-BuOOH, 4 Å MS
CH2Cl2, –15 °C, 14 h
O
OTBS
HO
Me
1. I2 , PPh3, imidazole
CH2Cl2, 23 °C, 1 h
2. Zn, NaI
MeOH, 65 °C, 1 h
88% yield
(over 3 steps)
86% ee
OH
OTBS
Me

49 **52** **44**

Chiral allylic alcohol 44. The title compound was obtained using the procedure described above for its $^{13}C_4$ analog starting from 1.53 g (6.64 mmol) of allylic alcohol **49**. The following reagents were used with the indicated quantities: Ti(O*i*-Pr)$_4$ (0.14 mL, 0.46 mmol, 0.14 equiv); (−)-DIPT (0.13 mL, 0.60 mmol, 0.18 equiv); *t*-BuOOH (2.6 mL of 5.14 M solution, 13.28 mmol, 2.0 equiv); iodine (5.0 g, 19.92 mmol, 3.0 equiv); triphenylphosphine (5.2 g, 19.92 mmol, 3.0 equiv); imidazole (3.4 g, 49.8 mmol, 7.5 equiv); zinc (2.16 g, 33.2 mmol, 5.0 equiv); sodium iodide (2.5 g, 16.6 mmol, 2.5 equiv). Pure allylic alcohol **44** was obtained in 85% yield (1.30 g, 5.64 mmol) as a clear oil over 3 steps. The enantiopurity of the material (86% ee) was measured by HPLC trace analysis after derivatization to compound **S7** (see page 132).

^{1}H NMR (500 MHz, $CDCl_3$, mixture of diastereomers): δ 5.91–5.78 (m, 2H), 5.32–5.22 (m, 2H), 5.11–5.05 (m, 2H), 4.48–4.42 (m, 1H), 4.32–4.24 (m, 1H), 4.22–4.14 (m, 1H), 4.13–4.05 (m, 1H), 3.38 (s, 1H), 3.27 (s, 1H), 1.69–1.58 (m, 4H), 1.23 (d, J = 6.3 Hz, 3H), 1.19 (d, J = 6.1 Hz, 3H), 0.91 (s, 9H), 0.90 (s, 9H), 0.12 (s, 3H), 0.11 (s, 3H), 0.09 (s, 3H), 0.09 (s, 3H). ^{13}C NMR (150 MHz, $CDCl_3$, mixture of diastereomers): δ 141.3, 140.9, 114.1, 113.9, 72.3, 69.7, 69.6, 67.3, 46.1 44.6, 25.95, 25.94, 24.7, 23.2, 18.6, 18.0, −3.74, −4.3, −4.7 −4.8. HRMS–ESI (*m*/*z*): $[M + Na]^+$ calcd for $C_{12}H_{26}O_2SiNa$, 253.1600; found, 253.1604.

Racemic Allylic Alcohol 44:

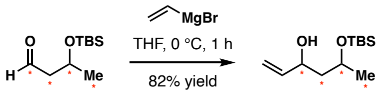

$[^{13}C_4]$-**48**

(±)-$[^{13}C_4]$-**44**

(±)-Alcohol-$[^{13}C_4]$-44.[120] A solution of vinylmagnesium bromide (0.97 M in THF, 1.55 mL, 1.50 mmol, 1.5 equiv) was added dropwise to a solution of aldehyde $[^{13}C_4]$-**48** (0.206 g, 1.00 mmol) in THF (3 mL) at −78 °C. The reaction mixture was then warmed to 0 °C and stirred for 45 min. A saturated aqueous solution of NH_4Cl was added to quench the reaction mixture. The layers were separated, and the aqueous layer was extracted with EtOAc (3 × 15 mL). The combined organic layers were washed with brine, dried over Na_2SO_4, and concentrated to dryness under reduced pressure. The crude product was purified by column chromatography on silica gel (1% EtOAc in hexanes to 5% EtOAc in hexanes) to give (±)-$[^{13}C_4]$-**44** (0.193 g, 0.823 mmol, 82% yield). The ^{1}H NMR, ^{13}C NMR, and mass spectral data are in full agreement with those for the compound obtained by method 1 (see page 123).

Determination of the Enantiopurity for Alcohol 44:

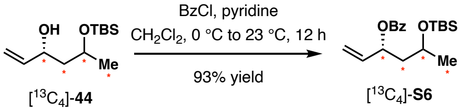

Allylic benzoate [$^{13}C_4$]-S6. Benzoyl chloride (0.050 mL, 0.43 mmol, 5.0 equiv) was added to a mixture of allylic alcohol [$^{13}C_4$]-**44** (20 mg, 0.085 mmol) and pyridine (0.14 mL, 1.71 mmol, 20 equiv) in CH_2Cl_2 (0.17 mL) at 0 °C. The reaction mixture was warmed to 23 °C and stirred for 12 h. The resulting solution was diluted with CH_2Cl_2 (5 mL), and the organic layer was then washed with a 1 M aqueous hydrochloric acid solution (5 mL), a saturated aqueous solution of $NaHCO_3$ (5 mL), and brine (5 mL). The combined organic layers were dried over Na_2SO_4 and concentrated to dryness under reduced pressure. The crude product was purified by column chromatography on silica gel (3% EtOAc in hexanes) to give [$^{13}C_4$]-**S6** (27 mg, 0.0807 mmol, 93% yield) as a colorless oil.

^{1}H NMR (500 MHz, $CDCl_3$, mixture of diastereomers): δ 8.10 (d, *J* = 7.5 Hz, 4H), 7.60 (t, *J* = 7.4 Hz, 2H), 7.49 (t, *J* = 7.7 Hz, 4H), 6.01–5.89 (m, 2H), 5.61 (dd, *J* = 149.5, 25.5 Hz, 2H), 5.37 (ddd, *J* = 24.2, 17.3, 6.9 Hz, 2H), 5.29–5.19 (m, 2H), 4.00 (dm, *J* = 140.0 Hz, 2H), 2.28–1.67 (m, 4H), 1.25 (dm, *J* = 125.6 Hz, 6H), 0.94 (s, 9H), 0.92 (s, 9H), 0.11 (s, 3H), 0.10 (s, 3H), 0.04 (s, 3H), 0.00 (s, 3H). ^{13}C NMR (150 MHz, $CDCl_3$, mixture of diastereomers): δ 165.8, 165.9, 137.1 (dd, *J* = 47.4, 3.1 Hz), 136.7 (dd, *J* = 47.6, 2.3 Hz), 133.0, 132.9, 130.8, 130.7, 129.71, 129.65, 128.48, 128.47, 117.0, 116.2, 73.0 (dd, *J* = 39.0, 2.2 Hz), 72.9 (dd, *J* = 39.8, 2.8 Hz), 65.3 (m), 44.7 (m), 26.03, 26.01, 24.5 (ddd, *J* = 39.2, 3.0, 1.5 Hz), 23.9 (ddd, *J* = 39.2, 2.3, 1.2 Hz).), 18.3, 18.1, −4.08, −4.11, −4.6, −4.8. HRMS–ESI (*m/z*): [M + Na]$^+$ calcd for $^{13}C_4C_{15}H_{30}O_3SiNa$, 361.1996; found, 361.1992.

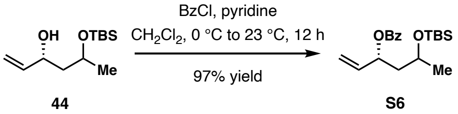

Allylic benzoate S6. The title compound was obtained using the procedure described above for its $^{13}C_4$ analog using 50.0 mg (0.22 mmol) of allylic alcohol **44**, 0.050 mL (0.43 mmol, 5.0 equiv) of benzoyl chloride, and 0.14 mL (1.71 mmol, 20 equiv) of pyridine in 0.17 mL of CH_2Cl_2. **S6** was obtained in 97% yield (70.4 mg, 0.21 mmol) as a clear oil.

^1H NMR (400 MHz, $CDCl_3$, mixture of diastereomers): δ 8.05 (d, J = 7.6 Hz, 4H), 7.56 (t, J = 7.4 Hz, 2H), 7.44 (t, J = 7.4 Hz, 4H), 5.97–5.85 (m, 2H), 5.64–5.51 (m, 2H), 5.39 – 5.14 (m, 4H), 4.03–3.89 (m, 2H), 2.10 – 2.01 (m, 2H), 1.95–1.73 (m, 2H), 1.21 (d, J = 2.56 Hz, 3H), 1.19 (d, J = 2.56 Hz, 3H), 0.90 (s, 9H), 0.87 (s, 9H), 0.07 (s, 3H), 0.06 (s, 3H), 0.00 (s, 3H), −0.05 (s, 3H). ^{13}C NMR (125 MHz, $CDCl_3$, mixture of diastereomers): δ 165.9, 165.8, 137.1, 136.7, 133.0, 132.9, 130.8, 130.7, 129.7, 129.7, 128.5, 128.5, 117.0, 116.2, 73.0, 72.9, 65.6, 65.1, 44.8, 44.6, 26.0, 26.0, 24.6, 23.9, 18.3, 18.1, −4.08, −4.09, −4.12, −4.6, −4.8. HRMS–ESI (*m/z*): $[M + Na]^+$ calcd for $C_{19}H_{30}O_3SiNa$, 357.1862; found, 357.1865.

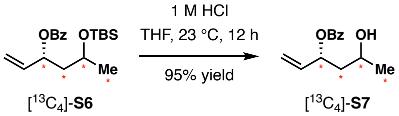

Alcohol [$^{13}C_4$]-S7. A 1 M hydrochloric acid solution (0.2 mL) was added to a solution of allylic benzoate [$^{13}C_4$]-**S6** (27 mg, 0.0807 mmol) in THF (2 mL) at 23 °C. The reaction mixture was stirred at 23 °C for 12 h. The resulting solution was diluted with EtOAc (8 mL), and the organic layer was washed with a saturated aqueous solution of $NaHCO_3$ (10 mL) and brine (10 mL). The combined organic layers were dried over Na_2SO_4 and concentrated to dryness under reduced pressure. The crude product was purified by column chromatography on silica gel (10%

EtOAc in hexanes to 35% EtOAc in hexanes) to give alcohol [$^{13}C_4$]-**S7** (17 mg, 0.0772 mmol, 95% yield) as a colorless oil. The enantiopurity of the material (86% ee) was measured by HPLC trace analysis [Chiralpak ® AD-H; 1% *i*-PrOH in hexanes; flow rate = 1 mL/min; 10 μL injection of a 1 mg/mL solution; detection at 254 nm; t_1 = 17.68 min (major), t_2 = 21.94 min (minor), t_3 = 27.47 min (major), t_4 = 29.84 min (minor)].

^1H NMR (600 MHz, $CDCl_3$, mixture of diastereomers): δ 8.06 (ddt, *J* = 10.9, 6.9, 1.4 Hz, 2H), 7.61–7.54 (m, 1H), 7.45 (q, *J* = 8.0 Hz, 2H), 6.01–5.91 (m, 1H), 5.91–5.49 (m, 1H), 5.43–5.33 (m, 1H), 5.29–5.18 (m, 1H), 4.16–3.63 (m, 1H), 2.21–1.59 (m, 3H), 1.34 (ddt, *J* = 23.5, 6.2, 4.5 Hz, 1.5H), 1.13 (ddt, *J* = 23.6, 6.2, 4.5 Hz, 1.5H). ^{13}C NMR (125 MHz, $CDCl_3$, mixture of diastereomers): δ 167.0, 165.9, 136.6 (dd, *J* = 48.3, 3.0 Hz), 136.4 (dd, *J* = 48.3, 2.5 Hz), 133.4, 133.2, 130.4, 130.1, 130.0, 129.7, 128.59, 128.55, 117.2 (d, *J* = 3.0 Hz), 116.6 (d, *J* = 3.0 Hz), 73.7 (dd, *J* = 38.9, 3.2 Hz), 72.7 (ddd, *J* = 39.1, 3.7, 1.5 Hz), 65.4 (t, *J* = 38.2 Hz), 63.7 (ddd, *J* = 39.3, 37.8, 1.4 Hz), 44.6 (ddd, *J* = 39.3, 37.7, 1.5 Hz), 43.6 (ddd, *J* = 39.0, 37.7, 1.1 Hz), 23.9 (ddd, *J* = 38.6, 3.2, 1.1 Hz), 23.2 (ddd, *J* = 39.4, 3.8, 1.5 Hz).

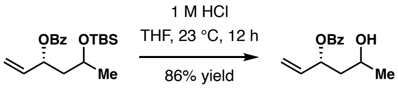

S6 S7

Alcohol S7. The title compound was obtained using the procedure described above for its $^{13}C_4$ analog using 65.0 mg (0.19 mmol) of allylic benzoate **S7** and 0.5 mL of a 1 M aqueous solution of hydrochloric acid in 5 mL of THF. Alcohol **S7** was obtained in 86% yield (37.0 mg, 0.17 mmol). The enantiopurity of the material (86% ee) was measured by HPLC trace analysis described for its $^{13}C_4$ analog with identical retention times (see page 132).

^1H NMR (500 MHz, $CDCl_3$, mixture of diastereomers): δ 8.06 (t, *J* = 7.48 Hz, 4H), 7.56 (q, *J* = 7.48 Hz, 2H), 7.44 (q, *J* = 7.48 Hz, 4H), 6.03–5.88 (M, 2H), 5.81–5.60 (m, 2H), 5.39 (dd, *J* =

5.04, 17.2 Hz, 2H), 5.23 (t, *J* = 10.28 Hz, 2H), 4.05–3.75 (m, 2H), 2.10–1.72 (m, 6H), 1.25 (d, *J* = 6.16 Hz, 3H), 1.21 (d, *J* = 6.16 Hz, 3H). ^{13}C NMR (125 MHz, $CDCl_3$, mixture of diastereomers): δ 166.9, 165.8, 136.6, 133.4, 130.4, 129.7, 128.5, 117.2, 116.5, 73.7, 72.7, 65.4, 63.7, 44.6, 43.7, 23.9, 23.2.

==== Shimadzu LCsolution Analysis Report ====

C:\LabSolutions\Data\Project1\Karen\kyc1-167a_AD-H1.lcd

Acquired by : Artur Mailyan
Sample Name : kyc1-167a_AD-H
Sample ID : kyc1-167a_AD-H
Vail # :
Injection Volume : 10 uL
Data File Name : kyc1-167a_AD-H1.lcd
Method File Name : brad.lcm
Batch File Name :
Report File Name : Default.lcr
Data Acquired : 10/4/2017 12:09:27 PM
Data Processed : 10/4/2017 1:03:27 PM

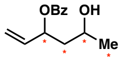

(±)-[$^{13}C_4$]-**S7**

<Chromatogram>

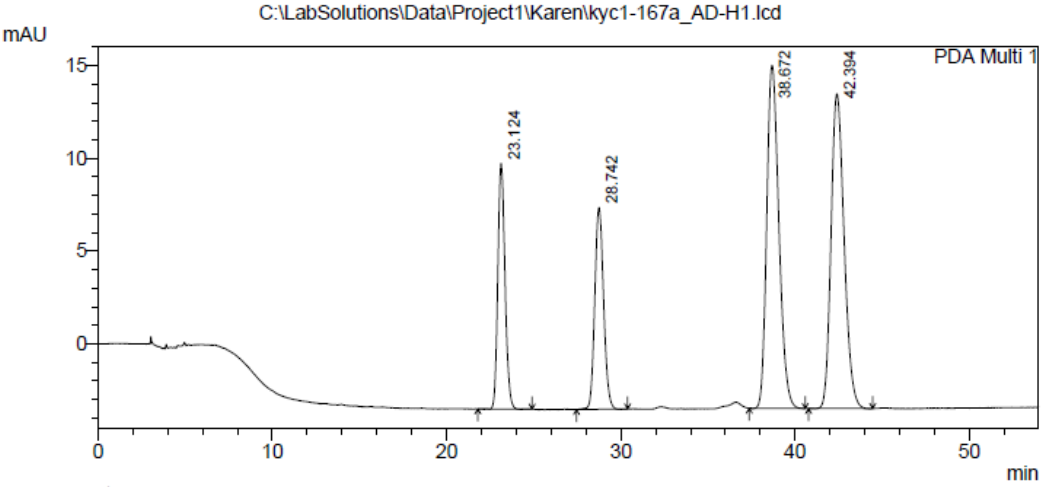

1 PDA Multi 1/254nm 4nm

PeakTable

PDA Ch1 254nm 4nm

Peak#	Ret. Time	Area	Height	Area %	Height %
1	23.124	377702	13247	14.876	22.221
2	28.742	383514	10881	15.105	18.253
3	38.672	893630	18509	35.197	31.047
4	42.394	884093	16978	34.821	28.479
Total		2538939	59616	100.000	100.000

==== Shimadzu LCsolution Analysis Report ====

C:\LabSolutions\Data\Project1\kyc2-8a.lcd

Acquired by : Karen Chen
Sample Name : kyc2-8a
Sample ID : kyc2-8a
Vail # :
Injection Volume : 10 uL
Data File Name : kyc2-8a.lcd
Method File Name : brad.lcm
Batch File Name :
Report File Name : Default.lcr
Data Acquired : 2/9/2018 6:30:51 PM
Data Processed : 2/9/2018 7:28:31 PM

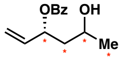

[$^{13}C_4$]-**S7**
from method 1
70% ee

<Chromatogram>

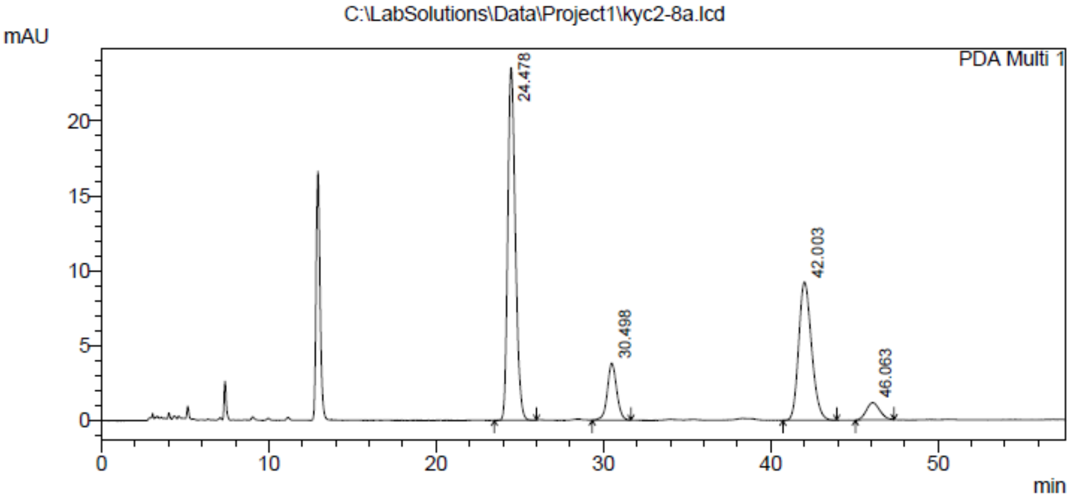

1 PDA Multi 1/254nm 4nm

PeakTable

PDA Ch1 254nm 4nm

Peak#	Ret. Time	Area	Height	Area %	Height %
1	24.478	739002	23526	51.171	62.352
2	30.498	146884	3810	10.171	10.097
3	42.003	493881	9238	34.198	24.483
4	46.063	64405	1157	4.460	3.068
Total		1444172	37730	100.000	100.000

==== Shimadzu LCsolution Analysis Report ====

C:\LabSolutions\Data\Project1\kyc2-151.lcd

Acquired by : Karen Chen
Sample Name : kyc2-151a
Sample ID : kyc2-151a
Vail # :
Injection Volume : 10 uL
Data File Name : kyc2-151.lcd
Method File Name : brad.lcm
Batch File Name :
Report File Name : Default.lcr
Data Acquired : 7/8/2018 12:13:19 PM
Data Processed : 7/8/2018 12:46:29 PM

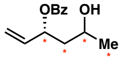

[$^{13}C_4$]-**S7**
from method 2
86% ee

<Chromatogram>

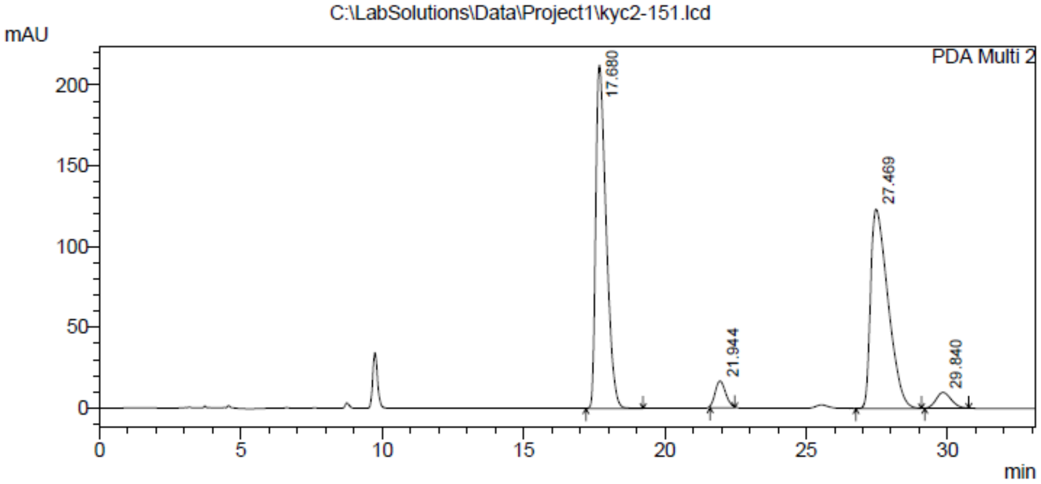

1 PDA Multi 2/254nm 4nm

PeakTable

PDA Ch2 254nm 4nm

Peak#	Ret. Time	Area	Height	Area %	Height %
1	17.680	5446840	212582	47.115	58.638
2	21.944	426679	16544	3.691	4.563
3	27.469	5312796	123514	45.955	34.070
4	29.840	374497	9896	3.239	2.730
Total		11560813	362535	100.000	100.000

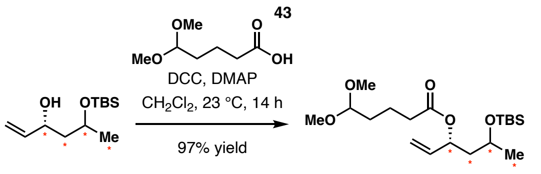

[$^{13}C_4$]-**44**

[$^{13}C_4$]-**42**

Ester [$^{13}C_4$]-42. DMAP (0.68 g, 5.55 mmol, 2.0 equiv) and *N*,*N*'-dicyclohexylcarbodiimide (1.14 g, 5.55 mmol, 2.0 equiv) were added sequentially to a solution of allylic alcohol [$^{13}C_4$]-**44** (0.650 g, 2.77 mmol) and 5,5-dimethoxypentanoic acid **43**[121] (0.900 g, 5.55 mmol, 2.0 equiv) in CH_2Cl_2 (14 mL) at 23 °C. The reaction mixture was stirred at 23 °C for 12 h. The resulting solution was filtered to remove the *N*,*N*'-dicyclohexylurea precipitate, and the filtrate was concentrated to dryness under reduced pressure. The crude product was purified by column chromatography on silica gel (10% EtOAc in hexanes) to give [$^{13}C_4$]-**42** (1.02 g, 2.69 mmol, 97% yield) as a colorless oil.

^{1}H NMR (600 MHz, $CDCl_3$, mixture of diastereomers): δ 5.81–5.71 (m, 2H), 5.49–5.38 (m, 1H), 5.26–5.07 (m, 5H), 4.35 (t, *J* = 5.5 Hz, 2H), 3.84 (dm, *J* = 141.8 Hz, 2H), 3.30 (s, 12H), 2.32 (t, *J* = 7.2 Hz, 4H), 2.02–1.48 (m, 12H), 1.14 (dm, *J* = 125.6 Hz, 6H), 0.87 (s, 9H), 0.86 (s, 9H), 0.03 (s, 6H), 0.02 (s, 3H), 0.00 (s, 3H). ^{13}C NMR (150 MHz, $CDCl_3$, mixture of diastereomers): δ 172.5, 172.4, 137.2 (dd, *J* = 47.4, 3.0 Hz), 136.7 (dd, *J* = 47.5, 2.3 Hz), 117.0 (d, *J* = 2.6 Hz), 116.2 (d, *J* = 2.6 Hz), 104.28, 104.26, 72.3 (dd, *J* = 39.0, 2.3 Hz), 72.2 (dd, *J* = 39.8, 2.9 Hz), 65.4 (t, *J* = 39.4 Hz), 64.9 (t, *J* = 39.4), 52.86 (d, *J* = 1.1 Hz), 52.80 (*J* = 2.2 Hz), 44.6 (td, *J* = 39.7, 1.2 Hz), 44.4 (td, *J* = 39.2, 0.8 Hz), 34.29, 34.24, 31.99, 31.96, 25.99, 25.98, 24.4 (ddd, *J* = 39.2, 3.0, 1.4 Hz), 23.8 (ddd, *J* = 39.2, 3.2, 1.1 Hz), 20.24, 20.20, 18.2, 18.1, −4.07, −4.10, −4.6, −4.8. HRMS–ESI (*m*/*z*): $[M + Na]^+$ calcd for $^{13}C_4C_{15}H_{38}O_5SiNa$, 401.2520; found, 401.2520.

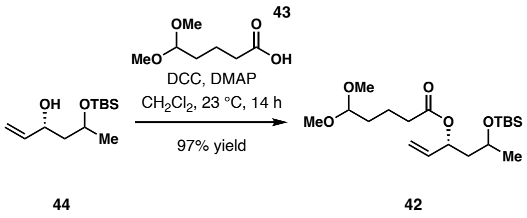
43
OMe
MeO
O
OH
DCC, DMAP
CH$_2$Cl$_2$, 23 °C, 14 h
97% yield
OH
OTBS
Me
44
OMe
MeO
O
O
OTBS
Me
42

Ester 42. The title compound was obtained using the procedure described above for its $^{13}C_4$ analog using 0.95 g (4.12 mmol) of allylic alcohol **44**, 1.00 g (6.18 mmol, 1.5 equiv) of 5,5-dimethoxypentanoic acid **43**, 0.75 g (6.18 mmol, 1.5 equiv) of DMAP, and 1.27 g (6.18 mmol, 1.5 equiv) of *N*,*N*'-dicyclohexylcarbodiimide in 21 mL of CH_2Cl_2. Ester **42** was obtained in 97% yield (1.50 g, 4.0 mmol).

^{1}H NMR (400 MHz, $CDCl_3$, mixture of diastereomers): δ 5.83–5.73 (m, 2H), 5.40–5.09 (m, 6H), 4.36 (t, *J* = 5.1 Hz, 2H), 3.92–3.79 (m, 2H), 3.31 (s, 12H), 2.33 (t, *J* = 7.2 Hz, 6H), 1.92–1.83 (m, 1H), 1.73–1.59 (m, 11H), 1.16 (d, *J* = 2.6 Hz, 3H), 1.14 (d, *J* = 2.6 Hz, 3H), 0.89 (s, 9H), 0.88 (s, 9H), 0.05 (s, 6H), 0.03 (s, 3H), 0.01 (s, 3H). ^{13}C NMR (150MHz, $CDCl_3$, mixture of diastereomers): δ 172.56, 172.49, 137.1, 136.7, 117.0, 116.2, 104.28, 104.26, 72.28, 72.21, 65.5, 64.9, 52.86, 52.81, 44.6, 44.4, 34.28, 34.24, 31.99, 31.96, 25.99, 25.97, 24.4, 23.9, 20.23, 20.20, 18.2, 18.1, −4.07, −4.11, −4.6, −4.8. HRMS–ESI (*m*/*z*): $[M + Na]^+$ calcd for $C_{19}H_{38}O_5SiNa$, 397.2386; found, 397.2393.

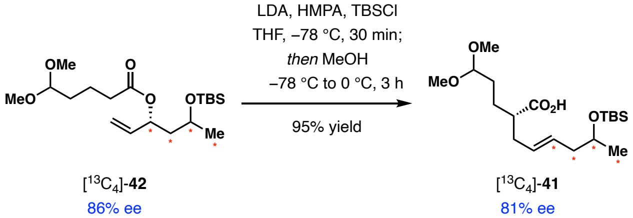
LDA, HMPA, TBSCl
THF, –78 °C, 30 min;
then MeOH
–78 °C to 0 °C, 3 h
95% yield
OMe
MeO
O
O
OTBS
Me
[^{13}C$_4$]-42
86% ee
OMe
MeO
CO$_2$H
OTBS
Me
[^{13}C$_4$]-41
81% ee

Acid [$^{13}C_4$]-41. A solution of ester [$^{13}C_4$]-**42** (0.500 g, 1.32 mmol) in THF (2 mL) was added dropwise to a solution of freshly prepared lithium diisopropylamide (2.64 mmol, 2.0 equiv) in THF (14 mL) at −78 °C. The mixture was stirred at −78 °C for 30 min before TBSCl (0.46 g, 3.04 mmol, 2.3 equiv) and HMPA (2.1 mL) were added sequentially. The resulting mixture was then stirred at −78 °C for an additional 30 min. Methanol (0.53 mL, 13.2 mmol, 10 equiv) was added dropwise over 1 min to quench excess LDA. The reaction mixture was then warmed to 0 °C and let stirred at 0 °C until complete disappearance of the starting material was observed by TLC (approximately 2 h). A solution of lithium hydroxide (63 mg, 2.64 mmol, 2.0 equiv) in water (1 mL) was then added to the reaction mixture at 0 °C to stir at 0 °C until complete hydrolysis of the silyl ester was observed by TLC (approximately 1 h). The resulting solution was then diluted with EtOAc (30 mL) and water (20 mL), then cooled to 0 °C. The aqueous layer was carefully acidified to pH = 5 with 1 M hydrochloric acid, then quickly extracted with EtOAc (3 × 20 mL). The combined organic layers were washed with brine (50 mL), dried over Na_2SO_4, and concentrated to dryness under reduced pressure. The crude product was purified by column chromatography on silica gel (15% EtOAc in hexanes to 50% EtOAc, 1% AcOH in hexanes) to give [$^{13}C_4$]-**41** (0.49 g, 1.31 mmol, 99% yield) as a pale yellow oil. The enantiopurity of the material (81% ee) was measured by HPLC trace analysis after derivatization to compound [$^{13}C_4$]-**S8** (see page 141).

^{1}H NMR (600 MHz, $CDCl_3$, mixture of diastereomers): δ 5.50 (dm, *J* = 137.3 Hz, 1H), 5.37 (m, 1H), 4.35 (t, *J* = 4.92 Hz, 1H), 3.77 (dm, *J* = 140.7 Hz, 1H), 3.31 (s, 3H), 3.30 (s, 3H), 2.45–2.15 (m, 4H), 2.10–1.92 (m, 1H), 1.70–1.52 (m, 4H), 1.09 (ddd, *J* = 125.4, 9.2, 4.4 Hz, 3H), 0.87 (s, 9H), 0.03 (s, 3H), 0.03 (s, 3H). ^{13}C NMR (150 MHz, $CDCl_3$, mixture of diastereomers): δ 181.32, 181.34, 130.1 (dd, *J* = 43.4, 1.9 Hz), 128.7 (d, *J* = 2.1 Hz), 104.3, 68.8 (t, *J* = 39.1 Hz), 53.0 (d, *J* = 2.2 Hz), 52.6 (d, *J* = 0.8 Hz), 45.3 (d, *J* = 2.6 Hz), 43.0 (ddd, *J* = 43.4, 38.7, 4.2 Hz), 35.3, 30.2, 26.4, 26.3, 26.02, 23.5 (dd, *J* = 39.8, 1.0 Hz), 18.3, −4.6, −4.4. HRMS–ESI (*m/z*): [M + Na]$^+$ calcd for $^{13}C_4C_{15}H_{38}O_5SiNa$, 401.2520; found, 401.2523.

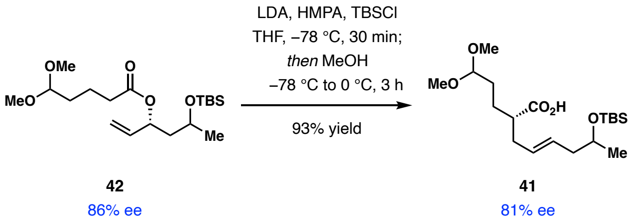
LDA, HMPA, TBSCl
THF, –78 °C, 30 min;
then MeOH
–78 °C to 0 °C, 3 h
93% yield
42
86% ee
41
81% ee

Acid 41. The title compound was obtained using the procedure described above for its $^{13}C_4$ analog using 2.0 g (5.34 mmol) of ester **42**, 2.0 equiv (10.68 mmol) of lithium diisopropylamide, 1.85 g (12.28 mol, 2.3 equiv) of TBSCl, and 8.0 mL of HMPA in 54 mL of THF. Acid **41** was obtained in 93% yield (1.86 g, 4.97 mmol). The enantiopurity of the material (81% ee) was measured by HPLC trace analysis after derivatization to compound [$^{13}C_4$]-**S8** (see page 141).

^{1}H NMR (400 MHz, $CDCl_3$, mixture of diastereomers): δ 5.52–5.44 (m, 1H), 5.42–5.34 (m, 1H), 4.35 (t, *J* = 5.2 Hz, 1H), 3.81–3.74 (m, 1H), 3.30 (s, 3H), 3.29 (s, 3H), 2.44–2.30 (m, 2H), 2.24–2.03 (m, 3H), 1.71–1.52 (m, 4H), 1.08 (d, *J* = 6.1 Hz, 3H), 0.87 (s, 9H), 0.03 (s, 3H), 0.02 (s, 3H). ^{13}C NMR (100 MHz, $CDCl_3$, mixture of diastereomers): δ 181.48, 181.46, 130.1, 128.6, 104.2, 68.8, 52.6, 52.6, 45.3, 43.00, 35.3, 30.2, 26.4, 26.3, 26.0, 23.4, 18.3, −4.4, −4.6. HRMS–ESI (*m*/*z*): $[M + Na]^+$ calcd for $C_{19}H_{38}O_5SiNa$, 397.2386; found, 397.2389.

Determination of the Enantiopurity for Acid 41:

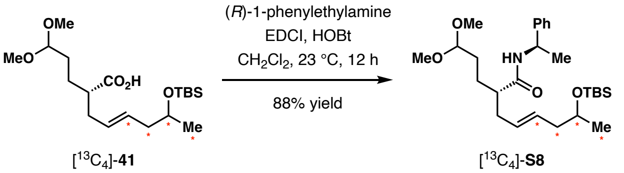
(*R*)-1-phenylethylamine
EDCI, HOBt
CH2Cl2, 23 °C, 12 h
88% yield
[13C4]-41
[13C4]-S8

Amide [$^{13}C_4$]-S8. EDCI hydrochloride (15.3 mg, 0.08 mmol, 3.0 equiv) was added to a solution of acid [$^{13}C_4$]-**41** (10 mg, 0.026 mmol), (*R*)-1-phenylethylamine (10.2 μL, 0.08 mmol, 3.0 equiv), and HOBt hydrate (11 mg, 0.08 mmol, 3.0 equiv) in CH_2Cl_2 (0.5 mL) at 23 °C. The reaction mixture was stirred at 23 °C for 12 h. The resulting solution was diluted with CH_2Cl_2 (7 mL), and the organic layer was washed with water (5 mL) and brine (5mL). The combined organic layer was then dried over Na_2SO_4 and concentrated to dryness under reduced pressure. The crude product was purified by column chromatography on silica gel (30% EtOAc in hexanes) to give [$^{13}C_4$]-**S8** (11.2 mg , 0.023 mmol, 88% yield) as a pale yellow oil. The enantiopurity of the material (81% ee) was measured by HPLC trace analysis [Chiralpak ® AD-H; 5% *i*-PrOH in hexanes; flow rate = 1 mL/min; 10 μL injection of a 1 mg/mL solution; detection at 210 nm; t_1 = 5.84 min (major), t_2 = 6.55 min (major), t_3 = 7.39 min (minor), t_4 = 9.44 min (minor)].

^{1}H NMR (500 MHz, $CDCl_3$, mixture of diastereomers): δ 7.37–7.22 (m, 5H), 5.78 (d, *J* = 6.3 Hz, 1H), 5.42 (dm, *J* = 134.0 Hz, 1H), 5.33–5.23 (m, 1H), 5.20–5.10 (m, 1H), 4.33 (t, *J* = 5.3 Hz, 1H), 3.71 (dm, *J* = 141.8 Hz, 1H), 3.32 (s, 3H), 3.30 (s, 3H), 2.34–1.82 (m, 5H), 1.72–1.51 (m, 3H), 1.48 (d, *J* = 6.9 Hz, 3H), 1.05 (ddd, *J* = 125.4, 10.2, 4.3 Hz, 3H), 0.87 (s, 9H), 0.02 (s, 3H), 0.01 (s, 3H). ^{13}C NMR (125 MHz, $CDCl_3$, mixtures of diastereomers): δ 174.03, 174.02, 143.4, 129.9 (dt, *J* = 5.7, 2.0 Hz), 129.5 (dt, *J* = 5.4, 2.1 Hz), 128.77, 128.76,, 127.46, 127.43, 126.36, 126.35, 104.8, 68.8 (m), 53.48, 53.46, 52.7, 48.62, 48.60, 47.74, 47.72, 43.1 (m), 36.3, 30.46, 30.45, 27.6, 27.5, 26.03, 26.02, 23.7 (dd, *J* = 9.2, 1.7 Hz), 23.3 (dd, *J* = 9.2, 3.1 Hz), 21.92, 21.87, 18.3, −4.4, −4.5. HRMS–ESI (*m*/*z*): [M + Na]$^+$ calcd for $^{13}C_4C_{23}H_{47}NO_4SiNa$, 504.3306; found, 504.3310.

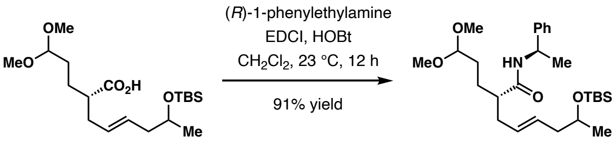

41

S8

Amide S8. The title compound was obtained using the procedure described above for its $^{13}C_4$ analog using 20 mg (0.053 mmol) of acid **41**, 30.7 mg (0.16 mmol, 3.0 equiv) of EDCI hydrochloride, 20.4 μL (0.16 mmol, 3.0 equiv) of (*R*)-1-phenylethylamine, and 22 mg (0.16 mmol, 3.0 equiv) of HOBt hydrate in 1 mL of CH_2Cl_2. **S8** was obtained in 91% yield (23.2 mg, 0.048 mmol). The enantiopurity of the material (81% ee) was measured by HPLC trace analysis described for its $^{13}C_4$ analog with identical retention times (see page 141).

^{1}H NMR (500 MHz, $CDCl_3$, mixture of diastereomers): δ 7.37–7.20 (m, 5H), 5.82 (d, *J* = 4.7 Hz, 1H), 5.47–5.36 (m, 1H), 5.33–5.23 (m, 1H), 5.20–5.07 (m, 1H), 4.33 (t, *J* = 5.3 Hz, 1H), 3.78–3.67 (m, 1H), 3.31 (s, 3H), 3.29 (s, 3H), 2.35–2.23 (m, 1H), 2.15–2.03 (m, 3H), 2.03–1.93 (m, 1H), 1.72–1.49 (m, 3H), 1.48 (d, *J* = 6.9 Hz, 3H), 1.06 (d, *J* = 6.1 Hz, 3H), 0.87 (s, 9H), 0.02 (s, 3H), 0.01 (s, 3H). ^{13}C NMR (125 MHz, $CDCl_3$): δ 174.0, 143.4, 129.6, 129.4, 128.7, 127.4, 126.3, 104.8, 68.8, 53.4, 52.6, 48.6, 47.7, 43.1, 36.3, 30.4, 27.5, 26.0, 23.4, 21.8, 18.3, −4.4, −4.6. HRMS–ESI (*m*/*z*): $[M + Na]^+$ calcd for $C_{27}H_{47}NO_4SiNa$, 500.3172; found, 500.3174.

==== Shimadzu LCsolution Analysis Report ====

C:\LabSolutions\Data\AKM\Anatoxin-a\AKM-09-133racemic1.lcd

Acquired by : Artur Mailyan
Sample Name : AKM-09-133racemic
Sample ID : AKM-09-133racemic
Vail # :
Injection Volume : 10 uL
Data File Name : AKM-09-133racemic1.lcd
Method File Name : brad.lcm
Batch File Name :
Report File Name : Default.lcr
Data Acquired : 6/21/2018 1:52:00 PM
Data Processed : 6/21/2018 2:09:20 PM

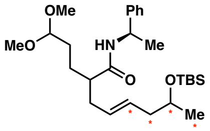

(±)-[$^{13}C_4$]-**S8**

<Chromatogram>

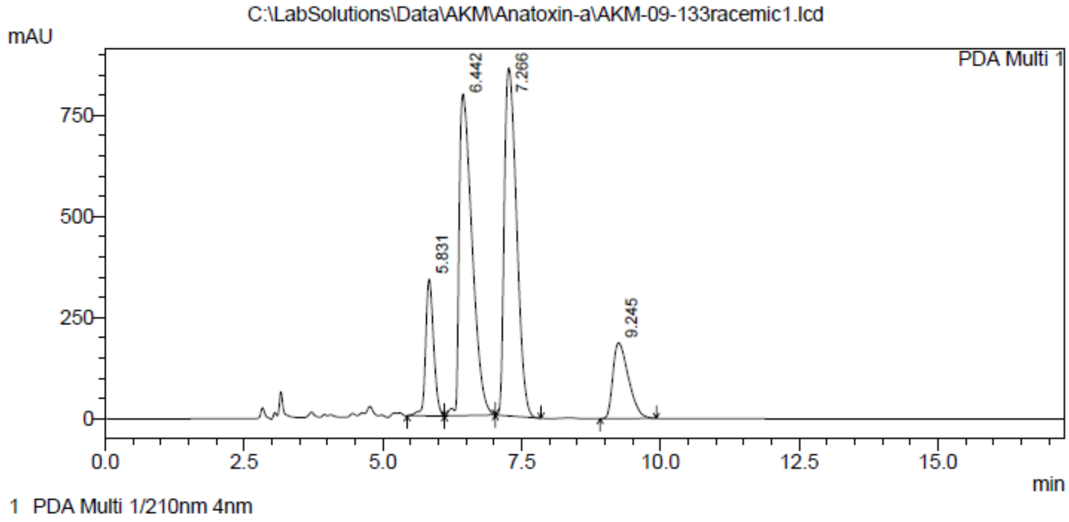

PeakTable

PDA Ch1 210nm 4nm

Peak#	Ret. Time	Area	Height	Area %	Height %
1	5.831	3369481	338182	10.165	15.501
2	6.442	12882099	795250	38.862	36.451
3	7.266	13234855	860867	39.927	39.458
4	9.245	3661508	187404	11.046	8.590
Total		33147943	2181703	100.000	100.000

==== Shimadzu LCsolution Analysis Report ====

C:\LabSolutions\Data\AKM\Anatoxin-a\AKM-09-133.2.lcd

Acquired by : Artur Mailyan
Sample Name : AKM-09-133.2
Sample ID : AKM-09-133.2
Vail # :
Injection Volume : 10 uL
Data File Name : AKM-09-133.2.lcd
Method File Name : brad.lcm
Batch File Name :
Report File Name : Default.lcr
Data Acquired : 6/20/2018 7:16:52 PM
Data Processed : 6/20/2018 7:31:18 PM

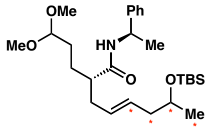

[$^{13}C_4$]-**S8**
81% ee

<Chromatogram>

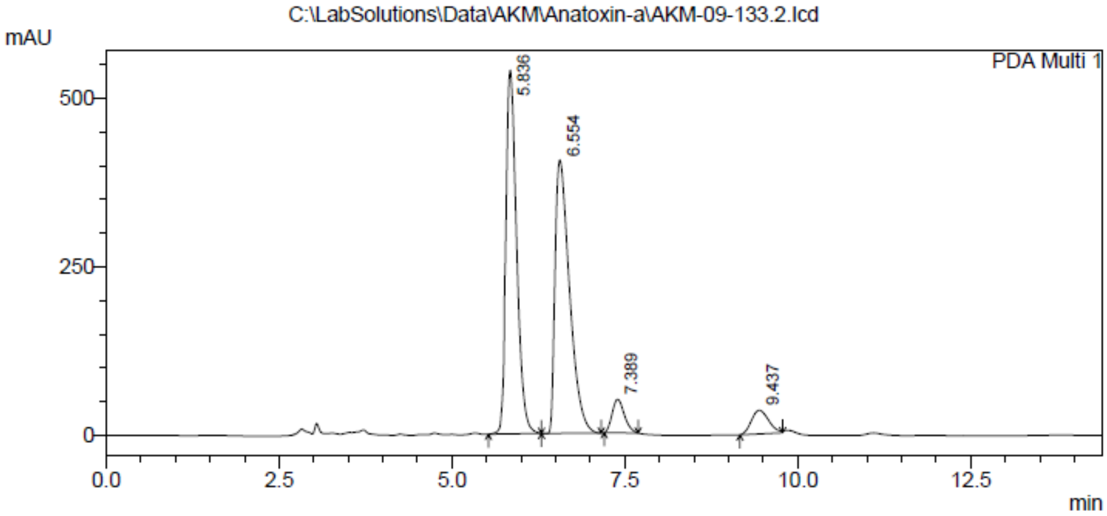

1 PDA Multi 1/210nm 4nm

PeakTable

PDA Ch1 210nm 4nm

Peak#	Ret. Time	Area	Height	Area %	Height %
1	5.836	5824115	539793	44.933	52.365
2	6.554	5912738	406052	45.617	39.391
3	7.389	611581	49751	4.718	4.826
4	9.437	613388	35226	4.732	3.417
Total		12961822	1030822	100.000	100.000

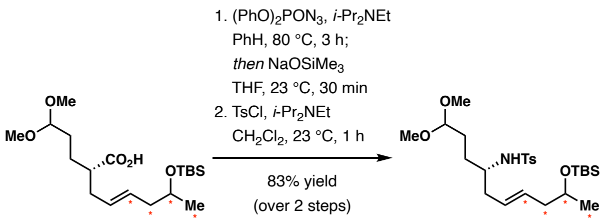

[$^{13}C_4$]-**41** [$^{13}C_4$]-**40**

Tosyl amine [$^{13}C_4$]-40. A solution of acid [$^{13}C_4$]-**41** (0.48 g, 1.27 mmol), diphenylphosphoryl azide (0.41 mL, 1.9 mmol, 1.5 equiv), and *i*-Pr_2NEt (0.44 mL, 2.54 mmol, 2.0 equiv) in benzene (12.7 mL) was heated at reflux for 3 h with a drying tube attached. The reaction mixture was then cooled to 23 °C, and a solution of $NaOSiMe_3$ (0.64 g, 5.7 mmol, 4.5 equiv) in THF (6.4 mL) was added in one portion, and the mixture was stirred at 23 °C for 20 min. The resulting solution was then diluted with EtOAc (20 mL) and quenched with water (20 mL). The layers were separated, and the aqueous layer was extracted with EtOAc (3 × 20 mL). The combined organic layers were washed with 3 M aqueous NaOH solution (50 mL) and brine (50 mL), dried over Na_2SO_4, and concentrated to dryness under reduced pressure. The crude amine was submitted to the next step without further purification.

i-Pr_2NEt (0.44 mL, 2.54 mmol, 2.0 equiv) and *p*-toluenesulfonyl chloride (0.31 g, 1.65 mmol, 1.3 equiv) were added sequentially to a solution of crude amine in CH_2Cl_2 (12.7 mL) at 23 °C. The reaction was stirred at 23 °C until the full consumption of the starting material was observed by TLC (approximately 1 h). The reaction mixture was concentrated under reduced pressure, and the residue was directly subjected to column chromatography on silica gel (15% EtOAc in hexanes to 35% EtOAc in hexanes) to afford [$^{13}C_4$]-**40** (0.53 g, 1.05 mmol, 83% yield) as a pale yellow oil.

^{1}H NMR (500 MHz, $CDCl_3$, mixture of diastereomers): δ 7.73 (d, *J* = 8.2 Hz, 2H), 7.28 (d, *J* = 8.2 Hz, 4H), 5.33 (dm, *J* = 151.8 Hz, 1H), 5.20–5.07 (m, 1H), 4.66–4.56 (m, 1H), 4.23 (t, *J* = 5.1 Hz, 1H), 3.74 (dm, *J* = 139.9 Hz, 1H), 3.25 (s, 6H), 3.24–3.17 (m, 1H), 2.41 (s, 3H), 2.01 (dm, *J* = 125.9 Hz, 2H), 2.08–1.06 (m, 2H), 1.58–1.46 (m, 3H), 1.43–1.34 (m, 2H), 1.06 (dm, *J* = 125.4 Hz, 3H), 0.86 (s, 9H), 0.02 (s, 3H), 0.00 (s, 3H). ^{13}C NMR (125 MHz, CDCl$_3$, mixture of diastereomers): δ 143.3, 131.8 (dd, *J* = 43.4, 10.9 Hz), 129.7 (d, *J* = 1.0 Hz), 127.2, 104.4, 68.6 (td, *J* = 39.1, 1.8 Hz), 68.4 (td, *J* = 39.1, 1.8 Hz), 53.6, 53.1, 53.0, 43.0 (ddd, *J* = 43.4, 38.5, 9.6 Hz), 38.17, 29.4, 28.6, 26.0, 23.5 (ddd, *J* = 39.8, 9.4, 1.1 Hz), 21.6, 18.3, −4.4, −4.6. HRMS–ESI (*m*/*z*): [M + Na]$^+$ calcd for ^{13}C$_4$C$_{21}$H$_{45}$NO$_5$SSiNa, 526.2820; found, 526.2827.

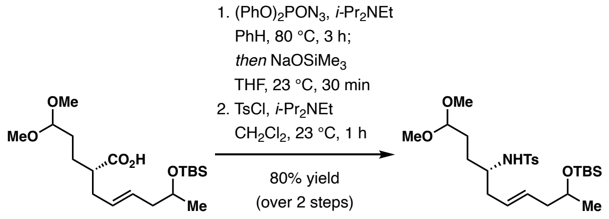
1. (PhO)$_2$PON$_3$, *i*-Pr$_2$NEt
PhH, 80 °C, 3 h;
then NaOSiMe$_3$
THF, 23 °C, 30 min
2. TsCl, *i*-Pr$_2$NEt
CH$_2$Cl$_2$, 23 °C, 1 h
80% yield
(over 2 steps)
OMe
MeO
CO$_2$H
OTBS
Me
OMe
MeO
NHTs
OTBS
Me

41 40

Tosyl amine 40. The title compound was obtained using the procedure described above for its ^{13}C$_4$ analog starting with 1.5 g (4.0 mmol) of acid **41**, 1.3 mL (6.0 mmol, 1.5 equiv) of diphenylphosphoryl azide, and 1.4 mL (8.0 mmol, 2.0 equiv) of *i*-Pr$_2$NEt in 40 mL of benzene, then 2.0 g (5.2 mmol, 1.3 equiv) of NaOSiMe$_3$ in 20 mL of THF for the first step. The second step was performed using 1.4 mL (8.0 mmol, 2.0 equiv) of *i*-Pr$_2$NEt, and 1.0 g (5.2 mmol, 1.3 equiv) of *p*-toluenesulfonyl chloride in 40 mL of CH$_2$Cl$_2$. **40** was obtained in 80% yield (1.6g, 3.20 mmol) over 2 steps.

^{1}H NMR (500 MHz, CDCl$_3$, mixture of diastereomers): δ 7.74 (d, *J* = 8.3 Hz, 4H), 7.29 (d, *J* = 8.1 Hz, 4H), 5.41–5.30 (m, 2H), 5.20–5.08 (m, 2H), 4.49 (d, *J* = 8.0 Hz, 1H), 4.45 (d, *J* = 7.8 Hz, 1H), 4.27–4.23 (m, 2H), 3.80–3.72 (m, 2H), 3.28–3.26 (s, 12H), 3.25–3.18 (m, 2H), 2.42 (s, 6H), 2.11–1.96 (m, 8H), 1.56–1.45 (m, 6H), 1.45–1.35 (m, 2H), 1.09 (d, *J* = 2.4 Hz, 3H), 1.07 (d, *J* = 2.4 Hz, 3H), 0.87 (s, 18H), 0.03 (s, 6H), 0.02 (s, 6H). ^{13}C NMR (125 MHz, CDCl$_3$, mixture of diastereomers): δ 143.34, 131.92, 129.74, 127.27, 126.69, 104.42, 68.44, 53.58, 53.14, 53.10, 43.07, 38.18, 29.48, 28.67, 26.02, 23.56, 21.65, 18.30, −4.37, −4.57. HRMS–ESI (*m*/*z*): [M + Na]$^+$ calcd for $C_{25}H_{45}NO_5SSiNa$, 522.2685; found, 522.2682.

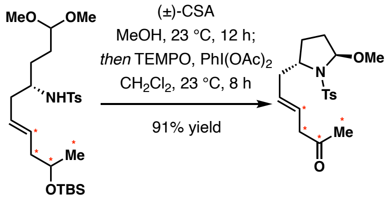

[$^{13}C_4$]-**40** [$^{13}C_4$]-**53**

***N*-Tosylpyrrolidine [$^{13}C_4$]-53.** (±)-10-Camphorsulfonic acid (10 mg, 0.04 mmol, 0.05 equiv) was added to a solution of tosyl amine [$^{13}C_4$]-**40** (0.450 g, 0.89 mmol) in MeOH (8.9 mmol) at 23 °C. The reaction mixture was stirred at 23 °C for 12 h. The solvent was evaporated under reduced pressure, and the dry residue was dissolved in CH_2Cl_2 (8.9 mL) at 23 °C. The solution was then treated with TEMPO (42 mg, 0.27 mmol, 0.3 equiv) and $PhI(OAc)_2$ (0.58 g, 1.79 mmol, 2.0 equiv). The reaction mixture was then stirred at 23 °C for 8 h. The reaction mixture was concentrated under reduced pressure, and the residue was directly subjected to column chromatography on silica gel (25% EtOAc in hexanes to 35% EtOAc in hexanes) to afford [$^{13}C_4$]-**53** (0.290 g, 0.81 mmol, 91% yield) as a pale yellow oil.

$[\alpha]^{21}_{D}$ −79.8 (*c* 1.0, $CHCl_3$). ^1H NMR (500 MHz, $CDCl_3$): δ 7.68 (d, *J* = 8.2 Hz, 2H), 7.30 (d, *J* = 8.0 Hz, 1H), 5.63 (dm, *J* = 126.5 Hz, 1H), 5.55–5.41 (m, 1H), 5.02 (d, *J* = 5.0 Hz, 1H), 3.56–3.46 (m, 1H), 3.41 (s, 3H), 3.12 (ddd, *J* = 126.4, 12.8, 6.4 Hz, 2H), 2.69–2.61 (m, 1H), 2.41 (s, 3H), 2.40–2.33 (m, 1H), 2.14 (ddd, *J* = 127.3, 5.8, 0.9 Hz, 3H), 1.82–1.69 (m, 3H), 1.15–1.02 (m, 1H). ^{13}C NMR (125 MHz, $CDCl_3$): δ 207.2 (t, *J* = 39.8 Hz), 143.7, 135.8, 130.3, 129.8, 127.4, 125.0 (dd, *J* = 43.3, 2.9 Hz), 92.8, 60.5, 54.8, 47.7 (ddd, *J* = 43.3, 38.8, 14.4 Hz), 40.1 (d, *J* = 39.8 Hz), 32.1, 29.4 (dd, *J* = 14.4, 40.8 Hz), 29.0, 21.6. HRMS–ESI (*m*/*z*): [M + Na]$^+$ calcd for $^{13}C_4C_{14}H_{25}NO_4SNa$, 378.1536; found, 378.1548.

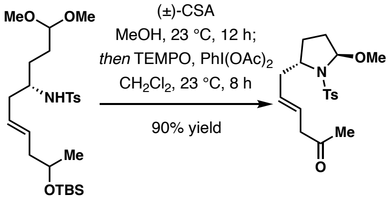

40 **53**

***N*-Tosylpyrrolidine 53.** The title compound was obtained using the procedure described above for its $^{13}C_4$ analog using 1.10 g (2.20 mmol) of tosyl amine **40** and 25.6 mg, (0.11 mmol, 0.05 equiv) of (±)-10-camphorsulfonic acid in 4.4 mL of MeOH, followed by treatment of 103 mg (0.66 mmol, 0.3 equiv) of TEMPO and 1.42 g (4.40 mmol, 2.0 equiv) of $PhI(OAc)_2$ in 22 mL of CH_2Cl_2. **53** was obtained in 90% yield (0.70 g, 1.98 mmol).

$[\alpha]_D^{21}$ −81.4 (*c* 1.0, $CHCl_3$). ^1H NMR (500 MHz, $CDCl_3$): δ 7.69 (d, *J* = 8.3 Hz, 2H), 7.31 (d, *J* = 8.3 Hz, 1H), 5.66–5.58 (m, 1H), 5.55–5.48 (m, 1H), 5.03 (d, *J* = 5.0 Hz, 1H), 3.56–3.48 (m, 1H), 3.41 (s, 3H), 3.12 (d, *J* = 6.8 Hz, 2H), 2.69–2.62 (m, 1H), 2.43 (s, 3H), 2.42–2.35 (m, 1H), 2.15 (s, 3H), 1.82–1.72 (m, 3H), 1.15–1.04 (m, 1H). ^{13}C NMR (125 MHz, $CDCl_3$): δ 207.2, 143.7, 135.7, 130.5, 129.8, 127.3, 125.1, 92.8, 60.5, 54.8, 47.7, 40.0, 32.1, 29.5, 29.0, 21.6. HRMS–ESI (*m/z*): $[M + Na]^+$ calcd for $C_{18}H_{25}NO_4SNa$, 374.1402; found, 374.1402.

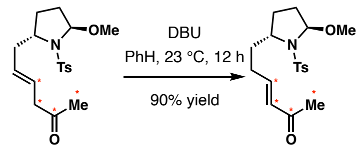

$[^{13}C_4]$-**53** $[^{13}C_4]$-**39**

Vinyl ketone $[^{13}C_4]$-39. DBU (0.63 mL, 4.2 mmol, 5.0 equiv) was added to a solution of *N*-tosylpyrrolidine $[^{13}C_4]$-**53** (0.300 g, 0.84 mmol) in benzene (8.4 mL) at 23 °C. The reaction mixture was stirred at 23 °C for 12 h. The resulting solution was diluted with EtOAc (35 mL). The organic layer was washed with a saturated aqueous solution of NH_4Cl (30 mL) and brine (30 mL), then dried over Na_2SO_4, and concentrated to dryness under reduced pressure. The crude product was purified by column chromatography on silica gel (35% EtOAc in hexanes to 50% EtOAc in hexanes) to give [$^{13}C_4$]-**39** (0.270 g, 0.76 mmol, 90% yield) as a pale yellow oil.

$[\alpha]_D^{21}$ −93.2 (*c* 1.0, MeOH). ^{1}H NMR (600 MHz, $CDCl_3$): δ 7.67 (d, *J* = 8.2 Hz, 2H), 7.31 (d, *J* = 8.2 Hz, 2H), 6.82 (ddt, *J* = 152.6, 15.9, 6.5 Hz, 1H), 6.09 (dd, *J* = 157.4, 16.0 Hz, 1H), 5.04 (d, *J* = 5.1 Hz, 1H), 3.54–3.46 (m, 1H), 3.42 (s, 3H), 2.43 (s, 3H), 2.26 (dd, *J* = 127.3, 5.8, 3H), 2.35–2.20 (m, 2H), 2.11–2.03 (m, 1H), 1.85–1.68 (m, 4H), 1.18–1.06 (m, 1H). ^{13}C NMR (150 MHz, $CDCl_3$): δ 198.7 (dd, *J* = 53.2, 42.1 Hz), 147.6 (dd, *J* = 67.9, 1.2 Hz), 143.8, 135.7, 131.6 (ddd, *J* = 67.9, 53.1, 14.7), 129.9, 127.4, 92.9, 60.4, 55.0, 35.3, 32.2, 28.5 (dd, *J* = 41.4, 5.7 Hz), 26.9 (dd, *J* = 42.1, 14.7), 27.0 (dd, *J* = 14.7, 42.1 Hz), 21.6. HRMS–ESI (*m/z*): $[M + Na]^+$ calcd for $^{13}C_4C_{14}H_{25}NO_4SNa$, 378.1536; found, 378.1529.

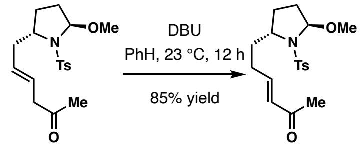

53 **39**

Vinyl ketone 39. The title compound was obtained using the procedure described above for its $^{13}C_4$ analog using 0.400 g (1.14 mmol) of *N*-tosylpyrrolidine **53** and 0.85 mL (5.69 mmol, 5.0 equiv) of DBU in 11.4 mL of benzene. **39** was obtained in 85% yield (0.340 g,0.97 mmol).

$[\alpha]_D^{21}$ −95.1 (*c* 1.0, MeOH). ^{1}H NMR (600 MHz, $CDCl_3$): δ 7.66 (d, *J* = 9.1 Hz, 2H), 7.29 (d, *J* = 9.4 Hz, 2H), 6.82 (dt, *J* = 16.0, 6.8 Hz, 1H), 6.08 (d, *J* = 16.0 Hz, 1H), 5.02 (d, *J* = 5.1 Hz, 1H), 3.54 – 3.44 (m, 1H), 3.41 (s, 3H), 2.41 (s, 3H), 2.37–2.27 (m, 1H), 2.27–2.18 (m, 4H), 2.12–2.03 (m, 1H), 1.84–1.67 (m, 4H), 1.16–1.05 (m, 1H). ^{13}C NMR (150 MHz, $CDCl_3$): δ 198.7, 147.7, 143.9, 135.7, 131.7, 129.9, 127.4, 92.9, 60.4, 55.0, 35.3, 32.2, 29.4, 28.6, 27.0, 21.6. HRMS–ESI (*m*/*z*): $[M + Na]^+$ calcd for $C_{18}H_{25}NO_4SNa$, 374.1402; found, 374.1398.

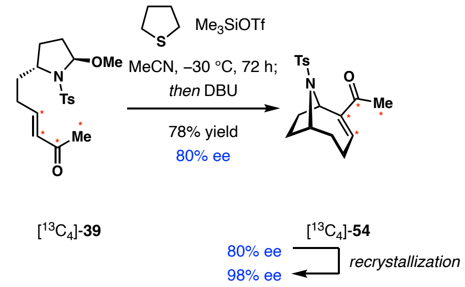

***N*-Tosylanatoxin-a $[^{13}C_4]$-54.** Me_3SiOTf (0.65 mL, 3.58 mmol, 2.5 equiv) was added to a solution of vinyl ketone $[^{13}C_4]$-**39** (0.510 g, 1.43 mmol) and tetrahydrothiophene (0.19 mL, 2.15 mmol, 1.5 equiv) in MeCN (14.3 mL) at −30 °C. The resulting mixture was stirred at −30 °C for 72 h. DBU (0.43 mL, 2.87 mmol, 2.0 equiv) was then added to quench the reaction mixture, and let stirred at 23 °C for 30 min. The resulting solution was diluted with EtOAc (40 mL). The organic layer was washed with a saturated aqueous solution of NH_4Cl (30 mL) and brine (30 mL), then dried over Na_2SO_4, and concentrated to dryness under reduced pressure. The crude product was purified by column chromatography on silica gel (35% EtOAc in hexanes) to give $[^{13}C_4]$-**54** (0.360 g, 1.11 mmol, 78% yield) as a white solid. The enantiopurity of the material (80% ee) was measured by HPLC trace analysis [Chiralpak ® AD-H; 10% *i*-PrOH in hexanes; flow rate = 1 mL/min; 10 μL injection of a 1 mg/mL solution; detection at 254 nm; t_1 = 16.6 min (minor), t_2 = 23.4 min (major)]. This material was then recrystallized using 5 mL of *i*-PrOH and 7 mL of hexanes to give 0.240 g (0.740 mmol, 67% recrystallization yield) of $[^{13}C_4]$-**54** with an enantiopurity of 98% ee.

$[\alpha]_D^{18}$ −14.6 (*c* 0.8, $CHCl_3$). ^1H NMR (500 MHz, $CDCl_3$): δ 7.71 (d, *J* = 8.3 Hz, 2H), 7.26 (d, *J* = 8.3 Hz, 2H), 6.86 (ddd, *J* = 152.6, 12.5, 6.4 Hz, 1H), 5.24–5.16 (m, 1H), 4.46–4.40 (m, 1H), 2.70–2.59 (m, 1H), 2.39 (s, 3H), 2.25 (dd, *J* = 127.7, 5.8 Hz, 3H), 2.39–2.31 (m, 1H), 2.20–2.13 (m, 1H), 1.77–1.58 (m, 3H), 1.55–1.43 (m, 2H). ^{13}C NMR (125 MHz, CDCl$_3$): δ 197.36 (ddd, *J* = 50.4, 43.3, 4.1 Hz), 147.3 (ddd, *J* = 69.6, 50.5, 12.2 Hz), 143.5 (dd, *J* = 69.6, 3.7 Hz), 143.4, 137.2, 129.7, 126.8, 58.9, 56.1, 33.3, 31.9, 29.6, 25.3 (dd, *J* = 43.3, 12.2 Hz), 24.3 (dd, *J* = 40.0, 5.6 Hz), 21.5. HRMS–ESI (*m*/*z*): [M + Na]$^+$ calcd for $^{13}C_4C_{13}H_{21}NO_3SNa$, 346.1274; found, 346.1276.

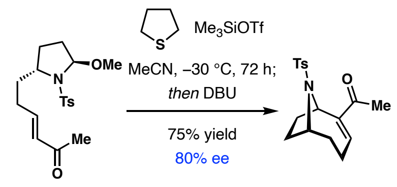

[^{13}C$_4$]-**39** [^{13}C$_4$]-**54**

***N*-Tosylanatoxin-a 54.** The title compound was obtained using the procedure described above for its ^{13}C$_4$ analog using 0.260 g (0.74 mmol) of vinyl ketone **39**, 0.34 mL (1.85 mmol, 2.5 equiv), and 98 μL (1.11 mmol, 1.5 equiv) of tetrahydrothiophene in 7.4 mL of MeCN, followed by treatment of 0.22 mL (1.48 mmol, 2.0 equiv) of DBU. **54** was obtained in 75% yield (0.177 g, 0.55 mmol). The enantiopurity of the material (80% ee) was measured by HPLC trace analysis described for its ^{13}C$_4$ analog with identical retention times (see page 150).

$[\alpha]_D^{20}$ –13.9 (*c* 0.8, CHCl$_3$). ^{1}H NMR (600 MHz, CDCl$_3$): δ 7.71 (d, *J* = 8.1 Hz, 2H), 7.26 (d, *J* = 8.1 Hz, 2H), 6.86 (t, *J* = 5.8 Hz, 1H), 5.21 (d, *J* = 8.7 Hz, 1H), 4.46–4.40 (m, 1H), 2.71–2.61 (m, 1H), 2.44–2.32 (m, 4H), 2.26 (s, 3H), 2.22–2.12 (m, 1H), 1.80–1.60 (m, 3H), 1.57–1.44 (m, 2H). ^{13}C NMR (150 MHz, CDCl$_3$): δ 197.6, 147.5, 143.4, 143.3, 137.4, 129.8, 127.1, 59.0, 56.5, 33.7, 32.1, 29.9, 25.5, 24.5, 21.6. HRMS–ESI (*m*/*z*): [M + Na]$^+$ calcd for $C_{17}H_{21}NO_3SNa$, 342.1140; found, 342.1136.

==== Shimadzu LCsolution Analysis Report ====

C:\LabSolutions\Data\AKM\Anatoxin-a\AKM-09-234.lcd

Acquired by	: Artur Mailyan
Sample Name	: AKM-09-234
Sample ID	: AKM-09-234
Vail #	:
Injection Volume	: 10 uL
Data File Name	: AKM-09-234.lcd
Method File Name	: brad.lcm
Batch File Name	:
Report File Name	: Default.lcr
Data Acquired	: 6/23/2018 11:18:55 AM
Data Processed	: 6/23/2018 11:54:50 AM

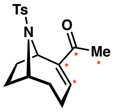

(±)-[$^{13}C_4$]-**54**

<Chromatogram>

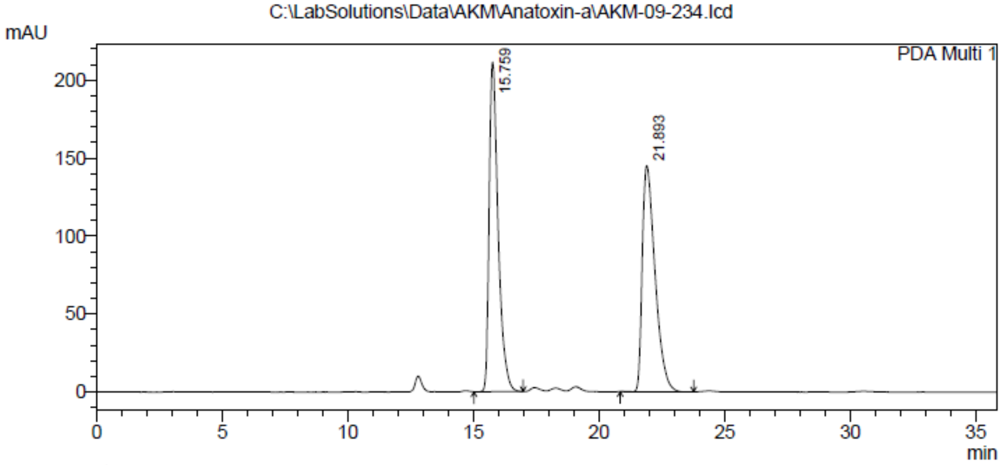

1 PDA Multi 1/254nm 4nm

PeakTable

PDA Ch1 254nm 4nm

Peak#	Ret. Time	Area	Height	Area %	Height %
1	15.759	5253735	211405	50.601	59.321
2	21.893	5128905	144968	49.399	40.679
Total		10382640	356373	100.000	100.000

==== Shimadzu LCsolution Analysis Report ====

	C:\LabSolutions\Data\AKM\Anatoxin-a\AKM-09-156_before_cryst2.lcd
Acquired by	: Artur Mailyan
Sample Name	: AKM-09-156_before_cryst2
Sample ID	: AKM-09-156_before_cryst2
Vail #	:
Injection Volume	: 10 uL
Data File Name	: AKM-09-156_before_cryst2.lcd
Method File Name	: brad.lcm
Batch File Name	:
Report File Name	: Default.lcr
Data Acquired	: 6/20/2018 3:49:25 PM
Data Processed	: 6/20/2018 4:17:32 PM

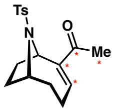

[$^{13}C_4$]-**54**

80% ee

<Chromatogram>

C:\LabSolutions\Data\AKM\Anatoxin-a\AKM-09-156_before_cryst2.lcd

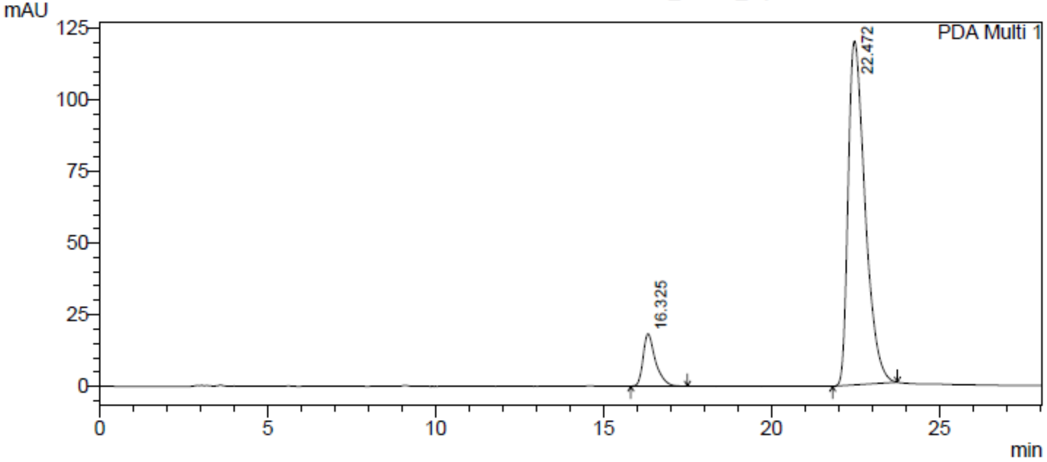

1 PDA Multi 1/254nm 4nm

PeakTable

PDA Ch1 254nm 4nm

Peak#	Ret. Time	Area	Height	Area %	Height %
1	16.325	469863	18309	10.031	13.228
2	22.472	4214128	120103	89.969	86.772
Total		4683991	138412	100.000	100.000

==== Shimadzu LCsolution Analysis Report ====

C:\LabSolutions\Data\AKM\Anatoxin-a\AKM-09-156_after_cryst2.lcd
Acquired by : Artur Mailyan
Sample Name : AKM-09-156_after_cryst2
Sample ID : AKM-09-156_after_cryst2
Vail # :
Injection Volume : 10 uL
Data File Name : AKM-09-156_after_cryst2.lcd
Method File Name : brad.lcm
Batch File Name :
Report File Name : Default.lcr
Data Acquired : 6/23/2018 12:40:32 PM
Data Processed : 6/23/2018 1:09:42 PM

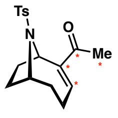

[$^{13}C_4$]-**54**
98% ee
(after recrystallization)

<Chromatogram>

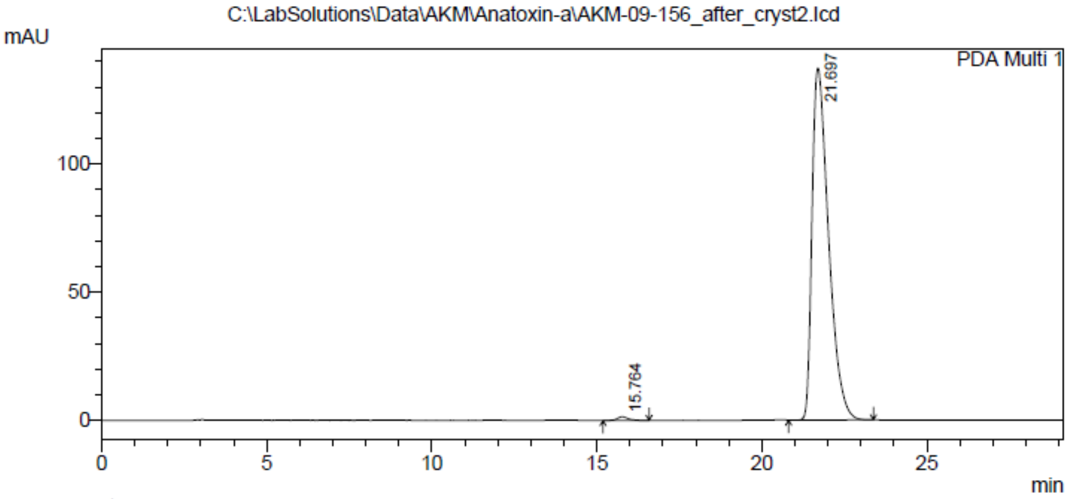

1 PDA Multi 1/254nm 4nm

PeakTable

PDA Ch1 254nm 4nm

Peak#	Ret. Time	Area	Height	Area %	Height %
1	15.764	31558	1408	0.657	1.015
2	21.697	4772383	137324	99.343	98.985
Total		4803941	138732	100.000	100.000

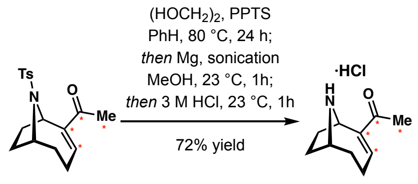

[^{13}C$_4$]-**54** [^{13}C$_4$]-**23·HCl**

(+)-[^{13}C$_4$]-Anatoxin-a hydrochloric salt ([^{13}C$_4$]-23·HCl): A mixture of *N*-tosylanatoxin-a [^{13}C$_4$]-**54** (0.240 g, 0.74 mmol), ethylene glycol (0.42 mL, 7.42 mmol, 10 equiv), and pyrdinium *p*-toluenesulfonate (19 mg, 0.074 mmol, 0.1 equiv) in benzene (10 mL) was heated to reflux with a Dean–Stark apparatus for 24 h. The reaction mixture was then cooled to 23 °C, and the solvent was evaporated under reduced pressure. The dry acetal residue was dissolved in MeOH (15 mL), and magnesium (0.530 g, 22.2 mmol, 30 equiv) was added to the solution ta 23 °C. The resulting suspension was sonicated at 23 °C for 1 h. The reaction solution was then quenched with 3 M aqueous hydrochloric acid (20 mL), and the resulting mixture was stirred at 23 °C for 1 h. The reaction solution was then carefully treated with solid K$_2$CO$_3$ until pH = 12. The mixture was filtered through celite to remove inorganic precipitates, and the aqueous layer was extracted with CH$_2$Cl$_2$ (4 × 20 mL). The combined organic layers were dried over Na$_2$SO$_4$ and concentrated to dryness under reduced pressure. The crude product was purified by reversed-phase column chromatography on C18 reversed-phase silica gel (1% MeOH, 0.1% trifluoroacetic acid in water to 3% MeOH, 0.3% trifluoroacetic acid in water). Treatment with a solution of 1 M hydrochloric acid in MeOH, followed by filtration of the precipitation from dry diethyl ether produced the hydrochloric salt of (+)-[^{13}C$_4$]-anatoxin-a ([^{13}C$_4$]-**23·HCl**) (0.110 g, 0.53 mmol, 72% yield) as a white solid.

$[\alpha]_{\mathrm{D}}^{21}$ +41.3 (*c* 1.0, MeOH). ^{1}H NMR (600 MHz, CD$_3$OD): δ 7.40 (dm, *J* = 157.4 Hz, 1H), 5.16–5.06 (m, 1H), 4.32–4.23 (m, 1H), 2.79–2.68 (m, 1H), 2.67–2.58 (m, 1H), 2.48–2.39 (m, 1H), 2.35 (dd, *J* = 128.0, 6.0 Hz, 3H), 2.30–2.20 (m, 1H), 2.19–2.11 (m, 1H), 2.05–1.89 (m, 3H). ^{13}C

NMR (150 MHz, CD$_3$OD): δ 198.4 (ddd, *J* = 51.2, 44.0, 3.8), 149.5 (d, *J* = 68.2 Hz), 144.7 (ddd, *J* = 68.1, 51.3, 13.0 Hz), 60.6 (d, *J* = 11.8 Hz), 53.7 (dd, *J* = 46.6, 15.8 Hz), 31.2, 29.0, 28.3, 25.42 (ddd, *J* = 44.0, 13.0, 5.4 Hz), 24.5 (dd, *J* = 39.0, 5.6 Hz). HRMS–ESI (*m/z*): $[M + H]^+$ calcd for $^{13}C_4C_6H_{16}NO$, 170.1366; found, 170.1365.

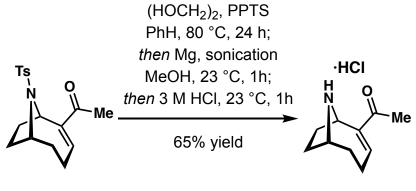

54

23·HCl

(+)-Anatoxin-a hydrochloric salt (23·HCl): The title compound was obtained using the procedure described above for its $^{13}C_4$ analog using 0.130 g (0.41 mmol) of *N*-tosylanatoxin-a (**54**), 0.23 mL (4.1 mmol, 10 equiv) of ethylene glycol, and 10.3 mg (0.041 mmol, 0.1 equiv) of pyridinium *p*-toluenesulfonate in 4.1 mL of benzene, followed by sonication with 0.295 g (12.3 mmol, 30 equiv) of magnesium in 7 mL of methanol. The hydrochloric salt of (+)-anatoxin-a (**23·HCl**) was obtained in 65% yield (54 mg, 0.27 mmol).

$[\alpha]^{23}_{D}$ +39.1 (*c* 1.0, MeOH). ^{1}H NMR (500 MHz, CD$_3$OD): δ 7.39 (dd, *J* = 8.6, 2.7 Hz, 1H), 5.10 (d, *J* = 9.3 Hz, 1H), 4.30–4.24 (m, 1H), 2.78–2.68 (m, 1H), 2.68–2.58 (m, 1H), 2.49–2.39 (m, 1H), 2.35 (s, 3H), 2.30–2.20 (m, 1H), 2.19–2.09 (m, 1H), 2.06–1.91 (m, 3H). ^{13}C NMR (125 MHz, CD$_3$OD): δ 198.5, 149.5, 144.7, 60.6, 53.7, 31.2, 29.0, 28.3, 25.5, 24.6. HRMS–ESI (*m/z*): $[M + H]^+$ calcd for $C_{10}H_{16}NO$, 166.1232; found, 166.1228.

Isotope Incorporation of (+)-[$^{13}C_4$]-Anatoxin-a ([$^{13}C_4$]-23) by HRMS:

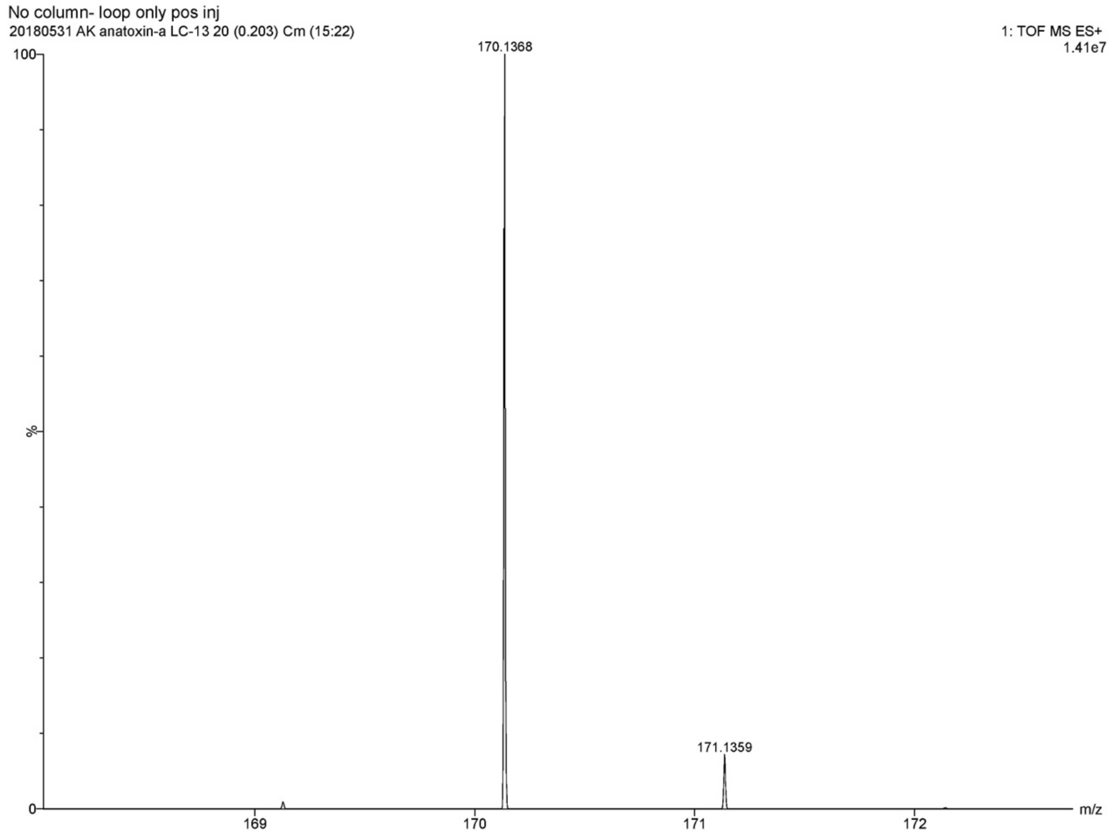

```
Spectrum Report                                        MassLynx MassLynx V4.1 SCN909
Data File:           Z:\Artur\20180531 AK anatoxin-a LC-13.raw
Acquired:            31-May-2018 12:18:50
Scan:                20 (0.203)
Function:            1: TOF MS (50:500) ES+
Process:             Cm (14:22)
Printed:             At              Thursday, May 31, 2018 12:59:01 Pacific Daylight Time

        Mass     Inten      %BPI    %TIC
--------------------------------------------------------------------------------------------------------------
    169.1220    4.03e4      0.26    0.07
    169.1247    9.46e4      0.61    0.15
    169.1273    1.42e5      0.91    0.23
    169.1300    1.30e5      0.83    0.21
    170.1315    5.19e6     33.24    8.40
    170.1341    1.23e7     78.74   19.89
    170.1368    1.56e7    100.00   25.26
    170.1395    8.18e6     52.39   13.23
    170.1421    2.57e6     16.45    4.16
```

Isotope incorporation was calculated from the peak intensities of *m/z* corresponding to (+)-[$^{13}C_4$]-anatoxin-a and (+)-[$^{13}C_3$]-anatoxin-a. The following values were obtained:

(+)-[$^{13}C_4$]-anatoxin-a (*m/z* = 170.1368)	99.1%
(+)-[$^{13}C_3$]-anatoxin-a (*m/z* = 169.1273)	0.9%
Total ^{13}C incorporation	> 99.8%

Enantioselective aza-MBH Cyclization:

Preparation of Chiral Sulfides for Enantioselective aza-MBH Cyclization:

Chiral sulfide **59** is commercially available and was purchased from TCI America. Sulfides **60**,[122] **61**,[123] and **62**[124] were prepared according to literatures. All other sulfides were synthesized according to the procedures outlined below. The absolute stereochemistry of thiolanes **63**, **64**, **65**, **66**, and **67** was not determined directly but was inferred through comparison of their specific rotations to the specific rotations of known 2,5-disubstituted thiolanes **62**,[124] **S9**,[125] **S10**,[126] **S11**,[127] and **S12**[126] (Figure 11). Preparative chiral HPLC purification was used to separate the enantiomeric thiolanes.

In all cases, the enantiomer which eluted first during chiral preparative HPLC purification was applied to the enantioselective aza-MBH cyclization of (±)-**39**. The measured specific rotation of our synthesized chiral sulfide **62** corresponded to the positive specific rotation previously reported; use of (+)-(*S*,*S*)-**62** for the aza-MBH cyclization produced the non-natural enantiomer of *N*-tosyl anatoxin-a (−)-**54** as the major product.[124] Chiral sulfides **63** and **64** were also measured to have positive specific rotations; employing thiolanes (+)-(*S*,*S*)-**63** and (+)-(*R*,*R*)-**64** in our enantioselective aza-MBH condition afforded (−)-**54**. Chiral sulfides **65**, **66**, and **67** measured to have negative specific rotations. Enantioselective aza-MBH cyclization performed with (−)-(*R*,*R*)-**64**, (−)-(*R*,*R*)-**65**, and (−)-(*R*,*R*)-**66** all yielded the natural enantiomer (+)-**54**. Our results suggest a high correlation between the measured optical rotations and the selectivity shown in the cyclized product **54**: a chiral sulfide with a positive optical rotation favors the formation of the (−)-**54**, while a chiral sulfide with a negative optical rotation favors the cyclization of the (+)-**54**.

Specific Rotations for Known 2,5-Disubstituted Thiolanes

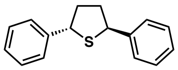

(+)-(2*S*,5*S*)-2,5-diphenylthiolane
(*S*,*S*)-**62**
$[\alpha]_D^{25} = +22.3$ (*c* 0.5, $CHCl_3$)

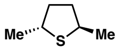

(+)-(2*R*,5*R*)-2,5-dimethylthiolane
(*R*,*R*)-**S9**
$[\alpha]_D^{25} = +119$ (*c* 4.0, pentane)

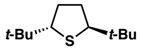

(+)-(2*S*,5*S*)-2,5-di-tert-butylthiolane
(*S*,*S*)-**S10**
$[\alpha]_D^{20} = +56$ (*c* 0.06, $CHCl_3$)

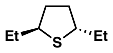

(–)-(2*S*,5*S*)-2,5-diethylthiolane
(*S*,*S*)-**S11**
$[\alpha]_D^{23} = -38$ (*c* 0.65, $CHCl_3$)

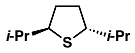

(–)-(2*R*,5*R*)-2,5-diisopropylthiolane
(*R*,*R*)-**S12**
$[\alpha]_D^{20} = -141$ (*c* 0.75, Et_2O)

Proposed Configurations for Newly Synthesized Thiolanes

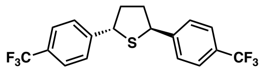

(+)-(2*S*,5*S*)-2,5-di(4-trifluoromethylphenyl)thiolane
(*S*,*S*)-**63**
$[\alpha]_D^{22} = +8.3$ (*c* 1.0, $CHCl_3$)

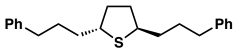

(+)-(2*R*,5*R*)-2,5-di(3-phenyl-1-propyl)thiolane
(*R*,*R*)-**64**
$[\alpha]_D^{24} = +100$ (*c* 1.0, $CHCl_3$)

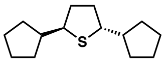

(–)-(2*R*,5*R*)-2,5-dicyclopentylthiolane
(*R*,*R*)-**65**
$[\alpha]_D^{22} = -150$ (*c* 1.0, $CHCl_3$)

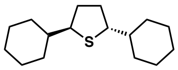

(–)-(2*R*,5*R*)-2,5-dicyclohexylthiolane
(*R*,*R*)-**66**
$[\alpha]_D^{20} = -168$ (*c* 1.0, $CHCl_3$)

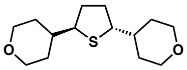

(–)-(2*R*,5*R*)-2,5-di(4-tetrahydropyranyl)thiolane
(*R*,*R*)-**67**
$[\alpha]_D^{25} = -159$ (*c* 1.0, $CHCl_3$)

Figure 11. Specific rotations of 2,5-disubstituted thiolanes.

Synthesis of Chiral Thiolanes 63–67:

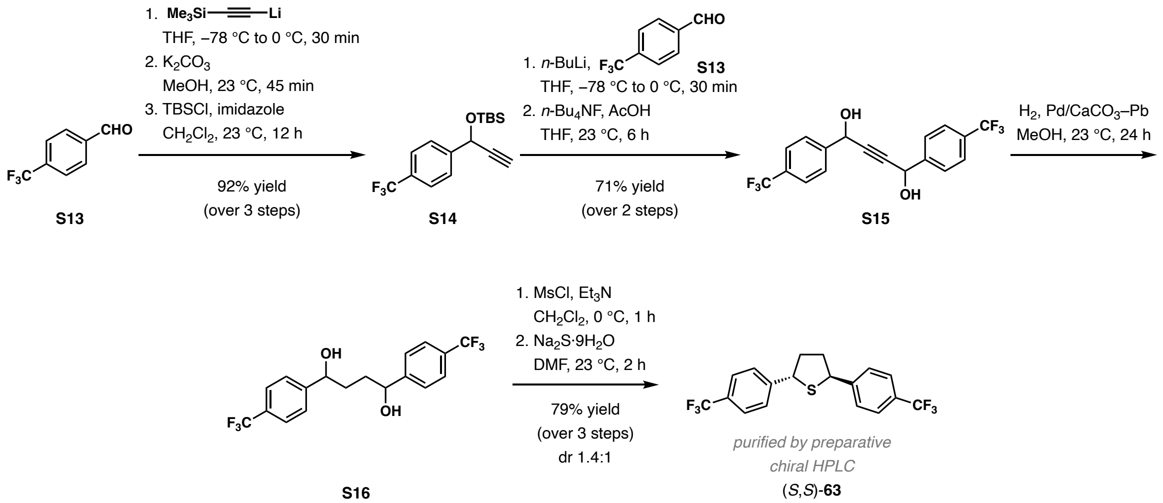
1. Me3Si—≡—Li
THF, –78 °C to 0 °C, 30 min
2. K2CO3
MeOH, 23 °C, 45 min
3. TBSCl, imidazole
CH2Cl2, 23 °C, 12 h
92% yield
(over 3 steps)
CHO
F3C
S13
OTBS
S14
1. n-BuLi, S13
THF, –78 °C to 0 °C, 30 min
2. n-Bu4NF, AcOH
THF, 23 °C, 6 h
71% yield
(over 2 steps)
OH
CF3
S15
H2, Pd/CaCO3–Pb
MeOH, 23 °C, 24 h
S16
1. MsCl, Et3N
CH2Cl2, 0 °C, 1 h
2. Na2S·9H2O
DMF, 23 °C, 2 h
79% yield
(over 3 steps)
dr 1.4:1
S
purified by preparative
chiral HPLC
(S,S)-63

Thiolane 63. *n*-Butyllithium (2.55 M in hexanes, 7.8 mL, 20.0 mmol, 2.0 equiv) was added dropwise to a solution of trimethylsilyl acetylene (2.16 g, 22.0 mmol, 2.2 equiv) in THF (40 mL) at −78 °C. The resulting mixture was stirred at −78 °C for 30 min before a solution of 4-(trifluoromethyl)benzaldehyde **S13** (1.74 g, 10.0 mmol) in THF (10 mL) was added dropwise at −78 °C. The reaction solution was warmed to 0 °C and stirred at 0 °C for 30 min. The resulting mixture was quenched with a saturated aqueous solution of NH_4Cl (75 mL). The layers were separated, and the aqueous layer was extracted with EtOAc (3 × 50 mL). The combined organic layers were washed with brine (200 mL), dried over Na_2SO_4, and concentrated to dryness under reduced pressure. The crude product was submitted to the next step without further purification.

The crude residue was redissolved in MeOH (100 mL) at 23 °C, and potassium carbonate (1.66 g, 12.0 mmol, 1.2 equiv) was added. The reaction mixture was stirred at 23 °C for 45 min. The solvent was evaporated under reduced pressure and the dry residue was dissolved in EtOAc (75 mL) and water (100 mL). The layers were separated, and the aqueous layer was extracted with EtOAc (3 × 50 mL). The combined organic layers were washed with brine (200 mL), dried over

Na_2SO_4, and concentrated to dryness under reduced pressure. The crude product was submitted to the next step without further purification.

The crude alcohol product was dissolved in CH_2Cl_2 (100 mL) at 23 °C, imidazole (1.63 g, 24.0 mmol, 2.4 equiv), and TBSCl (1.81 g, 12.0 mmol, 1.2 equiv) were added sequentially. The reaction mixture was stirred at 23 °C for 12 h before it was quenched with water (100 mL). The layers were separated, and the aqueous layer was extracted with CH_2Cl_2 (3 × 75 mL). The combined organic layers were dried over Na_2SO_4 and concentrated to dryness under reduced pressure. The crude product was purified by column chromatography on silica gel (20% EtOAc in hexanes) to give **S14** (2.91 g, 2.95 mmol, 92% yield over 3 steps).

n-Butyllithium (2.55 M in hexanes, 2.16 mL, 5.50 mmol, 1.1 equiv) was added dropwise to a solution of **S14** (1.57 g, 5.00 mmol) in THF (25 mL) at −78 °C. The resulting mixture was stirred at −78 °C before a solution of 4-(trifluoromethyl)benzaldehyde **S13** (1.31 g, 7.50 mmol, 1.5 equiv) in THF (10 mL) was added dropwise at −78 °C. The reaction solution was warmed to 0 °C and stirred at 0 °C for 30 min. The resulting mixture was quenched with a saturated aqueous solution of NH_4Cl (75 mL). The layers were separated, and the aqueous layer was extracted with EtOAc (3 × 50 mL). The combined organic layers were washed with brine (200 mL), dried over Na_2SO_4, and concentrated to dryness under reduced pressure. The crude product was submitted to the next step without further purification.

Acetic acid (0.43 mL, 7.50 mmol, 1.5 equiv) was added to a solution of the crude product from the previous step in THF (20 mL) at 23 °C, followed by the addition of a solution of *n*-$Bu_4NF \cdot xH_2O$ (1.57 g, 6.00 mmol, 1.2 equiv) in THF (5 mL). The reaction mixture was stirred at 23 °C for 6 h before it was quenched by a saturated aqueous solution of $NaHCO_3$ (50 mL) and diluted with EtOAc (30 mL). The layers were separated, and the aqueous layer was extracted with

EtOAc (3 × 50 mL). The combined organic layers were washed with brine (200 mL) and dried over Na_2SO_4. Silica (approximately 5.0 g) was added to the organic filtrate, and the solution was carefully concentrated under reduced pressure. The resulting crude residue was dry-loaded onto a silica gel column and purified by column chromatography on silica gel (25% EtOAc in hexanes to 50% EtOAc in hexanes) to afford diol **S15** (1.33 g, 3.56 mmol, 71% yield over 2 steps).

Palladium on calcium carbonate, poisoned with lead (5 wt % Pd, 0.783 g, 0.340 mmol, 10 mol %) was added to a solution of diol **S15** (1.24 g, 3.40 mmol) in MeOH (34 mL) at 23 °C. The reaction mixture was stirred under an atmosphere of hydrogen gas at 23 °C for 24 h. The resulting mixture was filtered through celite and concentrated under reduced pressure. The crude diol **S16** was submitted to the next step without further purification.

The crude diol **S16** was dissolved in CH_2Cl_2 (34 mL) and the solution was cooled to 0 °C. Triethylamine (1.90 mL, 13.6 mmol, 4.0 equiv) and methanesulfonyl chloride (0.80 mL, 10.2 mmol, 3.0 equiv) were added dropwise at 0 °C. The reaction mixture was stirred at 0 °C for 1 h. The resulting solution was diluted with CH_2Cl_2 (50 mL), and the organic layer was washed with 1 M aqueous hydrochloric acid solution (75 mL), a saturated aqueous solution of $NaHCO_3$ (75 mL), and brine (75 mL), then dried over Na_2SO_4 and concentrated to dryness under reduced pressure. The crude product was submitted to the next step without further purification.

The crude bismesylate from the previous step was dissolved in DMF (68 mL) at 23 °C and sparged with argon for 10 min. $Na_2S{\cdot}9H_2O$ (4.08 g, 17.0 mmol, 5.0 equiv) was added to the solution, and the reaction mixture was stirred at 23 °C for 2 h. The resulting solution was diluted with water (500 mL), and the aqueous layer was extracted with EtOAc (4 × 100 mL). The combined organic layers were washed with brine (3 × 200 mL), dried over Na_2SO_4, and concentrated to dryness under reduced pressure. The crude product mixture (dr 1.4:1) of

(±)-*trans*- to *cis*-**63** was purified by column chromatography on silica gel (8% toluene in hexanes to 10% toluene in hexanes to 12% toluene in hexanes) to first elute the pure (±)-*trans*-**63** (0.548 g, 1.46 mmol, 42% yield over 3 steps), then a 1:10 mixture of (±)-*trans*-**63** (44 mg, 0.117 mmol, 3.4 yield) and *cis*-**63** (0.439 g, 1.17 mmol, 34% yield). A portion of the pure (±)-*trans*-**63** (0.300 g, 0.797 mmol) was purified through preparative chiral HPLC [Chiralpak ® AD-H; 250 × 20 mm i.d.; 0.5% *i*-PrOH in hexanes; flow rate = 6 mL/min; 3 mL injection of a 10 mg/mL solution; detection at 210 nm; t_1 = 20.33 min (**63**), t_2 = 24.96 min (*ent*-**63**)] to afford 0.130 g (0.345 mmol, 43% yield) of **63** and *ent*-**63** each as enantiopure crystalline, white solids.

The enantiopurity of materials were measured by HPLC trace analysis [Chiralpak ® AD-H; 0.25% *i*-PrOH in hexanes; flow rate = 1 mL/min; 10 μL injection of a 1 mg/mL solution; detection at 254 nm; t_1 = 8.02 min (*cis*-**63**), t_2 = 8.49 min (**63**), t_3 = 16.25 min (*ent*-**63**)].

63: $[\alpha]_D^{22}$ +8.3 (*c* 1.0, $CHCl_3$). ^{1}H NMR (500 MHz, $CDCl_3$): δ 7.60 (s, 8H), 4.90 (t, *J* = 7.3 Hz, 2H), 2.64 (qd, *J* = 9.1, 5.6 Hz, 2H), 2.13 (p, *J* = 11.6 Hz, 2H). ^{13}C NMR (125 MHz, $CDCl_3$): δ 146.4, 129.7 (q, *J* = 32.5 Hz), 128.2, 125.7 (q, *J* = 3.8 Hz), 124.3 (q, *J* = 272.0 Hz), 54.0, 41.2. HRMS–ESI (*m/z*): $[M + C_2H_5]^+$ calcd for $C_{20}H_{19}F_6S$, 405.1112; found, 405.1107.

Preparative Chiral HPLC for (±)-*trans*-**63**:

SHIMADZU LabSolutions

Analysis Report

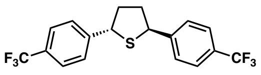

(±)-**63**

<Sample Information>

Sample Name	: JJL-6-287-preprun1
Sample ID	: JJL-6-287-preprun1
Data Filename	: JJL-6-287-preprun1.lcd
Method Filename	: JakePrep.lcm
Batch Filename	:
Vial #	: 1-1
Injection Volume	: 1500 uL
Date Acquired	: 11/16/2019 1:43:20 PM
Date Processed	: 11/16/2019 2:24:28 PM

Sample Type	: Unknown
Acquired by	: Jacob Lacharity
Processed by	: Jacob Lacharity

<Chromatogram>

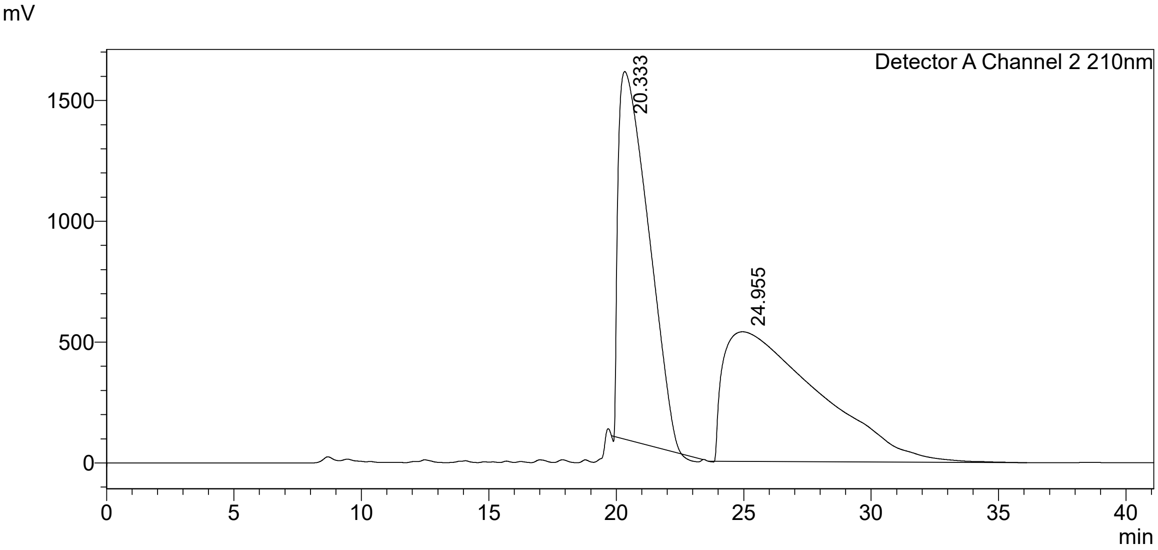

<Peak Table>

Detector A Channel 2 210nm

Peak#	Ret. Time	Area	Height	Area%	Height%
1	20.333	125395928	1521301	47.270	73.921
2	24.955	139881365	536699	52.730	26.079
Total		265277292	2058000	100.000	100.000

HPLC Trace Analysis for *cis*-**63** and (±)-*trans*-**63**:

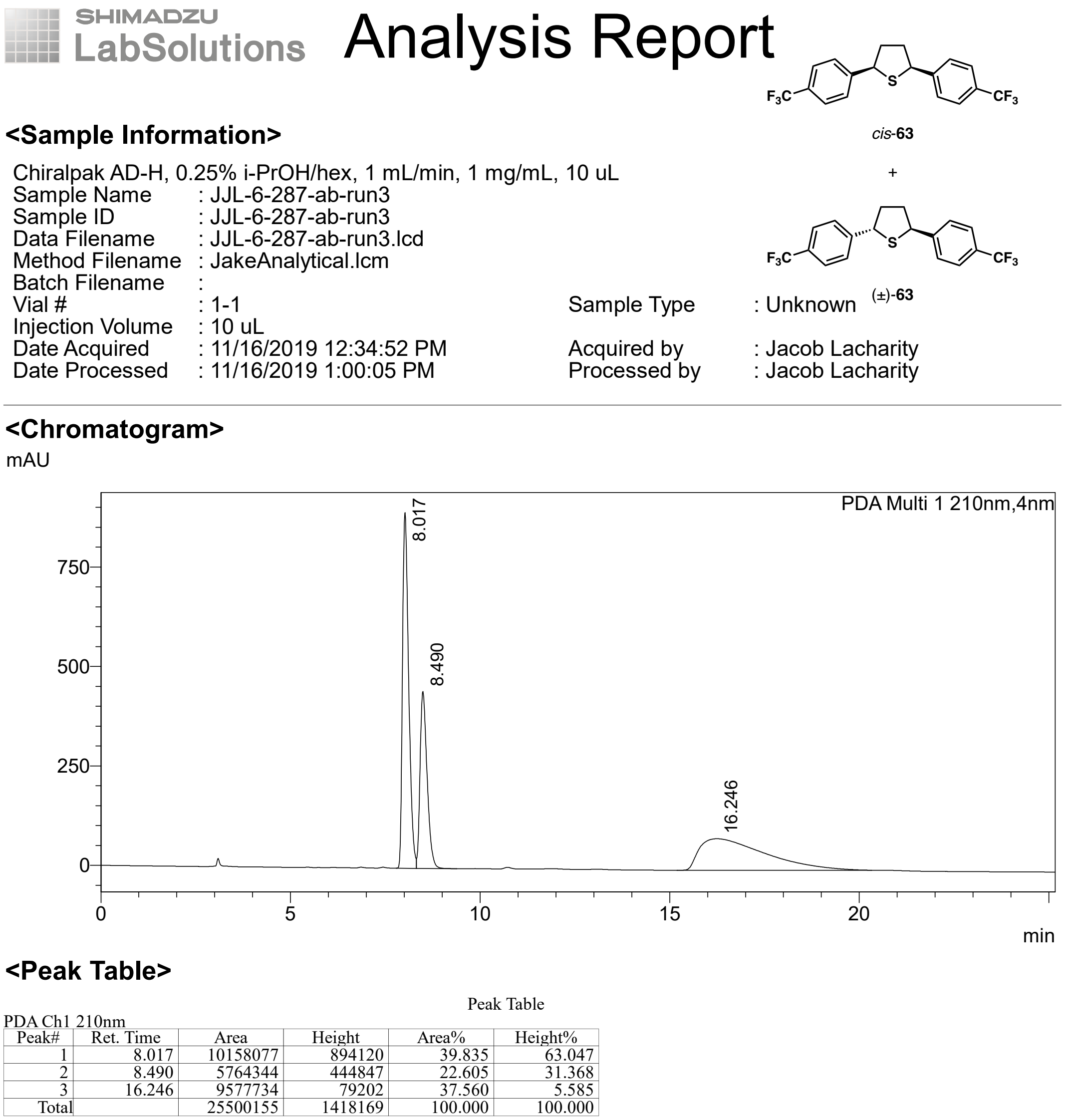

SHIMADZU LabSolutions

Analysis Report

<Sample Information>

Chiralpak AD-H, 0.25% i-PrOH/hex, 1 mL/min, 1 mg/mL, 10 uL

Sample Name : JJL-6-287-ab-run3
Sample ID : JJL-6-287-ab-run3
Data Filename : JJL-6-287-ab-run3.lcd
Method Filename : JakeAnalytical.lcm
Batch Filename :
Vial # : 1-1
Sample Type : Unknown
Injection Volume : 10 uL
Date Acquired : 11/16/2019 12:34:52 PM
Acquired by : Jacob Lacharity
Date Processed : 11/16/2019 1:00:05 PM
Processed by : Jacob Lacharity

<Chromatogram>

<Peak Table>

Peak Table

PDA Ch1 210nm

Peak#	Ret. Time	Area	Height	Area%	Height%
1	8.017	10158077	894120	39.835	63.047
2	8.490	5764344	444847	22.605	31.368
3	16.246	9577734	79202	37.560	5.585
Total		25500155	1418169	100.000	100.000

HPLC Trace Analysis of Enantioenriched **63**:

SHIMADZU
LabSolutions

Analysis Report

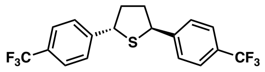

63

99% ee

<Sample Information>

Sample Name : JJL-6-293-prepHPLC-b
Sample ID : JJL-6-293-prepHPLC-b
Data Filename : JJL-6-293-prepHPLC-b.lcd
Method Filename : JakeAnalytical.lcm
Batch Filename :
Vial # : 1-1
Injection Volume : 10 uL
Date Acquired : 11/21/2019 4:40:40 PM
Date Processed : 11/21/2019 4:52:36 PM

Sample Type : Unknown
Acquired by : Jacob Lacharity
Processed by : Jacob Lacharity

<Chromatogram>

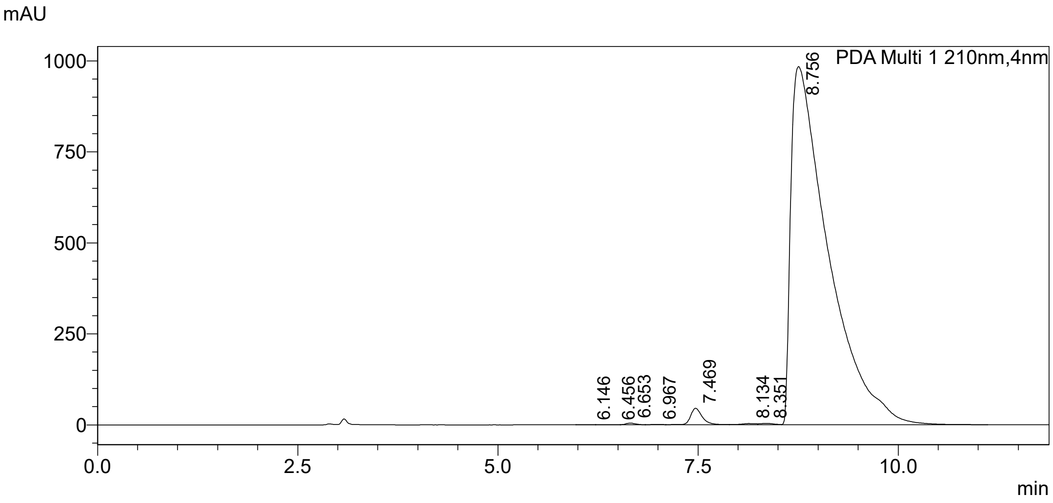

<Peak Table>

Peak Table

PDA Ch1 210nm

Peak#	Ret. Time	Area	Height	Area%	Height%
1	6.146	2225	210	0.007	0.020
2	6.456	5923	572	0.018	0.055
3	6.653	41270	4829	0.127	0.463
4	6.967	9725	789	0.030	0.076
5	7.469	469427	45449	1.440	4.357
6	8.134	45296	3393	0.139	0.325
7	8.351	45143	3775	0.138	0.362
8	8.756	31984663	984193	98.101	94.343
Total		32603671	1043211	100.000	100.000

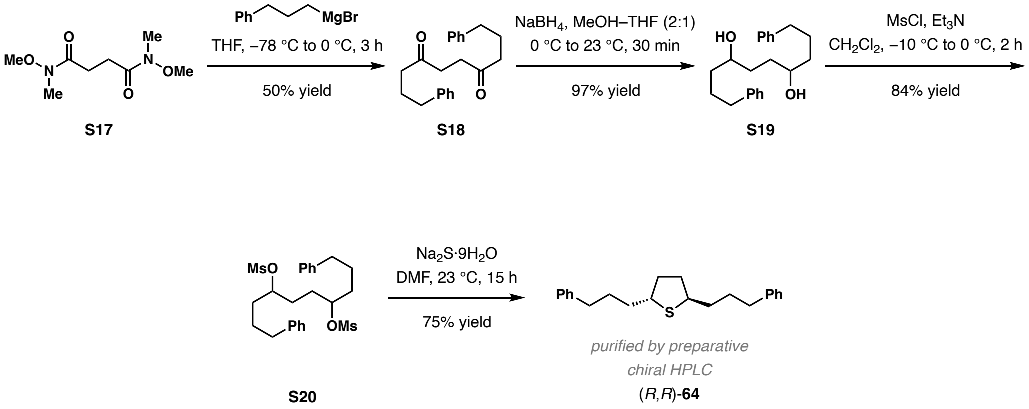
MgBr
THF, −78 °C to 0 °C, 3 h
50% yield
NaBH$_4$, MeOH–THF (2:1)
0 °C to 23 °C, 30 min
97% yield
MsCl, Et$_3$N
CH$_2$Cl$_2$, −10 °C to 0 °C, 2 h
84% yield
Na$_2$S·9H$_2$O
DMF, 23 °C, 15 h
75% yield
S17
S18
S19
S20
purified by preparative chiral HPLC
(R,R)-64

Thiolane 64. A solution of 3-phenylpropylmagnesium bromide (0.91 M in THF, 8.1 mL, 7.35 mmol, 3.0 equiv) was added dropwise to a solution of **S17**[128] (0.500 g, 2.45 mmol) in THF (12.3 mL) at −78 °C. The reaction mixture was warmed to 0 °C and stirred at 0 °C for 3 h before it was quenched with a saturated aqueous solution of NH_4Cl (25 mL). The layers were separated, and the aqueous layer was extracted with EtOAc (3 × 15 mL). The combined organic layers were washed with brine (60 mL), dried over Na_2SO_4, and concentrated to dryness under reduced pressure. The crude product was purified by column chromatography on silica gel (10% EtOAc in hexanes) to afford **S18** (0.396 g, 1.23 mmol, 50% yield). The spectral data were in full agreement with those reported in the literature.[129]

Sodium borohydride (93 mg, 2.46 mmol, 2.0 equiv) was added portion-wise to a solution of **S18** (0.396 g, 1.23 mmol) in MeOH (8.2 mL) and THF (4.1 mL) at 0 °C. The reaction mixture was warmed to 23 °C and stirred at 23 °C for 30 min. The solvent was evaporated under reduced pressure, and the dry residue was dissolved in a EtOAc (50 mL). The organic layer was washed with 1 M aqueous hydrochloric acid solution (30 mL), a saturated aqueous solution of $NaHCO_3$ (30 mL), and brine (30 mL), then dried over Na_2SO_4 and concentrated to dryness under reduced pressure. The crude product was purified by column chromatography on silica gel (50% EtOAc in hexanes) to afford diol **S19** (0.391 g, 1.20 mmol, 97% yield).

Diol **S19** (0.391 g, 1.20 mmol) was dissolved in CH_2Cl_2 (2.5 mL) and the solution was cooled to −10 °C. Triethylamine (0.67 mL, 3.58 mmol, 4.0 equiv) and methanesulfonyl chloride (0.28 mL, 3.58 mmol, 3.0 equiv) were added dropwise at −10 °C. The reaction mixture was warmed to 23 °C and stirred at 23 °C for 2 h. The resulting solution was diluted with CH_2Cl_2 (30 mL), and the organic layer was washed with 1 M aqueous hydrochloric acid solution (30 mL), a saturated aqueous solution of $NaHCO_3$ (30 mL), and brine (30 mL), then dried over Na_2SO_4 and concentrated to dryness under reduced pressure. The crude product was purified by column chromatography on silica gel (20% EtOAc in hexanes to 25% EtOAc in hexanes to 30% EtOAc in hexanes to 40% EtOAc in hexanes) to give **S20** (0.480 g, 0.994 mmol, 84% yield) as a clear oil.

$Na_2S\cdot 9H_2O$ (4.08 g, 17.0 mmol, 5.0 equiv) was added to a solution of bismesylate **S20** (0.467 g, 0.969 mmol) in DMF (49 mL) at 23 °C. The reaction mixture was stirred at 23 °C for 15 h. The resulting solution was diluted with water (300 mL), and the aqueous layer was extracted with EtOAc (4 × 75 mL). The combined organic layers were washed with brine (3 × 200 mL), dried over Na_2SO_4, and concentrated to dryness under reduced pressure. The crude product was purified by column chromatography on silica gel (2% EtOAc in hexanes) to afford a mixture (dr 1:1) of (±)-*trans*- to *cis*-**64** (0.234 g, 0.722 mmol, 75% yield). A portion of this mixture (95 mg, 0.294 mmol) was purified through preparative chiral HPLC [Chiralpak ® AD-H; 250 × 20 mm i.d.; 0.25% *i*-PrOH in hexanes; flow rate = 6 mL/min; 3 mL injection of a 10 mg/mL solution; detection at 210 nm; t_1 = 26.58 min (*cis*-**64**), t_2 = 34.00 min (**64**), t_3 = 43.14 min (*ent*-**64**)] to afford 20 mg (0.062 mmol, 21% yield) of **64** and 21 mg (0.065 mmol, 22% yield) of *ent*-**64** as enantiopure colorless oils.

The enantiopurity of **64** (99% ee) and *ent*-**64** (98% ee) were measured by HPLC trace analysis [Chiralpak ® AD-H; 0.25% *i*-PrOH in hexanes; flow rate = 1 mL/min; 10 μL injection of a 1 mg/mL solution; detection at 254 nm; t_1 = 9.95 min (*cis*-**64**), t_2 = 12.49 min (**64**), t_3 = 15.85 min (*ent*-**64**)].

64: $[\alpha]_D^{24}$ +100.7 (*c* 1.0, $CHCl_3$). ^1H NMR (600 MHz, $CDCl_3$): δ 7.28 (t, *J* = 7.8 Hz, 4H), 7.21–7.15 (m, 6H), 3.41 (tt, *J* = 8.4, 4.9 Hz, 2H), 2.63 (t, *J* = 6.7Hz, 4H), 2.17 (qd, *J* = 6.4, 3.7 Hz, 2H), 1.77–1.64 (m, 6H), 1.57 (tt, *J* =10.6, 4.9 Hz, 2H), 1.51 (t, *J* = 8.3 Hz, 2H). ^{13}C NMR (125 MHz, $CDCl_3$): δ 142.4, 128.5, 128.4, 125.8, 49.6, 37.4, 37.4, 35.9, 31.0. HRMS–ESI (*m/z*): $[M + H]^+$ calcd for $C_{22}H_{29}S$, 325.1990; found, 325.1987.

Preparative Chiral HPLC for *cis*-**64** and (±)-*trans*-**64**:

==== Shimadzu LCsolution Analysis Report ====

C:\LabSolutions\Data\Project1\kyc3-113a-prep1.lcd

Acquired by : Karen Chen
Sample Name : kyc3-113a-prep1
Sample ID : kyc3-113a-prep1
Vail # :
Injection Volume : 1 uL
Data File Name : kyc3-113a-prep1.lcd
Method File Name : JakeADHPrep.lcm
Batch File Name :
Report File Name : Default.lcr
Data Acquired : 4/10/2019 11:30:05 AM
Data Processed : 4/10/2019 12:49:56 PM

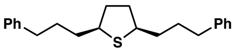

cis-**64**

+

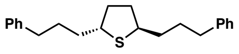

(±)-**64**

<Chromatogram>

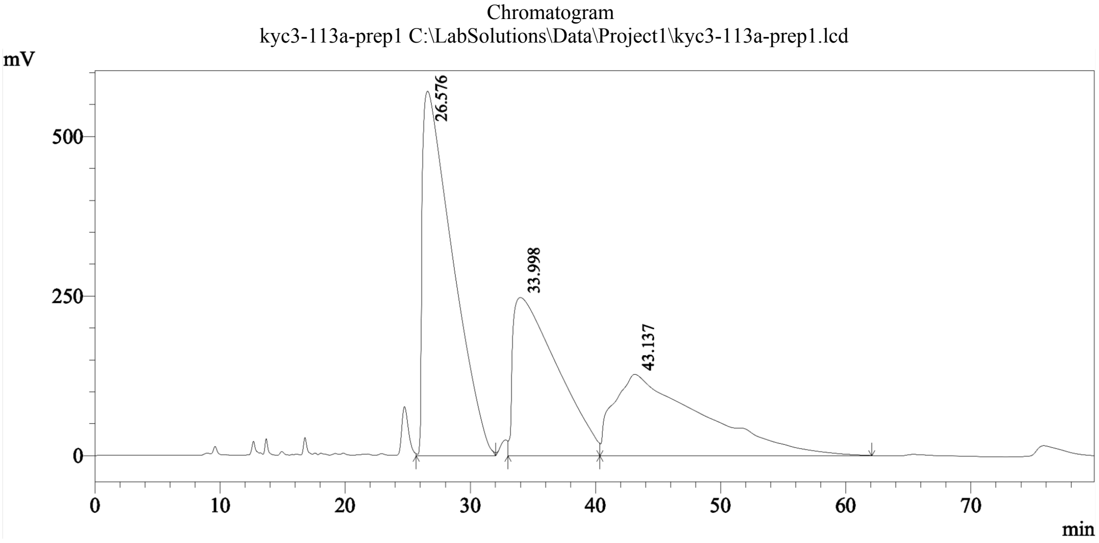

PeakTable

Detector A Ch2 210nm

Peak#	Ret. Time	Area	Height	Area %	Height %
1	26.576	95845877	571233	43.501	60.302
2	33.998	61076330	248192	27.720	26.200
3	43.137	63407337	127857	28.778	13.497
Total		220329544	947282	100.000	100.000

Note*: Thiolanes **64 and *ent*-**64** slightly overlap during preparative HPLC separation, hence, collected in fractions. The enantiopurity of **64** (99% ee) and *ent*-**64** (98% ee) were measured by HPLC trace analysis.

HPLC Trace Analysis for *cis*-**64** and (±)-*trans*-**64**:

==== Shimadzu LCsolution Analysis Report ====

C:\LabSolutions\Data\Project1\kyc3-113a.lcd

Acquired by : Karen Chen
Sample Name : kyc3-113a
Sample ID : kyc3-113a
Vail # :
Injection Volume : 10 uL
Data File Name : kyc3-113a.lcd
Method File Name : brad.lcm
Batch File Name :
Report File Name : Default.lcr
Data Acquired : 4/10/2019 10:05:27 AM
Data Processed : 4/10/2019 10:25:43 AM

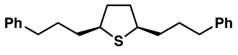

cis-**64**

+

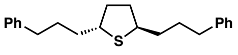

(±)-**64**

<Chromatogram>

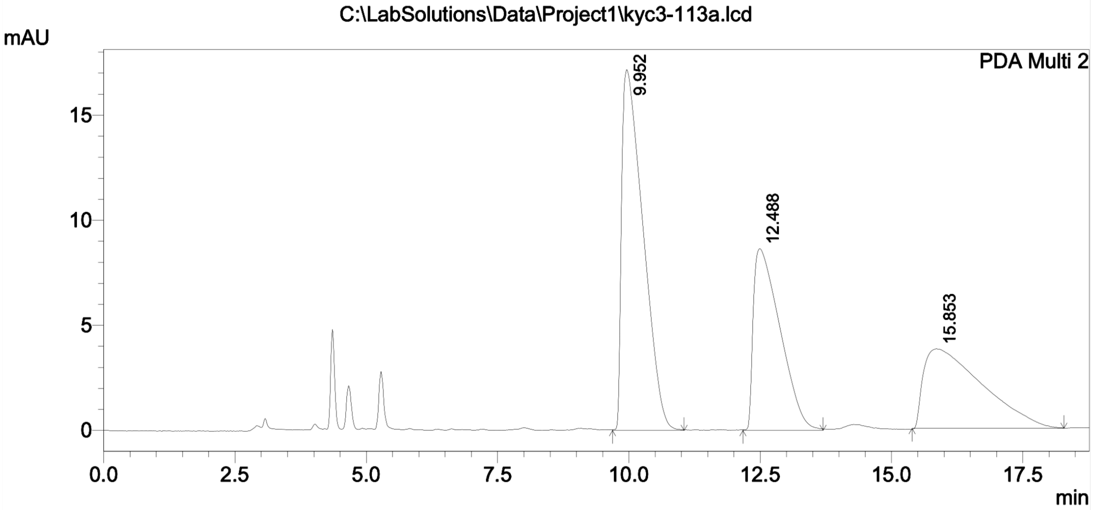

1 PDA Multi 2/254nm 4nm

PeakTable

PDA Ch2 254nm 4nm

Peak#	Ret. Time	Area	Height	Area %	Height %
1	9.952	487979	17174	44.804	58.002
2	12.488	305853	8648	28.082	29.206
3	15.853	295308	3788	27.114	12.793
Total		1089140	29609	100.000	100.000

HPLC Trace Analysis of Enantioenriched **64**:

==== Shimadzu LCsolution Analysis Report ====

C:\LabSolutions\Data\Project1\kyc3-113a-fB.lcd

Acquired by : Karen Chen
Sample Name : kyc3-113a-fB
Sample ID : kyc3-113a-fB
Vail # :
Injection Volume : 10 uL
Data File Name : kyc3-113a-fB.lcd
Method File Name : brad.lcm
Batch File Name :
Report File Name : Default.lcr
Data Acquired : 4/17/2019 8:30:14 PM
Data Processed : 4/17/2019 8:52:56 PM

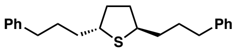

64

99% ee

<Chromatogram>

C:\LabSolutions\Data\Project1\kyc3-113a-fB.lcd

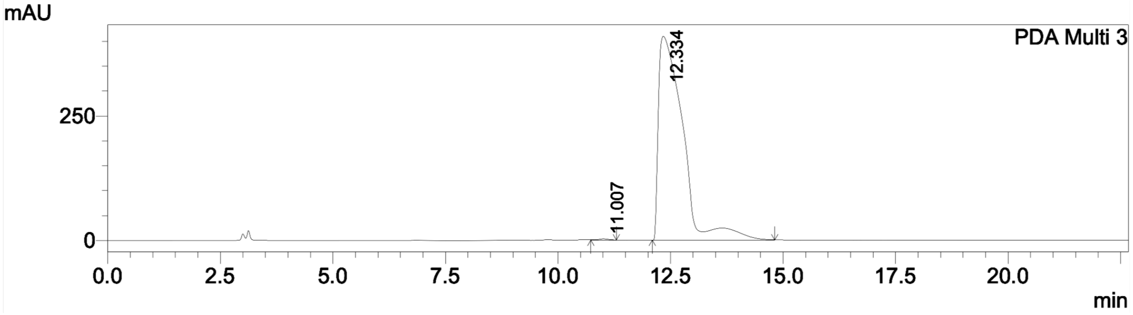

2 PDA Multi 3/210nm 4nm

PeakTable

PDA Ch3 210nm 4nm

Peak#	Ret. Time	Area	Height	Area %	Height %
1	11.007	37924	2389	0.247	0.580
2	12.334	15288956	409451	99.753	99.420
Total		15326880	411840	100.000	100.000

HPLC Trace Analysis of Enantioenriched *ent*-**64**:

==== Shimadzu LCsolution Analysis Report ====

C:\LabSolutions\Data\Project1\kyc3-114a-prep3-C2.lcd

Acquired by : Karen Chen
Sample Name : kyc3-114a-prep3-C2
Sample ID : kyc3-114a-prep3-C2
Vail # :
Injection Volume : 10 uL
Data File Name : kyc3-114a-prep3-C2.lcd
Method File Name : brad.lcm
Batch File Name :
Report File Name : Default.lcr
Data Acquired : 4/19/2019 11:13:52 AM
Data Processed : 4/19/2019 11:49:10 AM

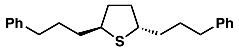

ent-**64**
98% ee

<Chromatogram>

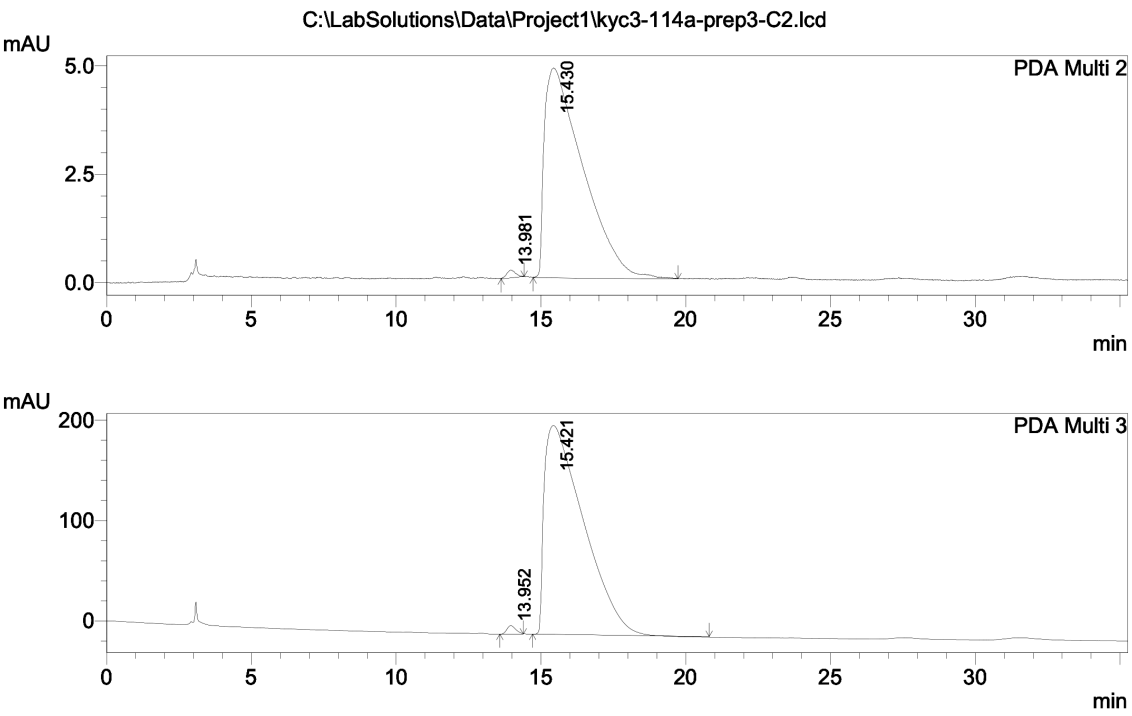

1 PDA Multi 2/254nm 4nm
2 PDA Multi 3/210nm 4nm

PeakTable

PDA Ch2 254nm 4nm

Peak#	Ret. Time	Area	Height	Area %	Height %
1	13.981	3890	181	0.858	3.602
2	15.430	449514	4848	99.142	96.398
Total		453404	5029	100.000	100.000

PeakTable

PDA Ch3 210nm 4nm

Peak#	Ret. Time	Area	Height	Area %	Height %
1	13.952	181507	8443	0.919	3.896
2	15.421	19576329	208238	99.081	96.104
Total		19757836	216681	100.000	100.000

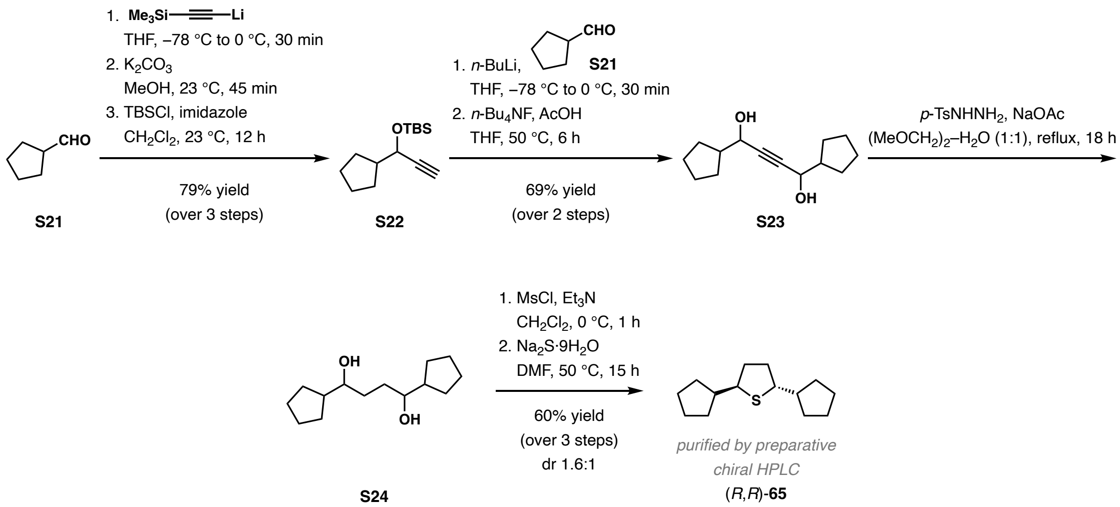
1. Me3Si—≡—Li
THF, −78 °C to 0 °C, 30 min
2. K2CO3
MeOH, 23 °C, 45 min
3. TBSCl, imidazole
CH2Cl2, 23 °C, 12 h
79% yield
(over 3 steps)
S21
CHO
OTBS
S22
1. n-BuLi, S21
THF, −78 °C to 0 °C, 30 min
2. n-Bu4NF, AcOH
THF, 50 °C, 6 h
69% yield
(over 2 steps)
OH
OH
S23
p-TsNHNH2, NaOAc
(MeOCH2)2–H2O (1:1), reflux, 18 h
OH
OH
S24
1. MsCl, Et3N
CH2Cl2, 0 °C, 1 h
2. Na2S·9H2O
DMF, 50 °C, 15 h
60% yield
(over 3 steps)
dr 1.6:1
S
purified by preparative
chiral HPLC
(R,R)-65

Thiolane 65. The title compound was prepared according to the procedures described above for thiolane **63**. Following the procedures described for **S14** (en route to thiolane **63**): 0.98 g (10.0 mmol) of cyclopentanecarbaldehyde **S21** was used with the following reagents with the indicated quantities: *n*-BuLi (2.55 M in hexanes, 7.8 mL, 20.0 mmol, 2.0 equiv); trimethylsilyl acetylene (2.16 g, 22.0 mmol, 2.2 equiv); potassium carbonate (1.66 g, 12.0 mmol, 1.2 equiv); imidazole (1.63 g, 24.0 mmol, 2.4 equiv); TBSCl (1.81 g, 12.0 mmol, 1.2 equiv). Silyl alcohol **S22** was obtained in 79% yield (1.88 g, 7.88 mmol) over 3 steps.

Diol **S23** was obtained using a modified procedure described for **S15**: starting with 1.88 g (7.88 mmol) of silyl alcohol **S22** and 1.20 equiv of *n*-butyllithium (2.55 M in hexanes, 3.71 mL, 9.46 mmol) in 30 mL of THF at −78 °C, 1.16 g (11.8 mmol, 1.5 equiv) of cyclopentanecarbaldehyde **S21** in 9 mL of THF was added at −78 °C before warming the resulting mixture to 0 °C to let stir for 30 min in the first step. The crude residue from the first step was dissolved in THF (30 mL) at 23 °C and treated with acetic acid (0.65 mL, 11.3 mmol, 1.5 equiv), followed by the addition of a solution of *n*-$Bu_4NF \cdot xH_2O$ (2.37 g, 9.06 mmol, 1.2 equiv) in THF (8 mL). The reaction mixture was heated to 50 °C and stirred at 50 °C for 6 h. The resulting solution was cooled to 23 °C before it was quenched by a saturated aqueous solution of

$NaHCO_3$ and diluted with EtOAc. The layers were separated, and the aqueous layer was extracted with EtOAc (3 × 75 mL). The combined organic layers were washed with brine, dried over Na_2SO_4, and concentrated to dryness under reduced pressure. The crude product was purified by column chromatography on silica gel (40% EtOAc in hexanes to 60% EtOAc in hexanes) to afford diol **S23** (1.22 g, 5.47 mmol, 72% yield over 2 steps).

A solution of diol **S23** (0.966 g, 4.51 mmol) in 1,2-dimethoxyethane (45 mL) and water (45 mL) was treated with *p*-toluenesulfonyl hydrazide (10.1 g, 54.1 mmol, 12.0 equiv) at 23 °C. The resulting mixture was then heated to reflux, and a solution of sodium acetate (9.20 g, 67.7 mmol, 15.0 equiv) was added over 5 h using a syringe pump. The reaction mixture was stirred for 18 h, then it was cooled to 23 °C and diluted with EtOAc (100 mL). The layers were separated, and the organic layer was washed with water (3 × 100 mL), dried over Na_2SO_4, and concentrated to dryness under reduced pressure. The crude diol **S24** was submitted to the next step without further purification.

Following a modified procedure described for thiolane **63** from diol **S16**. The crude diol **S24** obtained from the previous step was dissolved in 45 mL of CH_2Cl_2, followed by sequential addition of 2.51 mL (18.0 mmol, 4.0 equiv) of triethylamine and 1.05 mL (13.5 mmol, 3.0 equiv) of methanesulfonyl chloride for the first step. The resulting crude bismesylate was used directly without further purification: the crude residue was redissolved in DMF (225 mL) at 23 °C and treated with $Na_2S \cdot 9H_2O$ (5.42 g, 22.6 mmol, 5.0 equiv). The reaction mixture was then heated to 50 °C and stirred at 50 °C for 15 h. The resulting solution was then cooled to 23 °C then diluted with water, and the aqueous layer was extracted with EtOAc. The combined organic layers were washed with brine, dried over Na_2SO_4, and concentrated to dryness under reduced pressure. The crude product was purified by column chromatography on silica gel (100% hexanes) to afford a mixture (dr 1.6:1) of (±)-*trans*- to *cis*-**65** (0.603 g, 2.69 mmol, 60% yield over 3 steps). A portion of this mixture (0.300 g, 1.33 mmol) was purified through preparative chiral HPLC [Chiralpak ® AD-H; 250 × 20 mm i.d.; 0.05% *i*-PrOH in hexanes; flow rate = 6 mL/min; 3 mL injection of a 10 mg/mL solution; detection at 210 nm; t_1 = 17.38 min (*cis*-**65**), t_2 = 22.12 min (**65**), t_3 = 26.00 min (*ent*-**65**)] to afford 42 mg (0.187 mmol, 14% yield) of **65** and 40 mg (0.178 mmol, 13% yield) of *ent*-**65** as enantiopure white, crystalline solids.

The enantiopurity of **65** (> 99% ee) and *ent*-**65** (96% ee) were measured by HPLC trace analysis [Chiralpak ® AD-H; 0.15% *i*-PrOH in hexanes; flow rate = 1 mL/min; 10 μL injection of a 2 mg/mL solution; detection at 210 nm; t_1 = 5.36 min (*cis*-**65**), t_2 = 6.52 min (**65**), t_3 = 7.28 min (*ent*-**65**)].

65: $[\alpha]_D^{22}$ −150.0 (*c* 1.0, $CHCl_3$). ^1H NMR (600 MHz, $CDCl_3$): δ 3.28 (td, *J* = 9.1, 6.1 Hz, 2H), 2.17 (dp, *J* = 10.9, 5.5 Hz, 2H), 1.88 (h, *J* = 8.4 Hz, 2H), 1.78 (dp, *J* = 14.3, 5.6, 4.1 Hz, 4H), 1.66–1.55 (m, 4H), 1.51 (dtd, *J* = 9.8, 7.5, 3.2 Hz, 6H), 1.25 (dq, *J* = 12.1, 8.1 Hz, 2H), 1,16 (dq, 12.0, 8.3 Hz, 2H). ^{13}C NMR (125 MHz, $CDCl_3$): δ 55.8, 47.6, 37.1, 32.5, 31.9, 25.6, 25.5. HRMS–ESI (*m*/*z*): $[M + H]^+$ calcd for $C_{14}H_{25}S$, 225.1677; found, 225.1674.

Preparative Chiral HPLC for *cis*-**65** and (±)-*trans*-**65**:

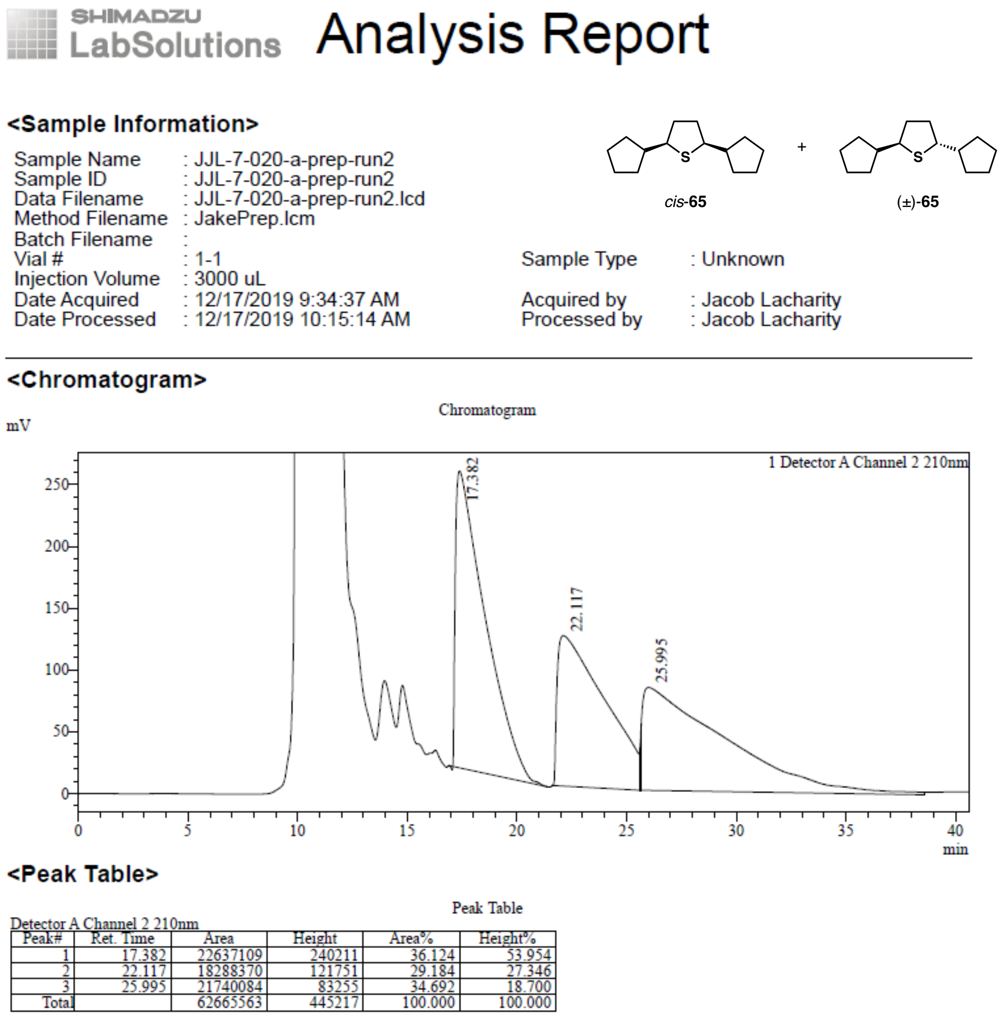

SHIMADZU LabSolutions

Analysis Report

<Sample Information>

Sample Name : JJL-7-020-a-prep-run2
Sample ID : JJL-7-020-a-prep-run2
Data Filename : JJL-7-020-a-prep-run2.lcd
Method Filename : JakePrep.lcm
Batch Filename :
Vial # : 1-1
Injection Volume : 3000 uL
Date Acquired : 12/17/2019 9:34:37 AM
Date Processed : 12/17/2019 10:15:14 AM

Sample Type : Unknown

Acquired by : Jacob Lacharity
Processed by : Jacob Lacharity

<Chromatogram>

Chromatogram
mV
1 Detector A Channel 2 210nm
250
200
150
100
50
0
17.382
22.117
25.995
0
5
10
15
20
25
30
35
40
min

<Peak Table>

Peak Table

Detector A Channel 2 210nm

Peak#	Ret. Time	Area	Height	Area%	Height%
1	17.382	22637109	240211	36.124	53.954
2	22.117	18288370	121751	29.184	27.346
3	25.995	21740084	83255	34.692	18.700
Total		62665563	445217	100.000	100.000

Note*: Thiolanes **65 and *ent*-**65** slightly overlap during preparative HPLC separation, hence, collected in fractions. The enantiopurity of **65** (> 99% ee) and *ent*-**65** (96% ee) were measured by HPLC trace analysis.

HPLC Trace Analysis for *cis*-**65** and (±)-*trans*-**65**:

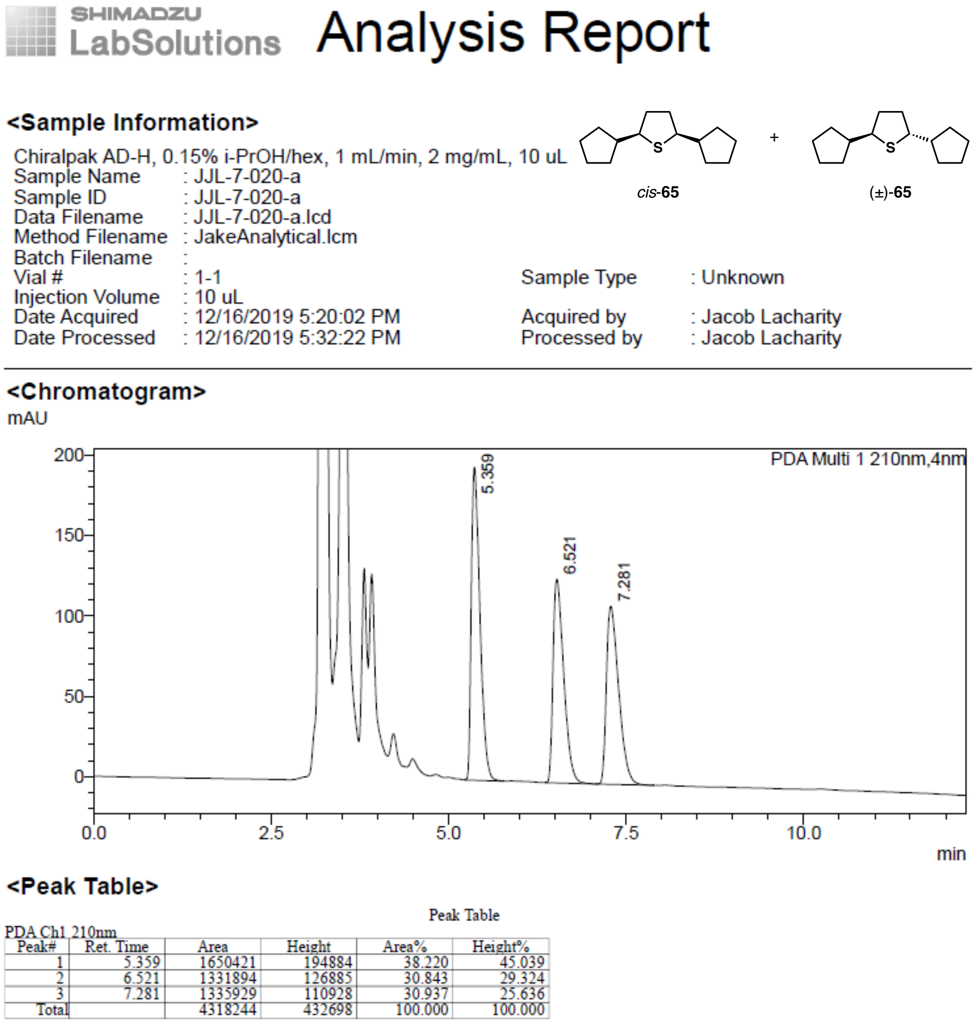

SHIMADZU LabSolutions **Analysis Report**

<Sample Information>

Chiralpak AD-H, 0.15% i-PrOH/hex, 1 mL/min, 2 mg/mL, 10 uL

cis-**65** + (±)-**65**

Sample Name : JJL-7-020-a
Sample ID : JJL-7-020-a
Data Filename : JJL-7-020-a.lcd
Method Filename : JakeAnalytical.lcm
Batch Filename :
Vial # : 1-1
Sample Type : Unknown
Injection Volume : 10 uL
Date Acquired : 12/16/2019 5:20:02 PM
Acquired by : Jacob Lacharity
Date Processed : 12/16/2019 5:32:22 PM
Processed by : Jacob Lacharity

<Chromatogram>

<Peak Table>

Peak Table

PDA Ch1 210nm

Peak#	Ret. Time	Area	Height	Area%	Height%
1	5.359	1650421	194884	38.220	45.039
2	6.521	1331894	126885	30.843	29.324
3	7.281	1335929	110928	30.937	25.636
Total		4318244	432698	100.000	100.000

HPLC Trace Analysis of Enantioenriched **65**:

SHIMADZU LabSolutions

Analysis Report

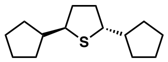

65

> 99% ee

<Sample Information>

Sample Name : JJL-7-020-prepHPLC-b
Sample ID : JJL-7-020-prepHPLC-b
Data Filename : JJL-7-020-prepHPLC-b.lcd
Method Filename : JakeAnalytical.lcm
Batch Filename :
Vial # : 1-1
Sample Type : Unknown
Injection Volume : 10 uL
Date Acquired : 12/18/2019 9:08:13 AM
Acquired by : Jacob Lacharity
Date Processed : 12/18/2019 9:23:21 AM
Processed by : Jacob Lacharity

<Chromatogram>

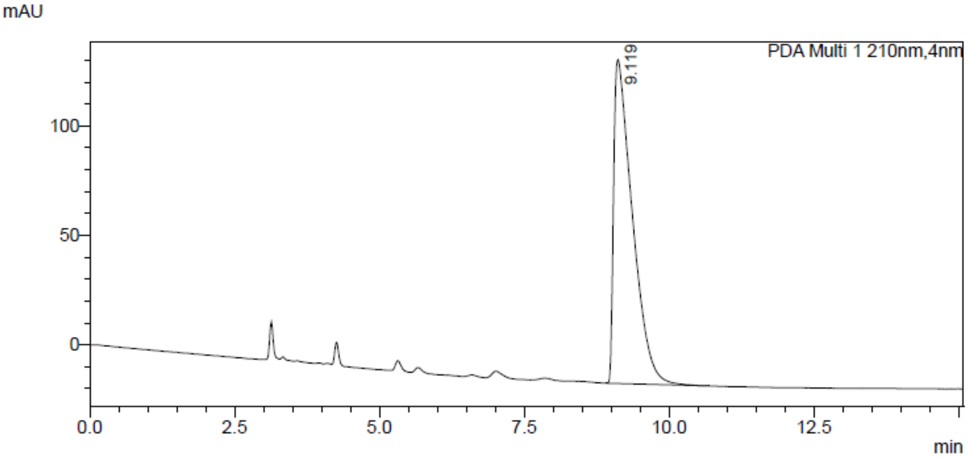

<Peak Table>

Peak Table

PDA Ch1 210nm

Peak#	Ret. Time	Area	Height	Area%	Height%
1	9.119	3328646	147851	100.000	100.000
Total		3328646	147851	100.000	100.000

HPLC Trace Analysis of Enantioenriched *ent*-**65**:

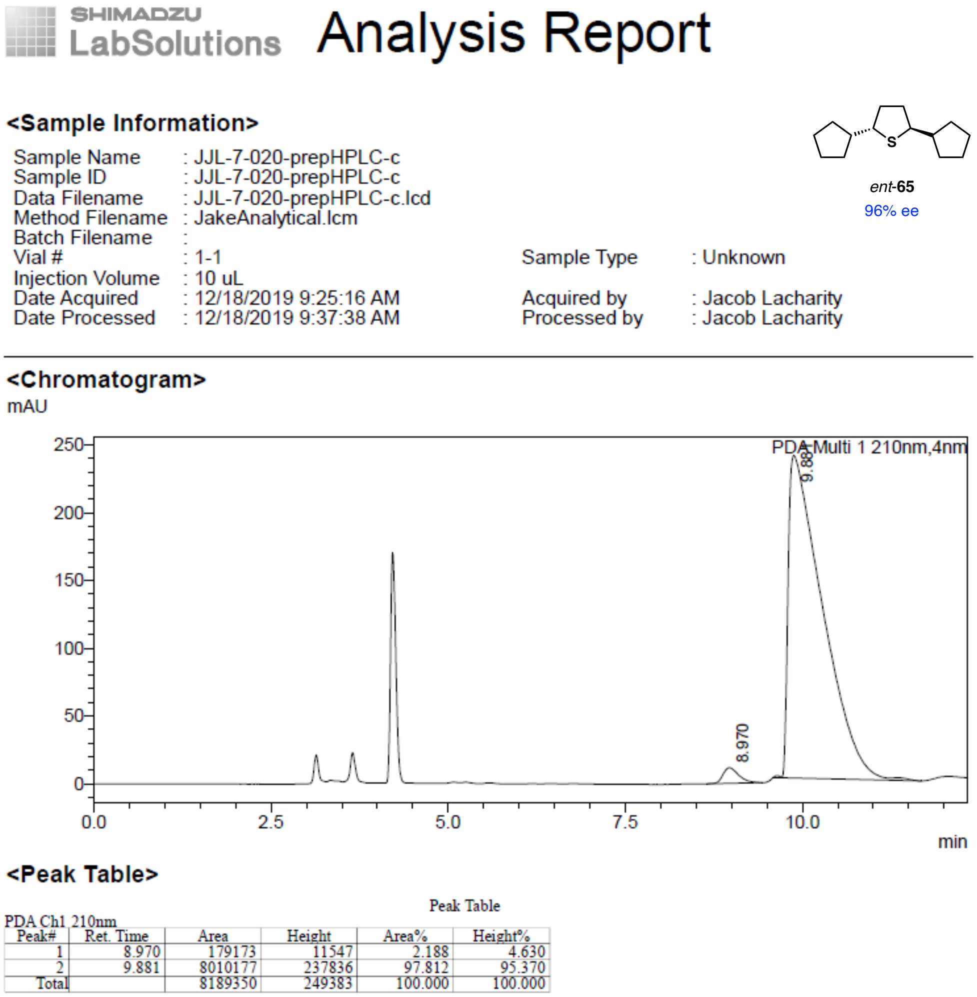

Analysis Report

<Sample Information>

ent-**65**

96% ee

Sample Name	: JJL-7-020-prepHPLC-c
Sample ID	: JJL-7-020-prepHPLC-c
Data Filename	: JJL-7-020-prepHPLC-c.lcd
Method Filename	: JakeAnalytical.lcm
Batch Filename	:
Vial #	: 1-1
Injection Volume	: 10 uL
Date Acquired	: 12/18/2019 9:25:16 AM
Date Processed	: 12/18/2019 9:37:38 AM
Sample Type	: Unknown
Acquired by	: Jacob Lacharity
Processed by	: Jacob Lacharity

<Chromatogram>

<Peak Table>

Peak Table

PDA Ch1 210nm

Peak#	Ret. Time	Area	Height	Area%	Height%
1	8.970	179173	11547	2.188	4.630
2	9.881	8010177	237836	97.812	95.370
Total		8189350	249383	100.000	100.000

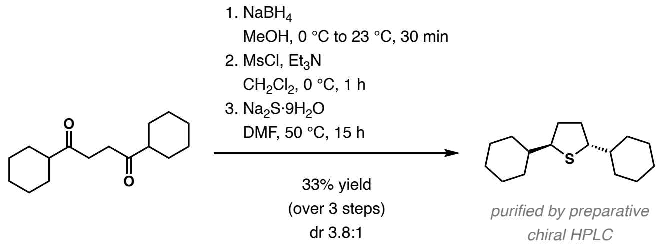

purified by preparative chiral HPLC

S25

(*R*,*R*)-**66**

Thiolane 66. Sodium borohydride (0.263 g, 6.94 mmol, 2.0 equiv) was added portion-wise to a solution of **S25**[130] (0.869 g, 3.47 mmol) in MeOH (18 mL) at 0 °C. The reaction mixture was then warmed to 23 °C and stirred at 23 °C for 30 min. The solvent was evaporated under reduced pressure, and the dry residue was dissolved in EtOAc (75 mL). The organic layer was washed with 1 M aqueous hydrochloric acid solution (50 mL), a saturated aqueous solution of $NaHCO_3$ (50 mL), and brine (50 mL), then dried over Na_2SO_4 and concentrated to dryness under reduced pressure. The crude diol was submitted to the next step without further purification.

The crude diol was dissolved in CH_2Cl_2 (17 mL), and the solution was cooled to 0 °C. Triethylamine (1.93 mL, 13.9 mmol, 4.0 equiv) and methanesulfonyl chloride (0.81 mL, 10.4 mmol, 3.0 equiv) were added dropwise at 0 °C. The reaction mixture was stirred at 0 °C for 1 h. The resulting solution was diluted with CH_2Cl_2 (50 mL), and the organic layer was washed with 1 M aqueous hydrochloric acid solution (30 mL), a saturated aqueous solution of $NaHCO_3$ (30 mL), and brine (30 mL), then dried over Na_2SO_4 and concentrated to dryness under reduced pressure. The crude product was submitted to the next step without further purification.

The crude bismesylate from the previous step was dissolved in DMF (170 mL) at 23 °C and sparged with argon for 10 min. $Na_2S·9H_2O$ (4.17 g, 17.4 mmol, 5.0 equiv) was added to the solution at 23 °C, then the reaction mixture was heated to 50 °C and stirred at 50 °C for 15 h. The resulting solution was then cooled to 23 °C then diluted with water (1000 mL), and the aqueous layer was extracted with EtOAc (4 × 200 mL). The combined organic layers were washed with brine (3 × 300 mL), dried over Na_2SO_4, and concentrated to dryness under reduced pressure.

The crude product was purified by column chromatography on silica gel (100% hexanes) to afford a mixture (dr 3.8:1) of (±)-*trans*- to *cis*-**66** (0.294 g, 1.16 mmol, 33% yield over 3 steps). This mixture was purified through preparative chiral HPLC [Chiralpak ® AD-H; 250 × 20 mm i.d.; 0.15% *i*-PrOH in hexanes; flow rate = 6 mL/min; 3 mL injection of a 10 mg/mL solution; detection at 210 nm; t_1 = 12.65 min (*cis*-**66**), t_2 = 16.48 min (**66**), t_3 = 20.68 min (*ent*-**66**)] to afford 75.1 mg (0.297 mmol, 26% yield) of **66** and *ent*-**66** each as enantiopure crystalline, white solids.

The enantiopurity of **66** (> 99% ee) and *ent*-**66** (99% ee) were measured by HPLC trace analysis [Chiralpak ® AD-H; 0.15% *i*-PrOH in hexanes; flow rate = 1 mL/min; 10 μL injection of a 1 mg/mL solution; detection at 254 nm; t_1 = 4.49 min (*cis*-**66**), t_2 = 7.26 min (**66**), t_3 = 9.59 min (*ent*-**66**)].

66: $[\alpha]_D^{20}$ −168.2 (*c* 1.0, $CHCl_3$). ^1H NMR (600 MHz, $CDCl_3$): δ 3.10 (td, *J* = 8.5, 4.7 Hz, 2H), 2.21 (ddd, *J* = 7.5, 4.4, 2.0 Hz, 2H), 1.81 (ddd, *J* = 11.1, 6.6, 3.2 Hz, 4H), 1.69 (dd, *J* = 8.4, 4.7 Hz, 4H), 1.63 (dddd, *J* = 12.5, 5.1, 3.3, 1.5 Hz, 2H), 1.45 (t, *J* = 9.3 Hz, 2H), 1.31 (tdt, *J* = 11.9, 8.7, 3.5 Hz, 2H), 1.22 (ddt, *J* =16.4, 12.5, 3.3 Hz, 4H), 1.14 (qt, *J* = 12.7, 3.3 Hz, 2H), 1.01 (qd, *J* = 12.7, 3.5 Hz, 2H), 0.93 (qd, *J* = 12.4, 3.6 Hz, 2H). ^{13}C NMR (125 MHz, $CDCl_3$): δ 55.9, 45.3, 35.7, 33.4, 31.7, 26.5, 26.3, 26.3. HRMS–ESI (*m*/*z*): $[M + C_2H_5]^+$ calcd for $C_{18}H_{33}S$, 281.2303; found, 281.2305.

Preparative Chiral HPLC for *cis*-**66** and (±)-*trans*-**66**:

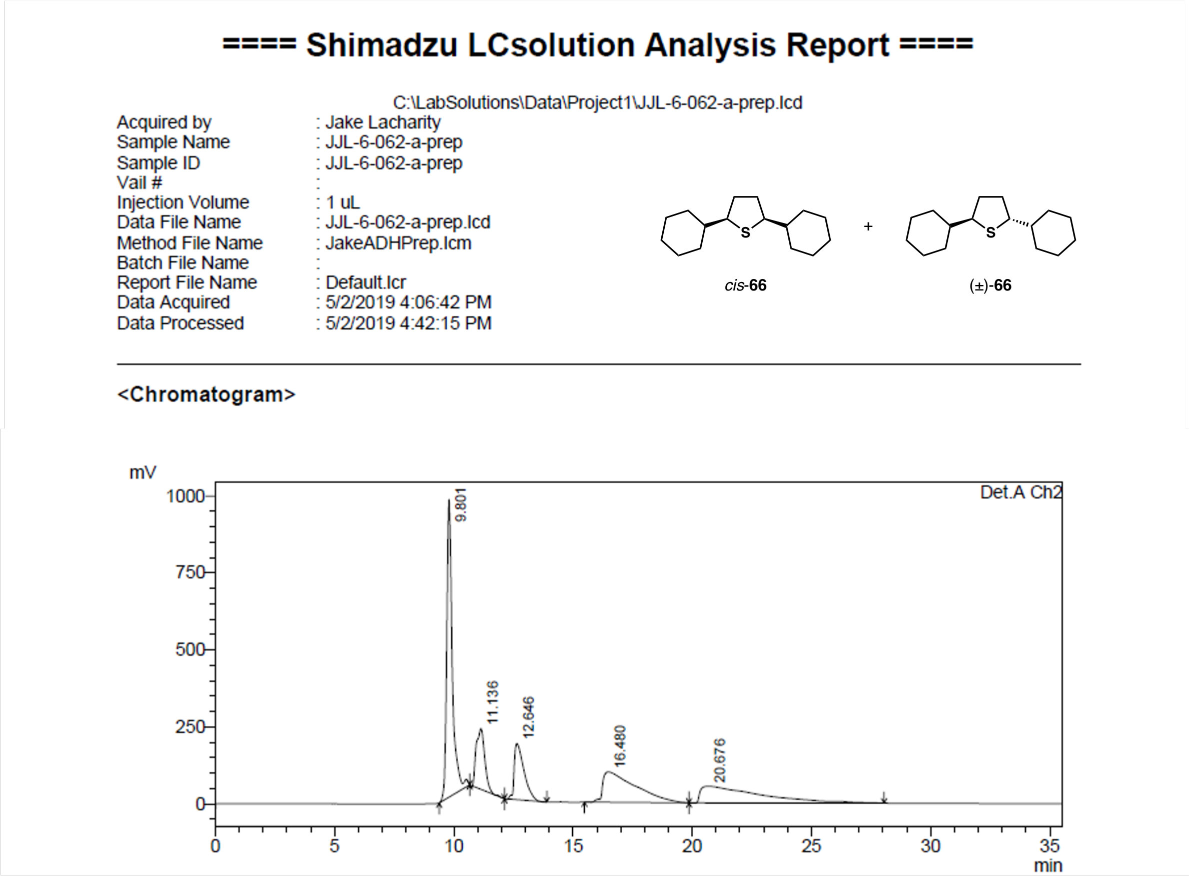

==== Shimadzu LCsolution Analysis Report ====

C:\LabSolutions\Data\Project1\JJL-6-062-a-prep.lcd

Acquired by : Jake Lacharity
Sample Name : JJL-6-062-a-prep
Sample ID : JJL-6-062-a-prep
Vail # :
Injection Volume : 1 uL
Data File Name : JJL-6-062-a-prep.lcd
Method File Name : JakeADHPrep.lcm
Batch File Name :
Report File Name : Default.lcr
Data Acquired : 5/2/2019 4:06:42 PM
Data Processed : 5/2/2019 4:42:15 PM

<Chromatogram>

mV
1000
750
500
250
0
Det.A Ch2
9.801
11.136
12.646
16.480
20.676
0
5
10
15
20
25
30
35
min

HPLC Analysis for *cis*-**66** and (±)-*trans*-**66**:

==== Shimadzu LCsolution Analysis Report ====

C:\LabSolutions\Data\Project1\JJL-6-062-a1.lcd

Acquired by	: Jake Lacharity
Sample Name	: JJL-6-062-a
Sample ID	: JJL-6-062-a
Vail #	:
Injection Volume	: 10 uL
Data File Name	: JJL-6-062-a1.lcd
Method File Name	: brad.lcm
Batch File Name	:
Report File Name	: Default.lcr
Data Acquired	: 5/2/2019 1:09:24 PM
Data Processed	: 5/2/2019 1:33:53 PM

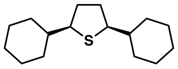

cis-**66**

+

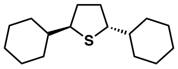

(±)-**66**

<Chromatogram>

C:\LabSolutions\Data\Project1\JJL-6-062-a1.lcd

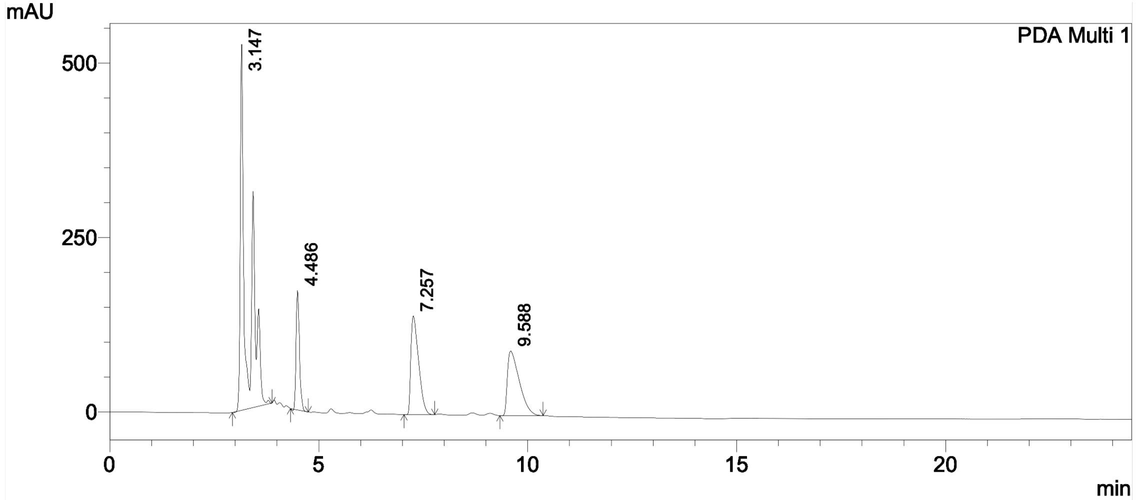

1 PDA Multi 1/210nm 4nm

PeakTable

PDA Ch1 210nm 4nm

Peak#	Ret. Time	Area	Height	Area %	Height %
1	3.147	5148950	523649	52.739	56.366
2	4.486	966510	171243	9.900	18.433
3	7.257	1813006	141526	18.570	15.234
4	9.588	1834699	92602	18.792	9.968
Total		9763165	929020	100.000	100.000

HPLC Trace Analysis of Enantioenriched **66**:

==== Shimadzu LCsolution Analysis Report ====

C:\LabSolutions\Data\Project1\JJL-6-062-prepHPLC-b-check1.lcd

Acquired by	: Jake Lacharity
Sample Name	: JJL-6-062-prepHPLC-b-check
Sample ID	: JJL-6-062-prepHPLC-b-check
Vail #	:
Injection Volume	: 10 uL
Data File Name	: JJL-6-062-prepHPLC-b-check1.lcd
Method File Name	: brad.lcm
Batch File Name	:
Report File Name	: Default.lcr
Data Acquired	: 5/4/2019 8:40:23 AM
Data Processed	: 5/4/2019 8:55:29 AM

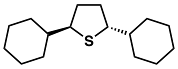

66

> 99% ee

<Chromatogram>

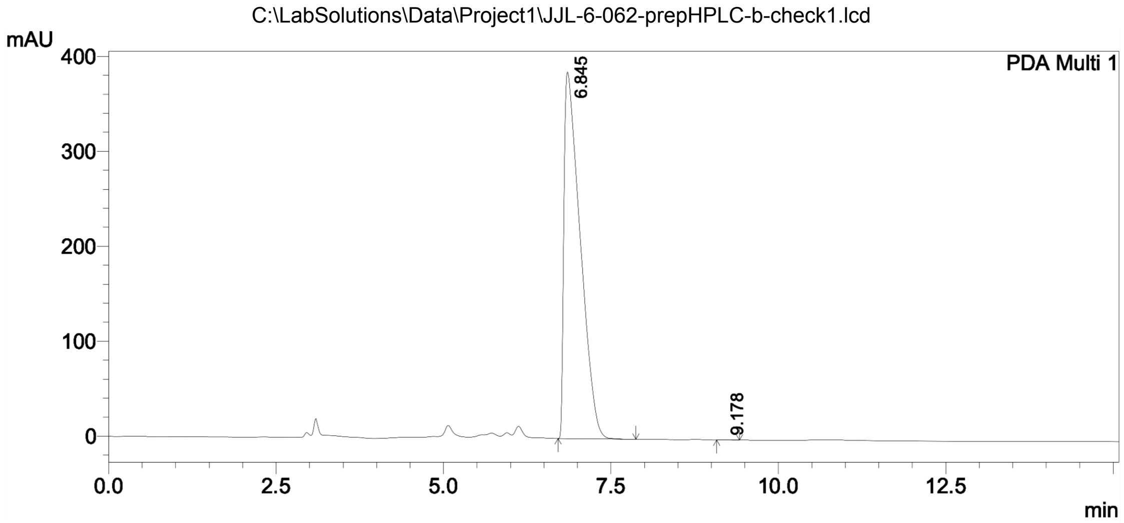

1 PDA Multi 1/210nm 4nm

PeakTable

PDA Ch1 210nm 4nm

Peak#	Ret. Time	Area	Height	Area %	Height %
1	6.845	6522871	386410	99.973	99.963
2	9.178	1789	144	0.027	0.037
Total		6524661	386554	100.000	100.000

HPLC Trace Analysis of Enantioenriched *ent*-**66**:

==== Shimadzu LCsolution Analysis Report ====

C:\LabSolutions\Data\Project1\JJL-6-062-prepHPLC-c-check1.lcd
Acquired by : Jake Lacharity
Sample Name : JJL-6-062-prepHPLC-c-check
Sample ID : JJL-6-062-prepHPLC-c-check
Vail # :
Injection Volume : 10 uL
Data File Name : JJL-6-062-prepHPLC-c-check1.lcd
Method File Name : brad.lcm
Batch File Name :
Report File Name : Default.lcr
Data Acquired : 5/4/2019 8:57:39 AM
Data Processed : 5/4/2019 9:09:56 AM

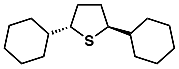

ent-**66**
99% ee

<Chromatogram>

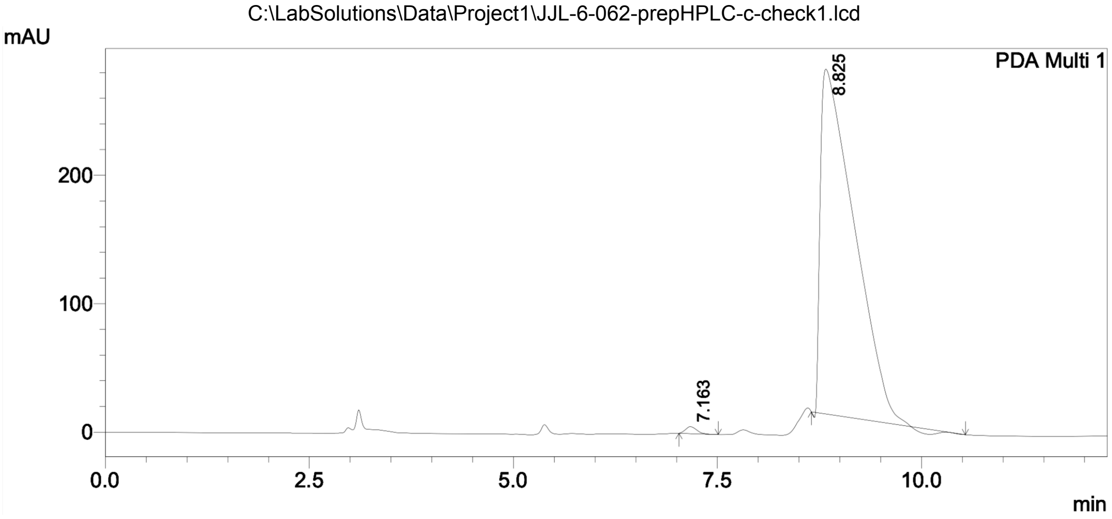

1 PDA Multi 1/210nm 4nm

PeakTable

PDA Ch1 210nm 4nm

Peak#	Ret. Time	Area	Height	Area %	Height %
1	7.163	51490	5455	0.663	1.991
2	8.825	7717342	268540	99.337	98.009
Total		7768833	273995	100.000	100.000

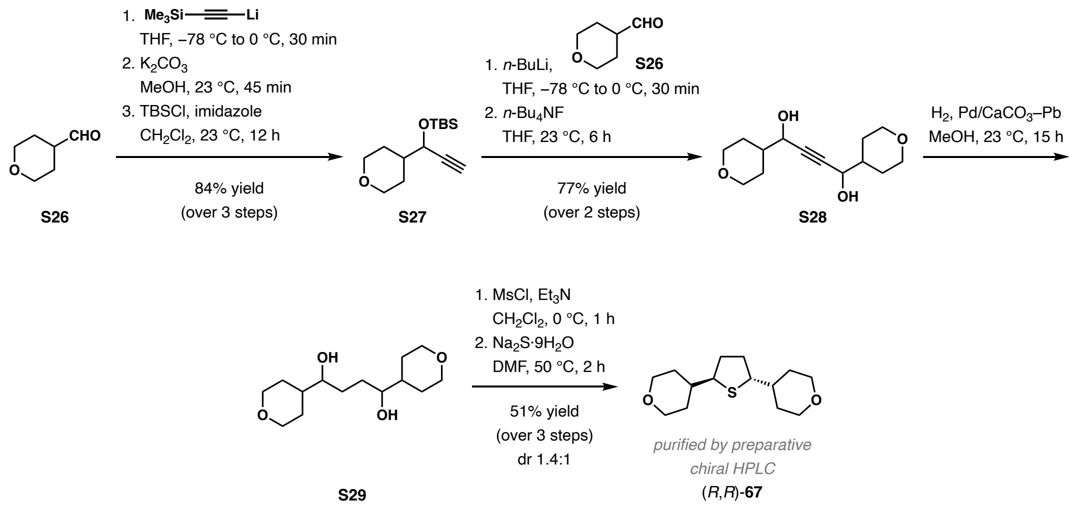

1. Me3Si—≡—Li
THF, −78 °C to 0 °C, 30 min
2. K2CO3
MeOH, 23 °C, 45 min
3. TBSCl, imidazole
CH2Cl2, 23 °C, 12 h
84% yield
(over 3 steps)
CHO
O
S26
OTBS
S27
1. n-BuLi,
S26
THF, −78 °C to 0 °C, 30 min
2. n-Bu4NF
THF, 23 °C, 6 h
77% yield
(over 2 steps)
OH
OH
S28
H2, Pd/CaCO3–Pb
MeOH, 23 °C, 15 h
OH
OH
S29
1. MsCl, Et3N
CH2Cl2, 0 °C, 1 h
2. Na2S·9H2O
DMF, 50 °C, 2 h
51% yield
(over 3 steps)
dr 1.4:1
S
purified by preparative
chiral HPLC
(R,R)-67

Thiolane 67. The title compound was prepared according to the procedures described above for thiolane **63**. Following the procedures described for **S14** (en route to thiolane **63**): 1.00 g (8.76 mmol) of aldehyde **S26**[131] was used with 1.81 g (18.4 mmol, 2.2 equiv) of trimethylsilyl acetylene, and 2.0 equiv of *n*-BuLi (2.55 M in hexanes, 6.9 mL, 17.5 mmol) in 40 mL of THF for the first step. The second step was performed with 1.45 g (10.5 mmol, 1.2 equiv) of potassium carbonate in 87 mL of MeOH. The third step was achieved 1.43 g (21.0 mmol, 2.4 equiv) of imidazole, and 1.58 g (10.5 mmol, 1.2 equiv) of TBSCl in 88 mL of CH_2Cl_2. Silyl alcohol **S27** was obtained in 84% yield (1.86 g, 7.33 mmol) over 3 steps.

Diol **S28** was obtained using a modified procedure described for **S15**: starting with 1.86 g (7.33 mmol) of silyl alcohol **S27** and 1.10 equiv of *n*-butyllithium (2.55 M in hexanes, 3.15 mL, 8.04 mmol) in 12 mL of THF at −78 °C, 1.03 g (9.0 mmol, 1.23 equiv) of aldehyde **S26** in 5 mL of THF was added at −78 °C before warming the resulting mixture to 0 °C to let stir for 30 min in the first step. The crude residue from the first step was dissolved in THF (35 mL) at 23 °C and treated with a solution of *n*-Bu_4NF (1 M in THF, 8.30 mL, 8.30 mmol, 1.2 equiv). The reaction mixture was stirred at 23 °C for 6 h before it was quenched by a saturated aqueous solution of $NaHCO_3$ and diluted with EtOAc. The layers were separated, and the aqueous layer was extracted with EtOAc (3 × 75 mL). The combined organic layers were washed with brine, dried over Na_2SO_4, and concentrated to dryness under reduced pressure. The crude product was purified by column chromatography on silica gel (5% MeOH in EtOAc) to afford diol **S28** (1.37 g, 5.38 mmol, 77% yield over 2 steps).

Following a modified procedure described for thiolane **63** from diol **S15**. A solution of diol **S24** (0.782 g, 3.08 mmol) in MeOH (30 mL) was treated with palladium on calcium carbonate, poisoned with lead (5 wt % Pd, 0.656 g, 0.308 mmol, 10 mol %) at 23 °C. The reaction mixture was stirred under an atmosphere of hydrogen gas at 23 °C for 15 h. The resulting mixture was filtered through celite and concentrated under reduced pressure. The crude diol **S29** was submitted to the next step without further purification.

The crude diol **S29** obtained from the previous step was dissolved in 30 mL of CH_2Cl_2, followed by sequential addition of 1.70 mL (12.3 mmol, 4.0 equiv) of triethylamine and 0.72 mL (13.5 mmol, 3.0 equiv) of methanesulfonyl chloride for the first step. The resulting crude bismesylate was used directly without further purification: a solution of crude bismesylate in DMF (154 mL) was sparged with argon for 10 min at 23 °C, then treated with $Na_2S{\cdot}9H_2O$ (3.70 g, 15.4 mmol, 5.0 equiv). The reaction mixture was then heated to 50 °C and stirred at 50 °C for 15 h. The resulting solution was then cooled to 23 °C then diluted with water (1000 mL), and the aqueous layer was extracted with EtOAc (4 × 200 mL). The combined organic layers were washed with brine (3 × 300 mL), dried over Na_2SO_4, and concentrated to dryness under reduced pressure. The crude product was purified by column chromatography on silica gel (30% EtOAc in hexanes) to afford a mixture (dr 3:1) of (±)-*trans*- to *cis*-**67** (0.400 g, 1.56 mmol, 51% yield over 3 steps). This mixture was purified through preparative chiral HPLC [Chiralpak ® AD-H; 250 × 20 mm i.d.; 5% *i*-PrOH in hexanes; flow rate = 6 mL/min; 3 mL injection of a 10 mg/mL solution;

detection at 210 nm; t_1 = 27.69 min (*cis*-**67**), t_2 = 43.39 min (**67**), t_3 = 57.15 min (*ent*-**67**)] to afford 0.112 g (0.437 mmol, 14% yield) of **67** and *ent*-**67** each as enantiopure white, crystalline solids. The enantiopurity of the material was measured by HPLC trace analysis [Chiralpak ® AD-H; 5% *i*-PrOH in hexanes; flow rate = 1 mL/min; 10 μL injection of a 1 mg/mL solution; detection at 254 nm; t_1 = 8.73 min (*cis*-**67**), t_2 = 14.46 min (**67**), t_3 = 19.29 min (*ent*-**67**)].

67: $[\alpha]_D^{22}$ −158.5 (*c* 1.0, $CHCl_3$). ^1H NMR (600 MHz, $CDCl_3$): δ 3.94 (dt, *J* = 11.3, 5.4 Hz, 4H), 3.34 (q, *J* = 11.5 Hz, 4H), 3.14 (td, *J* = 8.9, 5.1 Hz, 2H), 2.25 (tq, 11.1, 5.6 Hz, 2H), 1.75–1.62 (m, 4H), 1.60–1.44 (m, 4H), 1.35 (qd, *J* = 12.2, 4.5 Hz, 4H). ^{13}C NMR (125 MHz, $CDCl_3$): δ 68.0, 67.8, 55.1, 42.4, 34.9, 33.1, 31.6. HRMS–ESI (*m*/*z*): $[M + H]^+$ calcd for $C_{14}H_{25}O_2S$, 257.1575; found, 257.1575.

Preparative Chiral HPLC for *cis*-**67** and (±)-*trans*-**67**:

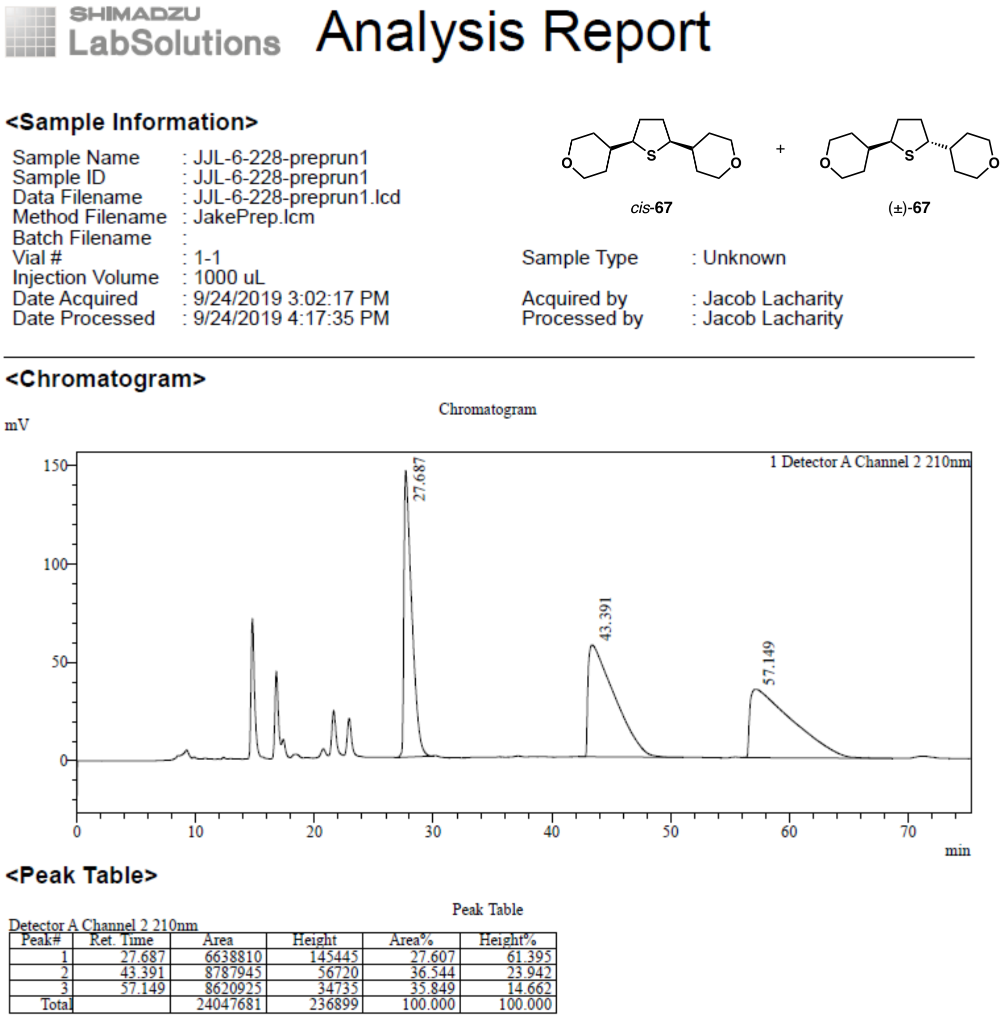
SHIMADZU
LabSolutions
O
S
O
+
O
S
O
cis-**67**
(±)-**67**
Chromatogram
mV
150
100
50
0
27.687
43.391
57.149
1 Detector A Channel 2 210nm
0
10
20
30
40
50
60
70
min

Analysis Report

<Sample Information>

Sample Name : JJL-6-228-preprun1
Sample ID : JJL-6-228-preprun1
Data Filename : JJL-6-228-preprun1.lcd
Method Filename : JakePrep.lcm
Batch Filename :
Vial # : 1-1
Injection Volume : 1000 uL
Date Acquired : 9/24/2019 3:02:17 PM
Date Processed : 9/24/2019 4:17:35 PM

Sample Type : Unknown

Acquired by : Jacob Lacharity
Processed by : Jacob Lacharity

<Chromatogram>

<Peak Table>

Peak Table

Detector A Channel 2 210nm

Peak#	Ret. Time	Area	Height	Area%	Height%
1	27.687	6638810	145445	27.607	61.395
2	43.391	8787945	56720	36.544	23.942
3	57.149	8620925	34735	35.849	14.662
Total		24047681	236899	100.000	100.000

HPLC Trace Analysis for *cis*-**67** and (±)-*trans*-**67**:

SHIMADZU
LabSolutions

Analysis Report

<Sample Information>

Sample Name : JJL-6-228-a
Sample ID : JJL-6-228-a
Data Filename : JJL-6-228-a.lcd
Method Filename : JakeAnalytical.lcm
Batch Filename :
Vial # : 1-1
Injection Volume : 10 uL
Date Acquired : 9/24/2019 11:02:10 AM
Date Processed : 9/24/2019 11:31:03 AM

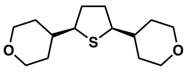

cis-**67**

+

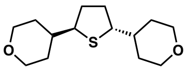

(±)-**67**

Sample Type : Unknown

Acquired by : Jacob Lacharity
Processed by : Jacob Lacharity

<Chromatogram>

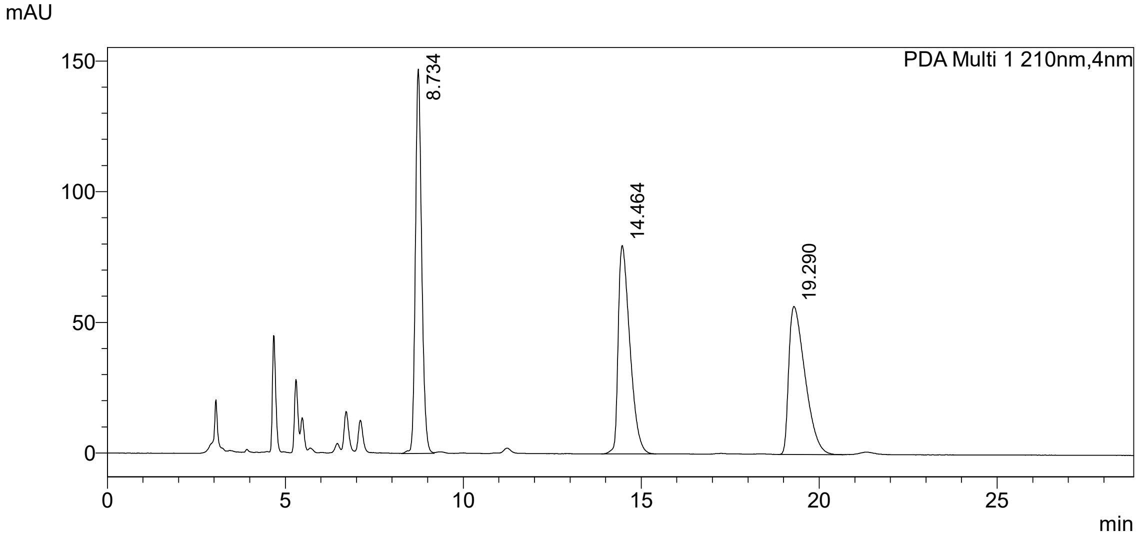

<Peak Table>

Peak Table

PDA Ch1 210nm

Peak#	Ret. Time	Area	Height	Area%	Height%
1	8.734	1810207	147060	33.375	51.879
2	14.464	1814038	79743	33.445	28.131
3	19.290	1799657	56666	33.180	19.990
Total		5423902	283469	100.000	100.000

General Procedure for Enantioselective aza-MBH Cyclization:

Table 8. Enantioselective aza-MBH Cyclization Conditions with Various Chiral Sulfides.

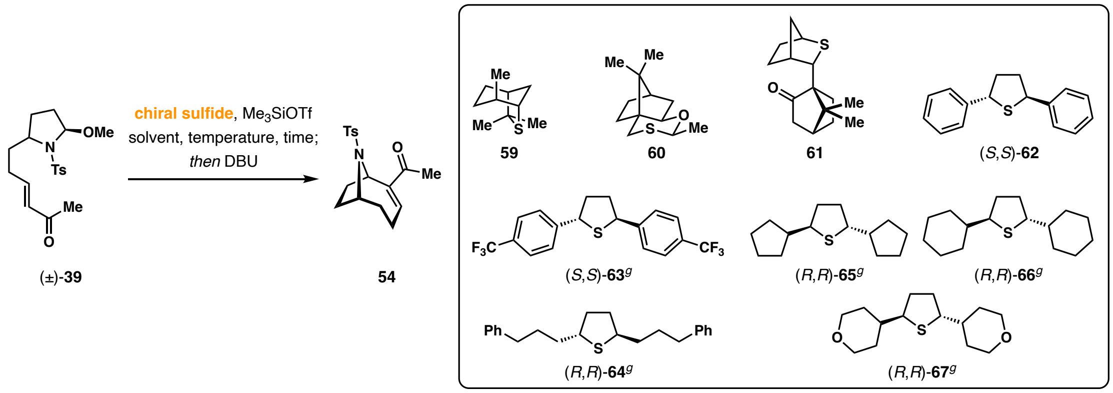

entry[a]	solvent	chiral sulfide	temperature (time)	yield	ee
1	MeCN	**59**	0 °C (2 h)	85%	–4%
2[b]	MeCN	**60**	0 °C (3 h)	24%	–14%
3[c]	MeCN	**61**	0 °C (4 h)	85%	0%
4[d]	MeCN	**62**	–20 °C (22 h)	53%	–21%
5	MeCN–CH_2Cl_2 (1:1)	**63**	–15 °C (24 h)	19%	0%
6	MeCN	**64**	0 °C (2 h)	68%	–9%
7	MeCN–CH_2Cl_2 (1:1)	**65**	0 °C (3 h)	59%	44%
8	MeCN–CH_2Cl_2 (1:1)	**65**	–10 °C (6 h)	42%	26%
9	MeCN–CH_2Cl_2 (1:1)	**65**	–20 °C (6 h)	68%	9%
10[e]	MeCN–PhMe (1:1)	**66**	0 °C (3 h)	40%	62%
11	MeCN–CH_2Cl_2 (1:1)	**67**	0 °C (3 h)	29%	82%
12	MeCN–PhMe (1:1)	**66**	–48 °C (24 h)	42%	70%
13	MeCN–CH_2Cl_2 (1:1)	**67**	–78 °C (4 h)	28%	93%
14[f]	MeCN–CH_2Cl_2 (1:1)	**67**	0 °C (2.5 h)	50%	78%

[a] Reactions were performed by treating a solution of (±)-**39** and 1.5 equiv of chiral sulfide (SR_2*) in solvent (0.1 M) with 2.5 equiv of Me_3SiOTf at the indicated temperature. [b] Chiral sulfide **59** was destroyed under the acidic reaction conditions. [c] Epimerization of chiral sulfide **60** was observed. [d] TBSOTf was used instead of Me_3SiOTf. [e] Solvent concentration was 0.03 M with respect to (±)-**39**. [f] Me_3SiOTf was added at –78 °C, and the reaction was performed at –78 °C for 1 h, then warmed to 0 °C to stir at 0 °C for another 75 min. [g] Thiolane configurations are proposed based on their optical rotations.

***N*-Tosylanatoxin-a 54.** A solution of vinyl ketone (±)-**39** (20 mg, 0.0569 mmol) and chiral sulfide (0.0854 mmol, 1.5 equiv) in the specified solvent (0.60 mL) was cooled to the indicated reaction temperature. Me_3SiOTf (26 μL, 0.142 mmol, 2.5 equiv) was added dropwise to the solution at the stated temperature to stirred for the indicated amount of time. The reaction mixture was then quenched with a saturated aqueous solution of $NaHCO_3$ and diluted with EtOAc (10 mL). The layers were separated, and the aqueous layer was extracted with EtOAc (3 × 10 mL). The combined organic layers were washed with brine (30 mL), dried over Na_2SO_4, and concentrated to dryness under reduced pressure. The dry residue was then redissolved in CH_2Cl_2

(0.60 mL) at 23 °C and treated with DBU (17 μL, 0.114 mmol, 2.0 equiv). The resulting mixture was stirred at 23 °C for 30 min. The solvent was evaporated under reduced pressure, and the crude residue was purified by column chromatography on silica gel (30% EtOAc in hexanes to 40% EtOAc in hexanes to 50% EtOAc in hexanes) to afford **54**. The enantiopurity of the material was measured by HPLC trace analysis [Chiralpak ® AD-H; 5% *i*-PrOH in hexanes; flow rate = 1 mL/min; 10 μL injection of a 1 mg/mL solution; detection at 254 nm; t_1 = 27.98 min (*ent*-**54**), t_2 = 40.62 min (**54**)]. The ^{1}H NMR, ^{13}C NMR, and mass spectral data are in full agreement with those for the compound obtained previously (see page 151).

==== Shimadzu LCsolution Analysis Report ====

C:\LabSolutions\Data\Project1\AKM-09-36a.lcd

Acquired by : Karen Chen
Sample Name : AKM-09-36a
Sample ID : AKM-09-36a
Vail # :
Injection Volume : 10 uL
Data File Name : AKM-09-36a.lcd
Method File Name : brad.lcm
Batch File Name :
Report File Name : Default.lcr
Data Acquired : 2/15/2018 11:11:21 AM
Data Processed : 2/15/2018 11:57:55 AM

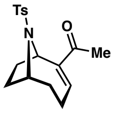

(±)-**54**

<Chromatogram>

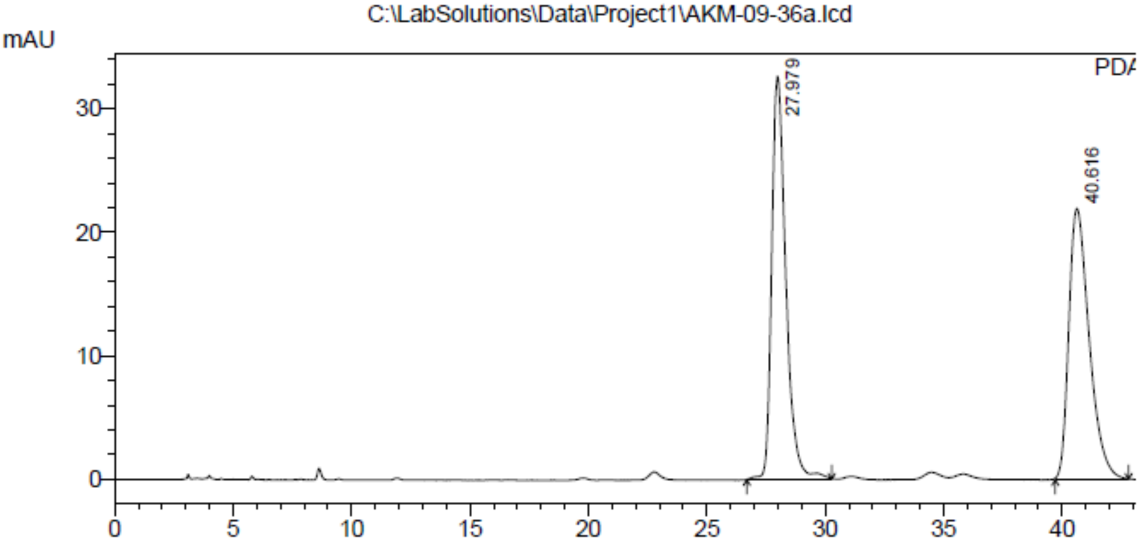

1 PDA Multi 2/254nm 4nm

PeakTable

PDA Ch2 254nm 4nm

Peak#	Ret. Time	Area	Height	Area %	Height %
1	27.979	1359037	32644	50.813	59.807
2	40.616	1315539	21938	49.187	40.193
Total		2674576	54582	100.000	100.000

SHIMADZU LabSolutions

Analysis Report

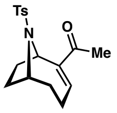

54

entry 14, thiolane **67**

78% ee

<Sample Information>

Sample Name : kyc3-242b
Sample ID : kyc3-242b
Data Filename : kyc3-242b.lcd
Method Filename : JakeAnalytical.lcm
Batch Filename :
Vial # : 1-1
Injection Volume : 10 uL
Date Acquired : 12/12/2019 10:18:15 AM
Date Processed : 12/12/2019 11:06:45 AM

Sample Type : Unknown

Acquired by : Karen Chen
Processed by : Karen Chen

<Chromatogram>

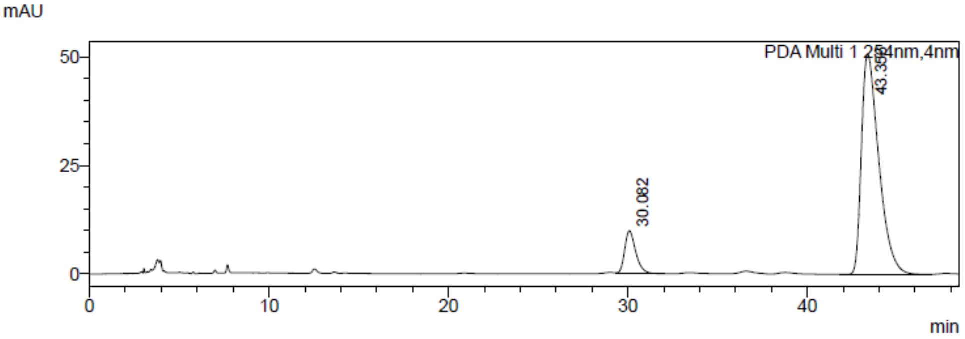

<Peak Table>

PDA Ch1 254nm

Peak#	Ret. Time	Area	Height	Height%	Area%
1	30.082	429370	9903	16.328	11.166
2	43.356	3416111	50746	83.672	88.834
Total		3845481	60649	100.000	100.000

SHIMADZU LabSolutions

Analysis Report

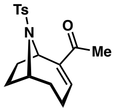

54

entry 13, thiolane **67**

93% ee

<Sample Information>

Sample Name : kyc3-244ba
Sample ID : kyc3-244ba
Data Filename : kyc3-244ba.lcd
Method Filename : JakeAnalytical.lcm
Batch Filename :
Vial # : 1-1
Injection Volume : 10 uL
Date Acquired : 1/10/2020 11:08:46 AM
Date Processed : 1/10/2020 11:55:56 AM

Sample Type : Unknown

Acquired by : Karen Chen
Processed by : Karen Chen

<Chromatogram>

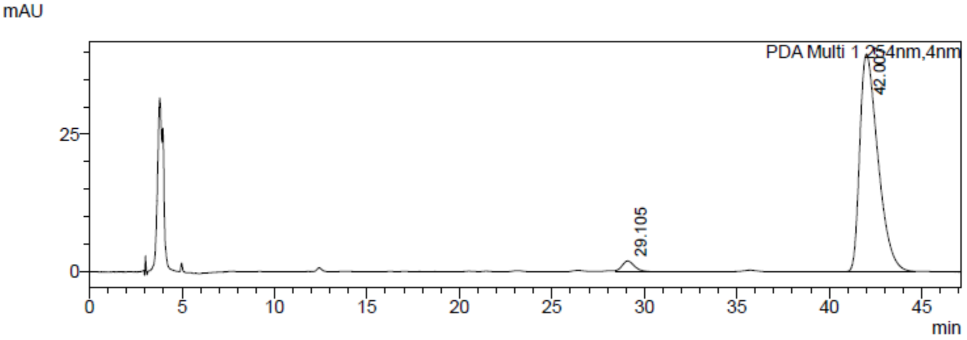

<Peak Table>

PDA Ch1 254nm

Peak#	Ret. Time	Area	Height	Height%	Area%
1	29.105	90684	1938	4.667	3.234
2	42.007	2713594	39582	95.333	96.766
Total		2804278	41520	100.000	100.000

Observed Epimerization of Thiolane 62:

We noticed thiolane **62** had epimerized upon subjecting to the aza-MBH cyclization condition. The recovered thiolane **62** following the aza-MBH reaction indicated a mixture (dr 14:86) of *cis*- and *trans*-**62** with 89% ee for the recovered *trans*-**62**, a drop from the 99% enantiopurity prior to reaction. We believe the epimerization took place via a ring-opening mechanism of the thiolane shown in Scheme 32, resulting in the formation of a carbocation at the benzylic carbon.

Scheme 32. Possible Epimerization Mechanism of Thiolane **62**.

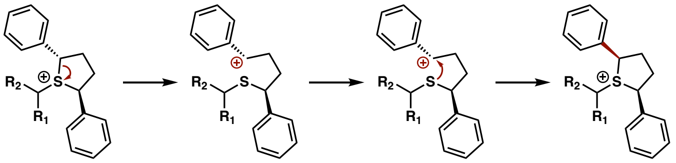

The enantiopurity (99% ee prior to aza-MBH cyclization, and dr 14:86 with 89% ee following aza-MBH cyclization) of the material was measured by HPLC trace analysis [Chiralpak ® AD-H; 5% *i*-PrOH in hexanes; flow rate = 1 mL/min; 10 μL injection of a 1 mg/mL solution; detection at 210 nm; t_1 = 8.46 min (*cis*-**62**), t_2 = 11.54 min (**62**), t_3 = 11.79 min (*ent*-**62**)].

HPLC Trace Analysis for *cis*-**62** and (±)-*trans*-**62**:

==== Shimadzu LCsolution Analysis Report ====

C:\LabSolutions\Data\Project1\JJL-6-007-a-run10.lcd

Acquired by : Jake Lacharity
Sample Name : JJL-6-007-a-run10
Sample ID : JJL-6-007-a-run10
Vail # :
Injection Volume : 10 uL
Data File Name : JJL-6-007-a-run10.lcd
Method File Name : brad.lcm
Batch File Name :
Report File Name : Default.lcr
Data Acquired : 4/1/2019 8:53:29 AM
Data Processed : 4/1/2019 9:07:38 AM

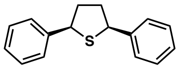

cis-**62**

+

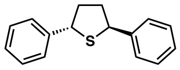

(±)-**62**

<Chromatogram>

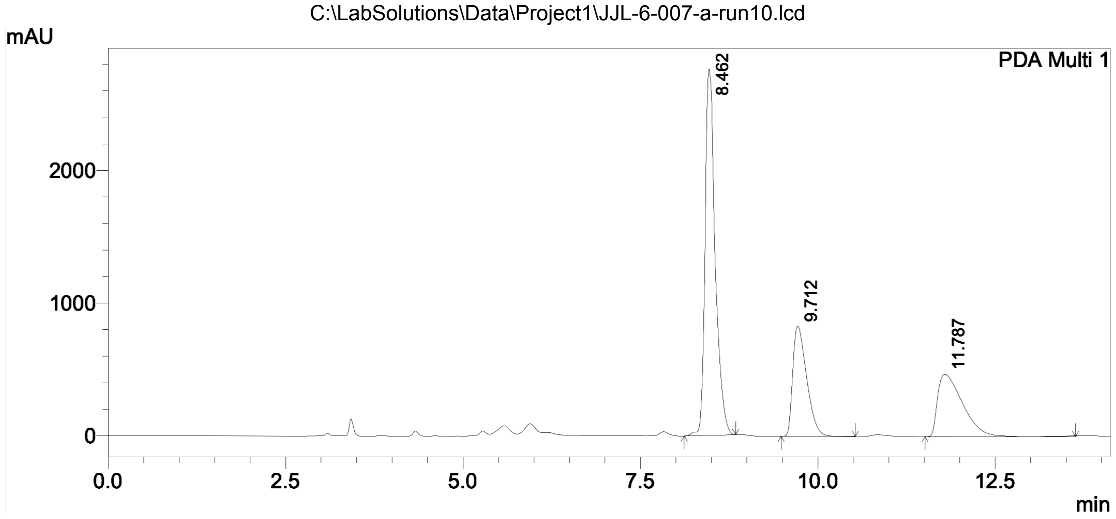

1 PDA Multi 1/210nm 4nm

PeakTable

PDA Ch1 210nm 4nm

Peak#	Ret. Time	Area	Height	Area %	Height %
1	8.462	27508802	2763740	54.742	68.008
2	9.712	11312450	831784	22.512	20.468
3	11.787	11430330	468344	22.746	11.525
Total		50251582	4063868	100.000	100.000

HPLC Trace Analysis of Enantioenriched **62**:

==== Shimadzu LCsolution Analysis Report ====

C:\LabSolutions\Data\Project1\JJL-6-007-HPLC-b1.lcd

Acquired by	: Jake Lacharity
Sample Name	: JJL-6-007-HPLC-b
Sample ID	: JJL-6-007-HPLC-b
Vail #	:
Injection Volume	: 10 uL
Data File Name	: JJL-6-007-HPLC-b1.lcd
Method File Name	: brad.lcm
Batch File Name	:
Report File Name	: Default.lcr
Data Acquired	: 4/3/2019 1:09:09 PM
Data Processed	: 4/3/2019 1:25:53 PM

Entiopure Thiolane **62** Prior to aza-MBH Cyclization:

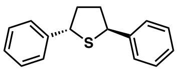

62

99% ee

<Chromatogram>

C:\LabSolutions\Data\Project1\JJL-6-007-HPLC-b1.lcd

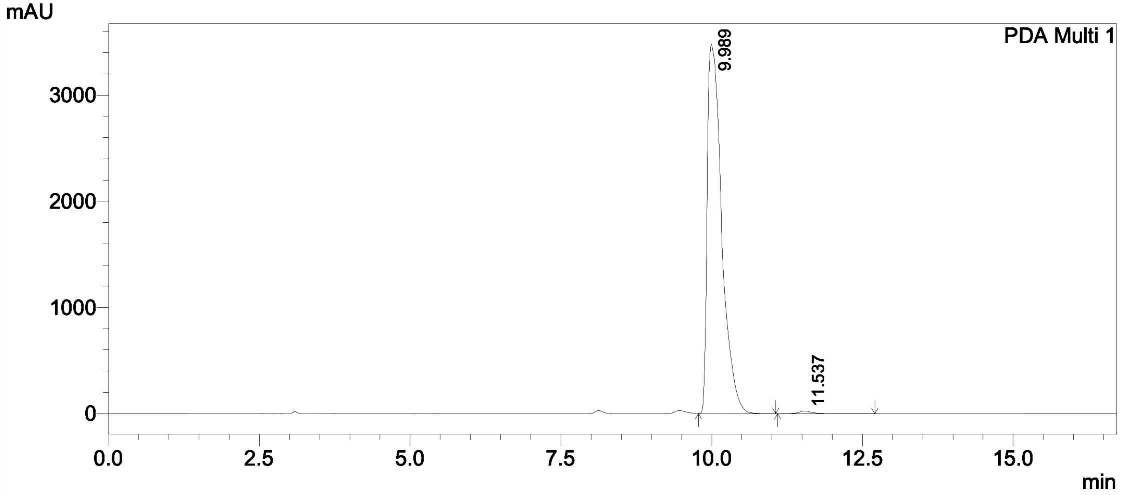

1 PDA Multi 1/210nm 4nm

PeakTable

PDA Ch1 210nm 4nm

Peak#	Ret. Time	Area	Height	Area %	Height %
1	9.989	57922876	3478428	99.341	99.319
2	11.537	384091	23843	0.659	0.681
Total		58306967	3502271	100.000	100.000

HPLC Trace Analysis of the Recovered **62**:

==== Shimadzu LCsolution Analysis Report ====

C:\LabSolutions\Data\Project1\kyc3-115a.lcd

Acquired by	: Karen Chen
Sample Name	: kyc3-115a
Sample ID	: kyc3-115a
Vail #	:
Injection Volume	: 10 uL
Data File Name	: kyc3-115a.lcd
Method File Name	: brad.lcm
Batch File Name	:
Report File Name	:
Data Acquired	: 4/17/2019 7:48:09 PM
Data Processed	: 4/17/2019 8:08:52 PM

Recovered Thiolane **62** Following aza-MBH Cyclization:

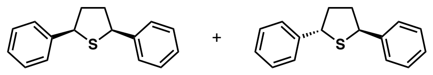

cis-**62** (±)-**62**

89% ee

cis:*trans* = 14:86

<Chromatogram>

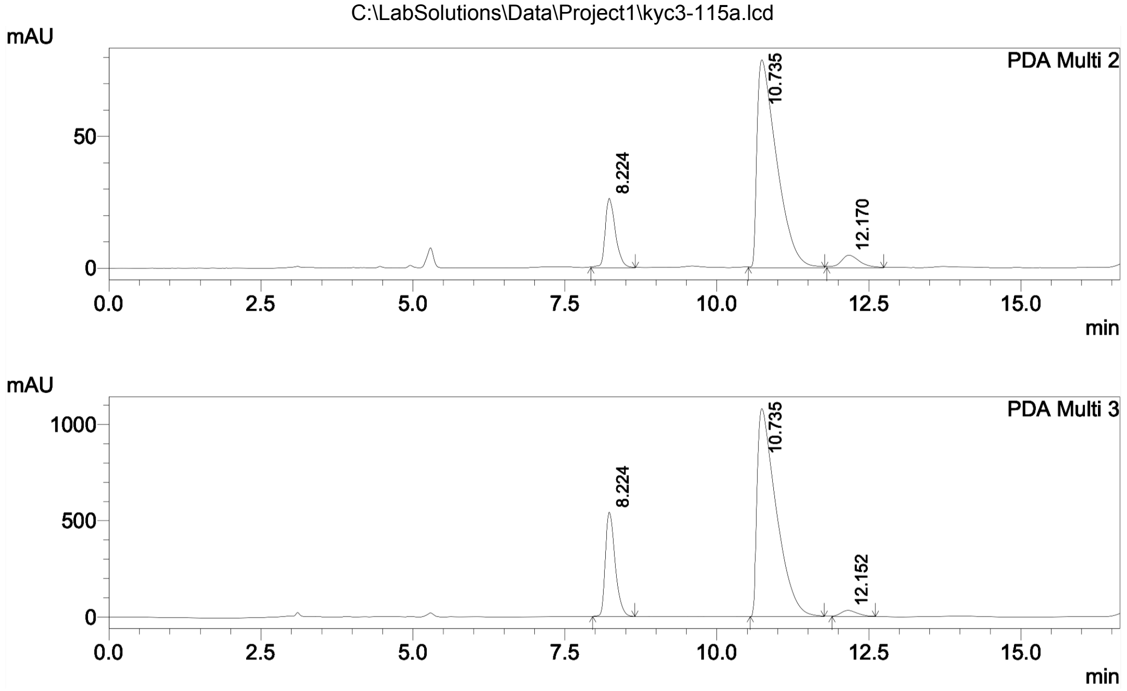

1 PDA Multi 2/254nm 4nm
2 PDA Multi 3/210nm 4nm

PeakTable

PDA Ch2 254nm 4nm

Peak#	Ret. Time	Area	Height	Area %	Height %
1	8.224	310178	26272	14.185	23.883
2	10.735	1773078	78974	81.089	71.792
3	12.170	103337	4757	4.726	4.324
Total		2186593	110003	100.000	100.000

PeakTable

PDA Ch2 254nm 4nm

Peak#	Ret. Time	Area	Height	Area %	Height %
1	8.224	310178	26272	14.185	23.883
2	10.735	1773078	78974	81.089	71.792
3	12.170	103337	4757	4.726	4.324
Total		2186593	110003	100.000	100.000

CHAPTER 3 EXPERIMENTAL PROCEDURES

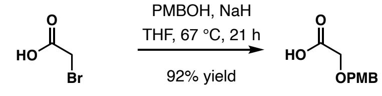

2-bromoacetic acid

118

2-((4-methoxybenzyl)oxy)acetic acid (118): The title compound was prepared according to a modification of the procedure reported by Griffin and co-workers:[132] Sodium hydride (7.0 g, 175 mmol, 2.4 equiv; 60% sodium hydride suspension in mineral oil was used) was added in portions to a solution of 2-bromoacetic acid (10.0 g, 72.0 mmol) and *p*-methoxybenzyl alcohol (9.9 g, 72.0 mmol, 1.0 equiv) in THF (130 mL) at 0 °C under argon. The resulting suspension was slowly warmed to 23 °C and then heated at reflux for 21 h. The resulting mixture was then cooled back to 23 °C and quenched with methanol (10 mL). The solvent was evaporated under reduced pressure, and the dry residue of white solids were redissolved in Et_2O (70 mL) and washed with water (3 × 70 mL). The combined aqueous layers were acidified to pH = 3 with 1 M aqueous hydrochloric acid solution and re-extracted with CH_2Cl_2 (3 × 100 mL). The combined organic layers were dried over Na_2SO_4 and concentrated to dryness under reduced pressure. The crude product **118** (13.0 g, 66.3 mmol, 92% yield) was a tinted white solid and was submitted to the next step without further purification.

^{1}H NMR (600 MHz, $CDCl_3$): δ 7.29 (d, *J* = 8.6 Hz, 1H), 6.90 (d, *J* = 8.6 Hz, 1H), 4.58 (s, 1H), 4.11 (s, 1H), 3.81 (s, 1H). The spectral data are in full agreement with those reported in the literature.[132]

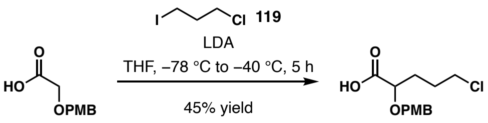

118

117

Acid 117. A solution of crude 2-((4-methoxybenzyl)oxy)acetic acid **118** (11.0 g, 56.1 mmol) in THF (140 mL, then 3 × 5.0 mL rinses) was added dropwise to a solution of freshly prepared lithium diisopropylamide (123 mmol, 2.2 equiv) in THF (125 mL) at −78 °C. The resulting solution was stirred at −78 °C for 1 h before 1-chloro-3-iodopropane **119** (18.0 mL, 168 mmol, 3.0 equiv) was added. The reaction mixture was stirred at −78 °C for an additional 1 h before warming to −50 °C to stir for 2 h, and then at −40 °C for 2 h. The reaction solution was diluted with EtOAc (100 mL) and washed with 1 M aqueous hydrochloric acid solution (150 mL). The organic layer was washed with brine (150 mL), dried over Na_2SO_4, and concentrated to dryness under reduced pressure. The crude product was purified by column chromatography on silica gel (60% EtOAc in hexanes to 60% EtOAc in hexanes with 0.5% AcOH) to give acid **117** (6.9 g, 25.3 mmol, 45% yield).

^{1}H NMR (600 MHz, $CDCl_3$): δ 7.30–7.26 (m, 2H), 6.92–6.89 (m, 2H), 4.65 (d, *J* = 11.2 Hz, 1H), 4.46 (d, *J* = 11.3 Hz, 1H), 4.02 (dd, *J* = 6.8, 4.5 Hz, 1H), 3.81 (s, 3H), 3.56–3.48 (m, 2H), 2.01 (ddt, *J* = 10.1, 8.0, 4.0 Hz, 1H), 1.97–1.86 (m, 3H).

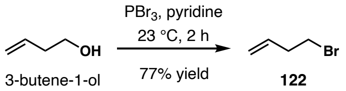

4-Bromobut-1-ene (122): The title compound was prepared according to a modification of the procedure reported by Rydon and co-workers:[133] Phosphorous tribromide (3.1 mL, 33.1 mmol, 0.4 equiv) was added dropwise to a mixture of 3-butene-1-ol (7.0 mL, 81.3 mmol) and pyridine (1.8 mL, 22.3 mmol, 0.28 equiv) at 0 °C. The reaction solution was then warmed to 23 °C and stirred at 23 °C for 2 h. The crude product was distilled under atmospheric pressure. The distillate collected was then washed with a saturated aqueous solution of $NaHCO_3$ and dried over Na_2SO_4 to afford bromobutene **122** (8.5 g, 63.0 mmol, 77% yield).

The spectral data are in full agreement with those reported in the literature.[133]

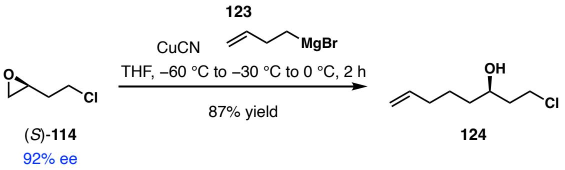

Alcohol 124. Bromobutene **122** (8.50 g, 63.0 mmol, 1.3 equiv) was added dropwise to a mixture of grounded Mg (1.47 g, 60.3 mmol, 1.25 equiv) and 4 mL of 1,2-dibromoethane in THF (60 mL) at 23 °C. The reaction mixture was heated at reflux for 2 h until all Mg turnings were consumed, at which point the solution was cooled to 23 °C. The resulting solution of Grignard reagent **123** in THF was submitted to next step.

The solution of Grignard reagent **123** from the previous step was added dropwise to a mixture of (*S*)-**114** (5.11 g, 47.9 mmol) and copper cyanide (0.216 g, 2.42 mmol, 0.05 equiv) in THF (210 mL) at −60 °C. The reaction mixture was gradually warmed to −30 °C over 20 min and stirred at −30 °C for an additional 20 min. Then it was warmed to 0 °C over 20 min and stirred at 0 °C for an additional 2 h. The resulting solution was quenched with a saturated aqueous solution of NH_4Cl at 0 °C. The layers were separated, and the aqueous layer was extracted with EtOAc. The combined organic layers were washed with brine, dried over Na_2SO_4, and concentrated to dryness under reduced pressure. The crude product was purified by column chromatography on silica gel (8% EtOAc in hexanes) to give alcohol **124** (6.63 g, 40.8 mmol, 85% yield).

^{1}H NMR (500 MHz, $CDCl_3$): δ 5.81(ddt, *J* = 16.9, 10.2, 6.7 Hz, 1H), 5.02 (dq, *J* = 17.1, 1.7 Hz, 1H), 4.97 (ddt, *J* = 10.2, 2.2, 1.3 Hz, 1H), 3.86 (dtd, *J* = 10.1, 8.7, 5.0 Hz, 1H), 3.75–3.63 (m, 2H), 2.14–2.05 (m, 2H), 1.96–1.81 (m, 2H), 1.60–1.40 (m, 5H).

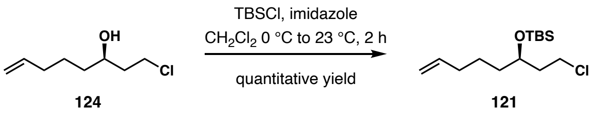
TBSCl, imidazole
CH2Cl2 0 °C to 23 °C, 2 h
quantitative yield
OH
Cl
124
OTBS
Cl
121

Alkene 121. Imidazole (8.0 g, 118 mmol, 3.2 equiv) and TBSCl (8.9 g, 59 mmol, 1.6 equiv) were added sequentially to a solution of alcohol **124** (6.0 g, 36.9 mmol) in CH_2Cl_2 at 0 °C. The reaction mixture was warmed to 23 °C and stirred at 23 °C for 2 h. The resulting solution was diluted with CH_2Cl_2. The organic layer was washed with water and brine, then dried over Na_2SO_4 and concentrated to dryness under reduced pressure. The crude product was purified by column chromatography on silica gel (100% hexanes to 1% EtOAc in hexanes) to give alkene **121** (10.2 g, 36.9 mmol, quantitative yield).

^{1}H NMR (600 MHz, $CDCl_3$): δ 5.79 (ddt, *J* = 16.9, 10.2, 6.6 Hz, 1H), 5.01 (dq, *J* = 17.1, 1.7 Hz, 1H), 4.96 (ddt, *J* = 10.2, 2.0, 1.2 Hz, 1H), 3.87 (p, *J* = 5.7 Hz, 1H), 3.63–3.56 (m, 2H), 2.07–2.02 (m, 2H), 1.90–1.84 (m, 2H), 1.51–1.45 (m, 2H), 1.44–1.38 (m, 2H), 0.89 (s, 9H), 0.08 (s, 3H), 0.07 (s, 3H).

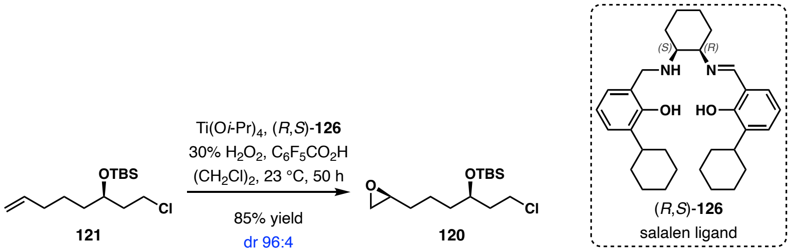
Ti(O*i*-Pr)4, (*R*,*S*)-**126**
30% H2O2, C6F5CO2H
(CH2Cl)2, 23 °C, 50 h
85% yield
dr 96:4
OTBS
Cl
121
O
OTBS
Cl
120
(S)
(R)
NH
N
OH
HO
(*R*,*S*)-**126**
salalen ligand

Epoxide 120. Ti(O*i*-Pr)$_4$ (0.054 mL, 0.18 mmol, 0.05 equiv) was added to a solution of (*R*,*S*)-**126**[134] (0.088 g, 0.18 mmol, 0.05 equiv) in CH_2Cl_2 (1.6 mL) at 23 °C under argon in a vial. The resulting mixture was stirred at 23 °C for 90 min. The solvent and other volatiles were evaporated at 23 °C by carefully applying manifold vacuum (approximately 10 mmHg), a modification to the "in situ/vac" procedure developed by Berkessel and co-workers.[134] The dry residue of Ti–salalen complex was dissolved in dichloroethane (0.6 mL) at 23 °C. Olefin **121** (1.0

g, 3.6 mmol) was added to the resulting solution at 23 °C followed by the sequential addition of pentafluorobenzoic acid (0.038 g, 0.18 mmol, 0.05 equiv) and 30% aqueous hydrogen peroxide (1.48 mL, 14.4 mmol, 4.0 equiv). The resulting mixture was vigorously stirred at 23 °C until full consumption of starting material was observed by TLC (approximately 40 h). The mixture was then diluted with CH_2Cl_2 (2 mL) and transferred to a separatory funnel. The layers were separated, and the aqueous layer as extracted with CH_2Cl_2 (3 × 3 mL). The combined organic layers were dried over Na_2SO_4 and concentrated to dryness under reduced pressure. The crude product was purified by column chromatography on silica gel (1% EtOAc in hexanes to 5% EtOAc in hexanes) to give epoxide **120** (0.921 g, 3.14 mmol, 87% yield). The diastereomeric ratio of the material (dr 96:4) was measured by HPLC trace analysis after derivatization to compound **S31** (see page 207).

^{1}H NMR (600 MHz, $CDCl_3$): δ 3.94–3.85 (m, 1H), 3.62–3.57 (m, 2H), 2.93–2.88 (m, 1H), 2.75 (dd, *J* = 5.0, 4.0 Hz, 1H), 2.47 (dd, *J* = 5.0, 2.7 Hz, 1H), 1.92–1.84 (m, 2H), 1.56–1.45 (m, 6H), 0.89 (s, 9H), 0.08 (s, 3H), 0.07 (s, 3H).

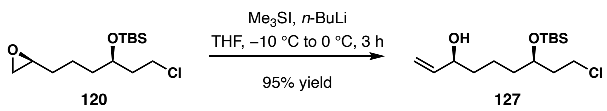

Allylic alcohol 127. *n*-Butyllithium (2.10 M in hexanes, 4.3 mL, 8.91 mmol, 3.0 equiv) was added to a solution of trimethylsulfonium iodide (1.9 g, 9.21 mmol, 3.1 equiv) in THF (9 mL) at −30 °C. The resulting solution was stirred at −30 °C for 40 min before warming it to −10 °C. A solution of epoxide **120** (0.870 g, 2.97 mmol) in THF (6 mL, then 3 × 1.0 mL rinses) was added dropwise at −10 °C. The reaction mixture was warmed to 0 °C and stirred at 0 °C for 3 h. The resulting mixture was quenched with a saturated aqueous solution of NH_4Cl (2 mL) at 0 °C ad diluted with Et_2O. The aqueous layer was extracted with Et_2O (3 × 15 mL). The combined organic layers were washed with brine, dried over Na_2SO_4, and concentrated to dryness under reduced pressure. The crude product was purified by column chromatography on silica gel (10% EtOAc in hexanes in 15% EtOAc in hexanes) to give **127** (0.823 g, 2.81 mmol, 95% yield) as a colorless oil.

^{1}H NMR (600 MHz, CDCl$_3$): δ 5.86 (ddd, *J* = 16.9, 10.4, 6.3 Hz, 1H), 5.23 (dt, *J* = 17.2, 1.4 Hz, 1H), 5.12 (dt, *J* = 10.4, 1.3 Hz, 1H), 4.10 (br s, 1H), 3.87 (p, *J* = 5.8 Hz, 1H), 3.64–3.56 (m, 2H), 1.87 (td, *J* = 7.0, 5.4 Hz, 2H), 1.55–1.44 (m, 6H), 0.89 (s, 9H), 0.07 (s, 3H), 0.06 (s, 3H).

Determination of Diastereomeric Ratio for Allylic Alcohol 127:

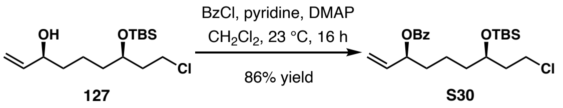

Allylic benzoate S30. Pyridine (0.030 mL, 0.34 mmol, 4.0 equiv) and benzoyl chloride (0.030 mL, 0.24 mmol, 2.8 equiv) were added sequentially to a mixture of allylic alcohol **127** (26 mg, 0.085 mmol) and DMAP (1 mg, 0.008 mmol, 0.1 equiv) in CH$_2$Cl$_2$ (0.85 mL) at 0 °C. The reaction mixture was warmed to 23 °C and stirred for 16 h. The resulting solution was diluted with CH$_2$Cl$_2$ (5 mL). The organic layer was then washed with a 1 M aqueous hydrochloric acid solution (5 mL), a saturated aqueous solution of NaHCO$_3$ (5 mL), and brine (5 mL). The combined organic layers were dried over Na$_2$SO$_4$ and concentrated to dryness under reduced pressure. The crude product was purified by column chromatography on silica gel (0.5% EtOAc in hexanes to 1% EtOAc in hexanes) to give **S30** (30 mg, 0.073 mmol, 86% yield) as a colorless oil.

^{1}H NMR (500 MHz, CDCl$_3$): δ 8.06 (d, *J* = 7.2 Hz, 2H), 7.56 (t, *J* = 7.4 Hz, 1H), 7.48–7.42 (m, 2H), 5.89 (ddd, *J* = 16.9, 10.6, 6.3 Hz, 1H), 5.50 (dt, *J* = 7.2, 5.8 Hz, 1H), 5.33 (dt, *J* = 17.2, 1.2 Hz, 1H), 5.21 (dt, *J* = 10.5, 1.2 Hz, 1H), 3.87 (dq, *J* = 7.5, 5.3 Hz, 1H), 3.62–3.55 (m, 2H), 1.93–1.69 (m, 4H), 1.68–1.55 (m, 2H), 1.54–1.38 (m, 2H), 0.85 (s, 9H), 0.06 (s, 3H), 0.03 (s, 3H).

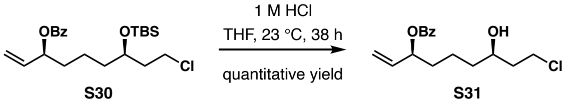

Alcohol S31. A 1 M hydrochloric acid solution (0.260 mL) was added to a solution of allylic benzoate **S30** (22 mg, 0.053 mmol) in THF (1.3 mL) at 23 °C. The reaction mixture was stirred at 23 °C for 38 h. The resulting solution was diluted with EtOAc (8 mL), and the organic layer was washed with a saturated aqueous solution of $NaHCO_3$ (10 mL) and brine (10 mL). The combined organic layers were dried over Na_2SO_4 and concentrated to dryness under reduced pressure. The crude product was purified by column chromatography on silica gel (17% EtOAc in hexanes) to give alcohol **S31** (16 mg, 0.053 mmol, quantitative yield) as a pale-yellow oil. The diastereomeric ratio of the material (dr 96:4) was measured by HPLC trace analysis [Chiralpak ® AD-H; 5% *i*-PrOH in hexanes; flow rate = 1 mL/min; 10 µL injection of a 1 mg/mL solution; detection at 273 nm; t_1 = 15.15 min (minor), t_2 = 20.11 min (major), t_3 = 21.42 min (major), t_4 = 29.64 min (minor)].

^{1}H NMR (600 MHz, $CDCl_3$): δ 8.08–8.03 (m, 2H), 7.59–7.54 (m, 1H), 7.48–7.41 (m, 2H), 5.90 (ddd, *J* = 17.0, 10.6, 6.2 Hz, 1H), 5.55–5.49 (m, 1H), 5.34 (dt, *J* = 17.2, 1.3 Hz, 1H), 5.22 (dt, *J* = 10.5, 1.2 Hz, 1H), 3.86 (br s, 1H),3.74–3.63 (m, 2H), 1.95–1.73 (m, 4H), 1.64–1.56 (m, 2H), 1.54–1.42 (m, 2H).

SHIMADZU LabSolutions

Analysis Report

<Sample Information>

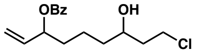

(±)-**S31**

Sample Name : kyc4-86a-4
Sample ID : kyc4-86a-4
Data Filename : kyc4-86a-4.lcd
Method Filename : JakeAnalytical.lcm
Batch Filename :
Vial # : 1-1
Injection Volume : 10 uL
Date Acquired : 5/18/2021 12:41:05 PM
Date Processed : 5/18/2021 1:24:26 PM

Sample Type : Unknown
Acquired by : Karen Chen
Processed by : Karen Chen

<Chromatogram>

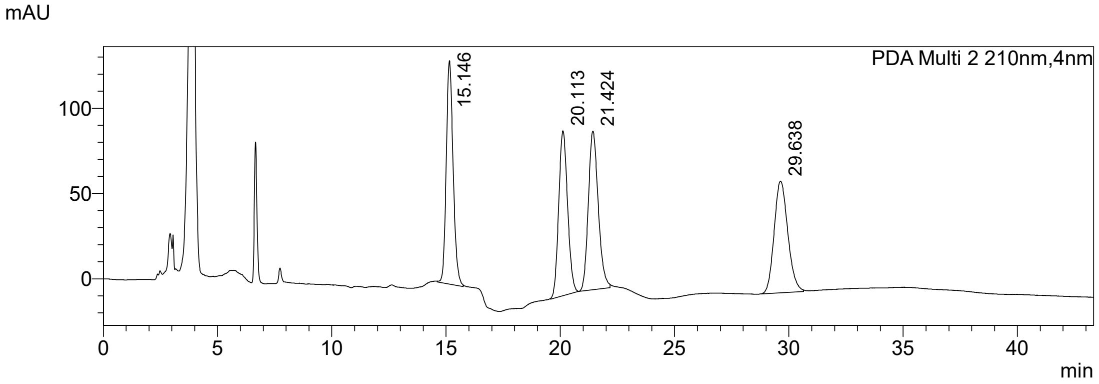

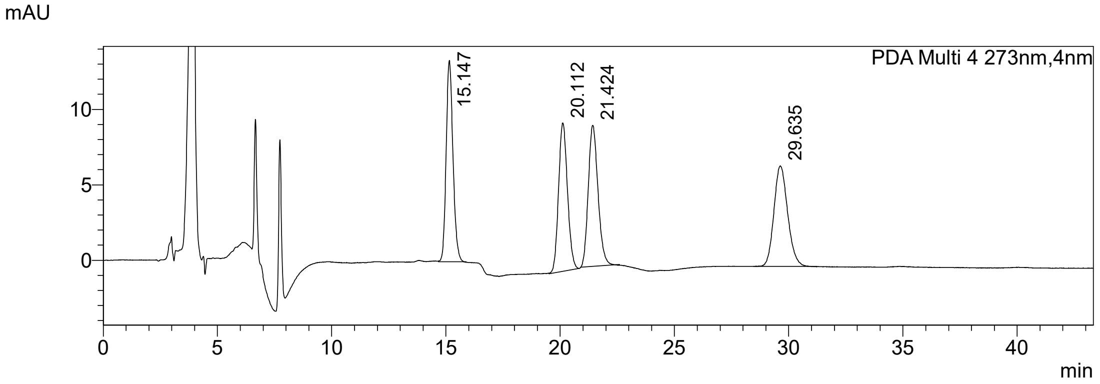

<Peak Table>

PDA Ch2 210nm

Peak#	Ret. Time	Area	Height	Height%	Area%
1	15.146	2742286	130988	33.907	25.183
2	20.113	2619909	96776	25.051	24.060
3	21.424	2809281	93052	24.087	25.799
4	29.638	2717809	65501	16.955	24.959
Total		10889285	386318	100.000	100.000

PDA Ch4 273nm

Peak#	Ret. Time	Area	Height	Height%	Area%
1	15.147	276852	13350	34.043	25.226
2	20.112	267379	9847	25.110	24.363
3	21.424	276289	9355	23.857	25.175
4	29.635	276958	6662	16.990	25.236
Total		1097478	39214	100.000	100.000

SHIMADZU LabSolutions

Analysis Report

<Sample Information>

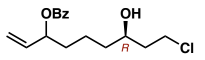

(±)-**S31**

Sample Name : kyc4-84a-6
Sample ID : kyc4-84a-6
Data Filename : kyc4-84a-6.lcd
Method Filename : JakeAnalytical.lcm
Batch Filename :
Vial # : 1-1
Sample Type : Unknown
Injection Volume : 10 uL
Date Acquired : 5/18/2021 2:00:51 PM
Acquired by : Karen Chen
Date Processed : 5/18/2021 2:52:03 PM
Processed by : Karen Chen

<Chromatogram>

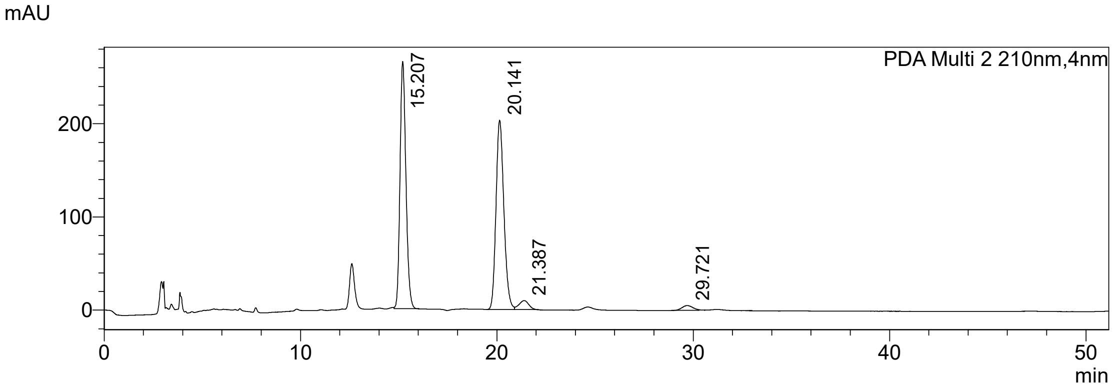

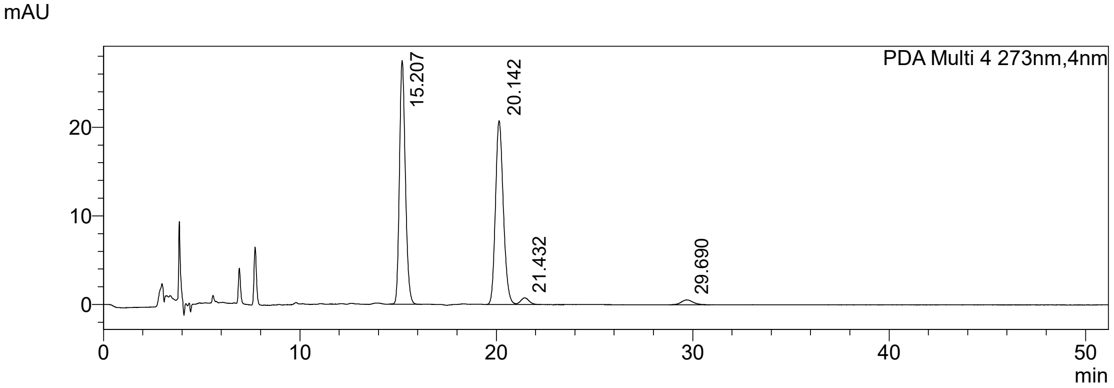

<Peak Table>

PDA Ch2 210nm

Peak#	Ret. Time	Area	Height	Height%	Area%
1	15.207	5544835	265064	54.859	47.159
2	20.141	5678034	203289	42.074	48.292
3	21.387	334848	9656	1.998	2.848
4	29.721	199966	5163	1.069	1.701
Total		11757683	483172	100.000	100.000

PDA Ch4 273nm

Peak#	Ret. Time	Area	Height	Height%	Area%
1	15.207	574856	27503	55.509	47.972
2	20.142	578103	20737	41.853	48.243
3	21.432	22268	758	1.529	1.858
4	29.690	23083	549	1.108	1.926
Total		1198311	49547	100.000	100.000

SHIMADZU LabSolutions

Analysis Report

<Sample Information>

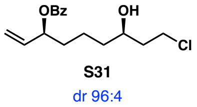

S31

dr 96:4

Sample Name : kyc4-155a
Sample ID : kyc4-155a
Data Filename : kyc4-155a.lcd
Method Filename : JakeAnalytical.lcm
Batch Filename :
Vial # : 1-1
Sample Type : Unknown
Injection Volume : 10 uL
Date Acquired : 9/30/2021 6:20:32 PM
Acquired by : Karen Chen
Date Processed : 9/30/2021 6:56:25 PM
Processed by : Karen Chen

<Chromatogram>

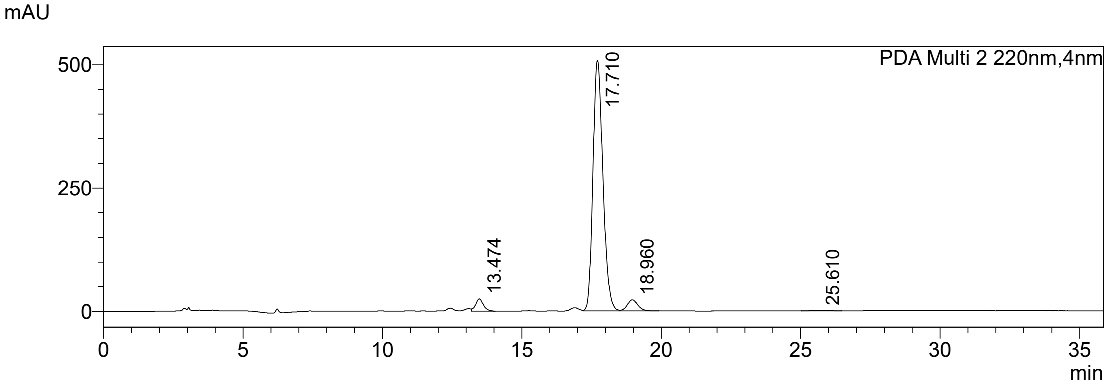

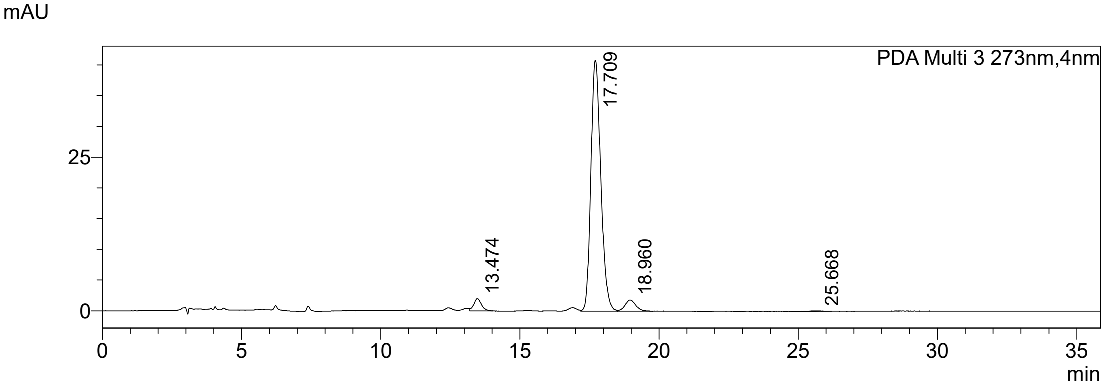

<Peak Table>

PDA Ch2 220nm

Peak#	Ret. Time	Area	Height	Height%	Area%
1	13.474	485604	24884	4.480	3.540
2	17.710	12616001	507447	91.359	91.958
3	18.960	589589	22362	4.026	4.298
4	25.610	28156	747	0.135	0.205
Total		13719351	555440	100.000	100.000

PDA Ch3 273nm

Peak#	Ret. Time	Area	Height	Height%	Area%
1	13.474	38679	1990	4.455	3.521
2	17.709	1010024	40811	91.373	91.935
3	18.960	48144	1805	4.042	4.382
4	25.668	1779	58	0.131	0.162
Total		1098626	44665	100.000	100.000

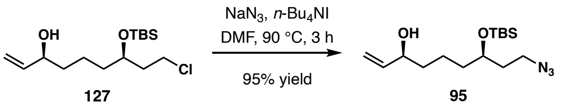

Azide 95. Sodium azide (0.200 g, 3.08 mmol, 1.1 equiv) and tetra-*n*-butylammonium iodide (0.009 g, 0.025 mmol, 0.9 mol %) were added to a solution of chloride **127** (0.820 g, 2.8 mmol) in DMF (1.8 mL) at 23 °C. The resulting mixture was heated at 90 °C for 3 h before cooling back to 23 °C and diluted with a solution of 20% EtOAc in hexanes (1 mL). The organic layer was washed with water (3 × 20 mL) and brine, dried over Na_2SO_4, and concentrated to dryness under reduced pressure. The crude product was purified by column chromatography on silica gel (15% EtOAc in hexanes) to give azide **95** (0.833 g, 2.66 mmol, 95% yield) as a pale-yellow oil.

^{1}H NMR (500 MHz, $CDCl_3$): δ 5.86 (ddd, *J* = 17.0, 10.4, 6.3 Hz, 1H), 5.23 (dt, *J* = 17.2, 1.4 Hz, 1H), 5.12 (dt, *J* = 10.4, 1.3 Hz, 1H), 4.10 (t, *J* = 5.5 Hz, 1H), 3.83–3.72 (m, 1H), 3.41–3.30 (m, 2H), 1.78–1.64 (m, 2H), 1.54–1.30 (m, 6H), 0.89 (s, 9H), 0.06 (s, 3H), 0.05 (s, 3H). The spectral data are in full agreement with those for the compound obtained by the reported synthetic route (the first generation synthesis).[94]

References

[111] Bindman, N. A.; Bobeica, S. C.; Liu, W. R.; van der Donk, W. A. *J. Am. Chem. Soc.* **2015**, *137*, 6975–6978.

[112] Dondoni, A.; Perrone, D. *Org. Synth.* **2000**, *77*, 64.

[113] Li, D. B.; Robinson, J. A. *Org. Biomol. Chem.* **2005**, *3*, 1233–1239.

[114] Montessuit, S.; Mazzei, G.; Magnenat, E.; Antonsson, B. *Protein Expression Purif.* **1999**, *15*, 202–206.

[115] Kabsch, W. Acta Crystallogr., Sect. D: Biol. Crystalloger. **2010**, D66, 133–144.

[116] (a) Winn, M. D.; Ballard, C. C.; Cowtan, K. D.; Dodson, E. J.; Emsley, P.; Evans, P. R.; Keegan, R. M.; Krissinel, E. B.; Leslie, A. G. W.; McCoy, A.; McNicholas, S. J.; Murshudov, G. N.; Pannu, N. S.; Potterton, E. A.; Powell, H. R.; Read, R. J.; Vagin, A.; Wilson, K. S. *Acta Crystallogr., Sect. D. Biol. Crystallogr.* **2011**, *D67*, 235–242. (b) Murshudov, G. N.; Vagin, A. A.; Dodson, E. J. *Acta Crystallogr., Sect. D. Biol. Crystallogr.* **1997**, *D53*, 240–255.

[117] Emsley, P.; Cowtan, K. Acta Crystallogr., Sect. D. Biol. Crystallogr. **2004**, D60, 2126–2132.

[118] Brubaker, J. D.; Myers, A. G. *Org. Lett.* **2007**, *9*, 3523–3525.

[119] Hanson, R. M.; Sharpless, K. B. *J. Org. Chem.* **1986**, *51*, 1922–1925.

[120] Fujino, A.; Sugai, T. *Adv. Synth. Catal.* **2008**, *350*, 1712–1716.

[121] Xu, G.; Micklatcher, M.; Silvestri, M. A.; Hartman, T. L.; Burrier, J.; Osterling, M. C.; Wargo, H.; Turpin, J. A.; Buckheit, R. W., Jr.; Cushman, M. *J. Med. Chem.* **2001**, *44*, 4092–4113.

[122] (a) Aggarwal, V. K.; Ford, J. G.; Thompson, A.; Jones, R. V. H.; Standen, M. C. H. *J. Am. Chem. Soc.* **1996**, *118*, 7004–7005. (b) Aggarwal, V. K.; Ford, J. G.; Fonquerna, S.; Adams, H.; Jones, R. V. H.; Fieldhouse, R. *J. Am. Chem. Soc.* **1998**, *120*, 8328–8339.

[123] (a) Aggarwal, V. K.; Alonso, E. Hynd, G.; Lydon, K. M.; Palmer, M. J.; Porcelloni, M.; Studley, J. R. *Angew. Chem. Int. Ed.* **2001**, *40*, 1430–1433. (b) Aggarwal, V. K.; Fang, G.; Kokotos, C. G.; Richardson, J.; Unthank, M. U. *Tetrahedron* **2006**, *62*, 11297–11303.

[124] Periasamy, M.; Ramani, G.; Muthukumaragopal, G. P. *Synthesis* **2009**, 1739–1743.

[125] Julienne, K.; Metzner, P. *J. Org. Chem.* **1998**, *63*, 4532–4534.

[126] Piccinini, A.; Kavanagh, S. A.; Connon, P. B.; Connon, S. J. *Org. Lett.* **2010**, *12*, 608–611.

[127] Brucks, A. P.; Treitler, D. S.; Liu, S.-A.; Snyder, S. A. *Synthesis* **2013**, *45*, 1886–1898.

[128] Wiesler, S.; Bau, M. A.; Younas, S. L.; Luu, H.-T.; Kratzert, D. Streuff, J. *Chem. Eur. J.* **2018**, *24*, 16532–16536.

[129] Satoh, T.; Taguchi, D.; Kurabayashi, A.; Kanoto, M. *Tetrahedron* **2002**, *58*, 4217–4224.

[130] Bach, J.; Berenguer, R.; Garcia, J.; López, M.; Manzanal, J.; Vilarrasa, J. *Tetrahedron* **1998**, *54*, 14947–14962.

[131] Morris, D. J.; Hayes, A. M.; Wills, M. *J. Org. Chem.* **2006**, *71*, 7035–7044.

[132] Stockley, M.; Clegg, W.; Fontana, G.; Golding, B. T.; Martin, N.; Rigoreau, L. J. M.; Smith, G. C. M.; Griffin, R. J. *Bioorg. Med. Chem. Lett.* **2001**, *11*, 2837–2841.

[133] Linstead, R. P.; Rydon, H. N. *J. Chem. Soc.* **1934**, 1995–2001.

[134] (a) Berkessel, A.; Günther, T.; Wang, Q.; Neudörfl, J.-M. *Angew. Chem. Int. Ed.* **2013**, *52*, 8467–8471. (b) Lansing, M.; Engler, H.; Leuther, T. M.; Neudörfl, J.-M.; Berkessel, A. *ChemCatChem* **2016**, *8*, 3706–3709.

^{1}H NMR and ^{13}C NMR Spectra

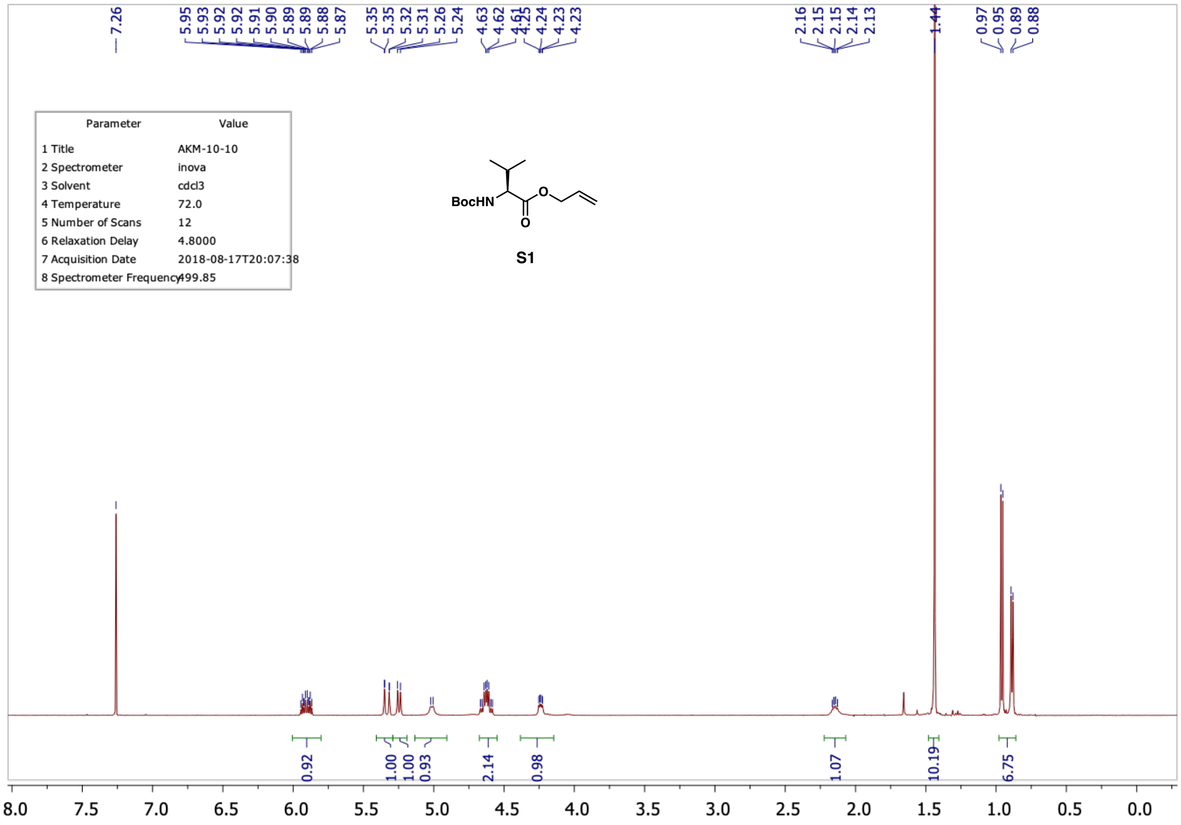

Parameter	Value
1 Title	AKM-10-10
2 Spectrometer	inova
3 Solvent	cdcl3
4 Temperature	72.0
5 Number of Scans	12
6 Relaxation Delay	4.8000
7 Acquisition Date	2018-08-17T20:07:38
8 Spectrometer Frequency	499.85

S1

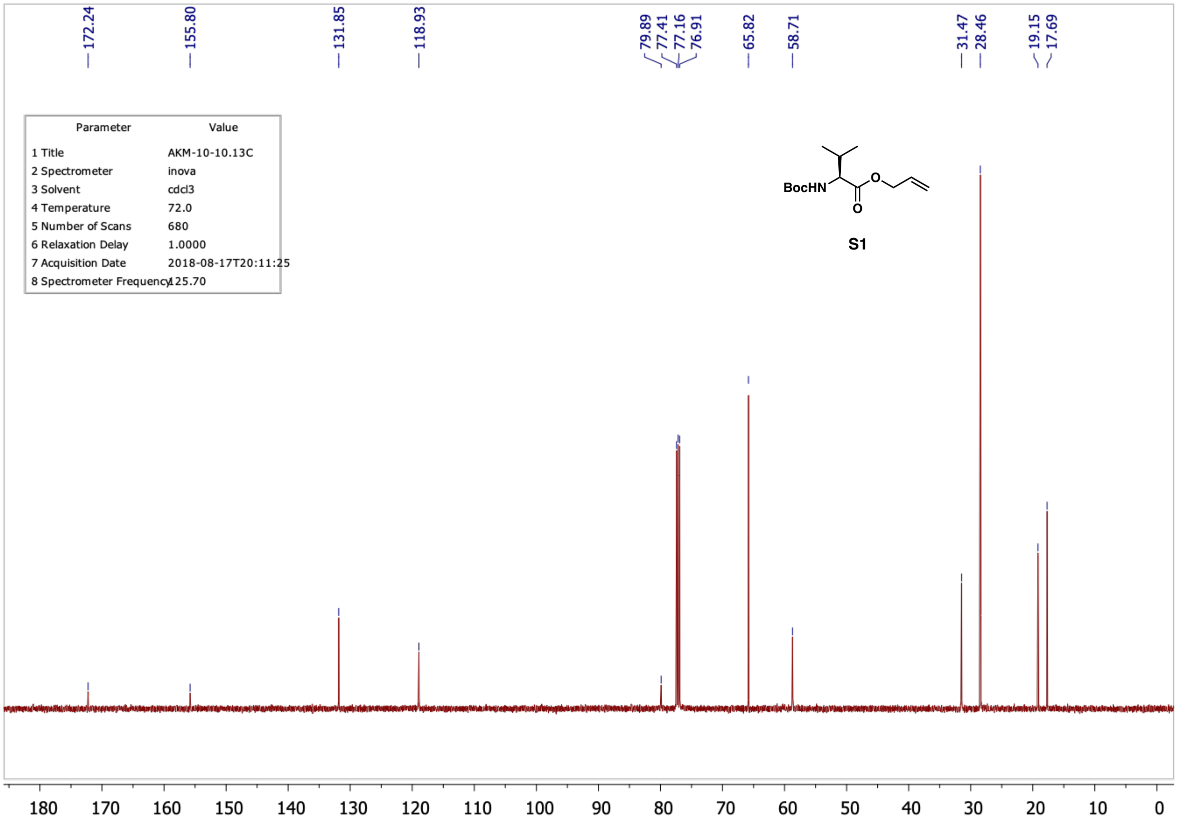

Parameter	Value
1 Title	AKM-10-10.13C
2 Spectrometer	inova
3 Solvent	cdcl3
4 Temperature	72.0
5 Number of Scans	680
6 Relaxation Delay	1.0000
7 Acquisition Date	2018-08-17T20:11:25
8 Spectrometer Frequency	125.70

S1

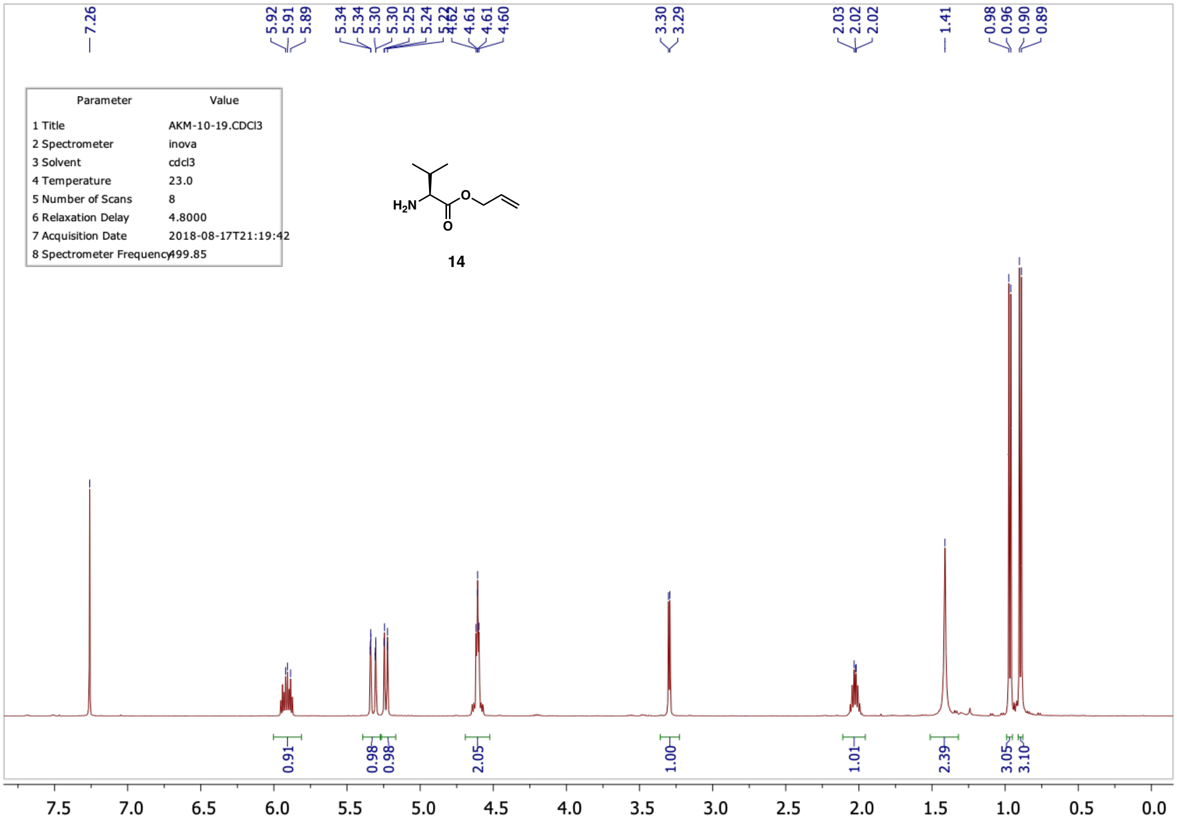

Parameter	Value
1 Title	AKM-10-19.CDCl3
2 Spectrometer	inova
3 Solvent	cdcl3
4 Temperature	23.0
5 Number of Scans	8
6 Relaxation Delay	4.8000
7 Acquisition Date	2018-08-17T21:19:42
8 Spectrometer Frequency	499.85

14

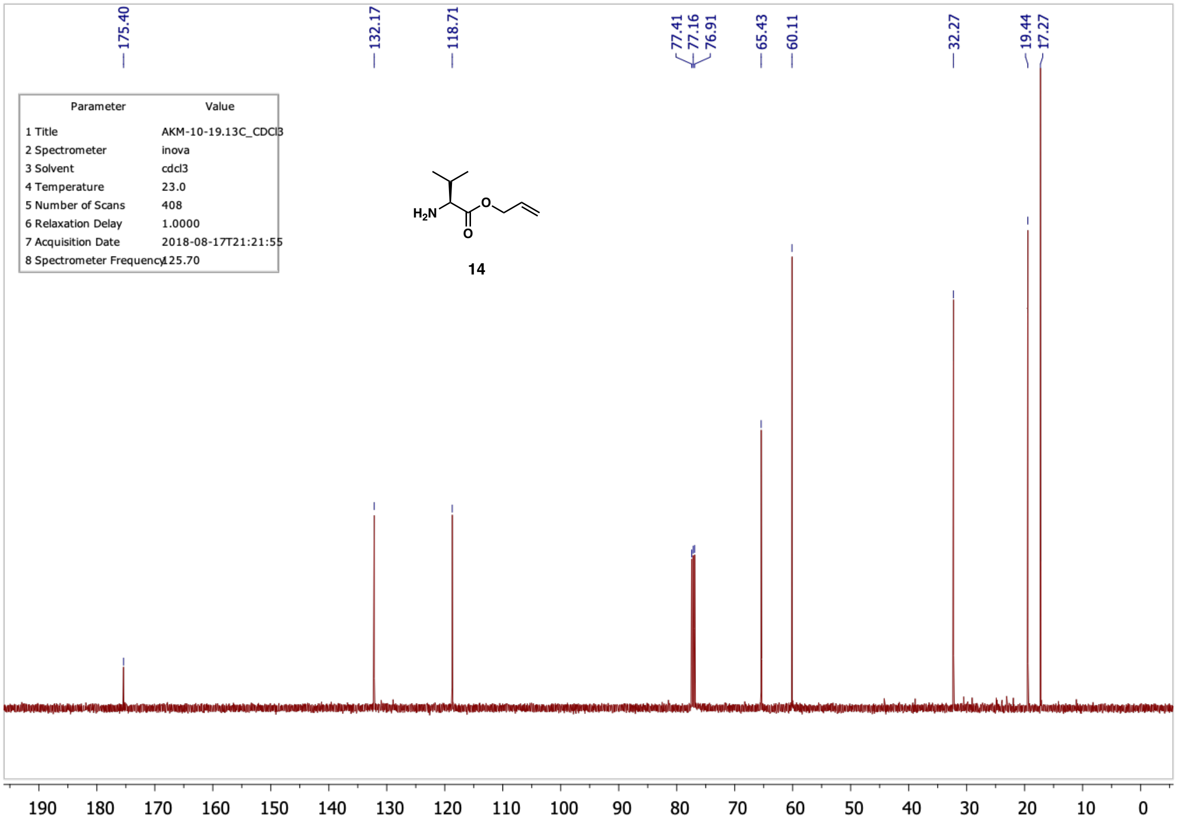

Parameter	Value
1 Title	AKM-10-19.13C_CDCl3
2 Spectrometer	inova
3 Solvent	cdcl3
4 Temperature	23.0
5 Number of Scans	408
6 Relaxation Delay	1.0000
7 Acquisition Date	2018-08-17T21:21:55
8 Spectrometer Frequency	125.70

14

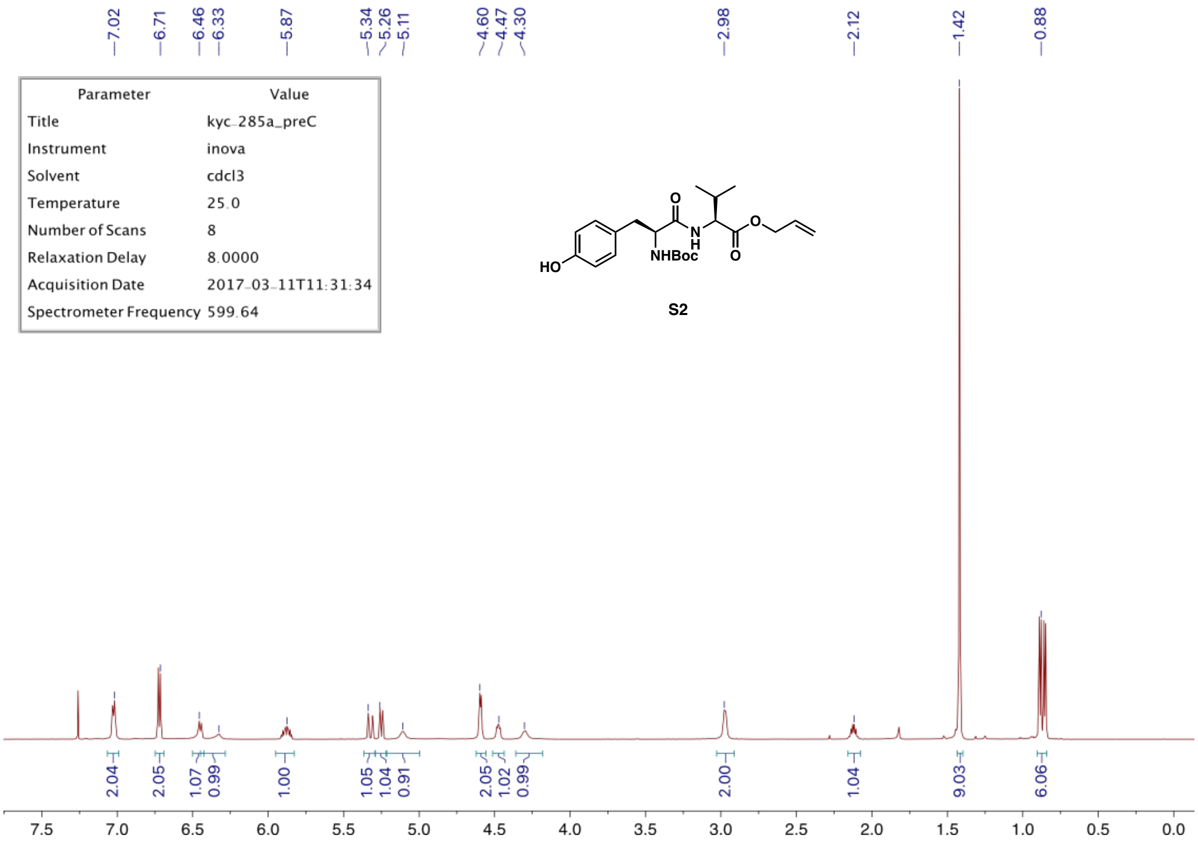

Parameter	Value
Title	kyc_285a_preC
Instrument	inova
Solvent	cdcl3
Temperature	25.0
Number of Scans	8
Relaxation Delay	8.0000
Acquisition Date	2017-03-11T11:31:34
Spectrometer Frequency	599.64

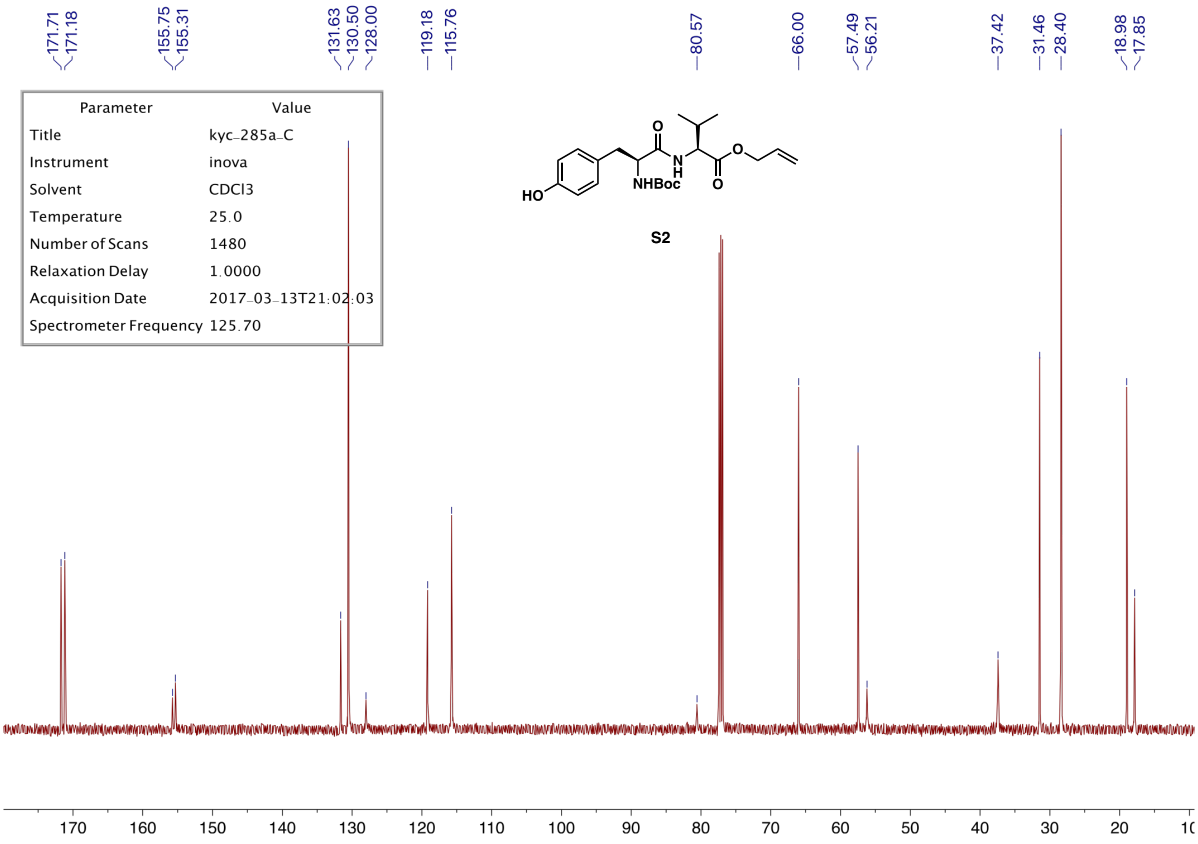

Parameter	Value
Title	kyc_285a_C
Instrument	inova
Solvent	CDCl3
Temperature	25.0
Number of Scans	1480
Relaxation Delay	1.0000
Acquisition Date	2017-03-13T21:02:03
Spectrometer Frequency	125.70

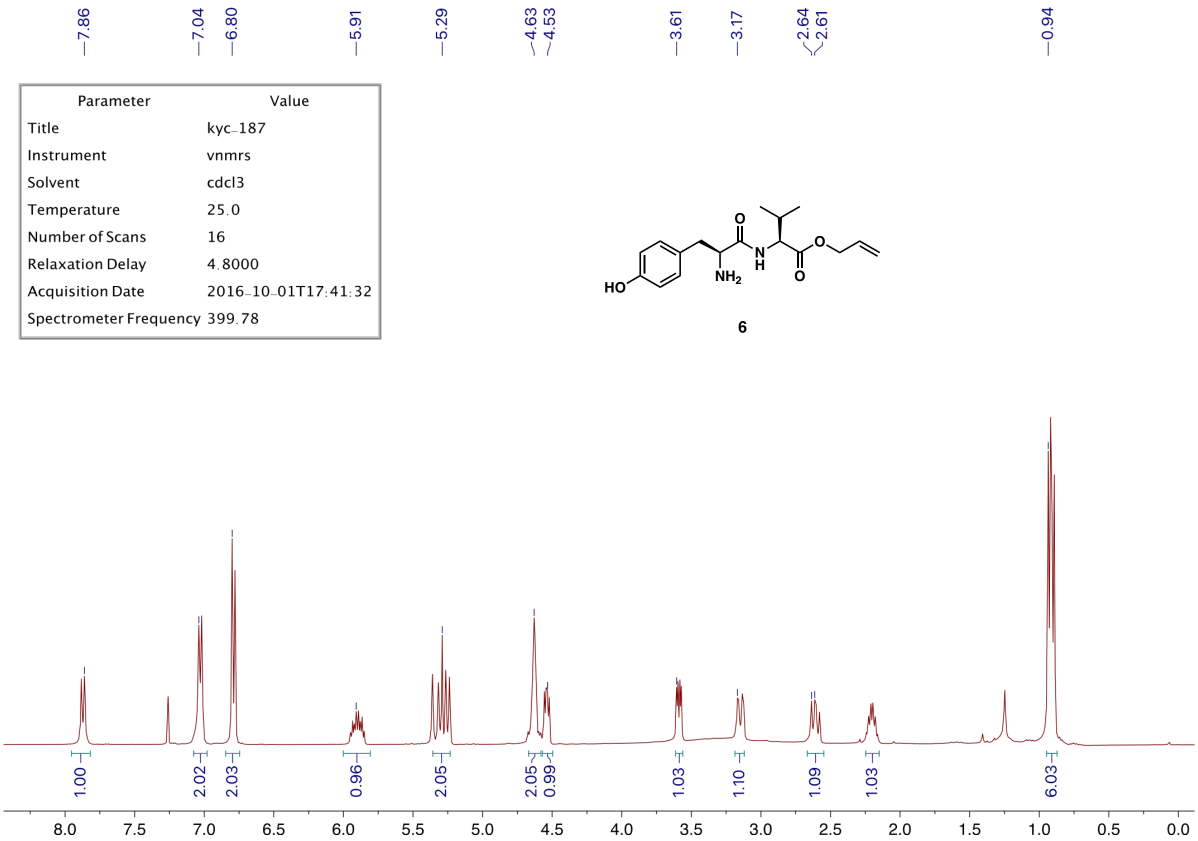

6

Parameter	Value
Title	kyc_187
Instrument	vnmrs
Solvent	cdcl3
Temperature	25.0
Number of Scans	16
Relaxation Delay	4.8000
Acquisition Date	2016_10_01T17:41:32
Spectrometer Frequency	399.78

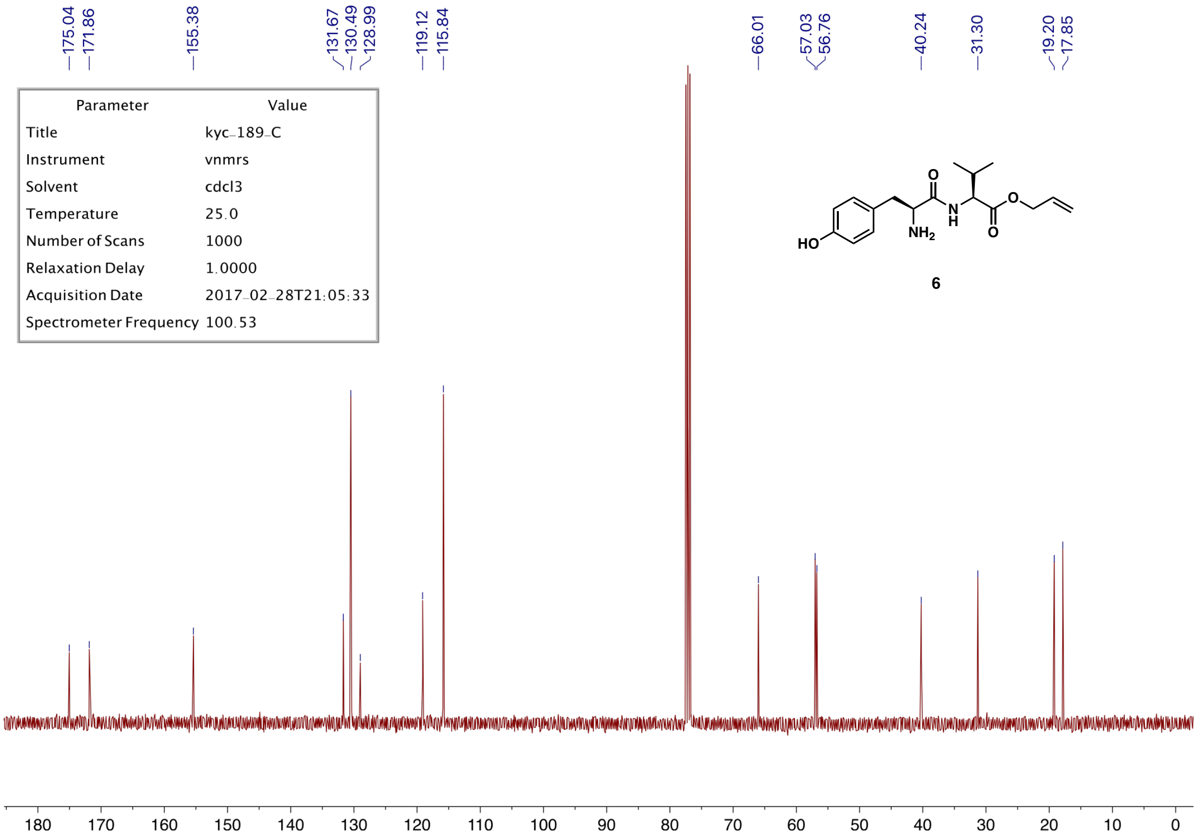

6

Parameter	Value
Title	kyc_189_C
Instrument	vnmrs
Solvent	cdcl3
Temperature	25.0
Number of Scans	1000
Relaxation Delay	1.0000
Acquisition Date	2017_02_28T21:05:33
Spectrometer Frequency	100.53

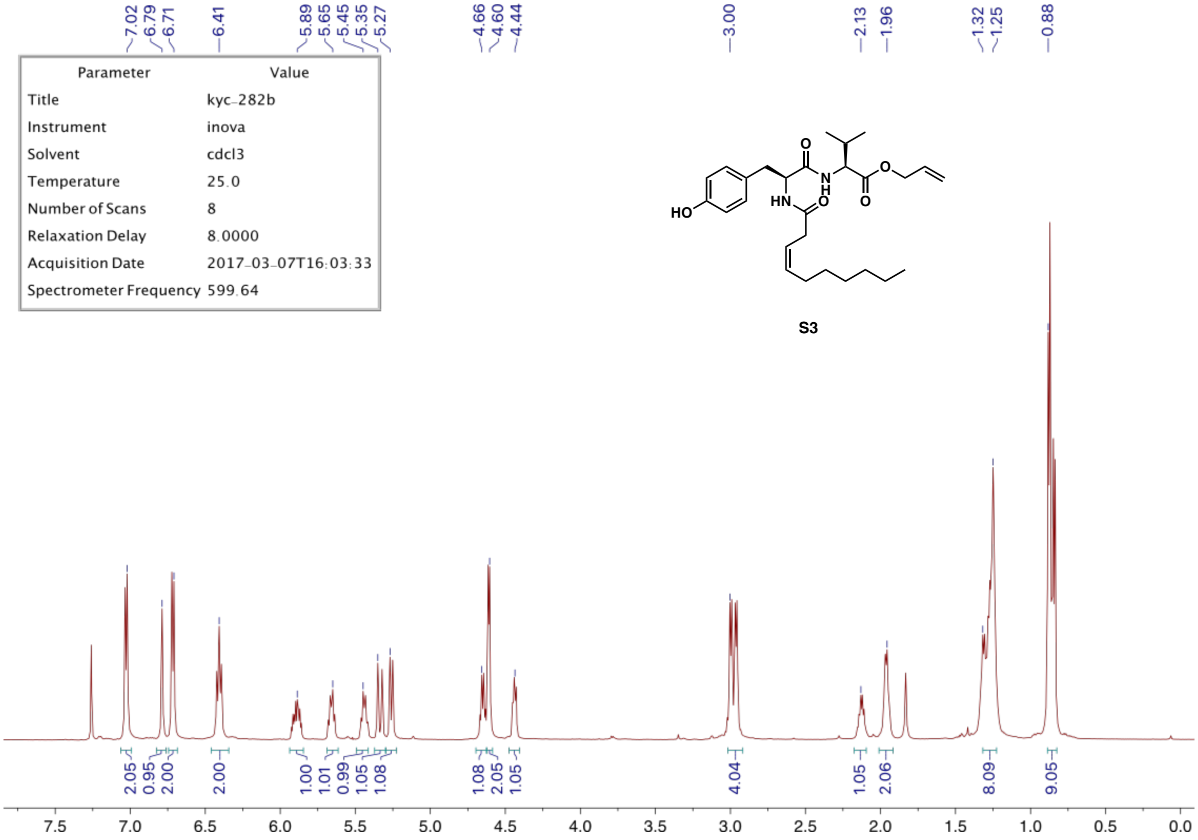

Parameter	Value
Title	kyc_282b
Instrument	inova
Solvent	cdcl3
Temperature	25.0
Number of Scans	8
Relaxation Delay	8.0000
Acquisition Date	2017_03_07T16:03:33
Spectrometer Frequency	599.64

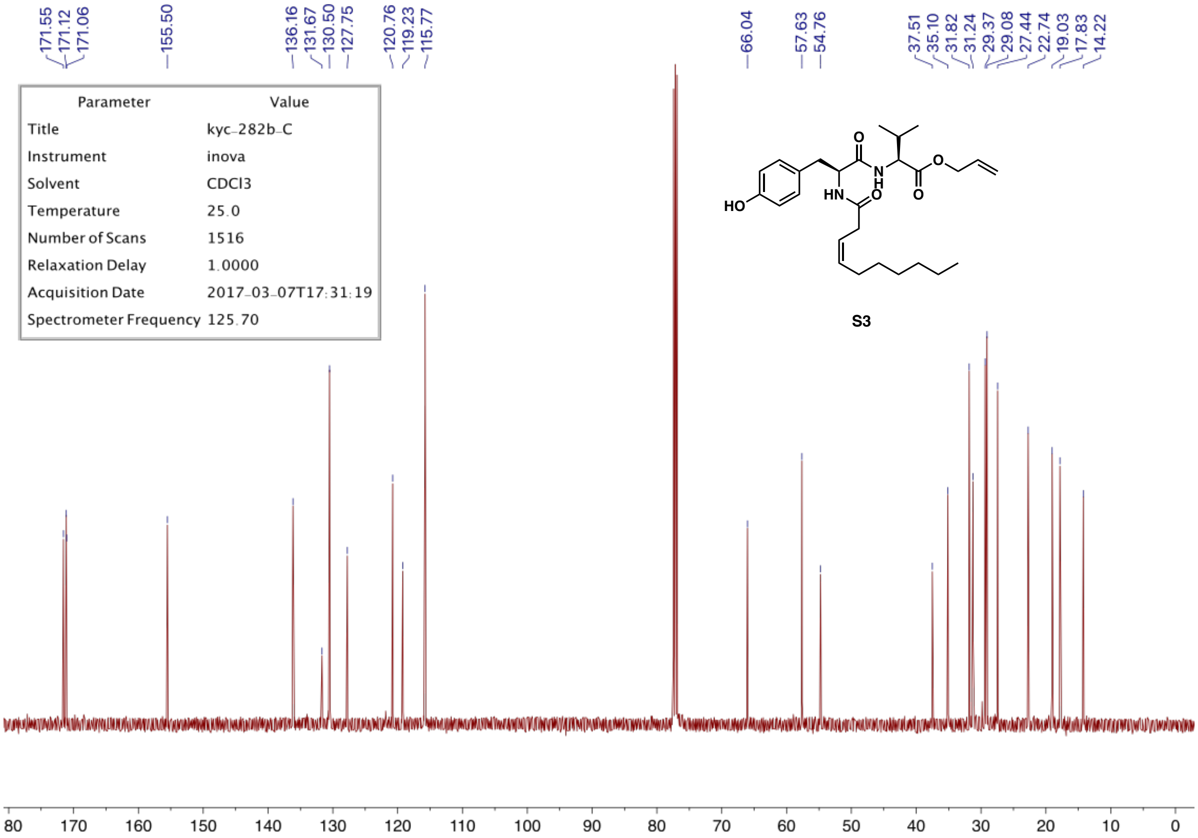

Parameter	Value
Title	kyc_282b_C
Instrument	inova
Solvent	CDCl3
Temperature	25.0
Number of Scans	1516
Relaxation Delay	1.0000
Acquisition Date	2017_03_07T17:31:19
Spectrometer Frequency	125.70

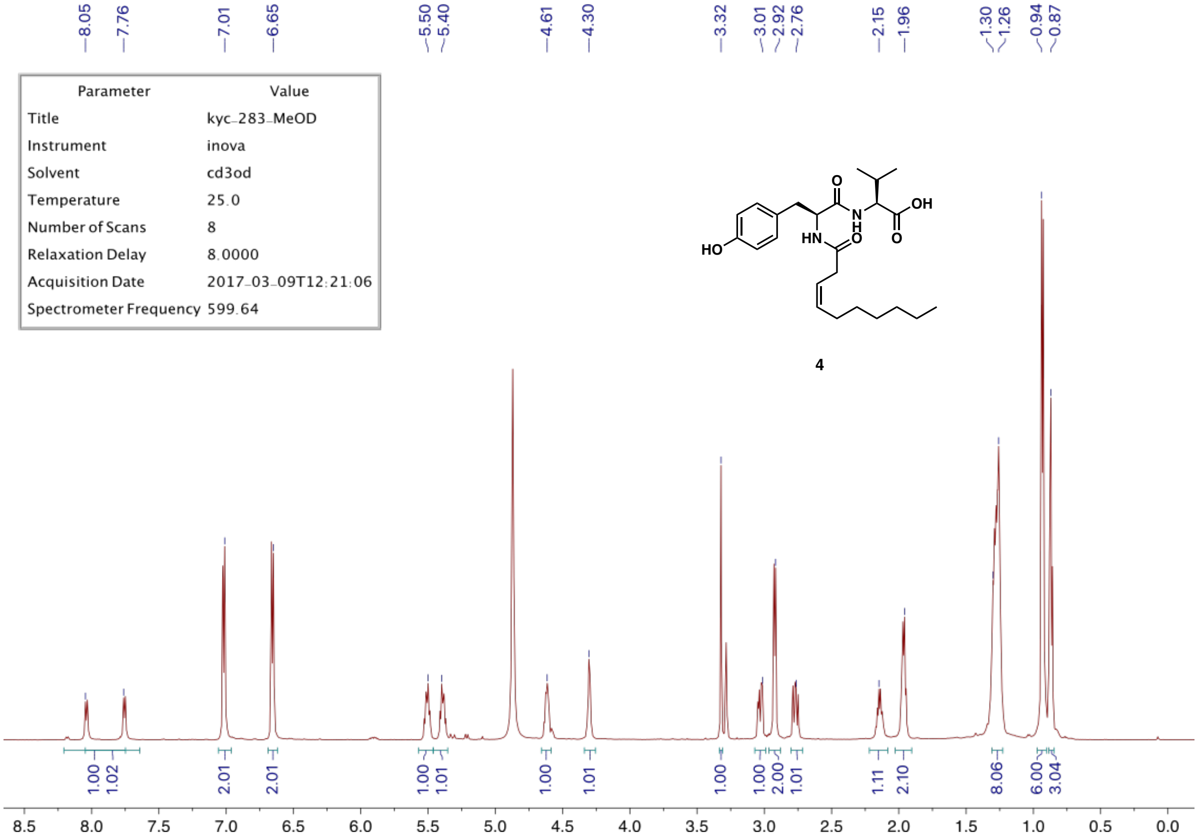

Parameter	Value
Title	kyc_283_MeOD
Instrument	inova
Solvent	cd3od
Temperature	25.0
Number of Scans	8
Relaxation Delay	8.0000
Acquisition Date	2017_03_09T12:21:06
Spectrometer Frequency	599.64

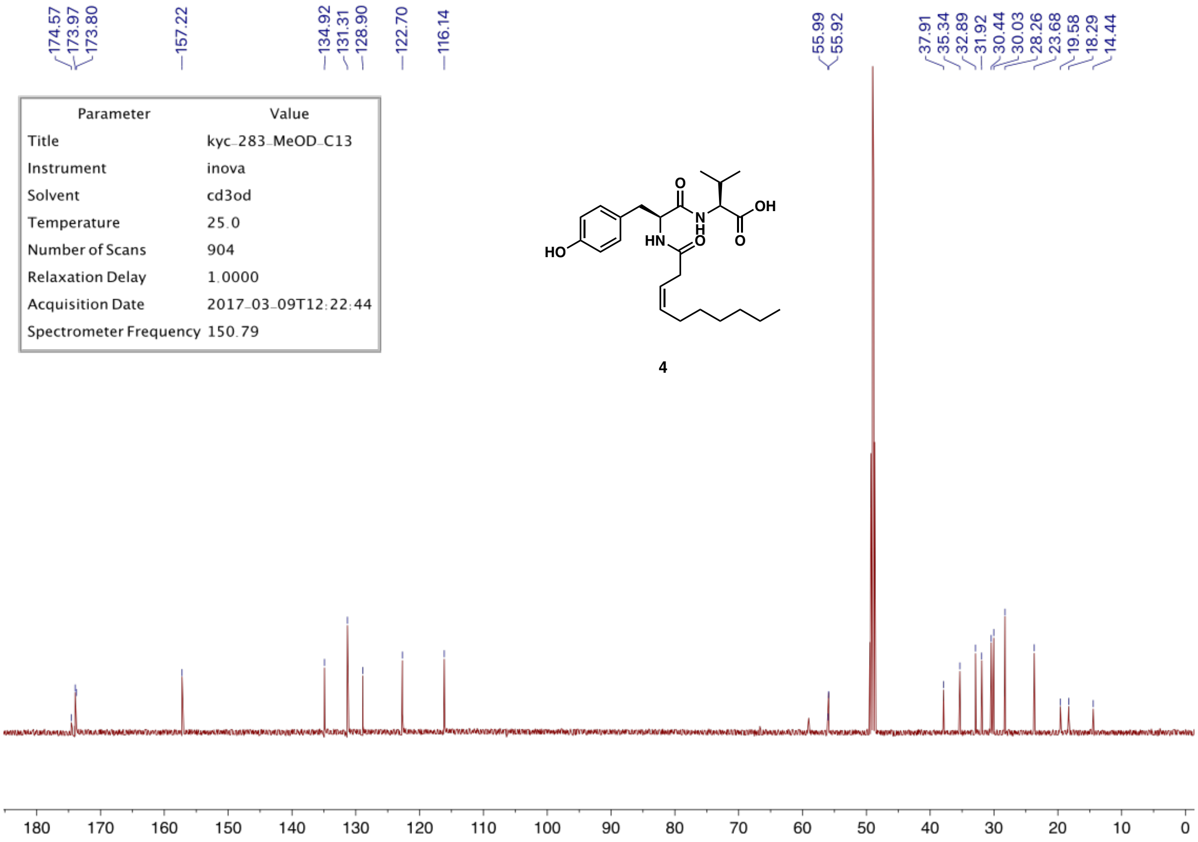

Parameter	Value
Title	kyc_283_MeOD_C13
Instrument	inova
Solvent	cd3od
Temperature	25.0
Number of Scans	904
Relaxation Delay	1.0000
Acquisition Date	2017_03_09T12:22:44
Spectrometer Frequency	150.79

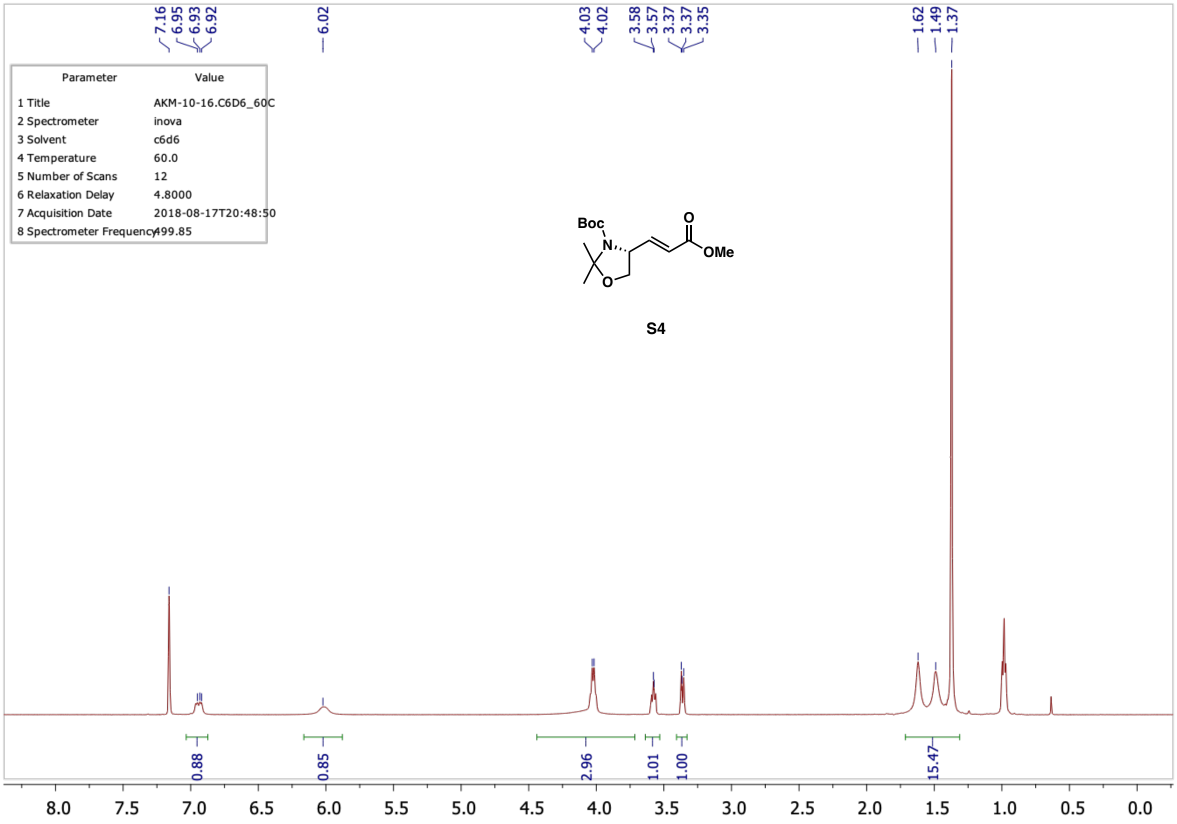

Parameter	Value
1 Title	AKM-10-16.C6D6_60C
2 Spectrometer	inova
3 Solvent	c6d6
4 Temperature	60.0
5 Number of Scans	12
6 Relaxation Delay	4.8000
7 Acquisition Date	2018-08-17T20:48:50
8 Spectrometer Frequency	499.85

S4

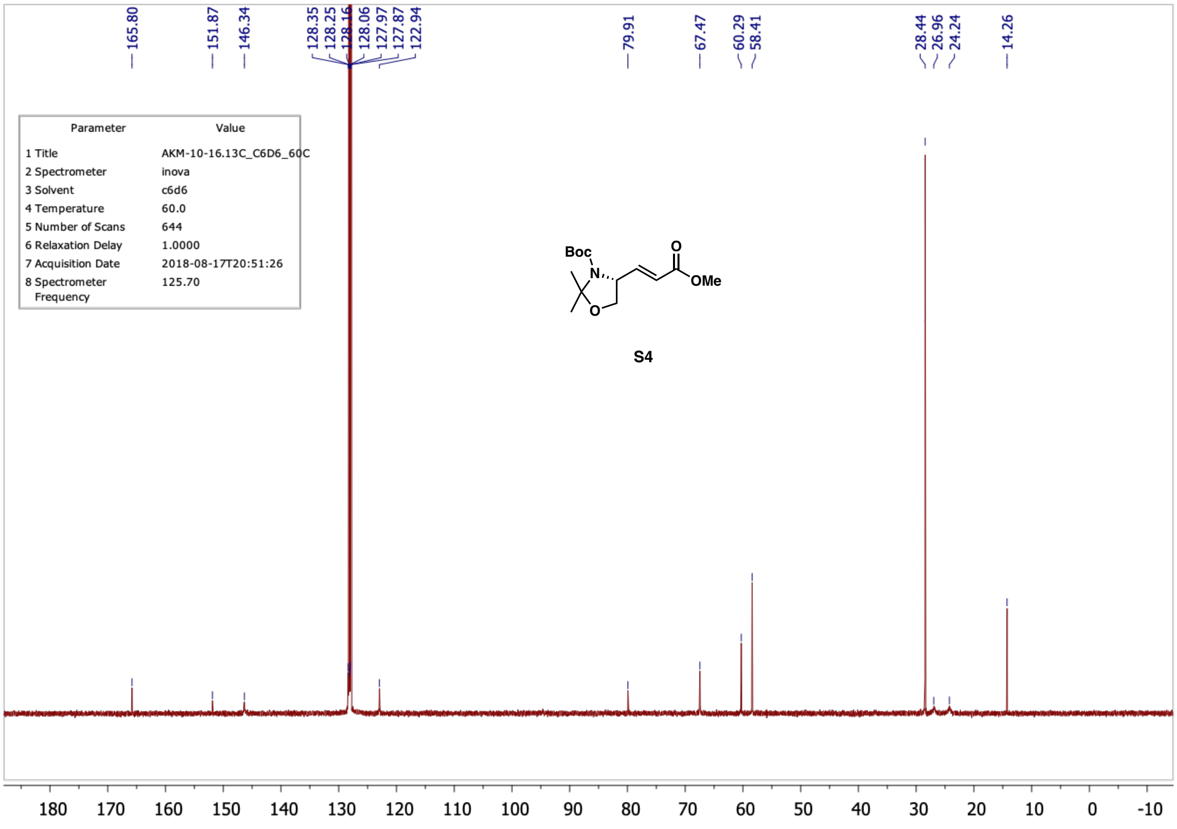

Parameter	Value
1 Title	AKM-10-16.13C_C6D6_60C
2 Spectrometer	inova
3 Solvent	c6d6
4 Temperature	60.0
5 Number of Scans	644
6 Relaxation Delay	1.0000
7 Acquisition Date	2018-08-17T20:51:26
8 Spectrometer Frequency	125.70

S4

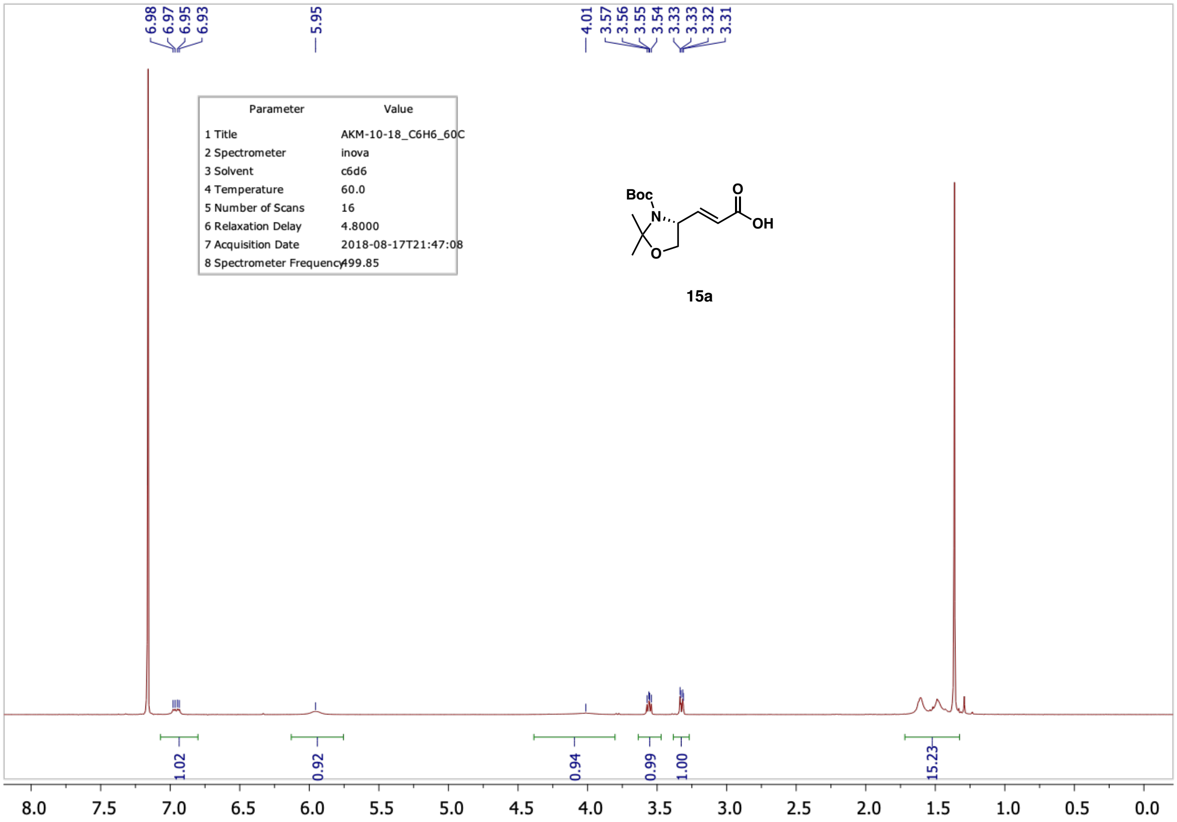

Parameter	Value
1 Title	AKM-10-18_C6H6_60C
2 Spectrometer	inova
3 Solvent	c6d6
4 Temperature	60.0
5 Number of Scans	16
6 Relaxation Delay	4.8000
7 Acquisition Date	2018-08-17T21:47:08
8 Spectrometer Frequency	499.85

15a

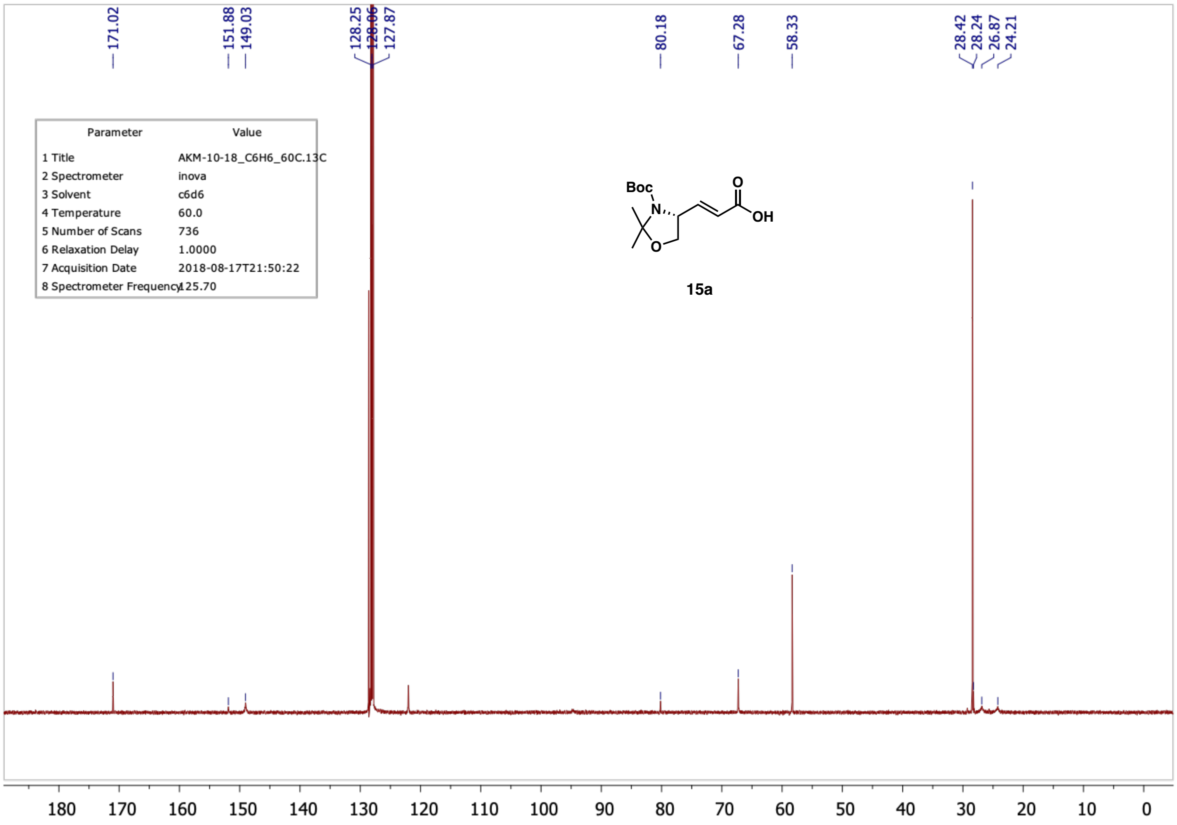

Parameter	Value
1 Title	AKM-10-18_C6H6_60C.13C
2 Spectrometer	inova
3 Solvent	c6d6
4 Temperature	60.0
5 Number of Scans	736
6 Relaxation Delay	1.0000
7 Acquisition Date	2018-08-17T21:50:22
8 Spectrometer Frequency	125.70

15a

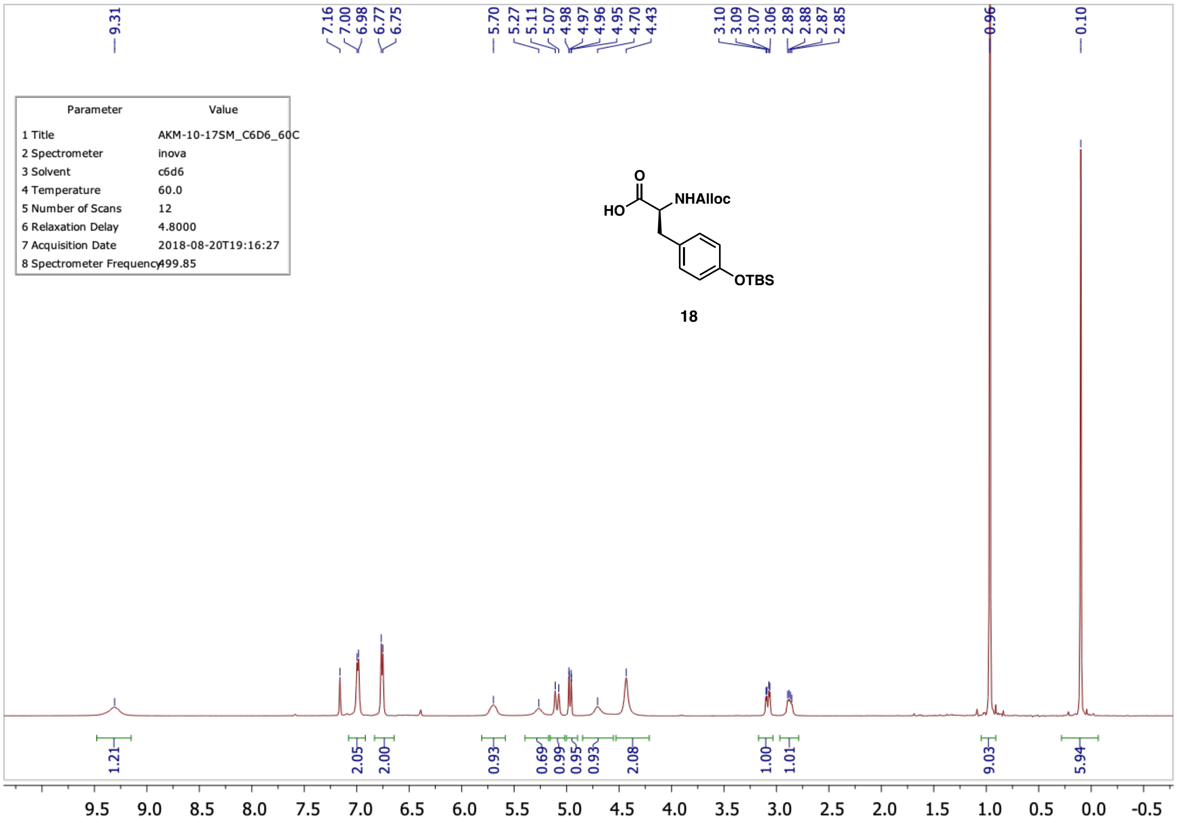

Parameter	Value
1 Title	AKM-10-17SM_C6D6_60C
2 Spectrometer	inova
3 Solvent	c6d6
4 Temperature	60.0
5 Number of Scans	12
6 Relaxation Delay	4.8000
7 Acquisition Date	2018-08-20T19:16:27
8 Spectrometer Frequency	499.85

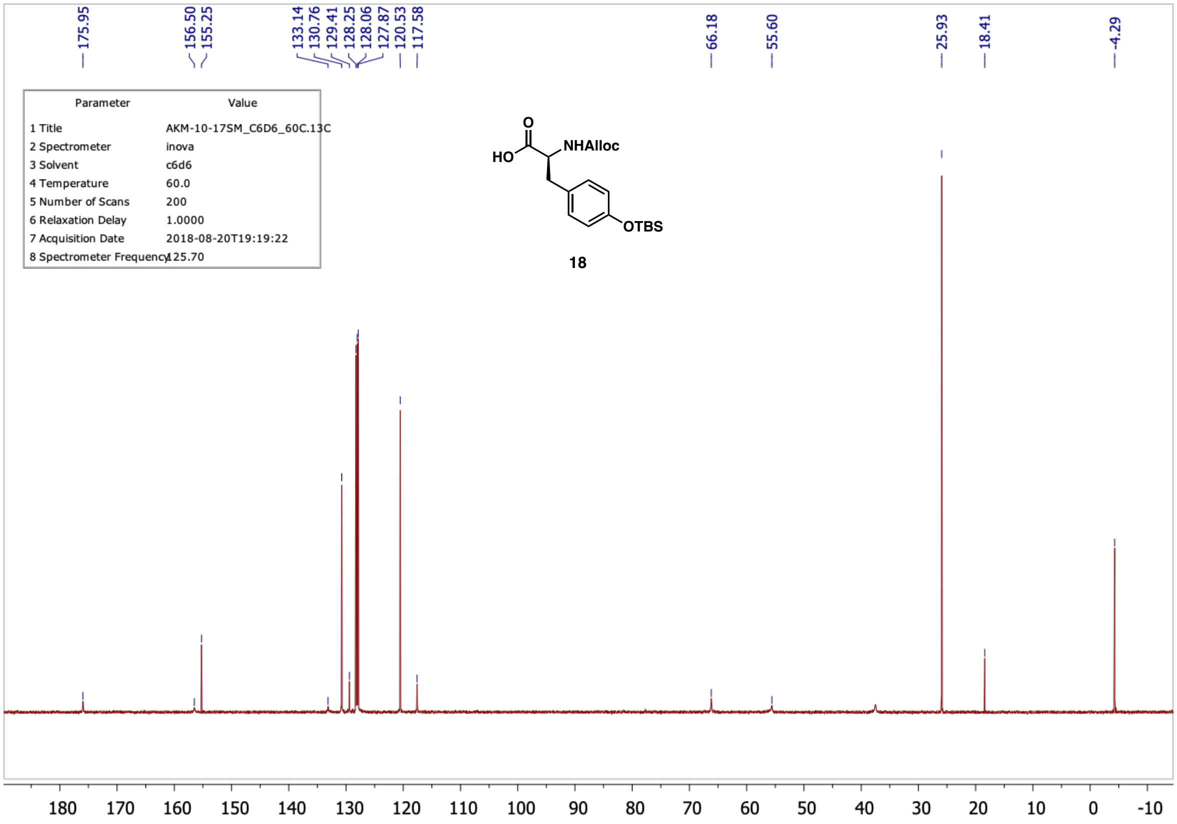

Parameter	Value
1 Title	AKM-10-17SM_C6D6_60C.13C
2 Spectrometer	inova
3 Solvent	c6d6
4 Temperature	60.0
5 Number of Scans	200
6 Relaxation Delay	1.0000
7 Acquisition Date	2018-08-20T19:19:22
8 Spectrometer Frequency	125.70

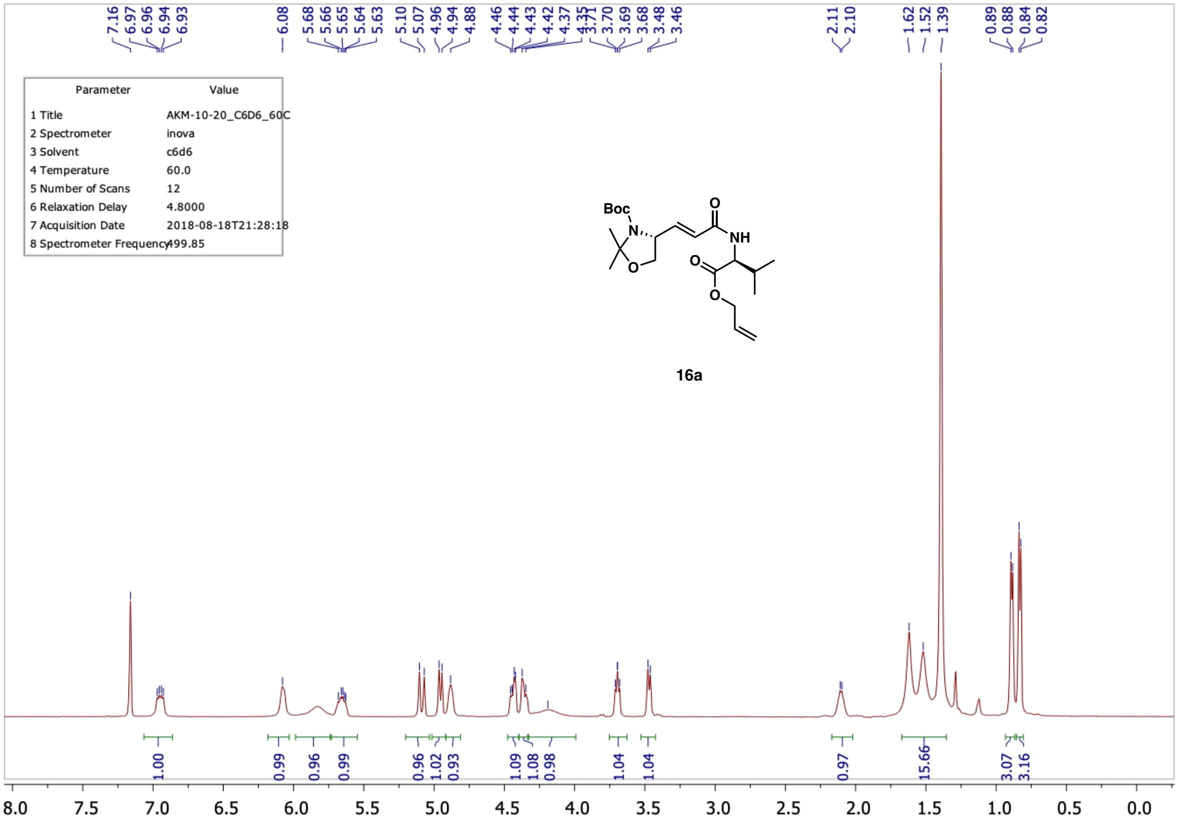

Parameter	Value
1 Title	AKM-10-20_C6D6_60C
2 Spectrometer	inova
3 Solvent	c6d6
4 Temperature	60.0
5 Number of Scans	12
6 Relaxation Delay	4.8000
7 Acquisition Date	2018-08-18T21:28:18
8 Spectrometer Frequency	499.85

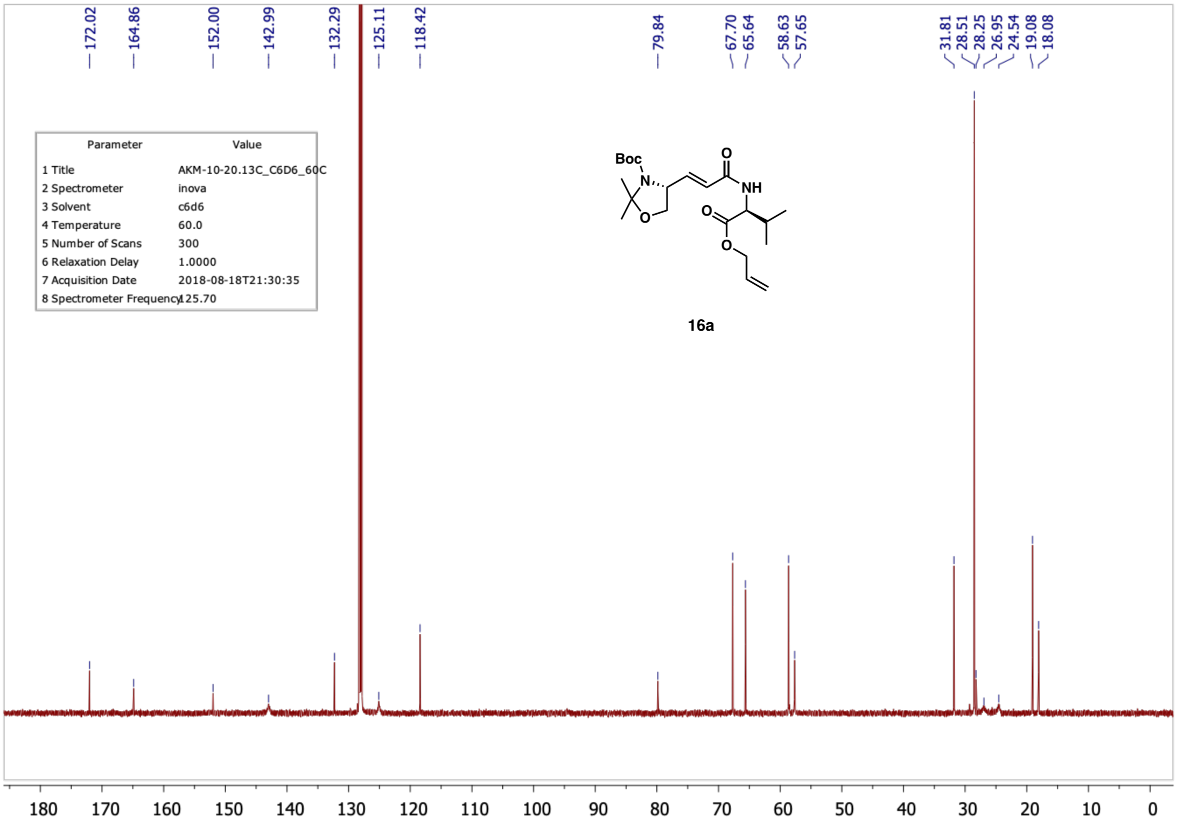

Parameter	Value
1 Title	AKM-10-20.13C_C6D6_60C
2 Spectrometer	inova
3 Solvent	c6d6
4 Temperature	60.0
5 Number of Scans	300
6 Relaxation Delay	1.0000
7 Acquisition Date	2018-08-18T21:30:35
8 Spectrometer Frequency	125.70

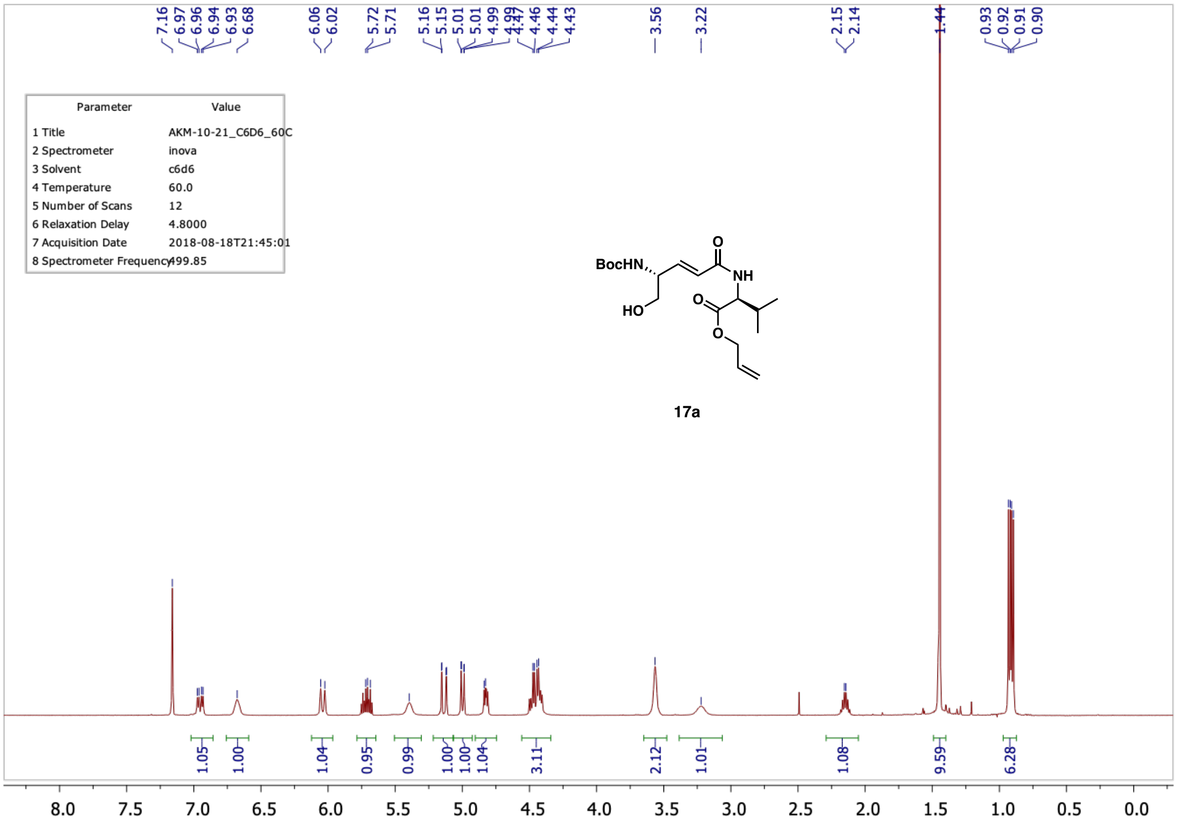

Parameter	Value
1 Title	AKM-10-21_C6D6_60C
2 Spectrometer	inova
3 Solvent	c6d6
4 Temperature	60.0
5 Number of Scans	12
6 Relaxation Delay	4.8000
7 Acquisition Date	2018-08-18T21:45:01
8 Spectrometer Frequency	499.85

17a

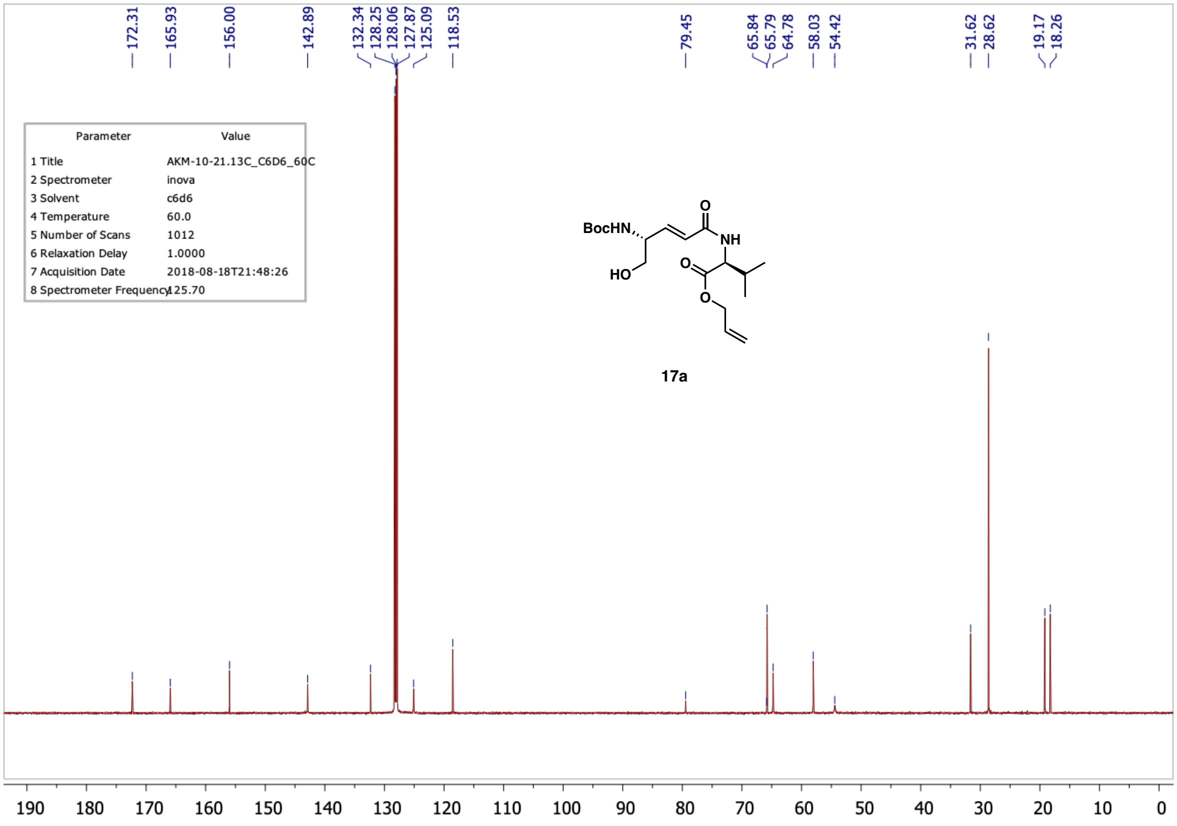

Parameter	Value
1 Title	AKM-10-21.13C_C6D6_60C
2 Spectrometer	inova
3 Solvent	c6d6
4 Temperature	60.0
5 Number of Scans	1012
6 Relaxation Delay	1.0000
7 Acquisition Date	2018-08-18T21:48:26
8 Spectrometer Frequency	125.70

17a

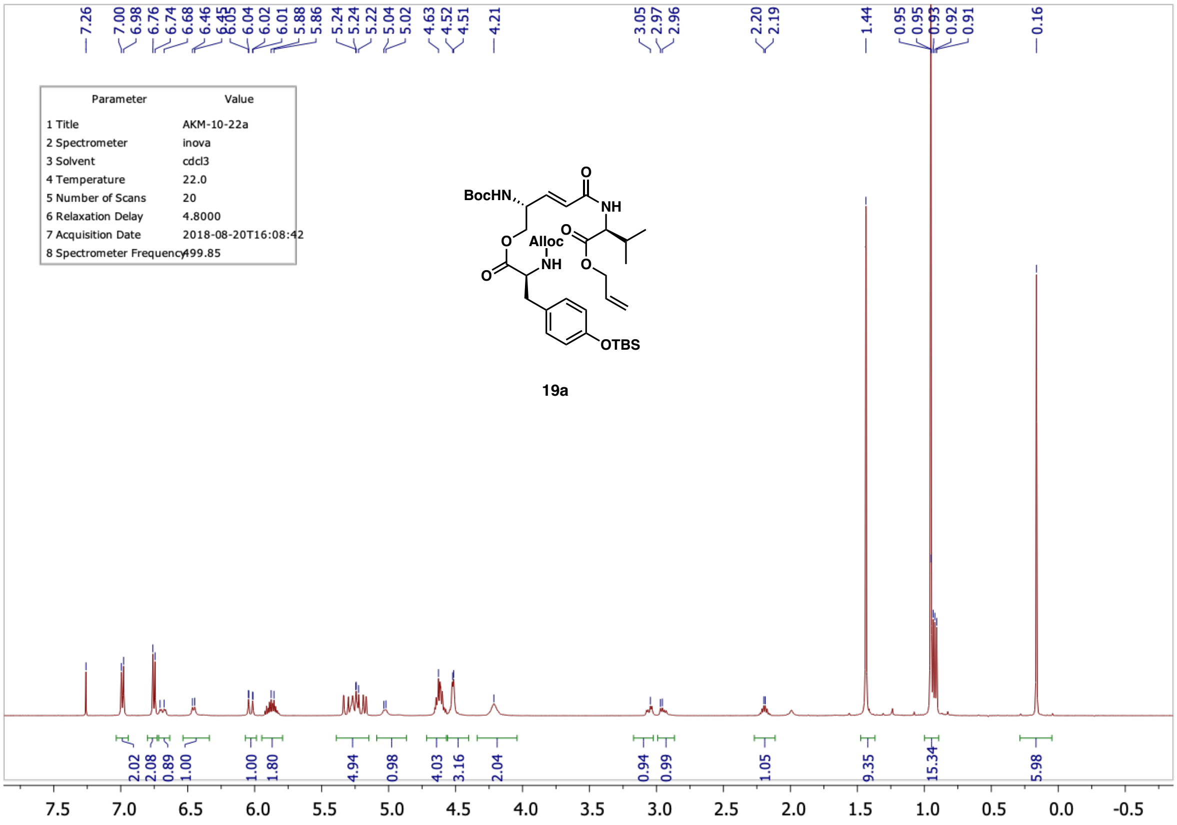

Parameter	Value
1 Title	AKM-10-22a
2 Spectrometer	inova
3 Solvent	cdcl3
4 Temperature	22.0
5 Number of Scans	20
6 Relaxation Delay	4.8000
7 Acquisition Date	2018-08-20T16:08:42
8 Spectrometer Frequency	499.85

19a

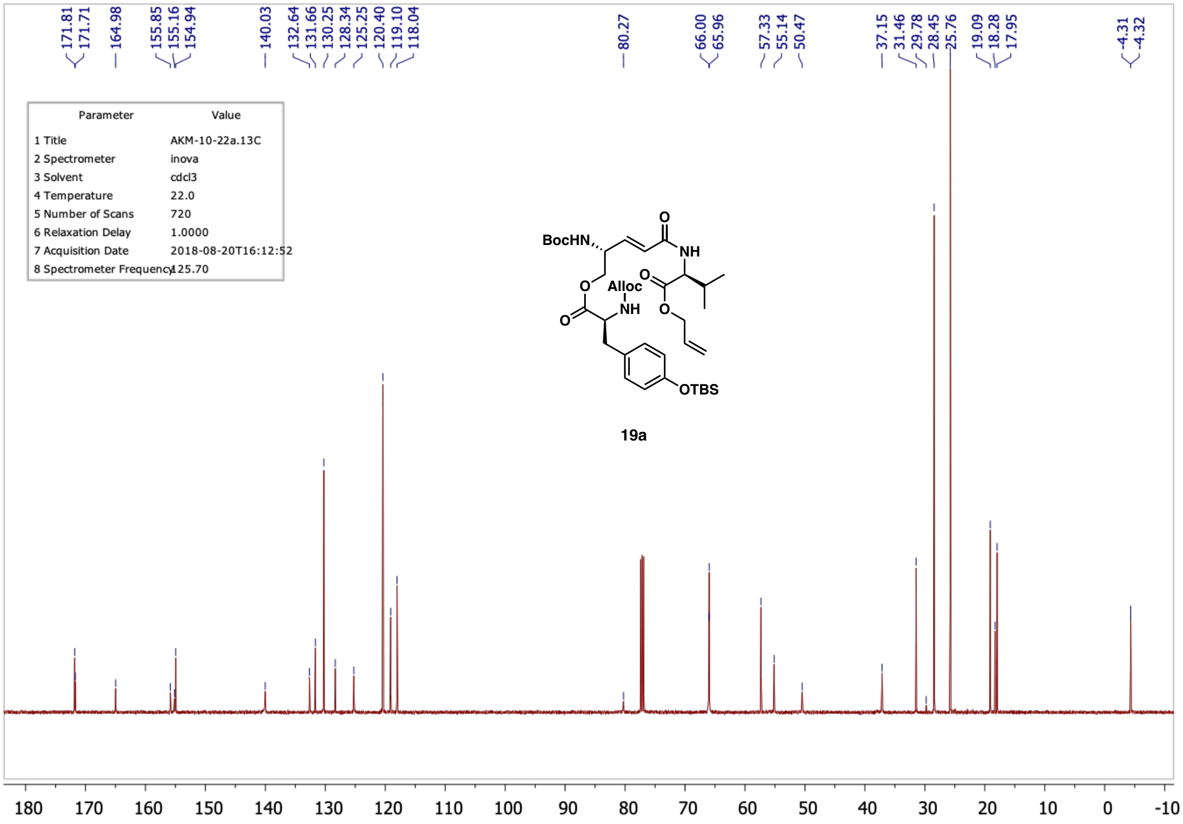

Parameter	Value
1 Title	AKM-10-22a.13C
2 Spectrometer	inova
3 Solvent	cdcl3
4 Temperature	22.0
5 Number of Scans	720
6 Relaxation Delay	1.0000
7 Acquisition Date	2018-08-20T16:12:52
8 Spectrometer Frequency	125.70

19a

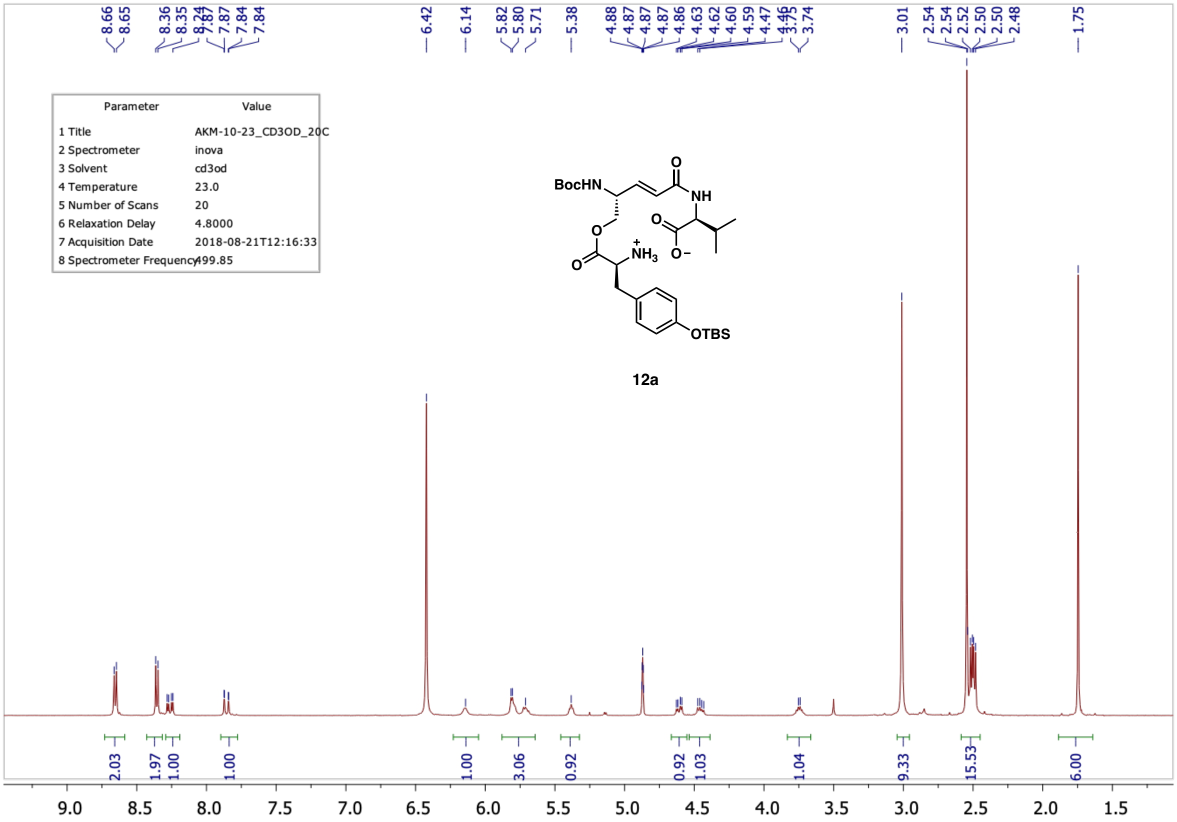

Parameter	Value
1 Title	AKM-10-23_CD3OD_20C
2 Spectrometer	inova
3 Solvent	cd3od
4 Temperature	23.0
5 Number of Scans	20
6 Relaxation Delay	4.8000
7 Acquisition Date	2018-08-21T12:16:33
8 Spectrometer Frequency	499.85

12a

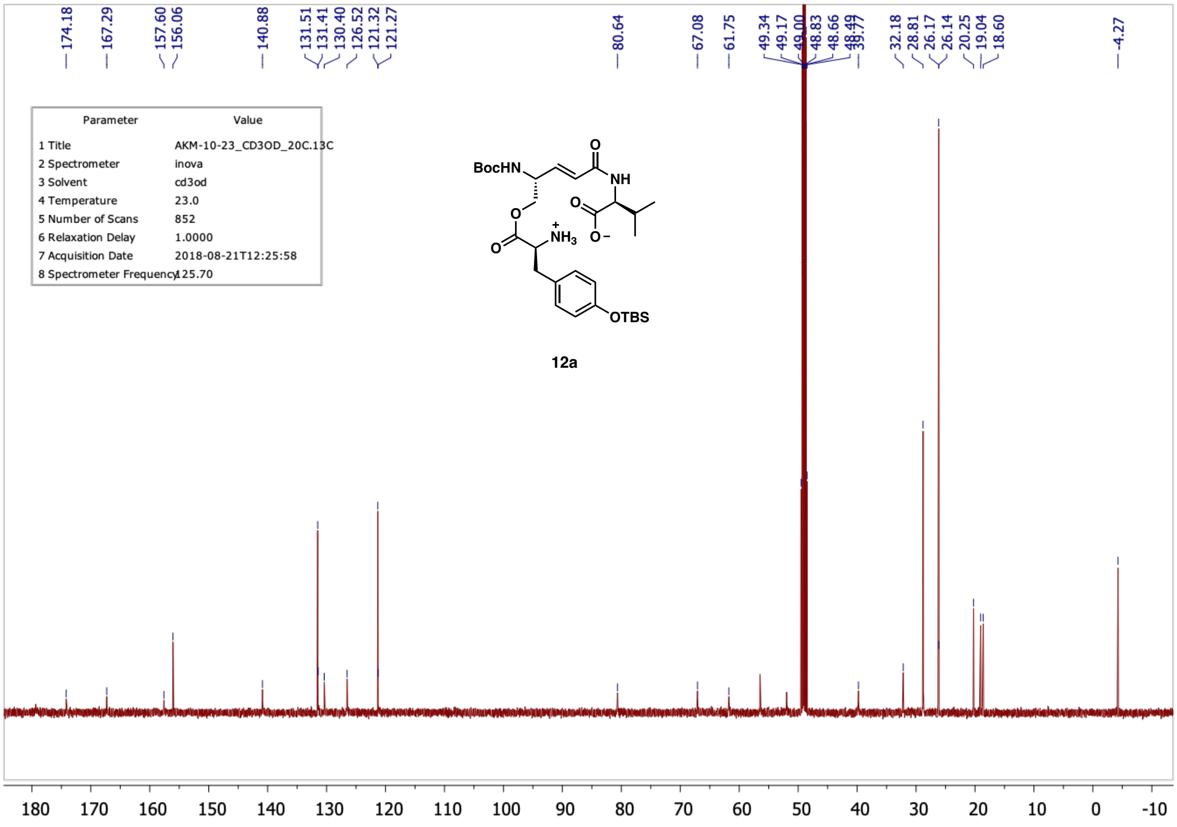

Parameter	Value
1 Title	AKM-10-23_CD3OD_20C.13C
2 Spectrometer	inova
3 Solvent	cd3od
4 Temperature	23.0
5 Number of Scans	852
6 Relaxation Delay	1.0000
7 Acquisition Date	2018-08-21T12:25:58
8 Spectrometer Frequency	125.70

12a

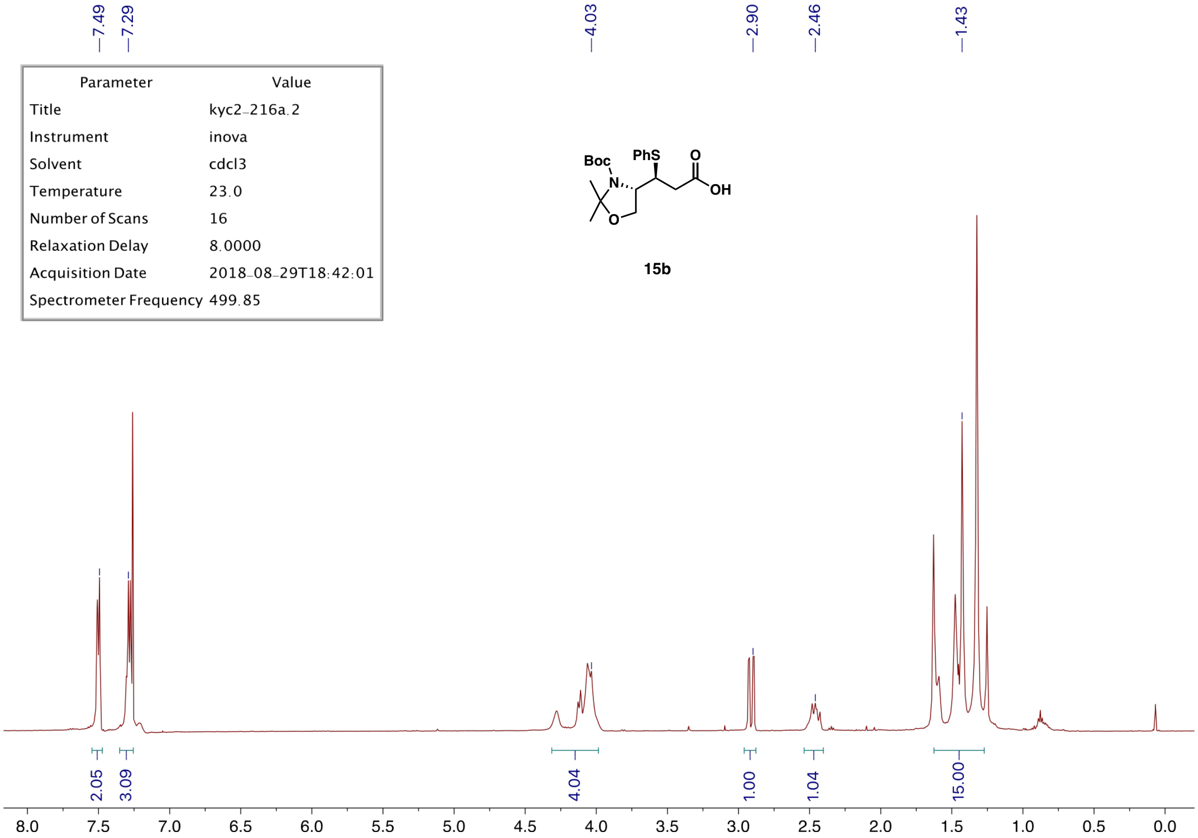

Parameter	Value
Title	kyc2_216a.2
Instrument	inova
Solvent	cdcl3
Temperature	23.0
Number of Scans	16
Relaxation Delay	8.0000
Acquisition Date	2018-08-29T18:42:01
Spectrometer Frequency	499.85

15b

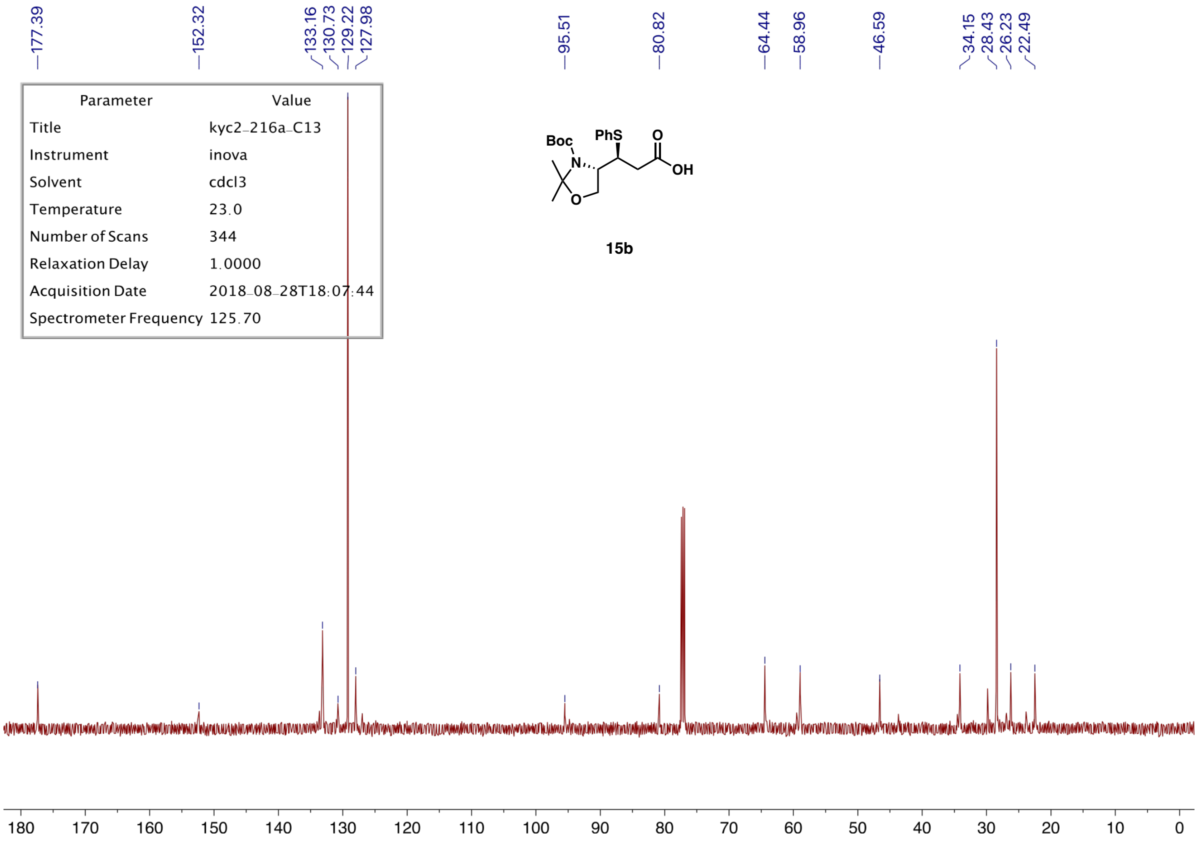

Parameter	Value
Title	kyc2_216a_C13
Instrument	inova
Solvent	cdcl3
Temperature	23.0
Number of Scans	344
Relaxation Delay	1.0000
Acquisition Date	2018-08-28T18:07:44
Spectrometer Frequency	125.70

15b

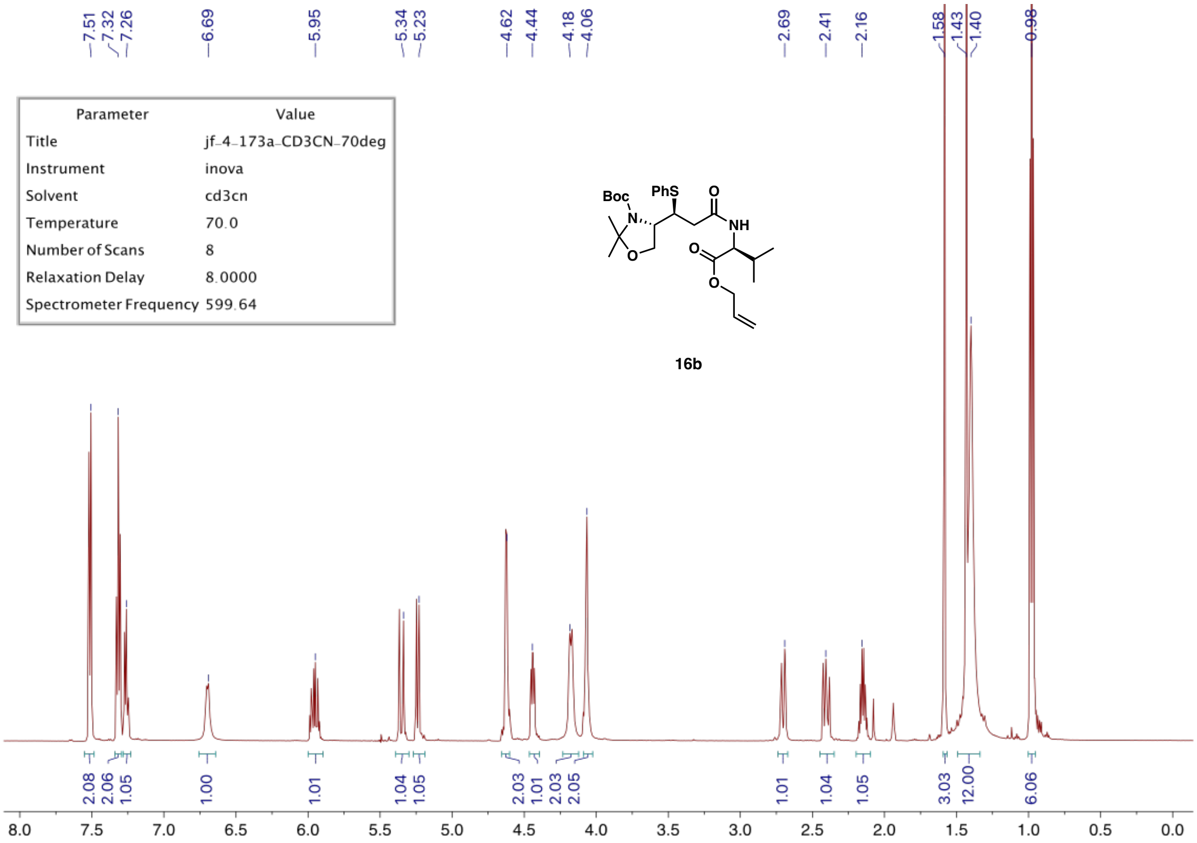

Parameter	Value
Title	jf_4_173a_CD3CN_70deg
Instrument	inova
Solvent	cd3cn
Temperature	70.0
Number of Scans	8
Relaxation Delay	8.0000
Spectrometer Frequency	599.64

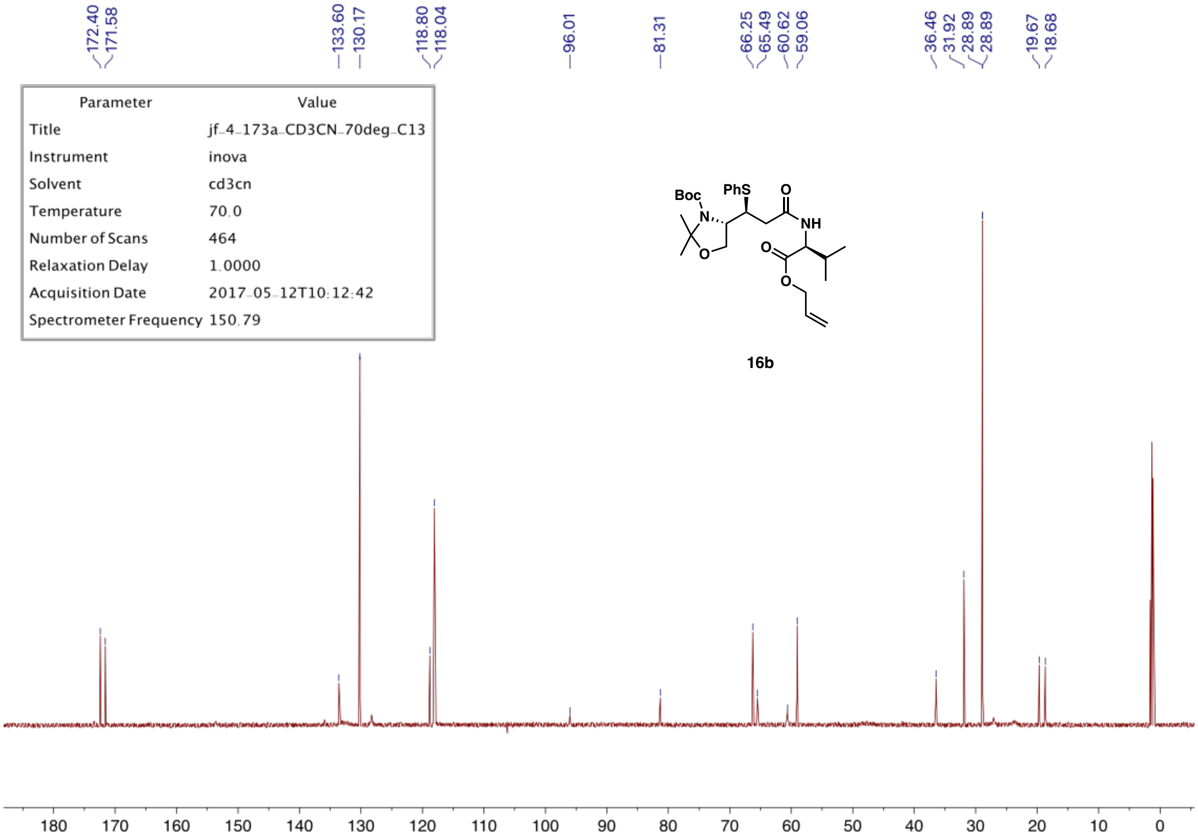

Parameter	Value
Title	jf_4_173a_CD3CN_70deg_C13
Instrument	inova
Solvent	cd3cn
Temperature	70.0
Number of Scans	464
Relaxation Delay	1.0000
Acquisition Date	2017_05_12T10:12:42
Spectrometer Frequency	150.79

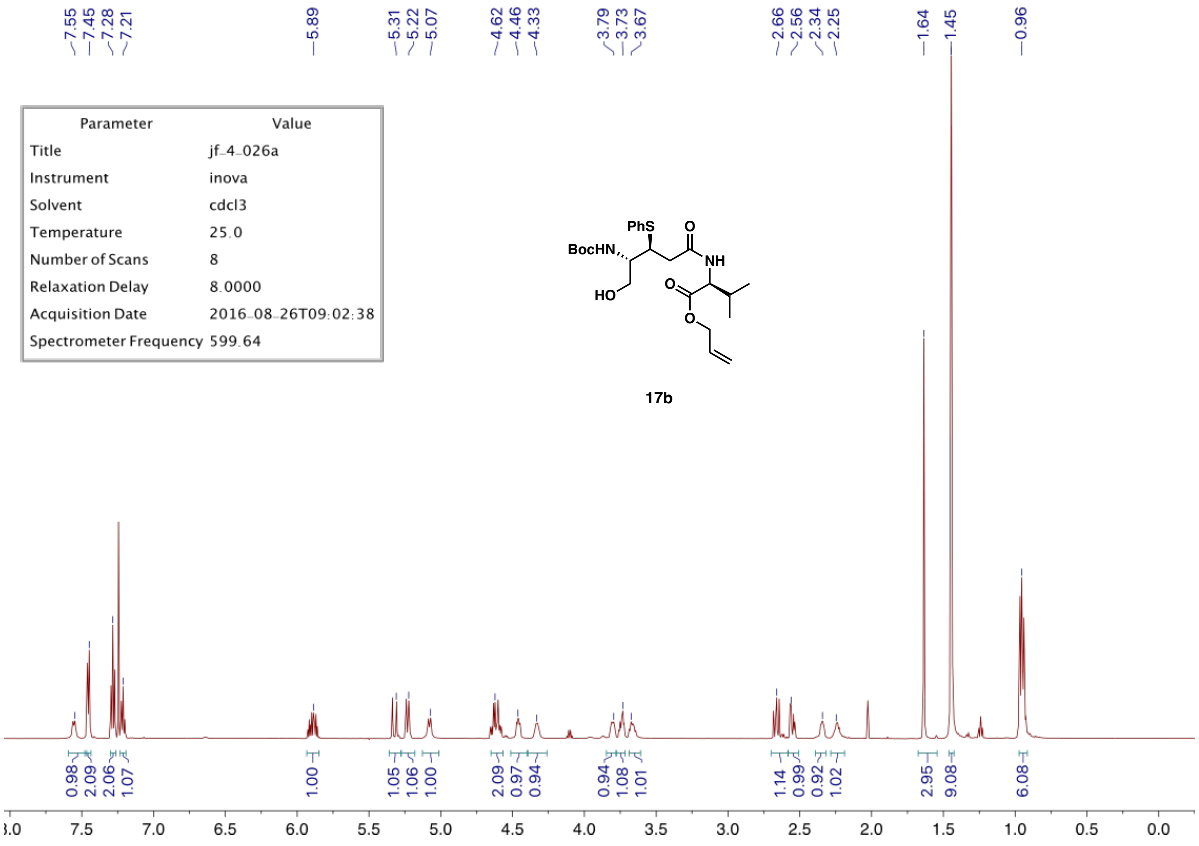

Parameter	Value
Title	jf_4_026a
Instrument	inova
Solvent	cdcl3
Temperature	25.0
Number of Scans	8
Relaxation Delay	8.0000
Acquisition Date	2016_08_26T09:02:38
Spectrometer Frequency	599.64

17b

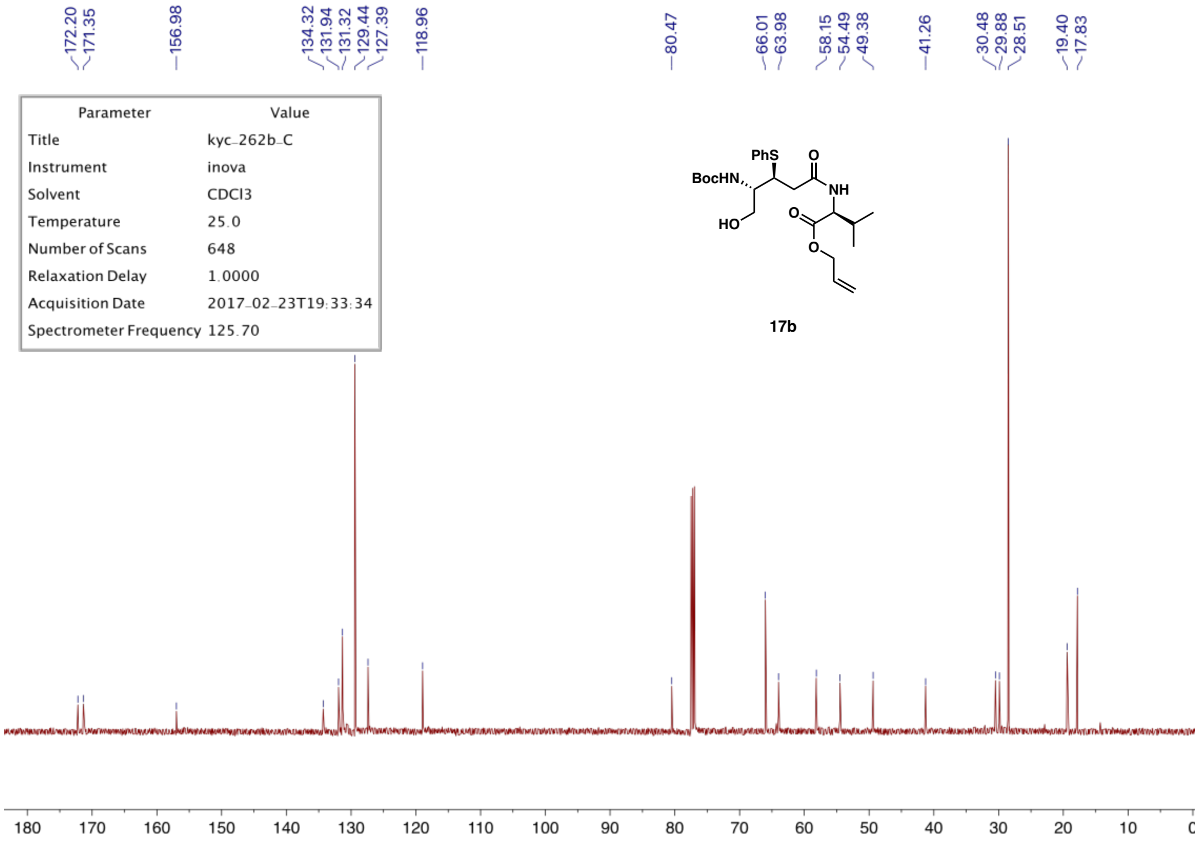

Parameter	Value
Title	kyc_262b_C
Instrument	inova
Solvent	CDCl3
Temperature	25.0
Number of Scans	648
Relaxation Delay	1.0000
Acquisition Date	2017_02_23T19:33:34
Spectrometer Frequency	125.70

17b

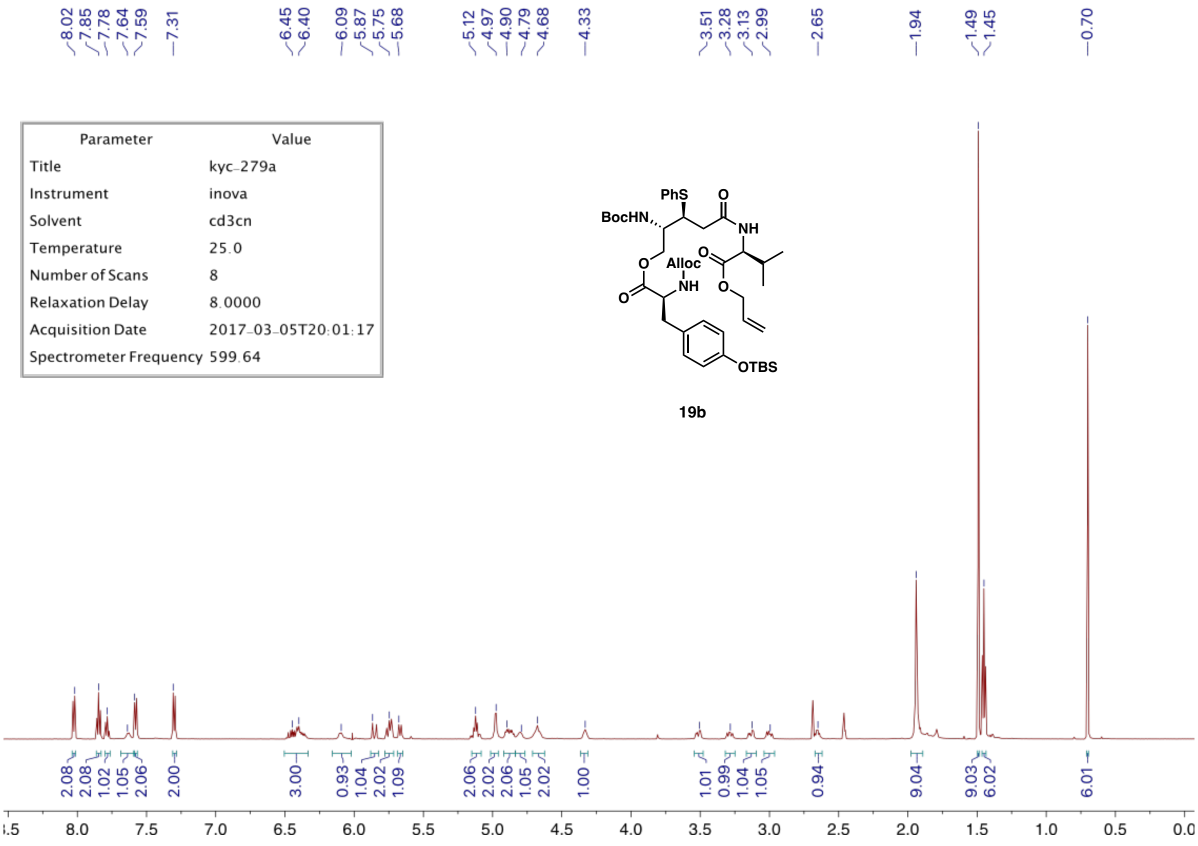

Parameter	Value
Title	kyc_279a
Instrument	inova
Solvent	cd3cn
Temperature	25.0
Number of Scans	8
Relaxation Delay	8.0000
Acquisition Date	2017-03-05T20:01:17
Spectrometer Frequency	599.64

19b

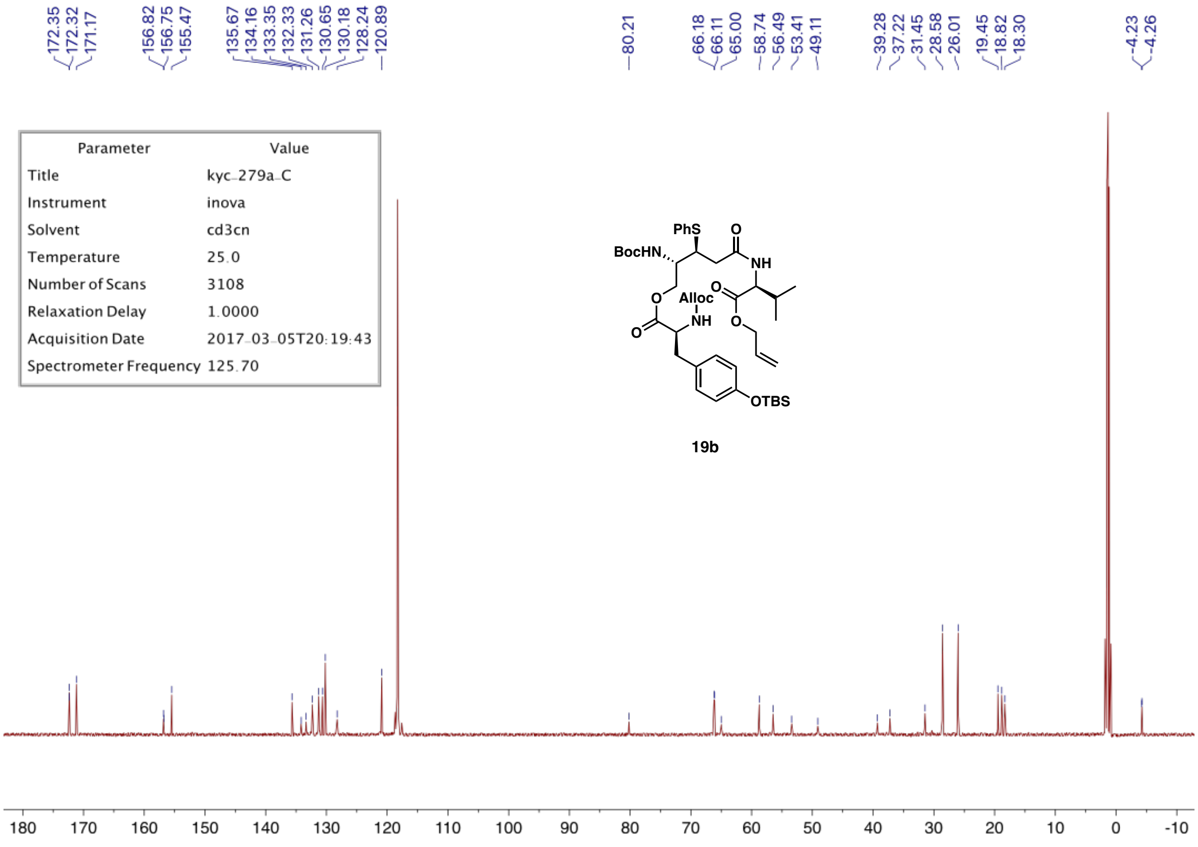

Parameter	Value
Title	kyc_279a_C
Instrument	inova
Solvent	cd3cn
Temperature	25.0
Number of Scans	3108
Relaxation Delay	1.0000
Acquisition Date	2017-03-05T20:19:43
Spectrometer Frequency	125.70

19b

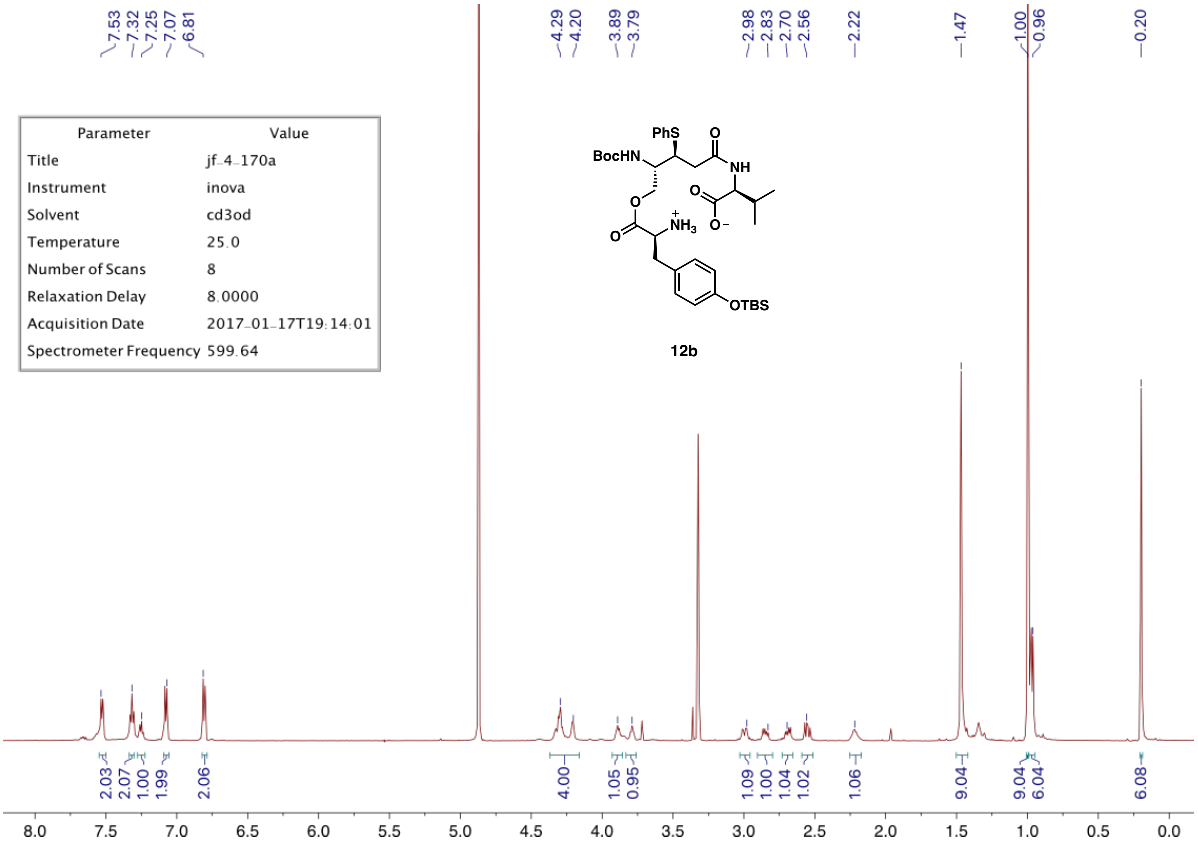

Parameter	Value
Title	jf_4_170a
Instrument	inova
Solvent	cd3od
Temperature	25.0
Number of Scans	8
Relaxation Delay	8.0000
Acquisition Date	2017_01_17T19:14:01
Spectrometer Frequency	599.64

12b

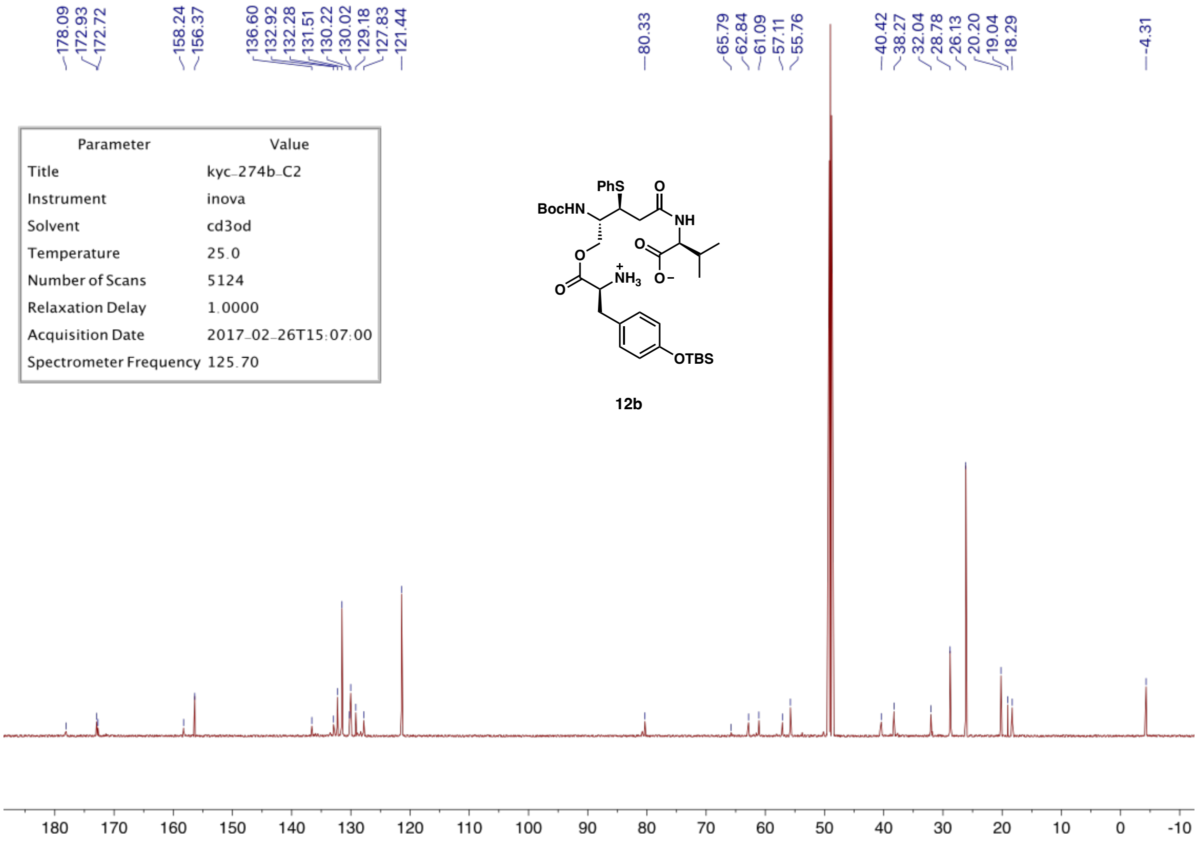

Parameter	Value
Title	kyc_274b_C2
Instrument	inova
Solvent	cd3od
Temperature	25.0
Number of Scans	5124
Relaxation Delay	1.0000
Acquisition Date	2017_02_26T15:07:00
Spectrometer Frequency	125.70

12b

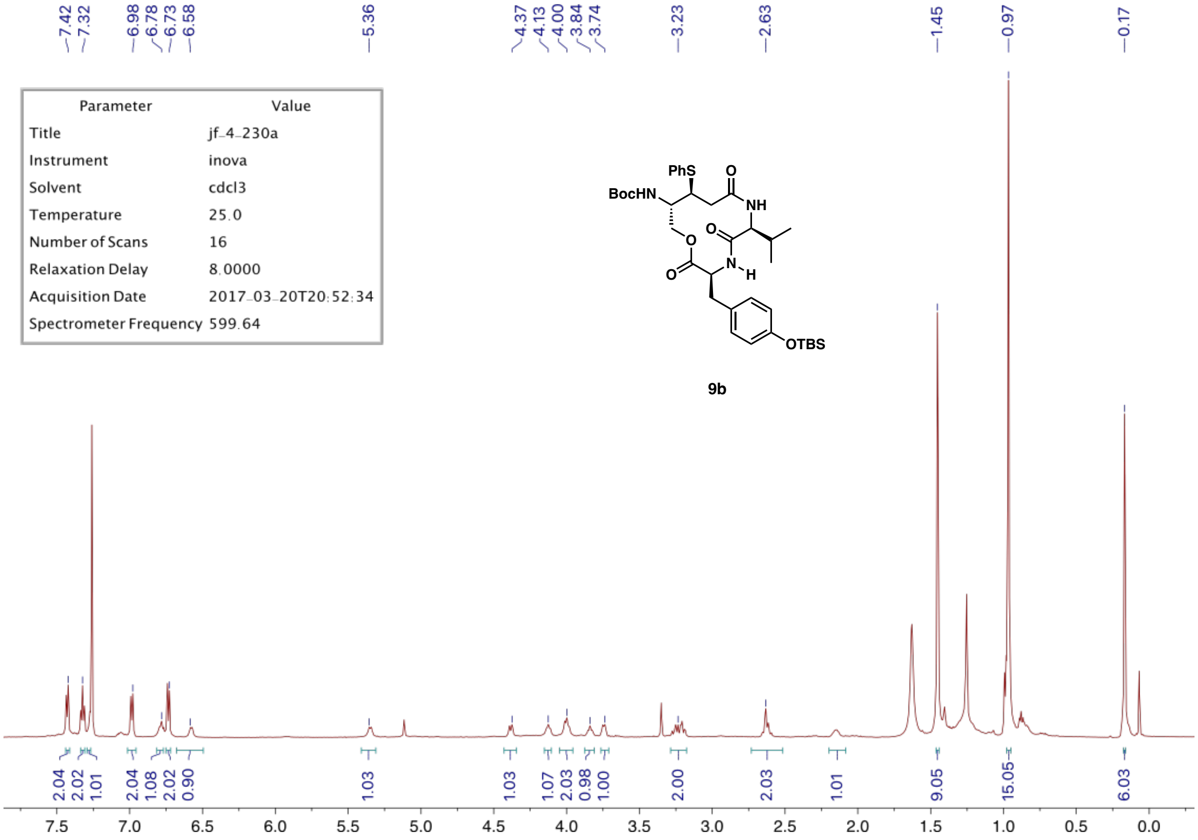

Parameter	Value
Title	jf_4_230a
Instrument	inova
Solvent	cdcl3
Temperature	25.0
Number of Scans	16
Relaxation Delay	8.0000
Acquisition Date	2017_03_20T20:52:34
Spectrometer Frequency	599.64

9b

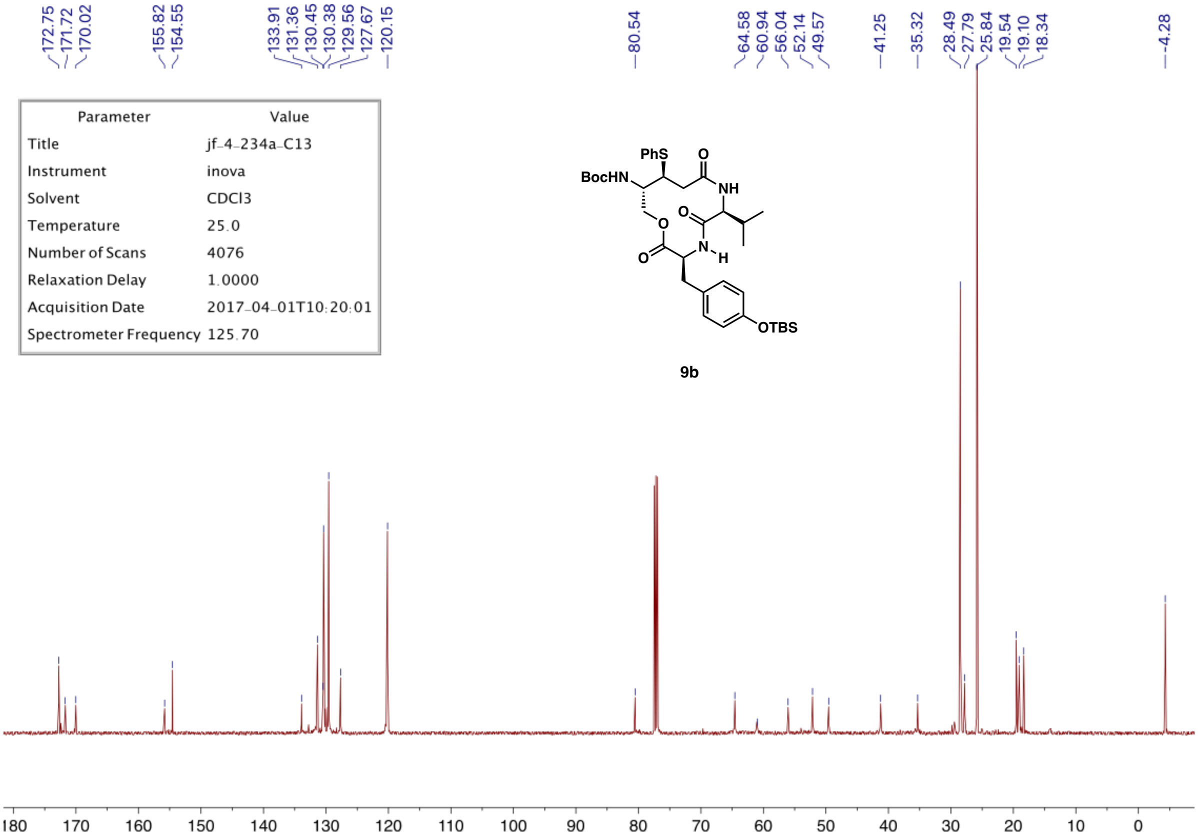

Parameter	Value
Title	jf_4_234a_C13
Instrument	inova
Solvent	CDCl3
Temperature	25.0
Number of Scans	4076
Relaxation Delay	1.0000
Acquisition Date	2017_04_01T10:20:01
Spectrometer Frequency	125.70

9b

Parameter	Value
Title	jf_4_246a
Instrument	inova
Solvent	cd3od
Temperature	25.0
Number of Scans	8
Relaxation Delay	8.0000
Acquisition Date	2017_04_01T16:28:13
Spectrometer Frequency	599.64

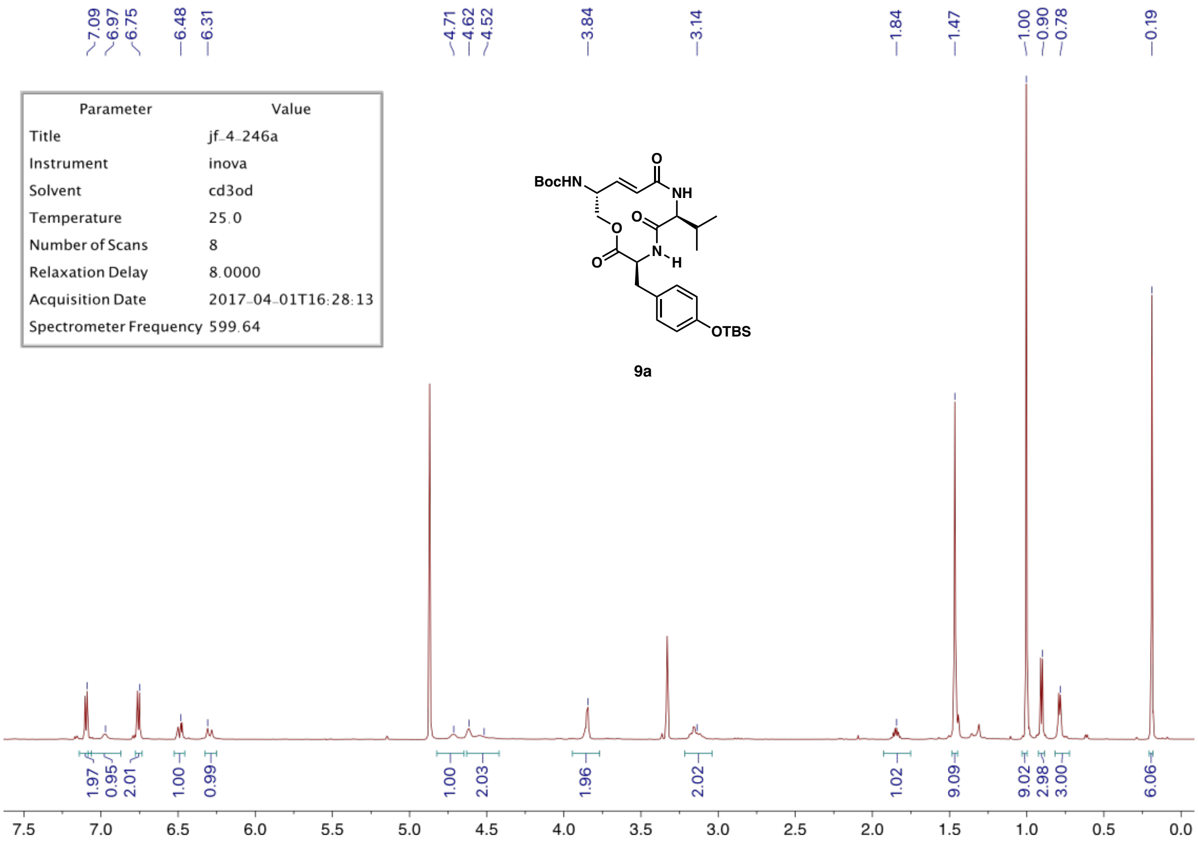

Parameter	Value
Title	kyc1_17a_C
Instrument	vnmrs
Solvent	cd3od
Temperature	25.0
Number of Scans	4676
Relaxation Delay	1.0000
Acquisition Date	2017_05_04T19:01:03
Spectrometer Frequency	100.54

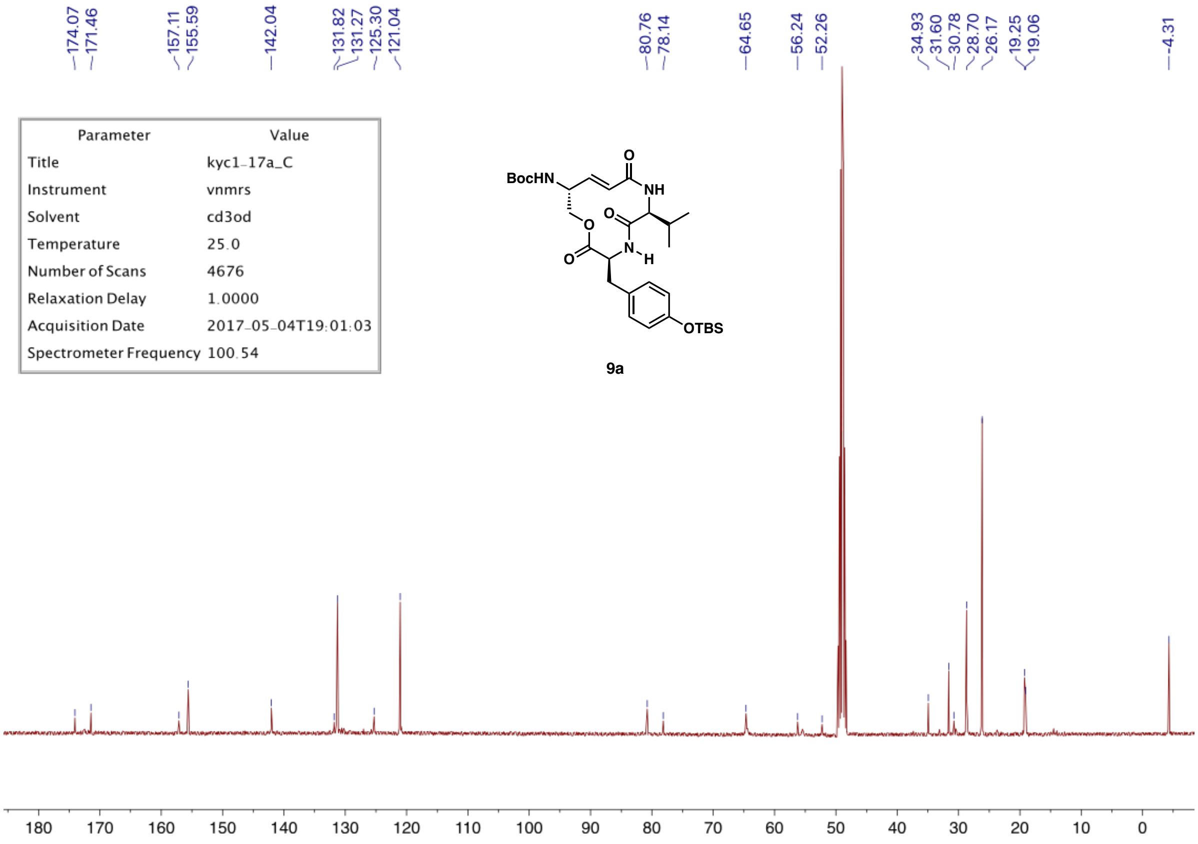

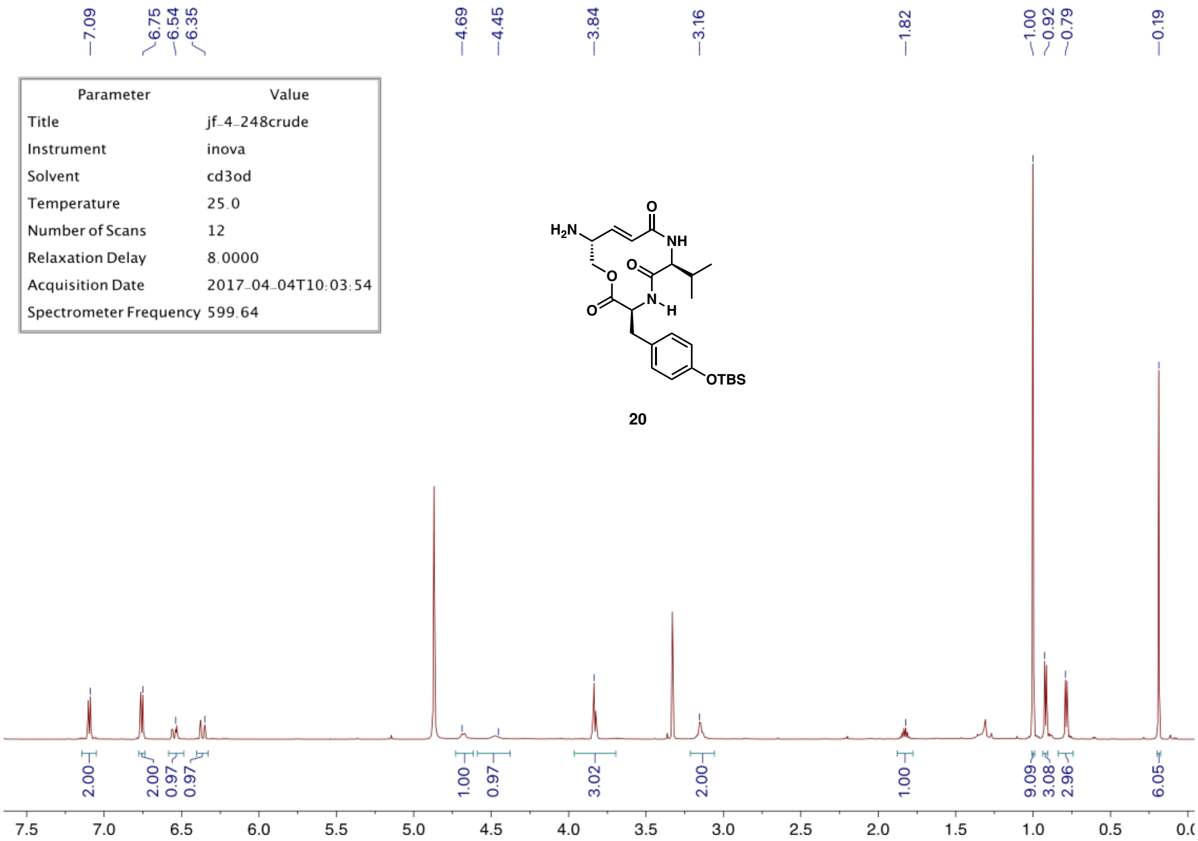

Parameter	Value
Title	jf_4_248crude
Instrument	inova
Solvent	cd3od
Temperature	25.0
Number of Scans	12
Relaxation Delay	8.0000
Acquisition Date	2017_04_04T10:03:54
Spectrometer Frequency	599.64

20

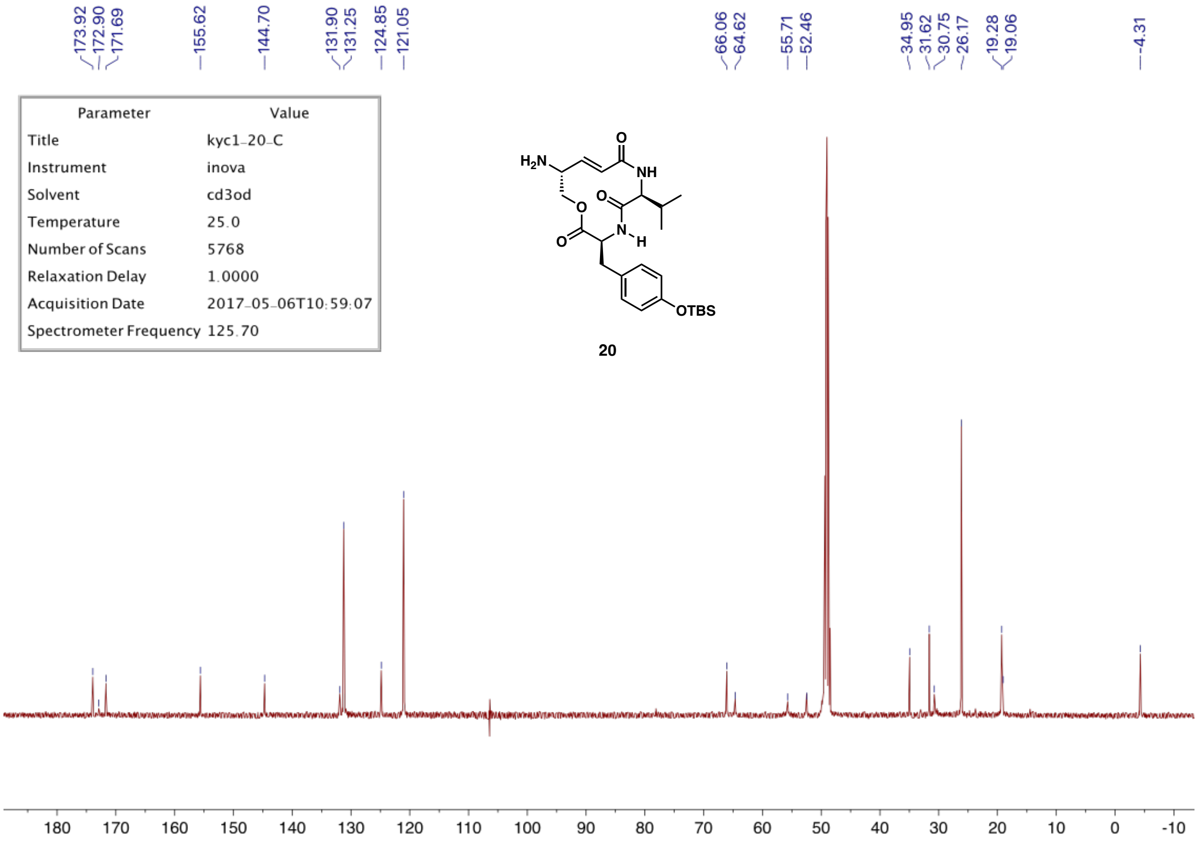

Parameter	Value
Title	kyc1_20_C
Instrument	inova
Solvent	cd3od
Temperature	25.0
Number of Scans	5768
Relaxation Delay	1.0000
Acquisition Date	2017_05_06T10:59:07
Spectrometer Frequency	125.70

20

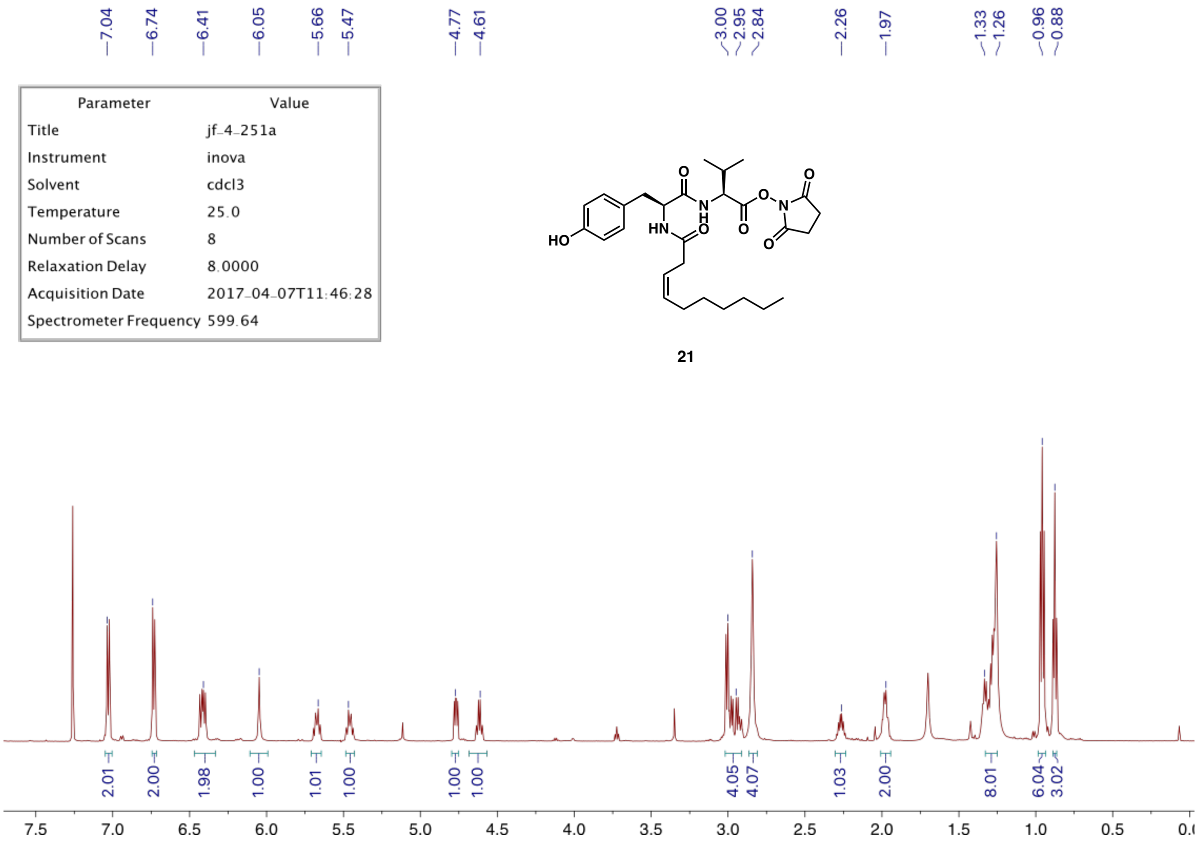

Parameter	Value
Title	jf_4_251a
Instrument	inova
Solvent	cdcl3
Temperature	25.0
Number of Scans	8
Relaxation Delay	8.0000
Acquisition Date	2017_04_07T11:46:28
Spectrometer Frequency	599.64

21

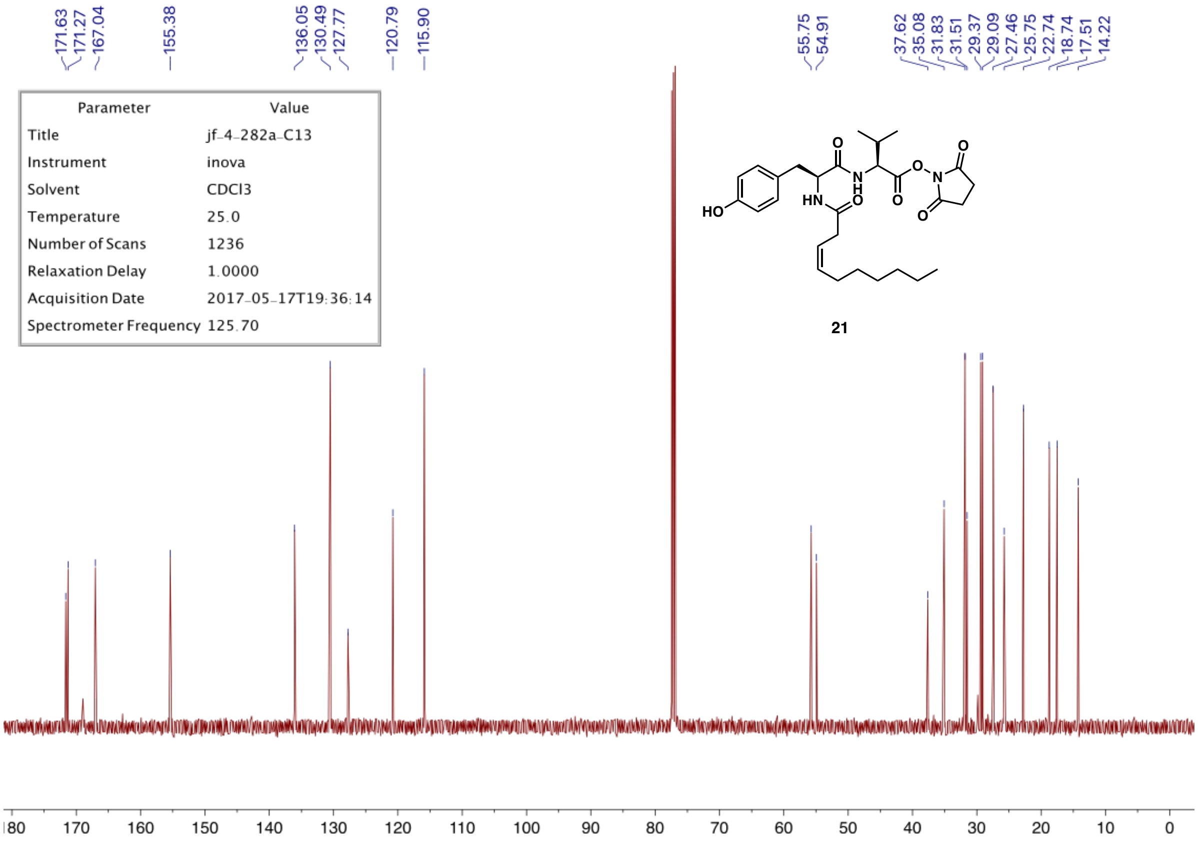

Parameter	Value
Title	jf_4_282a_C13
Instrument	inova
Solvent	CDCl3
Temperature	25.0
Number of Scans	1236
Relaxation Delay	1.0000
Acquisition Date	2017_05_17T19:36:14
Spectrometer Frequency	125.70

21

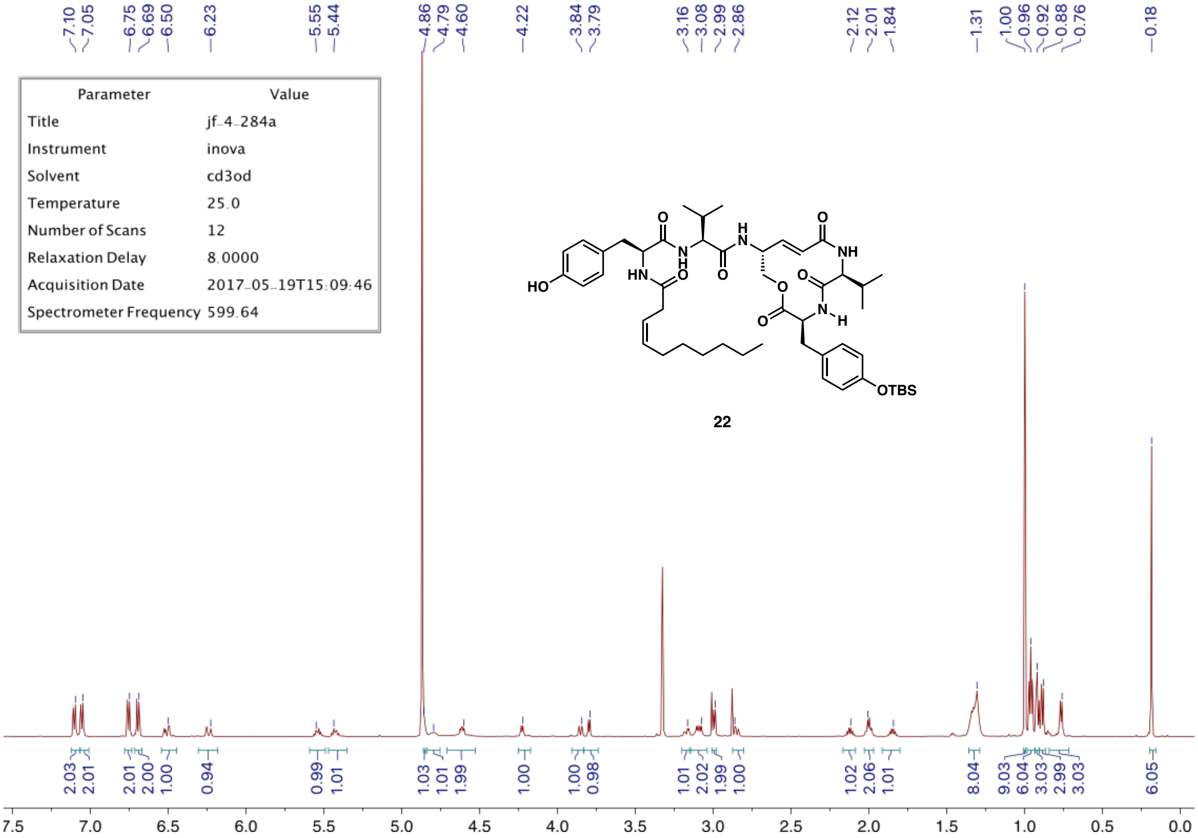

Parameter	Value
Title	jf_4_284a
Instrument	inova
Solvent	cd3od
Temperature	25.0
Number of Scans	12
Relaxation Delay	8.0000
Acquisition Date	2017_05_19T15:09:46
Spectrometer Frequency	599.64

22

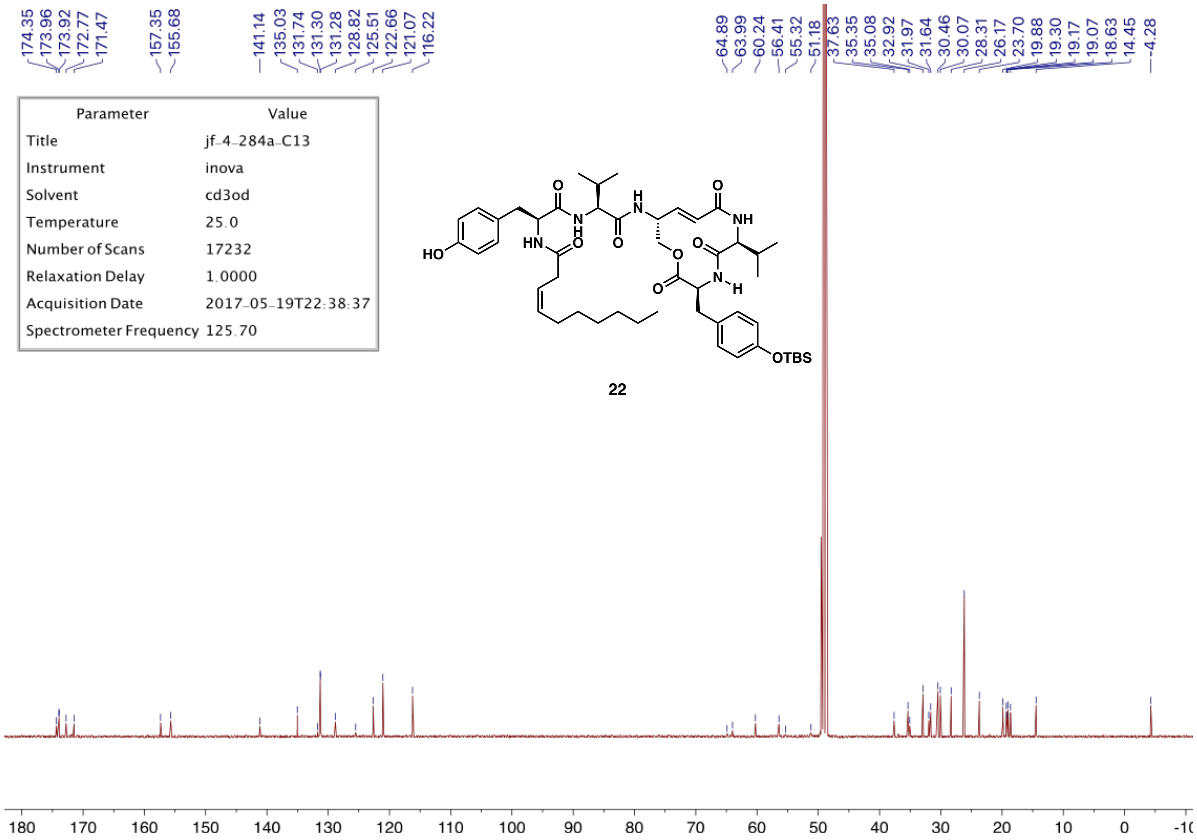

Parameter	Value
Title	jf_4_284a_C13
Instrument	inova
Solvent	cd3od
Temperature	25.0
Number of Scans	17232
Relaxation Delay	1.0000
Acquisition Date	2017_05_19T22:38:37
Spectrometer Frequency	125.70

22

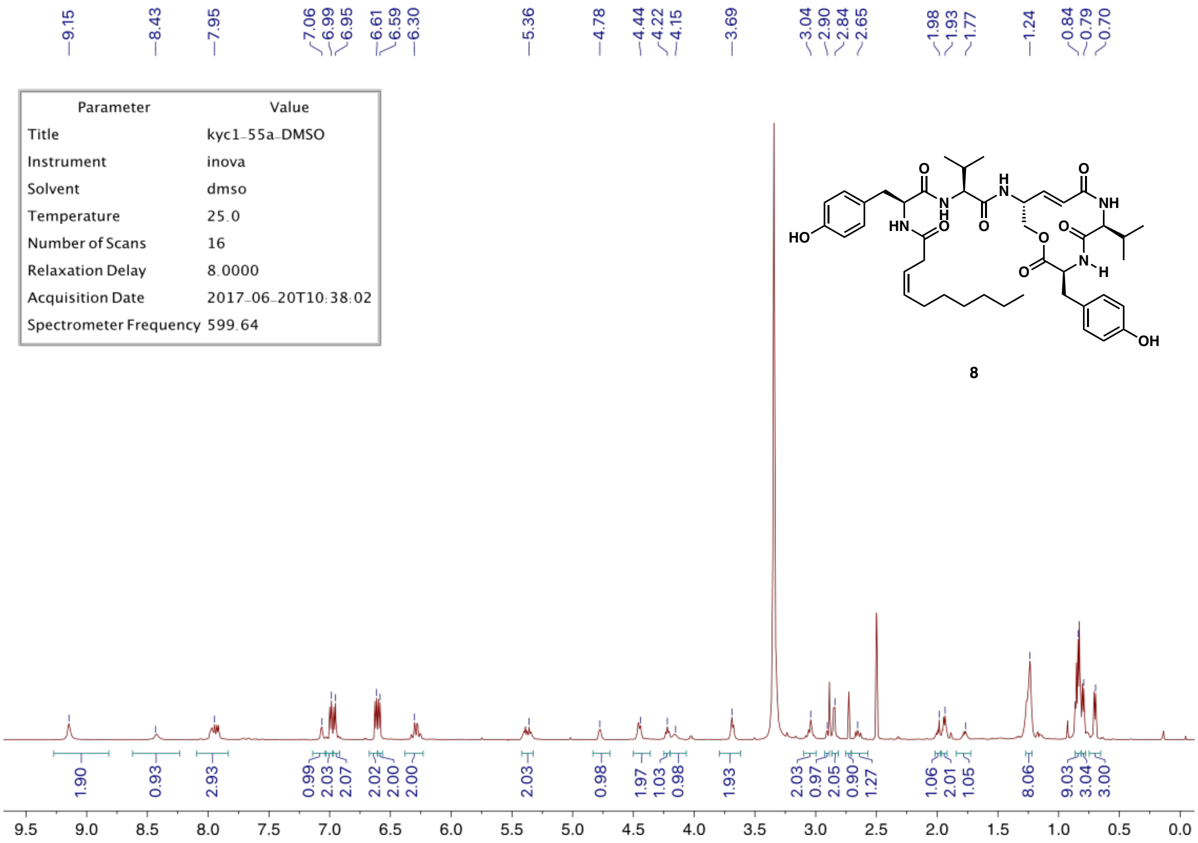

Parameter	Value
Title	kyc1_55a_DMSO
Instrument	inova
Solvent	dmso
Temperature	25.0
Number of Scans	16
Relaxation Delay	8.0000
Acquisition Date	2017_06_20T10:38:02
Spectrometer Frequency	599.64

8

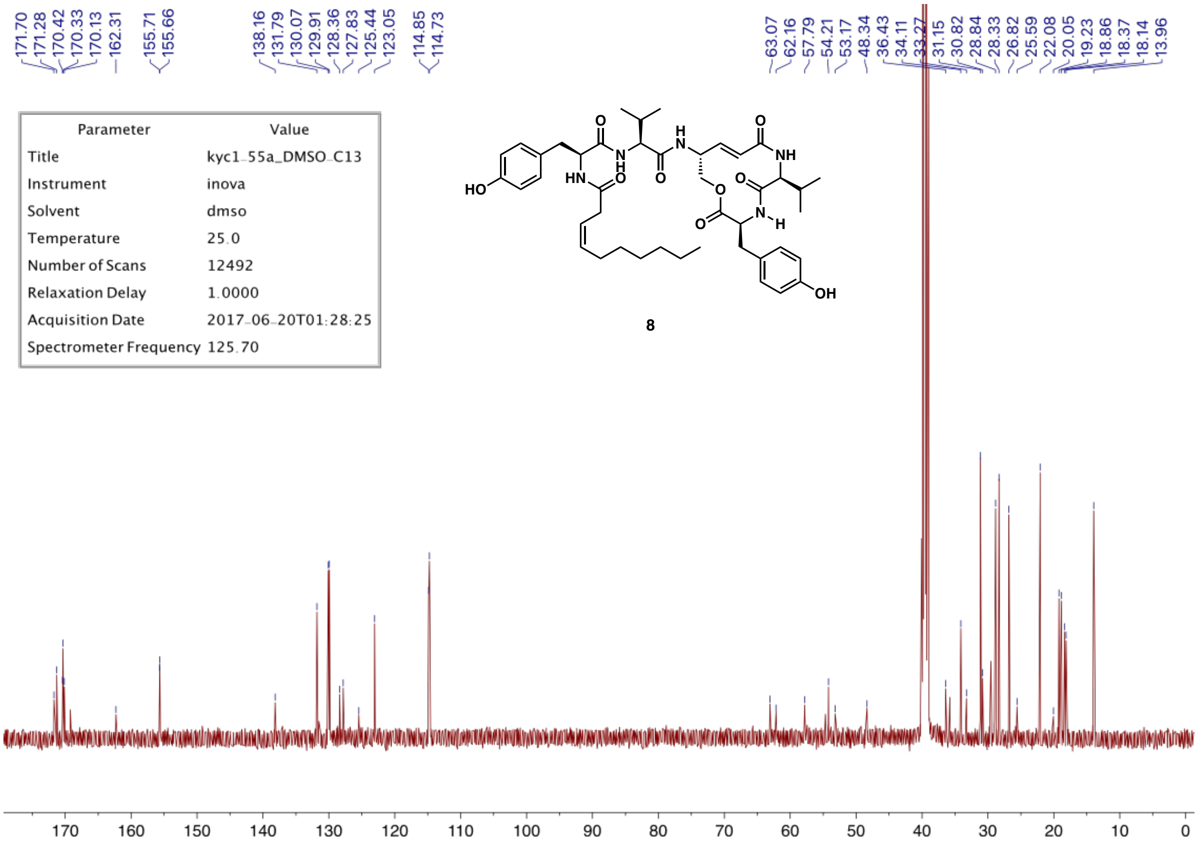

Parameter	Value
Title	kyc1_55a_DMSO_C13
Instrument	inova
Solvent	dmso
Temperature	25.0
Number of Scans	12492
Relaxation Delay	1.0000
Acquisition Date	2017_06_20T01:28:25
Spectrometer Frequency	125.70

8

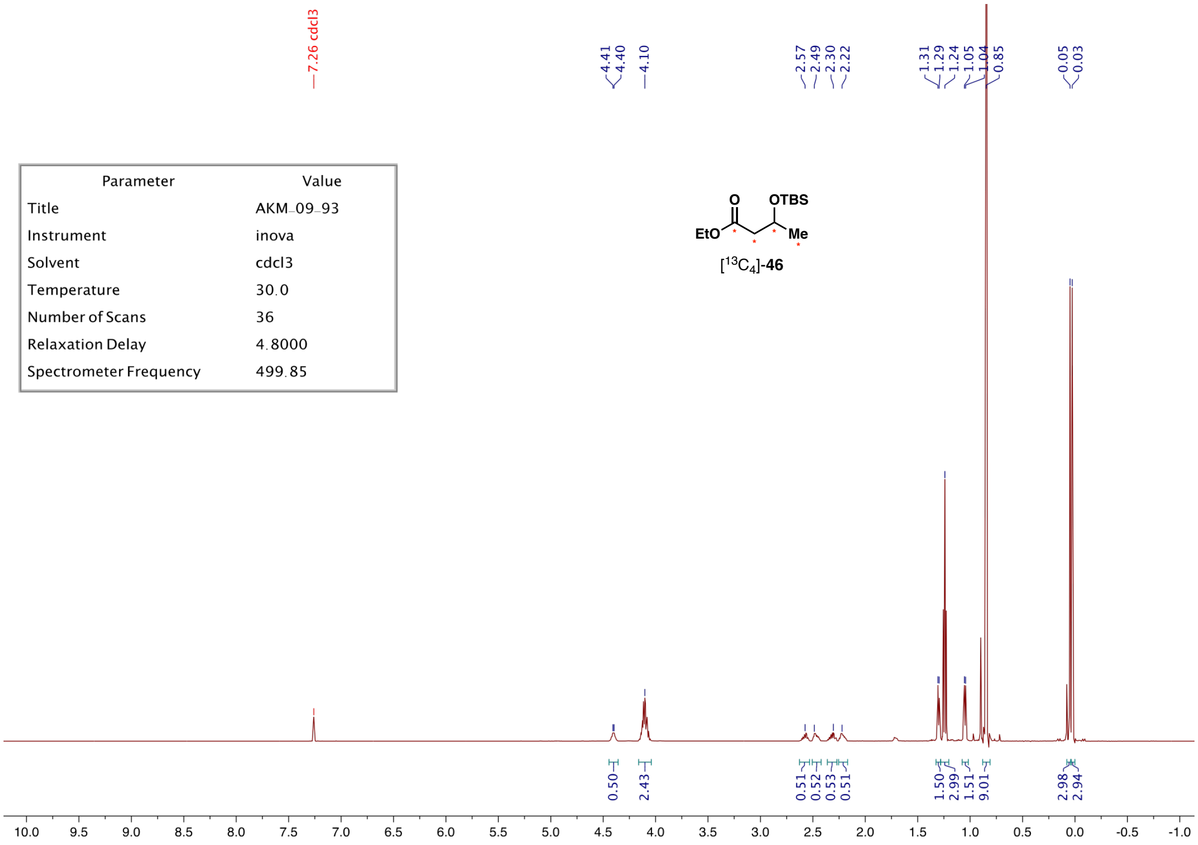

Parameter	Value
Title	AKM_09_93
Instrument	inova
Solvent	cdcl3
Temperature	30.0
Number of Scans	36
Relaxation Delay	4.8000
Spectrometer Frequency	499.85

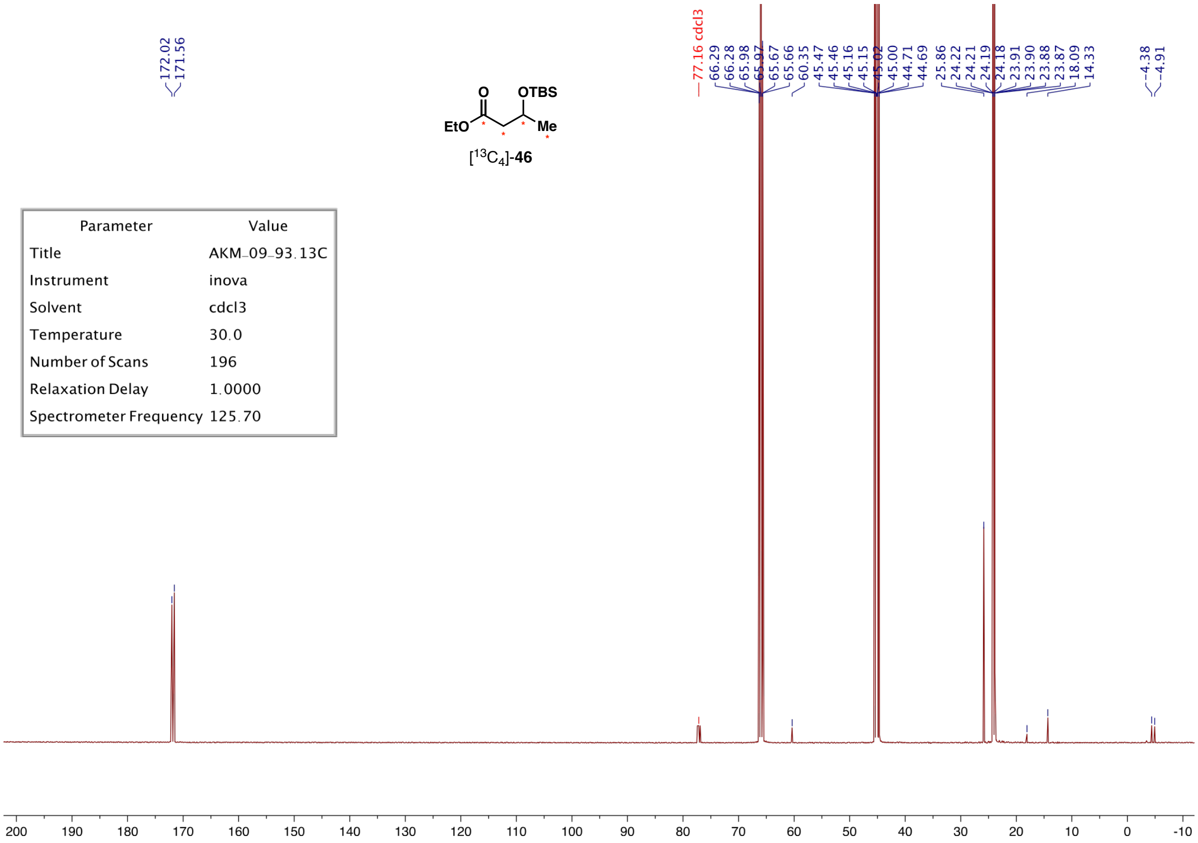

Parameter	Value
Title	AKM_09_93.13C
Instrument	inova
Solvent	cdcl3
Temperature	30.0
Number of Scans	196
Relaxation Delay	1.0000
Spectrometer Frequency	125.70

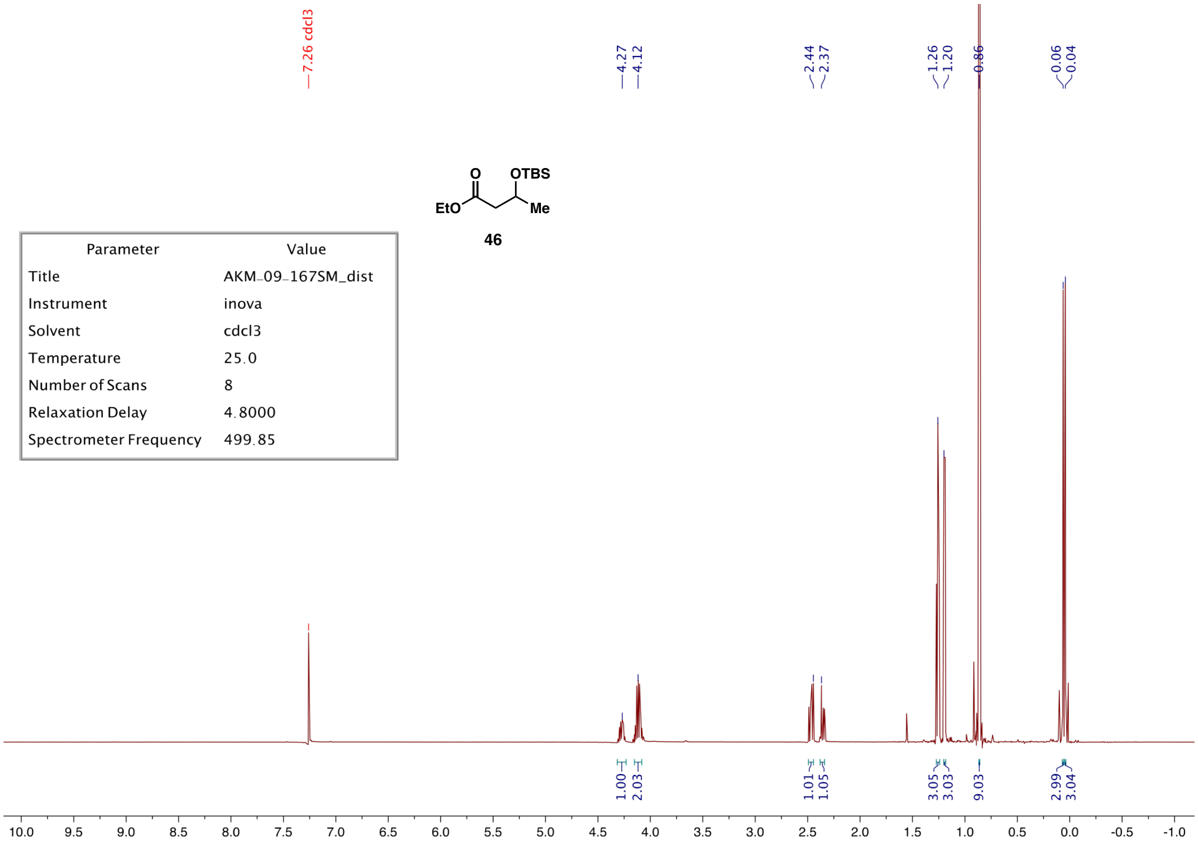

Parameter	Value
Title	AKM_09_167SM_dist
Instrument	inova
Solvent	cdcl3
Temperature	25.0
Number of Scans	8
Relaxation Delay	4.8000
Spectrometer Frequency	499.85

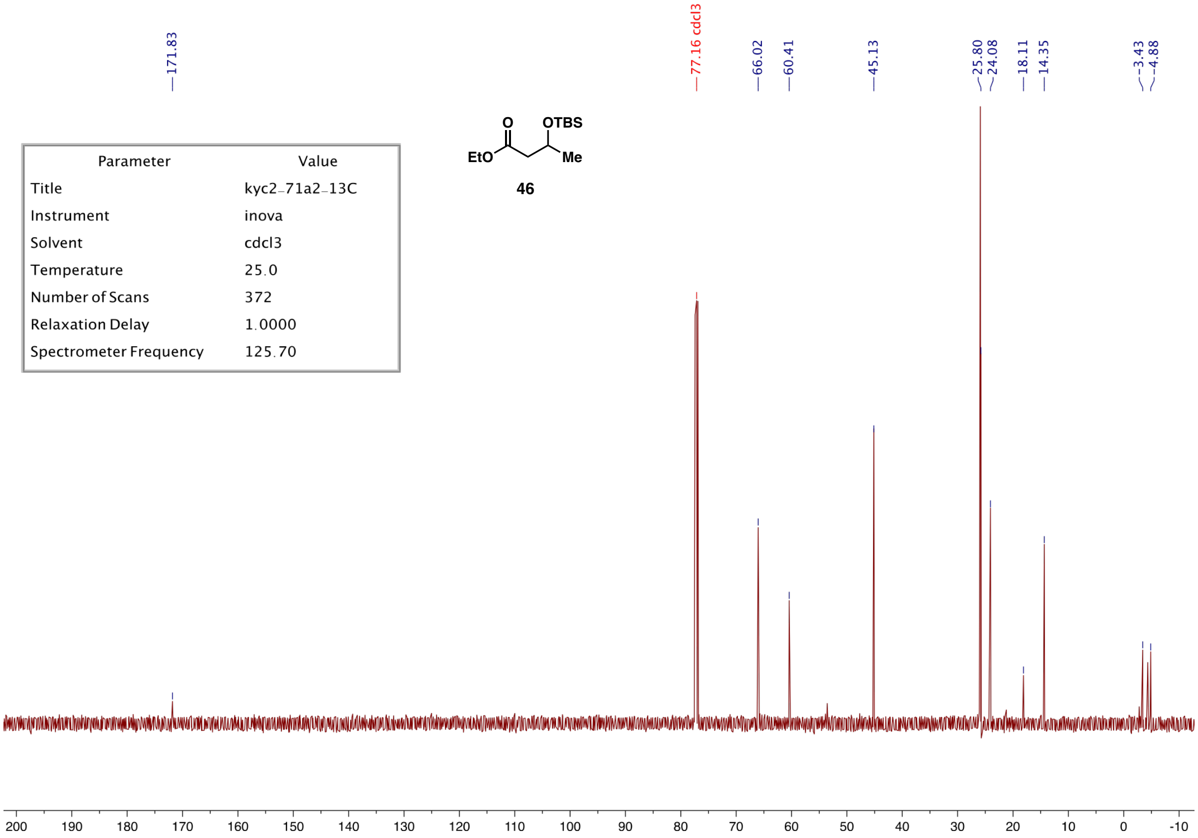

Parameter	Value
Title	kyc2_71a2_13C
Instrument	inova
Solvent	cdcl3
Temperature	25.0
Number of Scans	372
Relaxation Delay	1.0000
Spectrometer Frequency	125.70

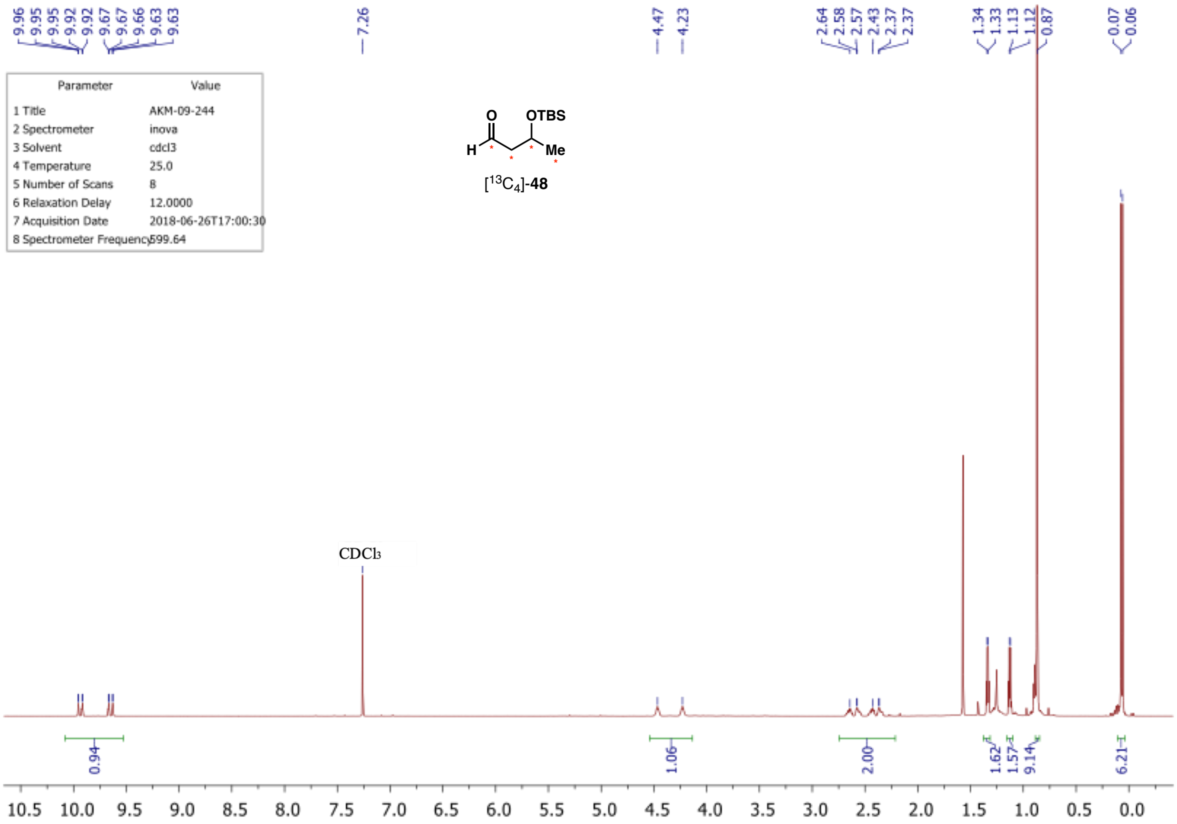

Parameter	Value
1 Title	AKM-09-244
2 Spectrometer	inova
3 Solvent	cdcl3
4 Temperature	25.0
5 Number of Scans	8
6 Relaxation Delay	12.0000
7 Acquisition Date	2018-06-26T17:00:30
8 Spectrometer Frequency	599.64

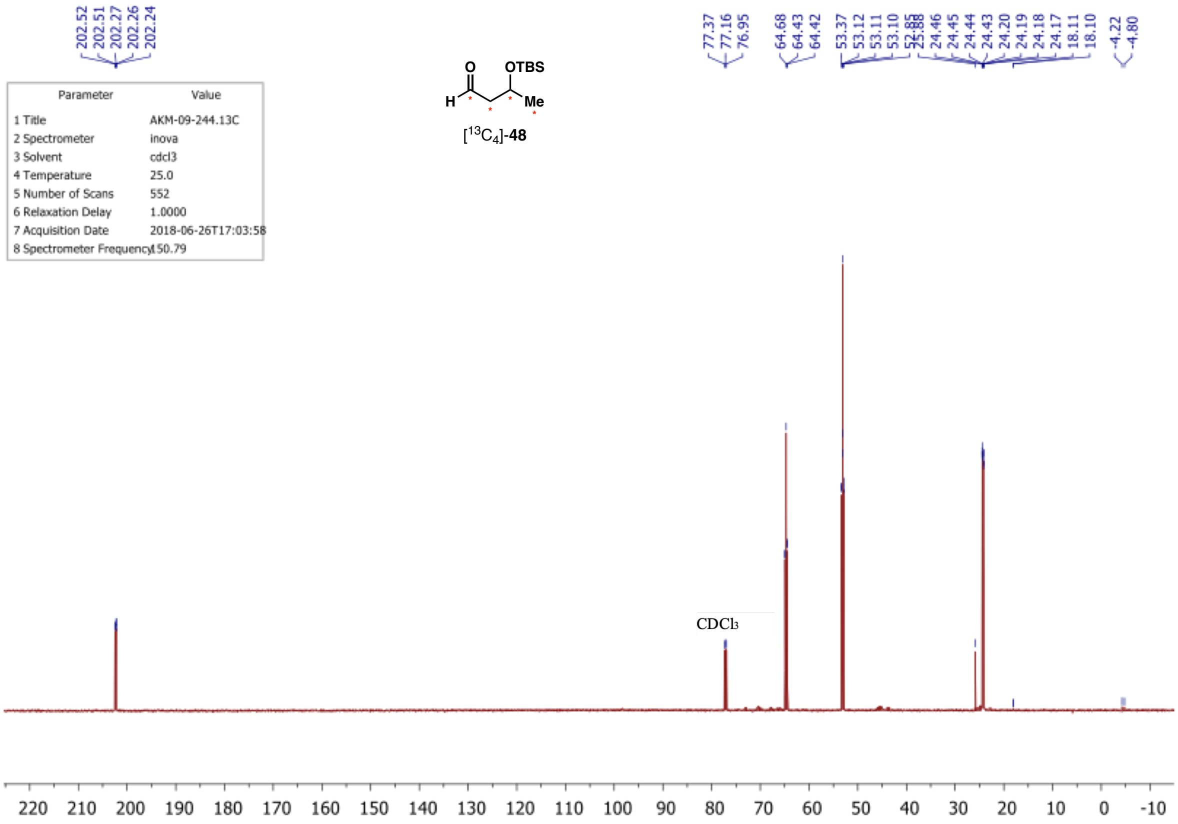

Parameter	Value
1 Title	AKM-09-244.13C
2 Spectrometer	inova
3 Solvent	cdcl3
4 Temperature	25.0
5 Number of Scans	552
6 Relaxation Delay	1.0000
7 Acquisition Date	2018-06-26T17:03:58
8 Spectrometer Frequency	150.79

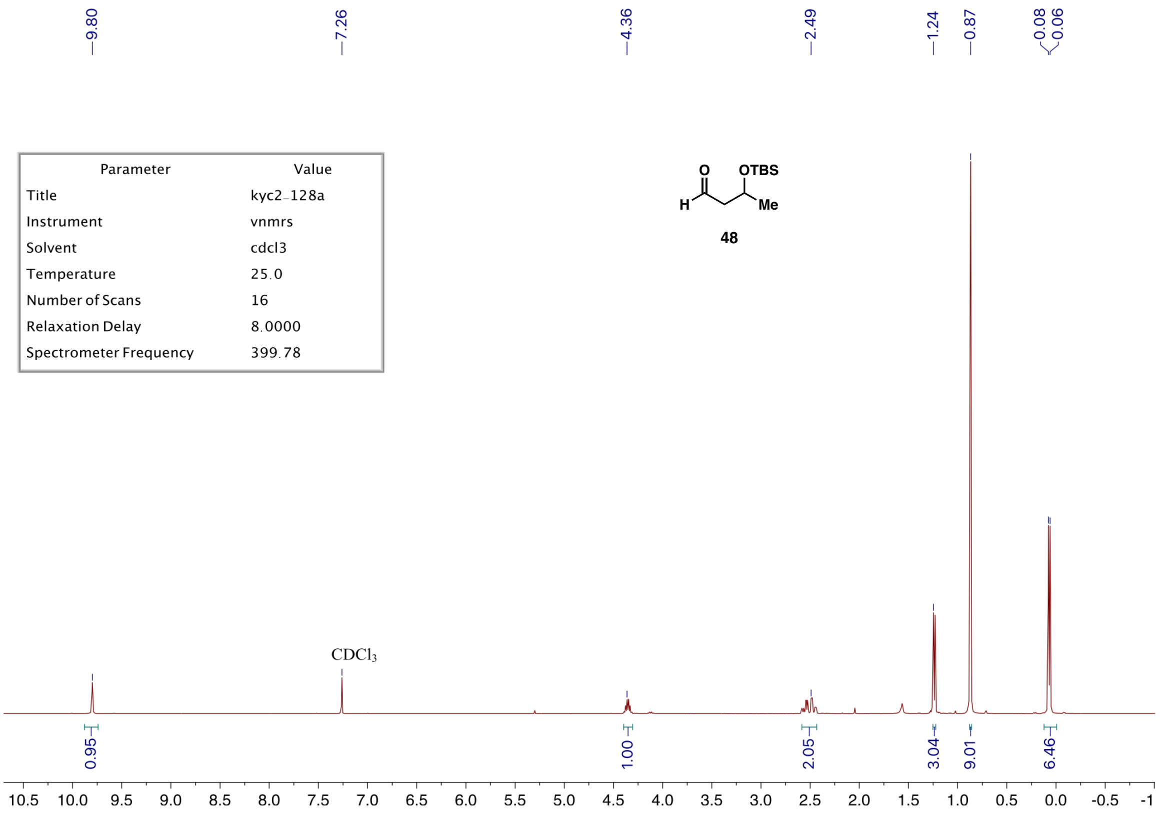

48

Parameter	Value
Title	kyc2_128a
Instrument	vnmrs
Solvent	cdcl3
Temperature	25.0
Number of Scans	16
Relaxation Delay	8.0000
Spectrometer Frequency	399.78

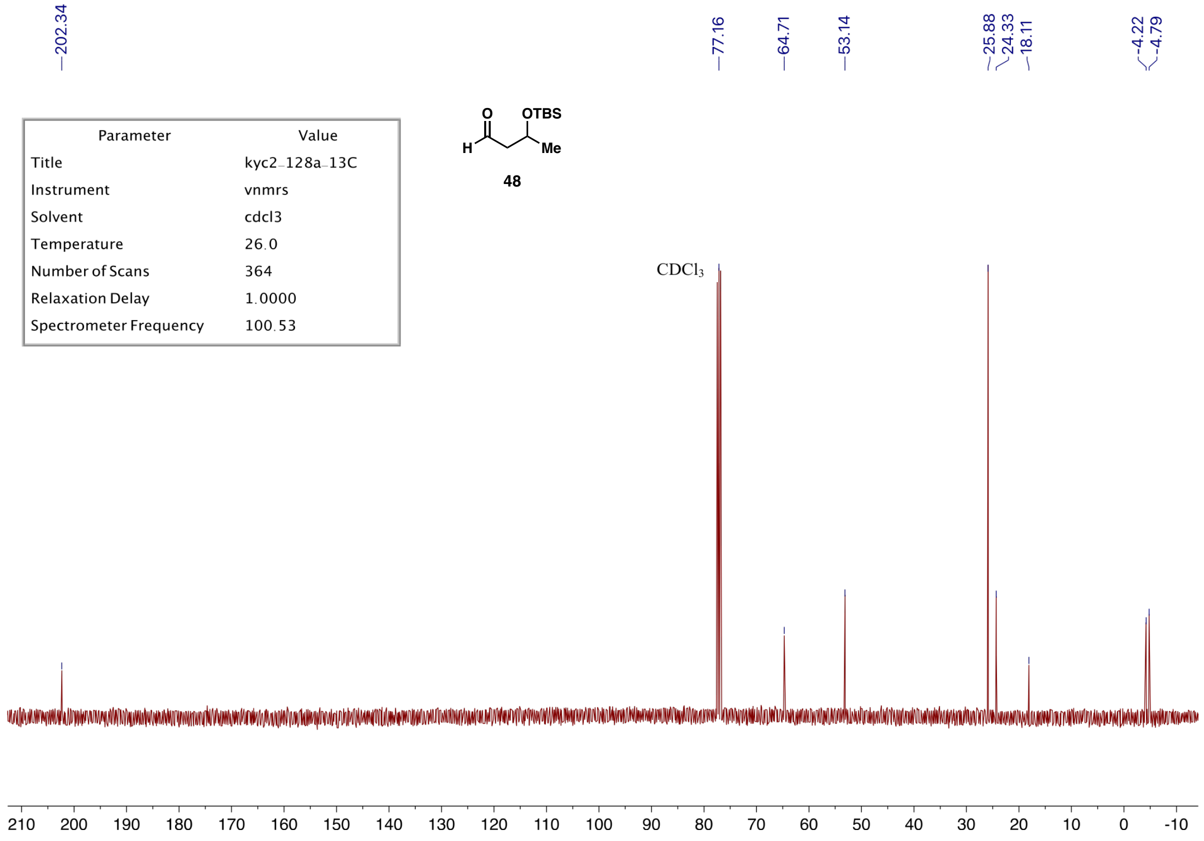

48

Parameter	Value
Title	kyc2_128a_13C
Instrument	vnmrs
Solvent	cdcl3
Temperature	26.0
Number of Scans	364
Relaxation Delay	1.0000
Spectrometer Frequency	100.53

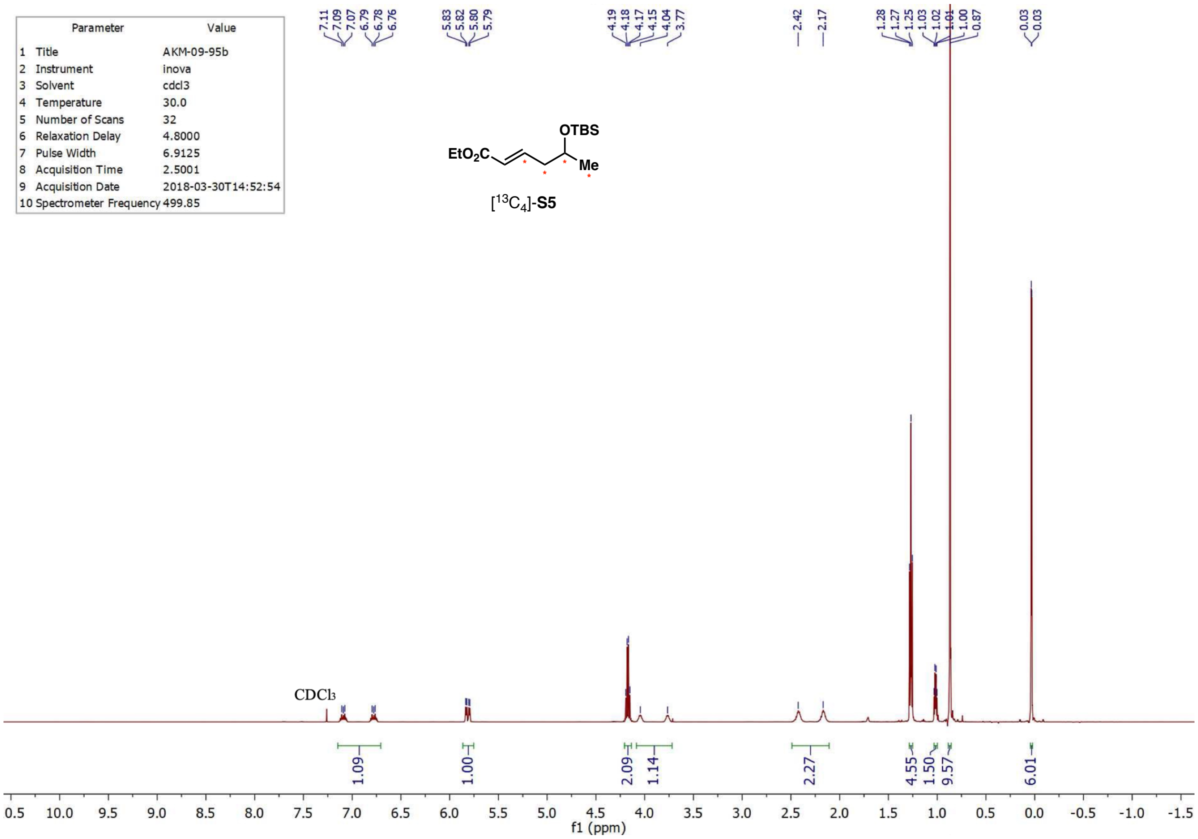

	Parameter	Value
1	Title	AKM-09-95b
2	Instrument	inova
3	Solvent	cdcl3
4	Temperature	30.0
5	Number of Scans	32
6	Relaxation Delay	4.8000
7	Pulse Width	6.9125
8	Acquisition Time	2.5001
9	Acquisition Date	2018-03-30T14:52:54
10	Spectrometer Frequency	499.85

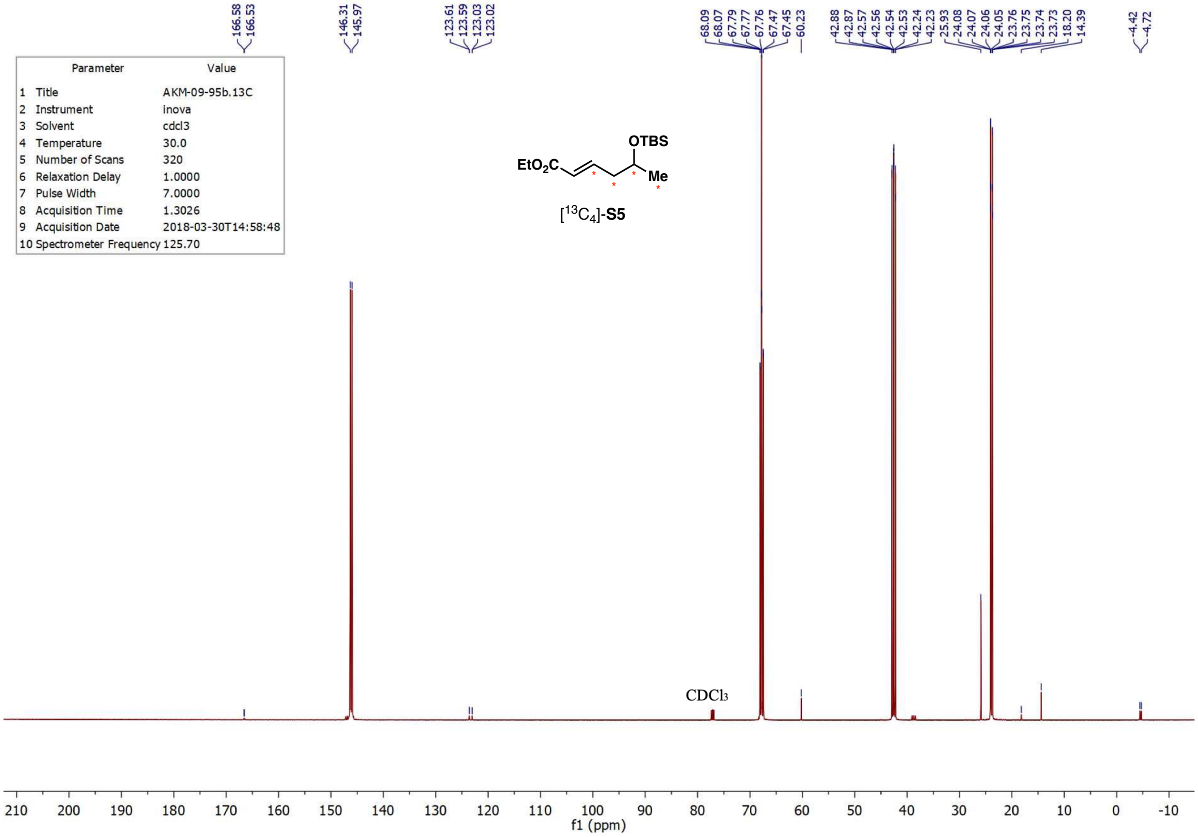

	Parameter	Value
1	Title	AKM-09-95b.13C
2	Instrument	inova
3	Solvent	cdcl3
4	Temperature	30.0
5	Number of Scans	320
6	Relaxation Delay	1.0000
7	Pulse Width	7.0000
8	Acquisition Time	1.3026
9	Acquisition Date	2018-03-30T14:58:48
10	Spectrometer Frequency	125.70

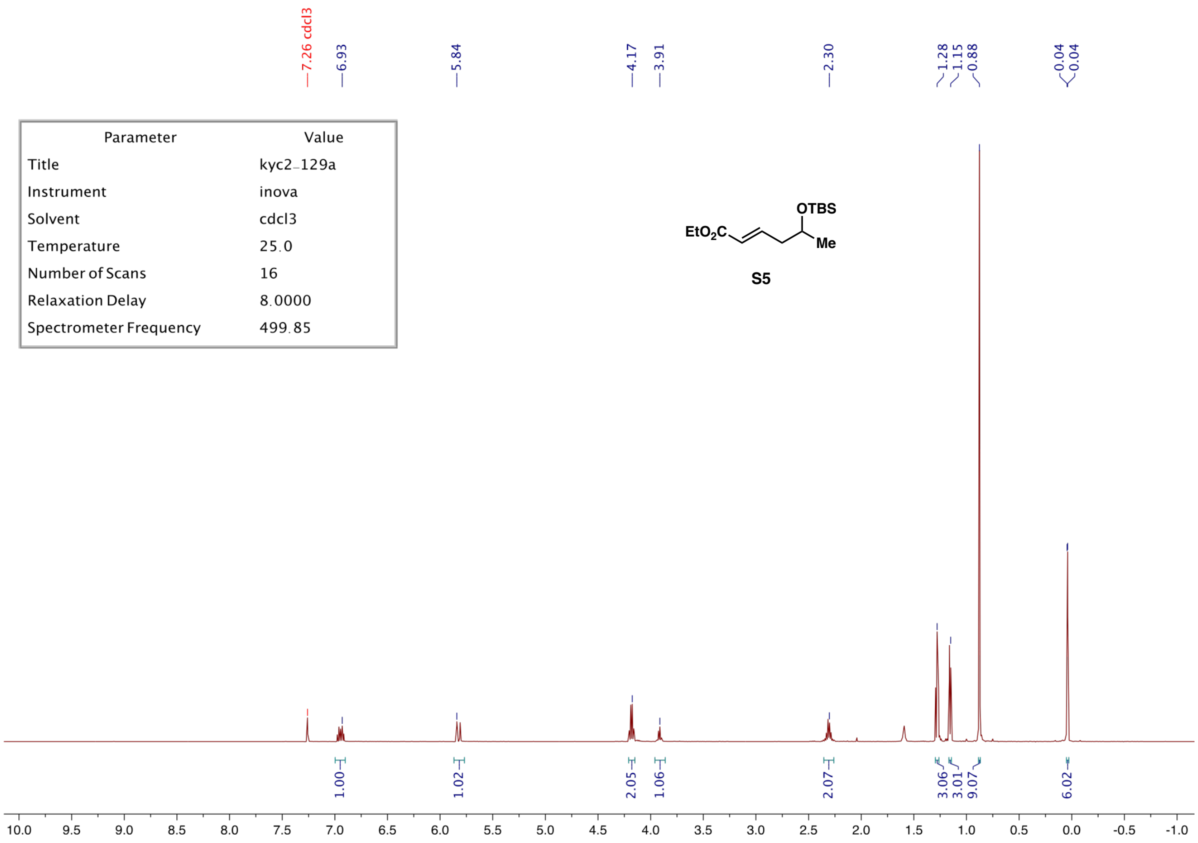

S5

Parameter	Value
Title	kyc2_129a
Instrument	inova
Solvent	cdcl3
Temperature	25.0
Number of Scans	16
Relaxation Delay	8.0000
Spectrometer Frequency	499.85

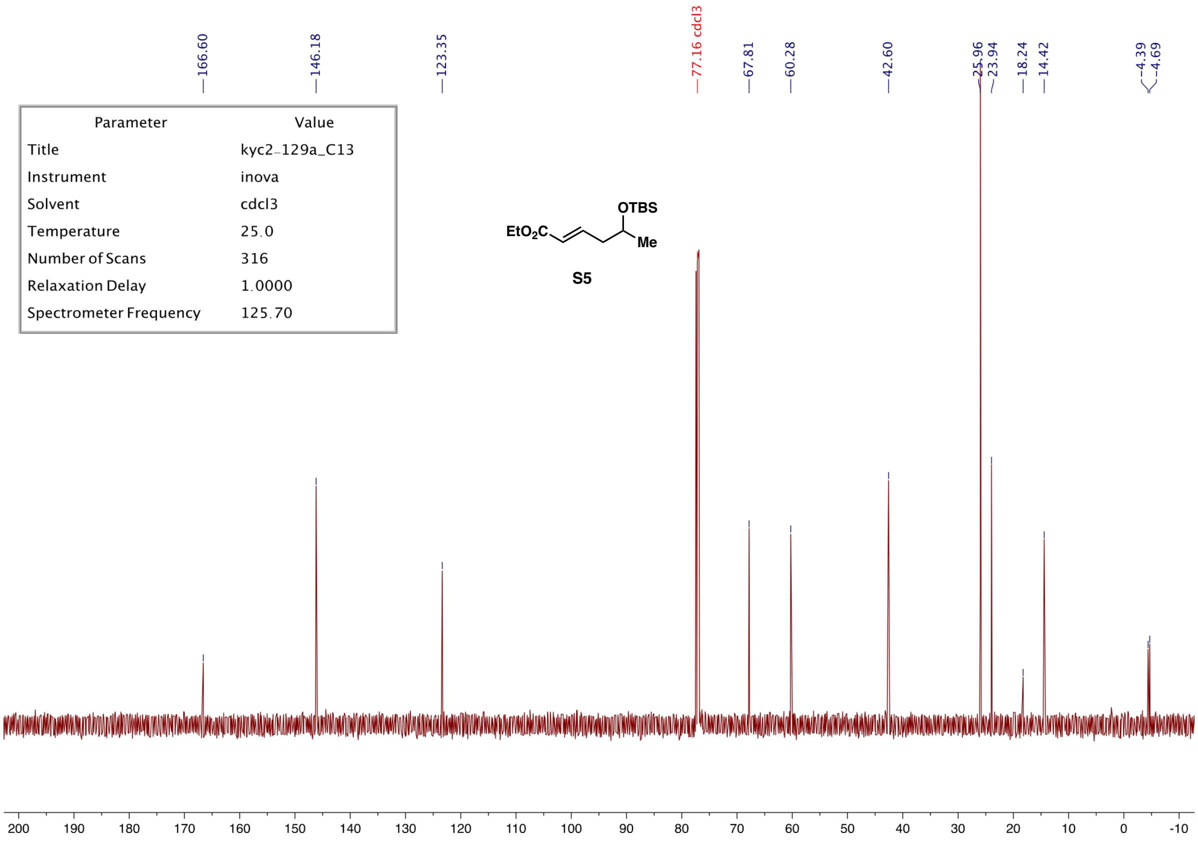

S5

Parameter	Value
Title	kyc2_129a_C13
Instrument	inova
Solvent	cdcl3
Temperature	25.0
Number of Scans	316
Relaxation Delay	1.0000
Spectrometer Frequency	125.70

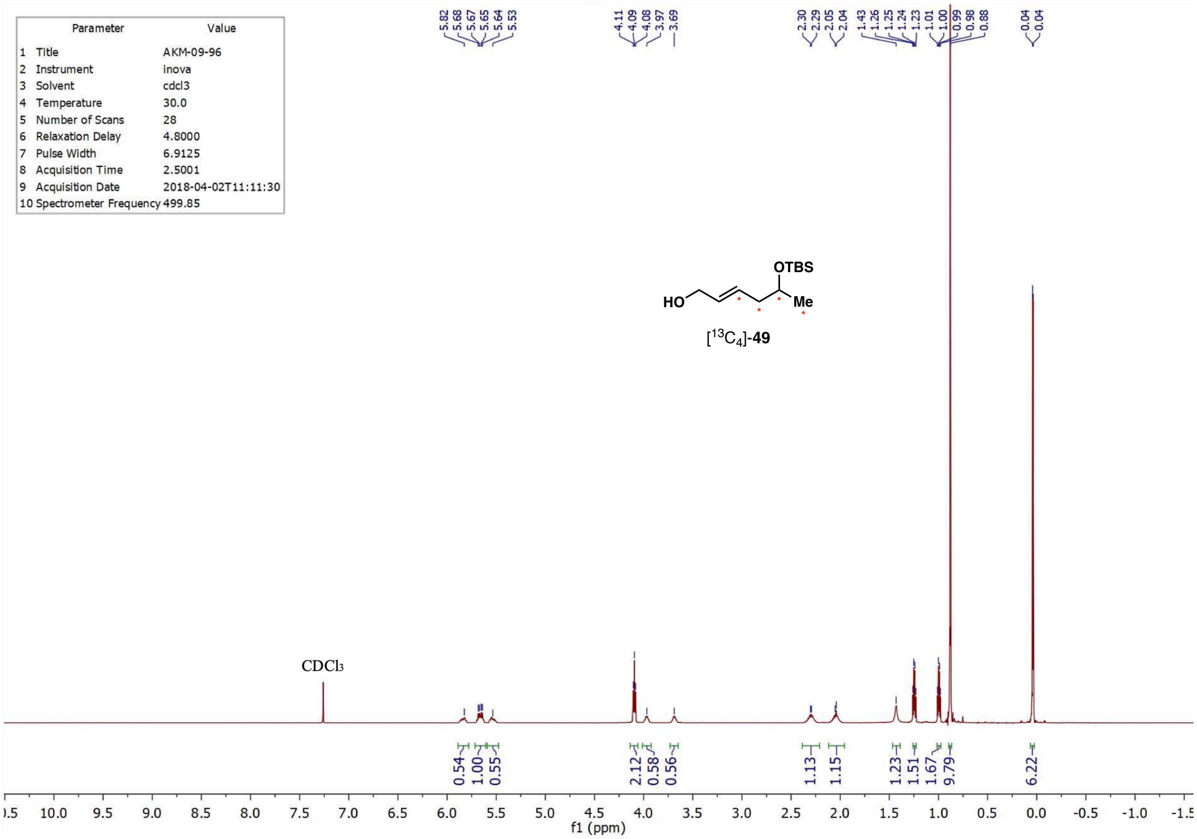

	Parameter	Value
1	Title	AKM-09-96
2	Instrument	inova
3	Solvent	cdcl3
4	Temperature	30.0
5	Number of Scans	28
6	Relaxation Delay	4.8000
7	Pulse Width	6.9125
8	Acquisition Time	2.5001
9	Acquisition Date	2018-04-02T11:11:30
10	Spectrometer Frequency	499.85

[$^{13}C_4$]-**49**

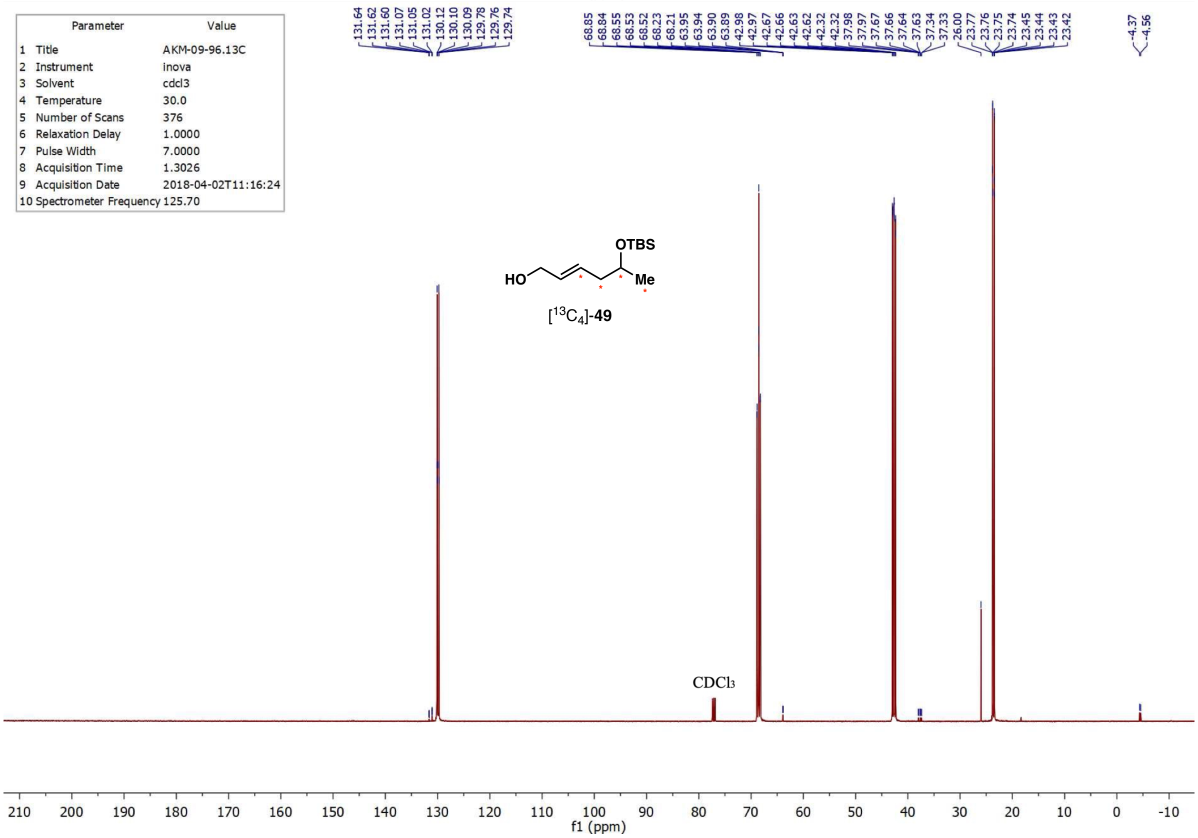

	Parameter	Value
1	Title	AKM-09-96.13C
2	Instrument	inova
3	Solvent	cdcl3
4	Temperature	30.0
5	Number of Scans	376
6	Relaxation Delay	1.0000
7	Pulse Width	7.0000
8	Acquisition Time	1.3026
9	Acquisition Date	2018-04-02T11:16:24
10	Spectrometer Frequency	125.70

[$^{13}C_4$]-**49**

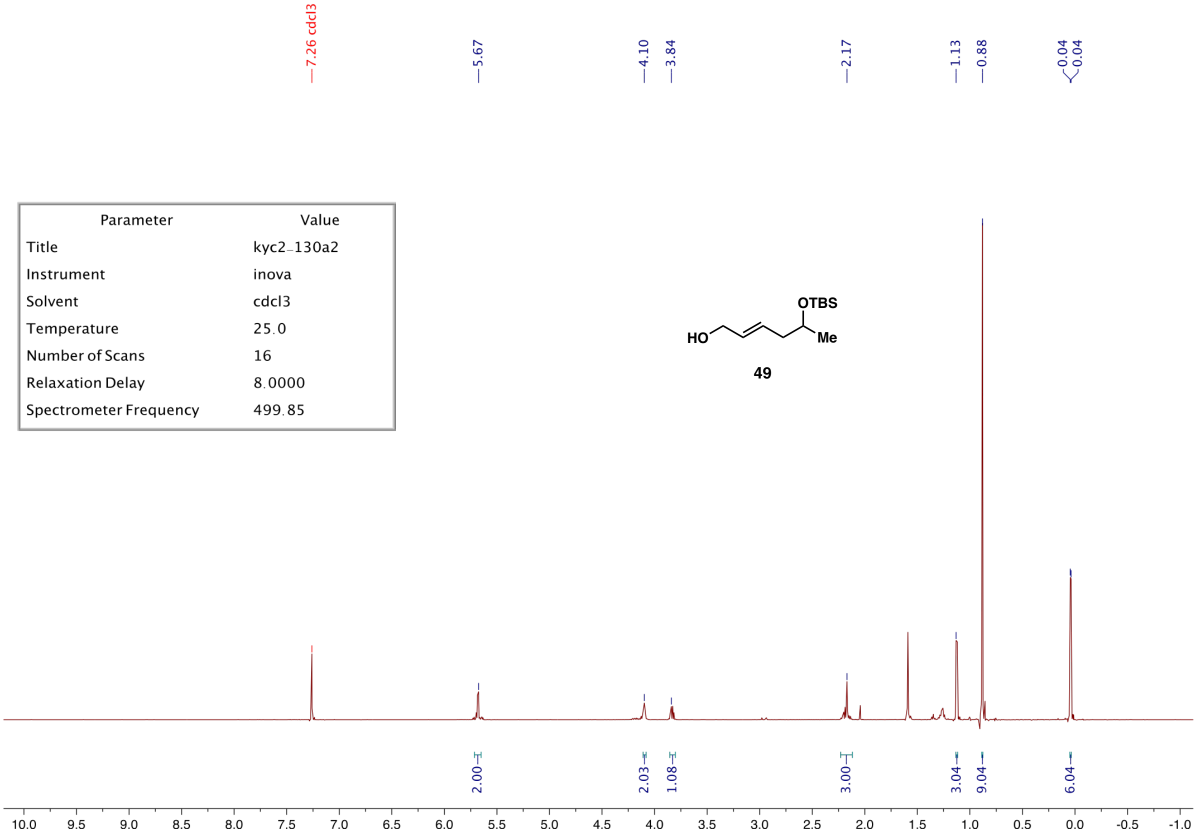

Parameter	Value
Title	kyc2_130a2
Instrument	inova
Solvent	cdcl3
Temperature	25.0
Number of Scans	16
Relaxation Delay	8.0000
Spectrometer Frequency	499.85

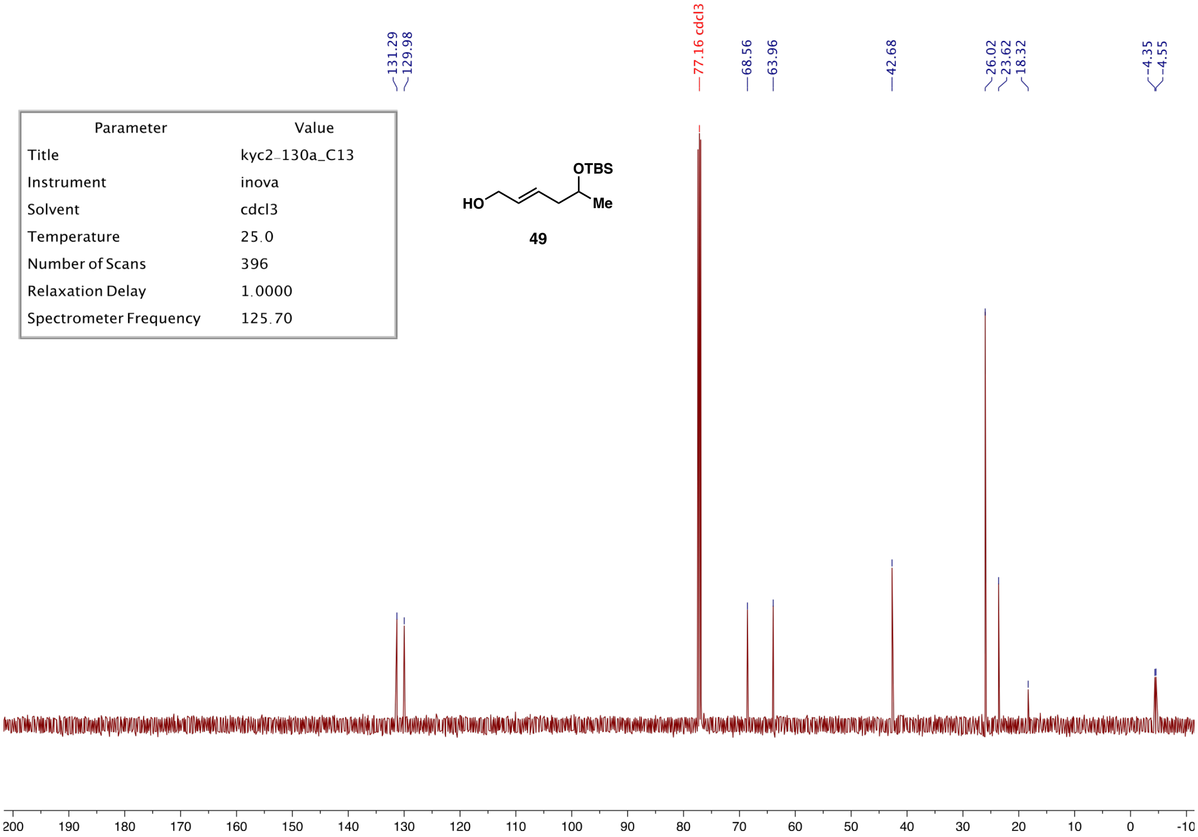

Parameter	Value
Title	kyc2_130a_C13
Instrument	inova
Solvent	cdcl3
Temperature	25.0
Number of Scans	396
Relaxation Delay	1.0000
Spectrometer Frequency	125.70

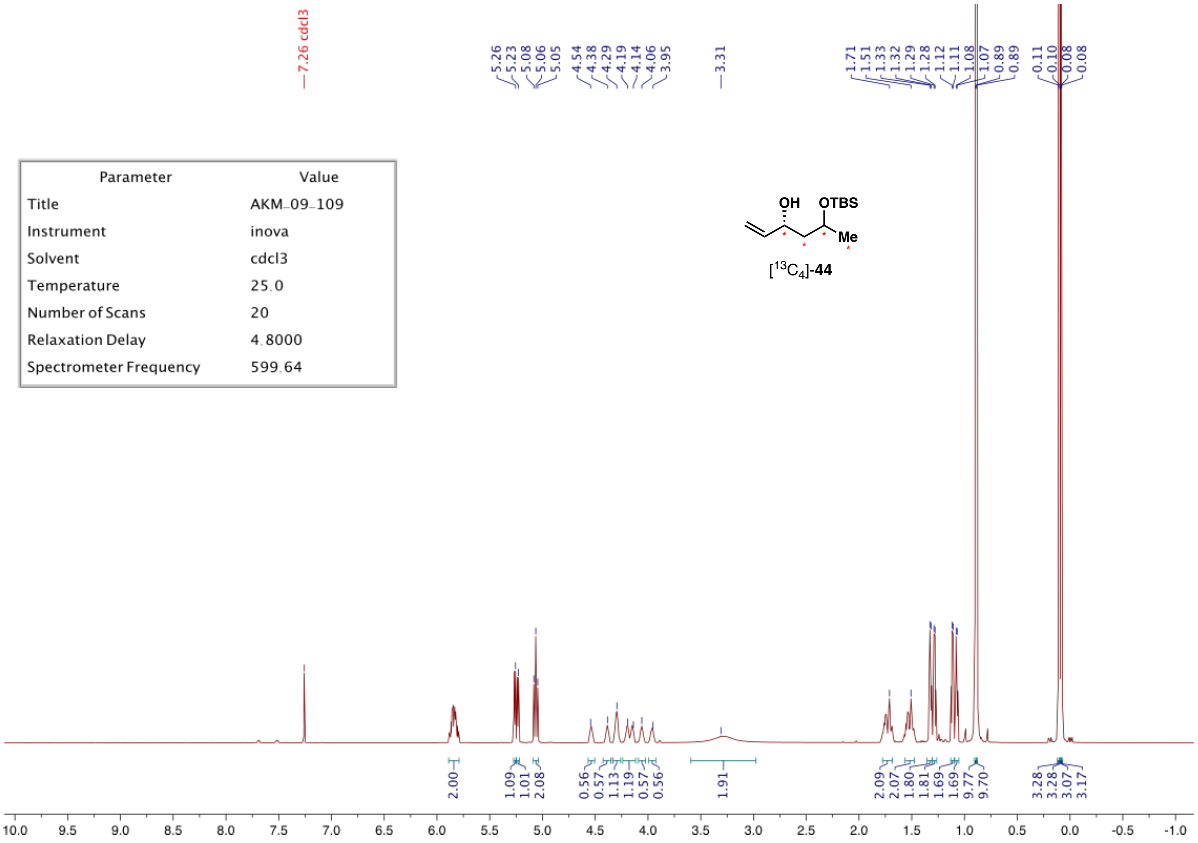

Parameter	Value
Title	AKM_09_109
Instrument	inova
Solvent	cdcl3
Temperature	25.0
Number of Scans	20
Relaxation Delay	4.8000
Spectrometer Frequency	599.64

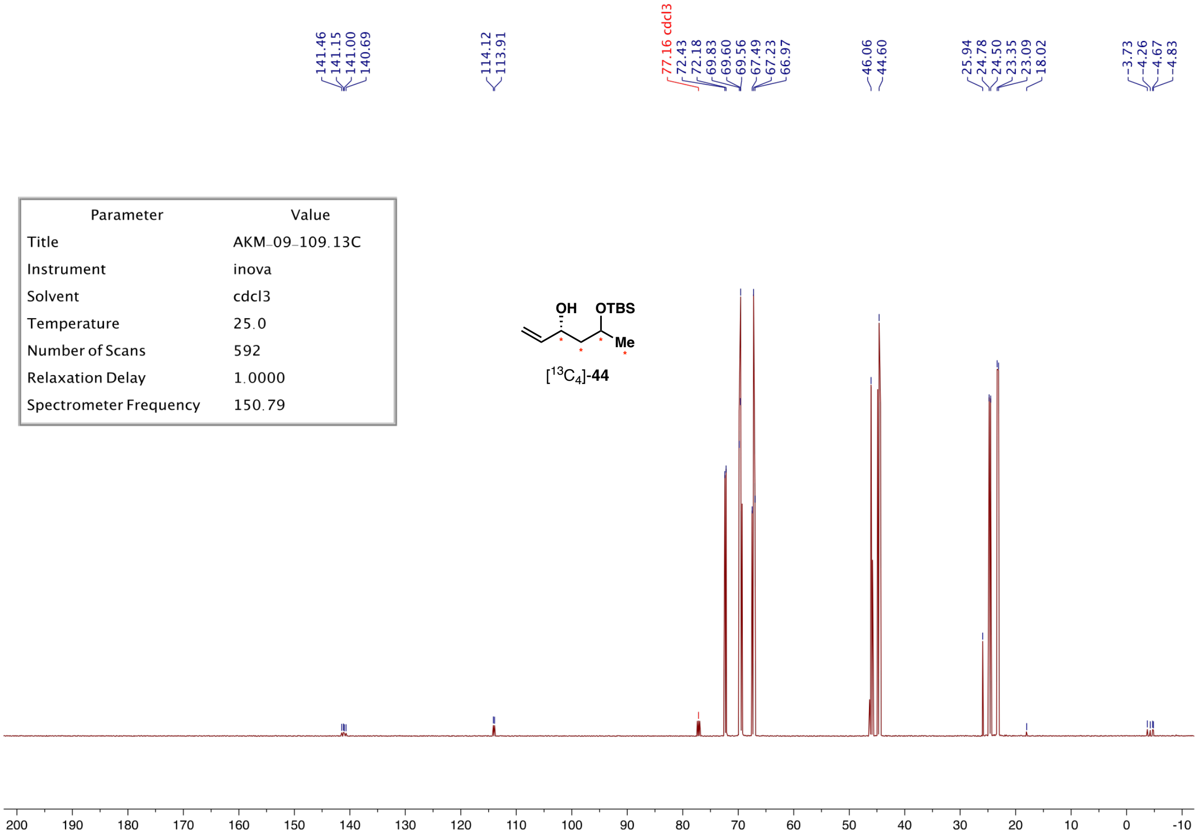

Parameter	Value
Title	AKM_09_109.13C
Instrument	inova
Solvent	cdcl3
Temperature	25.0
Number of Scans	592
Relaxation Delay	1.0000
Spectrometer Frequency	150.79

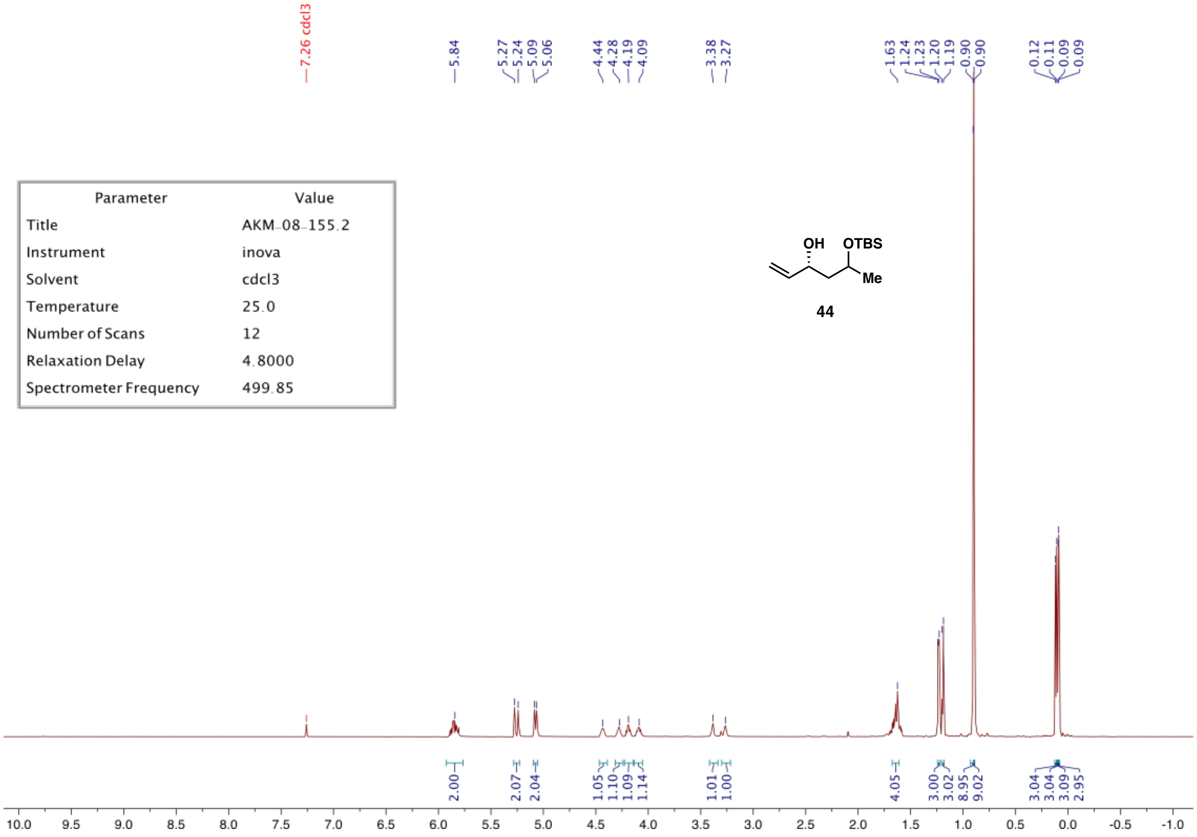

44

Parameter	Value
Title	AKM_08_155.2
Instrument	inova
Solvent	cdcl3
Temperature	25.0
Number of Scans	12
Relaxation Delay	4.8000
Spectrometer Frequency	499.85

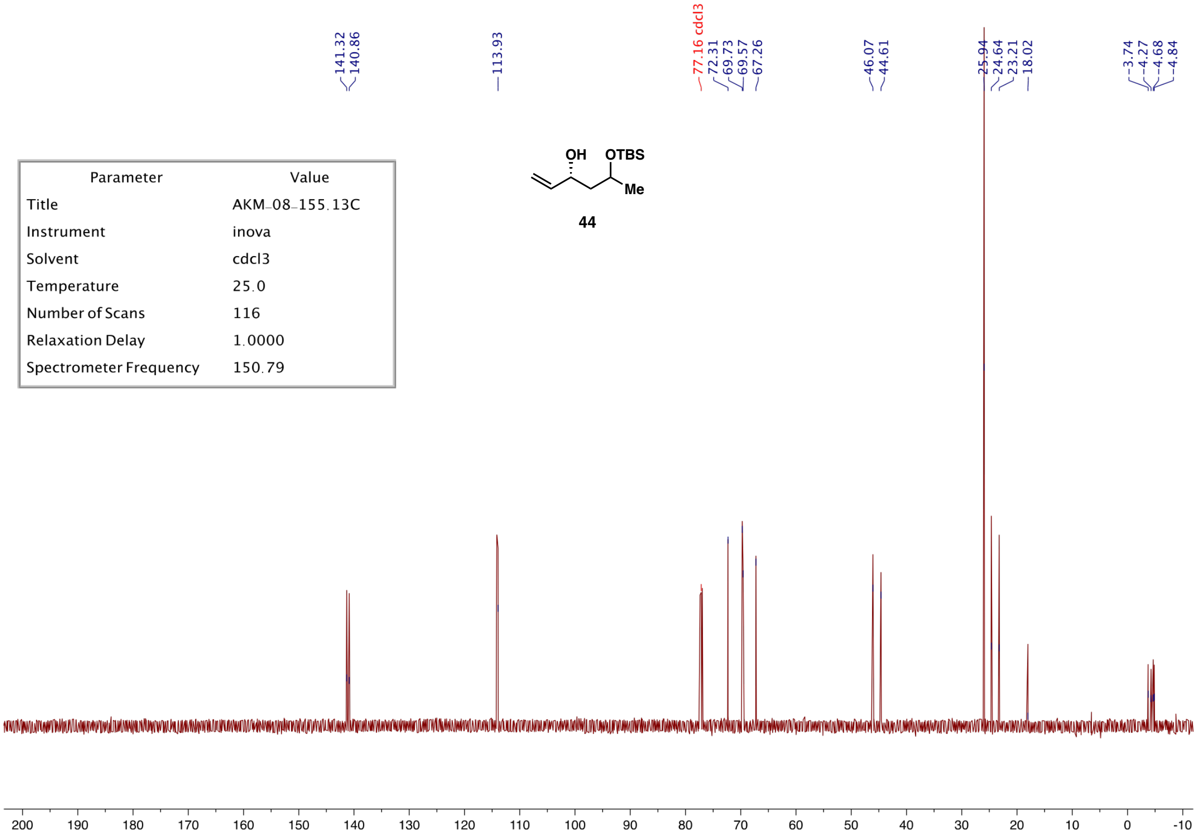

44

Parameter	Value
Title	AKM_08_155.13C
Instrument	inova
Solvent	cdcl3
Temperature	25.0
Number of Scans	116
Relaxation Delay	1.0000
Spectrometer Frequency	150.79

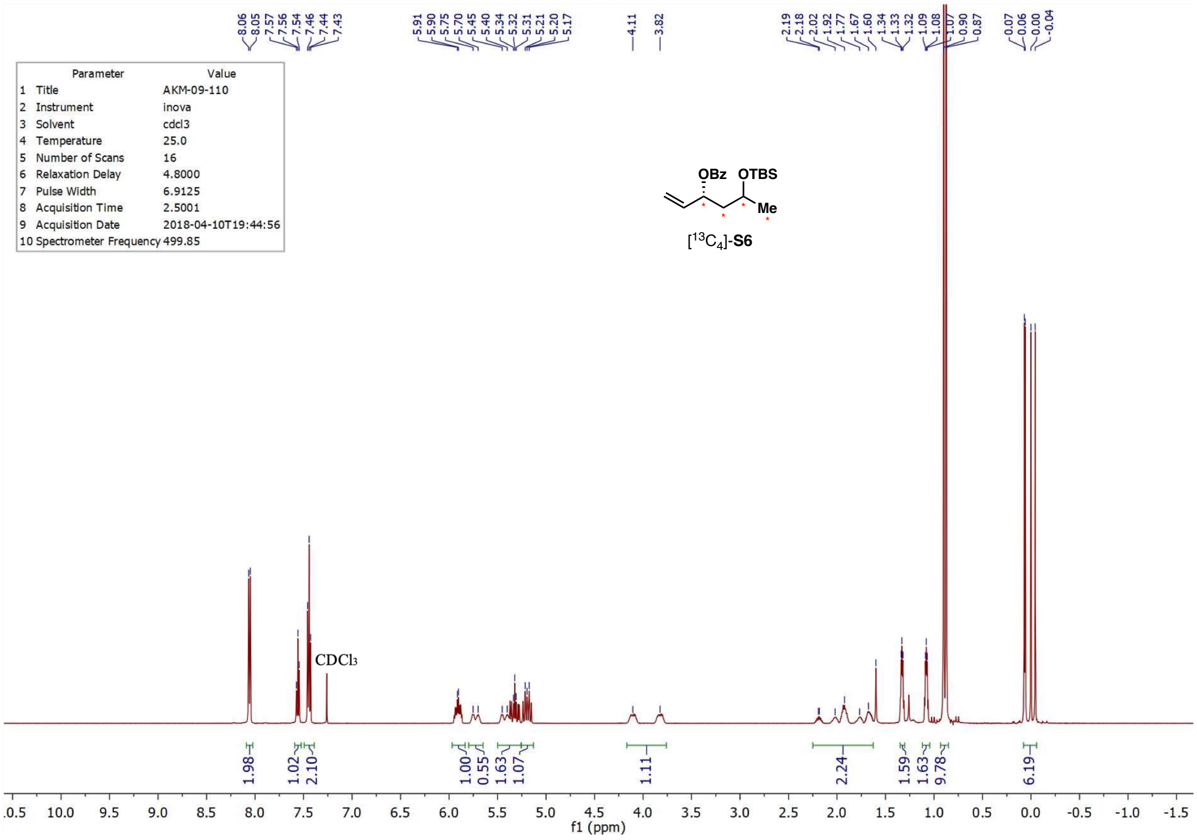

	Parameter	Value
1	Title	AKM-09-110
2	Instrument	inova
3	Solvent	cdcl3
4	Temperature	25.0
5	Number of Scans	16
6	Relaxation Delay	4.8000
7	Pulse Width	6.9125
8	Acquisition Time	2.5001
9	Acquisition Date	2018-04-10T19:44:56
10	Spectrometer Frequency	499.85

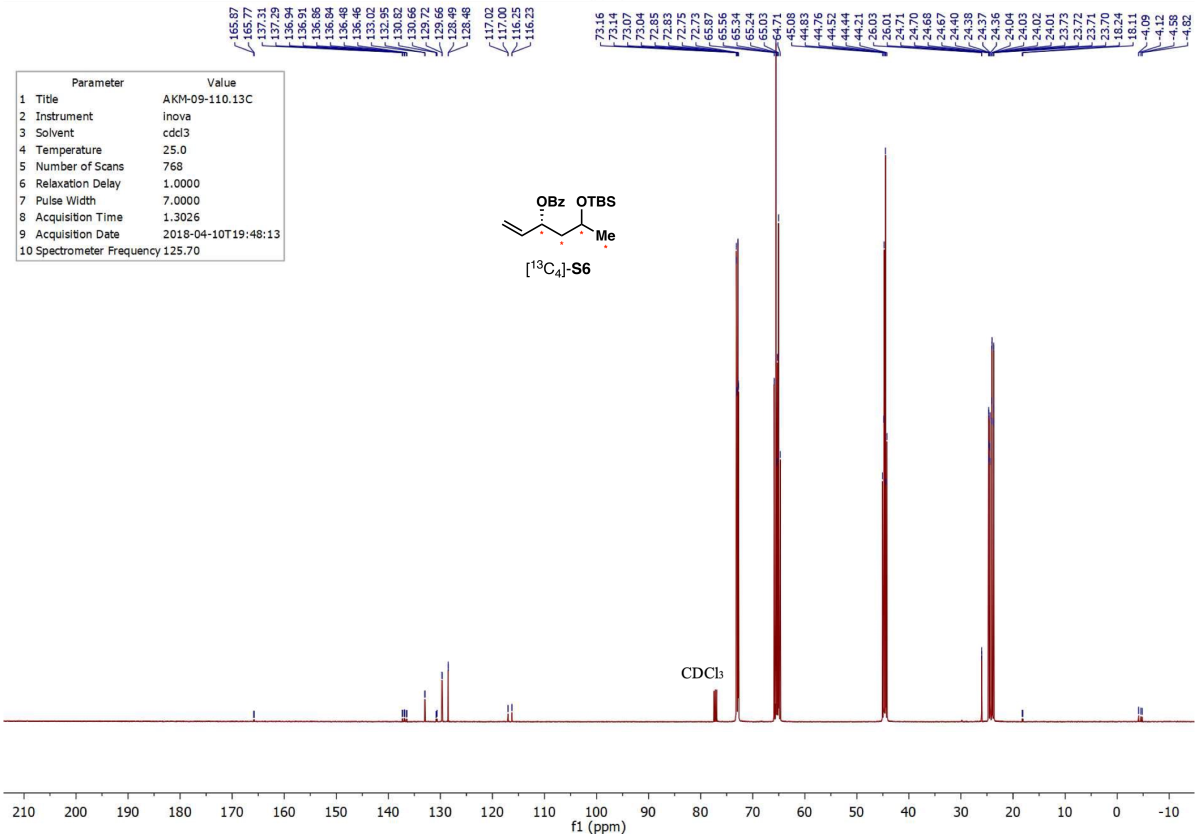

	Parameter	Value
1	Title	AKM-09-110.13C
2	Instrument	inova
3	Solvent	cdcl3
4	Temperature	25.0
5	Number of Scans	768
6	Relaxation Delay	1.0000
7	Pulse Width	7.0000
8	Acquisition Time	1.3026
9	Acquisition Date	2018-04-10T19:48:13
10	Spectrometer Frequency	125.70

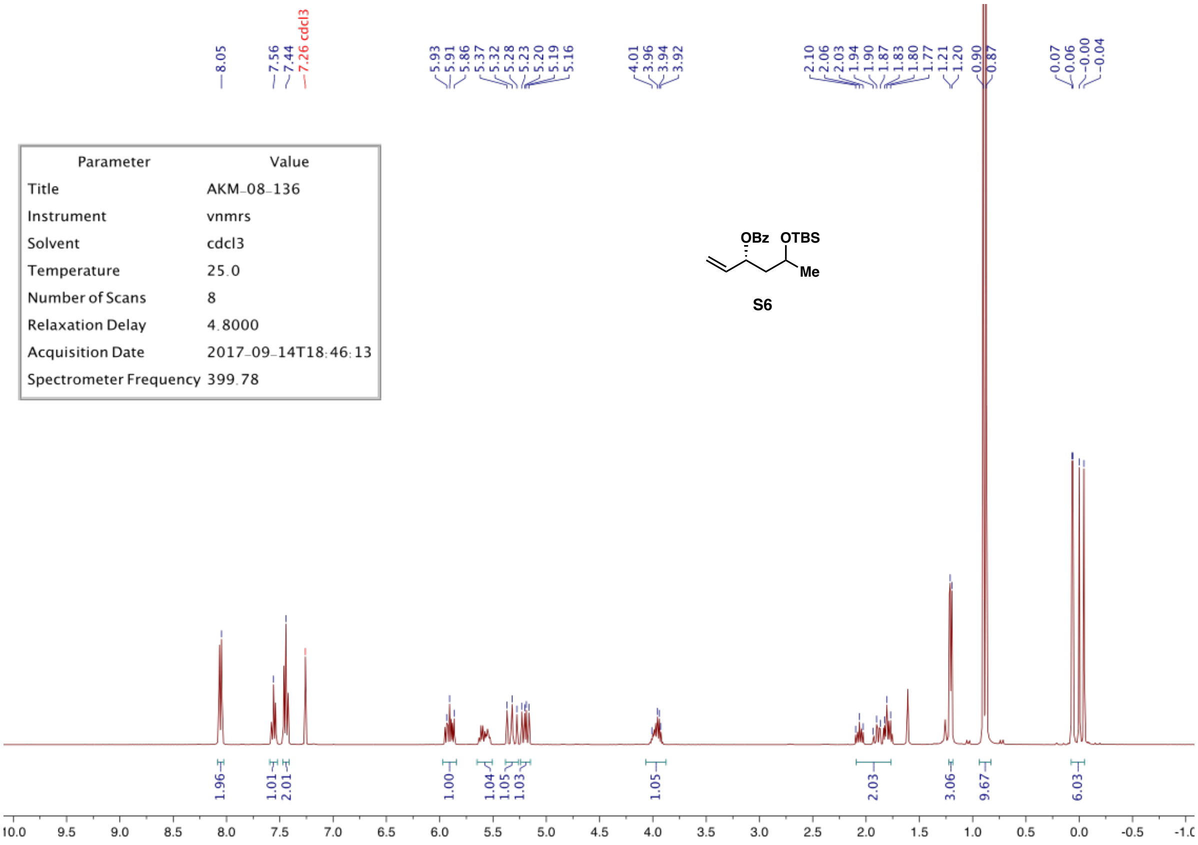

Parameter	Value
Title	AKM_08_136
Instrument	vnmrs
Solvent	cdcl3
Temperature	25.0
Number of Scans	8
Relaxation Delay	4.8000
Acquisition Date	2017_09_14T18:46:13
Spectrometer Frequency	399.78

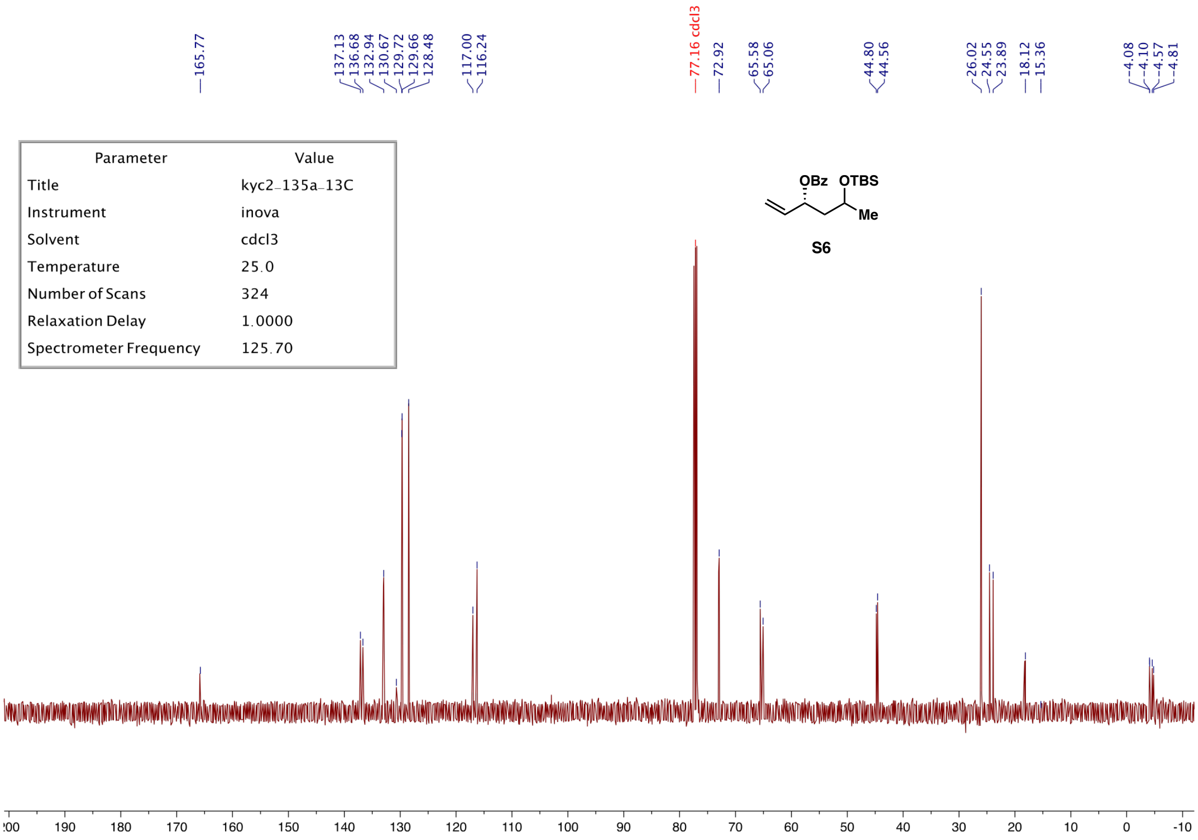

Parameter	Value
Title	kyc2_135a_13C
Instrument	inova
Solvent	cdcl3
Temperature	25.0
Number of Scans	324
Relaxation Delay	1.0000
Spectrometer Frequency	125.70

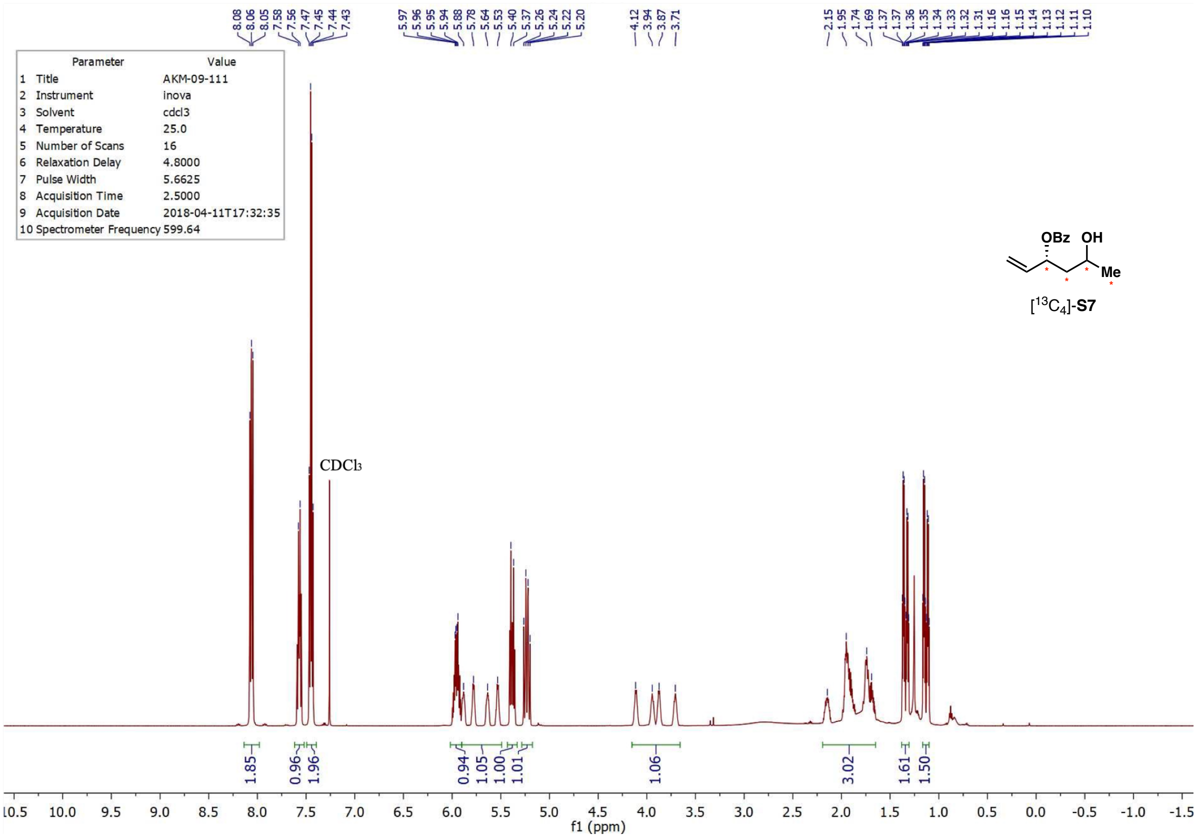

	Parameter	Value
1	Title	AKM-09-111
2	Instrument	inova
3	Solvent	cdcl3
4	Temperature	25.0
5	Number of Scans	16
6	Relaxation Delay	4.8000
7	Pulse Width	5.6625
8	Acquisition Time	2.5000
9	Acquisition Date	2018-04-11T17:32:35
10	Spectrometer Frequency	599.64

$[^{13}C_4]$-**S7**

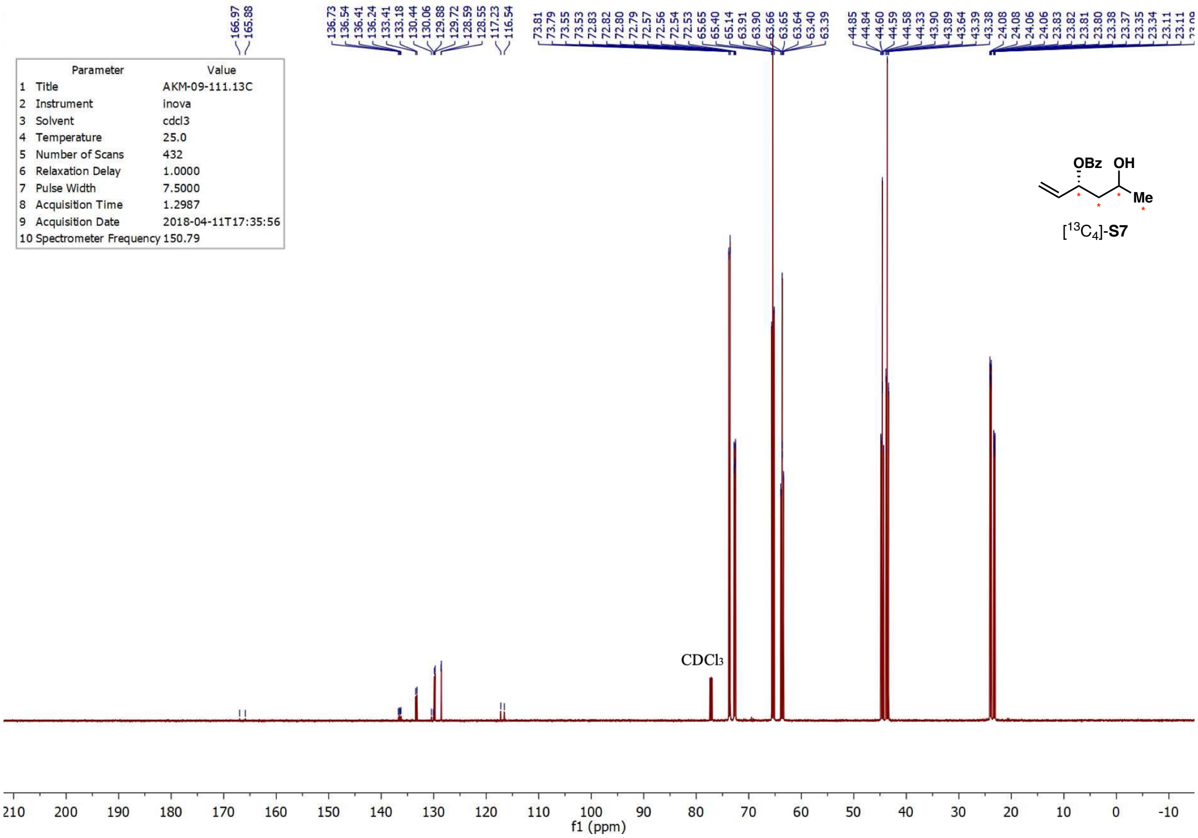

	Parameter	Value
1	Title	AKM-09-111.13C
2	Instrument	inova
3	Solvent	cdcl3
4	Temperature	25.0
5	Number of Scans	432
6	Relaxation Delay	1.0000
7	Pulse Width	7.5000
8	Acquisition Time	1.2987
9	Acquisition Date	2018-04-11T17:35:56
10	Spectrometer Frequency	150.79

$[^{13}C_4]$-**S7**

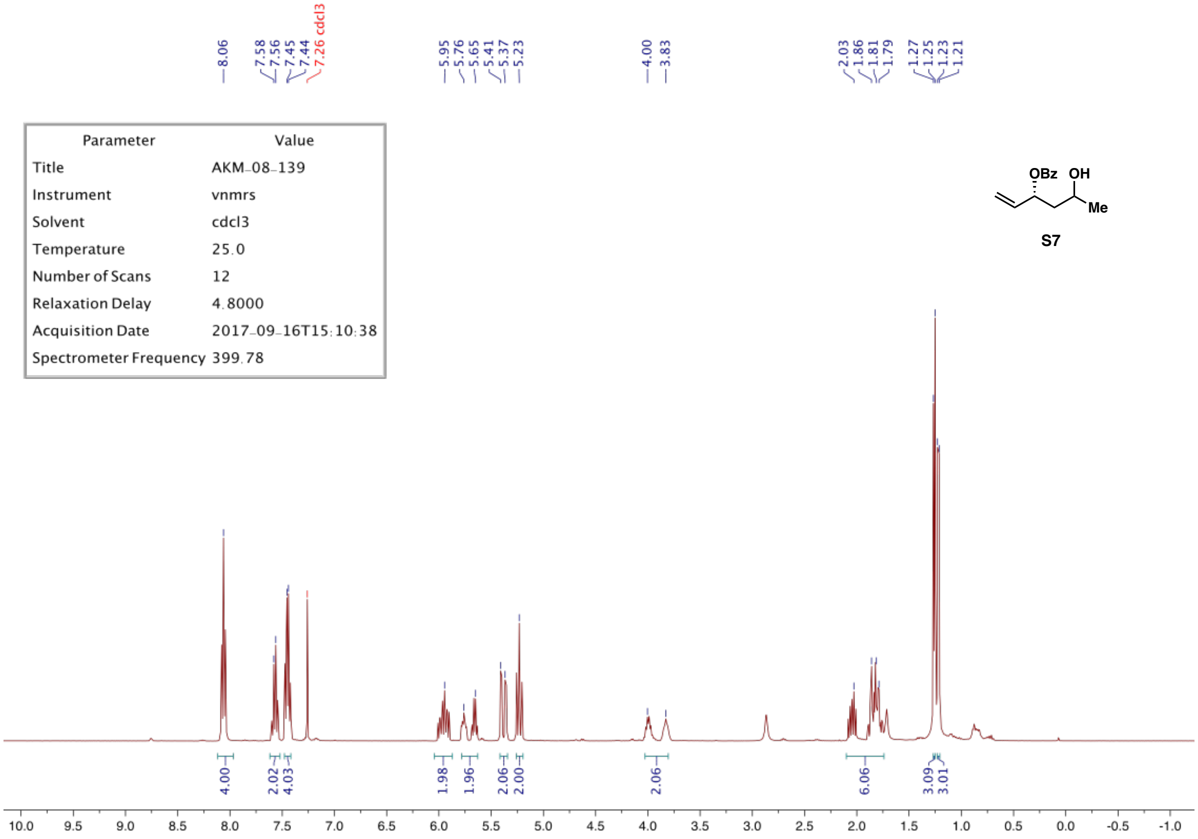

Parameter	Value
Title	AKM_08_139
Instrument	vnmrs
Solvent	cdcl3
Temperature	25.0
Number of Scans	12
Relaxation Delay	4.8000
Acquisition Date	2017-09-16T15:10:38
Spectrometer Frequency	399.78

S7

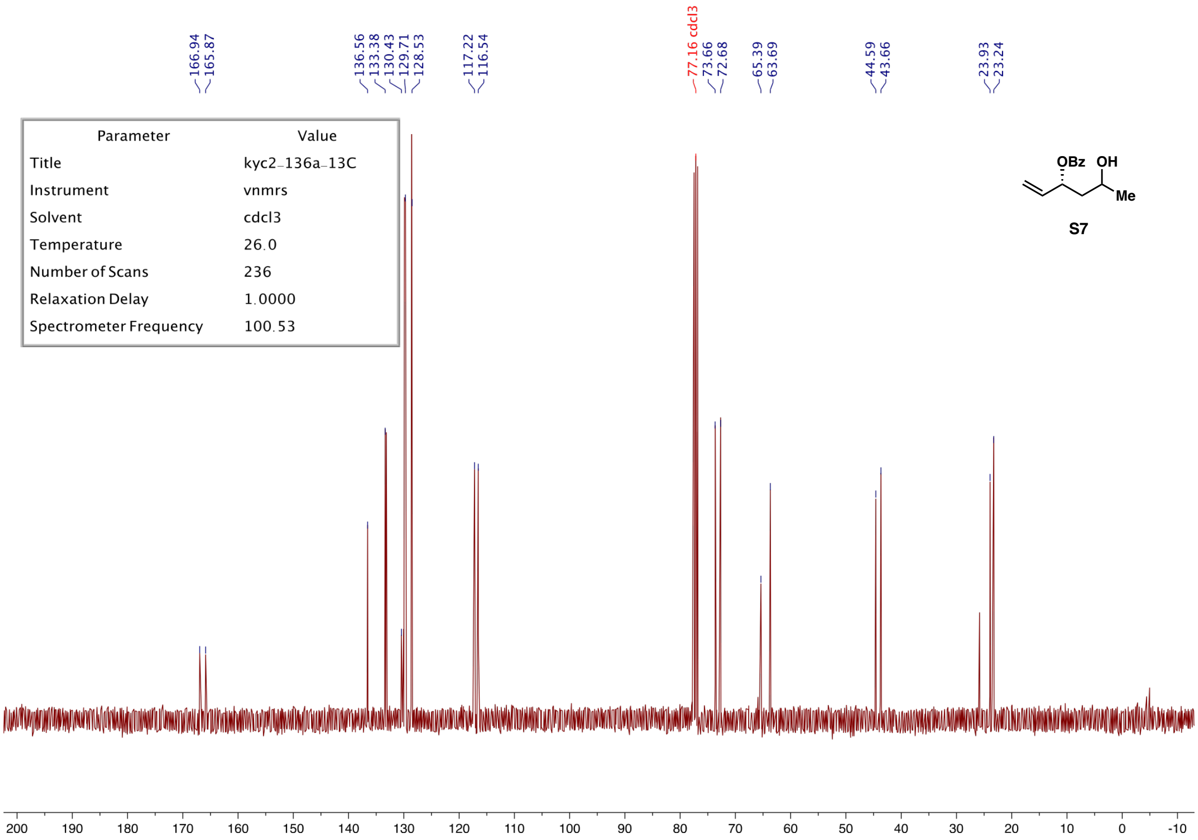

Parameter	Value
Title	kyc2_136a_13C
Instrument	vnmrs
Solvent	cdcl3
Temperature	26.0
Number of Scans	236
Relaxation Delay	1.0000
Spectrometer Frequency	100.53

S7

Parameter	Value
Title	AKM_09_114
Instrument	inova
Solvent	cdcl3
Temperature	25.0
Number of Scans	24
Relaxation Delay	4.8000
Spectrometer Frequency	599.64

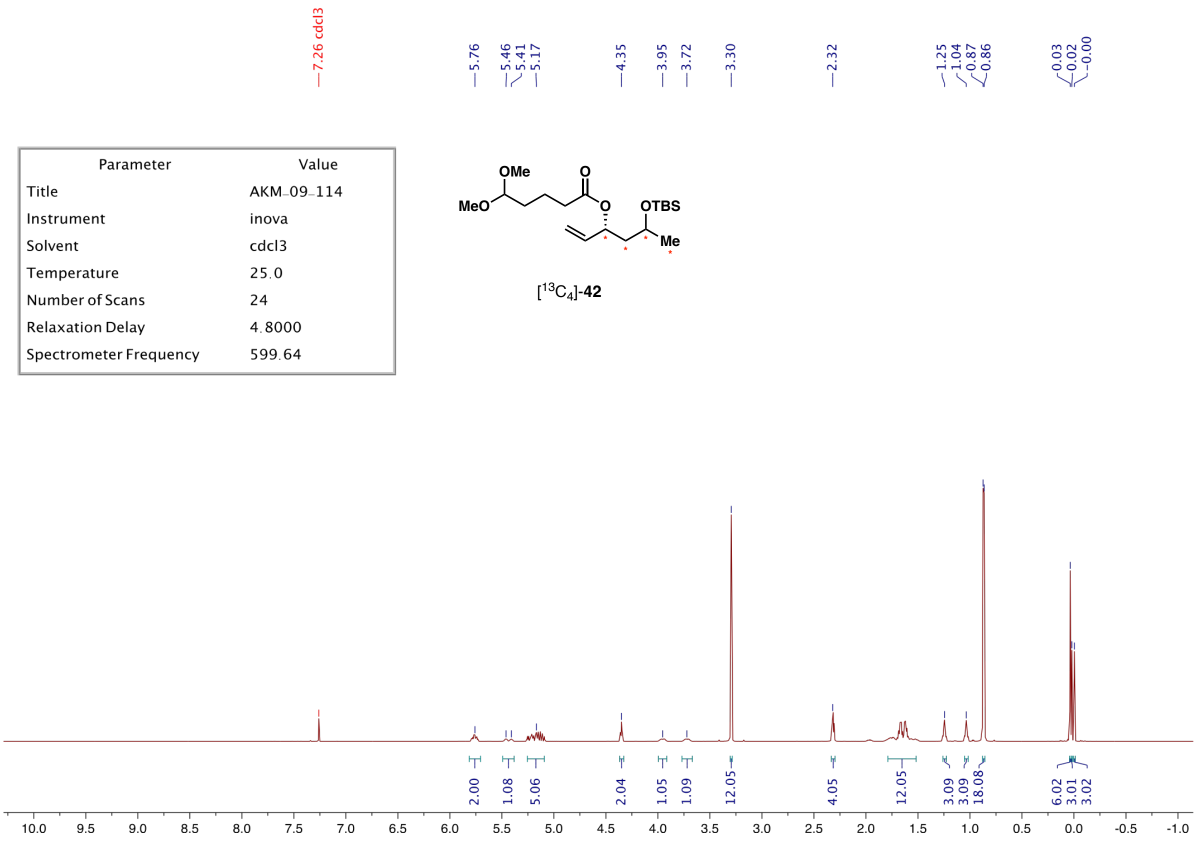

[$^{13}C_4$]-**42**

Parameter	Value
Title	AKM_09_114.13C
Instrument	inova
Solvent	cdcl3
Temperature	25.0
Number of Scans	340
Relaxation Delay	1.0000
Spectrometer Frequency	150.79

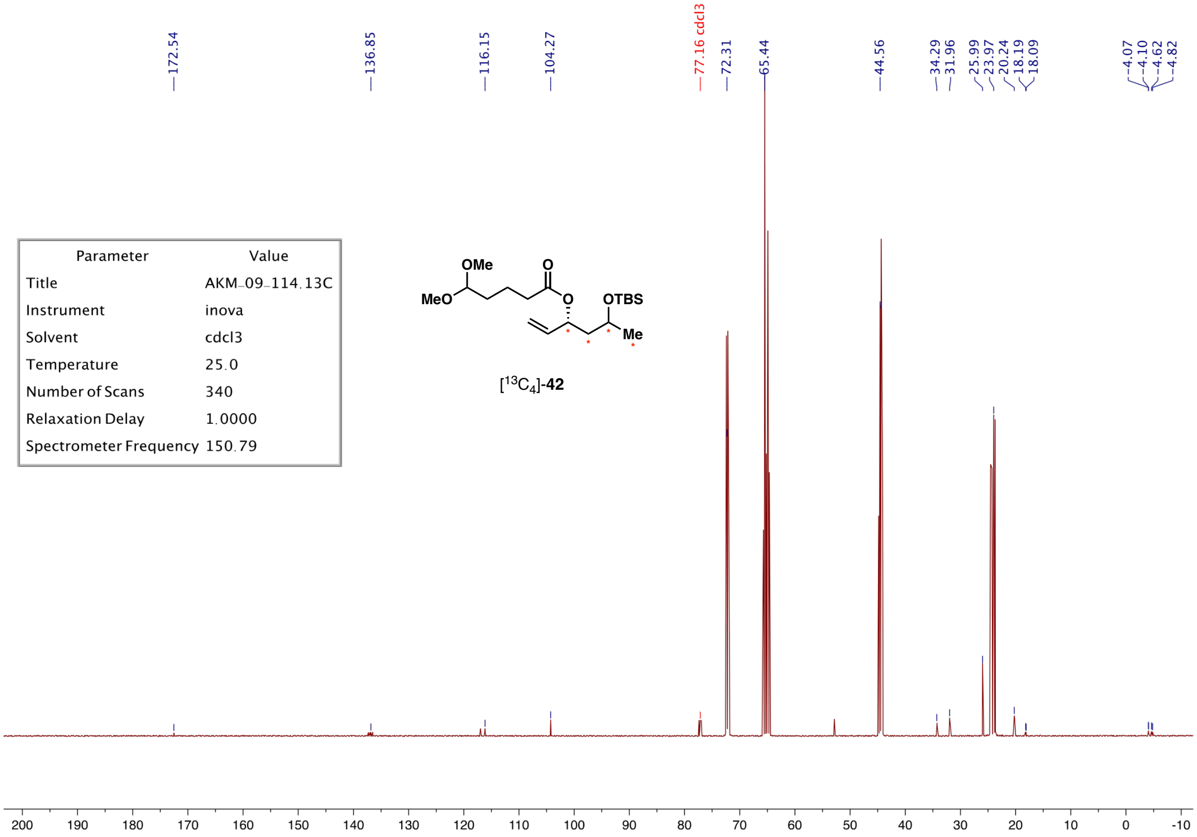

[$^{13}C_4$]-**42**

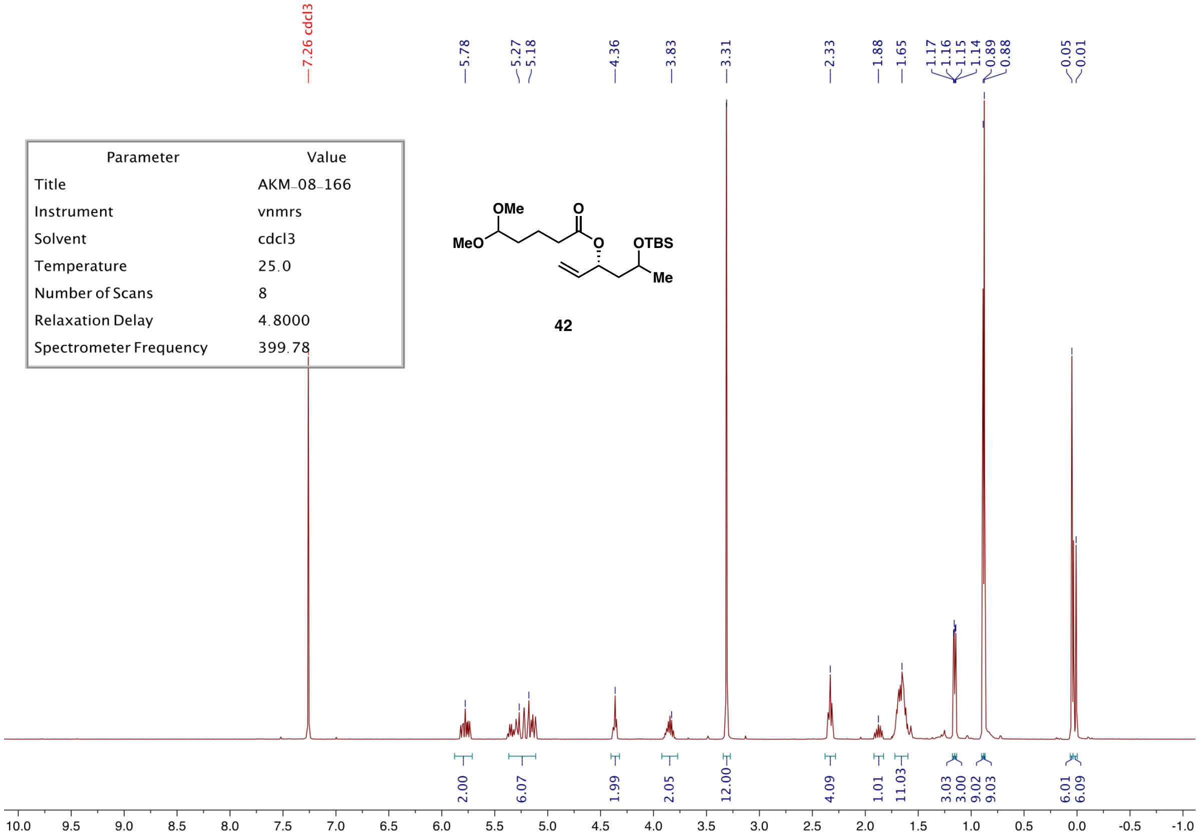

Parameter	Value
Title	AKM_08_166
Instrument	vnmrs
Solvent	cdcl3
Temperature	25.0
Number of Scans	8
Relaxation Delay	4.8000
Spectrometer Frequency	399.78

42

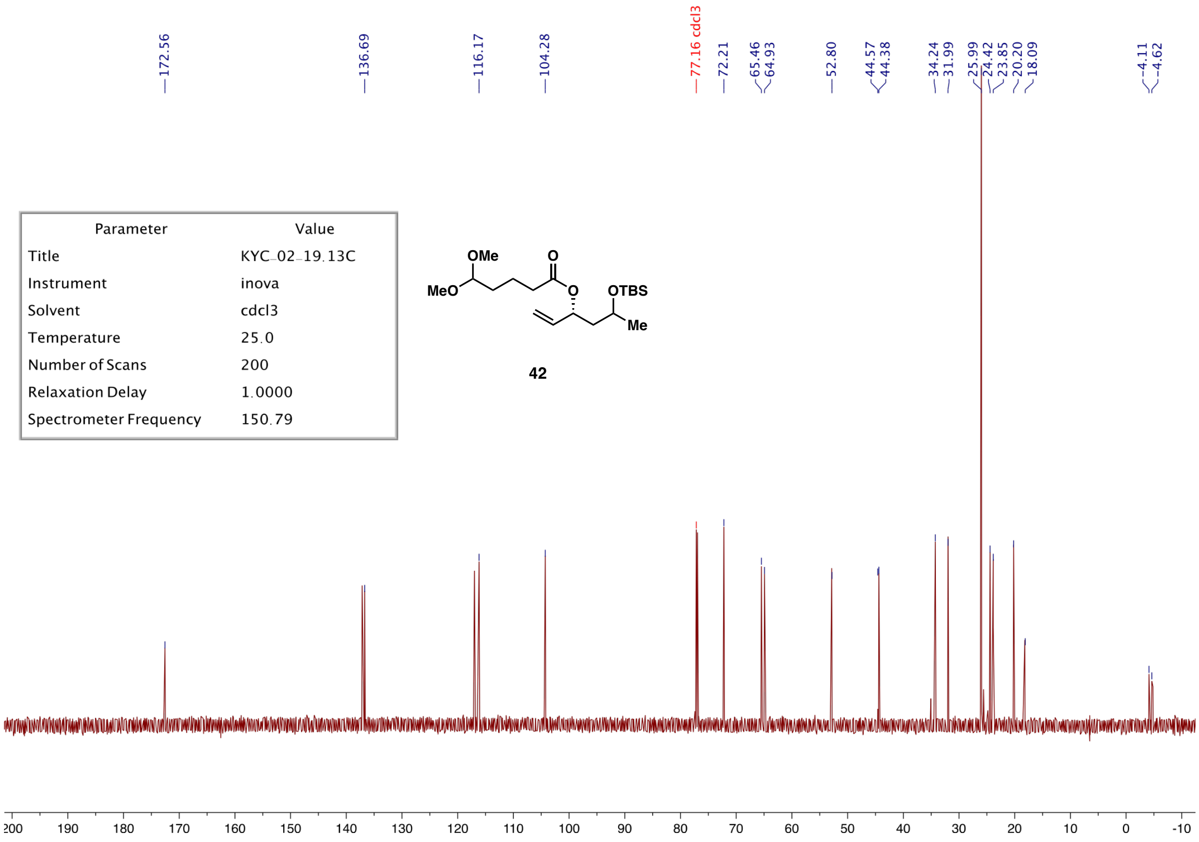

Parameter	Value
Title	KYC_02_19.13C
Instrument	inova
Solvent	cdcl3
Temperature	25.0
Number of Scans	200
Relaxation Delay	1.0000
Spectrometer Frequency	150.79

42

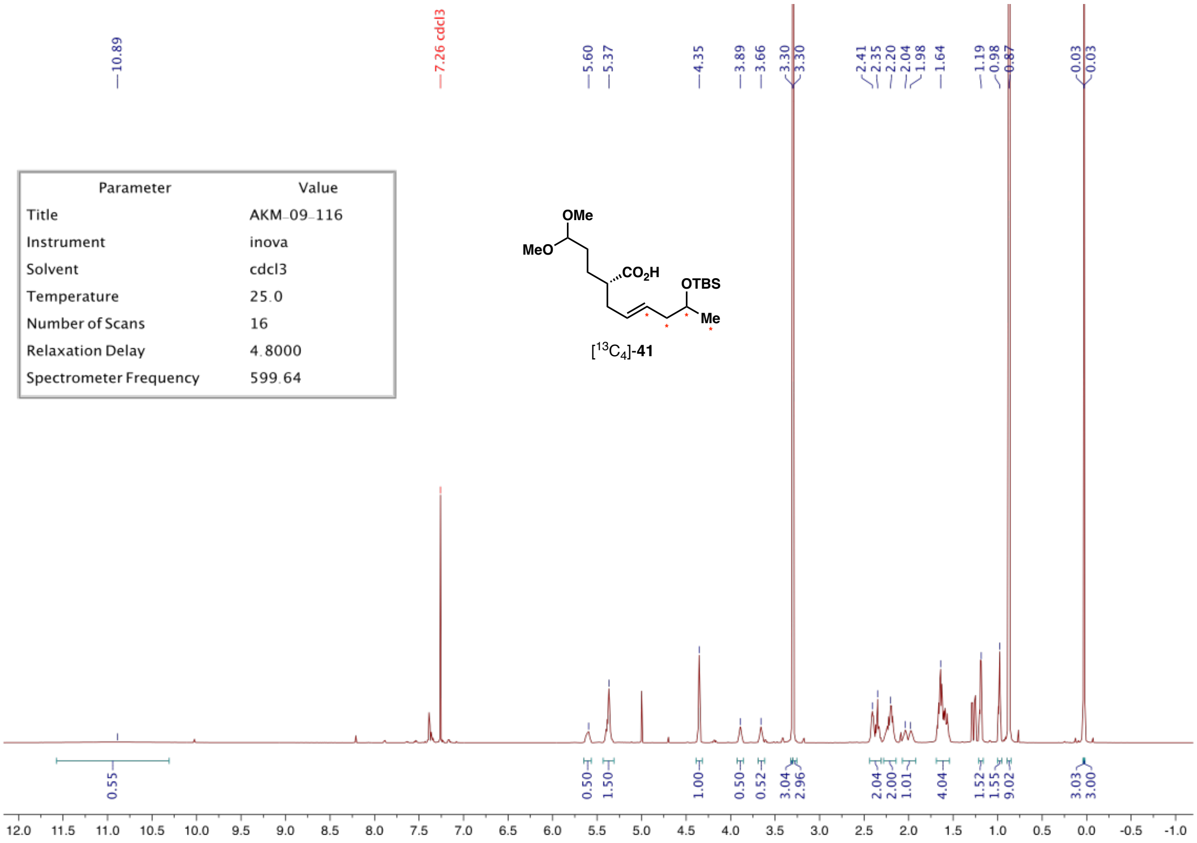

Parameter	Value
Title	AKM_09_116
Instrument	inova
Solvent	cdcl3
Temperature	25.0
Number of Scans	16
Relaxation Delay	4.8000
Spectrometer Frequency	599.64

$[^{13}C_4]$-**41**

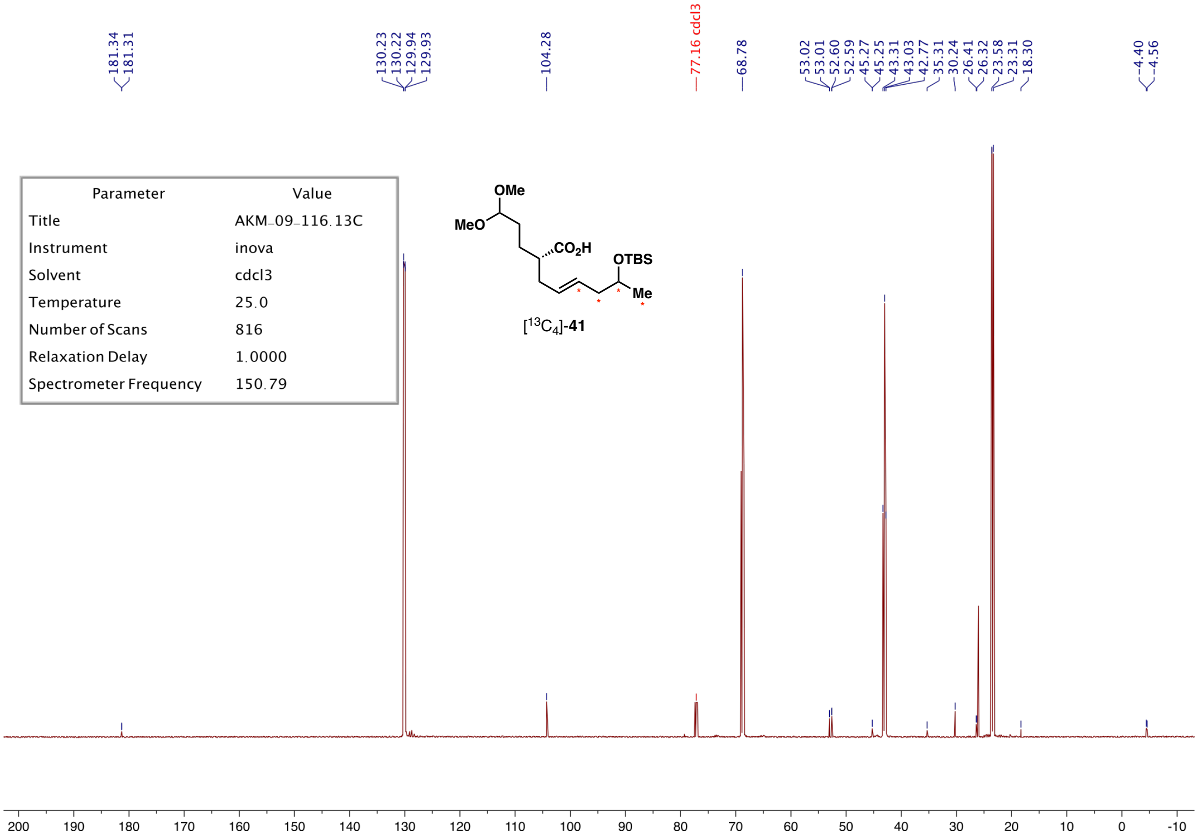

Parameter	Value
Title	AKM_09_116.13C
Instrument	inova
Solvent	cdcl3
Temperature	25.0
Number of Scans	816
Relaxation Delay	1.0000
Spectrometer Frequency	150.79

$[^{13}C_4]$-**41**

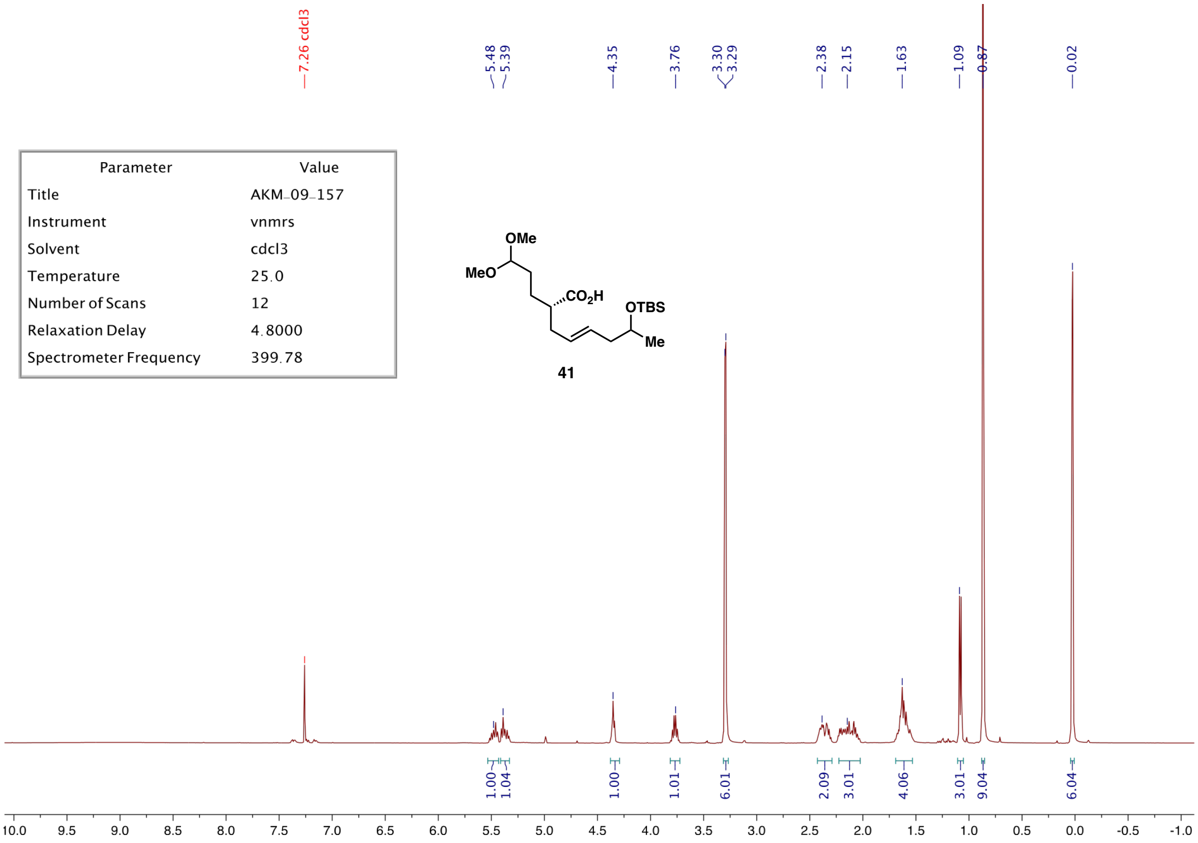

Parameter	Value
Title	AKM_09_157
Instrument	vnmrs
Solvent	cdcl3
Temperature	25.0
Number of Scans	12
Relaxation Delay	4.8000
Spectrometer Frequency	399.78

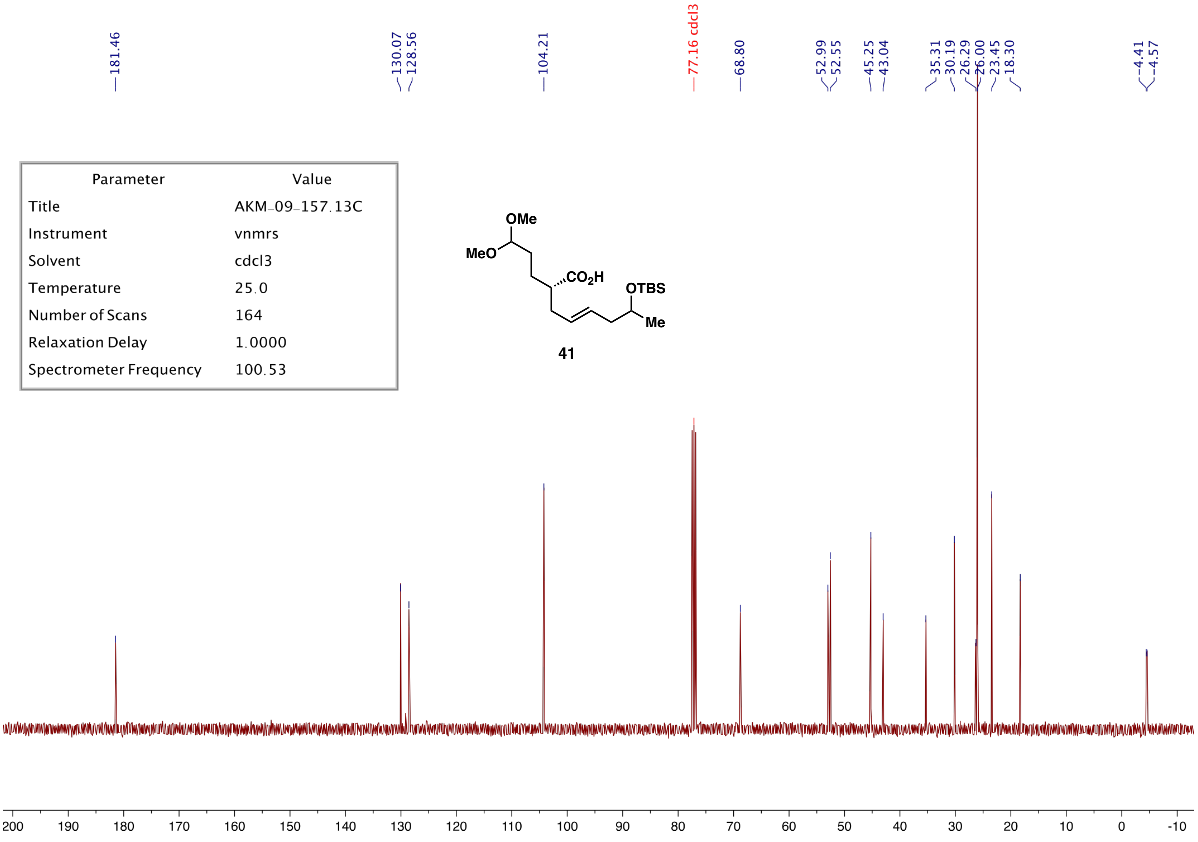

Parameter	Value
Title	AKM_09_157.13C
Instrument	vnmrs
Solvent	cdcl3
Temperature	25.0
Number of Scans	164
Relaxation Delay	1.0000
Spectrometer Frequency	100.53

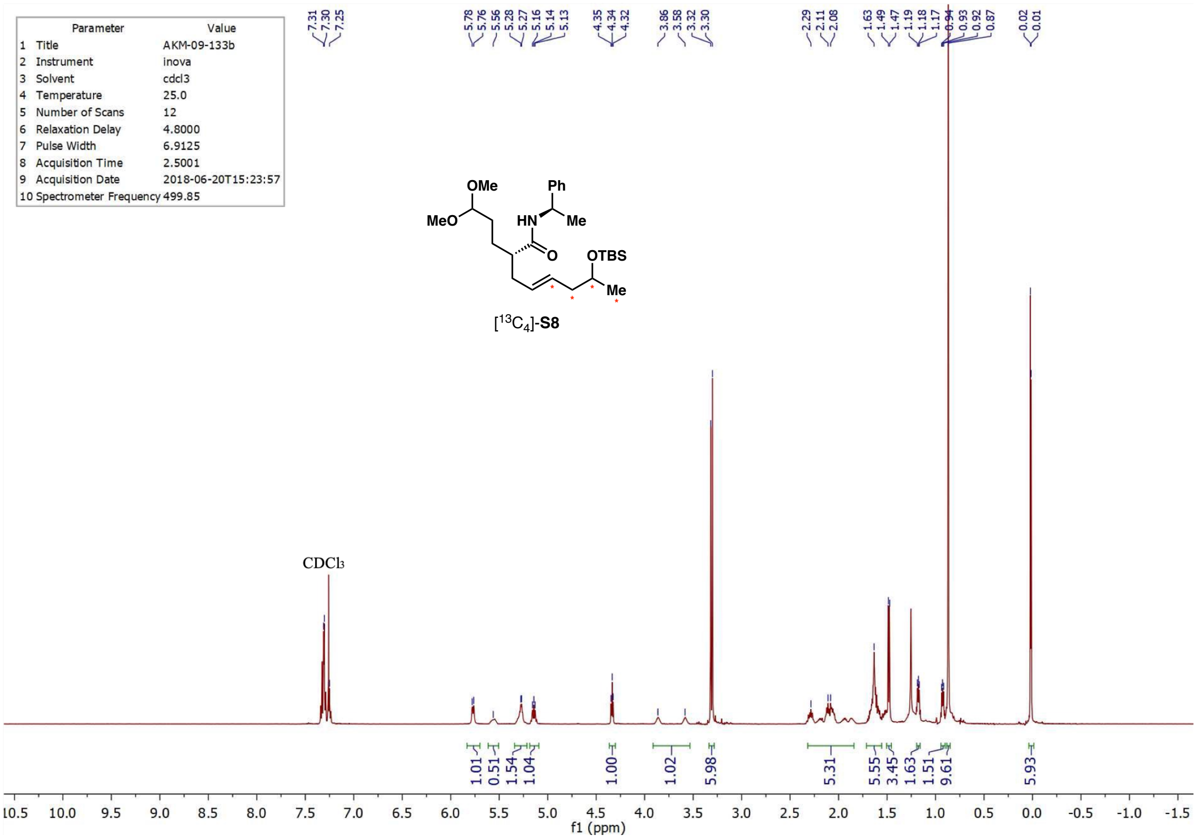

[$^{13}C_4$]-**S8**

	Parameter	Value
1	Title	AKM-09-133b
2	Instrument	inova
3	Solvent	cdcl3
4	Temperature	25.0
5	Number of Scans	12
6	Relaxation Delay	4.8000
7	Pulse Width	6.9125
8	Acquisition Time	2.5001
9	Acquisition Date	2018-06-20T15:23:57
10	Spectrometer Frequency	499.85

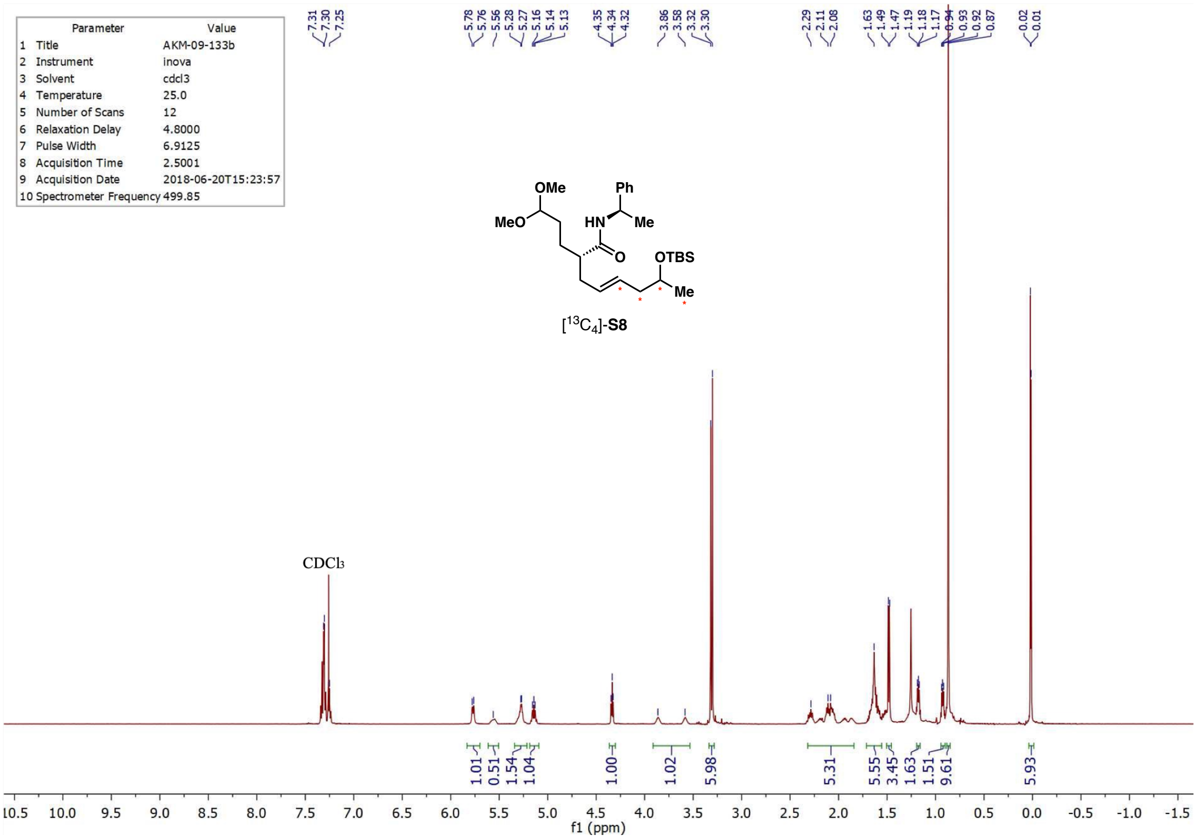
[$^{13}C_4$]-**S8**

	Parameter	Value
1	Title	AKM-09-133b
2	Instrument	inova
3	Solvent	cdcl3
4	Temperature	25.0
5	Number of Scans	12
6	Relaxation Delay	4.8000
7	Pulse Width	6.9125
8	Acquisition Time	2.5001
9	Acquisition Date	2018-06-20T15:23:57
10	Spectrometer Frequency	499.85

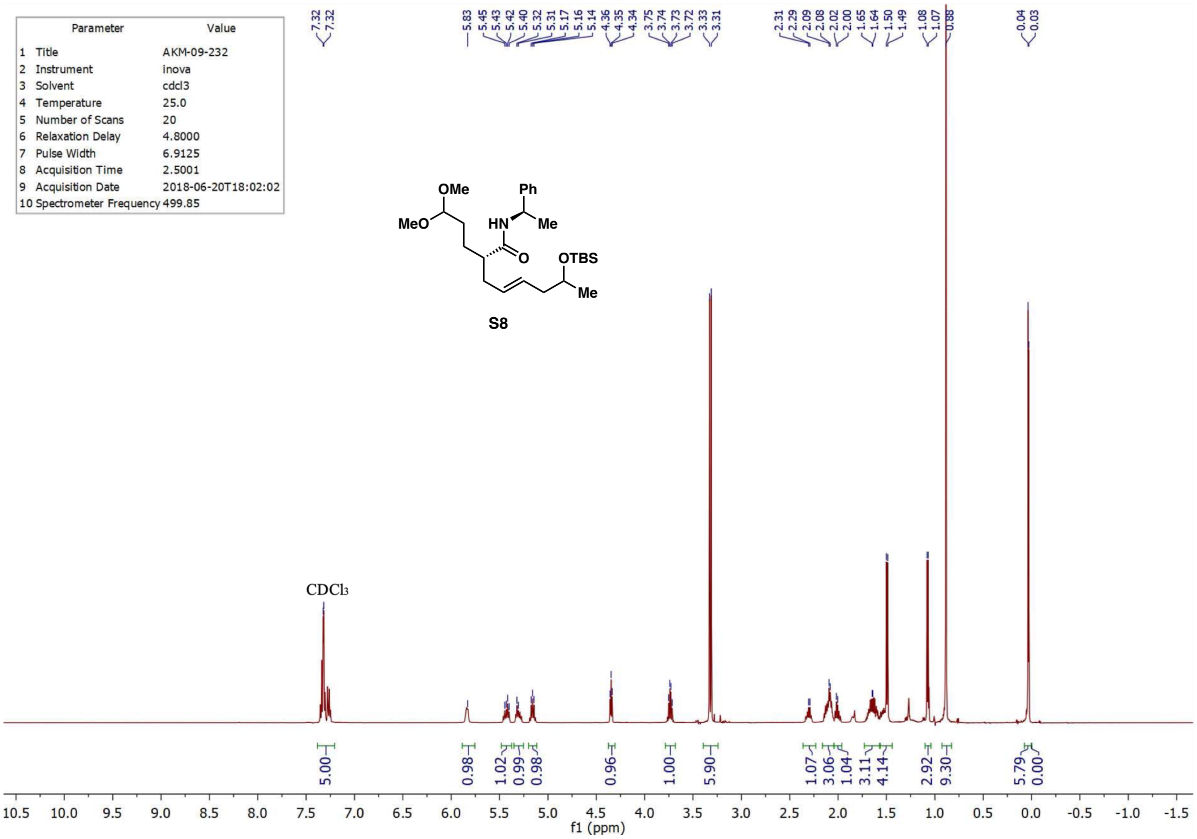

	Parameter	Value
1	Title	AKM-09-232
2	Instrument	inova
3	Solvent	cdcl3
4	Temperature	25.0
5	Number of Scans	20
6	Relaxation Delay	4.8000
7	Pulse Width	6.9125
8	Acquisition Time	2.5001
9	Acquisition Date	2018-06-20T18:02:02
10	Spectrometer Frequency	499.85

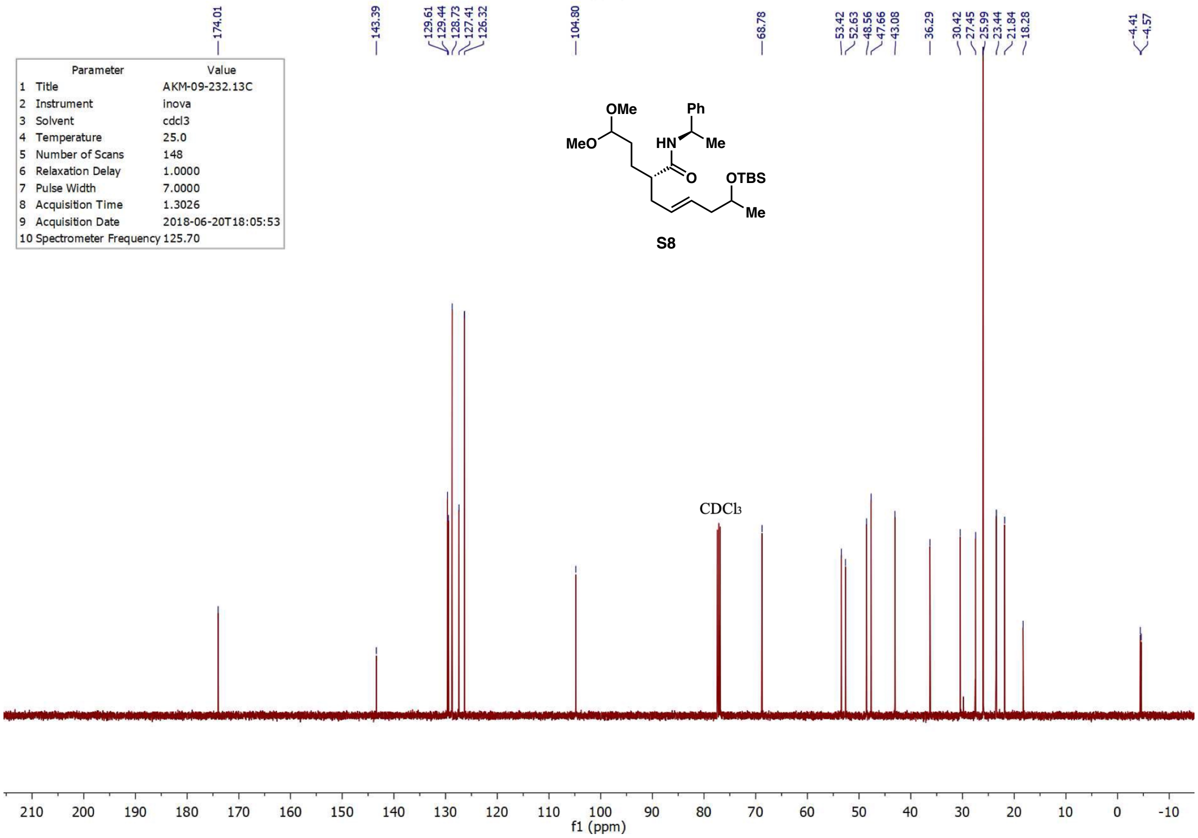

	Parameter	Value
1	Title	AKM-09-232.13C
2	Instrument	inova
3	Solvent	cdcl3
4	Temperature	25.0
5	Number of Scans	148
6	Relaxation Delay	1.0000
7	Pulse Width	7.0000
8	Acquisition Time	1.3026
9	Acquisition Date	2018-06-20T18:05:53
10	Spectrometer Frequency	125.70

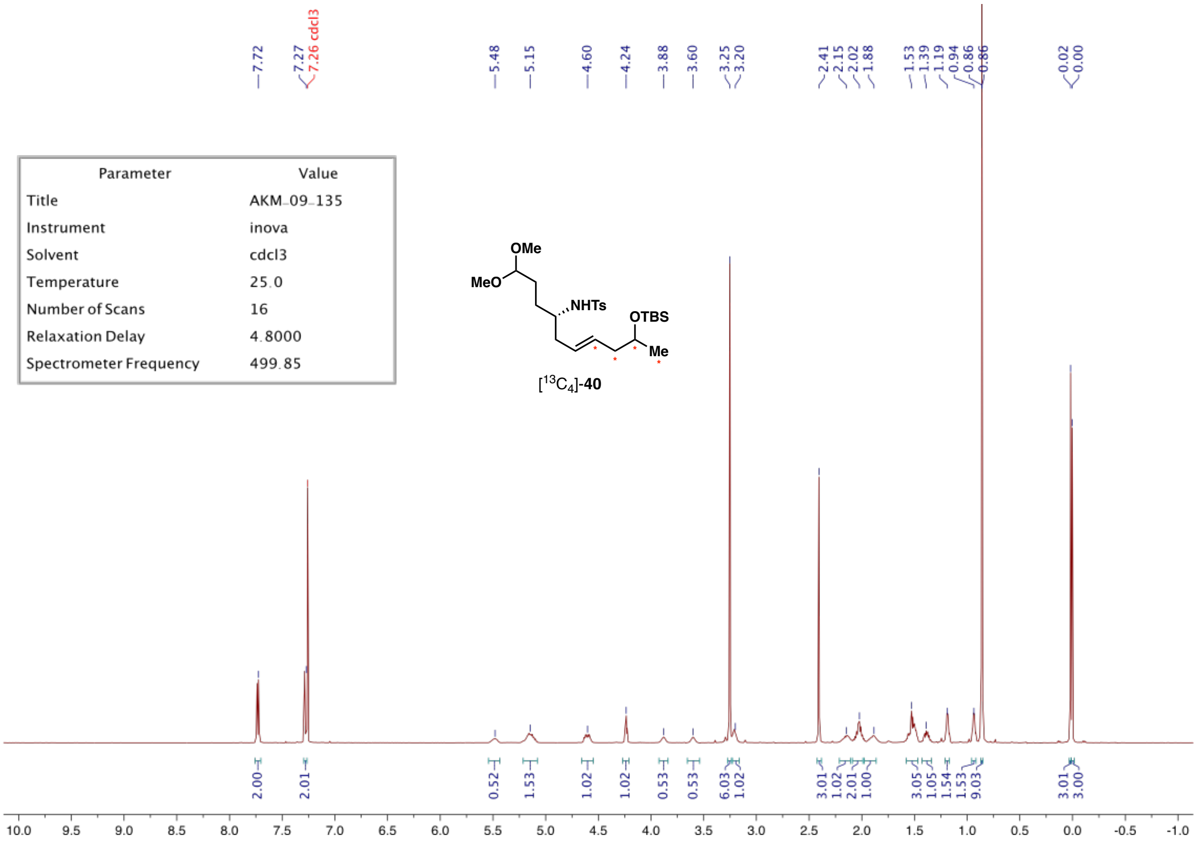

Parameter	Value
Title	AKM_09_135
Instrument	inova
Solvent	cdcl3
Temperature	25.0
Number of Scans	16
Relaxation Delay	4.8000
Spectrometer Frequency	499.85

[^{13}C$_4$]-**40**

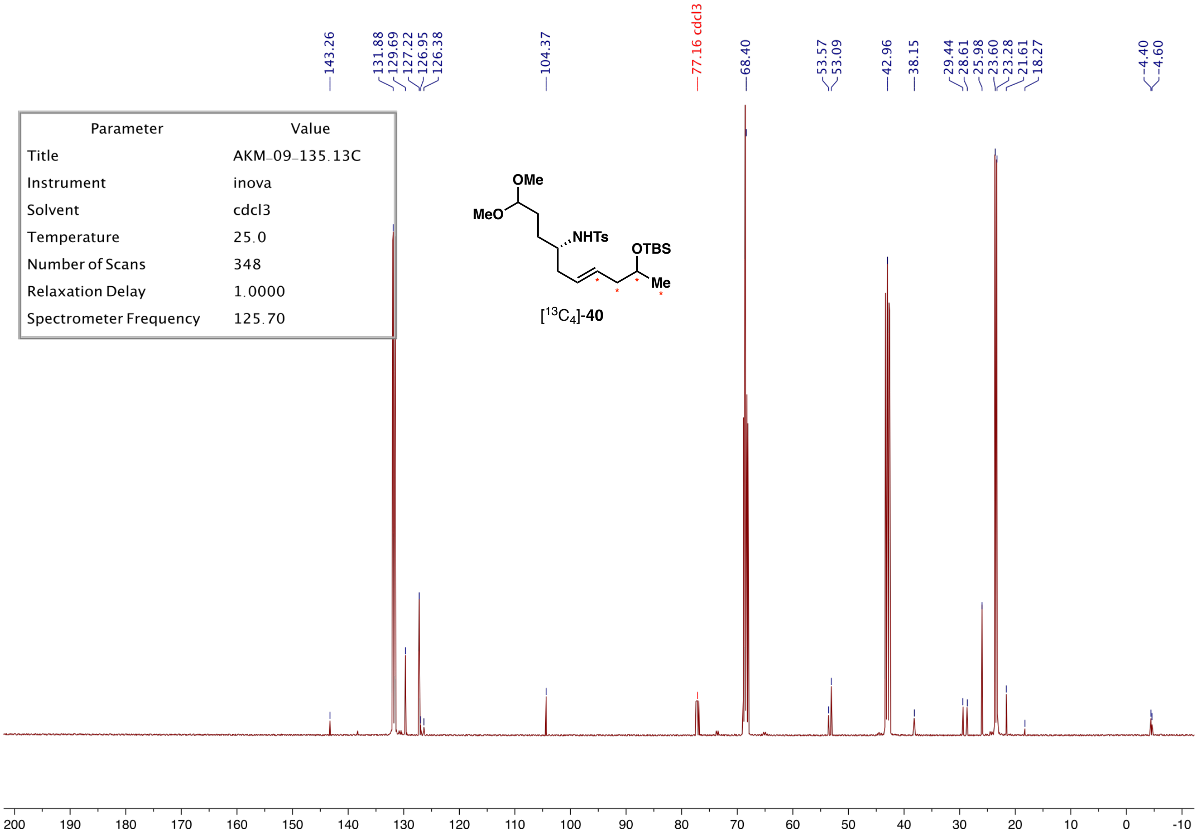

Parameter	Value
Title	AKM_09_135.13C
Instrument	inova
Solvent	cdcl3
Temperature	25.0
Number of Scans	348
Relaxation Delay	1.0000
Spectrometer Frequency	125.70

[^{13}C$_4$]-**40**

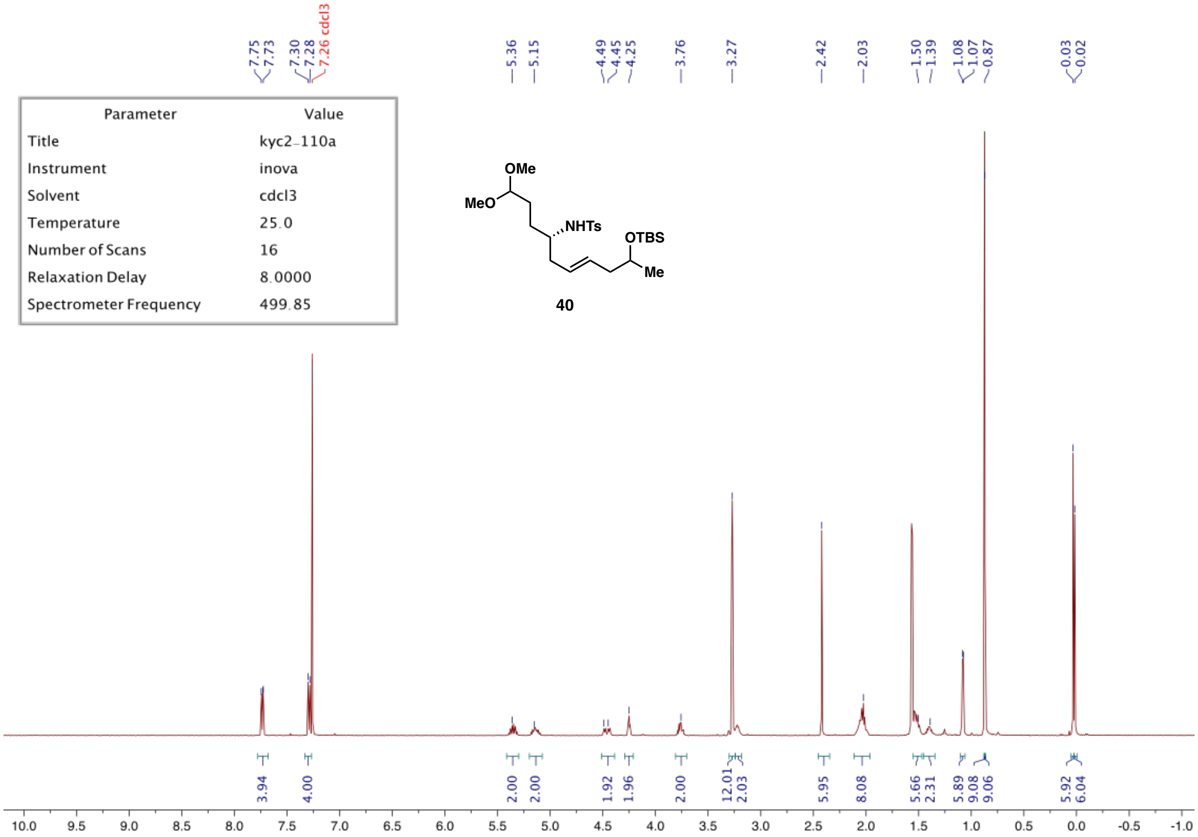

Parameter	Value
Title	kyc2_110a
Instrument	inova
Solvent	cdcl3
Temperature	25.0
Number of Scans	16
Relaxation Delay	8.0000
Spectrometer Frequency	499.85

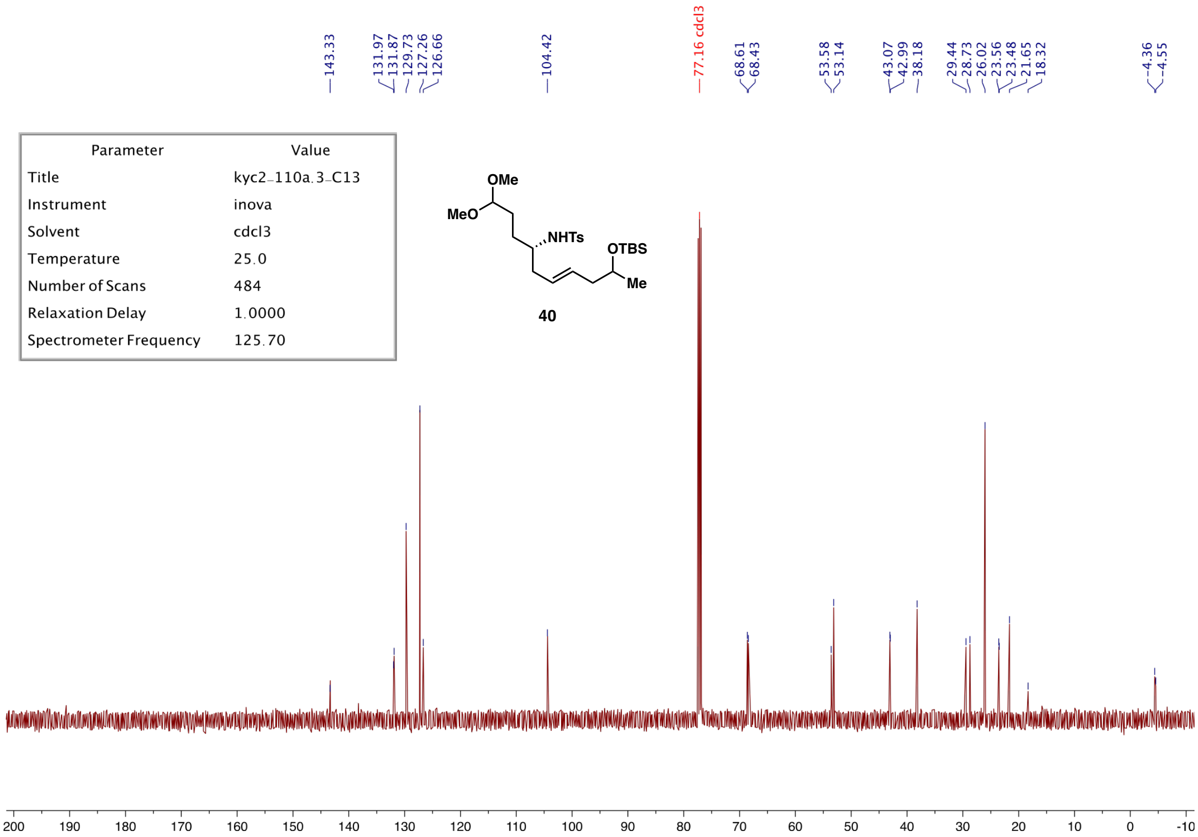

Parameter	Value
Title	kyc2_110a.3_C13
Instrument	inova
Solvent	cdcl3
Temperature	25.0
Number of Scans	484
Relaxation Delay	1.0000
Spectrometer Frequency	125.70

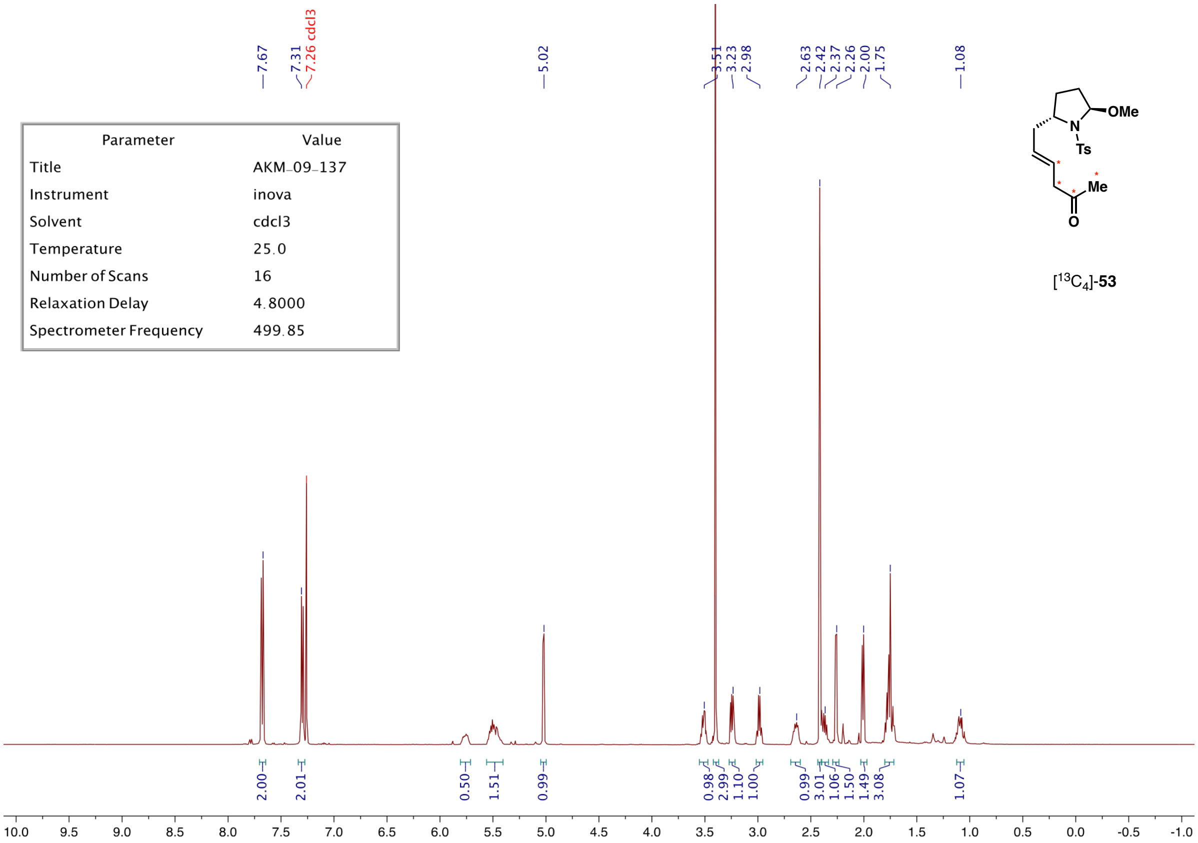

Parameter	Value
Title	AKM_09_137
Instrument	inova
Solvent	cdcl3
Temperature	25.0
Number of Scans	16
Relaxation Delay	4.8000
Spectrometer Frequency	499.85

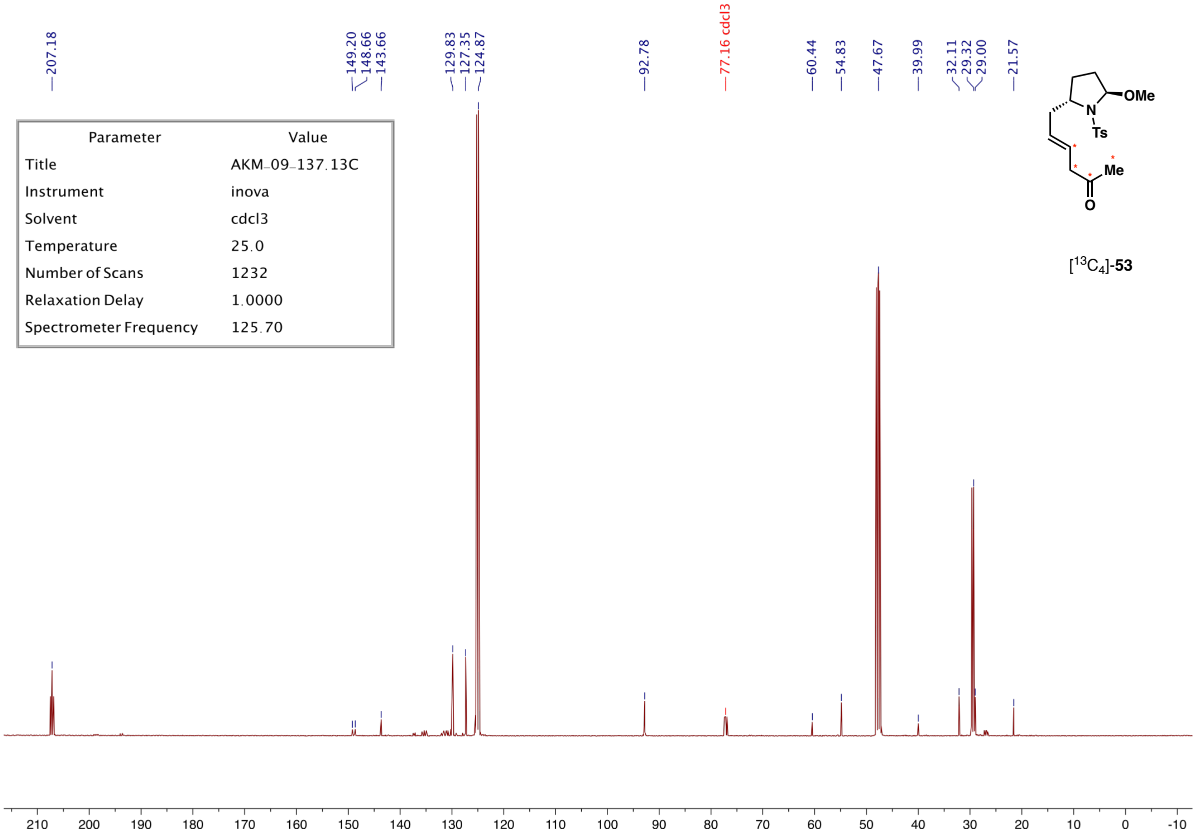

Parameter	Value
Title	AKM_09_137.13C
Instrument	inova
Solvent	cdcl3
Temperature	25.0
Number of Scans	1232
Relaxation Delay	1.0000
Spectrometer Frequency	125.70

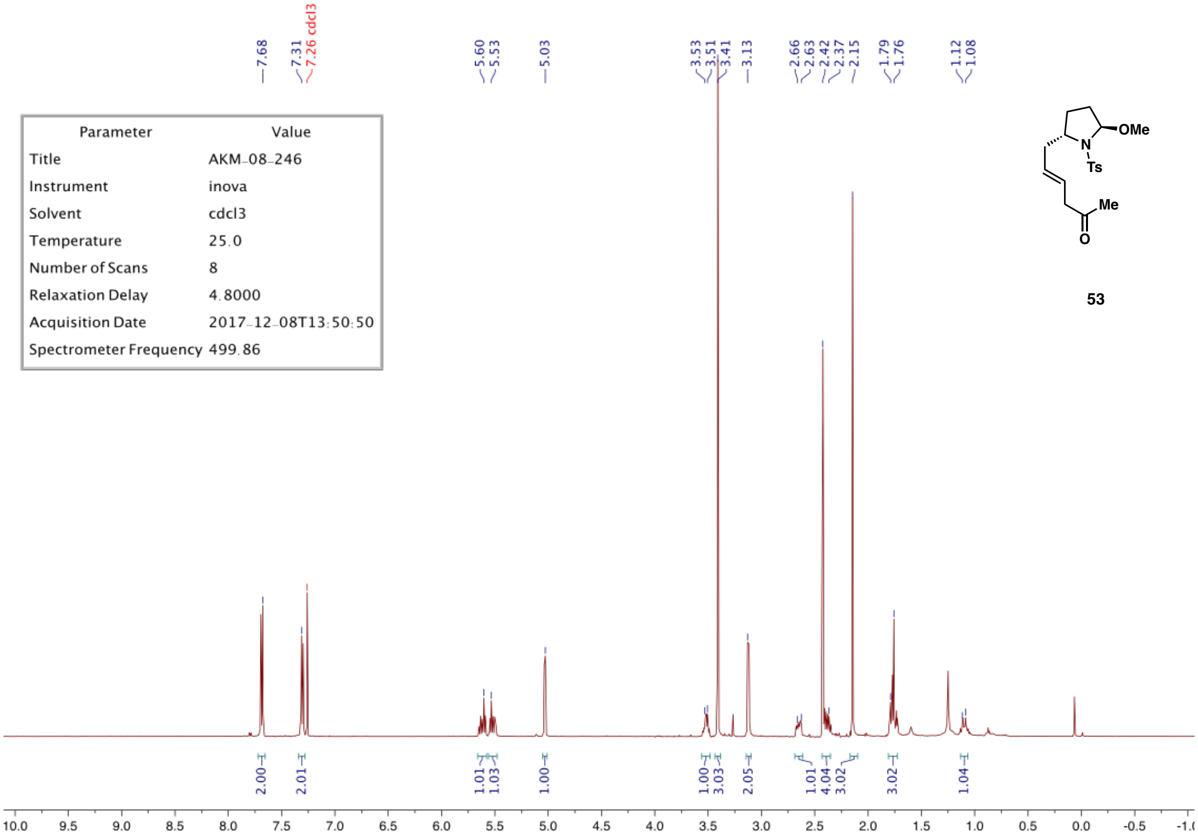

Parameter	Value
Title	AKM_08_246
Instrument	inova
Solvent	cdcl3
Temperature	25.0
Number of Scans	8
Relaxation Delay	4.8000
Acquisition Date	2017_12_08T13:50:50
Spectrometer Frequency	499.86

53

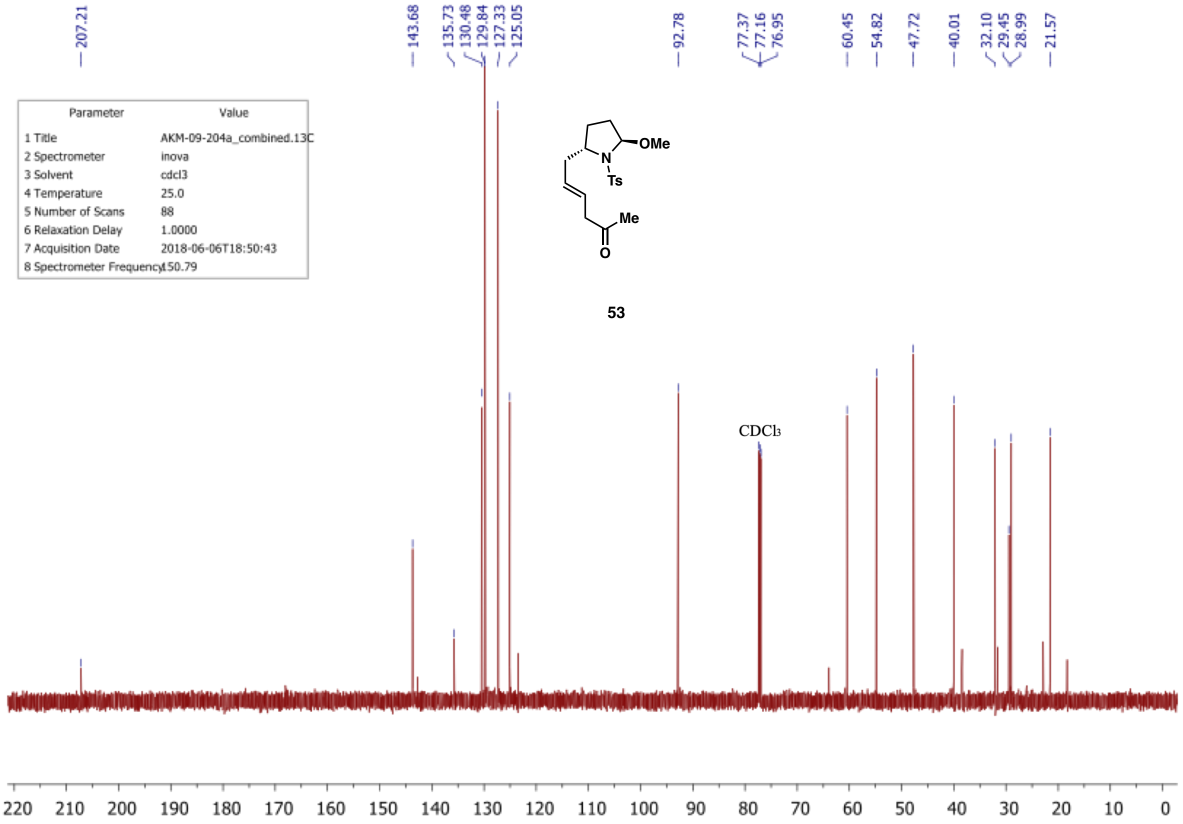

Parameter	Value
1 Title	AKM-09-204a_combined.13C
2 Spectrometer	inova
3 Solvent	cdcl3
4 Temperature	25.0
5 Number of Scans	88
6 Relaxation Delay	1.0000
7 Acquisition Date	2018-06-06T18:50:43
8 Spectrometer Frequency	150.79

53

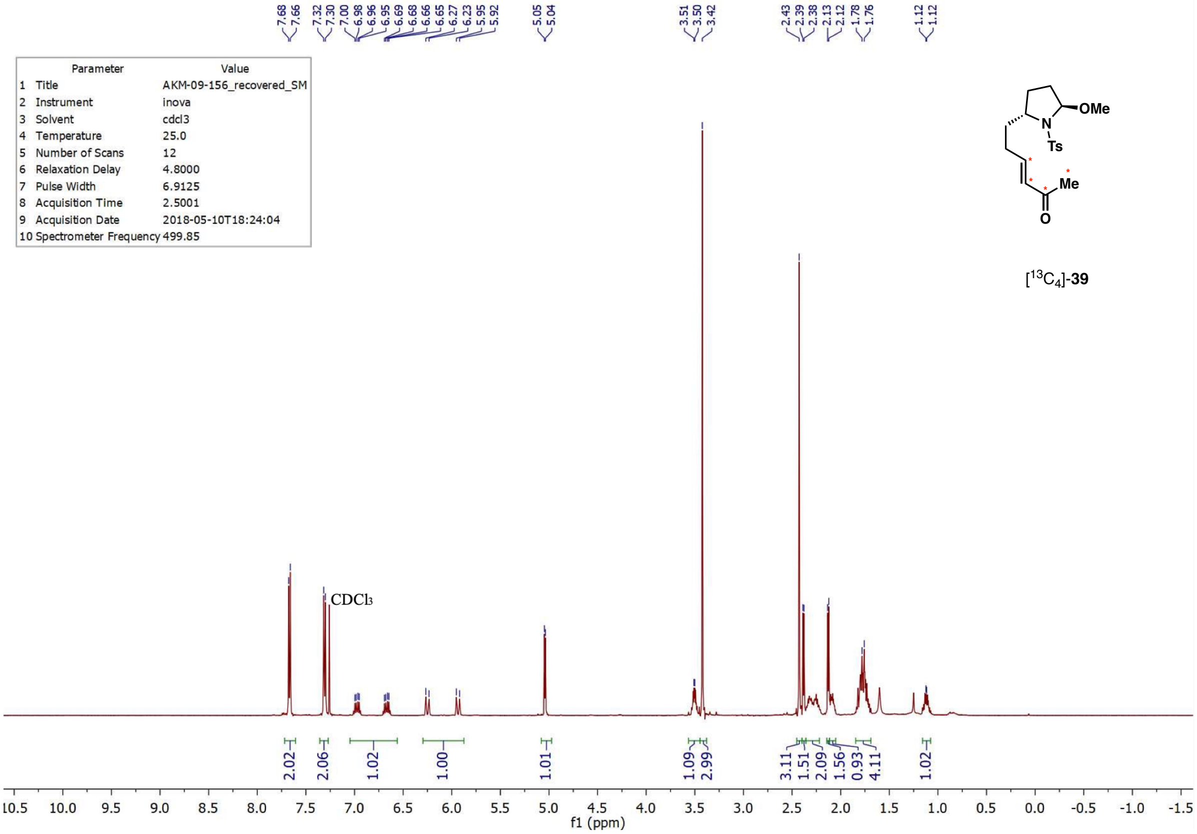

	Parameter	Value
1	Title	AKM-09-156_recovered_SM
2	Instrument	inova
3	Solvent	cdcl3
4	Temperature	25.0
5	Number of Scans	12
6	Relaxation Delay	4.8000
7	Pulse Width	6.9125
8	Acquisition Time	2.5001
9	Acquisition Date	2018-05-10T18:24:04
10	Spectrometer Frequency	499.85

[^{13}C$_4$]-**39**

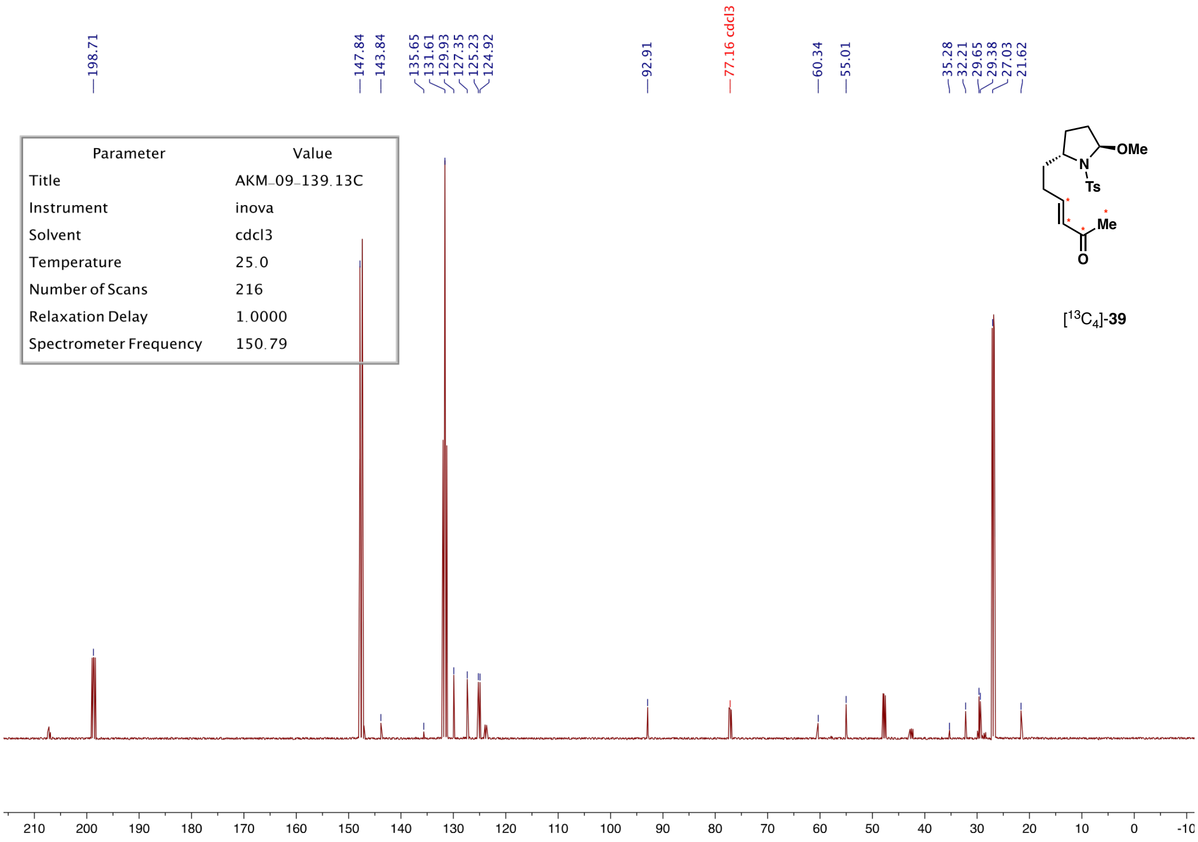

Parameter	Value
Title	AKM_09_139.13C
Instrument	inova
Solvent	cdcl3
Temperature	25.0
Number of Scans	216
Relaxation Delay	1.0000
Spectrometer Frequency	150.79

[^{13}C$_4$]-**39**

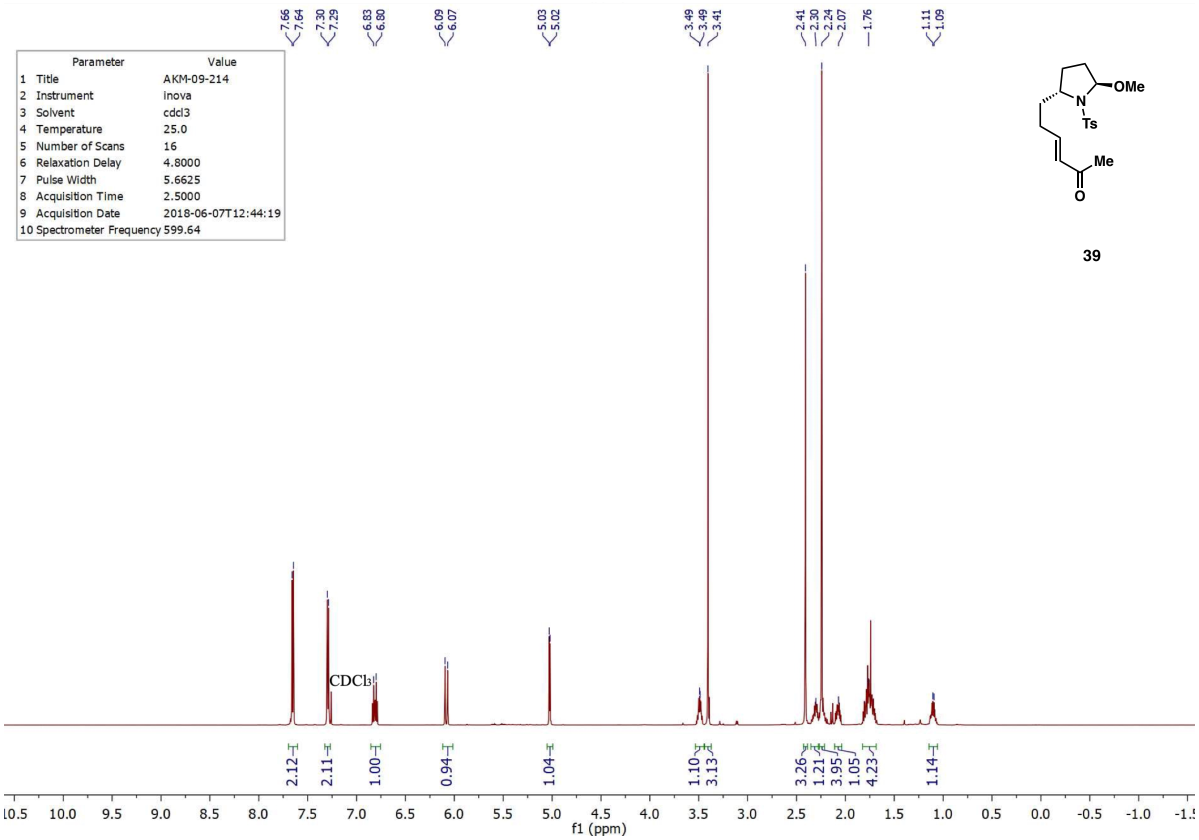

	Parameter	Value
1	Title	AKM-09-214
2	Instrument	inova
3	Solvent	cdcl3
4	Temperature	25.0
5	Number of Scans	16
6	Relaxation Delay	4.8000
7	Pulse Width	5.6625
8	Acquisition Time	2.5000
9	Acquisition Date	2018-06-07T12:44:19
10	Spectrometer Frequency	599.64

39

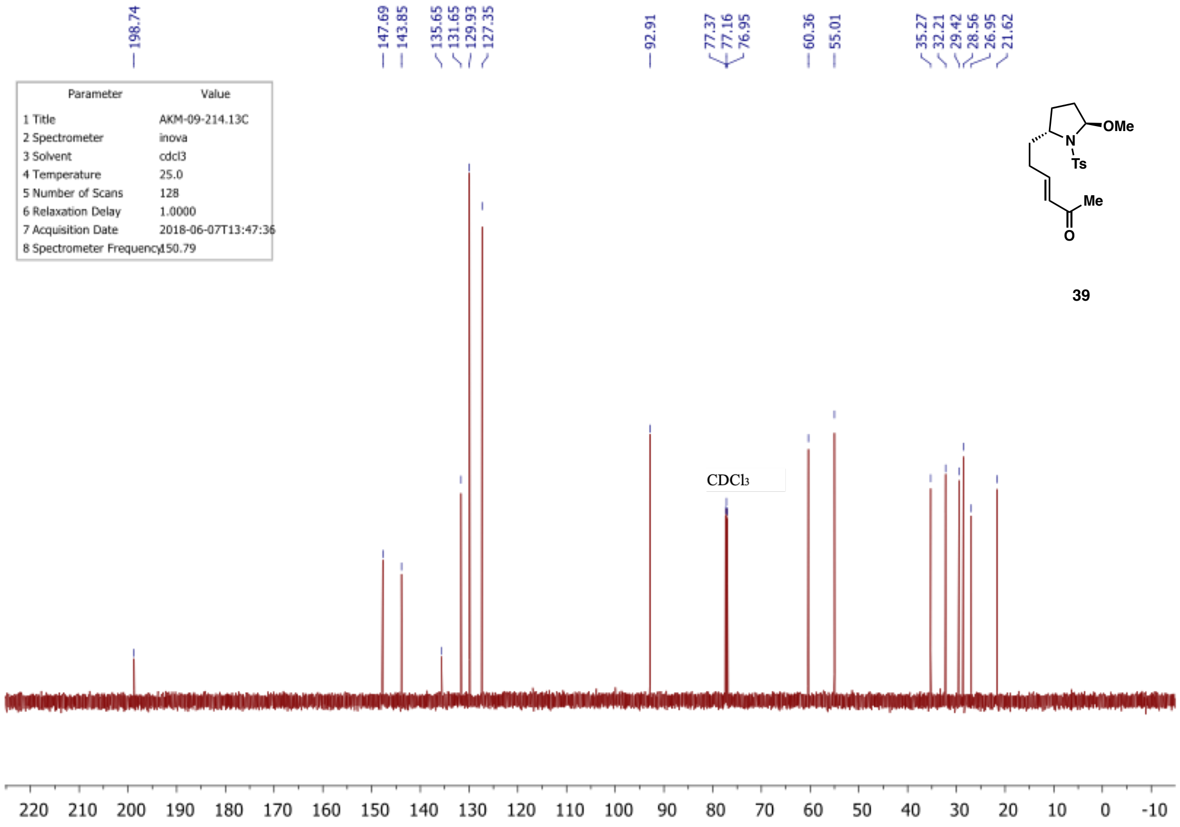

	Parameter	Value
1	Title	AKM-09-214.13C
2	Spectrometer	inova
3	Solvent	cdcl3
4	Temperature	25.0
5	Number of Scans	128
6	Relaxation Delay	1.0000
7	Acquisition Date	2018-06-07T13:47:36
8	Spectrometer Frequency	150.79

39

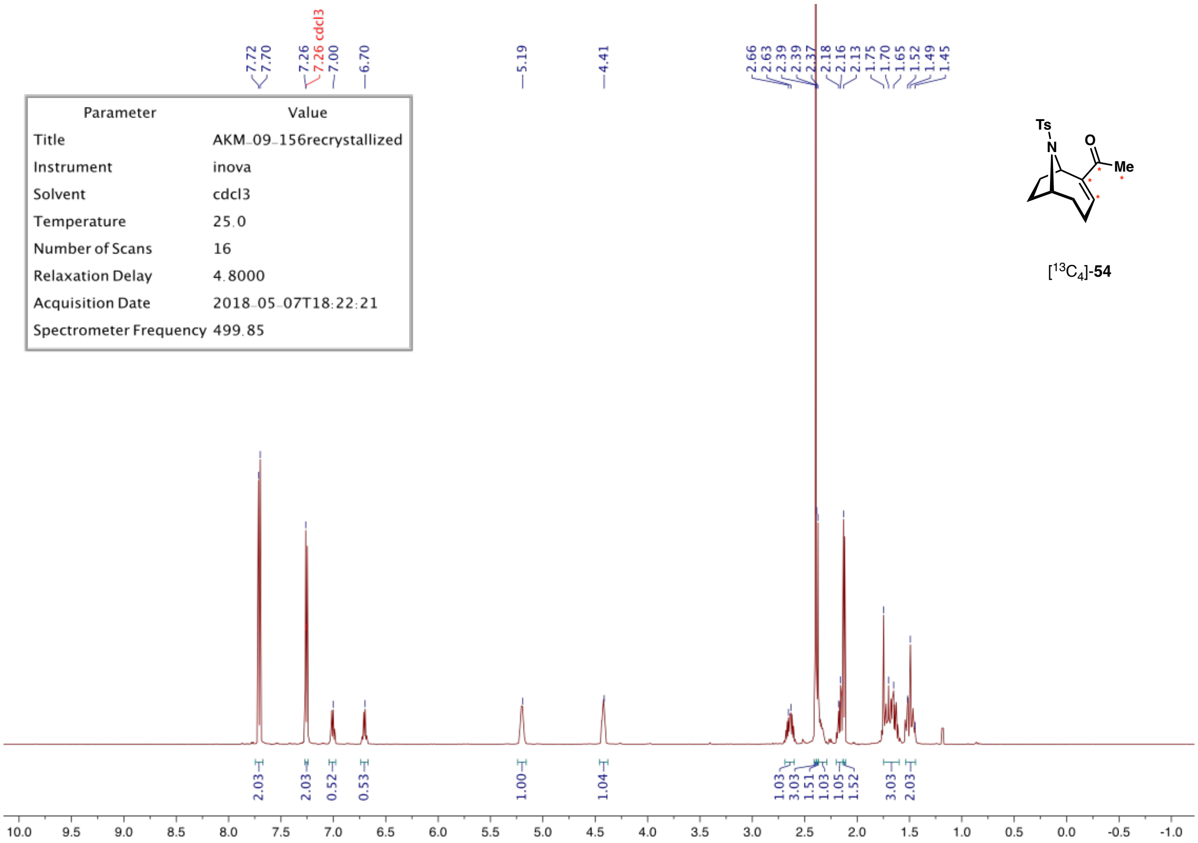

Parameter	Value
Title	AKM_09_156recrystallized
Instrument	inova
Solvent	cdcl3
Temperature	25.0
Number of Scans	16
Relaxation Delay	4.8000
Acquisition Date	2018_05_07T18:22:21
Spectrometer Frequency	499.85

[$^{13}C_4$]-**54**

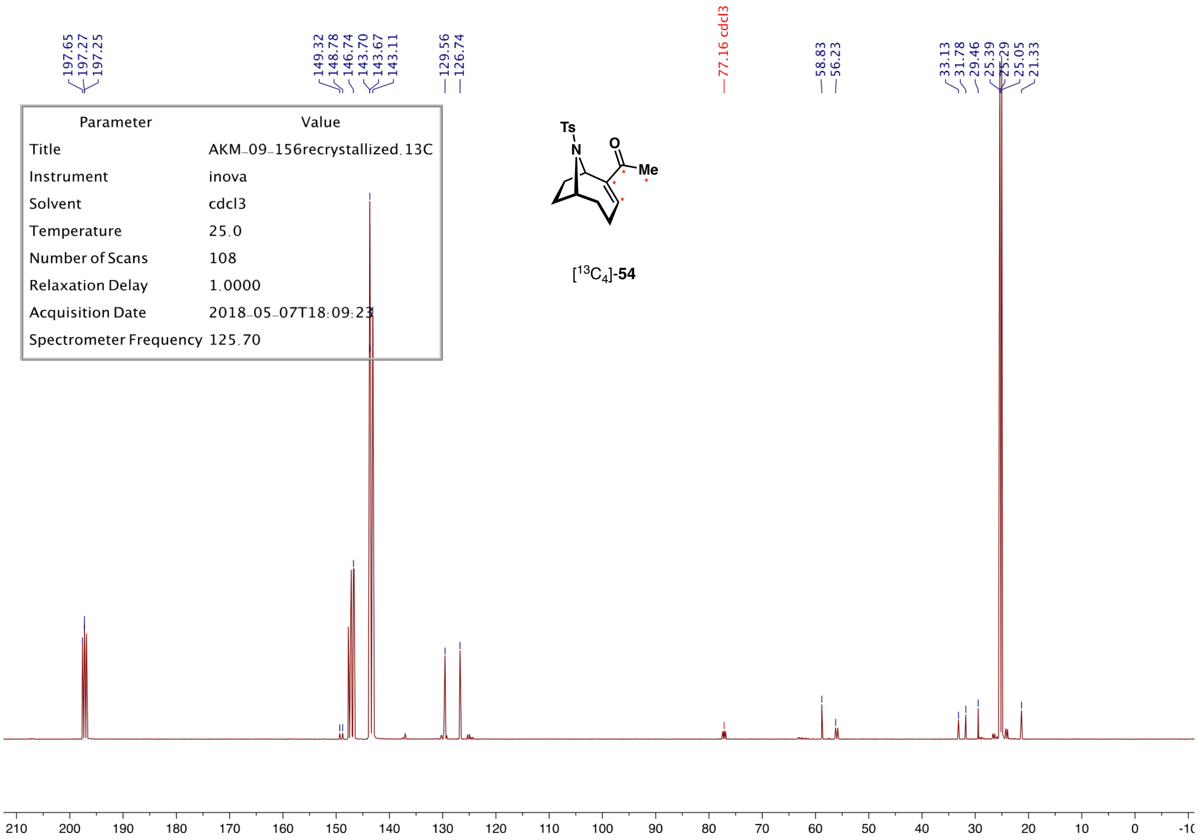

Parameter	Value
Title	AKM_09_156recrystallized.13C
Instrument	inova
Solvent	cdcl3
Temperature	25.0
Number of Scans	108
Relaxation Delay	1.0000
Acquisition Date	2018_05_07T18:09:23
Spectrometer Frequency	125.70

[$^{13}C_4$]-**54**

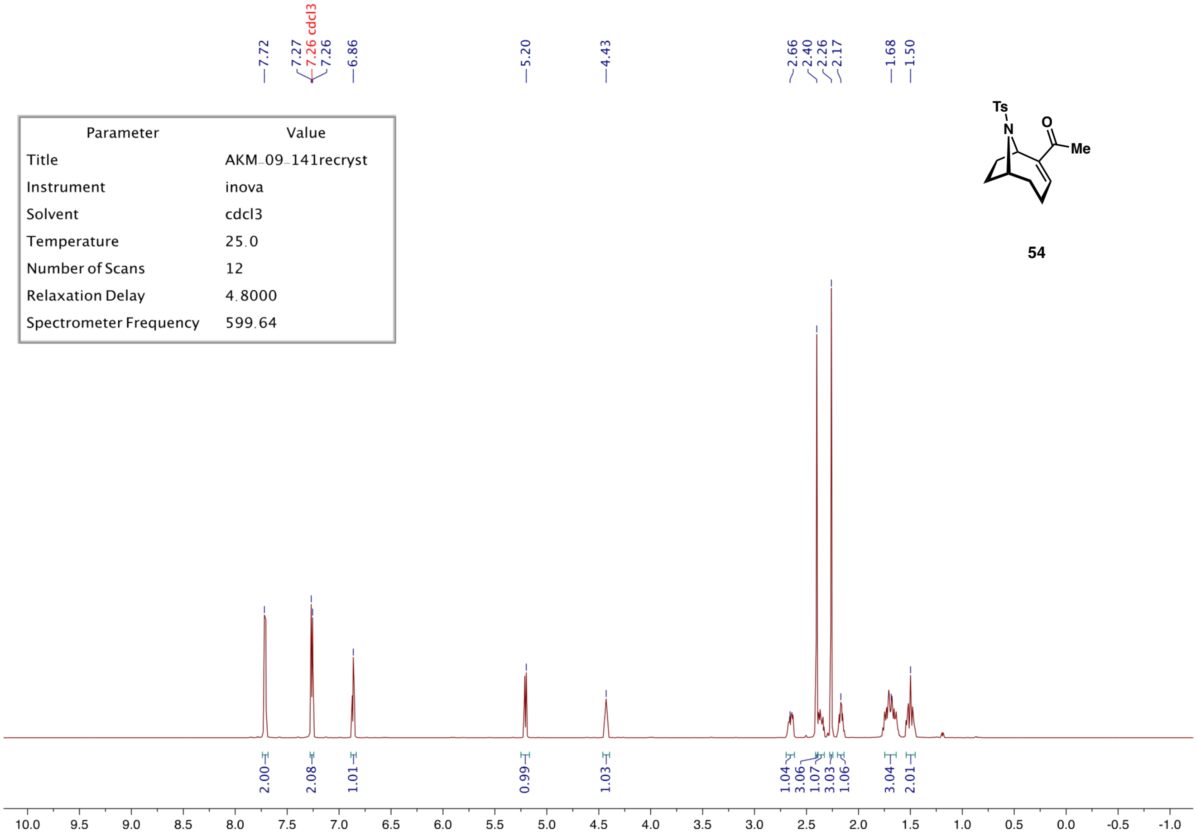

Parameter	Value
Title	AKM_09_141recryst
Instrument	inova
Solvent	cdcl3
Temperature	25.0
Number of Scans	12
Relaxation Delay	4.8000
Spectrometer Frequency	599.64

54

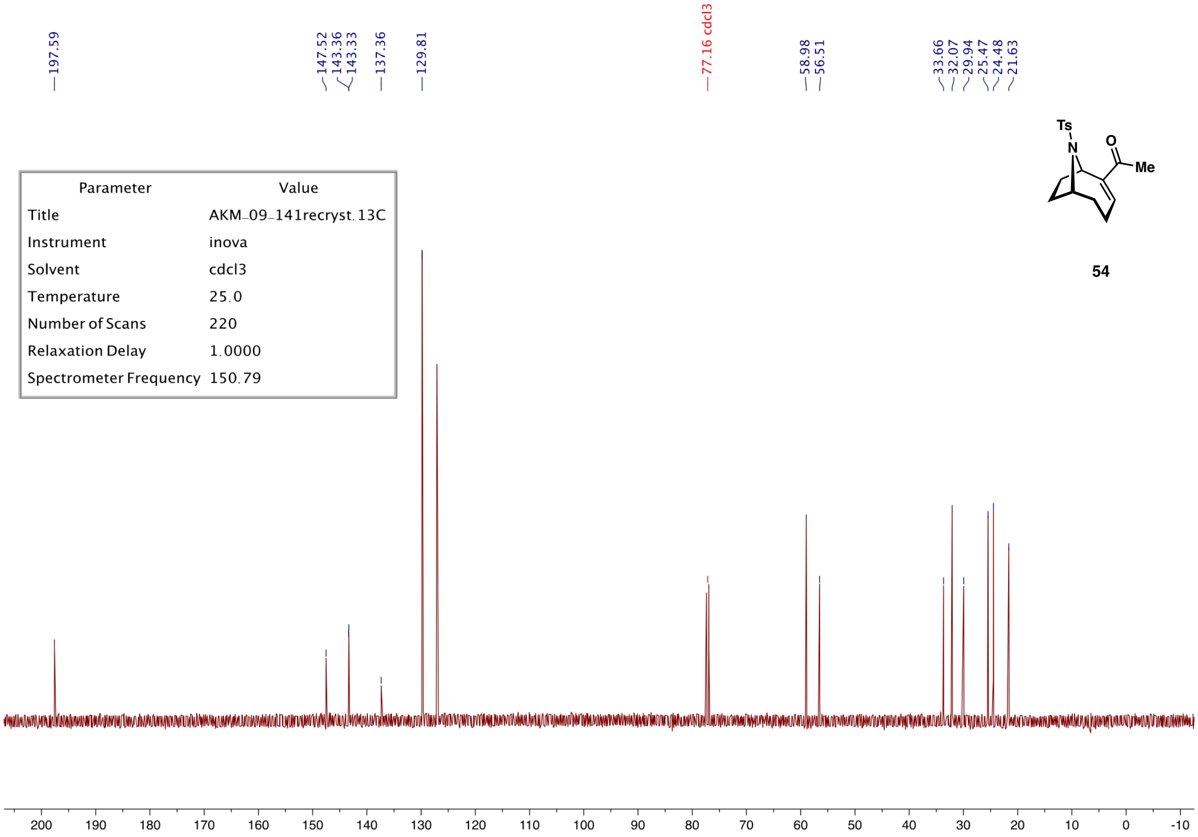

Parameter	Value
Title	AKM_09_141recryst.13C
Instrument	inova
Solvent	cdcl3
Temperature	25.0
Number of Scans	220
Relaxation Delay	1.0000
Spectrometer Frequency	150.79

54

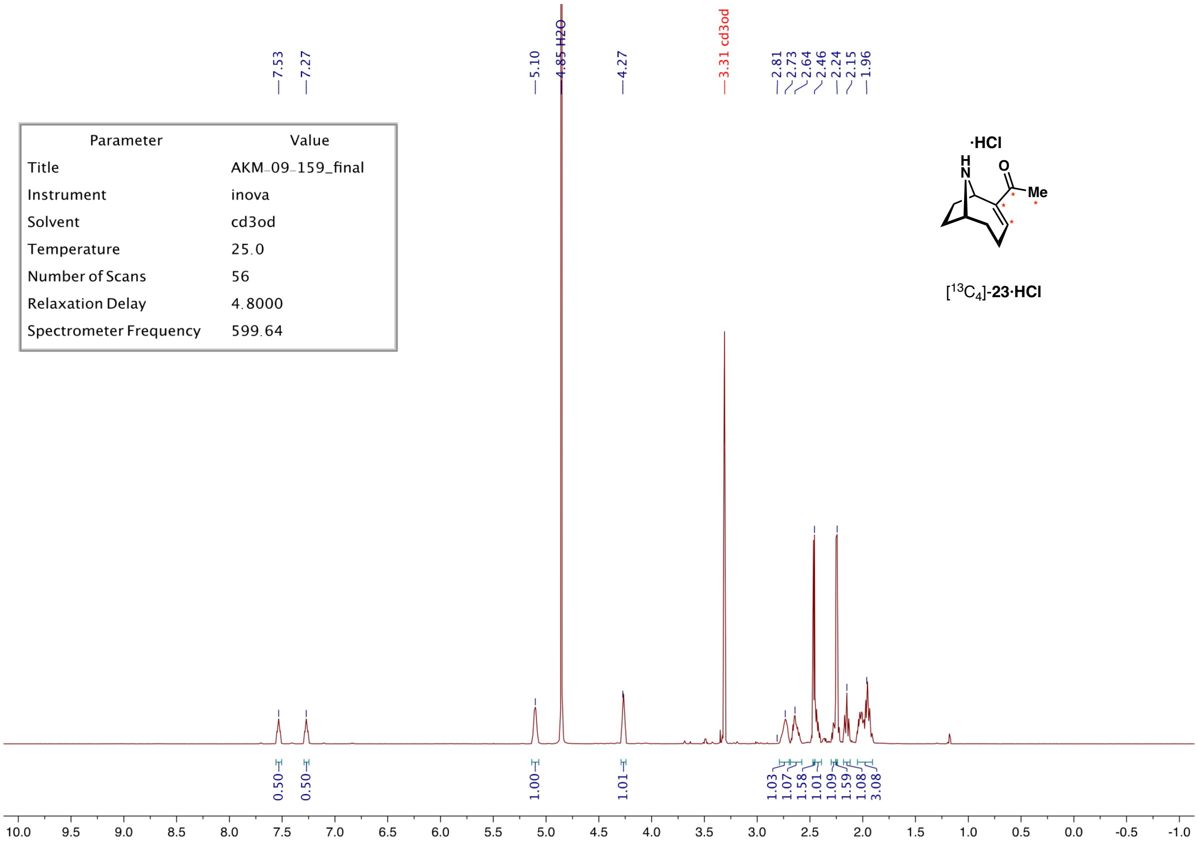

[$^{13}C_4$]-**23·HCl**

Parameter	Value
Title	AKM_09_159_final
Instrument	inova
Solvent	cd3od
Temperature	25.0
Number of Scans	56
Relaxation Delay	4.8000
Spectrometer Frequency	599.64

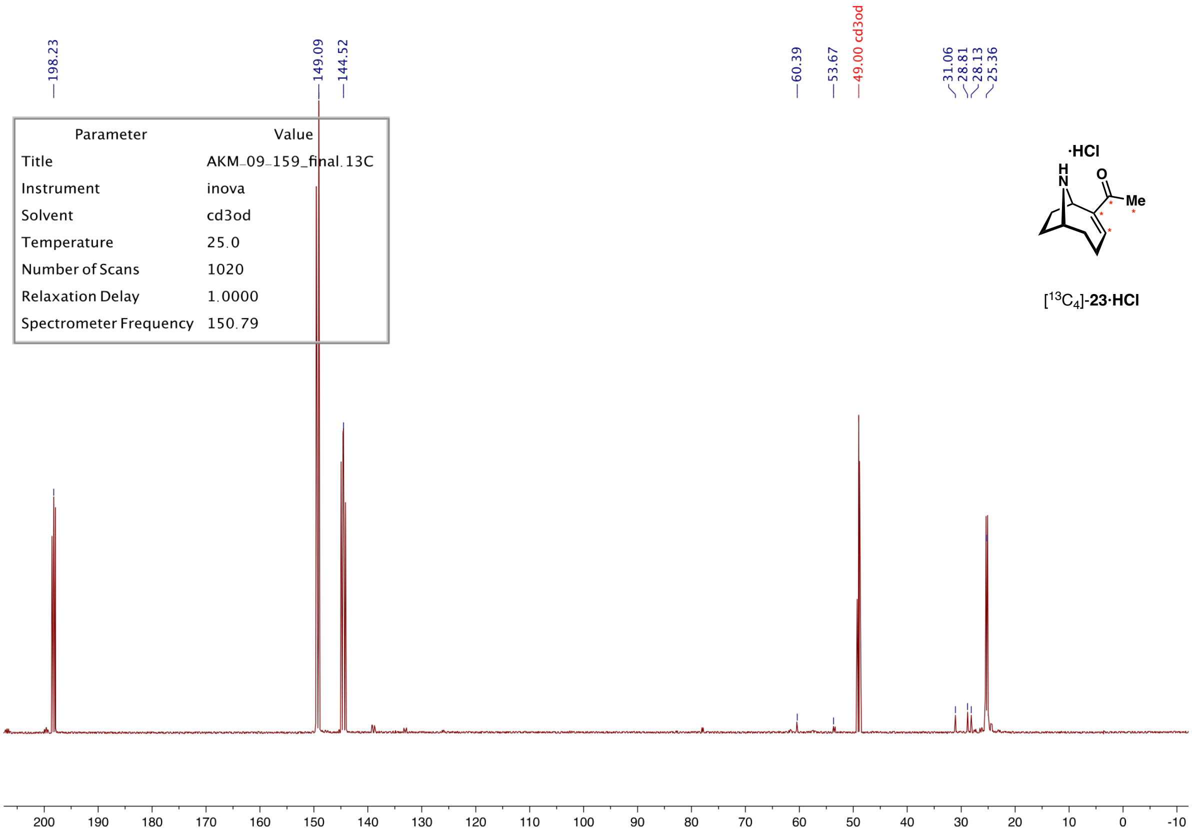

[$^{13}C_4$]-**23·HCl**

Parameter	Value
Title	AKM_09_159_final.13C
Instrument	inova
Solvent	cd3od
Temperature	25.0
Number of Scans	1020
Relaxation Delay	1.0000
Spectrometer Frequency	150.79

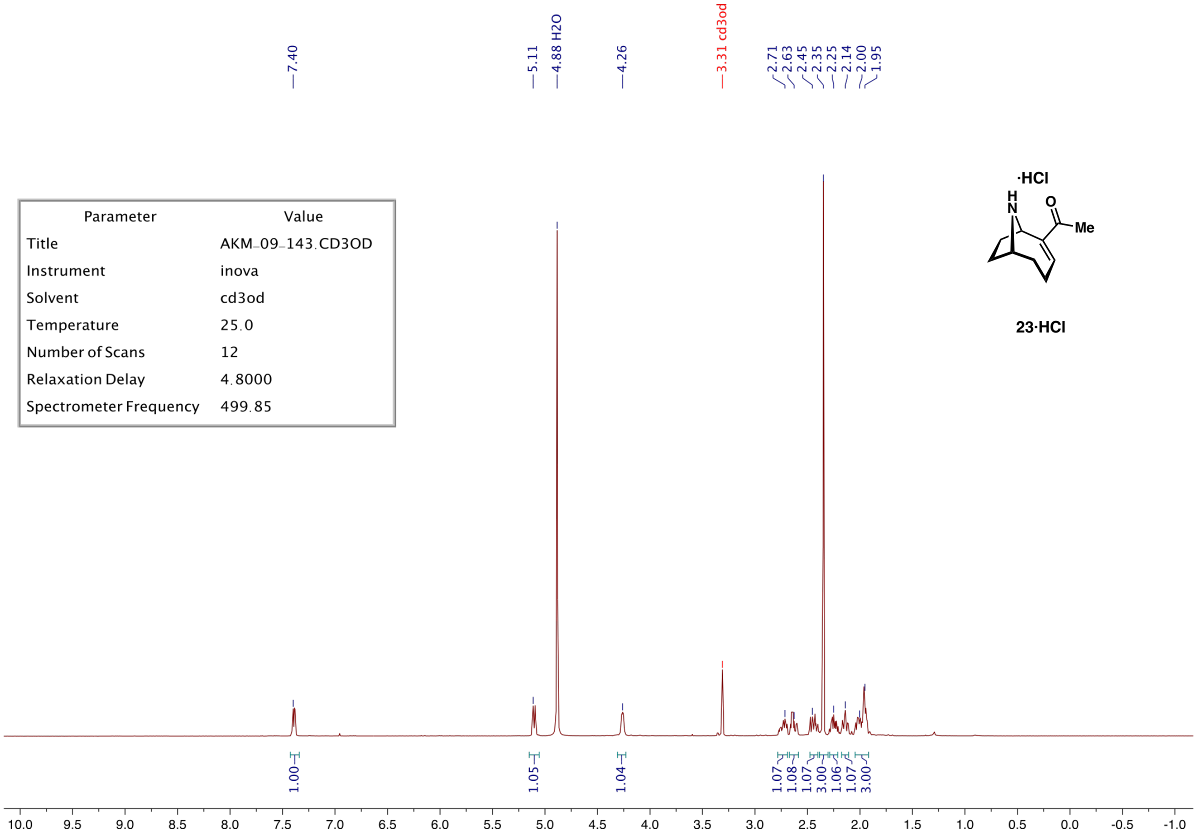

Parameter	Value
Title	AKM_09_143.CD3OD
Instrument	inova
Solvent	cd3od
Temperature	25.0
Number of Scans	12
Relaxation Delay	4.8000
Spectrometer Frequency	499.85

23·HCl

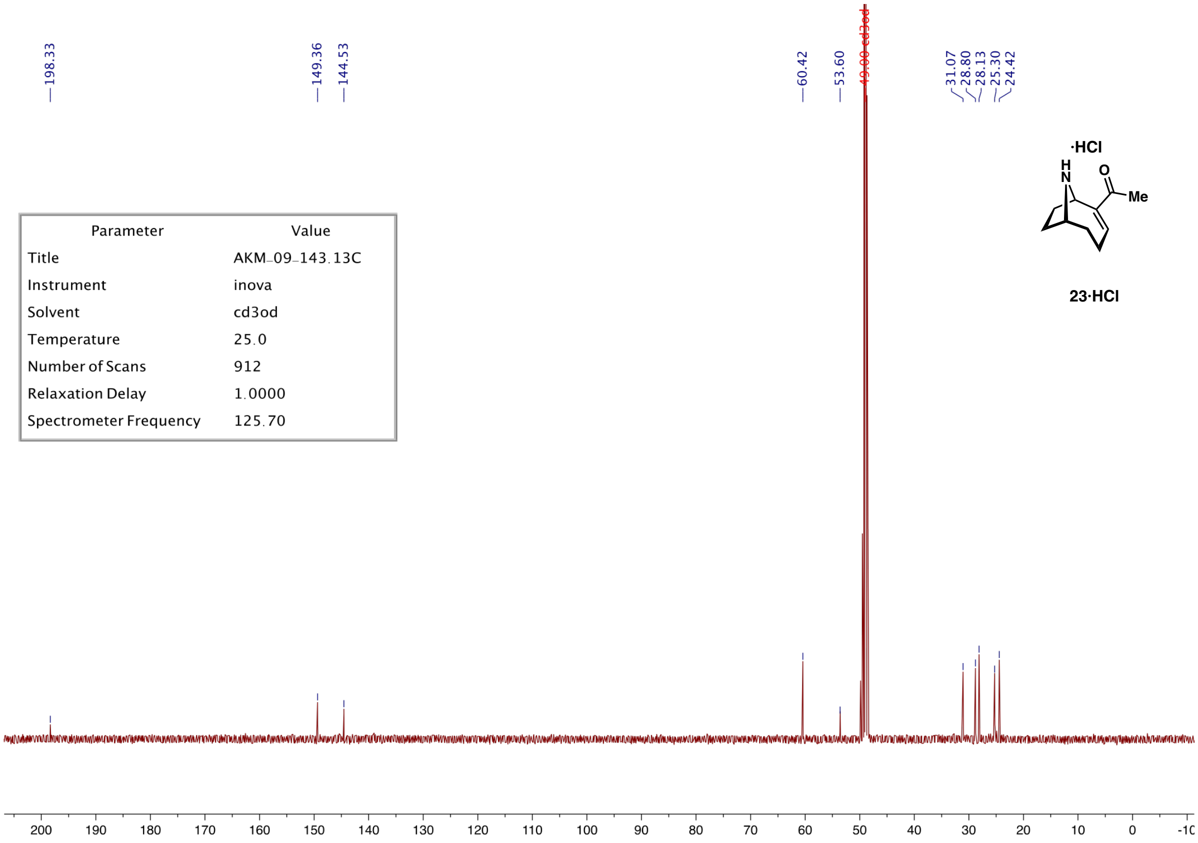

Parameter	Value
Title	AKM_09_143.13C
Instrument	inova
Solvent	cd3od
Temperature	25.0
Number of Scans	912
Relaxation Delay	1.0000
Spectrometer Frequency	125.70

23·HCl

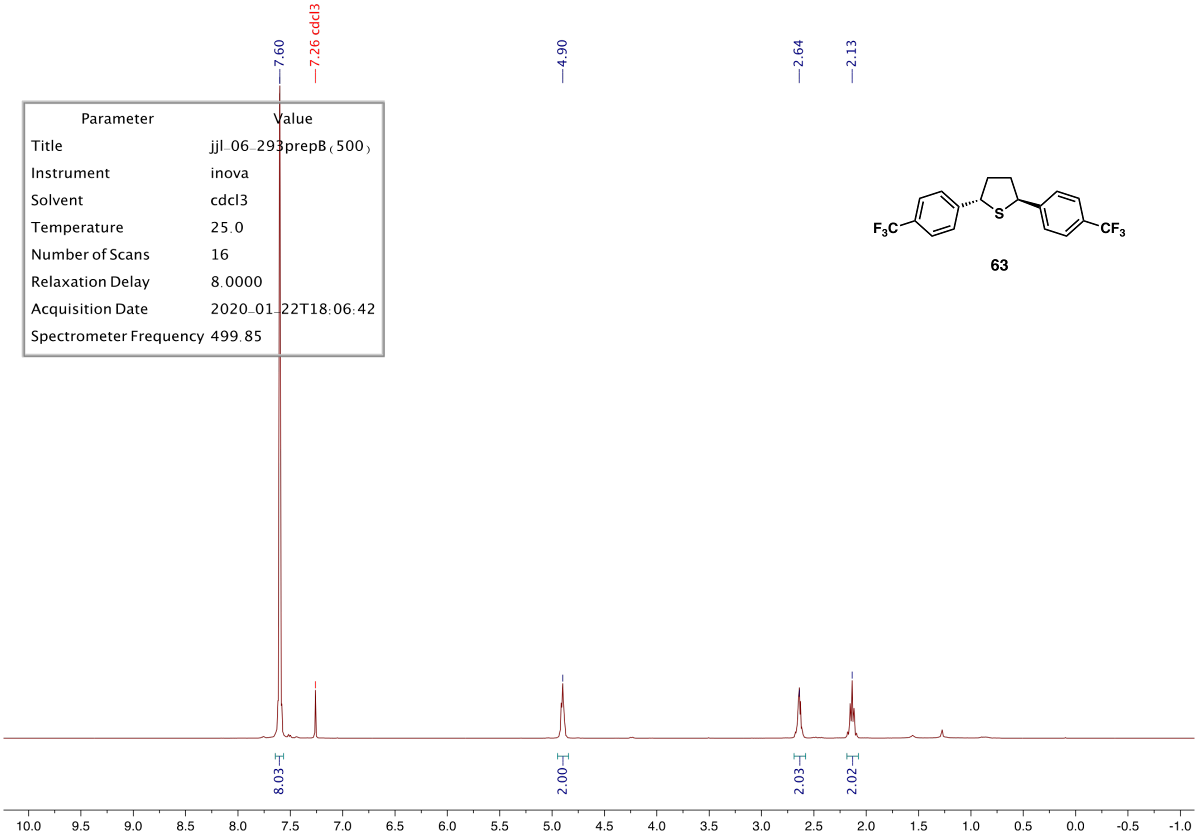

Parameter	Value
Title	jjl_06_293prepB(500)
Instrument	inova
Solvent	cdcl3
Temperature	25.0
Number of Scans	16
Relaxation Delay	8.0000
Acquisition Date	2020_01_22T18:06:42
Spectrometer Frequency	499.85

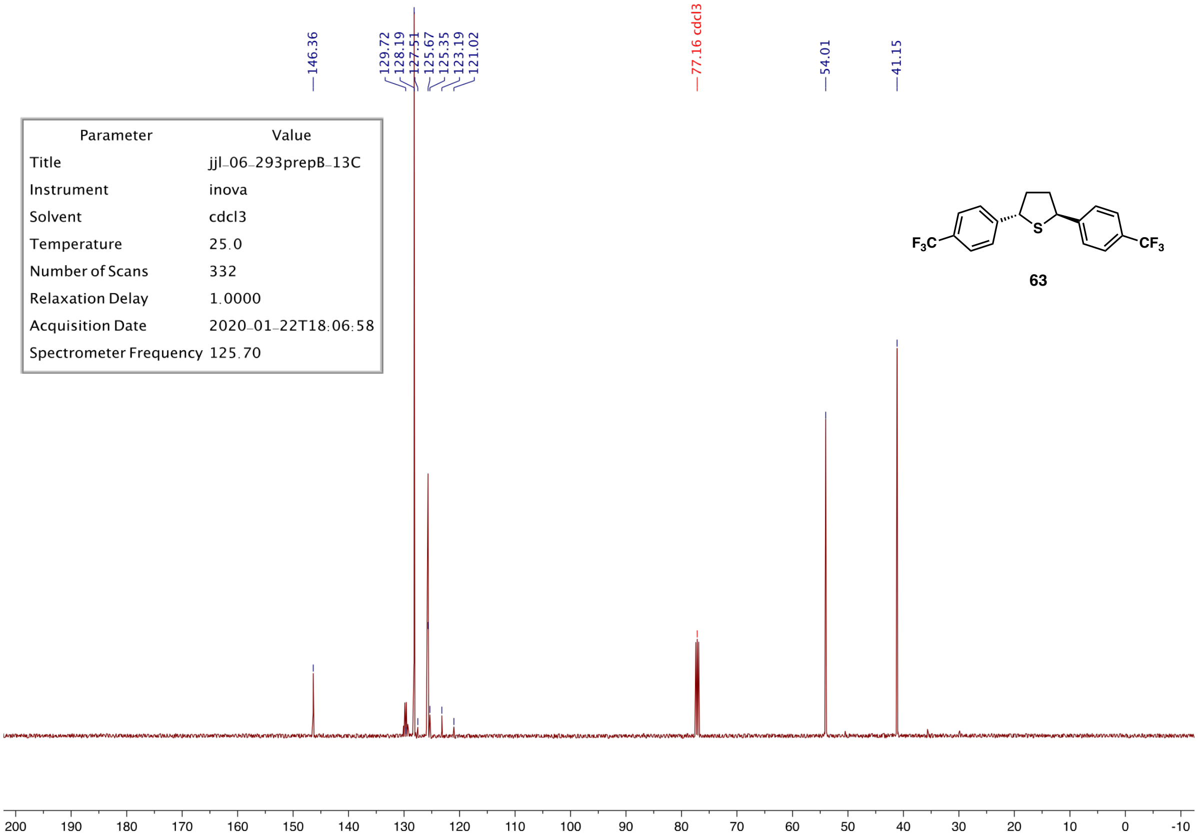

Parameter	Value
Title	jjl_06_293prepB_13C
Instrument	inova
Solvent	cdcl3
Temperature	25.0
Number of Scans	332
Relaxation Delay	1.0000
Acquisition Date	2020_01_22T18:06:58
Spectrometer Frequency	125.70

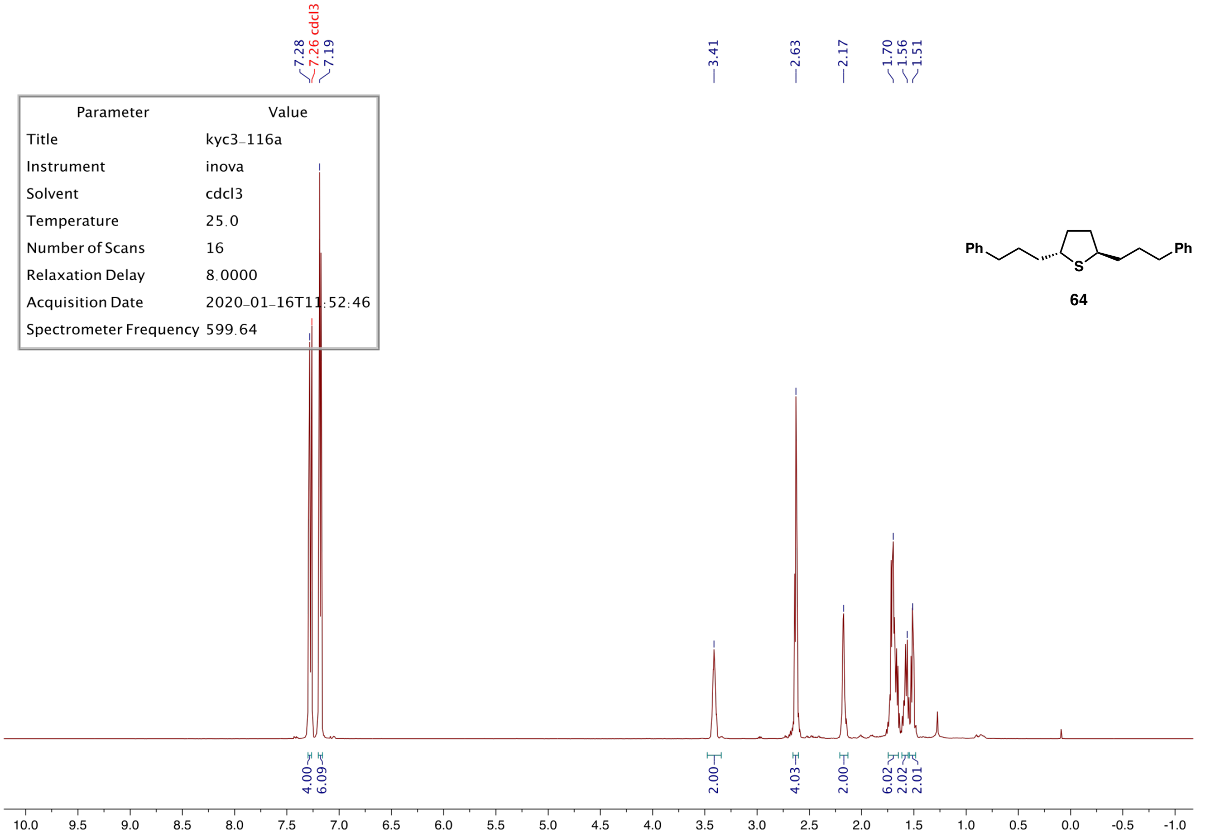

Parameter	Value
Title	kyc3_116a
Instrument	inova
Solvent	cdcl3
Temperature	25.0
Number of Scans	16
Relaxation Delay	8.0000
Acquisition Date	2020-01-16T11:52:46
Spectrometer Frequency	599.64

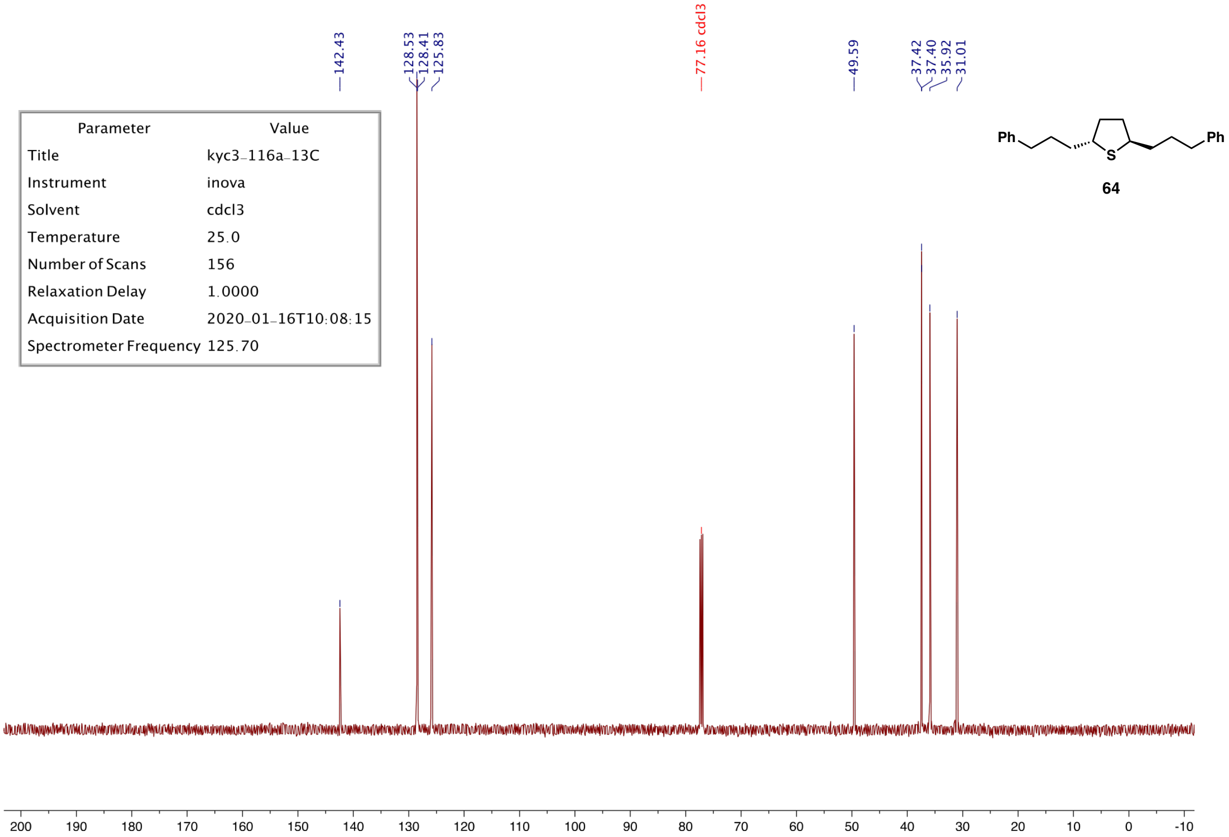

Parameter	Value
Title	kyc3_116a_13C
Instrument	inova
Solvent	cdcl3
Temperature	25.0
Number of Scans	156
Relaxation Delay	1.0000
Acquisition Date	2020-01-16T10:08:15
Spectrometer Frequency	125.70

Parameter	Value
Title	kyc3_248a2
Instrument	inova
Solvent	cdcl3
Temperature	25.0
Number of Scans	16
Relaxation Delay	8.0000
Acquisition Date	2020-01-19T14:19:48
Spectrometer Frequency	599.64

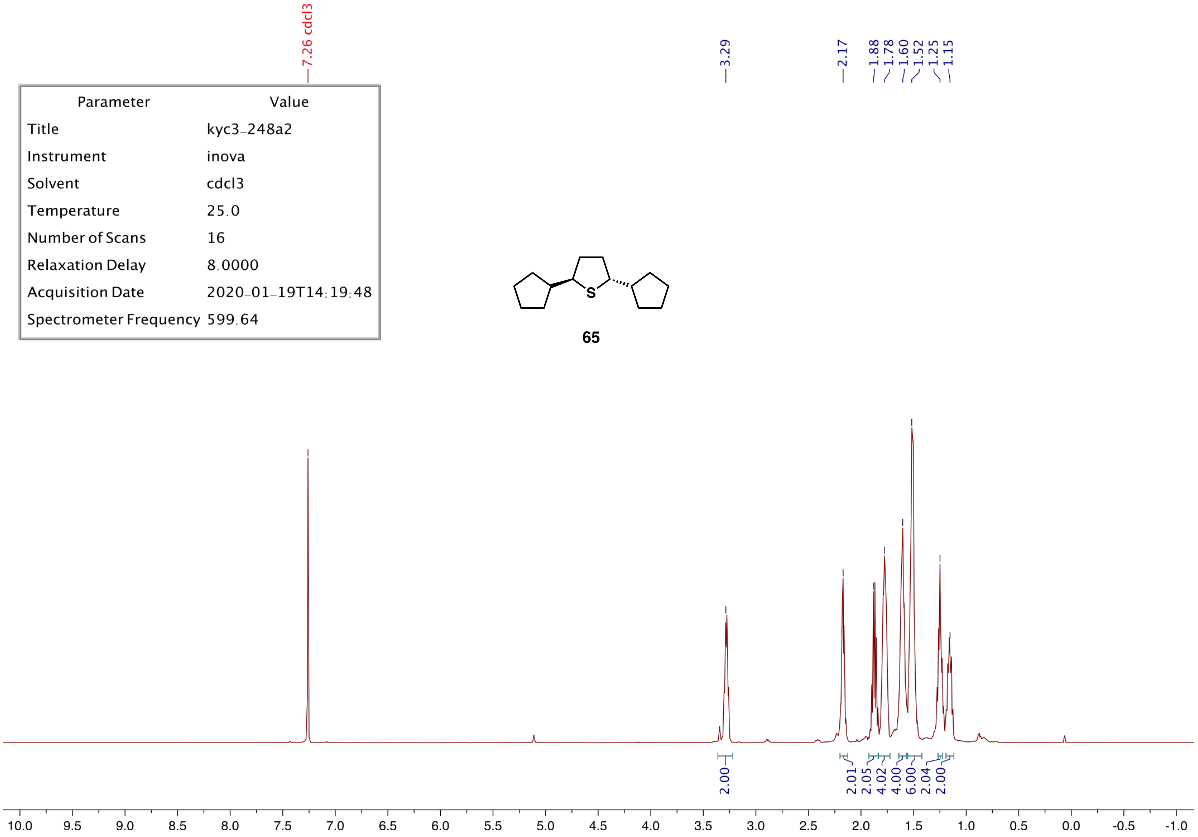

65

Parameter	Value
Title	kyc3_248a2_13C
Instrument	inova
Solvent	cdcl3
Temperature	25.0
Number of Scans	156
Relaxation Delay	1.0000
Acquisition Date	2020-01-19T13:30:22
Spectrometer Frequency	125.70

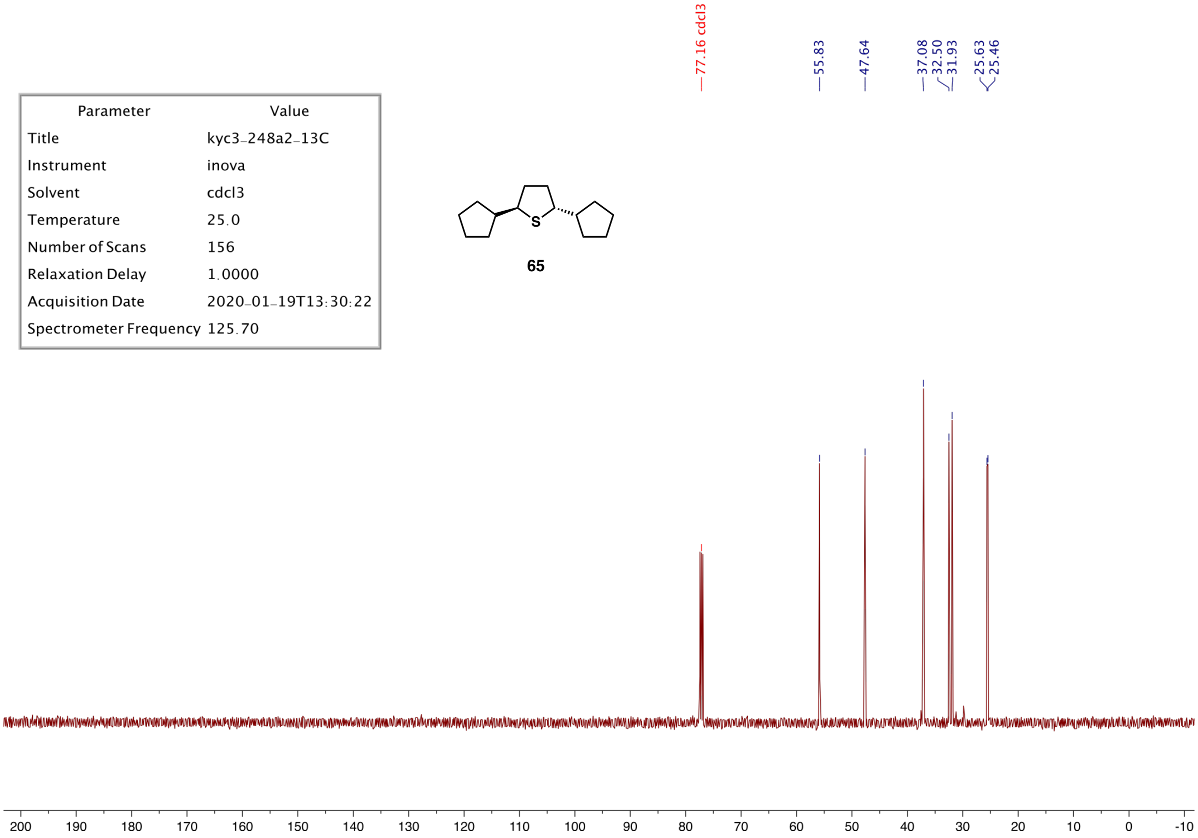

65

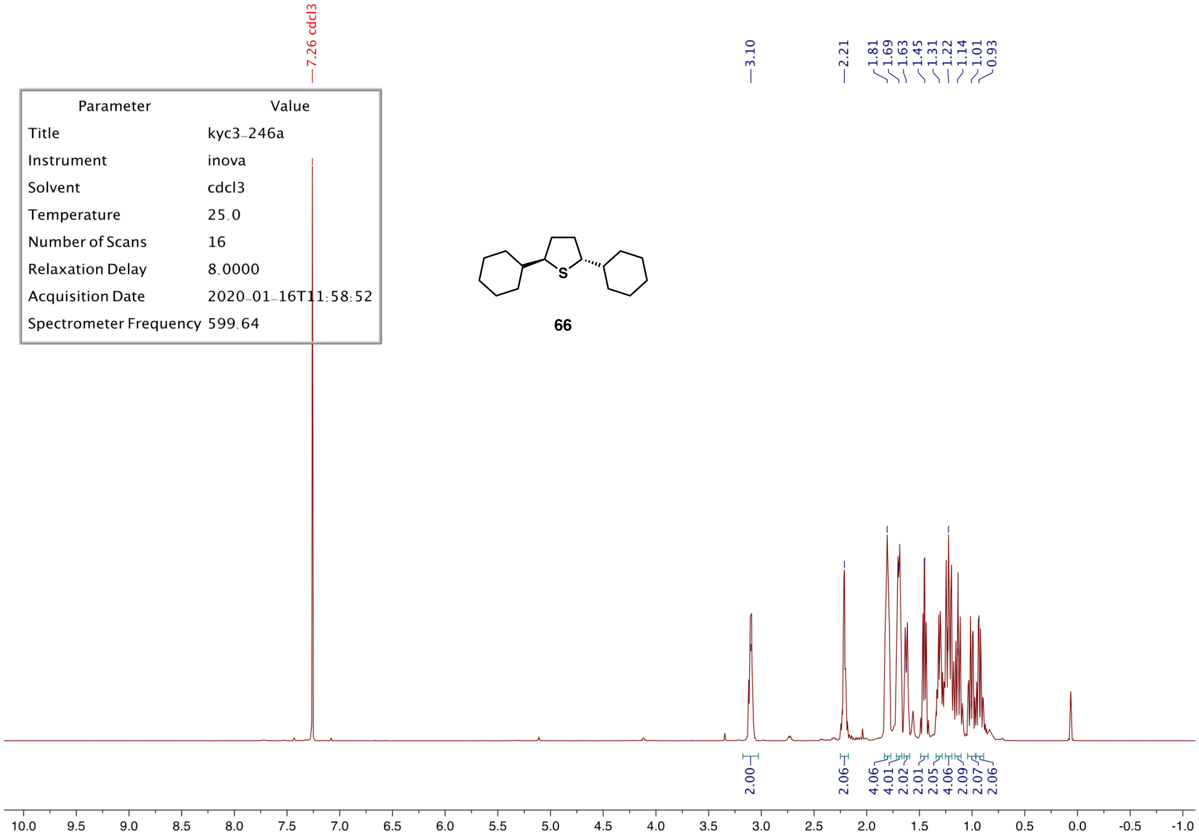

Parameter	Value
Title	kyc3_246a
Instrument	inova
Solvent	cdcl3
Temperature	25.0
Number of Scans	16
Relaxation Delay	8.0000
Acquisition Date	2020-01-16T11:58:52
Spectrometer Frequency	599.64

66

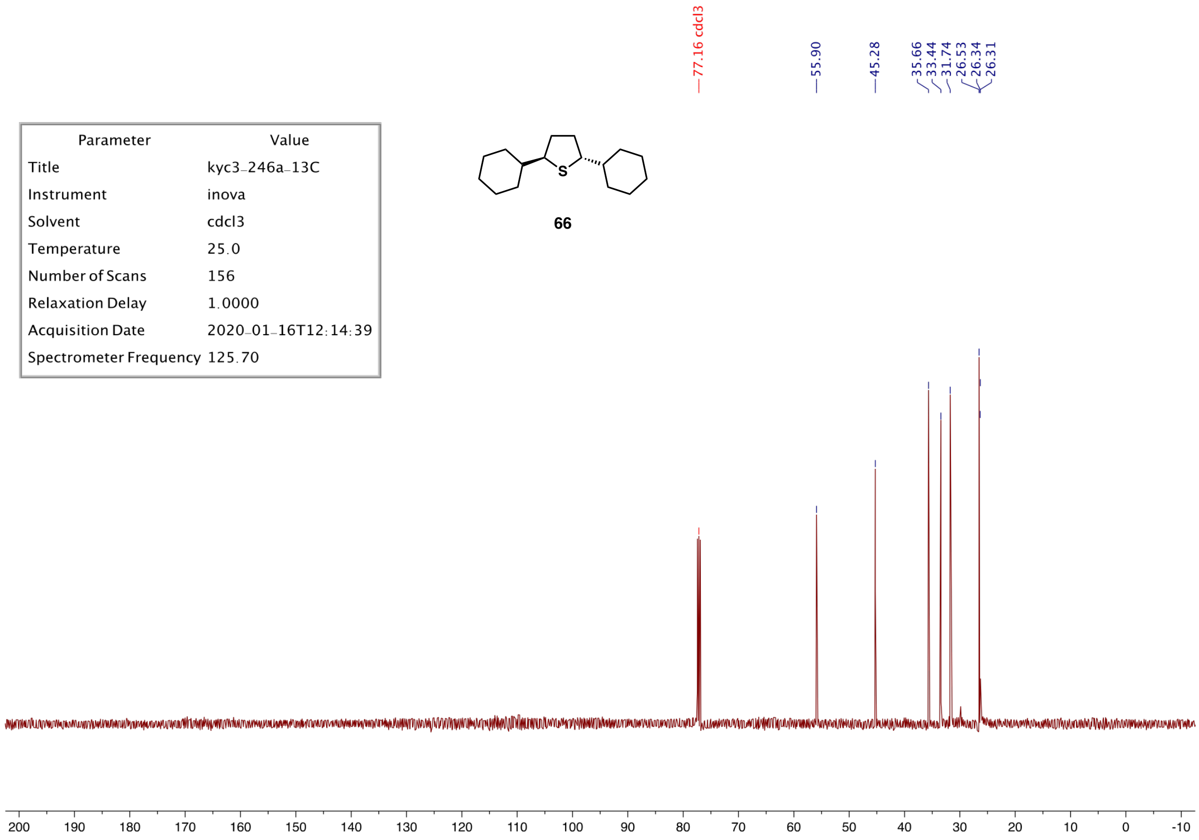

Parameter	Value
Title	kyc3_246a_13C
Instrument	inova
Solvent	cdcl3
Temperature	25.0
Number of Scans	156
Relaxation Delay	1.0000
Acquisition Date	2020-01-16T12:14:39
Spectrometer Frequency	125.70

66

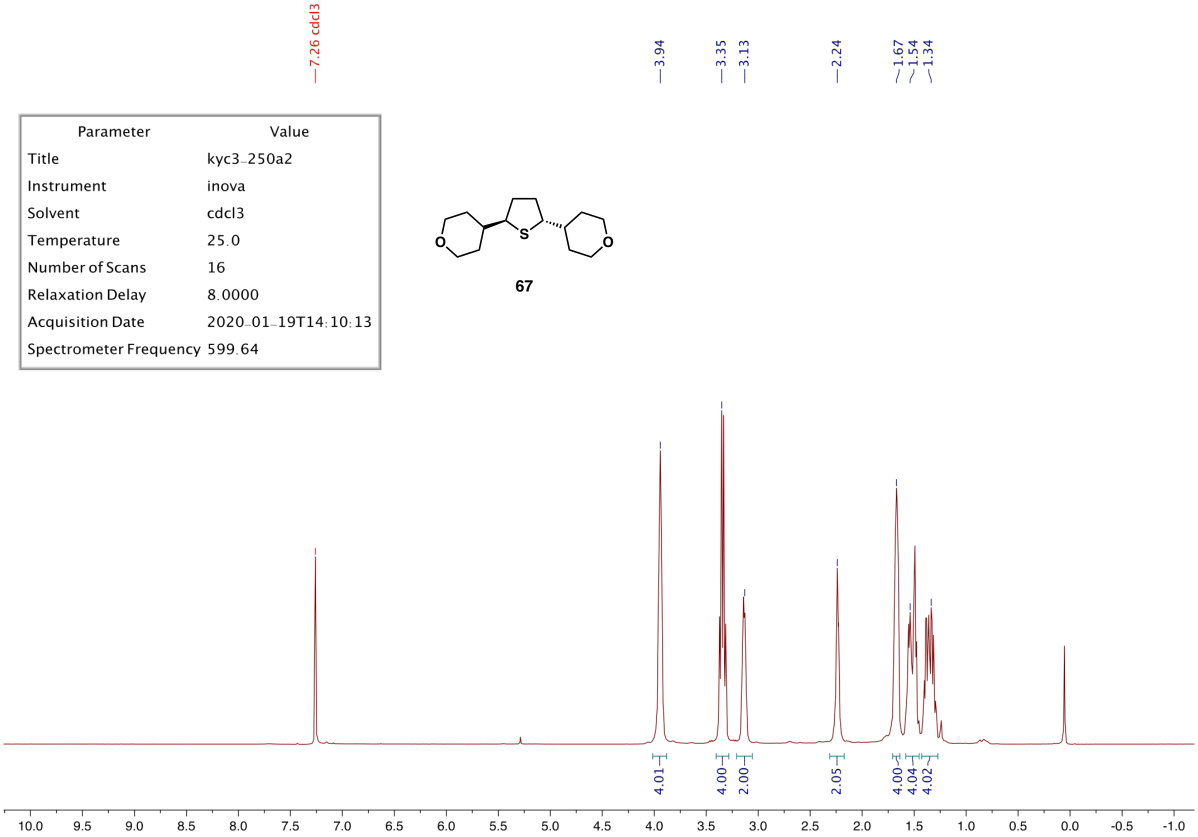

Parameter	Value
Title	kyc3_250a2
Instrument	inova
Solvent	cdcl3
Temperature	25.0
Number of Scans	16
Relaxation Delay	8.0000
Acquisition Date	2020-01-19T14:10:13
Spectrometer Frequency	599.64

67

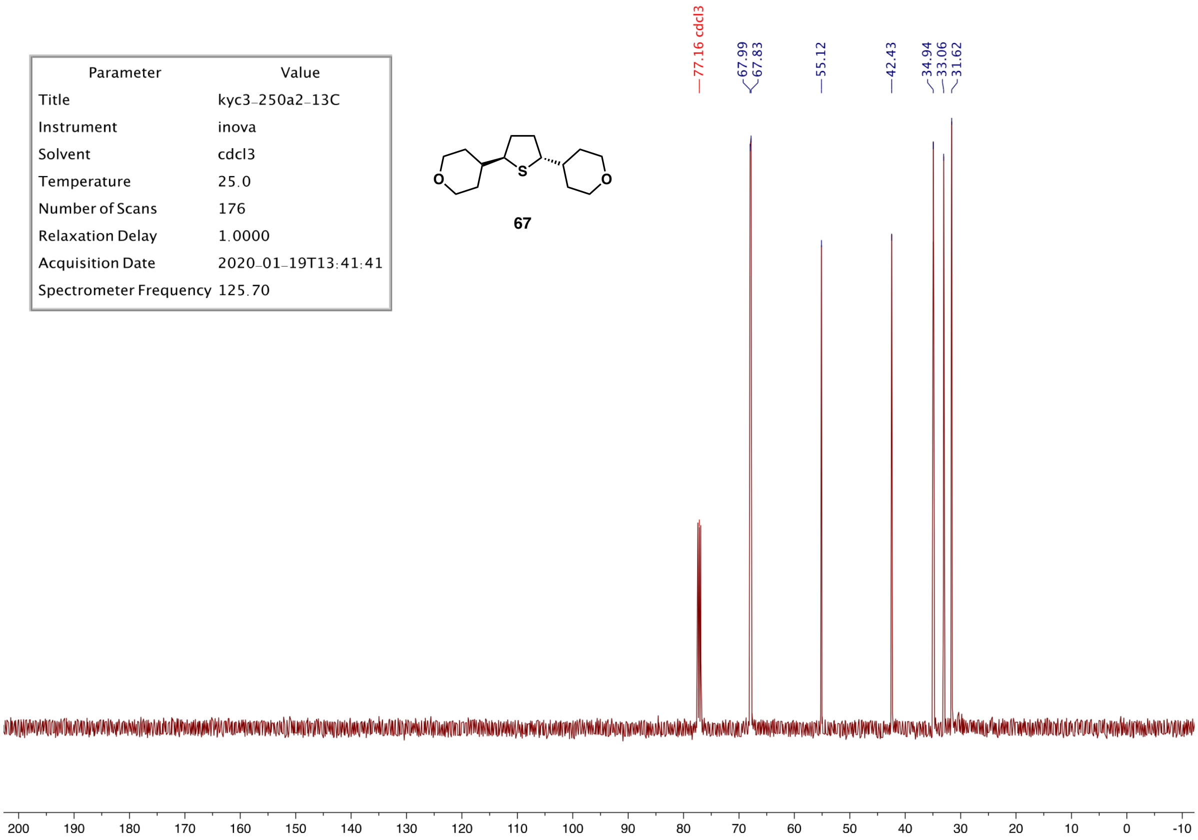

Parameter	Value
Title	kyc3_250a2_13C
Instrument	inova
Solvent	cdcl3
Temperature	25.0
Number of Scans	176
Relaxation Delay	1.0000
Acquisition Date	2020-01-19T13:41:41
Spectrometer Frequency	125.70

67

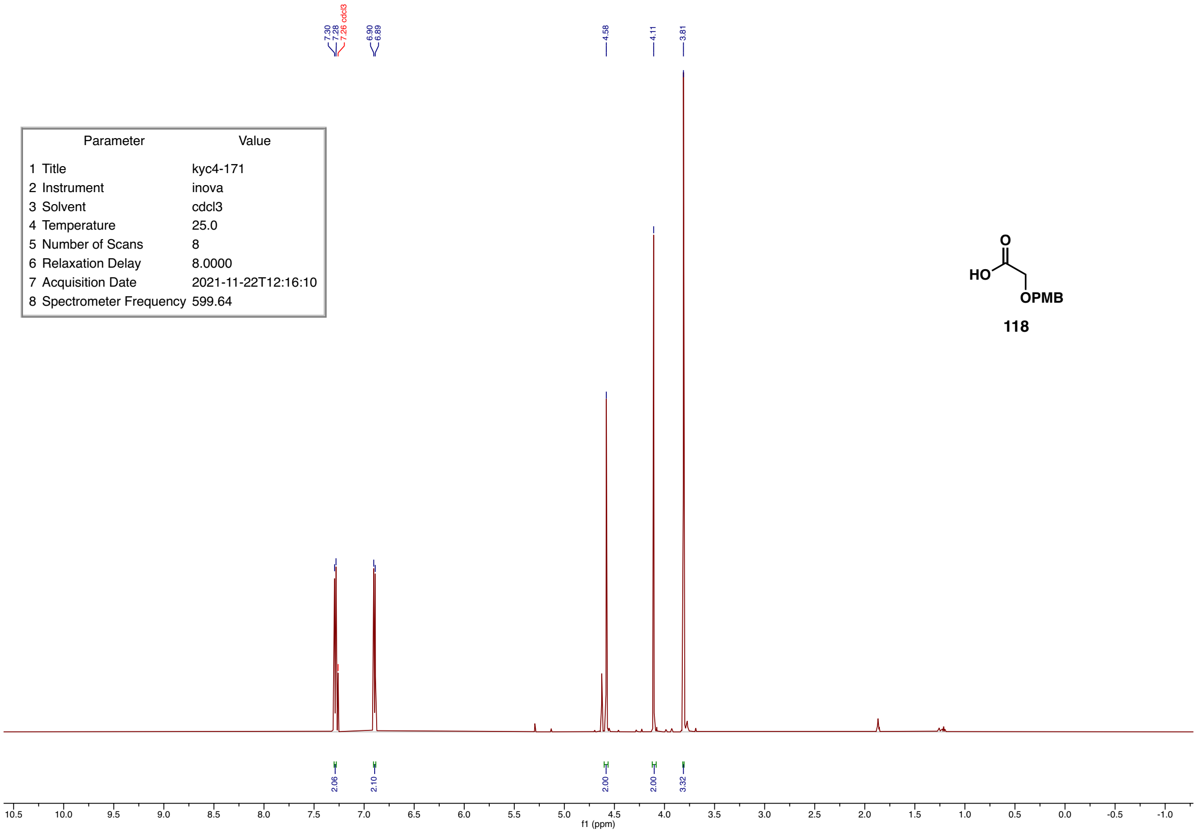

Parameter	Value
1 Title	kyc4-171
2 Instrument	inova
3 Solvent	cdcl3
4 Temperature	25.0
5 Number of Scans	8
6 Relaxation Delay	8.0000
7 Acquisition Date	2021-11-22T12:16:10
8 Spectrometer Frequency	599.64

118

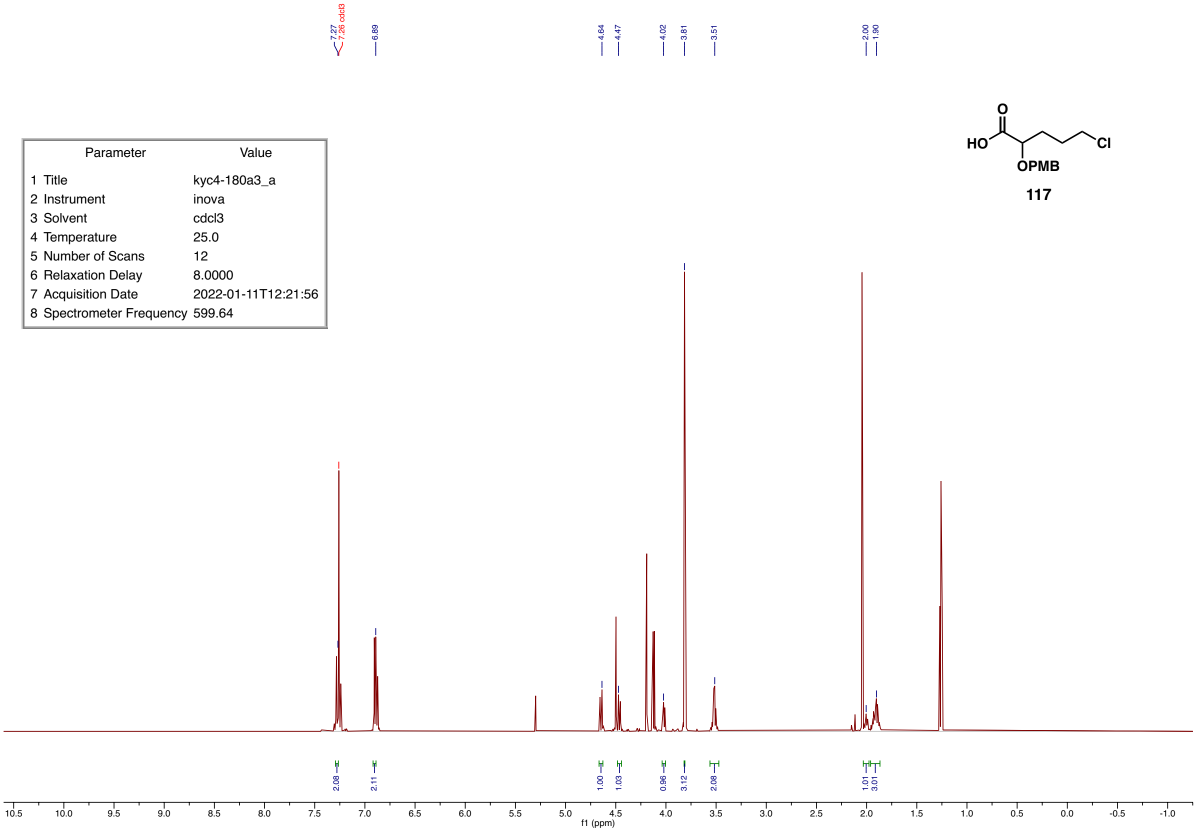

Parameter	Value
1 Title	kyc4-180a3_a
2 Instrument	inova
3 Solvent	cdcl3
4 Temperature	25.0
5 Number of Scans	12
6 Relaxation Delay	8.0000
7 Acquisition Date	2022-01-11T12:21:56
8 Spectrometer Frequency	599.64

117

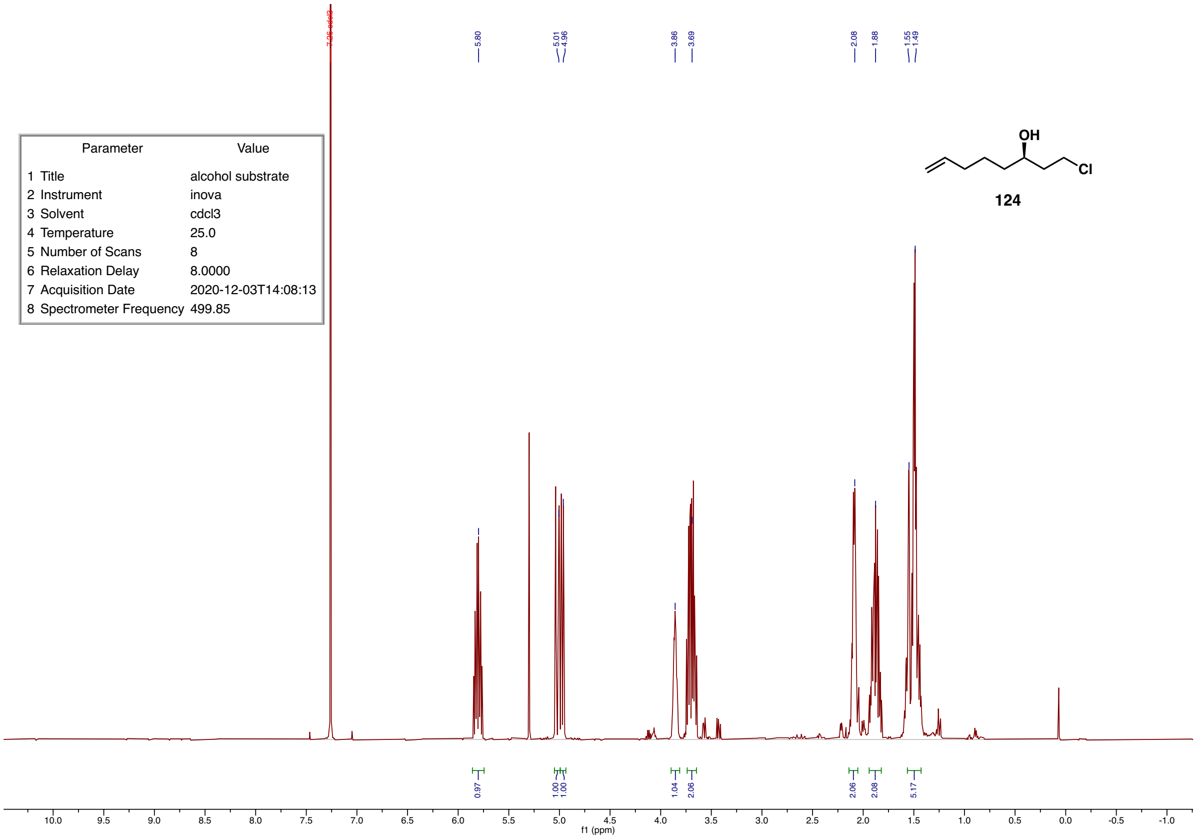

Parameter	Value
1 Title	alcohol substrate
2 Instrument	inova
3 Solvent	cdcl3
4 Temperature	25.0
5 Number of Scans	8
6 Relaxation Delay	8.0000
7 Acquisition Date	2020-12-03T14:08:13
8 Spectrometer Frequency	499.85

124

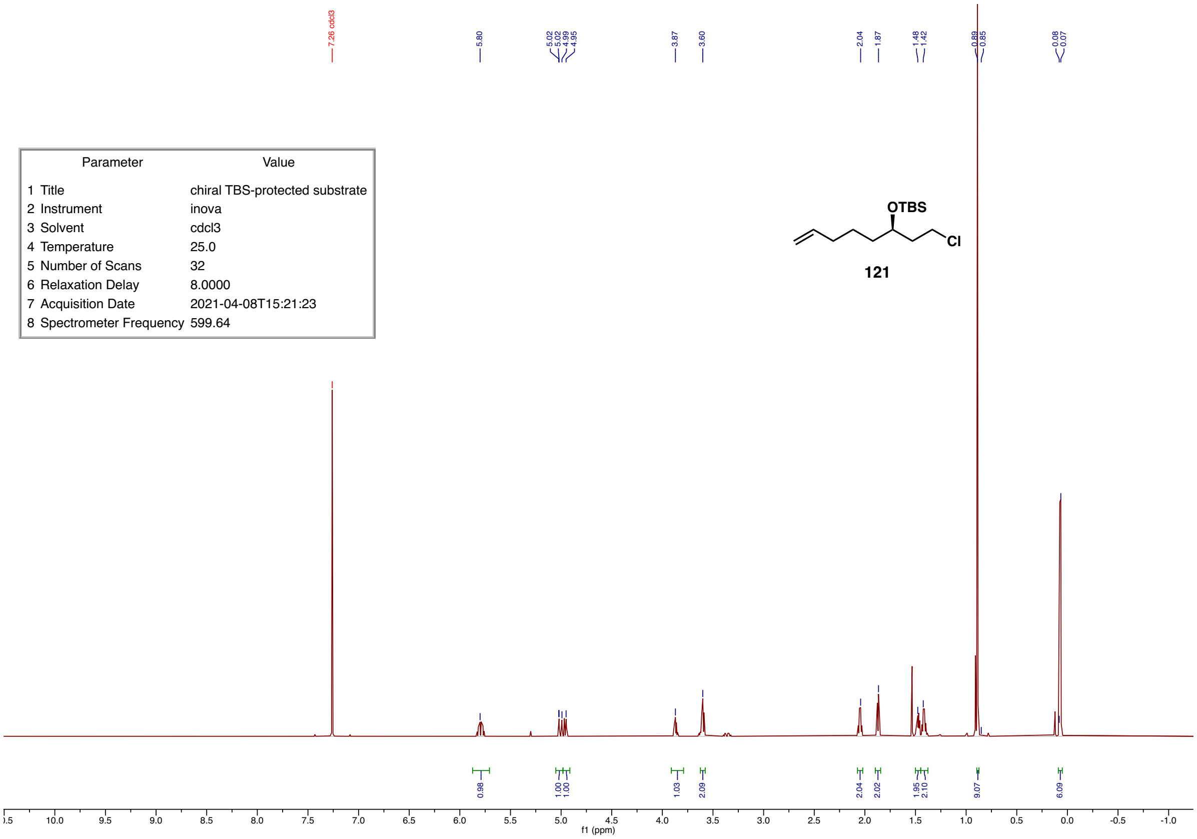

Parameter	Value
1 Title	chiral TBS-protected substrate
2 Instrument	inova
3 Solvent	cdcl3
4 Temperature	25.0
5 Number of Scans	32
6 Relaxation Delay	8.0000
7 Acquisition Date	2021-04-08T15:21:23
8 Spectrometer Frequency	599.64

121

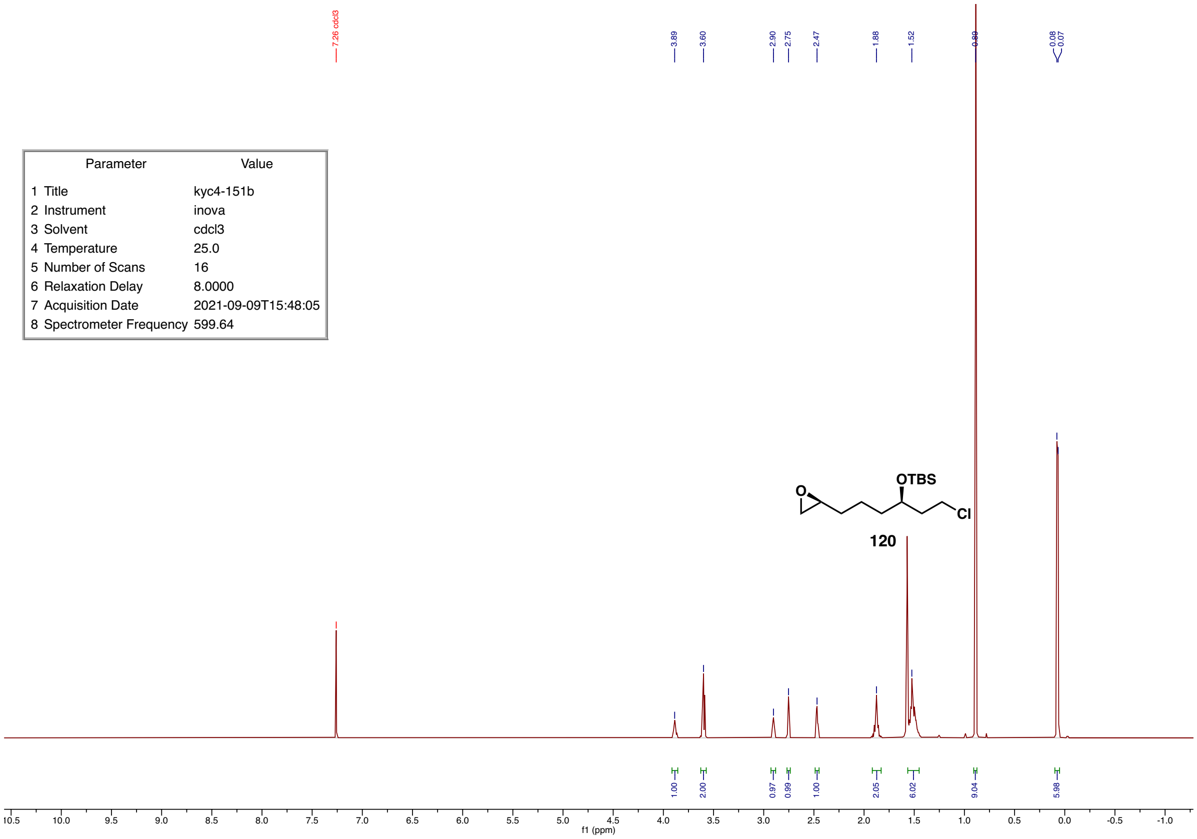

120

Parameter	Value
1 Title	kyc4-151b
2 Instrument	inova
3 Solvent	cdcl3
4 Temperature	25.0
5 Number of Scans	16
6 Relaxation Delay	8.0000
7 Acquisition Date	2021-09-09T15:48:05
8 Spectrometer Frequency	599.64

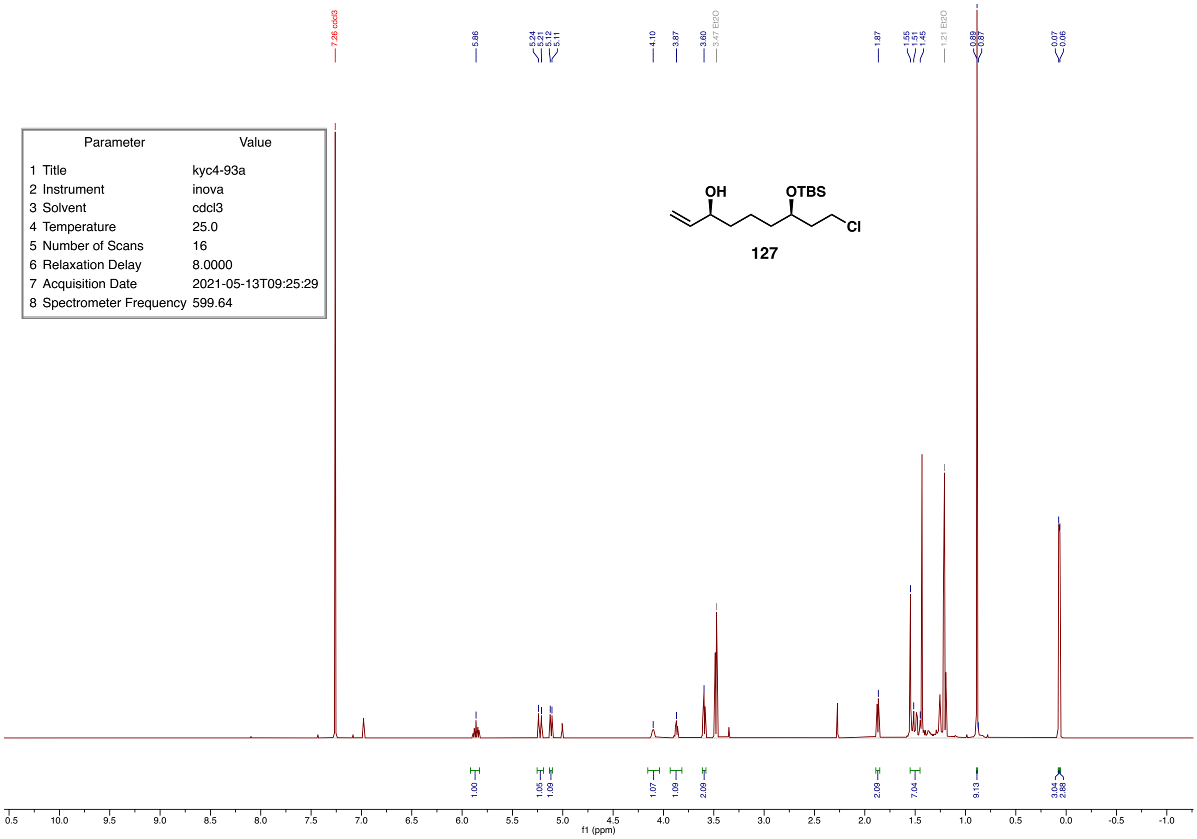

127

Parameter	Value
1 Title	kyc4-93a
2 Instrument	inova
3 Solvent	cdcl3
4 Temperature	25.0
5 Number of Scans	16
6 Relaxation Delay	8.0000
7 Acquisition Date	2021-05-13T09:25:29
8 Spectrometer Frequency	599.64

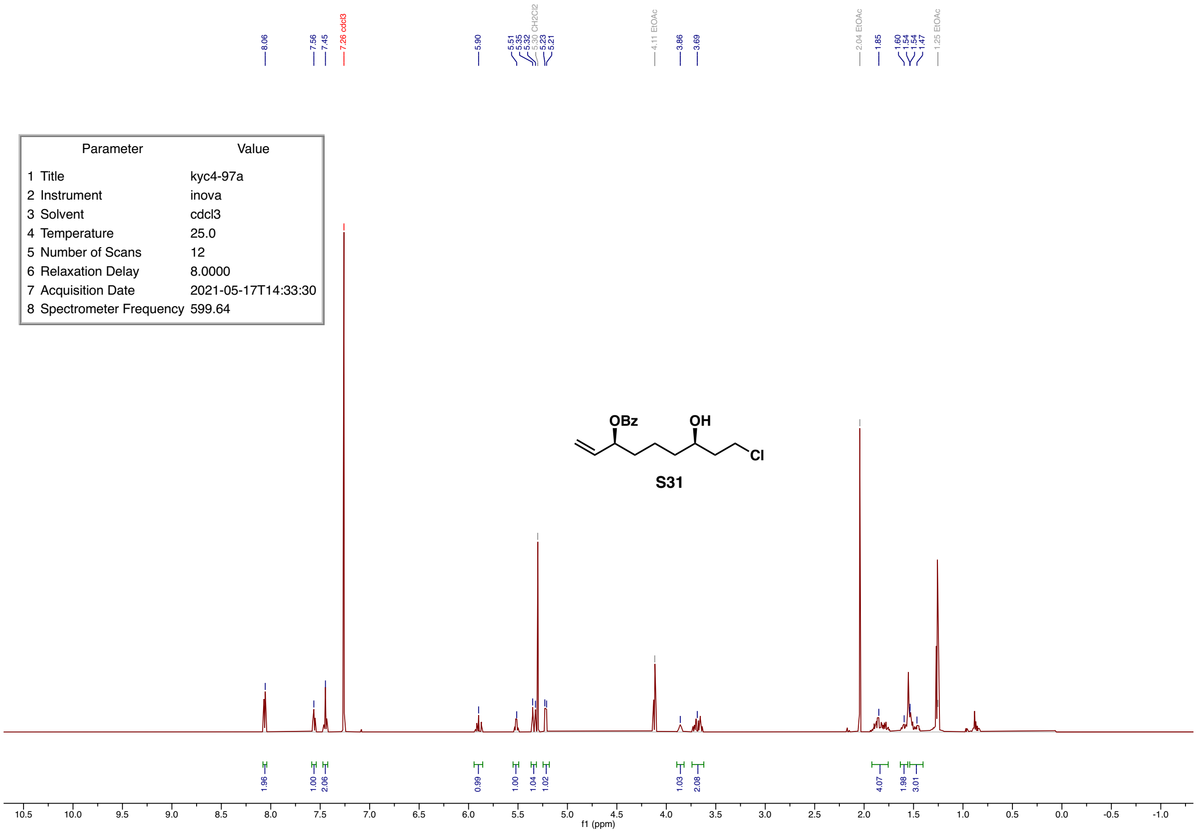

Parameter	Value
1 Title	kyc4-97a
2 Instrument	inova
3 Solvent	cdcl3
4 Temperature	25.0
5 Number of Scans	12
6 Relaxation Delay	8.0000
7 Acquisition Date	2021-05-17T14:33:30
8 Spectrometer Frequency	599.64

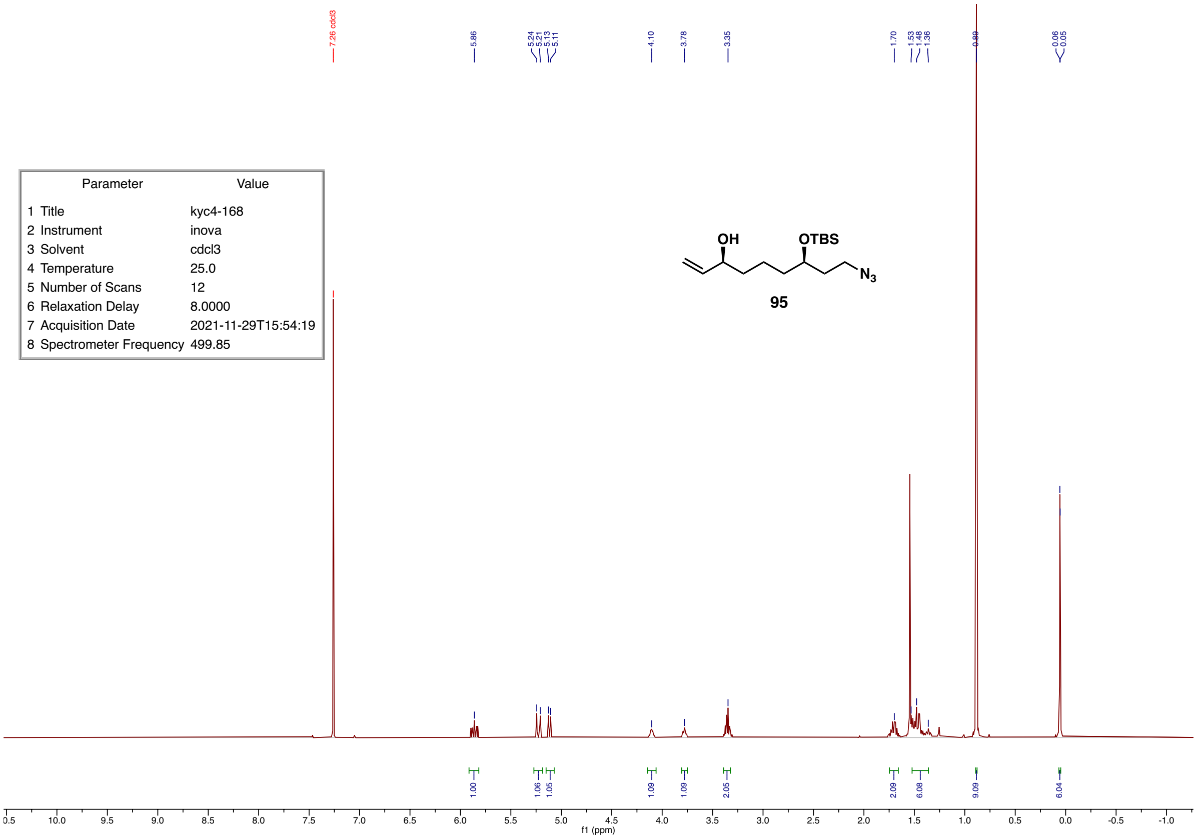

Parameter	Value
1 Title	kyc4-168
2 Instrument	inova
3 Solvent	cdcl3
4 Temperature	25.0
5 Number of Scans	12
6 Relaxation Delay	8.0000
7 Acquisition Date	2021-11-29T15:54:19
8 Spectrometer Frequency	499.85